

**Borrower is requested  
to check the book and  
get the signatures on the  
torned pages, if any.**

### Kashmere Gate, Delhi

**DUE DATE**

**For each day's delay after the due date a fine of 50 P. per Vol. Shall be charged for books of General Section and Re 1.00 for text books Section.**

Borrower's No.	Due Date	Borrower's No.	Due Date



*Centrifugal and Axial Flow*

P U M P S

THEORY, DESIGN, AND APPLICATION

*A. J. Stepanoff, Ph.D.*

*Melville Medalist 1932, A.S.M.E.*

*Ingersoll-Rand Company*

1948

NEW YORK • JOHN WILEY & SONS, INC.  
LONDON • CHAPMAN & HALL, LIMITED



COPYRIGHT, 1943  
BY  
ALEXEY J. STEPANOFF

---

*All Rights Reserved*

*This book or any part thereof must not  
be reproduced in any form without  
the written permission of the publisher.*

FOURTH PRINTING, NOVEMBER, 1954

PRINTED IN THE UNITED STATES OF AMERICA

## PREFACE

The progress in the design and application of centrifugal pumps has been so rapid that at present almost all limitations of pressure, capacity, temperature, nature of liquid, and speed of operation have disappeared. This advance in construction and application has presented numerous problems—mechanical, hydraulic, operating, and economic. None of the books on centrifugal pumps gives an adequate account of the progress of the art during recent years or deals with problems arising from new practices and uses of these pumps. To make possible this advance in pump design required theoretical and experimental studies of such subjects as: cavitation; operation outside the normal head-capacity and speed range; axial and radial thrust; effect of stuffing boxes on the critical speed of pump shafts; control of head-capacity and brake-horsepower curves; pumping viscous liquids.

The theoretical treatment of the centrifugal pump impeller presented herein deviates materially from that found in existing texts on the subject. The new method of attack is based on: a single pattern of flow; identical theoretical reasoning; and similar procedure of impeller layout for centrifugal, mixed flow, and axial flow pumps. As a result a simple diagram (Fig. 9.16) evolved which combines the important design elements and performance characteristics of all centrifugal pumps and is, in a sense, a "Mollier diagram" of centrifugal and axial flow pumps.

Chapters 6, 12, and 13 evolved from articles submitted by me to the Hydraulic Institute for the Annual Engineering Essay Contest; they were awarded first prize in the years 1941, 1942, and 1943, respectively. It is suggested that the reader become familiar with *Standards of the Hydraulic Institute* (90 West Street, New York, N.Y.) which contains a great volume of useful information not duplicated in this book.

I am indebted to Ingersoll-Rand Company, to Mr. D. R. Lowry, Executive Vice President, and to Mr. A. P. Brocklebank, Chief Engineer, whose interest and encouragement made this book possible. I wish to acknowledge also the help of my associates at Ingersoll-Rand Company and particularly that of Messrs. A. Brkich and H. A. Stahl who have participated in the discussion of all important phases of the book and have read the proofs.

The manuscript was critically reviewed by Professor J. W. Daily of Massachusetts Institute of Technology, Professor A. Hollander and Dr. D. E. Hudson of California Institute of Technology, and Mr. I. J. Karassik of Worthington Pump and Machinery Corporation who have furnished numerous corrections and improvements throughout the book.

Although great care has been exercised to check the manuscript and proofs, errors may be discovered. I shall appreciate it if these are called to my attention. I also invite criticism of the views presented in the book or suggestions which may lead to its improvement.

A. J. S.

*Phillipsburg, N. J.*

*November, 1947*

# CONTENTS

## Chapter 1    SELECTED TOPICS FROM HYDRAULICS

1.1	Bernoulli's Equation . . . . .	1
1.2	Reynolds' Number . . . . .	3
1.3	Flow through Elbows and Bends . . . . .	7
1.4	Energy Gradient . . . . .	10
1.5	Transition of Pressure in Liquid in Motion . . . . .	11
1.6	Pressure Energy . . . . .	13
1.7	Vortex Motion . . . . .	14
1.8	Losses . . . . .	18

## Chapter 2    DEFINITIONS AND TERMINOLOGY

2.1	Introduction . . . . .	21
2.2	Classification and Terminology . . . . .	21
2.3	Field of Application and Limitations . . . . .	25
2.4	Pump Characteristics . . . . .	25
2.5	Specific Speed . . . . .	29
2.6	Net Positive Suction Head . . . . .	30

## Chapter 3    THEORY OF THE CENTRIFUGAL PUMP IMPELLER

3.1	Velocity Triangles . . . . .	31
3.2	Theoretical Head of Centrifugal Pumps . . . . .	32
3.3	Theoretical Characteristic Curves . . . . .	35
3.4	Efficiencies . . . . .	37
3.5	Impeller Approach and Prerotation . . . . .	39
3.6	Discussion of Euler's Characteristics and Euler's Velocity Triangles . . . . .	44
3.7	Flow through the Impeller . . . . .	48
3.8	Pfleiderer's Correction to Euler's Equation . . . . .	55

## Chapter 4    VORTEX THEORY OF EULER'S HEAD

4.1	Radial Impeller . . . . .	58
4.2	Axial Flow Impeller . . . . .	63
4.3	Forced Vortex Axial Flow Impeller . . . . .	66
4.4	Special Cases . . . . .	72

## Chapter 5    SPECIFIC SPEED AND DESIGN CONSTANTS

5.1	Centrifugal Pump Constants from General Principles of Similitude . . . . .	76
5.2	Specific Speed, Unit Speed, and Unit Capacity . . . . .	82
5.3	Reduction of Impeller Diameter . . . . .	89
5.4	Design Constants . . . . .	93
5.5	Specific Speed in Terms of Design Constants . . . . .	99

## Chapter 6 DESIGN OF MIXED FLOW IMPELLERS FOR CENTRIFUGAL PUMPS

6.1	Introduction . . . . .	103
6.2	Geometrical Relationships . . . . .	104
6.3	Plain Vane Faults . . . . .	105
6.4	Mixed Flow Impellers . . . . .	106
6.5	Vane Development on a Cone . . . . .	108
6.6	Method of "Error Triangles" . . . . .	110
6.7	Application of Method of Error Triangles to the Design of Plain Vanes . . . . .	119

## Chapter 7 PUMP CASING

7.1	Suction Nozzle . . . . .	121
7.2	Volute . . . . .	122
7.3	Pressure Distribution and Radial Thrust in the Volute Casing . . . . .	128
7.4	Crossover . . . . .	136
7.5	Diffusion Casing . . . . .	138

## Chapter 8 AXIAL FLOW PUMPS

8.1	Range of Specific Speeds . . . . .	143
8.2	Factors Affecting Specific Speed . . . . .	143
8.3	Summary of Test Results . . . . .	149
8.4	Design Procedure for an Axial Flow Impeller . . . . .	154
8.5	Use of Airfoil Data for Impeller Design . . . . .	155
8.6	Discussion of Airfoil Theory . . . . .	161
8.7	Guide Vanes Ahead of the Impeller . . . . .	163
8.8	The Axial Flow Pump Casing . . . . .	165

## Chapter 9 HYDRAULIC PERFORMANCE OF CENTRIFUGAL PUMPS

9.1	Hydraulic Losses . . . . .	170
9.2	Total Head-Capacity Curve . . . . .	176
9.3	Hydraulic Efficiency . . . . .	178
9.4	Author's Diagram of Centrifugal Pump Characteristics . . . . .	184

## Chapter 10 LEAKAGE, DISK FRICTION, AND MECHANICAL LOSSES

10.1	Leakage Loss . . . . .	193
10.2	Disk Friction Loss . . . . .	201
10.3	Mechanical Losses . . . . .	205
10.4	Losses versus Capacity at Constant Speed . . . . .	209
10.5	Open Impeller Design . . . . .	213

## Chapter 11 AXIAL THRUST

11.1	Single-Stage Pumps . . . . .	218
11.2	Multistage Pumps . . . . .	223
11.3	Open Impellers . . . . .	236

**Chapter 12 CAVITATION IN CENTRIFUGAL PUMPS**

12.1	Introduction and Definition . . . . .	241
12.2	Signs of Cavitation . . . . .	242
12.3	Materials to Resist Cavitation Pitting . . . . .	250
12.4	Theoretical Relationship at Cavitation Conditions . . . . .	254
12.5	Factors Affecting Cavitation . . . . .	257
12.6	Predetermination of Cavitation Conditions from Velocity Considerations . . . . .	259
12.7	Thoma's Cavitation Constant . . . . .	262
12.8	Means of Avoiding or Reducing Cavitation . . . . .	269

**Chapter 13 SPECIAL OPERATING CONDITIONS OF CENTRIFUGAL PUMPS**

13.1	Introduction . . . . .	271
13.2	Complete Pump Characteristics; Representation of Test Results . . . . .	272
13.3	Mechanical Problems Connected with Pump Operation Outside the Normal Head-Capacity and Rotation Range . . . . .	272
13.4	Hydraulic Problems Arising during Unusual Pump Operating Conditions . . . . .	280
13.5	Starting of Centrifugal Pumps . . . . .	287
13.6	Effect of Specific Speed upon the Behavior of Centrifugal Pumps under Special Operating Conditions . . . . .	292

**Chapter 14 SPECIAL PROBLEMS OF PUMP DESIGN AND APPLICATION**

14.1	Unstable Head-Capacity Characteristics of Centrifugal Pumps . . . . .	296
14.2	Determining Operating Points of Centrifugal Pumps Working on Pipe Lines . . . . .	301
14.3	Variable Speed Engine Drive . . . . .	307
14.4	Pumping Viscous Liquids with Centrifugal Pumps . . . . .	310
14.5	Regulation of Capacity of Centrifugal Pumps . . . . .	319
14.6	Model Testing . . . . .	325

**Chapter 15 SHAFT DESIGN FOR CRITICAL SPEEDS**

15.1	Theoretical Relationships . . . . .	328
15.2	Main Factors Affecting the Critical Speed . . . . .	334
15.3	Calculation of Critical Speeds . . . . .	336
15.4	Example of Graphical Determination of the Critical Speed . . . . .	338
15.5	Critical Speed Tests . . . . .	344
15.6	The Three-Bearing Shaft . . . . .	345
15.7	Higher Critical Speeds . . . . .	346
15.8	Secondary Critical Speeds . . . . .	347
15.9	Secondary Factors Affecting Critical Speed . . . . .	349
15.10	Selection of Critical Speed . . . . .	351

**Chapter 16 SPECIAL PROBLEMS AND APPLICATIONS OF VERTICAL TURBINE AND AXIAL FLOW PUMPS**

16.1	Brake Horsepower at Zero Capacity . . . . .	354
16.2	Vertical Propeller Pumps versus Horizontal Pumps . . . . .	360
16.3	Suction Sump Design . . . . .	363

16.4	Adjustable Impeller Vane Axial Flow Pumps . . . . .	367
16.5	Examples of Propeller and Vertical Turbine Pumps . . . . .	371
16.6	Measuring Large Volumes of Water in the Field . . . . .	383
16.7	Field Performance of Vertical Turbine Pumps . . . . .	385

#### **Chapter 17      SPECIAL PROBLEMS AND APPLICATIONS OF CENTRIFUGAL PUMPS**

17.1	Hot-Oil Pumps . . . . .	388
17.2	Field Testing of Hot-Oil Pumps . . . . .	396
17.3	Boiler Feed Pumps . . . . .	397
17.4	Boiler Forced Circulation Pumps . . . . .	402
17.5	Examples of Centrifugal Pumps and Installations . . . . .	405

#### **Chapter 18      CENTRIFUGAL-JET PUMP WATER SYSTEMS**

18.1	General Arrangement . . . . .	413
18.2	Jet Pumps . . . . .	414
18.3	Performance of a Centrifugal-Jet Pump Combination . . . . .	419
18.4	Affinity Relations . . . . .	422
Index . . . . .		425

## CHAPTER 1

### SELECTED TOPICS FROM HYDRAULICS

A theoretical treatment of the flow through hydraulic machines is very difficult because most of the channels comprising such machines have variable and irregular sections and a curved mean path. Some of the channels are in a circular motion with power applied to or taken from the flow. Simple relationships established in hydraulics for idealized conditions, if applied directly to such flow, may not only give an incorrect quantitative answer but may also result in a false qualitative mental pattern of flow.

An oversimplified view of some of the flow problems in hydraulics has, in the past, resulted in a number of fallacies which still persist although there is ample experimental evidence to prove the erroneous reasoning behind such views.

In this chapter a number of subjects are treated which are either missing or not sufficiently emphasized in books on hydraulics. In several instances limitations of principles established in hydraulics, when applied to conditions of flow as found in centrifugal pumps, are stressed. A few of the most common fallacies are clarified.

#### 1.1 BERNOULLI'S EQUATION

When Bernoulli's equation is applied to the flow through various parts of hydraulic machines its limitations are frequently overlooked. Bernoulli's equation,

$$h + \frac{p}{\gamma} + \frac{v^2}{2g} = E = \text{constant} \quad (1.1)$$

represents the energy per unit of weight where  $h$  is the energy of position (or ability to do work when situated  $h$  feet above the arbitrary datum plane),  $p/\gamma$  is the pressure energy, and  $v^2/2g$  is the kinetic energy, or velocity head. All three are expressed in feet. The quantity  $E$  is the total energy in foot-pounds per pound of liquid. It does not depend on the specific weight of the liquid,  $\gamma$ . When applied to two points of the same tube, Bernoulli's equation expresses the law of conservation of energy for an *idealized* liquid. In actual liquids, variations of  $E$



between different streamlines occur and changes of the value of  $E$  may be produced by the action of viscosity. The following paragraphs deal with the limitations caused by actual liquids.

(a) Equation 1.1 is obtained from the power equation

$$Q\gamma h + Qp + Q\gamma \frac{v^2}{2g} = \text{constant} \quad (1.2)$$

by eliminating  $Q$  (volume per unit time) and  $\gamma$  (specific weight of the liquid).

Elimination of  $Q$  from equation 1.2, when applied to two points of the same stream tube, requires that continuity of volume be satisfied. This means that in a closed conduit no liquid escapes or is added between the two points. *Therefore, when Bernoulli's equation is applied to imaginary stream tubes or streamlines, this continuity requirement makes it necessary that the two points of comparison lie on the same streamline because the constant in Bernoulli's equation is not necessarily the same for different streamlines;* as, for example, in straight pipe flow the total energy carried by streamlines near the center of the pipe is greater than that at any point in the pipe section.

(b) Elimination of  $\gamma$  from equation 1.2 is possible only if  $\gamma$  is constant at all points of the flow. *This means that the liquid must be incompressible.* It is not sufficient that the product  $Q\gamma$  be constant, because this product represents the weight of the liquid which is constant for gases. Bernoulli's equation, as given in equation 1.1, does not apply for gases because it does not include thermodynamic changes which take place in flowing gas. From the above it follows that *Bernoulli's equation cannot be used in cases where the gases are liberated or absorbed along the flow path, as either process involves an energy change.*

(c) A *streamline* is defined as the path of the liquid particle made up of prevailing flow direction from point to point. A fluid is in steady motion when its streamlines permanently maintain their position and relative arrangement and velocities at each point on the streamline are the same. *Bernoulli's equation applies only to a steady flow.*

(d) *Bernoulli's equation applies only to an "absolute" flow.* In relative flow in a moving channel, depending on the form of the channel and the nature of its motion, energy is either applied to or absorbed from the flow. Thus the constant in Bernoulli's equation varies along the streamline and from one streamline to another.

(e) *With actual liquids, Bernoulli's equation is not applicable to curvilinear motion* because inertia forces come into play and centrifugal forces are developed. Streamlines do not maintain their relative posi-

tions; secondary crossflows appear; and the liquid may leave the walls of the channel.\*

(f) *Even when applied to the average flow of the whole channel, Bernoulli's equation is invalid if the conduit contains bends and turns, or is in motion, because local pressures and velocities (as measured at two points) may differ greatly from the average values for the whole flow.* Besides, the velocity head in Bernoulli's equation based on mean velocity does not represent the true kinetic energy of the flow which is equal to a summation of the kinetic energy of individual streamlines<sup>1</sup> and

$$\frac{v_m^2}{2g} < \sum \frac{v^2}{2g}$$

This expression means that the square of the mean is smaller than the mean of the squares. This can be verified easily by a numerical example.

## 1.2 REYNOLDS' NUMBER

Reynolds' number  $R = vd/\nu$ , where  $v$  is the velocity,  $d$  the diameter of pipe, and  $\nu$  the kinematic viscosity of liquid, is used as a criterion of the flow in closed conduits. The type of flow (laminar or turbulent) and the velocity distribution are similar for geometrically similar tubular sections, and the same friction coefficient  $f$  can be used in Darcy's formula

$$h = f \frac{L}{d} \frac{v^2}{2g}$$

if the Reynolds number is the same irrespective of the nature of the fluid or actual velocity or pipe size. A considerable amount of data on friction losses for round pipes has been accumulated and correlated with Reynolds' number as a basis. Evaluation of the pipe roughness is the only factor which makes the results uncertain to within  $\pm 10$  per cent.

(a) **Hydraulic Radius.** For conduits other than circular, it has been customary to use the hydraulic radius  $m = \text{area}/\text{wetted perimeter}$ , and to select the friction coefficient from round pipe data for  $d = 4m$ , the existence of similarity of flow pattern under such conditions being assumed. *There is no theoretical justification for such an assumption because geometrical similarity is the first prerequisite for similarity of flow.* Thus, for laminar flow it has been shown theoretically and proved

\* Equation 12.1 of Chapter 12, widely used in treatises on pumps, is an example of misapplication of Bernoulli's equation.

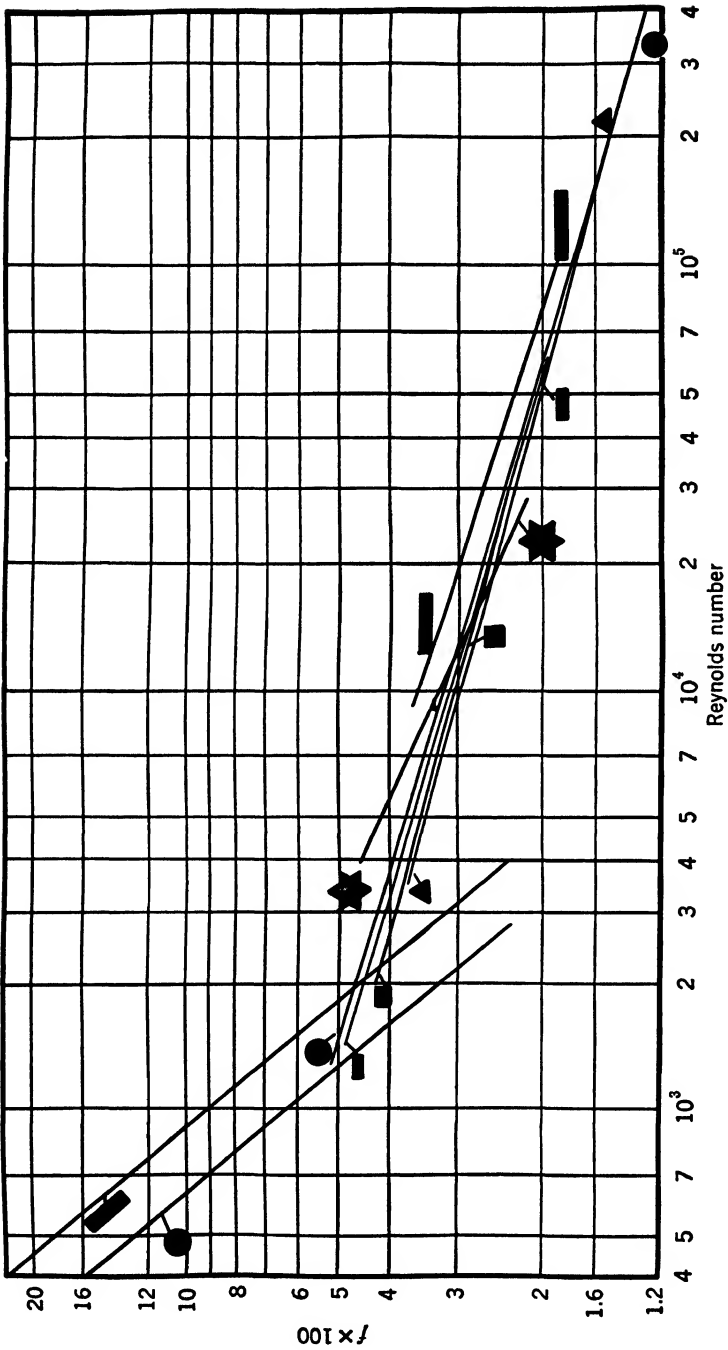


Fig. 1.1. Friction coefficient for smooth pipes of different cross section (Schiller).

experimentally that the friction coefficient for a rectangular channel section depends on the shape of the channel and is different from that for a round pipe.<sup>2</sup>

$$f = \frac{64}{R} \quad \text{for a round pipe}$$

$$f = 0.89 \frac{64}{R} \quad \text{for a square channel}$$

$$f = 1.5 \frac{64}{R} \quad \text{for an annulus, or two flat plates}$$

Schiller<sup>2</sup> investigated the flow through conduits of different sections—round, square, rectangular, triangular, and star-shaped—and found that the coefficients of friction  $f$ , plotted on the basis of  $d = 4m$ , do not coincide with those for round pipe, as is shown in Fig. 1.1, which represents Schiller's results. In the turbulent region the difference is not great and, for lack of better means, round pipe data may be used for flow in channels of other shape as an approximation, although the theoretical justification of such procedure is lacking.

**(b) Curvilinear Flow and Channels of Variable Cross Section.** *Anything that disturbs the velocity distribution of flow, such as a change in area or direction of flow, changes the pattern of flow through a conduit, and the Reynolds number based on the average velocity of steady flow ceases to be a criterion of the flow in the sense that it is used for straight pipe flow.* That is to say, the same Reynolds number is no assurance of similarity of flow because the change from laminar to turbulent flow may take place at vastly different Reynolds numbers when the pipe axis is not straight.<sup>3</sup> There is no way to estimate the friction coefficient  $f$  for such a flow; in fact, in some cases determination of the exact channel length or sectional area is impossible (example: impeller and volute channels). Moreover, the skin friction loss becomes secondary to additional eddy losses incurred by the disturbing element. The eddy losses follow laws different from those followed by friction losses. In a straight pipe flow a length of 20 to 40 pipe diameters (or even more according to some investigators) is necessary for the flow to assume its final velocity distribution. No such length is available in the channels comprising a centrifugal pump. Most of these are of irregular section, mostly divergent, some are stationary, and others are in rotary motion. There are a number of Reynolds numbers that can be assigned to a given pump, depending on what channel and which section of a given channel are taken for calculation of velocity and characteristic length for the Rey-

nolds number. Each of many possible Reynolds numbers, if used as a criterion of operation of a given type of pump, will reflect the summary effect of all channels comprising a pump. Properties of such criteria have never been determined and are different from those established for a straight pipe flow. Fortunately in a modern pump hydraulic friction losses are but a small fraction of the pump power input, and affect

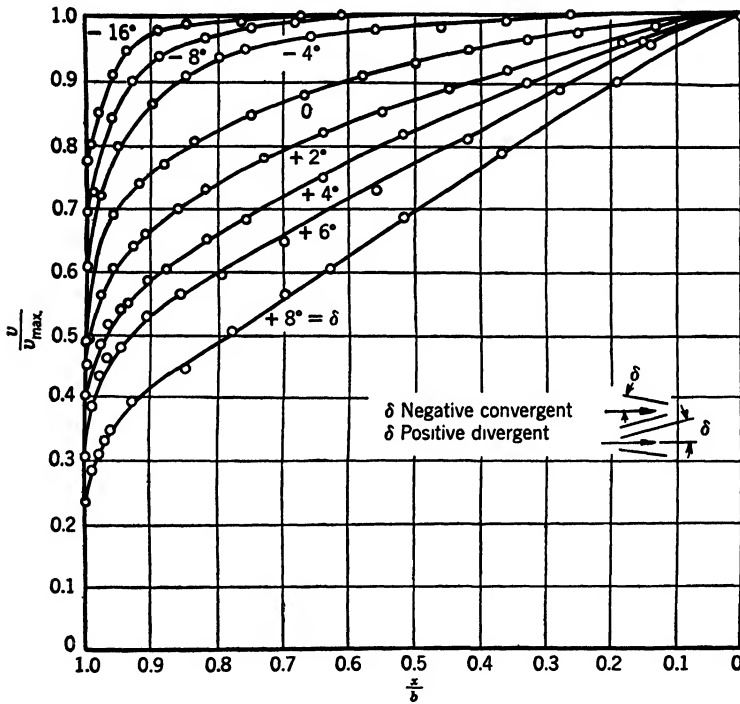


FIG. 1.2. Velocity distribution in convergent and divergent rectangular channels;  $b$  is one half of channel width,  $x$  is location of the point from the axis of the channel (Nikuradse).

little the laws of similarity governing the head generation which are the basis of the pump design. For that reason the dearth of accurate information about hydraulic losses in centrifugal pumps has not retarded appreciably the progress in their design.

To summarize, it can be stated that the velocity distribution, the loss of head (friction and eddy losses), and the pattern of flow (laminar or turbulent) cannot be established from the knowledge of Reynolds' number in curvilinear, divergent, or convergent flow. For some types of flow there is no generally accepted definition of Reynolds' <sup>1</sup> number;

for others, properties of Reynolds' number have never been determined in a sense commonly used for the straight pipe flow.

(c) **Convergent and Divergent Channels.** Figure 1.2 is reproduced from Nikuradse's work <sup>4</sup> to show the effect of channel section variation on the velocity distribution. The most uniform velocity across the channel is obtained in a convergent channel. The beneficial effect of convergent flow is made use of in designing impeller approach channels for the purpose of producing uniform velocity distribution. The author has found that a reducing suction elbow is just as efficient as a straight taper, an indication that the bad effect of an elbow on the velocity distribution is fully neutralized by the steadying effect of a convergent channel.

### 1.3 FLOW THROUGH ELBOWS AND BENDS

(a) **Velocity and Pressure Distribution.** The majority of investigations on flow through pipe bends and elbows were concerned with the losses of pressure through these parts. A theoretical pattern of flow,  $vr = \text{constant}$  (where  $v$  is the velocity of a streamline and  $r$  is the radius of curvature of its path), was generally assumed. However, more recent studies <sup>5</sup> have shown that such a pattern of flow exists only at very low velocities or where the ratio of the mean radius of curvature to the pipe diameters,  $r/d$ , is very large. At high velocities, or low values of  $r/d$ , the flow shifts toward the outer wall of the elbow in the second half of the turn (Figs. 1.3 and 1.4). With ideal liquids a change in the velocity distribution is followed by a change in pressure distribution in such a manner that an increase in velocities near the inner walls is accompanied by a pressure drop, and a reduction in velocities at the outer wall of the

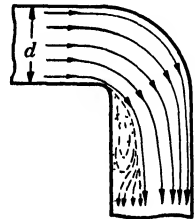


FIG. 1.3. Direction of streamlines in an elbow (Corrider).

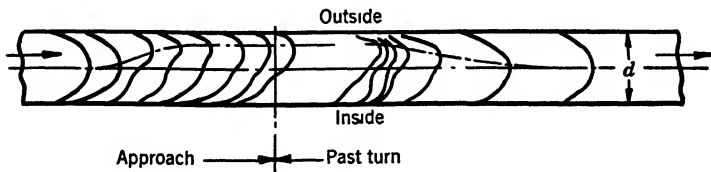


FIG. 1.4. Velocity distribution in an elbow; developed (Saph and Schoder).

turn is followed by a pressure increase. Such a velocity and pressure distribution begins to appear in the approach to the turn with low velocities and high  $r/d$  ratio.

In high velocities and sharp turns, although high velocities shift toward the outer wall, the pressure distribution is affected little by this change, and the maximum velocity and pressure both exist at the outer wall of the bend. The low pressure zone extends somewhat downstream,

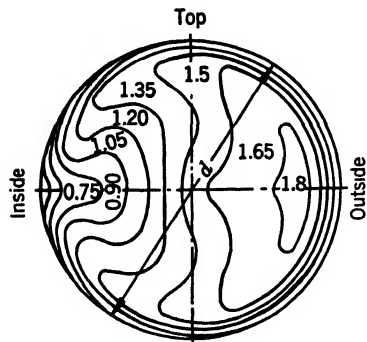


FIG. 1.5. Velocity distribution in the middle of an elbow; velocities in meters per second (Saph and Schoder).

resulting in a separation of flow from the inner wall and the formation of pockets filled with eddies (Figs. 1.5 and 1.6). Such behavior of liquid in a turn is caused by inertia of the flowing mass or centrifugal forces. In addition, two spiral cross-flow motions appear in the stream which are directed, in the middle, toward the outer wall of the turn and along the side walls of the pipe, toward the inner wall of the turn (Fig. 1.7).

Figure 1.8 shows the velocity and pressure distribution in a standard 6-in. elbow obtained by Yarnell.<sup>6</sup> Numbers under each section of pipe represent the location in feet from the beginning of the turn; negative when it is upstream, positive when downstream. High pressures and velocities are at the outer wall by the end of the turn. Six feet beyond the turn pressures are equalized, but it takes up to 10 ft. to restore the normal pipe velocity distribution.

Adler<sup>7</sup> observed higher velocities and pressures near the outer wall of the turn for laminar flow, very large radii of curvature  $r/d$  (25, 50,

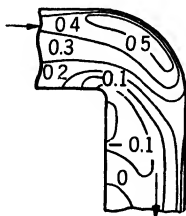


FIG. 1.6. Pressure distribution in an elbow. Pressures shown are in meters of water (Cordier).

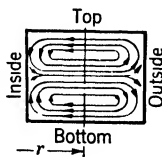


FIG. 1.7. Diagram of spiral cross flows in an elbow.

and 100), and Reynolds numbers 1930 to 3220. The critical values of velocities or ratio of  $r/d$  at which the theoretical velocity and pressure distribution is destroyed were not definitely established.

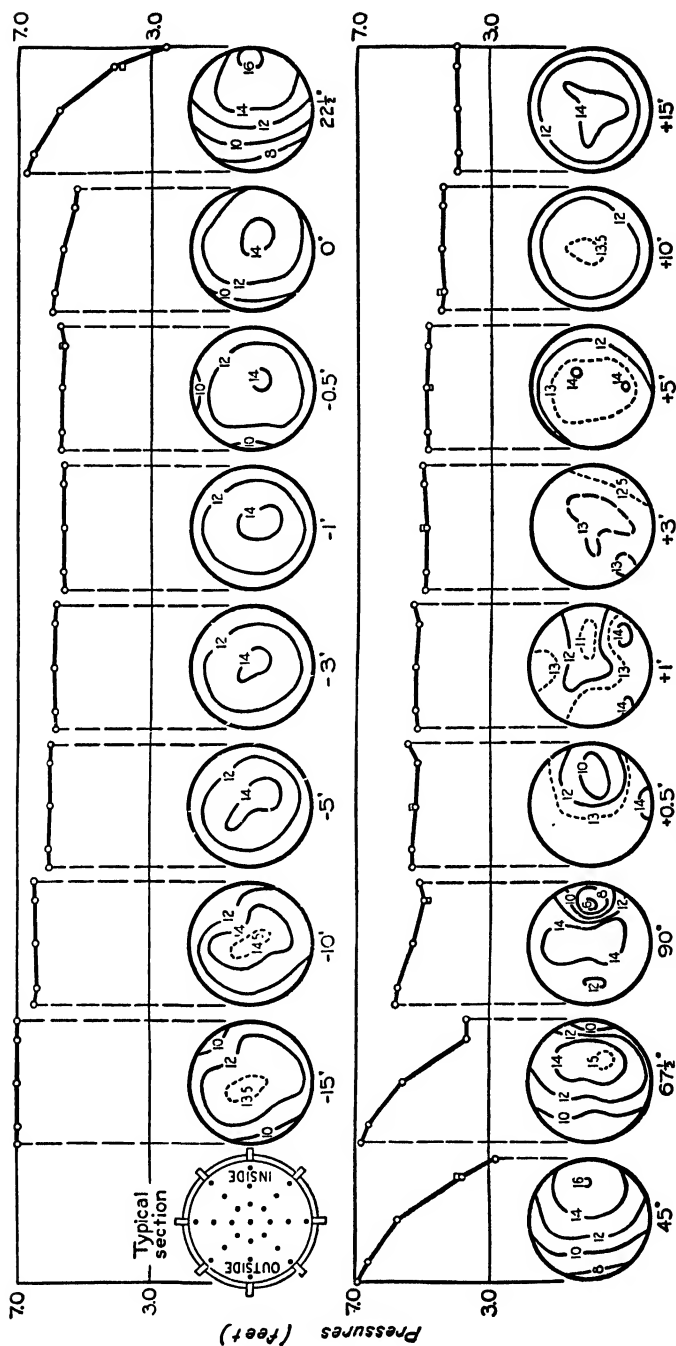


Fig. 1.8. Velocity distribution and peripheral pressures in standard bend; mean velocity, 12 ft. per sec.



*In centrifugal pumps, all passages in the impeller and casing are curvilinear and velocities are high. Therefore a theoretical velocity and pressure distribution is hardly ever encountered,*

**(b) Several Turns in Series.** When the flow of liquid follows several turns in succession in the same direction, which are located in different

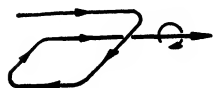


FIG. 1.9. Several elbows in series induce vortex motion.

planes as shown in Fig. 1.9, the liquid acquires a spiral motion which is superimposed on its forward velocity.<sup>8</sup> Such motion does not cause any additional losses in a channel with a circular cross section; in fact, it has a definite tendency to stabilize the flow. However, if the channel is square or rectangular, losses of head result because of excessive

eddies in the corners. In multistage centrifugal pumps of the volute type, such a succession of turns is found in the crossover passages from stage to stage. Round sections for the major portion of the crossovers should be used to reduce the losses.

#### 1.4 ENERGY GRADIENT

*To start and maintain flow in a channel, stationary or moving, there must be a drop in total energy content in the direction of flow below its initial level at zero flow.* The graphical representation of the total energy along the path of flow is the energy gradient. This should be distinguished from the hydraulic gradient, which shows only static pressures at different points of the path (Fig. 1.10). The hydraulic gradient may have a local drop and rise along the path, but the energy gradient drops continually and it determines the direction of flow. In actual pipe flow the energy gradient drop represents hydraulic losses along the flow path.

An idealized flow can be imagined to be produced by hydraulic (or pressure) gradient drop with the energy content remaining constant; for instance, the discharge from a vessel through a nozzle. But in every case where real liquids are concerned the process will follow the direction indicated by the energy gradient drop.

The presence of a pump in a system of conduits produces a jump in the energy gradient, but the flow is still maintained by the energy gradient drop ahead of the pump, through the pump, and beyond the pump. *In a movable channel, such as an impeller of a pump, the energy gradient drop is referred to the energy level when there is no flow.* When the flow

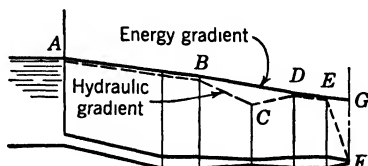


FIG. 1.10. Energy and hydraulic gradients.

starts, energy is absorbed by the flow at such a rate that the total energy remains, at all times and at all points, below its zero flow level. The use of the energy gradient concept simplifies a number of problems connected with the flow through a pump and will be elaborated further in later chapters (Figs. 1.11, 1.13; Fig. 7.11).

### 1.5 TRANSITION OF PRESSURE IN LIQUID IN MOTION

In a stationary body of liquid, pressure intensity is transmitted equally in all directions. In moving liquids, a difference in pressure may exist along the path of the flow and also across the section of the channel as a result of the dynamic forces developed by the flow. Pressure changes along the path of flow are a result of a change in kinetic energy as given by Bernoulli's equation, the total energy of each streamline remaining constant.

*Variation of pressure across a channel, however, can occur in such a manner that some streamlines will increase their pressure without decreasing their velocities, thus increasing their total energy, or the constant in Bernoulli's equation. But, since the total energy of the flow across the channel section remains the same, such an increase of pressure energy of one group of streamlines takes place at the expense of the pressure energy of the remaining streamlines. When the transition of pressure energy takes place in this manner without actual mixing of streamlines, pressure energy exchange might be called "conduction" by analogy to heat conduction. Both pressure energy and heat energy are due to molecular kinetic energy and are interchangeable, as is well known in thermodynamics of gases.*

*When the pressure energy exchange is effected by shifting or mixing of streamlines the process is similar to convection. There is still another mode of pressure transition which takes place without exchange of particles or mixing of streamlines, and that is by means of traveling pressure waves. This method might be called pressure radiation. Pressure waves follow all water-hammer phenomena and are treated in the extensive literature on the subject.*

The flow of pressure energy from a higher to a lower level takes place naturally like heat flow from a higher to a lower temperature, whereas the flow of pressure energy in the reverse direction usually takes place under the dynamic forces developed in a curvilinear or rotary motion. As soon as the tangential component of the velocity is taken out of the flow by special means, such as guide vanes or a straight length of pipe (Fig. 1.8) pressures are immediately equalized by a natural flow of the pressure energy from a higher to a lower level without mixing

of the streamlines, that is, by conduction. Conduction is responsible for the constant pressure across the section of a channel with a steady flow assumed in hydraulics.† Examples of conduction and convection of pressure energy follow. Figure 1.11 shows a straight pipe approach to an impeller of a centrifugal pump. At the section  $AB$ , sufficiently removed from the pump, pressure  $p_1$  is uniform across the section and a normal pipe velocity distribution prevails. At section  $CD$ , near the pump, the pressure  $p_2$ , as measured at the pipe wall, is higher than at

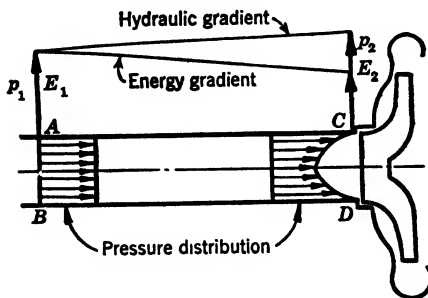


FIG. 1.11. Hydraulic and energy gradients along impeller approach.

section  $AB$ . But since the energy gradient decreases from  $AB$  to  $CD$ , the higher pressure at  $CD$  can appear only at the expense of the middle streamlines. A paraboloid of pressure distribution is developed at  $CD$  with the pressure at the periphery higher (and lower at the center) than the average original pressure. The absolute velocities at the periphery are higher than those in the middle as a result of the ad-

dition of a tangential component due to rotation of the stream. This pressure exchange takes place without mixing of streamlines or by conduction.‡

In Chapter 3, it will be shown that prerotation in the suction pipe is caused by the tendency of the liquid to follow a path of least resistance on its way to enter impeller channels. This becomes evident when the prerotation is in a direction opposite to that of the impeller. This occurs usually at pump capacities exceeding the normal capacity.

The process is reversed at the discharge of an axial flow pump. At the impeller discharge, pressure and velocities are higher at the periphery than at the hub. In the diffusion casing, part of the kinetic energy is converted into pressure, and pressures are equalized across the whole discharge pipe area. The exchange of pressure energy in the diffusion casing takes place without mixing of streamlines (by conduction), as

† Tests by Mayer with a straight transition channel from a rectangular to a circular section of constant area show that pressure unequalsities across the channel can be produced by the curvature of individual streamlines near walls caused by the change of the shape of the cross-sectional area. These changes in pressure are not compensated by the changes in local velocities. (N.A.C.A. Tech. Memo. 903, 1939, p. 25, translation of Verein deutscher Ingenieure Forschungsheft 389).

‡ An experimental illustration of the pattern of flow in the suction pipe is found in Art. 3.5 and Figs. 3.8 and 3.9.

visually observed by Schmidt,<sup>9</sup> by introducing smoke and sparks at a blower inlet.

Higher velocities and pressures near the outer wall of a turn observed by Adler<sup>7</sup> for laminar flow may serve as an illustration of the pressure transition by conduction, as there is no mixing of streamlines in the laminar flow.

Transition of pressure by convection takes place, for instance, in an elbow (Fig. 1.6). Beyond the turn, pressure and velocities are higher at the outer wall of the turn, the increase in energy being made at the expense of streamlines near the inner wall. This process is not efficient and is always followed by losses or degeneration of pressure energy into heat. Beyond the turn a uniform pressure is reestablished, partly by convection, partly by conduction.

## 1.6 PRESSURE ENERGY

**(a) Definition.** Pressure energy is defined by the term  $p/\gamma$  in Bernoulli's equation (1.1).§ It should be distinguished from the energy of compression as applied to gases. Energy of compression is due to the volume elasticity of fluids and is negligible for liquids. Both the pressure energy and the energy of compression are varieties of potential energy, which is stored energy. The difference between the two becomes apparent from the following example: a pound of water in an enclosed vessel under 100 p.s.i. static pressure possesses energy of compression only, which is negligible; but a pound of water at the bottom of a standpipe 231 ft. high possesses 231 ft.-lb. of pressure energy. The amount of potential energy of a pound of water in the standpipe is the same irrespective of its position in the standpipe but it is differently divided between the pressure energy and energy of position for different elevations in the standpipe. In both examples the amount of stored energy is equal to the amount of energy put in. Pressure is only an indication of the level at which energy is stored without any reference to the amount, in the same manner as temperature is no indication of the amount of heat in a body.

Pressure and pressure energy have been confused frequently.<sup>16, 17</sup> Pressure  $p$  (pounds per unit area) may stand for pressure energy in expressions such as Bernoulli's equation, where it means energy (foot-pounds) per unit volume in the same manner as head  $h$  in feet represents energy in foot-pounds per pound of liquid.

§ See Spannake, *Centrifugal Pumps, etc.*, M.I.T. Publication, 1934, p. 28; also King, *Hydraulics*, 1922, p. 56, and Hughes and Safford, *Hydraulics*, 1921, p. 20.

**(b) Solid-Liquid Mixtures.** Centrifugal pumps are widely used for transporting solids in suspension in a liquid. Dredging operations and pumping of paper pulp, ashes, and cement are examples of moving solids in suspension. Both mechanical and hydraulic performance of pumps are greatly affected by the presence of solids in the liquid.

*It is important to realize that solids in suspension in the liquid cannot absorb, store, or transmit pressure energy, which is a property of fluids.* Pressure exerted by a fluid on the walls of a container is caused by the bombardment of molecules freely moving in a confined space. Molecules of a solid being restricted in their movement by the molecular attraction cannot participate in maintaining or transmitting pressure energy, nor can they increase their own kinetic energy (disregarding the energy of compression) when surrounded with liquid carrying the pressure energy. A simple example will illustrate the point: in a standpipe a pound of solids at the top of the standpipe has as much potential energy of position as a pound of water (referred to the bottom of the standpipe). At the bottom of the standpipe a pound of water possesses as much potential energy as a pound of water at the top of the standpipe, but a pound of solids at the bottom of standpipe does not possess any energy referred to the same datum. If a mixture of solids and water is pumped into the standpipe a pound of solids would not carry any energy into the standpipe except a small amount of kinetic energy which is wasted at the discharge. In a standpipe filled with a solid-liquid mixture of an average specific gravity of, say, 1.1, the pressure gage at the bottom of the standpipe will register a pressure 1.1 times that of the clear water. But this pressure increase is due to the extra pressure energy of the liquid required to move and support solids in suspension. The potential energy of solids is all due to position and is all wasted when solids settle to the bottom of the standpipe.

*Note that, having no part in maintaining or transmitting pressure energy, solids in suspension cannot convert their kinetic energy into pressure.* This question becomes important and will be further elaborated in the discussion of pumping solids in suspension with centrifugal pumps in Chapter 4, Art. 4.4 (c).

## 1.7 VORTEX MOTION

Movement of water in a circular path is known as a vortex motion. All particles of liquid describing circles of the same radius form stream cylinders. Particles of the same stream cylinder move with the same tangential and angular velocity. These velocities may vary from one cylinder to another. *Variation in the linear or angular velocity deter-*

mines the pressure distribution along the radius, or the shape of the free surface if the vessel containing the liquid is open to atmosphere.

The condition of equilibrium requires that, for each particle, the centrifugal force must be balanced by the pressure or static liquid column at the same point.

$$\frac{dp}{dr} = \frac{\gamma}{g} \frac{v^2}{r} = \frac{\gamma}{g} \omega^2 r \quad (1.3)$$

where  $p$  is pressure at radius  $r$ ,  $v$  is the tangential velocity, and  $\omega$  is the angular velocity.

If the variation of angular velocity with radius is known, substitution of this value of  $\omega$  into equation 1.3 will permit integration, and the pressure distribution along the radius will be obtained. In Table 1, results of the integration of equation 1.3 are tabulated for a velocity distribution given by an equation:

$$\omega = Cr^m \quad (1.4)$$

or

$$vr^n = C \quad (1.5)$$

where

$$n = -(m + 1)$$

*Different values of  $m$  result in different types of vortices. The free vortex and forced vortex described in textbooks on hydraulics are special cases of this series. The first one is determined by a condition*

$$vr = C_3 \quad (1.6)$$

and the pressure distribution is obtained from

$$h + \frac{p}{\gamma} + \frac{v^2}{2g} = E = \text{constant} \quad (1.7)$$

which states that all particles possess the same amount of energy. If such a vortex is superimposed upon an axial flow with a uniform velocity, equation 1.7 will require either that no energy be added to the liquid or that energy be added at a constant rate. Such a pattern of flow is sometimes assumed for axial flow pumps.

In a forced vortex the angular velocity is constant, or

$$\omega = \text{constant} \quad (1.8)$$

This means that the liquid is revolving as a solid body. After the liquid is set in motion, disregarding losses, no power is required to maintain such a vortex. The pressure distribution curve is a square parabola;

TABLE 1. VORTEX MOTION

Curve No. on Figs. 1.12 (a) and 1.12 (b)	Angular Velocity Distribution $\omega = C r^m$	Peripheral Velocity Distribution $vr^n = C$	Pressure Distribution $\int dp = \int \frac{\gamma}{g} \omega^2 r dr$	Type of Vortex	Remarks
1	$\omega = C_1 r^{-\infty}$	$vr^\infty = C_1$	$\frac{p}{\gamma} = C_1^2 + h_1 = \text{constant}$	$\omega = 0$ , stationary	
2	$\omega = C_2 r^{-3/2}$	$vr^{3/2} = C_2$	$\frac{p}{\gamma} = -\frac{C_2^2}{3gr^{3/2}} + h_2$		
3	$\omega = C_3 r^{-2}$	$vr = C_3$	$\frac{p}{\gamma} = -\frac{C_3^2}{2gr^2} + h_3$	$\frac{v^2}{\gamma} + \frac{p}{\gamma} = \text{constant}$ , free vortex	$\omega$ is higher toward center for 1, 2, 3, 4, 5, and 6
4	$\omega = C_4 r^{-3/2}$	$vr^{3/2} = C_4$	$\frac{p}{\gamma} = -\frac{C_4^2}{gr} + h_4$		
5	$\omega = C_5 r^{-1}$	$vr^0 = C_5$	$\frac{p}{\gamma} = \frac{C_5^2}{g} \log r + h_5$	$v = \text{constant}$	
6	$\omega = C_6 r^{-1/2}$	$vr^{-1/2} = C_6$	$\frac{p}{\gamma} = \frac{C_6^2 r}{g} + h_6$	$\frac{v^2}{r} = \text{constant} = \text{centrifugal force}$	
7	$\omega = C_7 r^0$	$vr^{-1} = C_7$	$\frac{p}{\gamma} = \frac{C_7^2 r^2}{2g} + h_7$	$\omega = \text{constant}$ , forced vortex	$\omega = \text{constant}$
8	$\omega = C_8 r^{1/2}$	$vr^{-3/2} = C_8$	$\frac{p}{\gamma} = \frac{C_8^2 r^3}{3g} + h_8$	Super-forced vortex	
9	$\omega = C_9 r$	$vr^{-2} = C_9$	$\frac{p}{\gamma} = \frac{C_9^2 r^4}{4g} + h_9$	Super-forced vortex	$\omega$ is higher toward periphery for 8, 9, and 10
10	$\omega = C r^m$	$vr^{-(m+1)} = C$	$\frac{p}{\gamma} = \frac{C^2 r^{2(m+1)}}{2(m+1)g} + h$	A general form of vortex equation	

see Fig. 1.12 (a), curve 7. Forced vortex motion may be superimposed upon a radial outward flow; the resulting motion is a spiral forced vortex. Such a pattern of flow is found in centrifugal pumps. Disregarding losses, particles at the periphery carry the total amount of energy applied

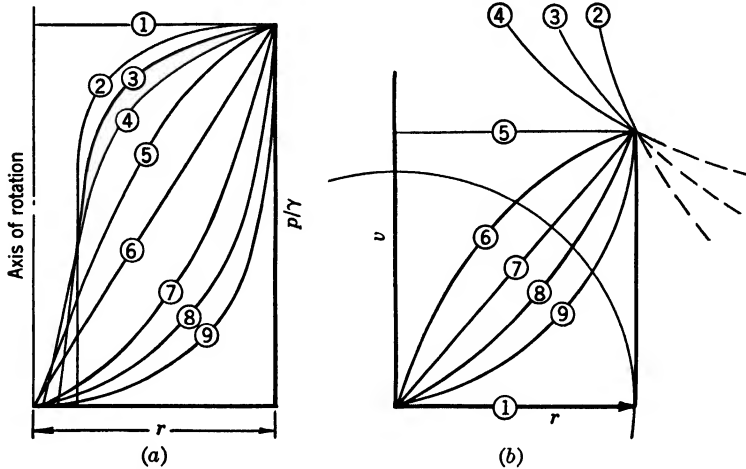


FIG. 1.12. (a) Vortex pressure distribution-elevation; (b) vortex velocity distribution,  $v^n = C$ , plan view.

to the liquid. To make possible a radial outward flow against higher pressures the energy gradient must be below the forced vortex pressure paraboloid (Fig. 1.13). The latter represents a state of static equilibrium for a forced vortex in the same manner as a horizontal plane does for a stationary liquid. To produce flow the energy gradient must fall in the direction of flow below its value at zero flow.

If a forced vortex is superimposed upon a uniform axial flow in a cylindrical conduit an axial spiral forced vortex is obtained. This type of flow is observed in axial flow pumps. Power is applied to maintain this flow. Particles carry different amounts of energy at different radii, with a maximum at the periphery.

A free spiral vortex motion is observed when water flows through a hole in the bottom of a vessel. The vortex usually starts naturally, some initial disturbance giving the direction of rotation. Water moves spirally toward the opening, friction limiting velocities near the axis to some finite values.

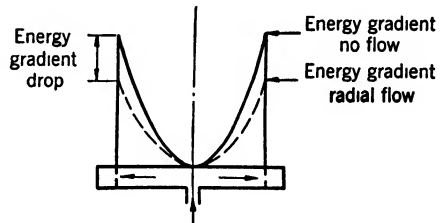


FIG. 1.13. Energy gradient, forced vortex.



When large vertical pumps of the propeller type are operated with a low submergence, free spiral vortices are formed in the suction sump. Air is drawn into the pump suction bell through the funnels formed at the axes of these vortices. A wooden board float around the pump column usually prevents formation of vortices under such circumstances. Also, suitable baffling of the pump suction bell or of the channel of approach will eliminate the tendency toward formation of vortices in the sump. Other forms of vortices can be produced with axial flow impellers having different vane curvature and vane twist along the radius. *All these vortices are stable and without cross flows as all satisfy equation 1.3*, but means of producing various vortices in this manner may not be equally efficient.

### 1.8 LOSSES

(a) **Elbow Losses.** Figure 1.14 is a compilation of information on hydraulic losses in elbows of various design. The losses are expressed by means of a dimensionless coefficient  $C$  in the formula

$$\text{Loss} = C \frac{v^2}{2g} \text{ feet} \quad (1.9)$$

The data of several investigators are consistent and have an accuracy comparable to that observed on pipe friction experiments. Emphasis

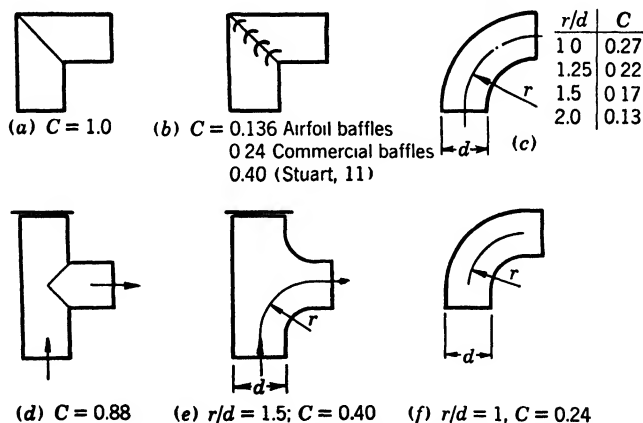


FIG. 1.14. Elbow losses. Data by N.A.C.A.,<sup>10</sup> Stuart,<sup>11</sup> Freeman,<sup>12</sup> Nordell,<sup>13</sup> and Madison.<sup>14</sup>

is placed on the relative value of several designs rather than on the absolute value of the losses. For example, a sharp 90° elbow with several short guide baffles of commercial design, Fig. 1.14 (b), and with

vanes of uniform thickness, has no advantage over a regular elbow with a radius ratio  $r/d = 1.25$  or higher, Fig. 1.14 (c). The primary function of such baffles is to maintain a uniform velocity throughout the section.

One wide baffle in the middle of the section of a regular elbow with a radius ratio of 1.5 or greater, Fig. 1.14 (f), has little or no advantage over a plain elbow, Fig. 1.14 (c). The effect of guide baffles in this case is to increase the radius ratio.

Nordell<sup>13</sup> has found that channels of square or rectangular section have the same total loss of head as circular turns of the same radius ratio.

(b) **Sudden Enlargement or Reduction of the Channel Area.** When the area of a channel is changed abruptly as in Fig. 1.15, the loss of head can be expressed by the formula

$$h_l = C \frac{(v_1 - v_2)^2}{2g} \quad (1.10)$$

The value of  $C = 1.0$  for a sudden enlargement and the value of  $C = 0.4$  to 0.5 for a sudden reduction of area.<sup>15</sup>

The loss due to a sudden reduction in area is about half that due to a sudden enlargement. It has been the practice in the past, when a

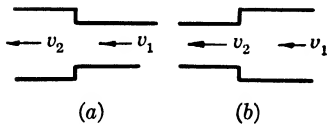


FIG. 1.15. Sudden enlargement and contraction.

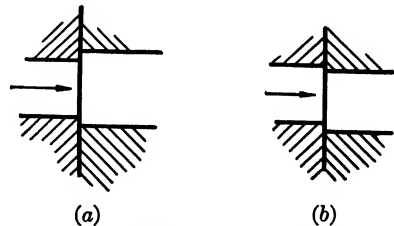


FIG. 1.16. Mismatched channel sections.

channel is formed by two or more parts, to make the section of the upstream part slightly smaller to avoid liquid "hitting the corner," Fig. 1.16 (a). Evidently such devices make the flow conditions worse instead of improving it. If two parts are of the same area, but sections are not matched because of manufacturing inaccuracies, Fig. 1.16 (b), the hydraulic loss is smaller than in the case shown on Fig. 1.16 (a).

## REFERENCES

1. BORIS BAKHMETEFF, *Trans. A.S.M.E., Hydraulics*, 54-4, Aug. 15, 1932, p. 57.
2. HUGO RICHTER, *Rohrhydraulik*, Berlin, Julius Springer, 1934, pp. 130-133, 124-125.

3. L. PRANDTL and O. G. TIETJENS, *Applied Hydro- and Aeromechanics*, New York, McGraw-Hill, 1934, pp. 43, 52, 53.
4. J. NIKURADSE, "Untersuchung über die Strömungen des Wassers in konvergenten und divergenten Kanälen," Berlin, Verein deutscher Ingenieure, 1929, Bulletin 289.
5. H. NIPPERT, "Über den Strömungsverlust in gekrümmten Kanälen," Berlin, Verein deutscher Ingenieure, 1929, Bulletin 320, pp. 1, 2.
6. DAVID L. YARNELL, "Flow of Water through 6 Inch Pipe Bends," U. S. Dept. of Agriculture, Washington, D. C., Oct. 1937, Tech. Bull. 577.
7. M. ADLER, "Strömung in gekrümmten Rohren," *Z. angew. Math. Mech.*, Vol. 14, Oct. 1934, p. 257.
8. H. FÖTTINGER, "Hydraulische Probleme, Diskussion über Kavitation," Berlin, Verein deutscher Ingenieure, 1926, p. 110.
9. HENRY F. SCHMIDT, "Some Screw Propeller Experiments," *Jour. Am. Soc. Nav. Eng.*, Vol. XL, No. 1, 1928, p. 15.
10. N.A.C.A. Tech. Mem. 722, p. 28.
11. M. C. STUART *et al.*, ASHVE Meeting, June 1942.
12. JOHN F. FREEMAN, "Experiments upon the Flow of Water in Pipes, *Trans. A.S.M.E.*, 1941, p. 173.
13. CARL H. NORDELL, "Curved Flow in Conduits of Constant Cross Section," *Oil and Gas Jour.*, May 16 and June 13, 1940.
14. R. D. MADISON and J. R. PARKER, "Pressure Losses in Rectangular Elbows," *Trans. A.S.M.E.*, Vol. 58, No. 3, April 1936, p. 167.
15. C. PFLEIDERER, *Die Kreiselpumpen*, Berlin, Julius Springer, 1932, p. 41.
16. A. F. SHERZER, *Trans. A.S.M.E.*, Vol. 64, 1942, p. 592.
17. HUNTER ROUSE, *Elementary Mechanics of Fluids*, John Wiley & Sons, 1946, p. 114.

## CHAPTER 2

### DEFINITIONS AND TERMINOLOGY

#### 2.1 INTRODUCTION

Centrifugal pumps comprise a very wide class of pumps in which pumping of liquids or generation of pressure is effected by a rotary motion of one or several impellers. In the early stage of centrifugal pump development, pumping was ascribed to centrifugal forces. Later this class of pumps was extended to include axial flow pumps, and the conception of the centrifugal action of the impeller was inadequate to explain the operation of axial flow pumps. However, treatment of axial flow pumps as a class by themselves was not justified, because hydraulically they represent one extreme of a continuous series of pump types. This continuity applies to both theoretical treatment and design methods. Some intermediate types are called mixed flow pumps. In these the flow through the impeller has both radial and axial components and the impeller resembles a ship propeller.

#### 2.2 CLASSIFICATION AND TERMINOLOGY

The great variety of centrifugal pumps built for various applications may be reduced to a few fundamental hydraulic types. The difference in design details is dictated mostly by the application and mechanical requirements. Every pump consists of two principal parts: an impeller, which forces the liquid into a rotary motion by impelling action, and the pump casing, which directs the liquid to the impeller and leads it away under a higher pressure (Fig. 2.1). The impeller is mounted on a shaft which is supported by bearings and driven through a flexible or rigid coupling by a driver. The pump casing includes suction and discharge nozzles, supports the bearings, and houses the rotor assembly. The casing has to be packed around the shaft to prevent external leakage. Closely fitted rings called wearing rings (Fig. 2.2) are mounted on the impeller and fitted in the casing to restrict leakage of high pressure liquid back to the pump suction. Liquid is directed to the impeller eye by the suction nozzle and is brought into a circular motion by the impeller vanes. The impeller vanes and impeller side walls, or shrouds,

form the impeller channels. In a double-suction impeller, liquid is introduced at both sides (Fig. 2.3). Frequently impellers are built "open" that is, with the front shroud removed. Impeller vanes are

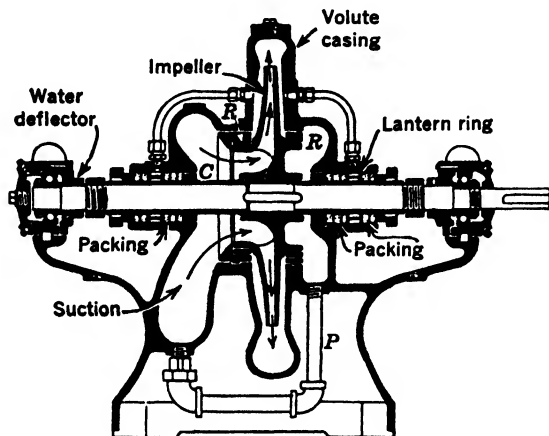


FIG. 2.1. Single-suction pump.

always curved backwards and are called plain or radial (erroneously) if they are of single curvature (Fig. 2.4). Wider impellers have vanes of double curvature, the suction ends being twisted. Such vanes are also called mixed flow vanes or Francis type, after James B. Francis, who introduced double-curvature vanes for water turbines known as Francis' turbines.

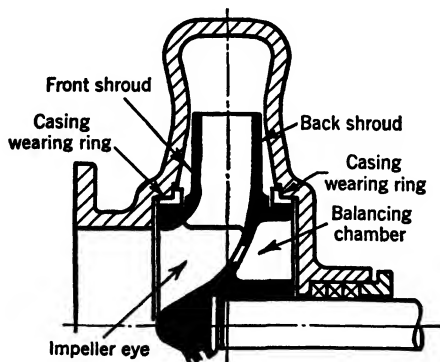


FIG. 2.2. Single-suction impeller with a balancing chamber on the back.

An impeller is designated as radial if the shrouds are essentially normal to the shaft axis, being only slightly curved at the entrance. These impellers usually have plain vanes. In an axial flow pump, liquid

approaches the impeller axially and the forward component of velocity through the impeller is parallel to the shaft axis. Mixed flow impellers occupy an intermediate position in the continuous range of types from

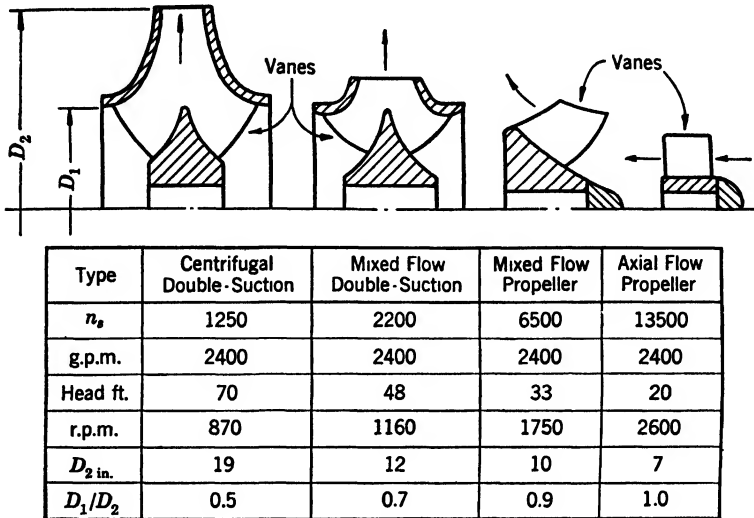


FIG. 2.3. Impellers of different specific speeds.

radial to axial flow. These always have Francis-type vanes. Extreme mixed flow and axial flow pumps are also called propeller pumps. Both types are built almost exclusively with open impellers.

As a result of the impeller action, liquid leaves the impeller at a higher pressure and higher velocity than exists at its entrance. The velocity

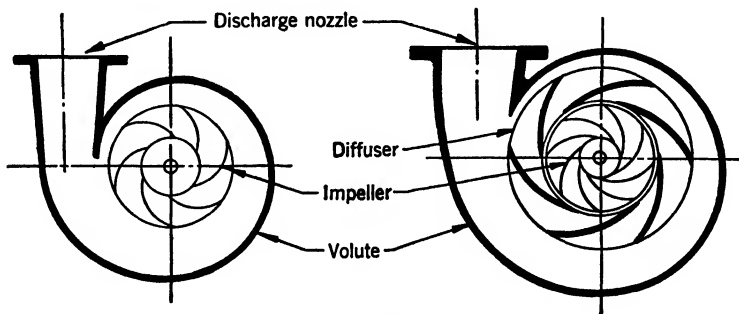


FIG. 2.4. Volute and diffusion casing pumps.

is partly converted into pressure by the pump casing before it leaves the pump through the discharge nozzle. This conversion of velocity into pressure is accomplished either in a volute casing or in a diffusion

**casing.** In a volute casing (Fig. 2.4) the impeller discharges into a single casing channel of gradually increasing area called a volute, and the major part of the conversion takes place in the conical discharge nozzle. When the impeller discharges into a channel provided with vanes, a major part of the conversion of velocity into pressure takes place between the diffusion vanes (Fig. 2.4). The diffusion vane casing was introduced into pump design from water turbine practice where diffusion vanes are indispensable. Early pumps equipped with diffusion vanes were known as turbine pumps. The trend is definitely away

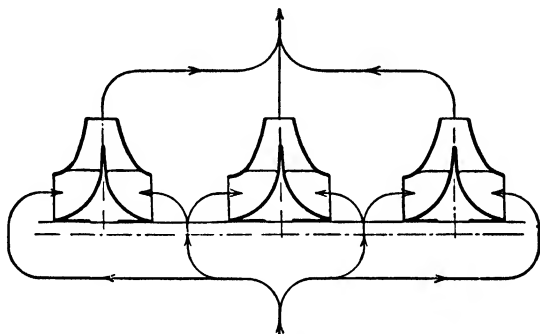


FIG. 2.5. Parallel arrangement of impellers.

from the diffusion vane casing for horizontal pumps, but for vertical pumps of the mixed flow and axial flow types the diffusion casing gives a more compact design and is predominant (Fig. 16.27).

When the total pressure cannot be efficiently produced by one impeller, several impellers are arranged in series; the result is a multistage pump (Figs. 17.10 and 17.12). In some designs, for hydraulic reasons, the total pump capacity is divided among two or three impellers operating in parallel (Fig. 2.5). Such pumps are rarely used today because modern propeller pumps are particularly suited for low head and high capacity.

Any centrifugal pump can be arranged with either a horizontal or a vertical shaft, depending on the application, type of driver, and other requirements. But there is one type of pump—the vertical turbine pump (Figs. 16.27 and 16.28)—which was specifically developed for vertical operation. Originally these pumps were designed to fit deep wells of limited inside diameter. Considering the space limitations, these pumps have reached a high degree of perfection and, owing to their efficient hydraulic performance, are now used widely for a variety of services for which horizontal pumps have been used in the past.

### 2.3 FIELD OF APPLICATION AND LIMITATIONS

There are few limits to maximum or minimum head or capacity produced by modern centrifugal pumps. Centrifugal pumps developing 5400 p.s.i. are used for operation of hydraulic presses (Fig. 17.18). The largest pumps installed in the United States are those of the Colorado River Aqueduct which were designed to deliver 90,000 g.p.m. at a 444-ft. head and are driven by 12,500-hp. vertical motors (Fig. 17.14). Considerably larger pumps are contemplated for the Grand Coulee project, each to deliver 607,000 g.p.m. against a 310-ft. head and to be driven by 65,000-hp. motors. Centrifugal pumps leave a very small field for reciprocating pumps, a field where capacities are too low and pressures too high to permit a favorable type for a centrifugal pump. However, this field is being gradually reduced.

Such progress in the development and application of centrifugal pumps is due to several factors: (1) their high adaptability for high speed electric motor and steam turbine drive; (2) minimum of moving parts; and (3) small size and low cost for the amount of liquid moved.

### 2.4 PUMP CHARACTERISTICS

**(a) Capacity.** The volume of liquid pumped is referred to as capacity and is generally measured in gallons per minute (g.p.m.). Large capacities are frequently stated in cubic feet per second, or millions of gallons per day. When referring to the pumping of petroleum oils, the capacity is sometimes specified in barrels (42-gal.) per day. The following are the conversion factors.

$$1 \text{ cubic foot per second} = 448.8 \text{ g.p.m.}$$

$$1,000,000 \text{ gallons per day} = 694.4 \text{ g.p.m.}$$

$$1,000 \text{ barrels per day} = 29.2 \text{ g.p.m.}$$

The height to which liquid can be raised by a centrifugal pump is called head and is measured in feet. This does not depend on the nature of the liquid (its specific gravity) so long as the liquid viscosity is not higher than that of water. Water performance of centrifugal pumps is used as a standard of comparison because practically all commercial testing of pumps is done with water. When a pump is not used for actual lifting of the liquid but for generation of pressure, the head can also be expressed in feet of liquid, or pounds per square inch. Determination of the pump total head depends on the method of measuring pressures ahead and beyond the pump, and varies for several types of pumps.



**(b) Total Dynamic Head.** For a horizontal pump the total dynamic head is defined as

$$H = H_d - H_s + \frac{v_d^2}{2g} - \frac{v_s^2}{2g} \quad (2.1)$$

$H_d$  is the discharge head as measured at the discharge nozzle and referred to the pump shaft centerline, and is expressed in feet;  $H_s$  is the suction

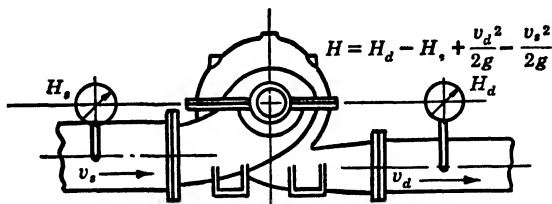


FIG. 2.6. Total dynamic head of horizontal pumps.

head expressed in feet as measured at the suction nozzle and referred to the same datum. If the suction head is negative, the term  $H_s$  in equation 2.1 becomes positive.

The last two terms in equation 2.1 represent the difference in the kinetic energy or velocity heads at the discharge and suction nozzles.

As expressed by equation 2.1, the total dynamic head is the energy imparted to liquid by the impeller between the points where suction and discharge heads are measured (Fig. 2.6). Note that the losses in the suction pipe are not charged against the pump.

For a vertical pump with the pumping element submerged (Fig. 2.7) the total dynamic head is given by

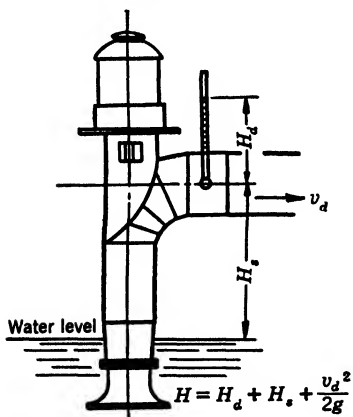


FIG. 2.7. Total dynamic head of vertical pumps.

$$H = H_d + H_s + \frac{v_d^2}{2g} \quad (2.2)$$

where  $H_s$  is the distance from the suction liquid level to the centerline of the discharge elbow and  $H_d$  is the discharge head in feet referred to the center of the discharge elbow. The last term in equation 2.2 represents the velocity head at the discharge. In this case the loss in the suction bell and the discharge column, up to the point where the discharge head is measured, is charged against the pump.

The method of arriving at the total dynamic head varies for different pump arrangements and means used for measuring head. The Hydraulic Institute Test Code gives a detailed procedure for head determination for all possible practical cases.

**(c) Efficiency.** The degree of hydraulic and mechanical perfection of a pump is judged by its efficiency. This is defined as a ratio of pump energy output to the energy input applied to the pump shaft. The latter is the same as the driver's output and is termed brake horsepower (b.hp.), as it is generally determined by a brake test.

$$\begin{aligned}\text{Efficiency } e &= \frac{\text{pump output}}{\text{b.hp.}} \\ &= \frac{Q\gamma H}{550 \times \text{b.hp.}}\end{aligned}\quad (2.3)$$

where  $Q$  is capacity in cubic feet per second,  $\gamma$  is the specific weight of the liquid (for cold water = 62.4 lb./cu. ft.), and  $Q\gamma$  is the weight of liquid pumped per second. If the capacity is measured in gallons per minute, equation 2.3 for water becomes

$$e = \frac{\text{g.p.m.} \times 8.33 \times H}{60 \times 550 \times \text{b.hp.}} = \frac{\text{g.p.m.} \times H}{3960 \times \text{b.hp.}}\quad (2.4)$$

In equation 2.4,  $(\text{g.p.m.} \times H)/3960$  is the pump output expressed in horsepower and is referred to as water horsepower (w.hp.). If a liquid other than cold water is used, the water horsepower should be multiplied by the specific gravity of the liquid to obtain the pump output or liquid horsepower.

The pump efficiency as defined by equations 2.3 and 2.4 is a gross efficiency. This is used by engineers for the comparison of performance of centrifugal pumps. Besides this there are a number of partial efficiencies used by designers and experts; these describe only one phase of pump performance—hydraulic, mechanical, volumetric—and are of no interest to the users of pumps but are important in the study of pump performance and will be defined in a later chapter.

**(d) Performance Curves.** Variation of the head with capacity at a constant speed is called the pump characteristic (Fig. 2.8). A complete characteristic includes also efficiency and brake horsepower curves. Head and capacity of a pump vary with the speed in such a way that the performance curves retain their characteristic features. The variation of head, capacity, and brake horsepower with speed follows definite rules known as affinity laws.\* These were originally found experi-

\* See Chapter 5 for development of these laws.

mentally but have a rigorous theoretical background. When applied to every point on the head-capacity curve these laws state: When speed

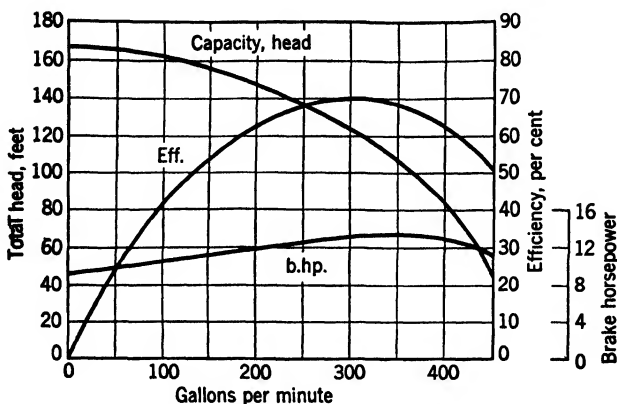


FIG. 2.8. Centrifugal pump characteristics; 3-in. pump at 1750 r.p.m.

is changed, capacity varies directly as the speed, the head varies directly as the square of the speed, and the brake horsepower varies directly as the cube of the speed. The cube of the speed is based on the assump-

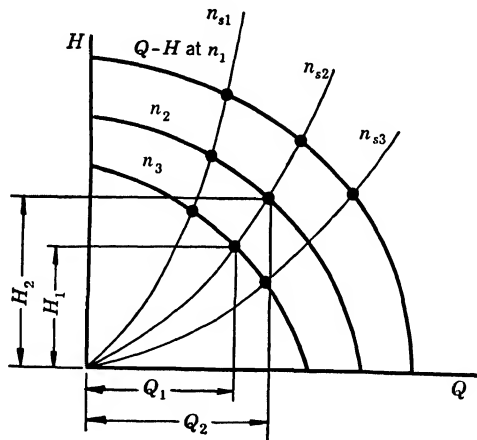


FIG. 2.9. Head and capacity variations with the speed.

tion that efficiency stays constant with speed for each point. The affinity laws are expressed by the following formulas.

$$\frac{Q_1}{Q_2} = \frac{n_1}{n_2} \quad \frac{H_1}{H_2} = \frac{n_1^2}{n_2^2} \quad \frac{(\text{b.hp.})_1}{(\text{b.hp.})_2} = \frac{n_1^3}{n_2^3} \quad (2.5)$$

Figure 2.9 shows three head-capacity curves at speeds  $n_1$ ,  $n_2$ , and  $n_3$ . Points connected by the affinity laws are called corresponding points and are connected by curved lines which are square parabolas. These points have the same efficiency and are of the same specific speed.

## 2.5 SPECIFIC SPEED

In the early stages of pump development it was customary to classify pumps according to their hydraulic-type ratios, such as a ratio of the impeller width at discharge to the impeller outside diameter ( $b_2/D_2$ ). Ratios of the impeller eye diameter to the impeller outside diameter ( $D_1/D_2$ ) were also used for the same purpose. Camerer † introduced a new characteristic to describe the hydraulic type of water turbines which was later applied to centrifugal pumps. It is called specific speed and is defined as

$$n_s = \frac{n\sqrt{Q}}{H^{3/4}} \quad (2.6)$$

where  $n$  is revolutions per minute,  $Q$  is capacity in gallons per minute, and  $H$  is head in feet. The physical meaning of specific speed is: revolutions per minute to produce 1 g.p.m. at 1-ft. head with an impeller similar to the one under consideration but reduced in size. The physical meaning of specific speed has no practical value and the number is used as a "type" number. The specific speed as a type number is constant for all similar pumps and does not change with the speed for the same pump. Figure 2.3 shows several impellers of different specific speeds. With each specific speed are associated definite proportions of leading impeller dimensions such as  $b_2/D_2$  or  $D_1/D_2$ .

In the study of pump performance and classification of all important design constants, specific speed is a criterion of similarity for centrifugal pumps in the manner that Reynolds' number is a criterion for pipe flow. When used as a type number, specific speed is calculated for the best efficiency point. For a multistage pump, specific speed is calculated on the basis of the head per stage. When the specific speed of a double-suction impeller is compared with that of a single-suction impeller the capacity of the first should be divided by 2 or its specific speed should be divided by  $\sqrt{2}$ . All important pump design and performance characteristics are so closely connected with the specific speed that it is impossible to discuss certain features without reference to it.

From equation 2.6 it follows that, for the same head-capacity requirements, higher specific speed pumps will run at a higher speed and will

† R. Camerer, *Z. ges. Turbinenwes.*, 1915, p. 217.

be of smaller physical dimensions. Also, for the same speed and capacity, higher specific speed pumps will operate at a lower head or, for the same speed and head, a higher specific speed pump will deliver a higher capacity.

Development of the formula for the specific speed and further discussion are presented in Chapter 5.

## 2.6 NET POSITIVE SUCTION HEAD

NPSH, a term accepted by the pump industry, stands for "net positive suction head." It is defined as the gage reading in feet taken on the suction nozzle referred to the pump center line, minus the gage vapor pressure in feet corresponding to the temperature of the liquid, plus velocity head at this point. When boiling liquids are being pumped from a closed vessel NPSH is the static liquid head in the vessel above the pump center line minus losses of head in the suction pipe. Hydraulic Institute Charts B-24, B-25, B-26, and B-27 give NPSH values recommended for boiler feed and condensate pumps (see Reference 7, Chapter 17). This subject is further discussed in Chapters 12 and 17.

## CHAPTER 3

### THEORY OF THE CENTRIFUGAL PUMP IMPELLER

#### 3.1 VELOCITY TRIANGLES

A study of the several component velocities of flow through an impeller is best carried out graphically by means of velocity vectors. The shape of such vector diagrams is triangular and they are called velocity triangles. They can be drawn for any point of the flow path through the impeller, but usually attention is focused on the entrance and discharge part of the impeller vanes, and the velocity triangles are called entrance and discharge triangles.

It is necessary to distinguish between absolute and relative velocities. The relative velocity of flow is considered relative to the impeller. The

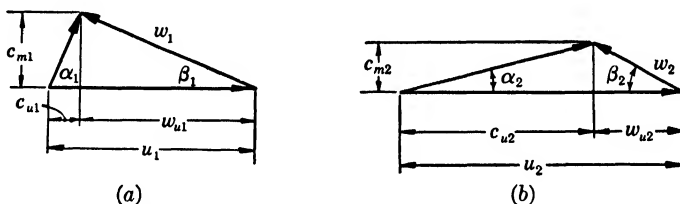


Fig. 3.1. (a) Entrance velocity triangle; (b) discharge velocity triangle.

absolute velocity of flow is taken with respect to the pump casing and is always equal to the vectorial sum of the relative velocity and the peripheral velocity of the impeller. Any point on the impeller will describe a circle about the shaft axis and will have a peripheral velocity

$$u = \frac{\pi D}{12} \times \text{r.p.s.} \quad \text{or} \quad u = \frac{D \times \text{r.p.m.}}{229} \text{ ft. per sec.}$$

where  $D$  is the diameter of the circle in inches.

Figure 3.1 (a) shows an entrance triangle and Fig. 3.1 (b) a discharge triangle. The following notation is adopted.

$u$  = peripheral velocity of impeller (ft. per sec.)

$w$  = relative velocity of flow (ft. per sec.)

$c$  = absolute velocity of flow (ft. per sec.)

Subscript 1 refers to the entrance; subscript 2 to the discharge. Tangential components of relative and absolute velocities are given another subscript,  $u$ . Components of the absolute velocity normal to the peripheral velocity are designated as  $c_{m1}$  and  $c_{m2}$  for entrance and discharge diagrams. This component is radial in a radial impeller and axial in an axial impeller. It will be referred to, in general, as meridional, and will have the subscript  $m$ .

Unless specifically stated, all velocities are considered average velocities for the section normal to the general direction of flow at a specified point. *This is one of the approximations made for theoretical studies and practical design which is not true in practice. A uniform velocity across a channel section does not exist for actual liquids, even in the case of straight pipe flow.*

### 3.2 THEORETICAL HEAD OF CENTRIFUGAL PUMPS

An expression for the theoretical head of a centrifugal pump is obtained by applying the principle of angular momentum to the mass of liquid going through the impeller passages. This principle states that the time rate of change of angular momentum of a body with respect to the axis of rotation is equal to the torque of the resultant force on the body with respect to the same axis.

Let us consider a mass of liquid filling the space between two adjacent impeller vanes (Fig. 3.2). At time  $t = 0$  its position is  $abcd$ , and after a time interval  $dt$  its position has changed to  $efgh$ . Denote the mass of an infinitely thin layer of liquid  $abef$  just leaving the impeller channel  $dm$ . This is equal to the mass of liquid just entering the channel in the same interval of time  $dt$ , as represented by  $cdgh$ . The part  $abgh$  of the liquid contained between the two impeller vanes does not change its moment of momentum in time interval  $dt$ ; thus the change in moment of momentum of the whole content of the channel is given by the change of moment of momentum of the mass  $dm$  entering the impeller ( $cdgh$ ) and mass  $dm$  leaving the impeller ( $abef$ ). This change of moment of momentum is equal to the moment of all external forces applied to the liquid contained between the two impeller vanes. The moment of external forces being denoted by  $T$ , the above is stated mathematically by

$$T = \frac{dm}{dt} (r_2 c_2 \cos \alpha_2 - r_1 c_1 \cos \alpha_1) \quad (3.1)$$

The external forces applied to the liquid contained between the vanes are: (1) the difference in pressure on two sides of each vane ( $p_f$  and  $p_b$ );

(2) pressures  $p_a$  and  $p_s$ , on the faces  $ab$  and  $cd$  of the elementary liquid section respectively, which are radial forces and have no moment about the axis of rotation; and (3) hydraulic friction forces, which oppose the relative flow and produce torque in addition to that exerted by the impeller vanes. Friction forces are neglected in idealized flow.\*

The term  $dm/dt$ , when extended to all impeller channels, represents the constant time rate of mass flow through the impeller which is  $Q\gamma/g$ .

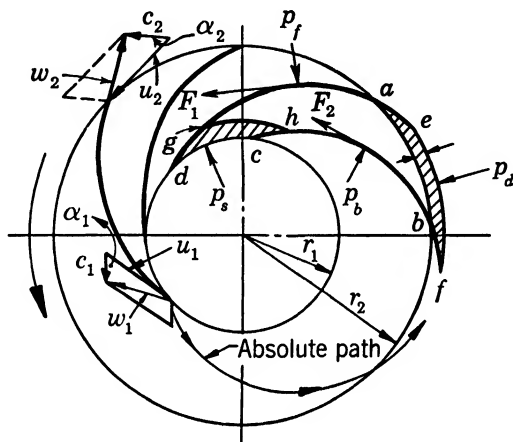


FIG. 3.2. Forces and velocities in an impeller.

Substituting this into equation 3.1 and multiplying both sides of it by  $\omega$ , the angular velocity of the impeller, we obtain

$$T\omega = \frac{Q\gamma}{g} \omega(r_2 c_2 \cos \alpha_2 - r_1 c_1 \cos \alpha_1) \quad (3.2)$$

The left-hand side of equation 3.2 represents power input  $P$  applied to the liquid by the impeller vanes. Substituting  $u_2 = \omega r_2$ ,  $c_2 \cos \alpha_2 = c_{u2}$ ,  $u_1 = \omega r_1$ , and  $c_1 \cos \alpha_1 = c_{u1}$  into equation 3.2, we obtain

$$P = \frac{Q\gamma}{g} (u_2 c_{u2} - u_1 c_{u1}) \quad (3.3)$$

Assuming that there is no loss of head between the impeller and the

\* In an actual pump, friction forces  $F_1$  and  $F_2$  have a moment about the axis, thus requiring power from the shaft. Therefore, not all the applied torque is converted into head. Statements to the contrary are found in books on hydraulics. (See references 1 and 2.)



point where the total dynamic head is measured, this power is available as the pump output of an idealized pump.

$$Q\gamma H_i = \frac{Q\gamma}{g} (u_2 c_{u2} - u_1 c_{u1}) \quad (3.4)$$

Eliminating  $Q\gamma$  we get an expression for head.

$$H_i = \frac{u_2 c_{u2} - u_1 c_{u1}}{g} \quad (3.5)$$

Since all hydraulic losses between the points where the actual total dynamic head of a pump is measured have been disregarded, the head  $H_i$  is a theoretical head; the equation is known as Euler's equation.

If the liquid enters the impeller without a tangential component, or if  $c_{u1} = 0$  (radially for a radial pump and axially for an axial flow pump), Euler's equation reduces to

$$H_i = \frac{u_2 c_{u2}}{g} \quad (3.6)$$

By geometric substitutions from the velocity triangles, Euler's equation 3.5 is transformed into another form more convenient for some discussions. From the velocity triangles we find

$$w_2^2 = c_2^2 + u_2^2 - 2u_2 c_2 \cos \alpha_2$$

$$w_1^2 = c_1^2 + u_1^2 - 2u_1 c_1 \cos \alpha_1$$

Making use of these, Euler's equation becomes

$$H_i = \frac{u_2^2 - u_1^2}{2g} + \frac{c_2^2 - c_1^2}{2g} + \frac{w_1^2 - w_2^2}{2g} \quad (3.7)$$

The first term in equation 3.7 represents the pressure gain due to centrifugal forces acting on the mass of liquid traveling from diameter  $D_1$  to  $D_2$ ; the second term shows the change in kinetic energy of flow from impeller eye to the impeller discharge; and the last term is a change in pressure due to relative velocity change of the flow while passing through the impeller. Equation 3.7 could be written directly by considering energy changes of the flow through the impeller.

If, in equations 3.1 and 3.2,  $c_1$  and  $c_2$  represent actual absolute velocities of all liquid particles and  $\alpha_1$  and  $\alpha_2$  are their true directions,  $P$  in equation 3.3 will represent the actual power input to the liquid by the impeller. In that case the theoretical head  $H_i$ , as given by equations 3.5, 3.6, and 3.7, will be the actual theoretical head of the pump, or the input

head. The term input head will be used in preference to actual theoretical head to avoid confusion, as different theories give different theoretical heads. However, for a given pump the input head  $H_i$  is a definite quantity independent of the formulas used for its calculation. In practice, however, the true velocities of flow and their directions are never known. Theoretical studies of impeller performance are based on the velocity triangles drawn on the vane angles, and the theoretical head is calculated by means of Euler's equations (3.5 or 3.7). Using velocities from such velocity triangles leads to a considerably higher head than the input head. To distinguish the two theoretical heads, the velocity triangles drawn on the vane angles will be called Euler's velocity triangles, and the head calculated by using velocities and angles from Euler's velocity triangles will be termed Euler's head and denoted by  $H_e$ .

*If velocities from Euler's velocity triangles are inserted in equation 3.3, P will not represent the actual power input to liquid, the equality will be destroyed, and the equation will lose its meaning.* Euler's velocity triangles are used mostly for graphical determination of the impeller vane shape, particularly in mixed flow and axial flow impellers.

### 3.3 THEORETICAL CHARACTERISTIC CURVES

By taking Euler's head equation in its simplest form as given in equation 3.6, it can be shown that it is the equation of a straight line which will give the variation of Euler's head with capacity. Substituting

$$c_{u2} = u_2 - w_{u2} = u_2 - \frac{c_{m2}}{\tan \beta_2}$$

into equation 3.6 we obtain

$$H_e = \frac{u_2^2}{g} - \frac{u_2 c_{m2}}{g \tan \beta_2} \quad (3.8)$$

In equation 3.8,  $c_{m2}$  is proportional to the capacity since  $Q$  is equal to the product of  $c_{m2}$  and the area normal to  $c_{m2}$ . Thus equation 3.8 is a linear equation which intersects the head axis at  $u_2^2/g$  and the  $c_{m2}$  axis at  $u_2 \times \tan \beta_2$  (Fig. 3.3). The slope of this line depends on the value of the angle  $\beta_2$ . When  $\beta_2 = 90^\circ$ , the head-capacity line is parallel to the axis of capacities, and  $H_e = u_2^2/g = \text{constant}$ . For  $\beta_2 < 90^\circ$ , the head decreases as the capacity increases. *With  $\beta_2 > 90^\circ$  the head increases with the capacity. This condition cannot be realized even in an idealized pump as flow cannot be started against a head higher than that at zero discharge.* The physical meaning of this can be appreciated by referring to Fig. 3.4. When  $\beta_2 > 90^\circ$ , the absolute velocity  $c_2$  and its tangential component  $c_{u2}$  are greater than  $u_2$ , thus the liquid moves faster than the impeller

vane. This can be realized only by impulse action with an impeller similar to the Pelton water wheel reversed. It is impossible to devise a pump casing which would catch the high velocity jets, convert velocity into pressure, and permit impulse action.

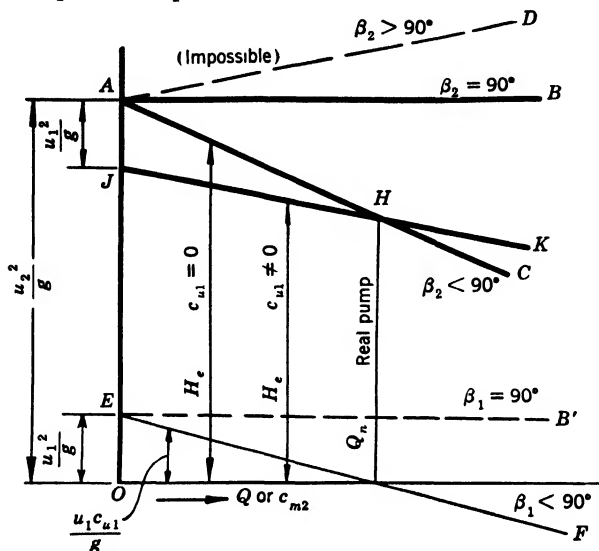


FIG. 3.3. Euler's head-capacity curves.

When the approach to the impeller eye is such that liquid has pre-rotation before being acted upon by the impeller, the subtractive term in equation 3.5 is not equal to zero and the head-capacity curve is obtained as follows. Let  $u_1 c_{u1}/g = H_1$ . Applying the same trigonometric substitution as used in equation 3.8, we get

$$H_1 = \frac{u_1^2}{g} - \frac{u_1 c_{m1}}{g \tan \beta_1} \quad (3.9)$$

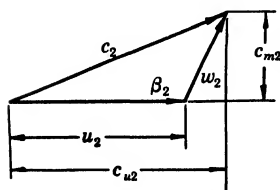


FIG. 3.4. Discharge triangle for  $\beta_2 > 90^\circ$ .

This equation is of the same type as equation 3.8 and represents a straight line cutting the head axis at  $u_1^2/g$ , which is parallel to axis of capacities for  $\beta_1 = 90^\circ$ , and which decreases for  $\beta_1 < 90^\circ$  (line  $EF$ , Fig. 3.3).

The Euler's head, line  $JK$ , is obtained by subtracting ordinates of the line  $EF$  from those of line  $AC$ . †

† At zero capacity the subtractive term  $u_1^2/g$  in Euler's equation requires full impeller angular velocity for the flow approaching the impeller eye. This can never be realized in actual pumps under the most favorable conditions. In normal designs prerotation is suppressed.

In practice the discharge angles  $\beta_2$  vary between  $35^\circ$  and  $15^\circ$ , the normal range being  $25^\circ > \beta_2 > 20^\circ$ . The entrance angle lies within the limits  $50^\circ > \beta_1 > 15^\circ$ .

In an idealized pump the input is equal to output, or brake horsepower equals water horsepower. The shape of the theoretical power

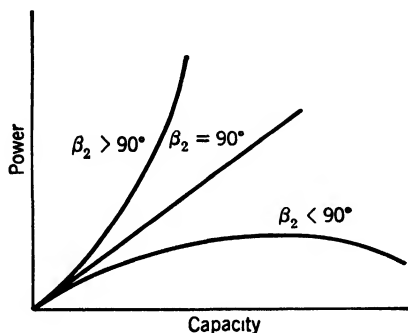


FIG. 3.5. Power to produce Euler's head.

curve is obtained by multiplying equation 3.8 by  $Q$ , or  $Kc_{m2}$ , where  $K$  is a constant for a given pump and can be accounted for by a proper selection of scales. Then

$$\frac{\text{w.hp.}}{K} = \frac{u_2^2 c_{m2}}{g} - \frac{u_2 c_{m2}^2}{g \tan \beta_2} \quad (3.10)$$

When  $\beta_2 = 90^\circ$ , equation 3.10 represents a straight line passing through the origin. For  $\beta_2 < 90^\circ$ , it is a parabola tangent to the above straight line at the origin (Fig. 3.5).

### 3.4 EFFICIENCIES

All the head in a centrifugal pump is generated by the impeller. The rest of the parts contribute nothing to the head but incur inevitable losses—hydraulic, mechanical, and leakage. All losses of head which take place between the points where the suction and discharge pressures are measured constitute hydraulic losses. These include skin friction losses along the liquid path from the suction to the discharge nozzle, losses due to sudden change in area or direction of flow, and all losses due to eddies whatever their causes. Hydraulic efficiency is defined as a ratio of the available total dynamic head to the input head, or

$$e_h = \frac{H}{H_i} = \frac{H_i - \text{hydraulic losses}}{H_i} \quad (3.11)$$

The ratio of the input head to Euler's head will be referred to as vane efficiency, or

$$\frac{H_i}{H_e} = e_{va} \quad (3.12)$$

In Fig. 3.6,  $AED$  is Euler's velocity triangle and  $AFD$  the input velocity triangle. The area  $AFB$  is proportional to the impeller input because  $H_i = u_2 c_{u2}' / g$  and  $Q = c_{m2} A_2$ , where  $A_2$  is the impeller discharge area normal to  $c_{m2}$ . Then

$$P = Q \gamma H_i = \frac{u_2 c_{u2}'}{g} \times c_{m2} \gamma A_2 = \frac{c_{u2}' c_{m2}}{2} \times K$$

In the above,  $K$  is a constant for a given pump and r.p.m.

Similarly, the area  $AEC$  is proportional to the input to produce Euler's head. Then the ratio of the two areas is the vane efficiency.

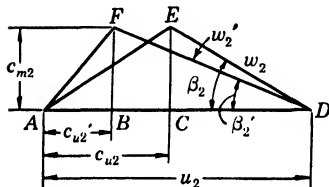


FIG. 3.6. Euler's and input velocity triangles.

$$\frac{AFB}{AEC} = \frac{H_i}{H_e} = \frac{c_{u2}'}{c_{u2}} \quad (3.12a)$$

This is similar to the cylinder or indicated efficiency of a steam engine which is defined as the ratio of the actual indicator diagram (corresponds to area  $AFB$  in our case) to the theoretical Rankine or Clausius pressure-volume diagram (area  $AEC$  on Euler's triangle).<sup>‡</sup>

Besides the losses of head there are losses of capacity in each pump known as leakage losses. These take place through the clearances between the rotating and stationary parts of the pump. The capacity available at the pump discharge is smaller than that passed through the impeller by the amount of leakage. The ratio of the two is called the volumetric efficiency.

$$\frac{Q}{Q_i} = \frac{Q}{Q + Q_L} = e_v \quad (3.13)$$

where  $Q_L$  is the amount of leakage.

Mechanical losses include loss of power in bearings and stuffing boxes, and the disk friction. The latter loss is hydraulic in nature but is grouped

<sup>‡</sup> The product of  $e_h e_{va} = e_{man}$  has been named manometric efficiency by several writers and defined as  $H/H_e = e_{man}$ . This has no physical meaning and frequently has been confused with hydraulic efficiency.

The difference between Euler's head  $H_e$  and the input head  $H_i$  is not a loss, therefore the ratio  $H_i/H_e$  could be termed vane effectiveness rather than vane efficiency. However, the latter term will be used for convenience.

with the mechanical losses since it is external to the flow through the pump and does not result in a loss of head. The mechanical efficiency is the ratio of the power actually absorbed by the impeller and converted into head and the power applied to the pump shaft, or

$$e_m = \frac{\text{b.hp.} - \text{mechanical losses}}{\text{b.hp.}} \quad (3.14)$$

The relationship between the efficiencies defined above and the gross pump efficiency can be established as follows.

$$e = \frac{\text{w.hp.}}{\text{b.hp.}}$$

where

$$\text{Water horsepower} = \frac{Q\gamma H}{550}$$

( $QH$  will be used to designate water horsepower for brevity). But

$$\text{b.hp.} - P_1 = (Q + Q_L)H_i \quad (3.15)$$

where  $P_1$  is a sum of all mechanical losses.

$$e = \frac{QH}{(Q + Q_L)H_i + P_1} \quad (3.16)$$

$$e_m = \frac{\text{b.hp.} - P_1}{\text{b.hp.}}$$

Hence

$$P_1 = \text{b.hp.} (1 - e_m) = \frac{QH}{e} (1 - e_m)$$

$$e = \frac{QH}{(Q + Q_L)H_i + \frac{QH}{e} (1 - e_m)}$$

$$\frac{1}{e} = \frac{Q + Q_L}{Q} \times \frac{H_i}{H} + \frac{1}{e} (1 - e_m) = \frac{1}{e_v} \times \frac{1}{e_h} + \frac{1}{e} (1 - e_m)$$

$$e_v e_h = e + e_v e_h - e_v e_h e_m \quad (3.17)$$

$$e = e_v e_h e_m$$

### 3.5 IMPELLER APPROACH AND PREROTATION

To study the effect of the impeller approach channel upon the impeller performance it is better to take into consideration part of the suction pipe because impeller reaction on the flow may extend a con-

siderable distance ahead of the impeller. *The flow toward the impeller, through the impeller, and beyond the impeller is caused by the drop of the energy gradient below its level at zero flow.*§ The drop in energy gradient permits liquid to proceed through the impeller against a gradually increasing head. *Following the energy gradient the liquid selects a path of least resistance to get to and through the impeller and out of the pump.* The liquid acquires prerotation to enter the impeller passages with a minimum disturbance and the direction depends on the impeller vane entrance angle  $\beta_1$ , the capacity going through, and the impeller peripheral velocity—all three of which determine the entrance velocity triangle. ||

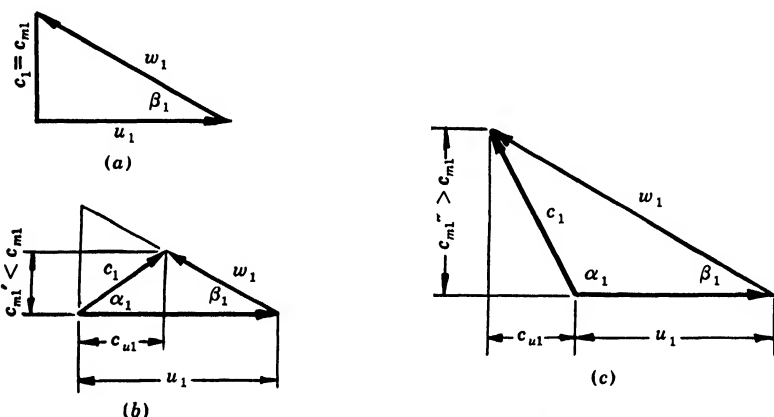


FIG. 3.7. Entrance velocity triangles.

It is evident that resistance to flow is a minimum if the liquid enters the impeller channel at an angle approaching the vane angle  $\beta_1$ . For a given impeller speed, there is only one capacity at which the liquid will approach the impeller meridionally, or without prerotation; see Fig. 3.7 (a). At a capacity considerably smaller than normal, the liquid should acquire prerotation in the direction of impeller rotation to be able to enter the channel at an angle approaching  $\beta_1$ ; see Fig. 3.7 (b). But at a capacity greater than normal, a prerotation in the opposite

§ It should be realized that liquids cannot transmit tension, therefore cannot be “pulled” or “sucked” but only “pushed” by the excess pressure from behind. Any devices that suck liquids accomplish only a local reduction of pressure, thus establishing an energy or hydraulic gradient necessary to produce flow.

|| The principle of least resistance is quite general when applied to the flow of energy; it is nothing more than a restatement of the second law of thermodynamics. Human beings and animals follow it by instinct; for instance, taking the shortest distance between two points, or boarding a moving train by running in the direction of the train motion. The latter is analogous to prerotation of flow in the impeller approach at partial capacities.

direction is necessary for the liquid to satisfy the "least resistance" requirement. The behavior of the liquid in actual pumps follows this pattern, modified somewhat by the effect of the suction nozzle and suction pipe design. *Note that the rotation of the liquid in the impeller approach is not derived from the impeller, as it is evident that an impeller cannot impart liquid rotation opposite to its own—a condition frequently observed at capacities above normal.*<sup>3</sup>

Stewart<sup>4</sup> with a special instrument, the "rotometer," established prerotation in a 6-in. suction pipe 18 in. ahead of the impeller. At zero capacity the rotometer showed 233 r.p.m. (impeller speed was 1135 r.p.m.), which gradually decreased to zero as capacity approached the

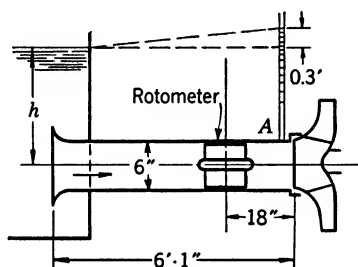


FIG. 3.8. Observation of prerotation in suction pipe by Stewart.

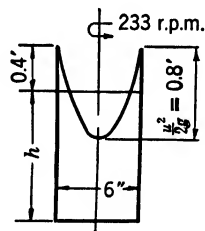


FIG. 3.9. Pressure rise in pipe due to rotation of liquid.

normal; then the rotometer speed increased again to 40 r.p.m. for capacities over normal. At that time (1909) it was not realized that the direction of prerotation changed when the best efficiency point was passed. The rotometer could record revolutions but not direction of rotation.

In these tests it was observed that the suction pressure at the pump suction nozzle was 0.3 ft. higher than the level in the suction tank (Fig. 3.8). On the basis of the above speed of prerotation of 233 r.p.m. and a 6-in. pipe diameter, the centrifugal head inside the pipe figures out to be 0.8 ft. =  $u^2/2g$ , which is the height of the paraboloid of pressures (Fig. 3.9). One half of it (0.4 ft.) is above the average pressure  $h$  (tank level) and the second half below the average. The difference between the calculated and actual pressure rise above the tank level (0.4 – 0.3 = 0.1 ft.) can be accounted for by losses in the suction pipe, or pipe wall drag effect on the paraboloid of pressures. The full meaning of Stewart's tests was not appreciated at that time.

If the suction pipe of a single-stage pump is such that a forced vortex can be set up, and if the suction pressure is measured at the suction



flange, the total head based on the suction head obtained in this way will be lower than its true value. The error is more pronounced at lower capacities, thus affecting the shape of the head-capacity and efficiency curves. With large pumps and Francis-type impeller operating with low velocities in the suction pipe, a forced vortex may develop in the suction pipe if no means are employed to prevent it. For instance, such a forced vortex was observed at the rated capacity during the field test on the large Colorado River Aqueduct pumps at Intake Station (Fig. 17.15). These pumps take their suction from a lake through a long radius elbow. The suction head, measured at four points around the suction flange, was higher than the static level in the lake, indicating the presence of the paraboloid of pressures caused by the vortex.

By referring to Figs. 3.8, 3.9 and 1.11, it will be observed that the energy gradient drop is greater along the streamlines in the middle of the suction pipe than along the streamlines near the pipe walls. Thus, higher velocities are expected in the middle of the impeller eye. At low capacities, approaching zero, the difference between the velocities in the suction pipe becomes more pronounced. This gives the impeller an opportunity to increase the tangential component of the velocity of flow near the periphery of the impeller eye by viscous drag of the liquid. *Thus, the energy of the streamlines near the pipe wall may increase and there may be no energy gradient drop available to maintain the flow along these streamlines. As a result, the flow near the impeller periphery may be reversed at capacities approaching zero. Such a back-flow has been observed by several investigators.*<sup>5</sup>

If the liquid approaching the impeller eye acquires prerotation in the direction of impeller rotation, the impeller will be deprived of the opportunity to impart that much of the tangential component to the flow and the entrance part of the impeller vanes will be inactive, taking no power from the shaft. This condition reduces the input head and consequently the available total head. It is immaterial whether prerotation is caused by the shape of the channel approach or by the exaggerated vane entrance angle. Lower input head will result, and the subtractive term in Euler's equation (3.5) will not equal zero.

An illustration of the above statements is given in Fig. 3.10 showing a water performance of a 4-in. paper stock pump shown in Fig. 3.11. This pump has a booster impeller in the suction nozzle ahead of the regular impeller. Comparison of the performance of this pump with and without the booster impeller shows that, although the booster impeller produces an appreciable head, the total combined head is not any higher than that without this impeller; in fact it is slightly lower by the amount of the additional hydraulic losses. The

brake horsepower at normal capacity is essentially the same in both cases. Thus the head of the regular impeller was reduced by the amount of head produced by the booster impeller, and the power demand by the first impeller was reduced in proportion to the reduced head.

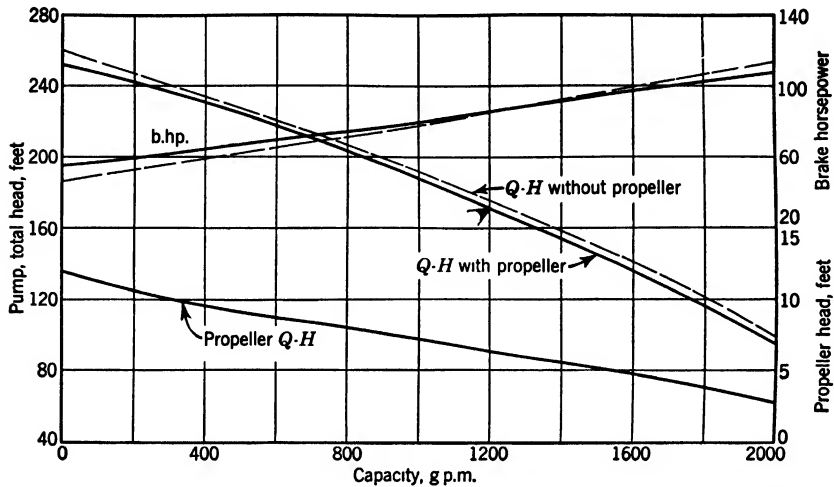


FIG. 3.10. Performance of 4-in. paper stock pump shown in Fig. 3.11, at 1750 r.p.m

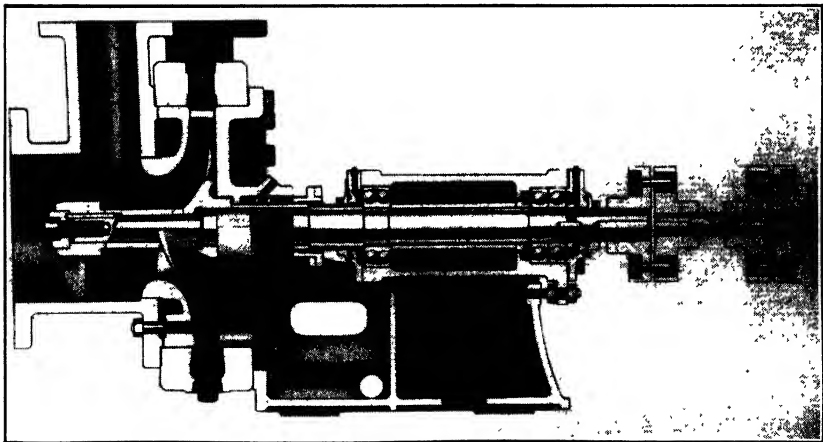


FIG. 3.11. Ingersoll-Rand 4-in. paper stock pump with a booster impeller in the suction nozzle. Performance in Fig. 3.10.

The direction of the flow in the impeller approach is impossible to estimate accurately from the configuration of the channel of approach, but it is rarely meridional (without prerotation). In modern high speed

pumps, entrance vane angles are exaggerated because small entrance angles result in a lower pump efficiency as vanes become unnecessarily long and passages between vanes narrow.¶

Prerotation as given by the subtractive term  $u_1 c_{u1}/g$  in Euler's equation (3.5) and equation 3.9 can never be fully realized in an actual pump. The design of suction nozzle and impeller approach in modern pumps is such that prerotation is suppressed to a great extent. Thus, although liquid seeks a path of least resistance to enter impeller channels, it is not given sufficient time and space to adjust itself for a shockless entrance at all capacities. As a result, separation of liquid from the impeller vane takes place at capacities other than normal, causing vane pitting as shown in Figs. 12.5 and 12.13.

### 3.6 DISCUSSION OF EULER'S CHARACTERISTICS AND EULER'S VELOCITY TRIANGLES

(a) **Head-Capacity Characteristics.** For simplicity assume no prerotation in the impeller approach. Euler's equation of head (3.8) represents a straight line intersecting the head axis at  $H_e = u_2^2/g$  and the axis of capacities at  $Q_{\max} = A_2 u_2 \tan \beta_2$ .

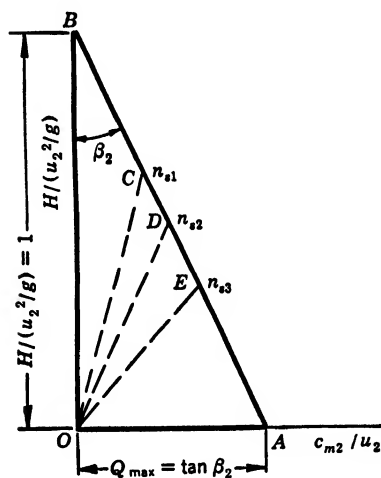


FIG. 3.12 (a). Euler's head-capacity characteristics.

$A_2$  is the impeller discharge area normal to  $c_{m2}$  and, since it is constant for a given pump, it can be omitted from the above relationship by incorporating it in a proper scale selection. The head-capacity characteristics, shown in Fig. 3.12 (a), are plotted on suitable dimensionless scales for a given impeller discharge angle  $\beta_2$  and apply to pumps of all specific speeds and sizes using the same angle  $\beta_2$  and consistent in design elements.

The specific speed is used here as a type number for actual pumps at the best efficiency point only and is determined by the conditions of minimum hydraulic losses. All points corresponding to the b.e.p. of different specific speeds ( $n_{s1}$ ,  $n_{s2}$ ,  $n_{s3}$ , etc.) are located on line BA, the specific speeds increasing from B to A.

¶ Figure 9.4 in Chapter 9 shows that the shockless entrance takes place always at a capacity greater than that at the best efficiency point (b.e.p.); therefore prerotation should be allowed at the b.e.p.

Similarly, Fig. 3.12 (b) shows Euler's discharge velocity triangles  $OCB$ ,  $ODB$ ,  $OEB$  for several capacities and applies to several specific speeds with their b.e.p. at points  $C$ ,  $D$ ,  $E$ , and so on. Each point on line  $AB$ , Fig. 3.12 (b), represents a different specific speed and fixes all important impeller characteristics.

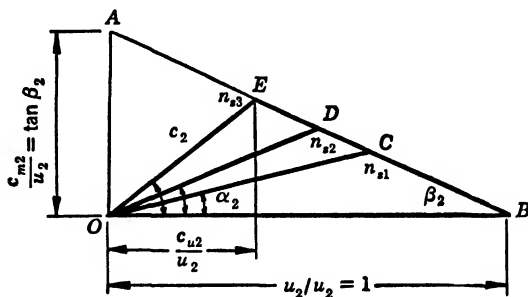


FIG. 3.12 (b). Euler's discharge velocity triangle.

**(b) Dimensionless Scales.** Thus line  $AB$  on Fig. 3.12 (b) represents the head-capacity curve for pumps of all specific speeds using the same angle  $\beta_2$  in the same manner as  $AB$  on Fig. 3.12 (a), but to a different scale. Conversely, by connecting points  $C$ ,  $D$ ,  $E$ , and so on, to point  $O$  on Fig. 3.12 (a), discharge velocity triangles  $OBC$ ,  $ODB$  and  $OBE$  are obtained if the scales for head and capacity are selected so that the angle  $OBA$  is equal to  $\beta_2$ . By using suitable scales Euler's head-capacity diagram and the discharge velocity diagrams become identical. This is an important property because certain features not clear on one diagram become more apparent on the other.

The following dimensionless scales (ratios) will bring both the head-capacity and the discharge velocity diagrams to the same scale. The meridional velocity  $c_{m2}$  will represent the capacity. On the head-capacity diagram, Fig. 3.12 (a), heads are expressed as ratios to shut-off head, or

$$\psi_e = \frac{H_e}{\frac{u_2^2}{g}} = \frac{u_2 c_{u2} g}{g u_2^2} = \frac{c_{u2}}{u_2} \quad (3.18)$$

which will be called the head coefficient. Then, on the velocity diagram, heads will be represented to the same scale by use of the ratio

$$\frac{c_{u2}}{u_2} = \psi_e$$

All velocities on the velocity diagram will be taken as ratios to  $u_2$ ; thus

$$\frac{c_{m2}}{u_2} = \phi_e \quad (3.19)$$

will be the meridional velocity on the velocity diagram and will represent capacity on both diagrams. This ratio is called the capacity coefficient. The peripheral velocity will be  $u_2/u_2 = 1$ . The shut-off head on the head-capacity diagram is also equal to unity. The maximum capacity and maximum meridional velocity are equal to

$$\left(\frac{c_{m2}}{u_2}\right)_{\max} = \tan \beta_2 \quad (3.20)$$

**(c) Vane Efficiency.** The input head-capacity curve  $DA$  for a given  $\beta_2$  is drawn on Fig. 3.13 (a). Both Euler's head-capacity curve  $BA$  and input head-capacity curve  $DA$  meet at zero head.\*\*

The direction of line  $DA$  can be determined by locating one point on this line. This point can be estimated, for instance, by assuming or

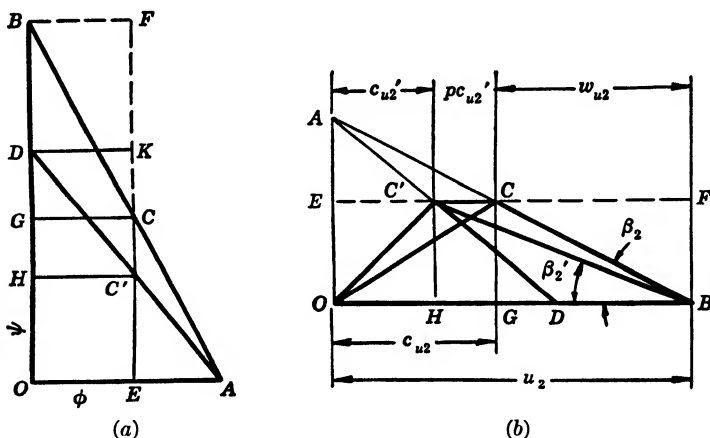


FIG. 3.13. (a) Euler's and input head-capacity curves; (b) Euler's and input discharge velocity triangles.

calculating the hydraulic efficiency for the best efficiency point of one existing pump of any specific speed. Then line  $DA$  will represent the input head-capacity curve for this particular pump. Moreover, it will represent the input head-capacity characteristics of pumps of all specific speeds having the same discharge vane angle  $\beta_2$ .

\*\* This assumption is made by several writers.<sup>6</sup>

The ratio of ordinates for any capacity will be the vane efficiency or  $e_{va} = DO/BO$ . This is equal for pumps of all specific speeds using the same  $\beta_2$  and consistent otherwise. Figure 3.13 (b) represents Euler's velocity triangle drawn to the same dimensionless scale as Fig. 3.13 (a). By transferring point  $D$  from Fig. 3.13 (a) to Fig. 3.13 (b), line  $DA$  becomes the locus of all  $c_{u2}'$  values for the input velocity triangles  $OC'B$  shown for one point  $C$ . The vane efficiency then is

$$e_{va} = \frac{H_i}{H_e} = \frac{c_{u2}'}{c_{u2}} \quad (3.21)$$

and is constant for all capacities for pumps of all specific speeds forming a continuous series in their hydraulic design.

**(d) Euler's and Input Work Diagrams.** Figures 3.13 (a) and 3.13 (b) may also serve as work diagrams for the impeller. On Fig. 3.13 (a), the area  $OHC'E$  represents to scale the impeller input to the liquid. Area  $OGCE$  is the maximum impeller input theoretically possible, which is Euler's head. The ratio of the two areas is the vane efficiency. Again resorting to the steam engine for an analogy, the area  $OHC'E$  corresponds to the area of the indicator diagram, and the area  $OGCE$  corresponds to the theoretical diagram of the Rankine or Clausius cycle. At no flow, energy is available at level  $OD$  (or  $OB$  as a maximum theoretical), but to produce flow of energy a difference in energy levels is necessary (energy gradient drop) in the same manner as a temperature difference is necessary to produce flow of heat. The energy represented by the area  $DKGC$  is not a loss but unavailable energy of the process, something like rejected heat in a Carnot heat cycle. Figure 3.13 (b) represents the same quantities of work similarly lettered. It is possible to use parts of velocity triangles for the analysis given above since the input work is proportional to the area  $OC'H$  and the maximum possible input necessary to produce Euler's head will be proportional to area  $OCG$ . The unavailable energy, representing the energy gradient, is area  $C'HD$ . Out of the total maximum possible energy input (area  $OC'B$ ) only the energy of the absolute flow (area  $C'HO$ ) is available outside of the pump. The balance (area  $C'HB$ ) is the energy of the relative flow, which never leaves the pump and does not take any power from the impeller vanes.

Impeller characteristics similar to those discussed can be constructed with prerotation allowed in the impeller approach as was shown earlier in this chapter. These will have the same properties as the characteristics without prerotation, but the diagrams become complicated and lose their value for illustrative purposes.

## 3.7 FLOW THROUGH THE IMPELLER

*The reason impeller vanes cannot apply, and liquid cannot absorb the power required to produce Euler's head, will be seen from the following considerations.*

**(a) Pressure Distribution.** In order to transmit power to the liquid, pressure  $p_f$  on the leading or front face of the vane should be higher than pressure  $p_b$  on the back of the vane (Fig. 3.14). Any force exerted by the vane on the liquid has an equal and opposing reaction from the liquid and this can exist only as a pressure difference on two

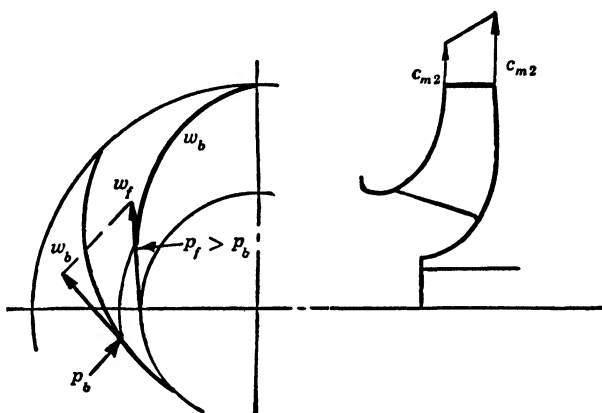


FIG. 3.14. Velocity distribution in an impeller channel.

sides of impeller vanes. The immediate effect of such a pressure distribution is that relative velocities near the back of the impeller vanes are higher than those near the front of the vane. The velocity triangle, Fig. 3.1 (b), will show that, for a given vane angle, the head produced is lower with higher meridional velocities. Therefore the higher relative velocity at the back of the vane will result in lower heads and the total integrated head will be lower than that calculated for an average velocity of flow, as will be shown later in this chapter.

**(b) Velocity Distribution.** Another cause for velocity distortion, which takes place even in an idealized pump, is the effect of turns in the impeller approach and impeller profile. In radial flow and mixed flow impellers the liquid must make nearly a full  $90^\circ$  turn before it is acted upon by the vane. An illustration of velocity distribution in a turn has been given in Chapter 1. The final result of uneven velocity distribution is again a reduction of the maximum head possible; see Fig. 3.14.

(c) **Relative Circulation.** The relative velocity distribution through an impeller channel is affected also by the relative circulation of the liquid due to the inertia effect of frictionless liquid particles; see Figs.

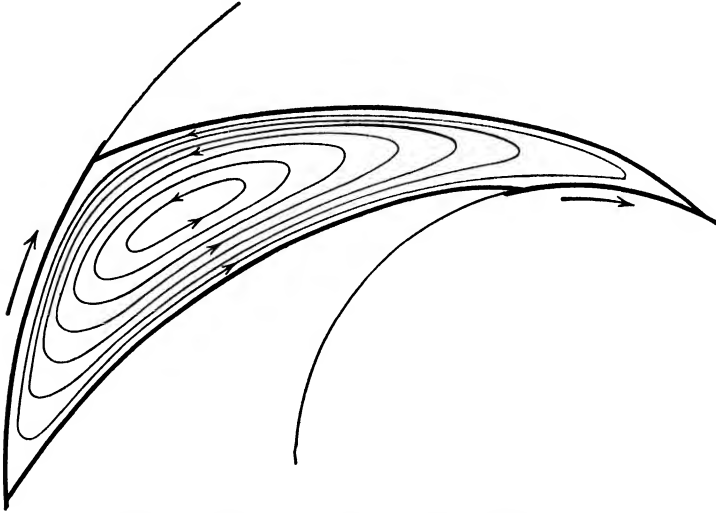


FIG. 3.15. Relative circulation within impeller channel.

3.15 and 3.16. The particles retain their orientation in space as shown in Fig. 3.17. Here, particle  $AB$ , shown as a sphere, has an arrow  $AB$  marked on its body and pointing radially outward from the center.

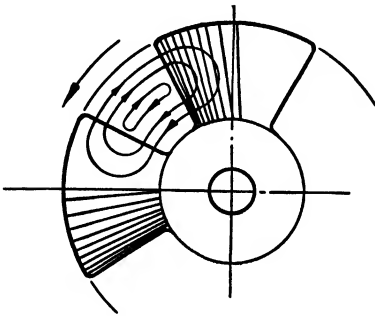


FIG. 3.16. Relative circulation within impeller channels of axial flow pump.

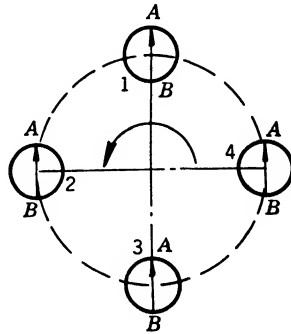


FIG. 3.17. Relative motion of particles is opposite to impeller rotation.

After half a revolution the same particle will have its arrow pointing toward the center, and after a complete revolution the arrow again will be pointing away from the center. The particle, while following the



impeller in its translatory movement around the axis, fails to turn with the impeller. This results in a turning movement relative to the impeller. Superimposition of flow through the impeller increases the

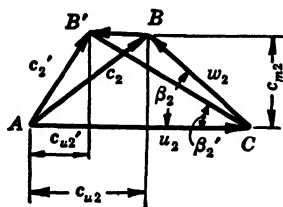


FIG. 3.18. Discharge velocity triangle.

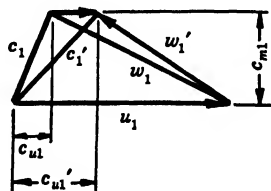


FIG. 3.19. Entrance velocity triangle.

velocity at the back of the vane and reduces the velocity at the front face of the vane. The result is a component in the tangential direction opposite to  $c_{u2}$  at the discharge (Fig. 3.18) and an additional component in the direction of  $c_{u1}$  at the entrance (Fig. 3.19). All these effects reduce the input head. Although the particle within the impeller

channel remains irrotational, it travels in a translatory motion in a circular path and therefore is subject to centrifugal force which causes outward flow through the impeller. Evidently the relative circulation is less with a greater number of vanes, hence the input head and the pump useful head are higher for a greater number of vanes. Also, it is reasonable to expect that relative circulation is smaller in a narrow impeller than in a wide one. For the same impeller diameter, the total head is greater with a narrow impeller (lower specific speed). The surface friction of shrouds has a decided effect on suppressing the relative circulation within the impeller channel and in imparting rotary motion to the liquid, thereby increasing the tangential component of the absolute velocity  $c_{u2}$  and the absolute velocity  $c_2$ .

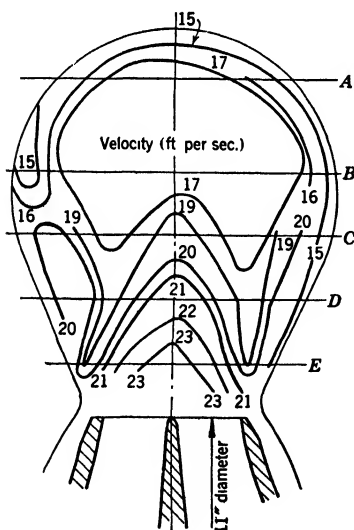


FIG. 3.20. Volute velocity distribution; double-suction impeller, 1950 g.p.m., 42 ft. head, 1180 r.p.m.

Special tests<sup>7</sup> have shown that higher absolute velocities exist near the shrouds at the impeller discharge. Figure 3.20 shows the observed velocity distribution for a given pump.

**(d) Actual Discharge Angle.** A study of Figs. 3.18 and 3.19 will reveal that the relative circulation of liquid within the impeller vanes has the effect of decreasing the liquid discharge angle from vane angle  $\beta_2$  to  $\beta_2'$ . The inlet angle  $\beta_1$ , on the other hand, is increased to  $\beta_1'$ , allowing more prerotation than indicated on Euler's velocity triangle. With actual liquids, power cannot be applied by the vane if the liquid moves in a path having the same relative angle  $\beta_2$  as the vane itself. In that case the liquid would move outward with the same velocity as the vane sweeps radial distances while turning. In an established flow, whether rotary or straight as in open channel flow, a body must move faster than the established velocity of flow in order to exert any force on the liquid flowing in the same direction. In other words, the vane must have "impelling" action.

It is important to realize that changing the vane angle from  $\beta_2$  to  $\beta_2'$  will mean only that the liquid will again lag behind the vane and discharge at a smaller angle  $\beta_2'' < \beta_2'$ .

**(e) Non-Active Part of Vane.** In an actual pump or an idealized one, the pressure difference on the two faces of a vane disappears at the vane tips where the two streams from adjacent impeller channels join. This

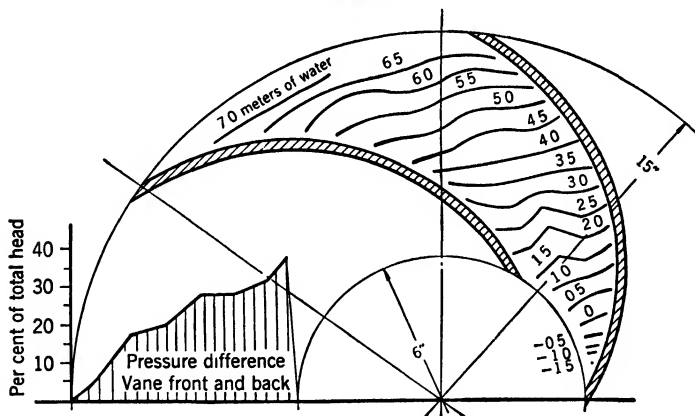


FIG. 3.21. Pressure distribution inside the impeller channel; 316 g.p.m., 28.6 ft head, 700 r.p.m., normal capacity 400 g.p.m. (Uchimaru).

means that not all of the vane is equally active; in fact, the vane discharge tips have to be inactive since no pressure difference exists there. To unload vane discharge ends the angle  $\beta_2$  must be reduced. In actual pumps it has been found advantageous to taper off the vane discharge ends, which has the effect of reducing the vane discharge angle.

Pressures on the impeller vanes, as measured by Uchimaru,<sup>8</sup> show that the pressure difference on the two faces has a maximum near the

suction end and tapers off to nothing near the discharge end (Fig. 3.21). Such pressure distribution in the actual pump does not entail any additional losses; it simply means that each vane can only transmit, and the liquid can only absorb, a fixed amount of energy. This is lower

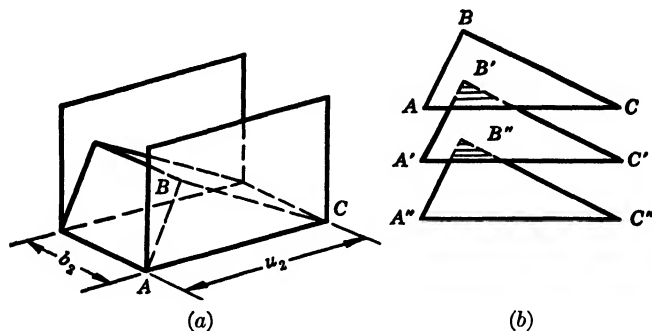


FIG. 3.22. (a) A grain scoop illustrating the vane loading; (b) series of scoops illustrating the vane interference.

than that given by Euler's equation. A simple analogy will illustrate the point. A scoop with two ends open, Fig. 3.22 (a), handling granular matter can lift only a fixed amount of grain which is dependent on the scoop width, its length, and the natural angle of repose of the grain. The work done in lifting the grain is proportional to the area  $ABC$  representing the outline of the grain heap. The outline  $ABC$  resembles the pressure distribution along an impeller vane. To produce Euler's head

the vane load is assumed to be uniform. Figure 3.22 (b) suggests the effect of vane interference on the head produced. Each vane does not carry its maximum load.

(f) **Theoretical Head with Non-Uniform Meridional Velocity.** It has been pointed out, in the previous article, that in an idealized pump the velocity distribution across the impeller channel is not uniform. Under such conditions the theoretical head  $H_t$  developed by the impeller is lower than that calculated on the basis of an average velocity.

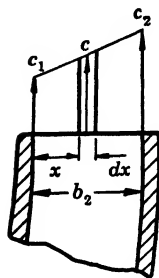


FIG. 3.23. Velocity distribution at impeller discharge.

Assuming that the radial velocity varies uniformly from  $c_1$  at one shroud to  $c_2$  at the other shroud (Fig. 3.23) and at some point located at a distance  $x$  from the shroud, the radial velocity is  $c = c_1 + ax$  where  $a = (c_2 - c_1)/b_2$ ,  $b_2$  being the impeller width at the discharge. The head produced at this point is

$$H_t = \frac{u_2 c u_2}{g} = \frac{u_2}{g} \left( u_2 - \frac{c}{\tan \beta_2} \right) = \frac{u_2^2}{g} - \frac{u_2 c}{g \tan \beta_2} \quad (3.22)$$

The volume of water discharged by an element  $dx$  of the impeller width is equal to

$$dQ = c\pi D_2 dx \quad (3.23)$$

The power output of this element is

$$dP = \gamma H_t dQ = \gamma H_t c\pi D_2 dx \quad (3.24)$$

Substituting for  $H_t$  its value from equation 3.22 we get

$$dP = \left( \frac{u_2^2}{g} - \frac{u_2 c}{g \tan \beta_2} \right) \gamma \pi D_2 c dx \quad (3.25)$$

For brevity,

$$\frac{u_2^2}{g} = A \quad \frac{u_2}{g \tan \beta_2} = B \quad \gamma \pi D_2 = C$$

The formula then takes the form

$$dP = (A - Bc)Ccdx = C(Ac - Bc^2)dx$$

Substituting for  $c$  its value  $c = c_1 + ax$ ,

$$dP = C[A(c_1 + ax) - B(c_1 + ax)^2]dx$$

Integrating between the limits 0 and  $b_2$ , we obtain the power output of the impeller.

$$\begin{aligned} P &= \int_0^{b_2} CA(c_1 + ax)dx - \int_0^{b_2} CB(c_1 + ax)^2 dx \\ &= CA \left[ \frac{(c_1 + ax)^2}{2a} \right]_0^{b_2} - BC \left[ \frac{(c_1 + ax)^3}{3a} \right]_0^{b_2} \\ &= CA \left[ \frac{(c_1 + ab_2)^2}{2a} - \frac{c_1^2}{2a} \right] - BC \left[ \frac{(c_1 + ab_2)^3}{3a} - \frac{c_1^3}{3a} \right] \end{aligned}$$

But  $c_1 + ab_2 = c_2$ ; then

$$P = CA \frac{(c_2^2 - c_1^2)}{2a} - CB \frac{(c_2^3 - c_1^3)}{3a}$$

Substituting for  $a$  its value  $a = (c_2 - c_1)/b_2$  and letting  $c_m$  denote  $(c_2 + c_1)/2$ , the mean radial velocity, the expression for the power output takes the form

$$\begin{aligned} P &= CA \frac{(c_2 - c_1)(c_2 + c_1)}{2a} - CB \frac{(c_2 - c_1)(c_2^2 + c_2c_1 + c_1^2)}{3a} \\ &= CAB_2 c_m - CBb_2 \frac{(c_2^2 + c_2c_1 + c_1^2)}{3} \end{aligned}$$

The average head produced by the impeller is obtained by dividing the impeller power output by the weight of liquid discharged  $W$ .

$$\begin{aligned}
 W &= \gamma \int_0^{b_2} dQ = \gamma \int_0^{b_2} c\pi D_2 dx \\
 &= \gamma \int_0^{b_2} D_2(c_1 + ax) dx = \gamma\pi D_2 \left( c_1 b_2 + \frac{ab_2^2}{2} \right) \\
 &= \gamma\pi D_2 \left[ c_1 b + \frac{(c_2 - c_1)b_2^2}{2b_2} \right] = \gamma\pi D_2 b_2 \frac{c_2 + c_1}{2} \\
 W &= \gamma\pi D_2 b_2 c_m = Cb_2 c_m \tag{3.26}
 \end{aligned}$$

which could be written at once, since the velocity involved is a linear function of  $x$ .

$$\begin{aligned}
 H_t &= \frac{P}{W} = A + \frac{B}{c_m} \left( \frac{c_2^2 + c_2 c_1 + c_1^2}{3} \right) \\
 &= A + \frac{B}{c_m} \left[ \frac{(c_2 + c_1)^2 - c_2 c_1}{3} \right] \\
 &= A + \frac{B}{c_m} \left[ \frac{3(c_2 + c_1)^2 + (c_2 + c_1)^2 - 4c_2 c_1}{12} \right] \\
 H_t &= A - \frac{B}{c_m} \left[ \left( \frac{c_2 + c_1}{2} \right)^2 + \frac{(c_2 - c_1)^2}{12} \right] \tag{3.27} \\
 &= A - \frac{B}{c_m} \left[ c_m^2 + \frac{(c_2 - c_1)^2}{12} \right] \\
 &= A - Bc_m \left[ 1 + \frac{(c_2 - c_1)^2}{12c_m^2} \right] \\
 H_t &= \frac{u_2^2}{g} - \frac{u_2 c_m}{g \tan \beta_2} \left[ 1 + \frac{(c_2 - c_1)^2}{12c_m^2} \right] \tag{3.28}
 \end{aligned}$$

A comparison of this formula with 3.22, shows that the average theoretical head produced by an impeller with radial velocity varying from  $c_1$  to  $c_2$  is smaller than that for the mean radial velocity  $c_m$ .

The difference in the head is greater for a greater difference between  $c_2$  and  $c_1$ , this difference disappearing when  $c_2$  is equal to  $c_1$ . The effect of the variable radial velocity on the head produced will be understood more clearly if it is kept in mind that the elementary formula 3.22

gives the head per pound of liquid pumped and that more pounds per second of the low pressure liquid are discharged by the impeller where the radial velocity is greater, since the head developed is smaller for a higher radial velocity.

From formula 3.28 it is seen that for the same ratio of  $c_2$  to  $c_1$  the correction factor is more effective for impellers for which the second term  $u_2 c_m / (g \tan \beta_2)$  is greater in comparison with the first or  $u_2^2 / g$ . In normal designs the second term is greater for impellers of high specific speed; hence the correction affects more the theoretical head for these impellers. In addition, the factor  $\left[ 1 + \frac{(c_2 - c_1)^2}{12 c_m^2} \right]$  is greater for wide impellers, since the velocity distortion is greater and the length of the water path is smaller for impellers of high specific speed. This explains the reason for a greater discrepancy between the theoretical and the actual heads for impellers of higher specific speed.

It is evident that formula 3.28 holds for the velocity distributions, with a linear relation between the maximum and minimum velocity. For any other relation between the minimum and maximum radial velocities the form of the expression for the correction factor will change, but the significance of the expression will remain the same.

### 3.8 PFLEIDERER'S CORRECTION TO EULER'S EQUATION

Pfleiderer<sup>9</sup> has developed a relationship between the input head and Euler's head in terms of the number of vanes, assuming that the force exerted by the vane on the liquid is the same per unit length along the whole vane length.††

$$H_e = H_i \left( 1 + \psi \frac{r_2^2}{zs} \right) = H_i (1 + p) \quad (3.29)$$

where  $r_2$  is the impeller radius

$z$  is the number of vanes

$s$  is the static moment of the middle streamline ( $CD$ , Fig. 3.24) about the axis of rotation

$\psi$  is an experimental coefficient to account for the inaccuracy of assumptions.

Pfleiderer gives values of  $\psi = 0.8$  to  $1.0$  for pumps with diffusion vanes. For volute pumps  $\psi$  is higher.††

†† In view of the vane pressure distribution as shown in Fig. 3.21 this assumption is a hardly justified simplification.

†† Since the pump casing has no part in head generation, this statement is questioned by the author.

The coefficient  $\psi$  depends on the impeller design. The effect of several impeller design elements upon  $\psi$  has not been determined. From equations 3.29 and 3.12 it is seen that

$$\frac{1}{1+p} = e_{va} = \frac{H_i}{H_e} = \frac{c_{u2}'}{c_{u2}} \quad (3.30)$$

and

$$c_{u2} = c_{u2}' + pc_{u2}' \quad (\text{Fig. 3.18}) \quad (3.31)$$

Having a fixed relationship with the vane efficiency, Pfeleiderer's correction factor  $\psi$  is constant for a continuous series of impellers of different specific speeds.

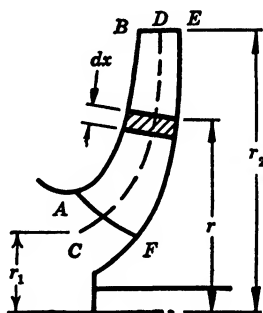


FIG. 3.24. Static moment of streamline  $s = \int_{r_1}^{r_2} r \, dx$ .

Experimental determination of  $\psi$  in Pfeleiderer's equation presents great difficulties. Evidently this requires knowledge of the input head  $H_i$  which cannot be measured because hydraulic losses are always present between the two points where the head is measured. Calculations of the input head from  $H_i = H +$  (hydraulic losses), by estimating several items comprising hydraulic losses, involves in turn a number of unknown experimental coefficients. In view of these difficulties, little progress has been made in devising means for determining the input head of centrifugal pumps. Probably the primary reason is that the art of designing centrifugal pumps on an entirely experimental basis has progressed to the point where a knowledge of the input head would have no effect on the designing procedure.

#### REFERENCES

1. A. H. GIBSON, *Hydraulics and Its Applications*, New York, D. Van Nostrand, 1925, p. 632.
2. JOSEPH N. LECONTE, *Hydraulics*, New York, McGraw-Hill, 1926, p. 252.
3. H. F. SCHMIDT, "Some Screw Propeller Experiments," *Jour. Am. Soc. Nav. Eng.*, Vol. XL, Feb. 1928, p. 16.

4. C. B. STEWART, "Investigation of Centrifugal Pumps," *Univ. of Wisc. Bull.* 318, Sept. 1909, p. 119.
5. KARL FISCHER, "Untersuchung der Strömung in einer Zentrifugalpumpe," *Mitt. Hyd. Inst. Tech. Hochschule Munchen Bull.* 4, Berlin, Oldenbourg, 1931, p. 13; the footnote on p. 221, of reference 9, quotes Vidmar's test of a blower, where back-flow from the impeller eye was observed (*Z. ges. Turbinenwes.* 1913, p. 150).
6. JOSEPH LICHTENSTEIN, "Method of Analyzing the Performance Curves of Centrifugal Pumps," *Trans. A.S.M.E.*, Vol. 50, No. 3, 1928, p. 3.
7. R. C. BINDER and R. T. KNAPP, "Experimental Determination of the Flow Characteristics in the Volute of Centrifugal Pumps," *Trans. A.S.M.E.*, Vol. 58, No. 8, Nov. 1936, p. 649.
8. SAICHIRO UCHIMARU, "Experimental Research on the Distribution of Water Pressure in a Centrifugal Pump Impeller," *Jour. Faculty Eng. Tokyo Imp. Univ.*, Vol. XVI, No. 1928.
9. C. PFLEIDERER, *Die Kreiselpumpen*, Berlin, Julius Springer, 1932, p. 115.



## CHAPTER 4

### VORTEX THEORY OF EULER'S HEAD

#### 4.1 RADIAL IMPELLER

*Flow through the impeller can be considered as consisting of two components: a circular motion around the axis as a result of the impelling action of the vanes, and through-flow or meridional flow caused by the energy gradient drop. The circular component of flow forms a vortex motion. The type of vortex depends on the velocity and pressure distribution and can be established from a study of Euler's equation. For simplicity, consider first a straight radial impeller in which the flow approaches the impeller eye without prerotation. Euler's equation for this case, Fig. 3.1 (b), is*

$$H_e = \frac{u_2 c_{u2}}{g} = \frac{u_2^2}{g} - \frac{u_2 c_{m2}}{g \tan \beta_2} = \frac{u_2^2}{g} - \frac{u_2 w_{u2}}{g} \quad (4.1)$$

Only tangential velocities appear in equation 4.1, indicating that all head is produced by vortex action in planes normal to the axis of rotation. It will be shown that this is true, in general, for all centrifugal pumps, including straight axial flow pumps.

When the flow is zero ( $w_{u2} = 0$ ), Euler's head becomes

$$H_e = \frac{u_2^2}{g} = 2 \frac{u_2^2}{2g} \quad (4.2)$$

and the total head at any radius  $r$  is equal to

$$H = 2 \frac{u^2}{2g} \quad (4.2a)$$

where  $u$  is the peripheral velocity at radius  $r$ . This head is equally divided between static and kinetic heads. Such energy distribution along the radius is typical for a forced vortex and is represented by a square parabola  $OA$  in Fig. 4.1. When flow starts, the head drops by an amount  $u_2 w_{u2}/g$ , where  $w_{u2}$  is proportional to the flow. *This drop of head is the energy gradient drop necessary to produce flow, because even an idealized pump (no losses) cannot start flow against a head higher than*



direction of flow as it exists in the pump impeller, the direction of rotation due to turbine reaction will be the same as that of the pump. The torque developed by the turbine action will act in the same sense as the applied torque. As a result the impeller power input is reduced by the value of  $u_2 w_{u2}/g$  (Fig. 4.2). There being no losses in an idealized machine, the turbine reaction returns to the shaft the energy put into it by the flow caused by the energy gradient drop.

*The turbine reaction of a pump impeller is analogous to the armature reaction of a direct-current generator.* Figure 4.3 shows a relationship

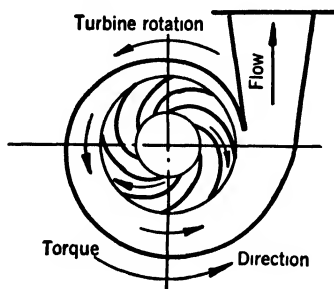


FIG. 4.2. Turbine reaction of impeller.

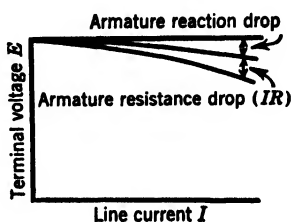


FIG. 4.3. Regulation curve of a direct-current generator.

between the voltage  $E$  (corresponding to the pump head) and current  $I$  (corresponding to the pump capacity) for a direct-current generator. The general appearance of  $E$ - $I$  curves resembles that of the  $Q$ - $H$  curve representing Euler's equation in Fig. 3.3.

For any rate of flow,

$$\frac{u_2^2}{g} = \frac{u_2 c_{u2}}{g} + \frac{u_2 w_{u2}}{g} \quad (4.3)$$

$$\frac{u_2^2}{g} = \text{pump action} + \text{turbine reaction}$$

Note the similarity of the algebraic expression for the first and second terms of the right-hand part of equation 4.3 representing pumping action and turbine reaction.\*

\* Applying the same reasoning to a hydraulic turbine runner, it can be stated that the runner, while rotating under applied head, generates a centrifugal head analogous to the back-electromotive force of an electric motor. The flow through the runner is determined by the difference between the head applied and the centrifugal head developed by the runner. A further reference to this subject is found in Chapter 13.

If prerotation is allowed in the impeller approach, Euler's equation takes the form

$$H_e = \frac{u_2 c_{u2}}{g} - \frac{u_1 c_{u1}}{g} = \frac{u_2^2}{g} - \frac{u_2 w_{u2}}{g} - \frac{u_1 c_{u1}}{g}$$

hence

$$\begin{aligned} \frac{u_2^2}{g} &= \left( \frac{u_2 c_{u2}}{g} - \frac{u_1 c_{u1}}{g} \right) + \left( \frac{u_2 w_{u2}}{g} + \frac{u_1 c_{u1}}{g} \right) \\ &= \text{pump action} + \text{turbine reaction} \end{aligned}$$

Figure 4.4 represents the same relationship graphically.

Thus with prerotation the pump action is reduced by  $u_1 c_{u1}/g$  but the turbine reaction is increased by the same amount. An increase in turbine reaction due to prerotation in the impeller approach is easily under-

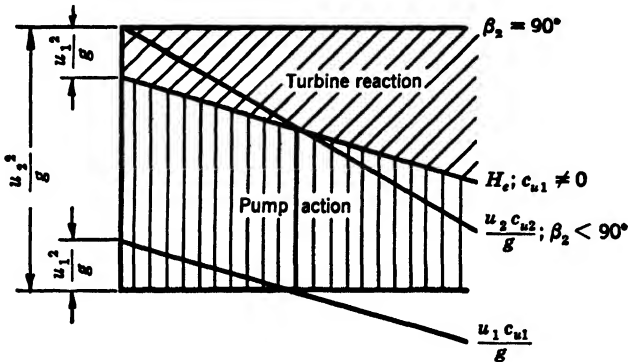


FIG. 4.4. Pump action and turbine reaction with prerotation allowed.

stood, as in normal water turbines water is given prerotation by the guide vanes. Again considering turbine reaction an energy gradient drop to produce the flow, an impeller in which prerotation is allowed will require a greater energy gradient drop to produce the same flow because absolute velocities are increased by prerotation.

Figure 3.3 shows the variation of  $H_e$  with capacity. This is given by the straight line  $AC$  below line  $AB$  for constant  $u_2^2/g$ . The latter can be approached theoretically with vane angles approaching  $90^\circ$  as a limit. The head-capacity curve above line  $AB$  for vane angles  $\beta_2 > 90^\circ$  ( $AD$  on Fig. 3.3) is impossible, even theoretically, as no energy gradient is available to produce the flow. It has been pointed out in Chapter 3 that impulse action is required to produce a rising characteristic. This principle cannot be realized in a centrifugal pump.

In contrast to the impulse action, all centrifugal pumps operate on a pressure or reaction principle, a term used in reference to hydraulic turbines. These represent a closed system under pressure. The total energy is partly pressure and partly kinetic, whereas in impulse water turbines all energy is converted to kinetic energy of high velocity jets which impinge upon the buckets at atmospheric pressure. Pumps with a vane angle  $\beta_2 > 90^\circ$  have been built which had rising head-

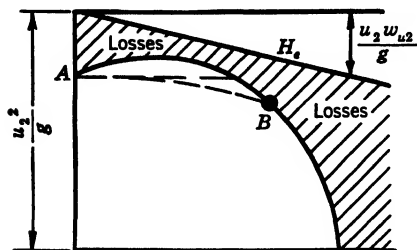


FIG. 4.5. Pump characteristics with  $\beta_2 > 90^\circ$ .

capacity curves (Fig. 4.5). However, the actual discharge angle of the liquid in these pumps was less than  $90^\circ$  and their maximum head never approached  $u_2^2/g$ . In other words their Euler head-capacity curves had an energy gradient drop. Such pumps can be started only against heads lower than their shut-off head, but after starting they can produce

higher heads on their head-capacity curves to the left of point B. Besides being inferior in efficiency, pumps with high discharge angles have undesirable characteristics and for that reason were abandoned many years ago.

If the flow approaching the impeller eye is not radial, or prerotation is allowed, Euler's equation (4.1) will change to

$$H_e = \frac{u_2 c_{u2}}{g} - \frac{u_1 c_{u1}}{g} \quad (4.4)$$

It will be noticed that the second or subtractive term is similar to the first term. Following the same reasoning applied to the first term will reveal that the subtractive term represents the part  $OC'$  of the parabolic head curve  $OC$  (Fig. 4.1), and thus the total head will be obtained as the difference  $CE - C'E' = H_e$ .

For each capacity there is a parabolic curve located somewhere between  $OA$  and  $OE$  representing the head variation along the impeller radius. The line  $OE$  is reached at zero head or when  $w_{u2} = u_2$  in equation 4.1.

By using Euler's head equation in the expanded form,

$$H_e = \frac{u_2^2 - u_1^2}{2g} + \frac{c_2^2 - c_1^2}{2g} + \frac{w_1^2 - w_2^2}{2g} \quad (4.5)$$

it can be shown that each component part of the total head as it appears

in this equation represents a vortex motion. By making use of the geometrical relationships

$$\begin{aligned} c_1^2 &= c_{u1}^2 + c_{m1}^2 & w_1^2 &= w_{u1}^2 + c_{m1}^2 \\ c_2^2 &= c_{u2}^2 + c_{m2}^2 & w_2^2 &= w_{u2}^2 + c_{m2}^2 \end{aligned}$$

equation 4.4 can be changed to

$$H_e = \frac{u_2^2 - u_1^2}{2g} + \frac{c_{u2}^2 - c_{u1}^2}{2g} + \frac{w_{u1}^2 - w_{u2}^2}{2g} \quad (4.6)$$

Only tangential velocities appear in this equation and the radial velocities at entrance and discharge, not equal in general, cancel out. This shows again that all changes in velocities as a result of impeller action take place in planes normal to the axis of rotation producing a vortex motion. With radial approach  $c_{u1} = 0$  and  $w_{u1} = u_1$ , equation 4.5 reduces to

$$H_e = \frac{u_2^2}{2g} + \frac{c_{u2}^2}{2g} - \frac{w_{u2}^2}{2g} \quad (4.7)$$

As the capacity approaches zero,  $w_{u2}$  approaches zero, and  $c_{u2}$  approaches  $u_2$ . So at zero flow

$$H_e = \frac{u_2^2}{g} = \frac{u_2^2}{2g} + \frac{c_{u2}^2}{2g} \quad (4.7a)$$

showing that at zero capacity the total head is equally divided between static head and kinetic energy. At zero head,  $c_{u2} = 0$  and  $w_{u2} = u_2$ ; then

$$H_e = \frac{u_2^2}{2g} - \frac{w_{u2}^2}{2g} = 0 \quad (4.7b)$$

showing that the flow is meridional, under energy gradient, and there is no vortex produced by the impeller.

## 4.2 AXIAL FLOW IMPELLER

In an axial flow pump, liquid particles leave the impeller at the same radius at which they enter. Applying Euler's equation (4.5) to a point on the impeller periphery and noting that  $u_2 = u_1$  we get

$$H_e = \frac{c_{u2}^2 - c_{u1}^2}{2g} + \frac{w_{u1}^2 - w_{u2}^2}{2g} \quad (4.8)$$



design both  $w_{u2}$  and  $u_2$  vary directly as the radius. Therefore the energy gradient drop  $u_2 w_{u2}/g$  varies directly as the square of the radius (curve  $O'C$ ), and the curve of heads  $OC$  is a square parabola. This is a characteristic of a forced vortex when all particles rotate with the same angular velocity.

Although the head distribution along the radii is similar for radial and axial pumps there is an important difference between the final results of the two. In a radial impeller all particles reach the same maximum head at the periphery of the impeller. In an axial flow pump, liquid particles enter and leave at the same radii and the heads produced at different radii are different, being a maximum at the periphery and a minimum at the hub. The pump total head is an integrated average. The hydraulic integration of the head over the whole impeller area takes place in the discharge casing, where the tangential component of the absolute velocity is converted into pressure and the pressure is equalized over the whole area of the discharge pipe. In an efficient diffusion casing, this equalization of pressure occurs without mixing of streamlines, as demonstrated with axial blowers by admitting smoke and sparks into the suction.<sup>1</sup> Evidently the pressure equalization takes place by conduction. (See Chapter 1.) Figure 4.7 shows a diagram of hydraulic integration. The volume of the liquid in the two legs of the U-tube is the same. In the left leg liquid is in rotation. The column of liquid at the center of the left leg supports a higher head  $H$  in the right-hand leg of the tube. The integrated head of the impeller in Fig. 4.6 is equal to the average of the head at the hub ( $H_h$ ) and the head at the periphery ( $H_o$ ). This follows from the geometrical properties of a square paraboloid.

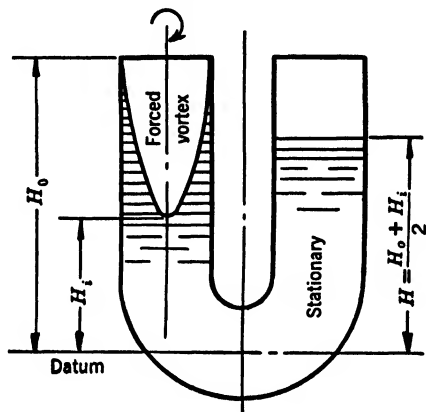


FIG. 4.7. Diagram of hydraulic integration.

$$H_e = \frac{H_h + H_o}{2} \quad (4.10)$$

If the liquid approaches the impeller with prerotation, Euler's head for an axial flow impeller is given by equation 4.4 which is the same as for the radial impeller. The subtractive term is of the same appearance as the first term, and represents a square parabola of suction heads at



different radii ( $FF'$ , Fig. 4.6). The net Euler's head at different radii is represented by ordinates between the curves  $CC'$  and  $FF'$ . The curve of the net Euler's head will remain a square parabola.

### 4.3 FORCED VORTEX AXIAL FLOW IMPELLER

(a) **Inlet and Outlet Pitch, Pitch per Second.** All theoretical discussion and practical design of axial flow pumps is based on the assumption of constant axial velocity through the impeller. The axial velocity of approach to the impeller and beyond the impeller is assumed to be equal to that through the impeller. This assumption is reasonable with a

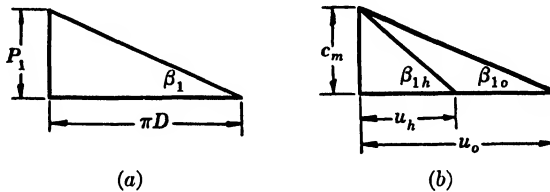


FIG. 4.8. (a) Inlet pitch; (b) inlet velocity triangle for axial flow pump.

normal design except for the effects of frictional drag at the casing and impeller walls. Such distribution has been actually observed on axial flow blowers. To maintain a uniform axial velocity the impeller vane should have the same inlet pitch at different radii. The latter is defined as  $P_1 = \pi D \tan \beta_1$  where  $P_1$  is inlet pitch,  $D$  is impeller diameter, and  $\beta_1$  is the vane entrance angle, Fig. 4.8 (a).

There is a definite relationship between the axial velocity  $c_m$  at normal capacity and pitch  $P_1$ . From the entrance velocity triangle, Fig. 4.8 (b),

$$\frac{c_m}{u_o} = \tan \beta_{1o} \quad \text{and} \quad \frac{c_m}{u_h} = \tan \beta_{1h} \quad (4.11)$$

where subscript  $o$  refers to the outside diameter and  $h$  refers to the hub. But

$$u_h = \pi D_h \times \text{r.p.s.} \quad u_o = \pi D_o \times \text{r.p.s.} \quad (4.12)$$

and

$$\tan \beta_{1h} = \frac{P_h}{\pi D_h} \quad \tan \beta_{1o} = \frac{P_o}{\pi D_o} \quad (4.13)$$

$$c_m = P_h \times \text{r.p.s.} = P_o \times \text{r.p.s.} = P_1 \times \text{r.p.s.} = P_{1s} \quad (4.14)$$

Thus, to maintain a constant axial velocity  $c_m$ , the vane inlet pitch at all radii should be constant.

To provide impelling action, the impeller vane angles should increase gradually from inlet toward discharge or the vane pitch should increase. To maintain the same axial velocity along the radii the pitch for all radii should remain constant to assure the same degree of impelling action for several streamlines of different radii. Thus by definition (Fig. 4.9)

$$P_2 = \pi D_h \tan \beta_{2h} = \pi D_o \tan \beta_{2o} \quad (4.15)$$

and, multiplying by the revolutions per second, we obtain (Fig. 4.10)

$$P_2 \times \text{r.p.s.} = u_h \tan \beta_{2h} = u_o \tan \beta_{2o} = P_{2s} \quad (4.16)$$

$P_{2s}$  may be called discharge pitch per second, a term which will be used in discussing axial flow impeller geometry. Similarly  $P_1 \times \text{r.p.s.} = P_{1s}$  may be called inlet pitch per second. With an axial inlet velocity,  $P_{1s} = c_m$  at normal capacity.

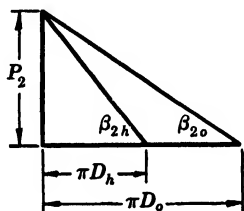


FIG. 4.9. Outlet pitch.

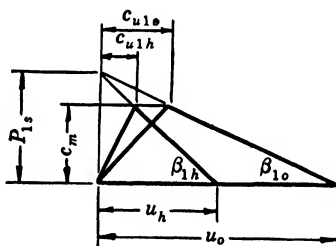


FIG. 4.10. Axial flow pump entrance triangle with prerotation.

If some prerotation is allowed ahead of the impeller, and the vane entrance angles are so selected that the entrance pitch is constant along the radius, the entrance velocity triangle will be as shown on Fig. 4.10 where  $P_{1s} > c_m$  at normal capacity.

The differences  $(P_{1s} - c_m)$  and  $(P_{2s} - c_m)$  are frequently referred to as axial slip. This term is misleading as slip is usually associated with loss of capacity and corresponding drop in volumetric efficiency. However, with axial flow pumps there is no connection between  $(P_{1s} - c_m)$  and volumetric efficiency. Thus at half-normal capacity the slip  $[(P_{1s} - c_m)/c_m]$  may be more than one half but a pump gross efficiency considerably over 50 per cent is quite common. Also, at a capacity over the normal,  $(P_{1s} - c_m)$  is negative while the efficiency is decreasing after reaching a maximum at the normal capacity.

**(b) Forced Vortex Action.** A constant pitch  $P_1$  at entrance and  $P_2$  at discharge, where  $P_2 > P_1$ , assures a forced vortex motion of the liquid by the impeller. Assuming an axial inlet, it follows from con-

sideration of two pairs of similar triangles  $OEB$  and  $EFD$ ,  $OEA$  and  $EFC$  of Fig. 4.11, that

$$\frac{c_{u2h}}{u_h} = \frac{c_{u2o}}{u_o} = \frac{P_{2s} - c_m}{P_{2s}} \quad (4.17)$$

hence

$$\frac{c_{u2h}}{r_h} = \frac{c_{u2o}}{r_o} = \omega' \quad (4.18)$$

where  $\omega'$  is the angular velocity of the absolute flow leaving the impeller which is constant for all streamlines at different radii. This is the requirement for a forced vortex.

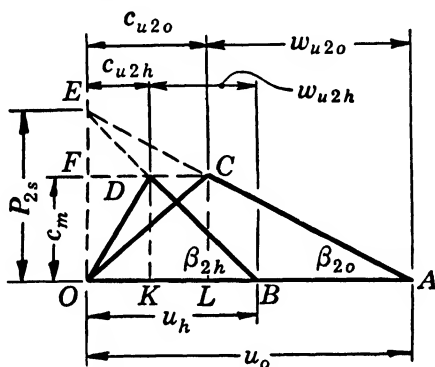


FIG. 4.11. Discharge velocity triangle, axial flow pump.

From similar triangles  $EBO$  and  $DBK$ ,  $EAO$  and  $CLA$  (Fig. 4.11),

$$\frac{w_{u2h}}{u_h} = \frac{w_{u2o}}{u_o} = \frac{c_m}{P_{2s}} \quad \text{and} \quad \frac{w_{u2h}}{r_h} = \frac{w_{u2o}}{r_o} = \omega''$$

also

$$\omega' + \omega'' = \omega \quad (4.19)$$

$\omega''$  is the relative angular velocity of flow, also constant for all streamlines.

The forced vortex regime is maintained at all capacities, or all values of  $c_m$ . Zero head ( $c_u = 0$ ) occurs simultaneously at all streamlines at  $c_m = P_{2s}$ . Also, zero capacity takes place at the same time at all points on different radii when  $c_m = 0$ .

To summarize: *Euler's head in an axial flow pump can be generated by a forced vortex motion. To produce a forced vortex the impeller has to be of constant pitch along the radius, the pitch increasing from suction to discharge. The pitch at the suction edge fixes the axial velocity at normal capacity. The ratio of the pitch per second at discharge  $P_{2s}$  to the axial*

velocity  $c_m$  is a measure of the impelling action of the vane and will be referred to as an impelling ratio.

$$\frac{P_{2s}}{c_m} = \text{impelling ratio} \quad (4.20)$$

For the axial flow impellers without prerotation, the impelling ratio becomes the pitch ratio, since

$$\frac{P_{2s}}{c_m} = \frac{P_{2s}}{P_{1s}} = \frac{P_2}{P_1} = \frac{\tan \beta_2}{\tan \beta_1} \quad (4.20a)$$

The impelling ratio varies with the capacity, increasing as the capacity  $c_m$  is decreasing. It is equal to unity at zero head point since the axial velocity  $c_m$  at that point is equal to  $P_{2s}$ . There is no impelling action when the impelling ratio is equal to unity.

Thus when there is no slip ( $P_{2s} - c_m = 0$ ) there is no impelling action, and impelling action is increasing as the slip is increasing.

**(c) Mixed Flow Impellers.** It has been shown that the action of impellers is the same in a straight radial flow and a straight axial flow pump. This action consists in producing a forced vortex which is superimposed on a radial outward flow in the first case and upon a uniform axial flow in the latter case. The mixed flow impellers occupy an intermediate position between the above two types. Therefore all the deductions for radial and axial flow pumps apply as well to the mixed flow types. The meridional velocity at the entrance  $c_{m1}$  is not equal to that at discharge; normally  $c_{m1} > c_{m2}$ . In drawing the discharge angles, the same procedure is followed as in Fig. 4.11 for axial flow impellers, the impelling ratio  $P_{2s}/c_m$  being selected. It should be noted that with mixed flow impellers a vane having a prescribed impelling ratio may have a discharge angle at the hub lower than the entrance angle  $\beta_{2h} < \beta_{1h}$ . This depends on the relative values of  $c_{m2}$  and  $c_{m1}$  and impeller profile.

With radial impellers  $\beta_2 < \beta_1$  is a most frequent occurrence. The impelling ratio as defined by equation 4.20 applies equally to the radial impellers. The pitch per second at discharge  $P_{2s}$  for radial impellers is defined in the same manner as for axial flow impellers.

$$P_{2s} = u_2 \tan \beta_2$$

and the impelling ratio is

$$\frac{P_{2s}}{c_{m2}} = \frac{u_2 \tan \beta_2}{c_{m2}} = \frac{\tan \beta_2}{\frac{c_{m2}}{u_2}} = \frac{\tan \beta_2}{\phi_e} \quad (4.20b)$$

where  $\phi_e$  is capacity coefficient, defined by equation 3.19.

The impelling ratio increases as the specific speed at b.e.p. decreases. The impelling ratio is discussed further in Chapter 9, in connection with other design elements incorporated in the author's diagram of centrifugal pump characteristics represented in Fig. 9.16.

**(d) Free Vortex Pattern of Flow through the Axial Flow Impeller.**

The forced vortex pattern of flow, as a basis of the impeller action on the liquid, is not the only one possible when applied to straight axial flow pumps. A free vortex pattern of flow for axial flow pumps is assumed by many writers on the subject mostly in connection with the airfoil theory. According to this, the tangential velocity distribution along the radius follows the law

$$c_{u2}r = \text{constant} \quad (4.21)$$

This is arrived at by assuming that the same head is generated at all radii, or

$$uc_{u2} = gH = \text{constant} \quad (4.21a)$$

which is Euler's head equation with an axial inlet velocity. Both assumptions are motivated by reasoning that only at these conditions is the flow stable or free from cross flows. In Chapter 1 it has been shown

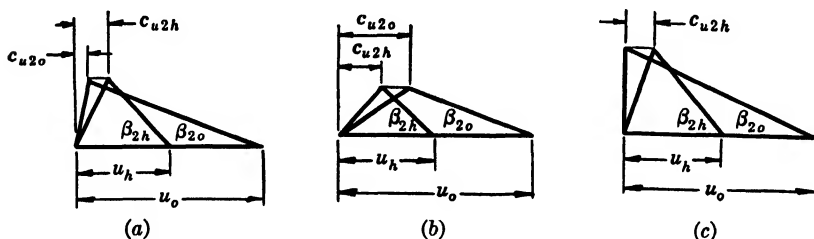


FIG. 4.12. (a) Discharge velocity triangle at rated point, free vortex; (b) velocity triangle at partial capacity; (c) velocity triangle at capacity over the normal.

that a free vortex is only one mode of circular motion of liquids out of a great many possible ones, all of which are stable. There are several objections to a free vortex flow pattern as a basis for the theoretical reasoning of the axial flow pump impeller action, some of which have been pointed out in more recent writings on the subject.<sup>2</sup> †

† A statement by C. W. Smith, of General Electric Company, may serve as an example. "The Vortex Theory (free vortex) is not the best on which to base a design, at least in its present simple form." Minutes of Axial Flow Compressor Meeting of 26 June, on German Articles primarily by Bruno Eckert and Group P.40, published by Navy Department, Code 445A, Bureau of Ships, 1946, Washington 25, D. C.

(1) Free vortex motion of liquid at the impeller discharge can exist at one point on the head-capacity curve only. If Fig. 4.12 (a) represents Euler's velocity triangle, at the design point

$$c_{u2h}r_h = c_{u2o}r_o = \text{constant} = C \quad (4.22)$$

which means that the tangential component is inversely proportional to the radius. Then at partial capacity  $c_{u2o}$  becomes greater than  $c_{u2h}$ , and the regime approaches a forced vortex; Fig. 4.12 (b). At zero capacity the flow becomes a forced vortex.

At capacities over the rated,  $c_{u2o}$  will become zero, while  $c_{u2h}$  is not; Fig. 4.12 (c). At a still greater capacity,  $c_{u2o}$  becomes negative.

(2) Actual test curves show that at capacities below one half of normal (Fig. 4.13) the total head  $H$  is equal to or exceeds  $u_h^2/g$ . This is a maximum possible theoretical head at the hub. Evidently a theory assuming a constant head for all radii does not hold at capacities less than normal and some different assumption is required.

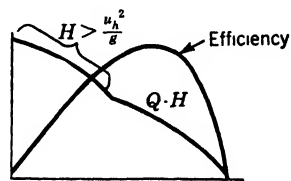


FIG. 4.13. Axial flow pump characteristics.

(3) Since the tangential components vary inversely as the radius at the best efficiency point, the angular velocity of the absolute flow will vary inversely as the square of radius, as the following relationships show. From equation 4.22

$$\omega_h = \frac{c_{u2h}}{r_h} = \frac{C}{r_h^2}$$

and

$$\omega_o = \frac{c_{u2o}}{r_o} = \frac{C}{r_o^2} \quad (4.23)$$

Such an angular velocity distribution is not easy to visualize in view of the constant angular velocity of the impeller which is responsible for all changes in velocities.

(4) The advocates of the free vortex pattern of flow for axial flow pumps usually resort to selection of impeller vane sections from airfoil test data. This procedure is not applicable to extreme mixed flow impellers or straight radial flow impellers. Thus the pump designer is left to his own resources in filling the gap between the straight radial and straight axial impeller types.

The forced vortex reasoning of impeller action is free from these drawbacks because

(1) It applies equally well to straight centrifugal, mixed flow, and straight axial flow pumps.

(2) With axial flow pumps the forced vortex regime is maintained for the whole head-capacity range. Zero head and zero capacity points occur at the same time at the hub and periphery of the impeller.

(3) A constant absolute angular velocity is maintained at all capacities ahead, through, and beyond the impeller, this velocity increasing as the capacity decreases.

(4) Head generated at different radii of the impeller expressed as a fraction of the maximum head at zero capacity is constant:

$$\psi_e = \frac{H_e}{\frac{u_2^2}{g}} = \frac{c_{u2}}{u_2} = \text{constant}$$

where  $\psi_e$ , the head coefficient defined by equation 3.18, is constant for all radii and at all capacities. Thus, at each radius the impeller vane elements contribute their share to the total integrated head "according to their ability" or, stated differently, *the "dimensionless head"  $\psi_e$  produced at different radii is constant at all capacities.*

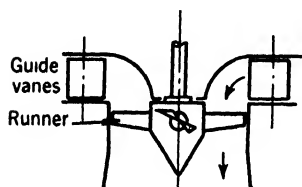


FIG. 4.14. Axial flow water turbine.

(5) Using a forced vortex pattern of flow leads to a geometrical procedure of impeller vane layout which is valid for straight axial flow impellers as well as for mixed

flow impellers of any profile.

The use of a free vortex theoretical treatment of operation of hydraulic axial flow water turbines is the only one possible because the same head is actually applied to all streamlines. Radial guide vanes (Fig. 4.14) give the water the same tangential component for all streamlines. The flow between the guide vanes and the impeller follows closely the law  $c_u r = \text{constant}$ . The impeller vane curvature is selected with due regard to the velocity distribution of the approaching flow. The difference in problems confronting the axial flow pump designer and the axial flow water turbine designer have a direct bearing upon the impeller design.

#### 4.4 SPECIAL CASES

All the examples considered here appear to contradict the theory and established experimental knowledge; however, on close examination they reveal misapplication of the theory or misunderstanding of the method of operation of the pump.

(a) **High Head Pump.** Figures 4.15 and 4.16 show a small single-stage pump which develops unusually high head for a centrifugal pump,

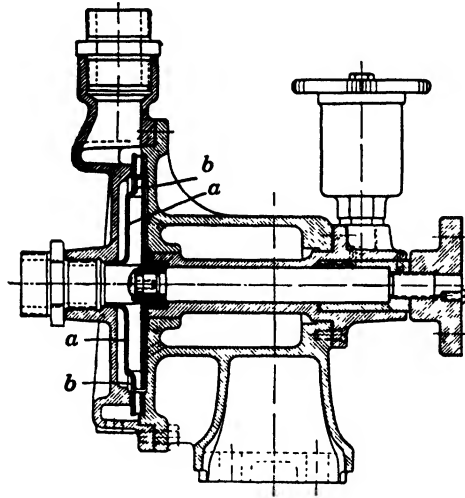


FIG. 4.15. A pump generating head  $H = 0.958 (u_2^2/g)$ .

reaching 95.8 per cent of  $u_2^2/g$ , whereas an average low specific speed pump will produce about 63 per cent of  $u_2^2/g$ .<sup>3, 4</sup> This pump in small size is rated to deliver 15 g.p.m. at 115 ft., 3000 r.p.m. with an efficiency of 48 per cent. The impeller and diffusion casing passages are milled out. The high head of this pump is explained by the fact that, in addition to a normal centrifugal head, the impeller works as a "turbine" pump (a misnomer) known as Westco type. The multivane impeller rotates closely fitted to the diffusion vanes. Liquid leaves and reenters spaces between the vanes absorbing additional energy from the vanes, viscosity playing an important part in this exchange of energy. At the cut-water the high pressure liquid is taken off into the nozzle.<sup>5</sup>

If the clearance between the impeller and the casing diffusion vanes is increased, the head drops off rapidly and the performance approaches that of a normal centrifugal pump with high impeller vane angles. There are blowers which work on

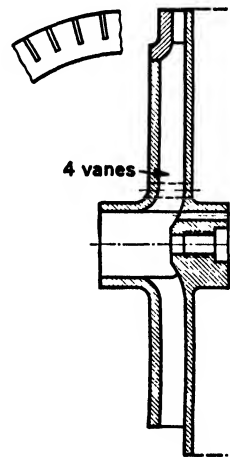


FIG. 4.16. Impeller for pump in Fig. 4.15; 4 long vanes and 48 short vanes.



the same principle with a great many (64) forward curved short vanes producing heads in excess of  $1.1(u_2^2/g)$ .

**(b) Reverse Rotation.** Since the theoretical head at shut-off does not depend on the impeller vane angle one may expect that an impeller running in a direction opposite to that of normal should develop the same head at zero capacity. In practice, however, it has been found that the pump develops only about one half of the shut-off head under

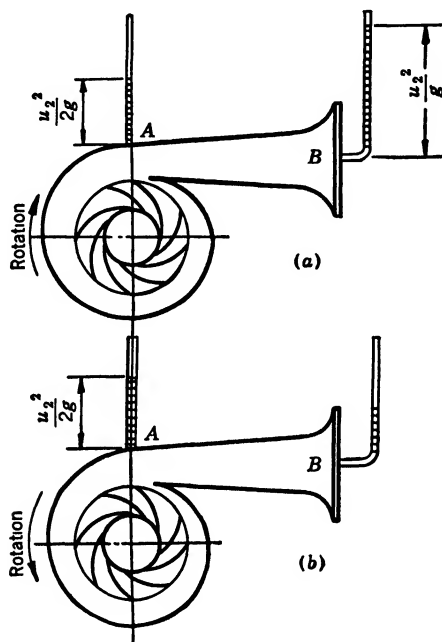


Fig. 4.17. Pump head at zero capacity with a correct and reverse rotation.

normal operation. The difference is not in the impeller performance but in the casing and method of measuring heads. Thus in a normally operated pump, losses being disregarded and an impeller developing full  $u_2^2/g$  shut-off head being assumed, a gage at A, Fig. 4.17 (a), will register only the static head  $u_2^2/2g$ . A gage at B will register both the static and the dynamic head or  $u_2^2/g$ .

When the impeller rotation is reversed, Fig. 4.17 (b), the pressure at A will remain the same or  $u_2^2/2g$ , but pressure at B will be lower than at A because of a negative dynamic head or suction exerted by the flow on the nozzle in the same manner as a pitot tube facing backwards will show a pressure lower than the static pressure by the amount of the velocity head. Thus the difference in the head at normal and backward

rotation is caused by the casing, the impeller behavior being quite normal in both cases.

**(c) Remarks on Pumping Solid-Liquid Mixtures.** In a centrifugal pump, power applied to the shaft is converted by the impeller into pressure energy and kinetic energy of the liquid. In Art. 1.6 it has been shown that *in solid-liquid mixtures solids cannot possess or transmit any pressure energy; therefore when solid-liquid mixtures are being pumped solids can acquire only kinetic energy. But since solids cannot convert their kinetic energy into pressure the major part of the latter is wasted. Solids are moved through the pump and beyond almost entirely at the expense of the energy imparted to the liquid by the impeller.* For that reason the energy per pound of mixture (total head) is considerably lower than that for the liquid alone. Transportation of solids in a liquid results in additional hydraulic losses due to the relative motion of the liquid with respect to the solids, which, in a sense, are obstructions to the flow of the liquid. These losses expressed as a percentage of the impeller input increase with the concentration of solids in the mixture. The pump gross efficiency decreases rapidly when concentration of solids in the mixture is increased.<sup>6</sup>

#### REFERENCES

1. HENRY F. SCHMIDT, "Some Screw Propeller Experiments with Particular Reference to Pumps and Blowers," *Jour. Am. Soc. Nav. Eng.*, Vol. XL, No. 1, Feb. 1928, p. 15.
2. G. F. WISLICENUS, "A Study of the Theory of Axial-Flow Pumps," *Trans. A.S.M.E.*, Vol. 67, No. 6, Aug. 1945, p. 451.
3. C. PFLEIDERER, *Die Kreiselpumpen*, Berlin, Julius Springer, 1932, p. 382.
4. F. LAWACZEK, *Turbinen und Pumpen*, Berlin, Julius Springer, 1932, pp. 157, 161, 167.
5. KARL SCHMIDT, "Über Luftansaugende Kreiselpumpen," doctoral dissertation, Tech. Hochschule zu Hannover, 1932; Robert Noske, Universitätsverlag in Borna-Leipzig.
6. M. P. O'BRIEN and D. G. FOLSOM, "The Transportation of Sand in Pipe Lines," *Univ. of Calif. Publ. in Eng.*, Vol. 3, No. 7, 1937, pp. 343-384; available in bulletin form.

## CHAPTER 5

### SPECIFIC SPEED AND DESIGN CONSTANTS

#### 5.1 CENTRIFUGAL PUMP CONSTANTS FROM GENERAL PRINCIPLES OF SIMILITUDE

Dimensional analysis applied to problems of similitude in hydraulics proved to be a useful tool in many instances. It disclosed the functional relationship among the quantities involved and established dimensionless criteria of flow, found already experimentally in many cases, for conditions known as dynamically similar. One of the important contributions of dimensional analysis to our knowledge of model testing is that it indicated the limitations of the theory of similitude, showed the way to evaluate the various factors affecting the flow, and, sometimes, by destroying the geometrical similarity (one of the requisites for dynamic similarity), to obtain the desired information from model testing. *Applied to centrifugal pumps, the dimensional analysis did not contribute anything new* but it established from the very general principle the constants in a dimensionless form, and facilitated, from experience with water, the drawing of conclusions regarding the behavior of pumps when pumping liquids of different viscosities. The affinity laws follow from these constants.

Use will be made of the method of procedure proposed by Buckingham.<sup>1</sup> *The principle of dimensional analysis requires that all the terms of a correct and complete physical equation shall have the same dimensions. This implies that the object to be studied by dimensional analysis should be known well enough to permit assumption of the physical quantities expected to affect the phenomenon under consideration.* In the case of centrifugal pumps the quantities involved are

$H$	pump head (length) . . . . .	$l$
$Q$	capacity (volume per unit time). . . . .	$l^3/t$
$n$	speed in revolutions per minute (number per unit time)	$1/t$
$D$	impeller diameter representing the pump size for a series of similar pumps . . . . .	$l$
$g$	acceleration due to gravity, constant. . . . .	$l/t^2$

$\rho$	liquid density (mass per unit volume) . . . . .	$m/l^3$
$\mu$	absolute viscosity (viscosity coefficient) . . . . .	$m/lt$
$E$	energy applied (to the shaft) and obtained in the form of pump output measured in foot-pounds or $H \times \text{mg.}$ or per unit mass $E = gH$ which differs from the head by a constant $g$ ; its dimension is . . . . .	$l^2/t^2$

Energy per unit mass  $E = gH$  will be used instead of head because of its more general character and because it includes the effect of the acceleration due to gravity. It should be remembered that all equations for the head developed by an impeller are based on the law of conservation of energy which, for an incompressible fluid with a constant acceleration due to gravity, reduces to the height the liquid can be raised by the pump. Thus the number of quantities necessary to describe the operation of a centrifugal pump reduces to six:  $Q$ ,  $E$ ,  $n$ ,  $D$ ,  $\rho$ , and  $\mu$ . These are measured by three fundamental units: length ( $l$ ), time ( $t$ ), and mass ( $m$ ). The relation among these quantities may be expressed by a general functional equation

$$f(Q, E, n, D, \rho, \mu) = 0 \quad (5.1)$$

According to a theorem of dimensional analysis a complete equation describing the relation among  $n$  different quantities (six in this case) measured with  $k$  fundamental units (three here) can be reduced to the form

$$f(\Pi_1, \Pi_2, \dots \Pi_{n-k}) = 0$$

or in this case

$$f(\Pi_1, \Pi_2, \Pi_3) = 0 \quad (5.2)$$

where  $\Pi$  (Greek capital letter pi) represents a dimensionless product of the form

$$\Pi = Q^a E^b n^c d^d \rho^e \mu^g$$

where  $a$ ,  $b$ ,  $c$ ,  $d$ ,  $e$ , and  $g$  are whole numbers or fractions or equal to zero, in which case the corresponding factor is equal to unity;  $f$  is some unknown function to be found by experiment. If we select  $E$ ,  $D$ ,  $\rho$  as three independents, the dimensionless quantities  $\Pi_1$ ,  $\Pi_2$ ,  $\Pi_3$  can be put in the form

$$\begin{aligned} \Pi_1 &= E^{x_1} D^{y_1} \rho^{z_1} Q \\ \Pi_2 &= E^{x_2} D^{y_2} \rho^{z_2} n \\ \Pi_3 &= E^{x_3} D^{y_3} \rho^{z_3} \mu \end{aligned} \quad (5.3)$$

where  $x_1, y_1, z_1, x_2$ , etc., are the unknown exponents to be determined now. To do this we express  $E, D, \rho, Q, n$ , and  $\mu$  in terms of their dimensional formulas.

$$\begin{aligned}\Pi_1 &= \left(\frac{l^2}{t^2}\right)^{x_1} (l)^{y_1} \left(\frac{m}{l^3}\right)^{z_1} \left(\frac{l^3}{t}\right) = l^{2x_1+y_1-3z_1+3} t^{-2x_1-1} m^{z_1} \\ \Pi_2 &= \left(\frac{l^2}{t^2}\right)^{x_2} (l)^{y_2} \left(\frac{m}{l^3}\right)^{z_2} \left(\frac{1}{t}\right) = l^{2x_2+y_2-3z_2} t^{-2x_2-1} m^{z_2} \\ \Pi_3 &= \left(\frac{l^2}{t^2}\right)^{x_3} (l)^{y_3} \left(\frac{m}{l^3}\right)^{z_3} \left(\frac{m}{lt}\right) = l^{2x_3+y_3-3z_3-1} t^{-2x_3-1} m^{z_3+1}\end{aligned}\quad (5.4)$$

To make  $\Pi_1, \Pi_2$ , and  $\Pi_3$  dimensionless the exponents of  $l, t$ , and  $m$  must be equal to zero. For  $\Pi_1$  we obtain three simultaneous equations for determination of  $x_1, y_1$ , and  $z_1$ .

$$2x_1 + y_1 - 3z_1 + 3 = 0$$

$$-2x_1 - 1 = 0$$

$$z_1 = 0$$

from which we get

$$x_1 = -\frac{1}{2} \quad y_1 = -2 \quad z_1 = 0$$

Substituting these in the expression for  $\Pi_1$  in equation 5.3 we obtain

$$\Pi_1 = E^{-1/2} D^{-2} \rho^0 Q = \frac{Q}{E^{1/2} D^2} = \frac{Q}{(gH)^{1/2} D^2} \quad (5.5)$$

Similarly for  $\Pi_2$  the equations for the determination of  $x_2, y_2, z_2$  are

$$2x_2 + y_2 - 3z_2 = 0$$

$$-2x_2 - 1 = 0$$

$$z_2 = 0$$

Hence

$$x_2 = -\frac{1}{2} \quad y_2 = 1 \quad z_2 = 0$$

and

$$\Pi_2 = \frac{nD}{E^{1/2}} = \frac{nD}{(gH)^{1/2}} \quad (5.6)$$

$x_3, y_3$ , and  $z_3$  are found from

$$2x_3 + y_3 - 3z_3 - 1 = 0$$

$$-2x_3 - 1 = 0$$

$$z_3 + 1 = 0$$

Hence

$$x_3 = -\frac{1}{2} \quad y_3 = -1 \quad z_3 = -1$$

and

$$\Pi_3 = \frac{\mu}{\rho D E^{1/2}} = \frac{\nu}{D(gH)^{1/2}} \quad (5.7)$$

where  $\nu$  (kinematic viscosity) =  $\mu/\rho$ . Substituting these expressions for  $\Pi_1$ ,  $\Pi_2$ , and  $\Pi_3$  in equation 5.2 we obtain equation 5.8, which gives the relationship among the quantities involved.

$$f \left[ \frac{Q}{(gH)^{1/2} D^2}, \frac{nD}{(gH)^{1/2}}, \frac{\nu}{(gH)^{1/2} D} \right] = 0 \quad (5.8)$$

The relationship expressed by equation 5.2 can be given the form

$$f[\Pi_1, (\Pi_2 \Pi_1^{1/2}), (\Pi_3^{-1} \Pi_1)] = 0 \quad (5.9)$$

Substituting their values for  $\Pi_1$ ,  $\Pi_2$ ,  $\Pi_3$  we obtain

$$f \left[ \frac{Q}{(gH)^{1/2} D^2}, \frac{nQ^{1/2}}{(gH)^{1/4}}, \frac{DQ}{\nu D^2} \right] = 0 \quad (5.10)$$

Let

$$\frac{nQ^{1/2}}{(gH)^{1/4}} = \Pi_2' \quad \frac{DQ}{\nu D^2} = \Pi_3' = \frac{Q}{\nu D}$$

(a) It will be noticed that  $\Pi_2'$  is the dimensionless expression for specific speed and  $\Pi_3'$  is the Reynolds number, as for similar pumps  $Q/D^2$  is proportional to the velocities at corresponding points. For a true dynamic similarity  $\Pi_1$ ,  $\Pi_2'$  (or  $\Pi_2$ ) and  $\Pi_3'$  (or  $\Pi_3$ ) should be equal for similar pumps or for the same pump at different speeds. This condition is impossible to satisfy because, for the same liquid, if the size or speed is varied,  $\Pi_1$  and  $\Pi_2$  will stay constant while Reynolds' number  $\Pi_3'$  will increase with an increase of speed or pump size. However, it will be shown that Reynolds' number affects only a small part of the total power input, when pumping water that consumed by the hydraulic resistance to the flow through the pump. If this is neglected, the conditions for the similarity of flow are  $\Pi_1 = \text{constant}$  and  $\Pi_2 = \text{constant}$  or  $\Pi_1 = \text{constant}$ , and  $\Pi_2' = \text{constant}$ . This is true in practice with a degree of accuracy quite sufficient for all practical purposes. Although the disk friction of the impeller is of a hydraulic nature it is not considered here, being "external" to the flow through the pump.

(b) If the hydraulic losses are neglected, then the quantities necessary to describe the operation of the pump are  $H$  (or  $gH$ ),  $Q$ ,  $n$ , and  $D$ , four in number, which can be measured with two fundamental units,

length  $l$  and time  $t$ . Hence the operation of a pump can be expressed by an equation similar to 5.2.

$$f'(\Pi_1, \Pi_2) = 0 \quad (5.11)$$

which contains two dimensionless products. If the same procedure as before is followed, expressions for  $\Pi_1$  and  $\Pi_2$  will be found to be the same as when hydraulic resistance is considered, or

$$\Pi_1 = \frac{Q}{(gH)^{1/2} D^2} \quad \text{and} \quad \Pi_2 = \frac{nD}{(gH)^{1/4}} \quad (5.12)$$

For  $\Pi_2'$  the same expression will be obtained.

$$\Pi_2' = \frac{nQ^{1/2}}{(gH)^{3/4}} \quad (5.12a)$$

(c) Equation 5.11 can be presented in the form

$$\Pi_1 = f''(\Pi_2), \quad \text{or} \quad \frac{Q}{(gH)^{1/2} D^2} = f'' \left[ \frac{nD}{(gH)^{1/4}} \right] \quad (5.13)$$

and

$$Q = (gH)^{1/2} D^2 f'' \left[ \frac{nD}{(gH)^{1/4}} \right]$$

The functions  $f$ ,  $f'$ , and  $f''$ , in equations 5.2, 5.11, and 5.13 should be determined by experiment and, for a constant acceleration due to gravity  $g$  and a given pump (constant  $D$ ) operated at a constant speed  $n$ , they represent a regular constant speed head-capacity curve.

(d) Similarly if a pump is pumping liquids of various viscosities, equation 5.8, for constant  $g$ ,  $n$ , and  $D$ , represents a series of  $Q$ - $H$  curves which must be determined by test. Thus, the relationship between head and capacities for water and any viscous liquid for corresponding points (points of maximum efficiency for instance) is an experimental one.

(e) Once determined, the head-capacity curves for any size and speed, constant or variable, are determined from  $\Pi_1 = \text{constant}$  and  $\Pi_2 = \text{constant}$  from which the affinity laws follow. By dividing  $\Pi_1$  by  $\Pi_2$  we obtain

$$\frac{Q}{nD^3} = \text{constant} \quad (5.14)$$

which indicates that for a given pump ( $D = \text{constant}$ ) the capacity varies directly as the speed, and for a constant speed  $n$  the capacity varies directly as the cube of the diameters, or the cube of the factor.

From  $\Pi_2 = \text{constant}$  we obtain

$$\frac{n^2 D^2}{H} = g \text{ constant} = \text{constant} \quad (5.15)$$

which shows that for a given pump the head varies directly as the square of the speed, and for a constant speed the head varies directly as the square of the diameters.

(f) If, when water is being pumped, the speed or size of the pump is varied,  $\Pi_1$  and  $\Pi_2$  remain constant but Reynolds' number  $\Pi_3' = (Q/D^2)(D/\nu)$  changes directly as the speed and as the square of the size of the pump. If, instead of the speed or size, viscosity  $\nu$  is changed to  $\nu_1$  to produce the same Reynolds number change,  $\Pi_1$  and  $\Pi_2$  will remain constant, or affinity laws will hold. Following the same reasoning, if the affinity laws hold at viscosity  $\nu_1$  they will hold at viscosity  $\nu_2$  (perhaps with less accuracy), and so on. Thus *it can be stated in general that when viscosity is varied  $\Pi_1$  and  $\Pi_2$  remain constant and affinity laws hold.*

Again, when water is being pumped, affinity laws hold for pumps with low hydraulic efficiency (gross pump efficiency below 50 per cent). This happens when the pump is small and is operated at low speed. In such a case the Reynolds number is low. Now, it is reasonable to think that a good pump with high efficiency on water will follow the affinity laws when a viscous liquid is being pumped at a reduced efficiency and at the same Reynolds number as that of the small low speed pump pumping water. This suggests again that the affinity laws must hold when viscosity is varied. *It also means that the specific speed for the corresponding points (connected by the affinity laws), such as the best efficiency points, remains constant for all viscosities.* These are important relationships and their experimental proof and limitations for pumping viscous oils is given in Chapter 14.

(g) The dimensionless products  $\Pi_1$  and  $\Pi_2$  can be considered as criteria of the operation of centrifugal pumps in the same manner as Reynolds' number is for the pipe flow or Froude's number for the resistance of submerged bodies. These two constants could be rightly called Camerer's criteria because he introduced and defined them in their dimensional form for hydraulic turbines in 1912.<sup>2</sup> The physical meaning of these criteria as well as that of  $\Pi_2'$  or specific speed are of little importance. The numbers are used as constants connecting the head, capacity, speed, and size of a given type of pump.

(h) There is no available information showing at what Reynolds number the flow in centrifugal pumps will change from the streamline to the turbulent state. It is safe to state that it would be considera-



bly lower than that for the pipe flow on account of the many disturbing factors present and a very short path. Thus, it is hardly possible that streamline flow is ever encountered in centrifugal pumps.

(i) The criteria  $\Pi_1$  and  $\Pi_2$  (or  $\Pi_2' = n_s$ ) apply equally to hydraulic turbines. Moreover, they apply to all rotary pumps where the head is produced by virtue of velocity or inertia forces. This means that affinity laws hold also for pumps of tangential or impulse type, as confirmed by tests by Carl Ritter.<sup>3</sup>

## 5.2 SPECIFIC SPEED, UNIT SPEED, AND UNIT CAPACITY

The expression for the specific speed will be developed by making use of the affinity laws. Specific speed  $n_s$  is defined as that speed, in revolutions per minute, at which an impeller geometrically similar to the one under consideration and reduced in size will develop a head of 1 ft. at a capacity of 1 g.p.m. Suppose an impeller of diameter  $D_2$  operating at  $n$  revolutions per minute generates  $H$  feet of head and  $Q$  gallons per minute. From the definition of specific speed, an impeller similar to the first one but of diameter  $D_2'$  will develop a head  $H' = 1$  ft. and a capacity  $Q' = 1$  g.p.m. when operated at speed  $n_s$  (r.p.m.). If we denote the ratio of diameters by  $D_2'/D_2 = a$ , which is the reduction factor, and the ratio of speeds by  $n_s/n = b$ , the speed reduction factor, and recall that the head varies as  $a^2$  and  $b^2$  and the capacity changes as  $a^3$  and  $b$ , the following equations must be satisfied if both the speed and the pump size are changed to develop 1 ft. of head and deliver 1 g.p.m.:

$$Ha^2b^2 = 1 \quad (5.16)$$

$$Qa^3b = 1 \quad (5.17)$$

Solving these equations for  $b$  we have

$$b = \frac{n_s}{n} = \frac{Q'^{1/2}}{H'^{3/4}}$$

or

$$n_s = \frac{n\sqrt{Q}}{H^{3/4}} \quad (5.18)$$

which is the familiar expression for specific speed. For the reduction factor from the same equations we obtain

$$a = \frac{D_2'}{D_2} = \frac{n\sqrt{H'}}{n_s\sqrt{H}} = \frac{\frac{n}{\sqrt{H}}}{\frac{n_s}{\sqrt{H'}}}$$

or in general

$$a = \frac{\frac{n}{\sqrt{H}}}{\frac{n'}{\sqrt{H'}}} \quad (5.19)$$

The expression for the specific speed is sometimes given the form

$$n_s = \frac{n}{\sqrt{H}} \left( \frac{Q}{\sqrt{H}} \right)^{1/2} = n_1 \sqrt{q_1} \quad (5.20)$$

where  $n_1$  is called the unit speed and means the speed at which a given pump should operate to generate 1 ft. of head;  $q_1$  is called the unit capacity and represents the capacity at the unit speed and 1 ft. of head. The following information about the specific speed is important for the study and design of centrifugal pumps.

(a) The physical meaning of the specific speed as revolutions per minute to give 1 ft. of head and 1 g.p.m. capacity has no application or interest to the designer. The number is used merely as a type characteristic for impellers geometrically similar.

The term specific speed was introduced by R. Camerer<sup>4</sup> and was applied to hydraulic turbines in the form  $n_s = n\sqrt{N}/H^{5/4}$ . This is obtained by substitution of power  $N$  into the expression for  $n_s$  instead of capacity  $Q$  from  $N = (Q\gamma H)/550$ . Baashus,<sup>5</sup> independently of Camerer, used the same expression for the classification of hydraulic turbines, but called it *characteristic*.

(b) As a type number, specific speed is used to designate the operating characteristic for the best efficiency point only.

(c) For any impeller the specific speed varies from 0 to  $\infty$  for various points on the head-capacity curve, being zero when capacity is zero and infinity when the head is zero.

(d) For the same impeller, the specific speed does not change with the impeller speed. This can be checked by expressing the new head and capacity in terms of the old ones and the speed ratio and substituting in the expression for specific speed.

(e) For similar impellers the specific speed is constant for different speeds and sizes.

(f) Statements (e) and (d) presume the same hydraulic efficiency and apply to all points on the head-capacity curve. The points of the same specific speed of several  $Q$ - $H$  curves for different speeds of the same impeller or for several sizes of similar impellers are referred to as corresponding points, or points of the same efficiency (hydraulic).

(g) Inspection of the formula for specific speed shows that it increases with the capacity and decreases with the increase in head. A high specific speed impeller is characterized by large width as compared with the impeller diameter, a high ratio  $D_1/D_2$ , and a small number of vanes. If the same head and capacity requirements are met with pumps of different types, high specific speed pumps will run at a higher speed and will be smaller in size, hence cheaper, and will require smaller high speed motors (see Fig. 2.3).

(h) In general, any head-capacity requirements can be met with any one of many types of impellers of different sizes operating at different speeds. But some will lead to unpractical speeds and sizes. As an illustration, suppose an impeller of 15-in. diameter at 1800 r.p.m. develops 200 ft. of head and 2500 g.p.m. capacity. What will be the speed and size of a similar impeller to give 10,000 g.p.m. capacity at 15 ft. of head? The specific speed of the given impeller is

$$n_s = 1700$$

The speed  $n$  of the new impeller is obtained from

$$n_s = 1700 = \frac{n\sqrt{10,000}}{(15)^{3/4}} \quad n = 129.5 \text{ r.p.m.}$$

The factor

$$b = \frac{n_1}{n_1'} = \frac{\frac{1800}{\sqrt{200}}}{\frac{129.5}{\sqrt{15}}} = 3.8$$

or an impeller of  $15 \times 3.8 = 57$ -in. diameter will be necessary. The same conditions can be met with a high specific speed pump at 870 r.p.m. with an impeller of about 17 in.

One of the major problems of centrifugal pump engineering is the selection of the best type of pump, or specific speed, for a given set of head-capacity conditions. This problem presents the following conflicting considerations.

- (1) High specific speeds lead to smaller pumps.
- (2) Each specific speed has its limitations, depending on the cavitation characteristics (Chapter 12).
- (3) Driver speed selection has limitations, particularly when electric motors are used.
- (4) The optimum pump efficiency depends on the specific speed (Fig. 5.1).

(5) Specific speed may be varied by changing the number of stages or dividing capacity between several pumps.

(6) Placing the operating point off-peak and using a more efficient type may improve the operating point efficiency.

(i) For the same impeller for the points at best efficiency or corresponding points unit speed  $n_1 = n/\sqrt{H}$  and unit capacity  $q_1 = Q/\sqrt{H}$

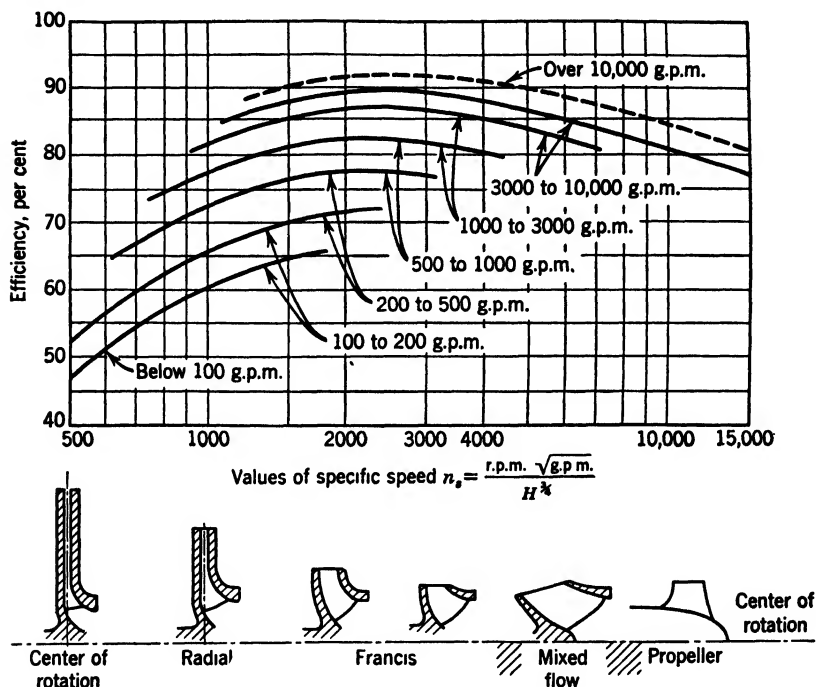


FIG. 5.1. Pump efficiency as affected by specific speed and pump size (Worthington).

do not change with the speed. For similar impellers unit speed and unit capacity vary with the size, as seen from the following. The reduction factor,

$$a = \frac{D_2'}{D_2} = \frac{n_1}{n_1'} \quad n_1 D_2 = n_1' D_2' = \text{constant} \quad (5.21)$$

That is, the unit speed varies inversely as the factor, and the product of the unit speed and impeller diameter is constant for impellers of the same type and different sizes.

The variation of the unit capacity is obtained from

$$n_s = n_1 \sqrt{q_1} = n_1' \sqrt{q_1'} = \text{constant}$$

Hence

$$\frac{n_1}{n_1'} = \frac{\sqrt{q_1'}}{\sqrt{q_1}} = a = \frac{D_2'}{D_2}$$

or

$$\frac{q_1'}{(D_2')^2} = \frac{q_1}{D_2^2} = \frac{Q'}{\sqrt{H'}(D_2')^2} = \frac{Q}{\sqrt{H}D_2^2} = \text{constant} \quad (5.22)$$

(j) It was for the products  $nD_2/\sqrt{H}$  and  $Q/\sqrt{H}D_2^2$ , as applied to hydraulic turbines, that Camerer introduced the names unit speed and unit capacity respectively. These were referred to centrifugal pumps, the first meaning speed in revolutions per minute to produce a head of 1 ft. with a geometrically similar impeller of 1-ft. diameter, and the second the capacity at unit speed or capacity given by a similar impeller of 1-ft. diameter at 1 ft. of head. The tendency, however, is to use the term unit speed for  $n/\sqrt{H}$  and unit capacity for  $Q/\sqrt{H}$ . To distinguish between the two, Camerer's notation might be called "type unit speed" and "type unit capacity," and the expression  $n/\sqrt{H}$  could have the name "impeller (or pump) unit speed" and  $Q/\sqrt{H}$  "impeller unit capacity."

(k) The expressions for unit speed  $n_{1h} = n/\sqrt{H}$  and unit capacity  $q_{1h} = Q/\sqrt{H}$  referred to 1 ft. of head were introduced into centrifugal pump practice from hydraulic turbine practice where the head is substantially constant. For centrifugal pumps, similar expressions can be obtained on the basis of a speed of 1 r.p.m. These are the unit capacity,  $q_{1n} = Q/n$ , and the unit head,  $h_{1n} = H/n^2$ .

The expression for specific speed in terms of unit capacity  $q_{1n}$  and unit head  $h_{1n}$  takes the form

$$n_s = \frac{q_{1n}^{1/2}}{h_{1n}^{1/4}} \quad (5.23)$$

For certain problems involving variable speed, such as predetermination of the performance of a centrifugal pump driven by an internal combustion engine with the throttle wide open, this form of the unit capacity and unit head has an advantage. (See Art. 14.3, Chapter 14.)

(l) By cutting the impeller diameter the specific speed is increased inversely as the diameter ratio. If an impeller of diameter  $D_2$  at speed  $n$  develops a head  $H$  and a capacity  $Q$ , with the diameter cut to  $D_2' = D_2\delta$ ,  $\delta < 1$  at the same speed it will give a head  $H' = H\delta^2$  and capacity  $Q' = Q\delta$ ; then the specific speed of the cut impeller will be

$$n_s' = \frac{n\sqrt{Q'}}{(H')^{1/4}} = \frac{n\sqrt{Q}\delta^{1/2}}{(H)^{1/4}\delta^{1/2}} = \frac{n_s}{\delta} \quad (5.24)$$

where  $n_s$  is the specific speed of the original impeller. Conversely, if the impeller diameter is extended, its specific speed will decrease inversely as the ratio of impeller diameters. Naturally this relationship is only approximate for large diameter cuts.

(m) *The introduction of the concept of specific speed, unit speed, and unit capacity did not add any new relationship between the head, capacity, and speed of the pump which could not be obtained from the affinity laws. The specific speed presents only a very convenient, generally accepted, impeller type characteristic instead of various ratios such as  $b_2/D_2$  or  $D_1/D_2$  previously employed.*

(n) Although by definition specific speed is a number of revolutions per minute its dimension is

$$\frac{l^{3/4}}{t^{3/2}}$$

or

$$\left(\frac{l}{t^2}\right)^{3/4}$$

and not  $1/t$  as revolutions per minute should be, because making  $H$  and  $Q$  equal to unity in the expression for specific speed does not change the dimension of the expression. The numerical value of the specific speed depends on the system of units used. In English units capacity is measured in gallons per minute and the head in feet, and specific speeds vary from 500 to 15,000, the latter figure referring to pumps of the axial flow type.

Specific speed was introduced first in Europe in application to hydraulic turbines. For turbines it is given the form

$$n_s = \frac{n\sqrt{\text{hp.}}}{H^{5/4}} \quad (5.25)$$

For centrifugal pumps specific speed is sometimes similarly expressed in terms of water horsepower.

$$n_s = \frac{n\sqrt{\text{w.hp.}}}{H^{5/4}} \quad (5.26)$$

the numerical value being 63 times smaller than that expressed in gallons per minute.

In comparing specific speeds of water turbines and pumps it is important to note the difference in the term  $H$  as applied to either machine. In a pump the head  $H$  is the output per pound of liquid flowing and

$$H = H_{teh}$$

where  $H_i$  is the input head of the impeller of an idealized pump (no losses). In a hydraulic turbine the head  $H'$  is the input per pound of liquid, and the head at the impeller is

$$H_i = H'e_h$$

Hence

$$H = H'e_h^2$$

Assuming  $e_h = \sqrt{e}$  for estimating purposes,

$$H = H'e \quad (5.27)$$

Thus a given impeller would have a lower specific speed when used in a hydraulic turbine than when used in a centrifugal pump.

In European treatises on pumps, specific speeds based on both horsepower and capacity are used. The following are the conversion factors where  $Q_m$  is capacity in cubic meters per second,  $H_{mt}$  is head in meters, and 1 hp. = 75 kg.-mt.,

$$n = \text{r.p.m.}$$

$$n_s(\text{metric})_{\text{hp.}} = \frac{n\sqrt{\text{hp.}}}{H_{\text{mt.}}^{3/4}} = \frac{n\sqrt{Q_m}}{H_{\text{mt.}}^{3/4}} \times 3.65 \quad \text{where } 3.65 = \left(\frac{1000}{75}\right)^{1/2}$$

$$n_s(\text{U.S.}) = \frac{n\sqrt{\text{g.p.m.}}}{H_{\text{ft.}}^{3/4}} = n_s(\text{metric})_{\text{hp.}} \times 14.15$$

$$\text{where } 14.15 = \frac{63}{(3.28)^{3/4}}$$

or

$$n_s(\text{U.S.}) = \frac{n\sqrt{\text{g.p.m.}}}{H_{\text{ft.}}^{3/4}} = n_s(\text{metric})_Q \times 52$$

$$\text{where } 52 = 3.65 \times 14.15$$

(o) For slide rule operation the formula for the specific speed can be presented in the form

$$n_s = \frac{n\sqrt{Q}\sqrt{\sqrt{H}}}{H}$$

By performing the operations in the following order

$$n_s = \sqrt{H} \left| \sqrt{\sqrt{H}} \left| \frac{1}{H} \right| \sqrt{Q} \right| n$$

the necessity of remembering or writing down the results of the intermediate operations is eliminated. The change of order of the last two operations sometimes saves one motion of the slide, depending on its

position. Slide rules of the Mannheim and Rietz type have an advantage for centrifugal pump calculations as they enable one to multiply or divide by square roots and squares directly by using square scales (last two operations in the above calculation) with the normal scales. The cube scale on the stationary part of the slide rule (stock or ruler) permits the calculation of  $\frac{3}{4}$  powers for heads without using the slide or logarithm scale by two motions of the cursor (glass) alone. The procedure is as follows: set the hair line of the cursor on the given number on the square scale of the stock and read the number under the hair line on the cube scale, which evidently is  $H^{\frac{3}{2}}$ ; take the square root of this number, which will be the  $\frac{3}{4}$  power of the given number; by reversing the procedure the  $\frac{3}{4}$  root of numbers can be found.

### 5.3 REDUCTION OF IMPELLER DIAMETER

In order to reduce the head and the capacity of a given centrifugal pump, the impeller diameter is generally reduced. Rules for estimating the performance of a pump for a given reduction in impeller diameter are closely associated with the affinity laws but are not so accurate. The error becomes greater the more the impeller diameter is reduced. The effect of reducing the impeller diameter is not the same for straight centrifugal, mixed flow and axial flow pumps, and each type will be discussed separately.

(a) **Radial Impellers.** When the impeller diameter is cut in a straight centrifugal pump a new but similar Euler's velocity triangle at the discharge is obtained which is constructed on a reduced peripheral velocity

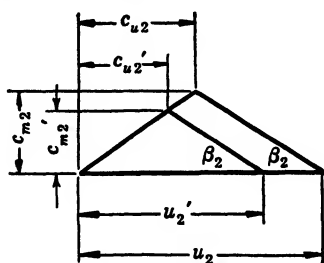


FIG. 5.2. The discharge velocity triangles for full and reduced impeller diameters.

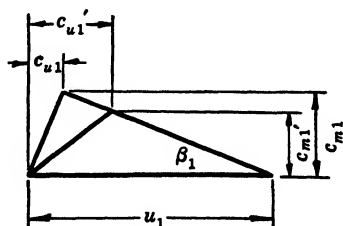


FIG. 5.3. Inlet velocity triangles for full and reduced impeller diameters.

vector  $u_2'$  (Fig. 5.2). All velocities of this new diagram are reduced in the ratio of the impeller diameters  $D_2'/D_2$ . If the subtractive term in Euler's equation ( $u_1 c_{u1}/g$ ) is omitted the following rules for predicting performance are obtained. The head varies directly as the square of



the diameter ratio, capacity varies directly as diameter ratio, and brake horsepower varies directly as the cube of the impeller diameter ratio. However, as the impeller diameter is reduced the rules become approximate only, because: (1) the hydraulic efficiency decreases with cut impellers (appearing as a loss in head) instead of remaining constant as assumed in the above rules; (2) the subtractive term in Euler's equation is seldom if ever zero, and when the impeller diameter is reduced,  $c_{u1}$  increases to  $c_{u1}'$  (Fig. 5.3), and the subtractive term  $u_1 c_{u1}/g$  becomes greater. The reduction in gross efficiency due to reduced impeller diameters is caused by several factors.

(1) Cutting impellers with streamlined tapered vanes results in blunt vane tips which cause more disturbance in the volute. This effect may

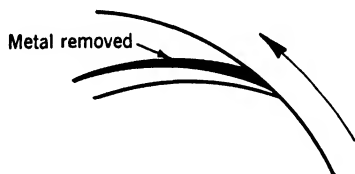


FIG. 5.4. Impeller vane overfiling.

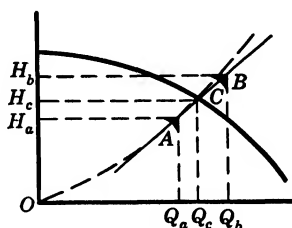


FIG. 5.5. Determination of impeller diameter cut.

be partly or entirely eliminated by again tapering the vanes after cutting by "overfiling" or removing the metal on the leading face of the vane (Fig. 5.4).

(2) A reduced impeller diameter results in a longer path for the liquid to travel in the volute casing before reaching the discharge nozzle.

(3) In general, in the case of exaggerated entrance vane angles, cutting the impellers moves the best efficiency point away from the "shockless" entrance conditions.

(4) A reduction in mechanical efficiency occurs with cut impellers because the mechanical losses, such as bearing and stuffing box losses, remain the same while the power output drops as the cube of impeller diameters.

The following procedure eliminates trial and error methods in calculating the impeller diameter required for a given head-capacity point. In Fig. 5.5, the specified point *A* is below the head-capacity curve *Q-H*. Take an arbitrary capacity  $Q_b$  higher than the given capacity  $Q_a$ , and calculate the head  $H_b$  by applying the affinity laws.

$$H_b = H_a \left( \frac{Q_b}{Q_a} \right)^2$$

Connect points  $B$  and  $A$  to obtain the point of intersection  $C$  on the  $Q$ - $H$  curve. The required impeller diameter ratio is  $Q_a/Q_c$ . The line  $AB$  is a part of a parabola connecting corresponding points or points of the same specific speed. The efficiency at the point  $A$  will be approximately the same as that at point  $C$ .

The calculated impeller diameter ratio  $Q_a/Q_c$  should be increased somewhat to compensate for the inaccuracy of the above established rules. Figure 5.6 gives the actual impeller diameter ratio in per cent plotted against calculated impeller diameter ratios. This correction again is approximate only, the accuracy decreasing with increased specific speed.

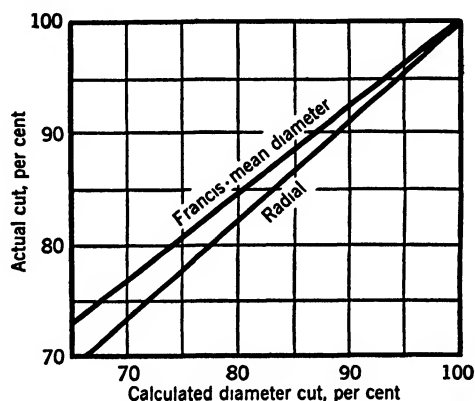


FIG. 5.6. Correction for calculated impeller diameter cut.

(b) **Axial Flow Impellers.** Reducing the outside diameter of an axial flow impeller would require a new casing (Fig. 5.7) or a liner to accommodate the reduced diameter. For that reason it is rarely used in practice. Referring to the preceding chapter and Fig. 4.6, the variation of the head and the capacity with cut impellers can be established: (1) the capacity varies directly as the net area swept by the impeller vane, the axial velocity remaining the same; (2) the head at the outside diameter will be reduced directly as the square of the diameters. The integrated head  $H'$  will be equal to the average of the head at the hub  $H_h$  (unchanged) and the new reduced head at the outside diameter  $= H_o(D_o'/D_o)^2$ .

$$2H' = H_h + H_o \left( \frac{D_o'}{D_o} \right)^2 \quad (5.28)$$

Axial flow impellers designed for a constant head at all radii at the design point will produce the same head as the full diameter impellers if cut.

It will be shown in Chapter 8 that the head produced by an axial flow impeller depends on the vane length. Cutting the vane length ( $CD$ , Fig. 5.7) is impractical because the streamlining of the vane is impaired to such a degree that the efficiency drop becomes excessive. Thus, to

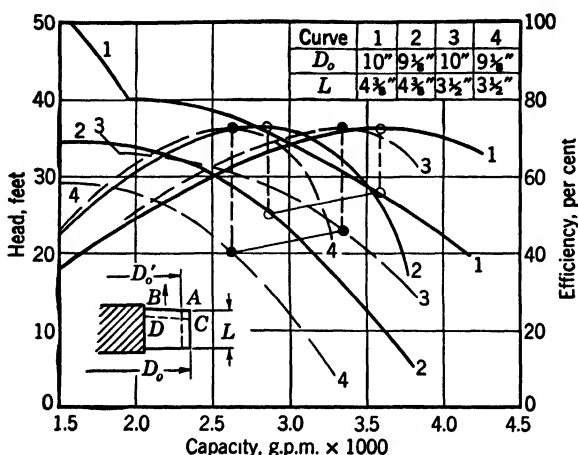


FIG. 5.7. Axial flow pump performance with full and cut impellers at 1760 r.p.m.

reduce the head-capacity output of an axial flow impeller a new casting is required with the vanes set at a lower angle. Figure 5.7 shows the performance of an axial flow pump with the impeller diameter reduced and with the vane length cut. The reduction of the head with the reduced impeller diameter indicates that the impeller is designed with a forced vortex pattern of flow.

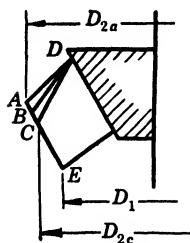


FIG. 5.8. Mixed flow impeller cutting.

**(c) Mixed Flow Impellers.** Mixed flow impellers can stand less reduction in diameter than radial impellers because the vane overlap is a great deal less. In calculating the impeller diameter ratio an average of the diameters of the outer and inner shrouds can be taken as an approximation and both diameters cut in the same ratio. With mixed flow propeller pumps it is better to cut more at the outside diameter and nothing at the hub. Figure

5.8 shows impeller cuts  $BD$ ,  $CD$ . The head and capacity reduction calculated on the basis of outside diameter ratios is not reliable. For a given profile, the vane length ratio  $BE/AE$ ,  $CE/AE$  may serve as a guide for estimating the necessary vane cut.

#### 5.4 DESIGN CONSTANTS

Selection of the specific speed value at the best efficiency point is the first step in the design of centrifugal pumps. This involves a selection of the rotative speed and a decision whether the required head should be produced in one or more stages. If the operating point is to be located off the peak efficiency point, the specific speed is established for the best efficiency point, which is then used as the design point. The impeller profile and vane layout is possible if the following elements are known: (1) meridional velocities at inlet and outlet, (2) impeller outside diameter, (3) impeller vane inlet and outlet angles. These same quantities determine both Euler's entrance and discharge triangles. For straight radial vanes, all particles of liquid enter and leave the impeller at the same diameter, and the vane is plain with single curvature. Thus only one entrance and discharge triangle determines the impeller design. For mixed flow and axial flow impellers, velocity triangles are drawn for several streamlines. Three streamlines usually suffice for an average mixed flow impeller but four or five are used for extreme mixed flow and axial flow impellers. Variation of vane angles along the radius determines vane curvature and "twist." The graphical problems connected with an impeller layout are presented in detail in Chapter 6. This article will deal with the selection of the impeller design elements listed above. These are chosen for the design point only. The head-capacity curve is estimated from previous experience and based on typical curves for different specific speeds such as appear in Fig. 9.1. The degree of perfection of a design is measured by the value of the gross pump efficiency. Control of the head-capacity or brake-horsepower characteristics, or designing for unusual suction conditions, belongs to the advanced stage of pump design and is treated in Chapter 14.

Pump designers, following hydraulic turbine practice, have established experimentally direct relationships between the pump total head and capacity at design points and Euler's velocity triangles. These are dimensionless velocity ratios, independent of the pump size and speed, which are correlated on the basis of specific speed. In addition, a number of ratios of important linear dimensions, not directly related to velocities, are found helpful in perfecting the hydraulic design of impellers. These too are entirely experimental and do not lend themselves to theoretical treatment.\* The progress in development of a theoretical relation between Euler's head and the pump total head has

\* Such design constants for water turbines were published first by Camerer.<sup>6</sup> Spannhake<sup>7</sup> gives similar data on both pumps and turbines. Fabrin's<sup>12</sup> curve of ratio  $D_1/D_2$  agrees with that in Fig. 5.9.

been slow. In the present state of the art it is unlikely that an advance in theory would bring any changes in the established design procedure.

(a) **Speed Constants.** A speed constant is a factor giving the relation between the pump total head and the impeller peripheral velocity. Several such constants are in use.

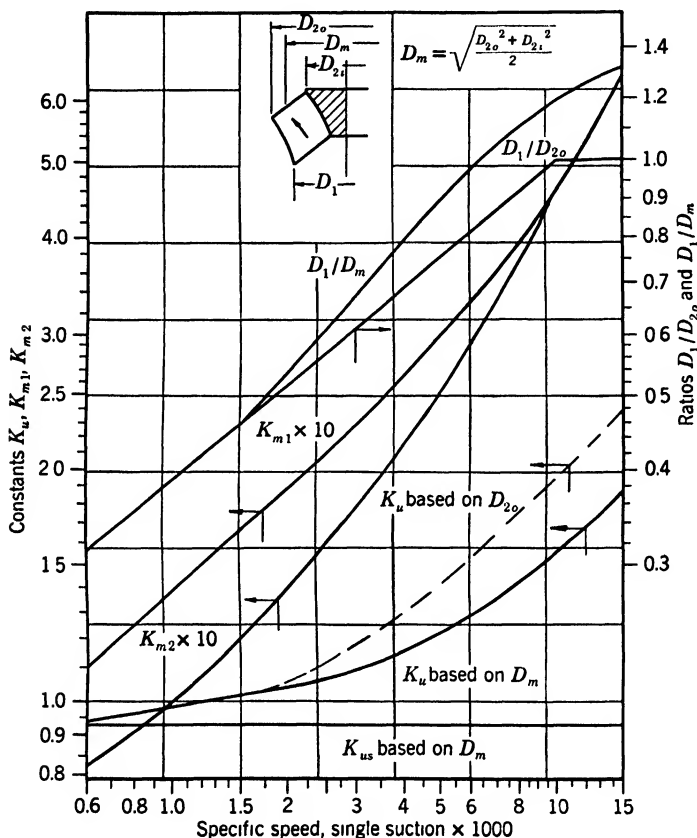


FIG. 5.9. Impeller constants.

The most widely used speed constant is defined as follows.

$$K_u = \frac{u_2}{\sqrt{2gH}} \quad \text{or} \quad u_2 = K_u \sqrt{2gH} \quad \text{and} \quad H = \frac{1}{K_u^2} \cdot \frac{u_2^2}{2g} \quad (5.29)$$

This was originally introduced for hydraulic turbines and later adopted by centrifugal pump engineers. In this definition,  $K_u$  is a ratio of  $u_2$  to the free jet velocity under head  $H$ . It is used for calculation of the

impeller diameter when the head  $H$  is given and the speed is selected.  $K_u$  increases with the specific speed.

In Fig. 5.9, curves for  $K_u$  are drawn for an average normal design and an impeller discharge angle  $\beta_2$  of approximately  $22\frac{1}{2}^\circ$ .  $K_u$  is affected by several design elements. (1)  $K_u$  increases for lower values of angle  $\beta_2$  since the normal head  $H$  is decreased. (2) Greater ratio of  $D_1/D_{2o}$  requires a higher value of  $K_u$ . Figure 5.9 gives ratios of the impeller eye diameter ( $D_1$ ) to the impeller discharge diameter ( $D_{2o}$  or  $D_m$ ) for normal design. (3)  $K_u$  is also affected by the number of vanes. This number depends on the vane load. With low vane discharge angles  $\beta_2$ , 6 vanes is probably a minimum for specific speeds up to 5000, whereas 8 vanes can be considered normal for the same range of specific speeds. For higher specific speeds, fewer vanes are used. Figure 8.1 shows the usual number of vanes for mixed and axial flow pumps. The number of vanes also depends on the pump size and the pump total head, smaller and lower head pumps requiring fewer vanes. For special services such as pumping paper stock or raw sewage, non-clogging impellers have frequently only two vanes (Fig. 9.15).

The value of  $K_u$  depends on the pump size, smaller pumps requiring higher value of  $K_u$ . Any reduction in gross pump efficiency of small pumps as compared with large pumps of the same specific speed is caused by a reduction of hydraulic efficiency. In order to compensate for a reduction of head due to increased hydraulic losses in small pumps, a larger impeller diameter or greater value of  $K_u$  is used.

**(b) Unit Peripheral Velocity.** This is defined as the peripheral velocity to produce 1 ft. of head, or

$$K_{u1} = \frac{u_2}{\sqrt{H}} \quad (5.30)$$

Evidently

$$K_{u1} = K_u \sqrt{2g} = 8.02K_u \quad (5.31)$$

The unit peripheral velocity  $K_{u1}$  is used as a design speed constant by several writers on hydraulic turbines.<sup>9, 10</sup>

**(c) The Head Coefficient.**

$$\psi = \frac{H}{\frac{u_2^2}{g}} \quad (5.32)$$

used already in Chapter 3 for plotting the head-capacity and velocity triangles of an idealized pump, can also be used as a speed constant for pump design.

$\psi$  expresses total head in terms of Euler's shut-off head, or

$$H = \psi \frac{u_2^2}{g} \quad (5.33)$$

It can also be shown that

$$\psi = \frac{1}{2K_u^2} \quad (5.34)$$

**(d) The Capacity Constant.** Capacity constant is defined by

$$K_{m2} = \frac{c_{m2}}{\sqrt{2gH}} \quad (5.35)$$

where  $c_{m2}$  is the meridional velocity at discharge. When  $c_{m2}$  is calculated from test data at the best efficiency point, the leakage is disregarded. Then, when a value of  $K_{m2}$  is selected from tabulated or plotted experimental data it is not necessary to consider the leakage.

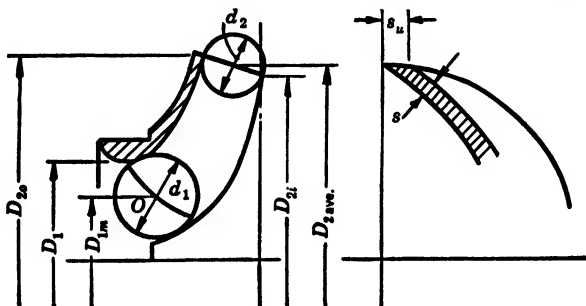


FIG. 5.10. Impeller inlet and outlet areas.

For practical use, experimental values of  $K_{m2}$  are plotted against specific speed (Fig. 5.9) for a continuous line of pumps. The continuity of type extends to the design of sealing rings. Any deviation from such general trend will introduce some inaccuracy which probably will not be any greater than that involved in calculations of leakage volume.

When  $c_{m2}$  or  $K_{m2}$  is calculated, the vane thickness should be considered in arriving at a net area normal to  $c_{m2}$ . For example, in Fig. 5.10

$$c_{m2} = \frac{Q}{A_2} = \frac{Q}{(D_{ave} \pi - z s_u) d_2} \quad (5.36)$$

where  $z$  is the number of vanes and  $s_u$  is the vane tangential thickness.

**(e) The Capacity Coefficient.** The ratio  $\phi = c_{m2}/u_2$  is frequently used as a capacity coefficient. It is connected to  $K_{m2}$  as follows.

$$\phi = \frac{K_{m2}}{K_u} \quad (5.37)$$

The head coefficient  $\psi$  and capacity coefficient  $\phi$  will be used as dimensionless head and dimensionless capacity for comparing characteristics of impellers of different specific speed irrespective of their size and rotational speed.†

**(f) The Entrance Velocity.** In order to complete the impeller profile the meridional velocity at entrance should be also known. This is given by the ratio

$$K_{m1} = \frac{c_{m1}}{\sqrt{2gH}} \quad (5.38)$$

This is calculated for the area at the vane entrance tips, again omitting the leakage. The vane thickness can be disregarded as the vane tips are usually tapered, and  $c_{m1}$  can be assumed to be the velocity just ahead of the vanes. Referring to Fig. 5.10,

$$c_{m1} = \frac{Q}{\pi D_{1m} d_1} \quad (5.39)$$

The velocity through the impeller eye is either equal to  $c_{m1}$  or slightly lower, depending on the impeller approach.

Neglecting leakage introduces an error in vane angles  $\beta_1$  and  $\beta_2$  for several streamlines as determined from Euler's velocity triangles. This error is negligible, and never over one degree on normal designs, and is certainly far smaller than the inaccuracy resulting from the assumption of a uniform meridional velocity for several streamlines.

**(g) The Vane Discharge Angle.** This angle is the most important single design element. It has been shown that the theoretical characteristics are determined by the vane angle alone. In actual pumps,  $\beta_2$  is still the deciding factor in design. *All the above design constants depend on the value of  $\beta_2$ . Therefore a choice of  $\beta_2$  is the first step in selecting impeller design constants.* This selection is based on consideration of the desired steepness of the head-capacity curve and whether or not a maximum output is desired from the impeller of a given diameter as both normal head and capacity increase with the angle  $\beta_2$ . If there are no such limitations selection of  $\beta_2$  is made for an optimum efficiency, or normal design. An average value of  $22\frac{1}{2}^\circ$  can be called normal for all specific speeds. For forced output this may be raised to  $27\frac{1}{2}^\circ$  without

† In axial blower literature  $\psi$  and  $\phi$  are used as pressure coefficient and flow coefficient respectively.<sup>11</sup> However,  $\psi$  is defined as  $\psi = H/(u^2/2g)$ , or is twice the value given by equation 5.32. In this form  $\psi$  does not possess properties described in Art. 3.6. Also, the diagram in Fig. 9.16 representing all essential design and performance features of impellers of all specific speeds discussed in Chapter 9, would be impossible with  $\psi$  defined as used by the writers on axial flow blowers.



affecting the efficiency appreciably. The lower limit of  $\beta_2$ , consistent with good design, is about  $17\frac{1}{2}^\circ$ .

**(h) The Entrance Vane Angle  $\beta_1$ .** This angle is established from the following considerations. (1) Except for the special case of low capacity impellers, prerotation should be allowed on the entrance velocity triangles.† (2) The ratio of relative velocities on Euler's triangles on good pumps is maintained within the limits

$$\frac{w_1}{w_2} = 1.15 \text{ to } 1.25 \quad (5.40)$$

higher ratios referring to higher specific speeds. With Francis vanes, when the several streamlines have different values of  $w_1$  and  $w_2$ , the ratio at the middle streamline is taken. (3) As a result of the above considerations the entrance angle at the outer streamline of pumps of specific speeds from 1500 to 6000 double suction are equal to the discharge angle, or  $\beta_1 \approx \beta_2$ .

**(i) Variation of Design Constants with  $n_s$ .** Since the speed constant  $K_u$  and the capacity constant  $K_{m2}$  represent velocity ratios to the same  $\sqrt{2gH}$ , the velocity triangle drawn on  $K_{m2}$  and  $K_u$  and selected angle  $\beta_2$  will represent to scale Euler's discharge triangle. This triangle will differ from the dimensionless discharge triangles in Fig. 3.12 (a) and 3.12 (b) only by its scale. Figure 3.12 (b) represents Euler's triangle for all specific speeds using the same angle  $\beta_2$ . Variation of the several velocities or design elements becomes apparent from this figure, thus

(1) The meridional velocity  $c_{m2}$  or  $\phi = (c_{m2}/u_2)$  increases for higher specific speeds.

(2) The absolute velocity of discharge  $OE$ ,  $OD$ ,  $OC$  on Fig. 3.12 (b) decreases as specific speed increases. This means that the casing velocity  $c_3$  will also decrease with the specific speed, and casing velocity constant  $K_3 = c_3/\sqrt{2gH}$  (discussed in Chapter 7) will decrease also.

(3) The absolute velocity discharge angle  $\alpha_v$  (volute angle) increases with the specific speed.

(4) For the same  $u_2$ , the shut-off head is the same for all specific speeds. If we introduce another speed constant in terms of shut-off head, or  $K_{us} = u_2/\sqrt{2gH_s}$ , where  $H_s$  is the shut-off head, we find this constant is also the same for all specific speeds (Fig. 5.9).<sup>5</sup> § If we define the steepness of the head-capacity curve as the ratio of  $H_s/H$ , then on

† Figure 9.4 shows that "shockless" entrance occurs at capacities greater than that at b.e.p., thus requiring larger angle  $\beta_1$  and prerotation at normal capacity.

§ A mean effective diameter  $D_m$ , defined in Chapter 8, equation 8.18, is used for calculation of  $u_2$  in the expression for  $K_{us}$ .

Euler's head-capacity curve, Fig. 3.12 (a), or on the input characteristics, Fig. 3.13 (a), impellers of higher specific speed have a steeper curve. Although hydraulic losses change the characteristic of the pump from that of the input curve, the above statements hold for actual pump test curves. This subject is treated in more detail in Chapter 9.

(j) **Type Characteristics.** The type unit speed  $n_1 = (nD_2)/\sqrt{H}$ , if plotted against the type unit capacity  $q_1 = Q/(\sqrt{H}D_2^2)$  will give a type performance curve. This applies for any size at any speed for the whole line of homologous pumps. Use of such type performance curves was discontinued in favor of curves showing head and capacities as ratio or percentage of the normal head and capacities. Such curves involve fewer calculations and are easy to read without special knowledge of pump constants or design factors. For a theoretical study, use of head and capacity coefficients  $\psi$  and  $\phi$  presents advantages, clearly demonstrated in Chapter 9.

## 5.5 SPECIFIC SPEED IN TERMS OF DESIGN CONSTANTS

It is possible to obtain an expression for specific speed in terms of design constants  $K_u$  and  $K_{m2}$  by substituting for the head and capacity their equivalents in terms of these constants.

$$u_2 = K_u \sqrt{2gH} \quad \text{and} \quad H = \frac{1}{K_u^2} \frac{u_2^2}{2g}$$

$$Q = c_{m2} A_2 = c_{m2} b_2 D_m \pi = K_{m2} \sqrt{2gH} b_2 D_m \pi \quad (5.41)$$

$$u_2 = \frac{\pi D_m n}{60} \quad n = \frac{60 u_2}{\pi D_m}$$

By substituting these values in the expression for specific speed and combining all constants into one, we obtain

$$n_s = C \left( \frac{b_2}{D_m} \right)^{1/2} \sqrt{K_{m2}} \times K_u$$

where  $C$  is a numerical constant, and  $b_2/D_m$  is constant for each specific speed,<sup>8</sup> thus

$$n_s' = \sqrt{K_{m2}} \times K_u = \frac{n_s}{C} \left( \frac{D_m}{b_2} \right)^{1/2} \quad (5.42)$$

Note the similarity of this expression to equation 5.20. In like manner, an expression for the type number is obtained in terms of head and capacity coefficients  $\psi$  and  $\phi$ .

$$\omega_s = \frac{\sqrt{\phi}}{\psi^{1/4}} \quad (5.43)$$

Both expressions for the specific speed, equations 5.42 and 5.43, are dimensionless as is equation 5.12a. The latter has the advantage that it can be applied to the pump head-capacity requirements after the speed is selected whereas equations 5.42 and 5.43 depend on the design constants, not generally known, and different for different makes of pumps.

In practice, the expression for specific speed in gallons per minute and head in feet is used; all the dimensionless expressions are convenient in the theoretical studies.

Below are tabulated several impeller characteristics and the expression for specific speed in terms of these characteristics.

No.	Capacity Term	Head Term	Speed Term	Specific Speed	Reference
1	$Q$ g.p.m.	$H$ ft.	$n$ r.p.m.	$n_{s1} = \frac{n\sqrt{Q}}{H^{3/4}}$	Equation 5.18
2	$q_1 = \frac{Q}{\sqrt{H}}$	....	$n_1 = \frac{n}{\sqrt{H}}$	$n_{s2} = n_1\sqrt{q_1}$	Equation 5.20
3	$q_{1n} = \frac{Q}{n}$	$h_{1n} = \frac{H}{n^2}$	....	$n_{s3} = \frac{\sqrt{q_{1n}}}{h_{1n}^{3/4}}$	Equation 5.23
4	$\Pi_1 = \frac{Q}{\sqrt{\rho}HD^2}$	. .	$\Pi_2 = \frac{nD}{\sqrt{\rho}H}$	$n_{s4} = \Pi_2\sqrt{\Pi_1}$	Equations 5.5 and 5.6
5	$K_{m2} = \frac{cm^2}{\sqrt{2\rho}H}$	. . .	$K_u = \frac{u_2}{\sqrt{2\rho}H}$	$n_{s5} = K_u\sqrt{K_{m2}}$	Equation 5.42
6	$\phi = \frac{cm^2}{u_2}$	$\psi = \frac{H}{u_2^2/\rho}$	....	$n_{s6} = \omega_s = \frac{\sqrt{\phi}}{\psi^{3/4}}$	Equation 5.43

The numerical values of specific speeds  $n_{s1}$ ,  $n_{s2}$ ,  $n_{s3}$ , and  $n_{s4}$  are connected by a constant numerical factor, whereas numerical values of  $n_{s5}$  and  $n_{s6}$  vary with the impeller design used to meet the same head-capacity requirements. Thus the factor required to convert from the latter group to the first group will vary with the impeller profile. ||

REMARKS. (1) Curves of design constants as given on Fig. 5.9 were drawn as an average through a great many points not necessarily all obtained from impellers with a  $22\frac{1}{2}^\circ$  vane angle. Variations from these curves are expected, as there are always some factors which deviate from those which constitute a continuous row of types. This is particularly true of high specific speed pumps of the axial flow type.

|| A further treatment of this subject is found in Chapter 9.

There are a number of design elements, such as hub ratio, number of vanes, vane length, profile, and hub cone angles, which do not enter directly into the calculation of design constants but all of which have a marked effect on the pump performance. (Chapter 8 is devoted to the design of axial flow pumps.) The detection of these influences and the anticipation of their effect depends on the skill of the designer when he analyzes the performance of existing pumps and when he selects the design constants for new pumps.

(2) The measured shut-off head of a pump is different from that of the impeller as it is affected by the amount of leakage and the slope of the head-capacity curve. Figure 5.11 shows this very clearly. Also, impellers with an unstable head-capacity characteristic near shut-off (drooping head-capacity curve) have a lower shut-off head than impellers of the same diameter having a steadily rising head-capacity curve. The first show excessive losses, owing to faulty design, at the impeller discharge at and near zero capacity which do not occur with normal design.¶ The above reasons partly explain the scatter of the  $K_{us}$  values about their average level.

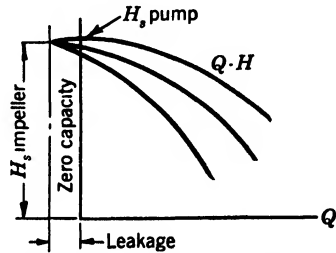


FIG. 5.11. Effect of leakage on shut-off head.

(3) The shut-off head is also affected by the casing design. The same impeller in a casing having a smaller volute will show a higher shut-off head. Also, a smaller diffusion vane angle results in a higher shut-off head. This is always followed by moving of the b.e.p. to a lower capacity and higher head. Figure 14.19 illustrates this point. In this example the pump casing is provided with adjustable diffusion vanes. Evidently the impeller shut-off head is the same for different diffusion vane angles. With smaller volute sections and lower diffusion vane angles (and hence a smaller net area between the diffusion vanes) a greater portion of the dynamic head is registered on the discharge pressure gage, as illustrated in Fig. 4.17. The quoted cases should be considered deviations from a normal optimum design, and should always be accompanied by a reduction of efficiency below the established optimum values.

## REFERENCES

1. E. BUCKINGHAM, "On Model Experiments and the Form of Empirical Equation," *Trans. A.S.M.E.*, Vol. 37, 1915, p. 263; or review by ALTON C. CHICK, *Hydraulic Laboratory Practice*, Appendix 15, A.S.M.E., 1929.

¶ This problem is discussed in Chapter 14,

2. *Starkstromtechnik, Taschenbuch für Electrotechniker*, 1912, p. 297.
3. CARL RITTER, *Flüssigkeitspumpen*, Leipzig, Max Jänecke, 1938.
4. *Z. Ver. deut. Ing.*, 1905, p. 380.
5. *Z. Ver. deut. Ing.*, 1905, p. 93.
6. R. CAMERER, *Vorlesungen über Wasserkraftmaschinen*, Leipzig, Wilhelm Engelmann, 1924, p. 248.
7. WILHELM SPANNHAKE, *Centrifugal Pumps, Turbines and Propellers*, Cambridge, Mass. Inst. of Tech., 1934, p. 208; German edition, Berlin, Julius Springer, 1931.
8. R. DEFELD in *A Practical Treatise on Single and Multistage Centrifugal Pumps* (London, Chapman and Hall, 1930) uses the ratio  $b_2/D_2$  to designate the impeller type in preference to specific speed, not mentioned in the book.
9. R. THOMANN, *Die Wasserturbinen und Turbinenpumpen*, Stuttgart, 1931.
10. VICTOR KAPLAN and ALFRED LECHNER, *Theorie und Bau von Turbinen-Schnellläufern*, Berlin, R. Oldenbourg.
11. CURT KELLER, *The Theory and Performance of Axial Flow Fans*, New York, McGraw-Hill, 1937, p. 8.
12. AXEL D. FABRIN, "Selecting Deep Well Centrifugal Pumps," *Water Works & Sewerage*, Oct. 1944, p. 348.

## CHAPTER 6

### DESIGN OF MIXED FLOW IMPELLERS FOR CENTRIFUGAL PUMPS

#### 6.1 INTRODUCTION

The layout of a mixed flow impeller on the drawing board is the most complicated drafting problem in centrifugal pump design. Two methods are in use. The first, or old, method is one in which the vane entrance and discharge tips are developed on a cone as a plain cylindrical vane and then transferred on the plan view, from which the vane pattern sections are constructed. In the second, or new, method, the vane plane development with true angularity, vane length, and thickness are assumed, and then the vane flow lines are replotted on the plan view. The principle of the new method was established in Europe about thirty years ago. It is not widely known in this country, although several German publications, listed as references, covered certain phases of it during recent years. This method, called by Kaplan the *method of error triangles*, has definite advantages over the old cone development and, it is believed, without it the high efficiencies recorded during recent years would have been impossible.

The design of a centrifugal pump impeller can be divided into two parts. The first is the selection of proper velocities and vane angles needed to obtain the desired performance with the best possible efficiency. The second is the layout of the impeller for the selected angles and areas. The first phase of the design will not be discussed here. For a given set of basic design elements it is possible to make several layouts which will differ in performance. Therefore, for best results, experience and skill are necessary to represent graphically the requirements for best efficiency.

The procedure for the construction of the vane on the drawing is the same for hydraulic turbines and centrifugal pumps. The method presented here was first developed for turbines and later applied to pumps.

The following are the minimum basic design elements necessary to define the impeller proportions; see Figs. 3.1 (a) and 3.1 (b).

- (1) Radial velocity at the impeller eye,  $c_{m1}$ .
- (2) Radial velocity at the impeller discharge,  $c_{m2}$ .

- (3) The impeller peripheral velocity  $u_2$  at the discharge or impeller diameter,  $D_2$ .
- (4) The vane angle at entrance,  $\beta_1$ .
- (5) The discharge angle  $\beta_2$ .

These quantities are sufficient to construct Euler's velocity triangles, the impeller profile, and the vane plan view.

## 6.2 GEOMETRICAL RELATIONSHIPS

Before the development of mixed flow vanes is described, several geometrical definitions and statements will be given. These are necessary for further discussion.

(a) The angle  $\alpha$  between two intersecting planes  $A$  and  $B$  (Fig. 6.1) is equal to the angle between the two normals  $CO$  and  $DO$  drawn at any

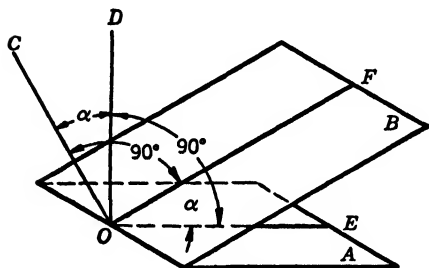


FIG. 6.1. Angle between two planes.

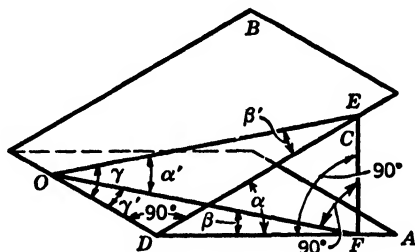


FIG. 6.2. Angle projections on a plane.

point on the common line of intersection of the two planes. Evidently both of these normals lie in a plane normal to both plane  $A$  and plane  $B$ . Traces of the normal plane on planes  $A$  and  $B$  (lines  $EO$  and  $FO$ ) form an angle  $\alpha$ .

(b) If two planes  $A$  and  $B$  (Fig. 6.2) have an angle  $\alpha$  between them and are sectioned with another plane  $C$  normal to plane  $A$ , the traces of plane  $C$  on planes  $A$  and  $B$  (lines  $OF$  and  $OE$  respectively) will form an angle  $\alpha'$  which is related to the angle  $\alpha$  in the following way:

$$\tan \alpha' = \tan \alpha \cos \beta \quad (6.1)$$

where  $\beta$  is an angle between the plane  $C$  and a plane normal to both plane  $A$  and plane  $B$ . If  $EDF$  lies in a plane normal to both  $A$  and  $B$ , then

$$\tan \alpha = \frac{EF}{DF} \quad \tan \alpha' = \frac{EF}{OF} \quad OF \cos \beta = DF$$

Hence

$$\frac{\tan \alpha'}{\tan \alpha} = \frac{DF}{OF} = \cos \beta$$

(c) If an angle  $\gamma$  on a plane  $B$  (Fig. 6.2) is projected on plane  $A$ , its projection angle  $\gamma'$  will be given by the relation

$$\tan \gamma' = \tan \gamma \cos \alpha \quad (6.2)$$

because

$$\frac{DE}{OD} = \tan \gamma \quad \frac{DF}{OD} = \tan \gamma' \quad \frac{DF}{DE} = \cos \alpha$$

and

$$\frac{\tan \gamma'}{\tan \gamma} = \cos \alpha$$

(d) Similarly, it can be shown that

$$\tan \beta \cos \alpha = \tan \beta' \quad (6.3)$$

Note that when one side of the angle is parallel to or coincides with  $OD$ , the common line of intersection of planes  $A$  and  $B$ , the angles in projection are smaller; but if none of the angle sides is parallel to the line of plane intersection  $OD$ , the angle in projection ( $\beta$  on plane  $A$ ) is greater than the projected angle  $\beta'$  on plane  $B$ .

The same definitions and theorems apply when one or both of the planes are replaced by curved surfaces except that tangent planes drawn at a common point on both surfaces are substituted for curved surfaces.

### 6.3 PLAIN VANE FAULTS

If the vane shown in Fig. 6.3 is laid out so that the entrance angle is  $\beta_1$  on the plan view for the flow lines near the front and back shrouds,

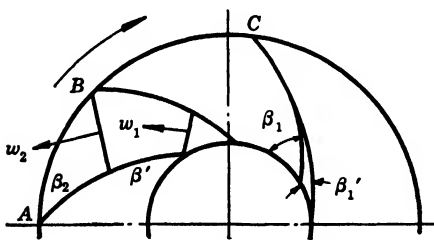


FIG. 6.3. Plain vane impeller.

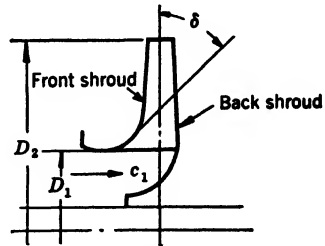


FIG. 6.4. Profile of a plain vane impeller.

the true angle between the vane and peripheral velocity at the entrance edge near the front shroud will be considerably greater than  $\beta_1$ , and is given, according to (c) in Art. 6.2, by the equation

$$\tan \beta_{1f} \cos \delta = \tan \beta_1 \quad (6.4)$$

where  $\delta$  is the angle between the tangent to the front shroud at the entrance edge (Fig. 6.4) and the plane normal to the impeller shaft axis.



Thus, if  $\beta_1 = 20^\circ$  and  $\delta = 45^\circ$ , which is quite usual for a plain vane impeller,  $\beta_{1f} = 27^\circ$ . But, since the peripheral velocity is constant for all points along the entrance edge, the vane angle should be constant for all points on the entrance edge to agree with the velocity triangle. To be equal in space the angle  $\beta_1'$  at the front shroud should be smaller on the plan view, so that

$$\tan \beta_1' = \tan \beta_1 \cos \delta \quad (6.5)$$

This is shown in Fig. 6.3, vane *C*. It means that the vane should have a double curvature. *Thus a plain vane impeller should have both shrouds normal to the shaft axis; such a condition seldom exists. With curved shrouds a mixed flow vane is necessary for "shockless entrance" even if the vane entrance edge is parallel to the axis.*

*In addition, if the front shroud is curved it is impossible to avoid sharp corners between the vane and the shroud with a plain vane; therefore the vane is extended into the impeller eye (Fig. 6.5) so that the entrance edge is no longer parallel to the axis, and the vane is curved so that the angles between the vane and the shrouds are nearly  $90^\circ$ .*

*With such a vane, different entrance angles will be required for several flow lines, such as  $a_1a_2$ ,  $b_1b_2$ , and  $c_1c_2$  (Fig. 6.5), for shockless entrance. The entrance angle varies in such a way that the vane becomes more nearly normal to both*

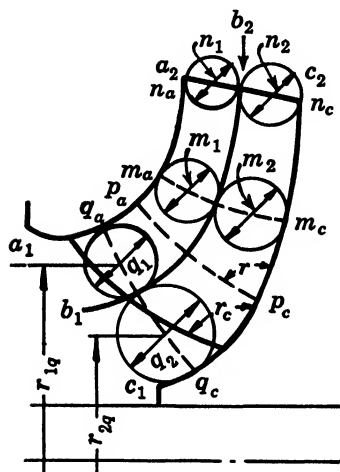


FIG. 6.5. Mixed flow impeller profile.

*shrouds.* The higher entrance angles required with mixed flow vanes result in wider openings between the vanes which are necessary for high specific speed impellers. Thus it follows that plain, single-curvature vanes can be used only with narrow impellers with both shrouds nearly normal to the axis and curved very little at the impeller eye. Such impellers are suited only to small pumps.

#### 6.4 MIXED FLOW IMPELLERS

To make a mixed flow vane pattern it is necessary to have drawings of the impeller and vane profile showing the layout of the front and back shrouds, the impeller vane entrance and exit edges, and the vane sections along contour lines on several planes drawn normal to the axis

The following points will be given consideration in developing the profile of an impeller of the mixed flow type.

(a) Extending the impeller vanes at the entrance into the impeller eye tends to improve efficiency by giving a greater overlap to the vanes and reducing the impeller outside diameter required for a given normal head. Shock losses take less power when the shock occurs at a smaller diameter, and disk friction will be less.

The effect of the impeller eye diameter on the total head will be seen from a consideration of the equation for the input head.

$$H_i = \frac{u_2 c_{u2} - u_1 c_{u1}}{g}$$

In a normal pump design it is impossible and inadvisable to suppress completely liquid prerotation at the impeller entrance; therefore  $c_{u1}$  is not equal to zero. In that case the subtractive term is smaller for lower values of  $u_1$ , and for a fixed outside diameter of the impeller the total head will be higher for smaller impeller entrance diameters. However, there is a limit to extending the vanes into the impeller eye beyond which further extension will reduce rather than improve the efficiency. This is because it is difficult to avoid sharp corners between the vanes and shrouds and, since vanes take up a considerable portion of the eye area, unnecessary vane friction is added, and the cleaning of the impeller casting becomes difficult. To provide the necessary entrance area a larger eye diameter is required.

(b) The profile of the impeller is drawn for given radial velocities  $c_{m1}$  at the entrance and  $c_{m2}$  at the discharge and in such a way that the change from  $c_{m1}$  to  $c_{m2}$  is gradual.

(c) The entrance edge of the vane on the profile is a circular projection of points which are not in one plane, but which are brought into the plane of the drawing by rotation about the axis of the impeller shaft. Similarly, the flow lines  $a_1a_2$ ,  $b_1b_2$ , and  $c_1c_2$  (Fig. 6.5) are circular projections of the paths of the water particles if they follow the vane in the manner prescribed by the design. The flow lines  $a_1a_2$  and  $c_1c_2$  represent the true radial sections through the impeller shrouds at the same time. The shroud curvature should be as gradual as possible to minimize uneven pressure and velocity distribution.

The edge of the vane is drawn so that the angles formed with the shrouds on the elevation view are about  $90^\circ$ .

(d) The flow lines are one set of construction lines used for the vane development on the drawing. The number of flow lines necessary to define accurately the vane surface depends on the width of the impeller and the actual impeller size. This is a matter of experience. The flow

lines are drawn in such a way that the surfaces of revolution formed by these lines divide the flow into equal parts. Following water turbine practice, where mixed flow impellers were first developed, it is assumed that the meridional velocity is constant along normals to the flow lines ( $n_a n_c$ ,  $m_a m_c$ ,  $p_a p_c$ , and  $q_a q_c$ , Fig. 6.5) and equal to the average velocity. From this it follows that the meridional velocities for several points along the entrance edge of the vane are the same only if the entrance edge coincides with one of the normals.

The normals are drawn first by eye. Then these are divided into parts (Fig. 6.5):  $n_1, n_2$ ;  $m_1, m_2$ ;  $q_1, q_2$ ; so that

$$2\pi r_{1q} q_1 = 2\pi r_{2q} q_2 \quad (6.6)$$

or

$$r_{1q} q_1 = r_{2q} q_2$$

where  $r_{1q}$  and  $r_{2q}$  are the radii of the centers of gravity of sections  $q_1$  and  $q_2$ . This is repeated for every normal.

For wide and large impellers requiring four or five flow lines, the work of adjusting the sections to comply with equation 6.6 requires much time and a great deal of patience. Accuracy within 3 to 5 per cent should be considered satisfactory.

### 6.5 VANE DEVELOPMENT ON A CONE

In indicating the flow lines on the plan view by the old method, tangents are drawn to the flow lines at the entrance and discharge edges.

For instance,  $OC$  is tangent to flow line  $b_1 b_2$ , Fig. 6.6 (a). Then the cone formed by revolution of line  $OC$  is developed into a plane, Fig. 6.6 (b), and the vane ends are drawn on this development in the same manner as if they were plain single-curvature vanes. The cones are drawn mostly tangent to the flow line at the vane edge. However, this is not necessary, and the line  $OC$  can be tangent at any point near the edge. The vane tip can be drawn as an involute on a base circle of the diameter  $d_1$ :

$$d_1 = 2R_1 \sin \beta_1 \quad (6.7)$$

The involute is a curve which is traced by the end of a cord when the cord is wound around the base circle. This means that any tangent to the base circle from any point on the curve is longer than the one passing through the vane tip by the distance the point of tangency moved on the base circle.

The involute can be replaced with the arc of a circle. For this, lay off the vane circular pitch  $t_1 = (2\pi r_1)/z$  along the arc of a circle with a

radius  $R_1$ , Fig. 6.6 (b), points  $A_1, A_2$ , etc. From these points draw tangents to the base circle. On these lines lay off  $p_1 + s'$  from equation 6.8.

$$p_1 + s' = t_1 \sin \beta_1 \quad (6.8)$$

Thus  $B_1$  and  $B_2$  are located. Through these points draw a circular arc with a radius tangent to the base circle and center lying near it. By laying off  $s'$ , the front side of the vane can be drawn.

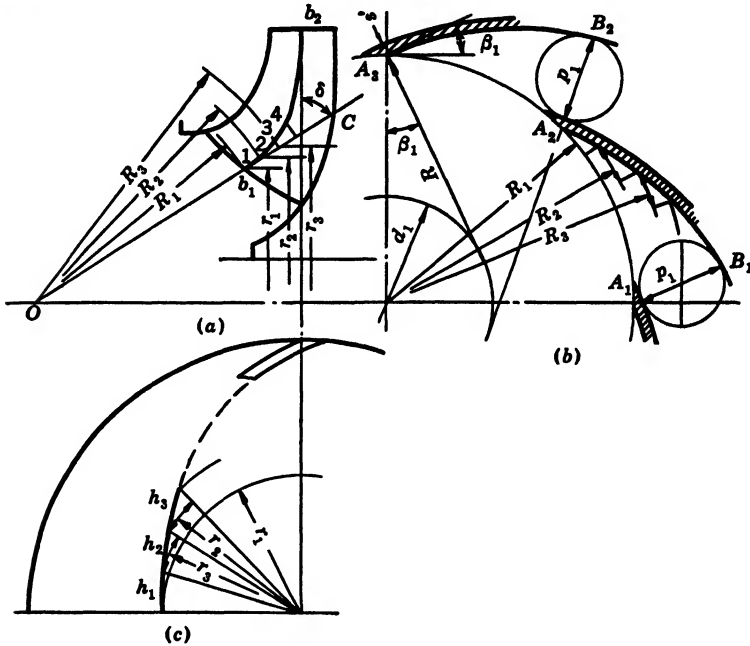


FIG. 6.6. Vane development on a cone.

After the vane ends are drawn on the cone development they are transferred to the plan view. In plotting points 1, 2, and 3 on the plan view note that they will be on arcs of radius  $r_1, r_2$ , and  $r_3$ , Fig. 6.6 (c). Their relative locations on these arcs are taken from the cone development where distances  $h_1, h_2, h_3$ , along arcs drawn with radii  $R_1, R_2, R_3$ , are obtained.

If the flow lines at the discharge are not lying in planes normal to the axis, they are also developed on cones and then transferred on the plan view in a similar manner. When both entrance and discharge ends of flow lines are drawn on the plan view, they are joined with a suitable smooth curve. This is accomplished better if one vane end is drawn on tracing paper which is moved back and forth over the other end of

the vane until a suitable joining line is possible. In this way all flow lines are drawn on the plan view. The additional steps in vane development are the same for both the old and new methods and will be described in connection with the new method. Thus, the difference lies in the manner in which the flow line projections are drawn on the plan view.

The disadvantages of the cone development method are as follows.

(1) There is no control over the middle portion of the vane projection. This is drawn as a joining line between the vane tips.

(2) There is no control over the vane thickness. This is usually assumed constant for the whole vane length.

(3) The designer has no view of the true vane length and angularity or channel shape along several flow lines, so he cannot get the experience required to choose the most efficient forms of vane. Without it the top efficiencies can be obtained only accidentally.

(4) The cone development method can hardly be applied to the development of the more complicated vane shapes, such as are used for diffusion casings of vertical deep-well or propeller pumps, because there is a considerable change of vane angularity between the vane entrance and exit tips which cannot be drawn in by eye on the plan view. The method of error triangles is equally accurate for simple and involved vane profiles.

It should be noted that the cone development enables the designer to draw vane entrance tips on a plan view, when the entrance angles are given in a plane inclined to the plane normal to the axis of the impeller, at an angle  $\delta$ , Fig. 6.6 (a). This may be done without going through the lengthy drafting procedure by using the geometrical relationships established above. Thus, if an angle  $\beta_1$  given in a plane OC, Fig. 6.6 (a), making an angle  $\delta$  with a plane normal to the impeller axis, is projected on to the normal plane, the angle  $\beta_1'$  on the plan view will be given by the equation

$$\tan \beta_1' = \tan \beta_1 \cos \delta \quad (6.9)$$

*Therefore the vane tip may be drawn by using angle  $\beta_1'$  as a plain single-curvature vane. The same procedure can be applied to the discharge vane ends, if they are not in a plane normal to the impeller axis.*

## 6.6 METHOD OF "ERROR TRIANGLES"

The principle of the new method will be described now. In Fig. 6.7 (a), suppose a flow line  $c_1c_2$  is shown in perspective on a surface of the back shroud of an impeller. By cutting the surface with a number

of parallel planes, the curve  $c_1c_2$  can be divided into sections  $f_1, f_2, \dots, f_6$ . The intersection of the planes with the surface of the shroud will form a number of parallel circles. Through the points of intersection of the curve  $c_1c_2$  with the parallel circles, a number of meridional planes may be drawn which will section the shroud surface along the curved lines  $g_1, g_2, \dots, g_6$ . These lines, together with the sections of the parallel

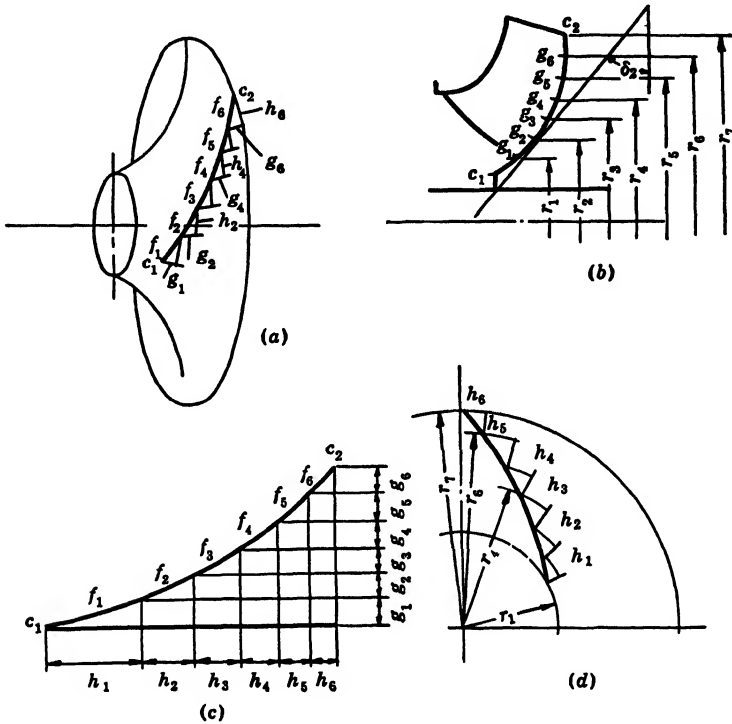


FIG. 6.7. Impeller flow line development on a plane.

circles  $h_1, h_2, \dots, h_6$  and the curve  $c_1c_2$ , form a number of curved triangles called by Kaplan "error triangles." Now suppose all these curved triangles are cut and transferred to a plane so that sections  $h_1, h_2, \dots, h_6$  of the parallel circles are arranged along horizontal parallel lines. The sections  $g_1, g_2, \dots, g_6$  of the curved vertical sides will become flat vertical lines, and the curves  $f_1, f_2, \dots, f_6$  will form a plane development of the curve  $c_1c_2$ , Fig. 6.7 (c). Obviously the greater the number of sections drawn through the flow line, the more accurate the plane development of the curve will be. The angles the curve  $c_1c_2$  makes with the parallel circles are the same on the plane development. Also, the length

of the flow line  $c_1c_2$  in the development is very nearly equal to the true length of the flow line in space.

On the elevation view, the flow line  $c_1c_2$  will appear as shown in Fig. 6.7 (b) where  $r_1, r_2, \dots, r_6$  are the radii of the parallel circles. A plan view of the flow line  $c_1c_2$  can now be drawn; Fig. 6.7 (d). Each point of the curve in the plan view is located by radii  $r_1, r_2, \dots, r_6$ . The displacement  $h_1, h_2, \dots, h_6$  of one meridional plane with respect to an adjacent one along the parallel circle is shown without distortion on the plane development, Fig. 6.7 (c), and appears in full length on the plan view, Fig. 6.7 (d). The intersections of the meridional planes with the parallel circles determine the points of the curve in the plan view.

To apply the method of error triangles to the impeller vane layout the following procedure is followed.

(a) The elevation view, or profile, of the impeller is drawn as described previously. The flow lines are drawn and checked in the same manner as for the vane development on cones, Fig. 6.8 (a).

(b) The vane development on a plane, Fig. 6.8 (b), is drawn to correspond to the profile and the vane angles at entrance and discharge. The vane thickness is shown on the plane development,  $s$  on Fig. 6.8 (b).

To draw the vane development divide one of the flow lines  $a_1a_2$  into a number of parts and then lay out the same distances along the rest of flow lines, points  $1a, 2a, \dots, 8a; 1b, 2b, \dots, 10b; 1c, 2c, \dots, 11c$ . In this way all the error triangles on the development will be of the same height. Parallel lines spaced  $g_1, g_2, g_3$ , etc., apart are drawn for the vane development on a plane, Fig. 6.8 (b). The vane development is first sketched in between the parallel lines limiting the flow lines on profile  $1a, 8a; 1b, 9b$ ; and  $1c, 10c$  for the flow lines  $a_1a_2, b_1b_2$ , and  $c_1c_2$ , respectively. The vane thickness is also shown for the flow line  $c_1c_2$  on Fig. 6.8 (b). This does not have to be the same for all flow lines or constant along the same flow line. The desired degree of streamlining can be given to the vane. Also, for molding reasons or strength, the vane thickness may vary from one flow line to the other. Although for the development it is more convenient to draw vane sections a certain distance apart, it is found helpful to put the vane development of several flow lines into their true relative positions, Fig. 6.8 (b). The suction ends of the developed flow lines should arrange themselves evenly spaced and the tips of flow lines should form a smooth curve to assure that the edge projection on the plan view will also be a smooth curve. Then the triangles are drawn for one side of the vane only, say the leading face,  $a_1a_2$ , Fig. 6.8 (b).

(c) The vane sections are transferred from the development to the plan view, Fig. 6.8 (c). An arbitrary starting point having been chosen, curved triangles are drawn. The arcs of parallel circles are drawn with

radii taken from the elevation view for points  $1a, 2a, \dots, 8a$ , etc. The displacement of one point with respect to the other is taken from the vane development ( $h_1, h_2, \dots, h_8$ ). By joining the points with a curved line the plan projection of the flow line is obtained.

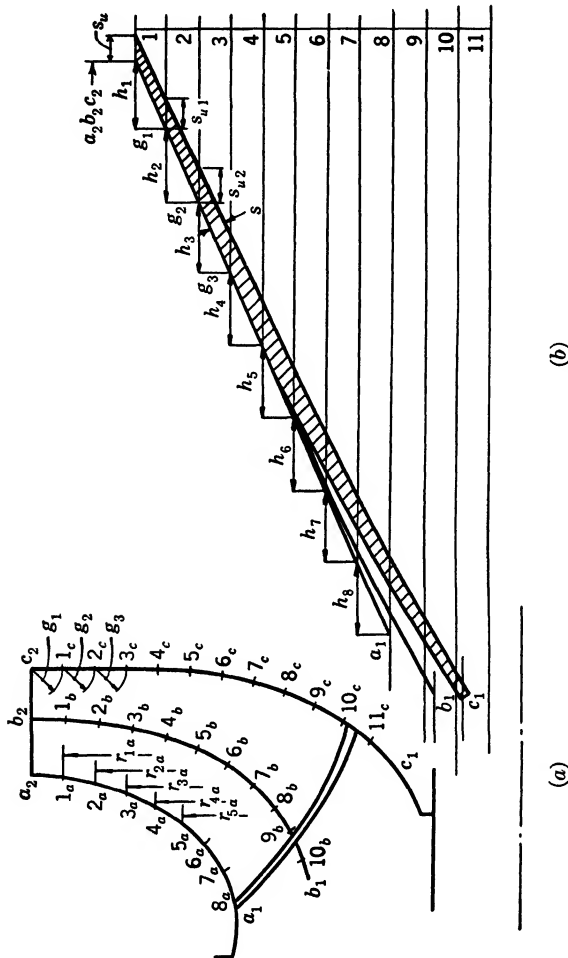


Fig. 6.8 (a and b). Mixed flow impeller profile and vane plane development.

To draw the back side of the vane, the vane thickness is laid off from points  $1a, 2a, \dots, 8a$  along the parallel circle arcs taken from the vane development ( $s_{u1}, s_{u2}$ , etc.). The flow lines  $b_1b_2$  and  $c_1c_2$  are plotted on the plan view in the same way.

(d) The flow lines on the elevation and plan view are the first set of construction lines used for plotting the vane pattern sections. As a second set of construction lines, a number of uniformly spaced (I, II,



III, etc.) radial sections are drawn on the plan view, Fig. 6.8 (e). The intersections of the flow lines, with the radial sections for both front and back of the vane, are plotted on the elevation view from the plan view, Fig. 6.8 (d). If the radial sections on the elevation view do not

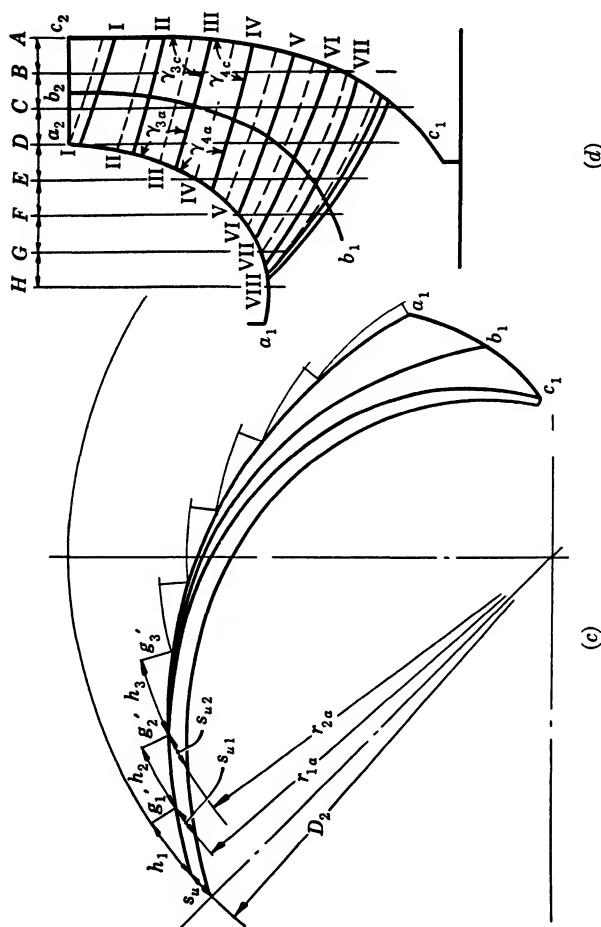


FIG. 6.8. (c) Impeller vane plan view; (d) radial sections on profile view.

form smooth lines, uniformly spaced, it is an indication that the change in vane angularity on the vane developments was too abrupt for one or more of the flow lines.

An alternate method of drawing the second set of construction lines may be mentioned. In this, the flow lines on the elevation view are divided into an equal number of parts and the corresponding points  $1a, 1b, 1c; 2a, 2b, 2c$ , etc., Fig. 6.8 (a), should form smooth curves on the plan view also. These curves are used for the second set of con-

struction lines for plotting the vane pattern sections. The advantage of this method is that no additional points are plotted, and those already on the drawing are utilized.

(e) The next step is to draw the vane pattern sections  $A, B, C, \dots, H$ , Fig. 6.8 (d). The vane is divided into a suitable number of boards, the number depending on the vane dimensions. Vane sections are drawn on the elevation view and then plotted on the plan view, the intersections of the board planes being located with the radial sections or any other construction lines. To avoid confusion of lines it may

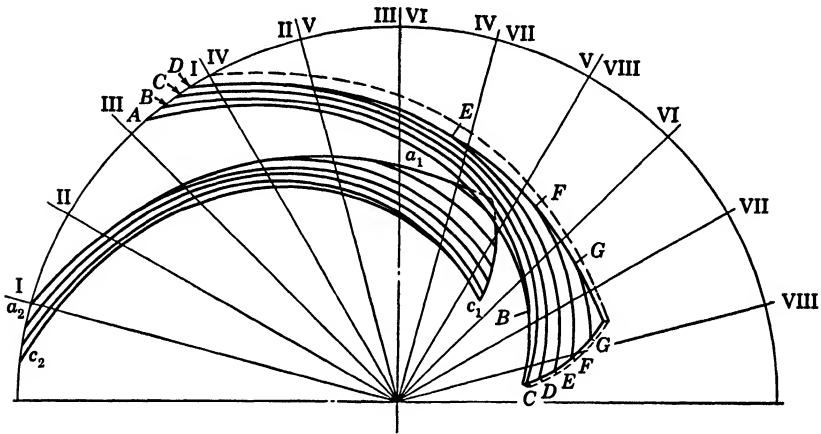


FIG. 6.8 (e). Vane pattern sections.

be advisable to separate the views of the front and back sides of the vane by showing the front side of one vane and back side of the next vane, Fig. 6.8 (e). In this way the channel between the two vanes will be defined.

The contour lines or the vane pattern sections on the plan view completely determine the shape of the vanes. If boards of the proper thickness are cut along these lines and stacked in the proper order and the corners of the boards are shaved off, the vane surface will be obtained for the front and back sides.

There are two ways to use these vane sections for building the impeller pattern. In one, a sectional core box is made for a single-vane channel. A number of cores equal to the number of vanes are made and assembled into one core, for the whole impeller. For this arrangement, views of the front and back sides of the vane as shown on Fig. 6.8 (*e*) are sufficient.

In the second method, used mostly for smaller impellers, one core is made for the whole impeller. This core is usually baked with metal

vanes in place and is then broken to remove the vanes, after which the parts of the core are pasted together. For a pattern of this type a wooden vane is first made, from which metal vanes are cast for the core box. To build the wooden vane, the vane sections are cut to the proper shape and thickness and, when they are glued together in the proper order and their corners are shaved off, they will give the vane shape.

The vane section drawings are obtained by placing the two views of the front and back sides of the vane in their proper relative position,

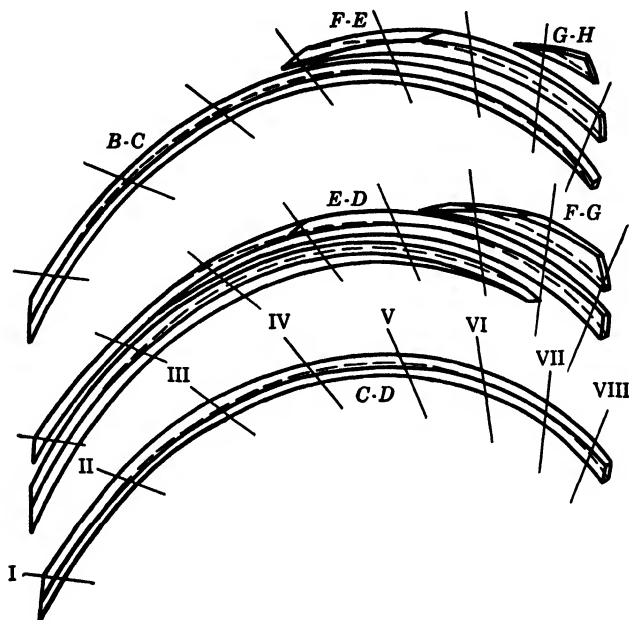


FIG. 6.8 (f). Vane pattern sections.

one on top of the other. From this the vane sections can be picked out for each board; Fig. 6.8 (f). Although only outer contour lines are necessary to cut the boards, the inside lines are also shown because they assist in locating the boards in their correct position. Also the radial lines I, II, III, etc., are shown on the vane section as additional guides in the assembly of the vane from the board sections.

(f) Hydraulically, the best form of the impeller channel is obtained when the true angles between the impeller vanes and shrouds are close to  $90^\circ$ . When the impeller profile is curved considerably this becomes difficult to accomplish. *The channel form may be improved by tilting the vane with respect to the shrouds. This is done by moving the flow lines on the plan view, Fig. 6.8 (c), through a certain angle, which will change*

the angle between the vane and the impeller shrouds without changing the vane angularity.

When heavy vanes are used, a slight inclination of the vanes to both impeller shrouds at the discharge results in quieter pump operation because the discharge from the individual impeller channels against the volute tongue is smoother. With thin streamlined vanes and ample space between the impeller and volute tongue, this consideration becomes unimportant.

To obtain a true picture of the impeller channel normal to the flow, the channel section should be drawn normal to some average flow line which passes somewhere in the middle of the channel. This section is not normal to either of the shrouds or vanes, as neither the shrouds nor two adjacent vanes are parallel. It is difficult to draw such a section on the drawing. However, to find the angles between the vanes and both shrouds, the radial sections I, II, III, etc., Fig. 6.8 (e), will give a satisfactory approximation. *It will be shown that the angles between the shrouds and the vane radial sections on the elevation view— $\gamma'_{4a}$  and  $\gamma'_{4c}$ , Fig. 6.8 (d)—are very nearly equal to the true angles in space between the vane and shroud surfaces  $\gamma_{4a}$  and  $\gamma_{4c}$  or, more accurately,*

$$\begin{aligned}\tan \gamma'_{4a} &= \tan \gamma_{4a} \times \cos \beta_{4a} \\ \tan \gamma'_{4c} &= \tan \gamma_{4c} \times \cos \beta_{4c}\end{aligned}\quad (6.10)$$

where  $\beta_{4a}$  and  $\beta_{4c}$  are the vane angles at section IV, Fig. 6.8 (d), taken for illustration.

This follows from the fact that the plane normal to the flow line  $a_1a_2$  intersects the plane normal to the peripheral velocity (radial plane) at an angle  $\beta$ , according to the definition of the angle between the two planes. Thus the true angle  $\gamma_{4a}$  between the vane and shroud taken in the plane normal to the flow line, if projected on the radial plane IV making an angle  $\gamma_{4a}$  to the normal plane, will be reduced as given by equation 6.10. It should be noticed that if  $\gamma$  is  $90^\circ$  ( $\tan \gamma = \infty$ ) or near it, its tangent is a very large number and  $\gamma' \approx \gamma$ . Below are tabulated several values of  $\gamma$  and  $\gamma'$  for different values of  $\beta$ .

$\gamma \backslash \gamma'$	$\beta = 20^\circ$	$\beta = 30^\circ$	$\beta = 45^\circ$	$\beta = 60^\circ$
$85^\circ$	84.7	84.3	83.0	80.0
$80^\circ$	79.4	78.5	76.0	70.6
$75^\circ$	74.1	72.8	69.3	61.8

Because the shrouds are not parallel it is impossible to make angles between one vane and both shrouds  $90^\circ$  without excessive vane bending. But, since  $\beta$  seldom exceeds  $30^\circ$  and  $\gamma$  is seldom smaller than  $75^\circ$ ,  $\gamma'$ , on the elevation view always will be, within a few degrees, equal to  $\gamma$ , the true angle between the vane and shrouds in space.

When laying out a vane with high angles, such as are used on diffusion casings of vertical turbine pumps, the profiles of both shrouds enclosing the vanes are very nearly parallel, in which case there is no difficulty in keeping  $\gamma$  near  $90^\circ$ ; but  $\gamma'$  on the elevation view will be considerably lower than  $\gamma$  in space, as  $\cos \beta$  is decreasing rapidly when vane angle  $\beta$  is approaching  $90^\circ$ .

(g) The vane angle  $\beta$  for any point on the flow lines appears on the plan view reduced to  $\beta'$  so that

$$\tan \beta' = \tan \beta \cos \delta \quad (6.12)$$

where  $\delta$  is the angle between the tangent to the flow line at that point on the elevation view and the plane normal to the impeller axis. Thus, for instance, on Figs. 6.8 (a), (b), (c), (d) for triangle (3),

$$\tan \beta = \frac{g_3}{h_3} \quad \tan \beta' = \frac{r_{2a} - r_{3a}}{h_3}$$

but

$$\frac{r_{2a} - r_{3a}}{g_3} = \cos \delta_3$$

hence

$$\tan \beta' = \tan \beta \cos \delta_3$$

(h) For a study of the impeller channel form variation along a flow line, a development of the channel along the flow line can be made by

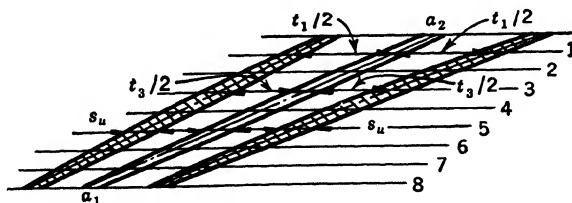


FIG. 6.9. Impeller channel development.

first drawing a middle line between the vane faces on the development (Fig. 6.9), and then laying off half of the circular pitch  $t/2$  for several points on the flow line. By drawing in the vane tangential thickness  $s_u$ , the developed view of the channel is obtained.

It has been found that for centrifugal pumps three flow lines will be sufficient for a vane layout in the majority of cases. Furthermore, the vane construction can be simplified by drawing the middle flow line as a curve equally spaced from both shrouds. For small and narrow impellers the middle flow line can be omitted. In that case the radial vane sections—lines I, II, III, etc., Figs. 6.8 (d) and 6.8 (e)—are drawn as straight lines or curves by eye on the elevation view. The accuracy of vane construction is not impaired by these short cuts, as can be proved by comparing layouts made with and without these simplifications.

### 6.7 APPLICATION OF METHOD OF ERROR TRIANGLES TO THE DESIGN OF PLAIN VANES

For a given entrance angle  $\beta_1$  and discharge angle  $\beta_2$  it is always possible to draw a vane as a circular arc with a single radius. However, such a vane has serious disadvantages. Figure 6.10 shows the con-

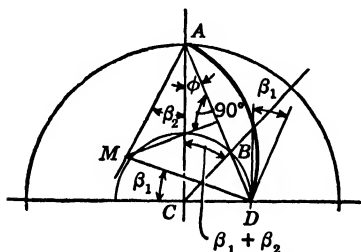


Fig. 6.10. Plain vane drawn as a circular arc.

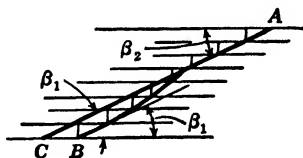


Fig. 6.11. Development of the vane in Fig. 6.10.

struction. From an arbitrary point  $A$  on the circle of the impeller outside diameter, draw one line  $AM$  at an angle  $\beta_2$  to the radius  $AC$ . At point  $C$ , construct an angle  $\beta_2 + \beta_1$  to the radius  $AC$ . The line will intersect the impeller eye circle at  $B$ . Draw a line  $AB$  to intersect the impeller eye circle at  $D$ . Draw a perpendicular line in the middle of  $AD$  to intersect line  $AM$  at  $M$ .  $MA$  will be the radius of the arc to give an angle  $\beta_2$  at discharge and an angle  $\beta_1$  at entrance.

The proof of this construction may be of interest.

$$\beta_1 + \beta_2 + \phi = \angle CBD = \angle CDB$$

$$\beta_2 + \phi = \angle MAD = \angle MDA$$

By subtraction

$$\beta_1 = \angle CDB - \angle MDA = \angle MDC$$

The method of error triangles can be advantageously applied to the analysis and construction of the plain vane. On Fig. 6.11,  $AB$  is the

development on a plane of the vane in Fig. 6.10 obtained by the use of error triangles. It will be noticed that the change in vane angularity is irregular. First, the vane angle increases rapidly, then slowly decreases to the discharge angle. This form of vane is not considered the most efficient. A vane with a gradual change in the vane angle,  $AC$  in Fig. 6.11, is preferred. To get a better vane shape for the plain vane impeller, it pays to draw first the vane development on a plane and then to replot it on a plan view by the method of error triangles. Although this method takes more time, its systematic use permits improving the vane shape to get the best performance.

### REFERENCES

1. VICTOR KAPLAN and ALFRED LECHNER, *Theorie und Bau von Turbinen-Schnelldauern*, Munich, R. Oldenbourg, 1931, pp. 125-129.
2. HERMAN SCHAEFER, *Kreiselmashinen*, Berlin, Julius Springer, 1930, pp. 29-37.
3. L. QUANTZ, *Kreiselpumpen*, Berlin, Julius Springer, 1930, pp. 18-20.
4. C. PFLEIDERER, *Die Kreiselpumpen*, Berlin, Julius Springer, 1932, pp. 266-279.
5. R. CAMERER, *Vorlesungen uber Wasserkraftmaschinen*, Leipzig, Wilhelm Engelmann, 1929, pp. 274, 275, 369.

## CHAPTER 7

### PUMP CASING

The purpose of the pump casing is to guide the liquid to the impeller, convert into pressure the high velocity kinetic energy of the flow from the impeller discharge, and lead the liquid away. *The casing takes no part in the generation of head, and all theoretical discussion of the casing deals with losses.*

#### 7.1 SUCTION NOZZLE

Since the liquid path between the suction flange and the impeller eye is short, and velocities in the suction nozzle are relatively low, the loss of head due to friction in the suction nozzle is very small. However, the design of the suction nozzle has an important bearing on the velocity distribution immediately ahead of the impeller, and in this way it may affect the impeller efficiency and pump cavitation characteristics. These effects are more pronounced in low head, high specific speed pumps. *With vertical pumps having only a short suction bell ahead of the impeller, the shape of the suction sump becomes an important part of the impeller approach and has a direct bearing on the hydraulic and mechanical performance of the pump.* There are numerous cases on record where large propeller pumps failed to meet the performance indicated by model tests, or by tests of similar pumps in different installations, owing entirely to the suction sump design.<sup>1</sup>

A straight, tapered, suction nozzle known as end suction nozzle is the best in every respect for single-inlet impellers. Such a nozzle, the area of which gradually reduces toward the impeller eye, has a definite steadying effect on the flow and assures a uniform liquid feed to the impeller.

A tapered, long-radius elbow is next best (Fig. 7.1). For low specific speeds (below 1500) the two are equivalent hydraulically; however, for

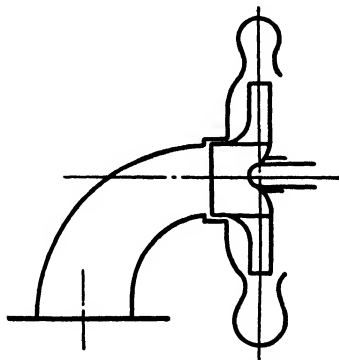


FIG. 7.1. Reducing suction elbow.



higher specific speeds and *particularly for propeller pumps, the optimum efficiency and maximum heads will be appreciably reduced with the elbow suction.* A flat elbow, or volute suction, as used with horizontally split pumps of multistage type (Fig. 7.2), is almost as efficient as a tapered elbow for low specific speed pumps, but for high specific speed pumps the bad effects of the sharp 90-degree turn become most pronounced. Propeller pumps are never built with flat elbow suction. In an elbow of this type it is essential to have the flow accelerated gradually, in order to suppress the tendency toward velocity distortion due to a

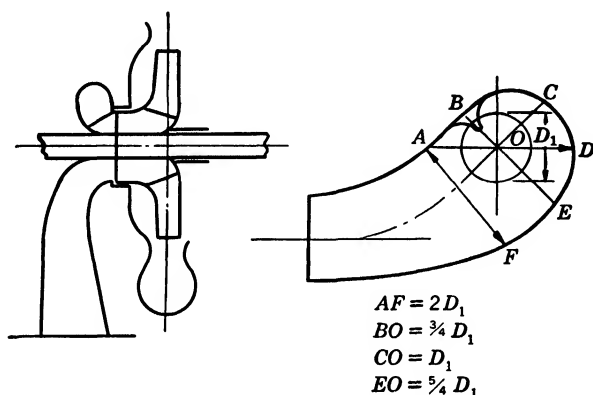


FIG. 7.2. Volute suction nozzle.

double turn just in front of the impeller eye. To effect a better distribution around the impeller eye section  $AF$ , Fig. 7.2, is given an area some 50 per cent or more greater than that of the impeller eye. At the same time the width of the nozzle at  $AF$  is about twice the impeller eye diameter. As a result of the turn, most of the flow shifts to the outer side; therefore the suction baffle or stop at  $B$  is placed about 90 degrees past the middle line of the nozzle  $OC$ .

## 7.2 VOLUTE

Except for vertical pumps of the turbine type, the majority of single-stage pumps built in the United States are of the volute type. There is likewise a definite trend toward volute casings for multistage pump construction. However, owing to the high cost of multistage patterns the change to volute pumps is taking place rather slowly. The main advantage of the volute casing, as compared with a casing having diffusion vanes, is its simplicity. Although efficiencies of pumps with

diffusion vane casings are equal to those of volute pumps, in several types they rarely exceed the efficiency of the latter. Higher efficiencies claimed for small low specific speed pumps with diffusion casings are usually attained by means of a high degree of finish on the diffusion vanes not possible with volute pumps.

There are several design elements of volute casings which determine their hydraulic characteristics, namely volute areas, volute angle  $\alpha_v$ ,

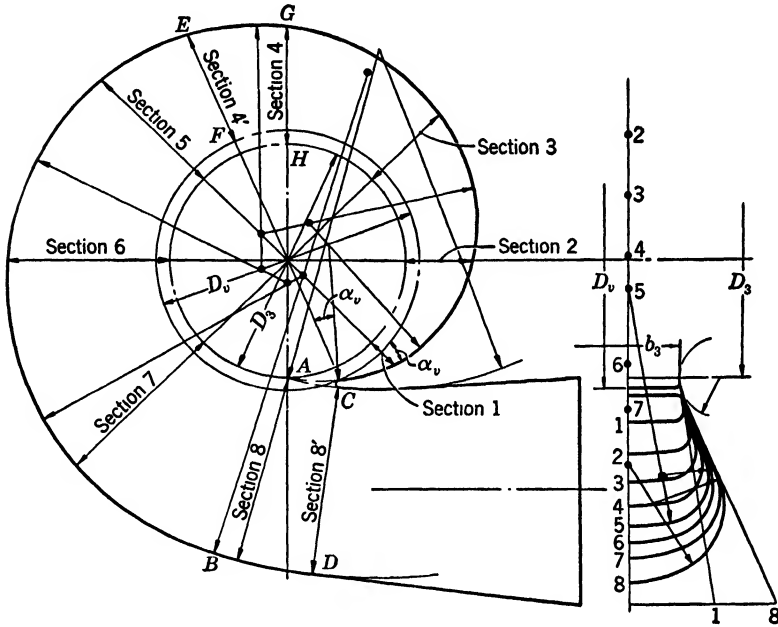


FIG. 7.3. Pump volute casing.

volute width  $b_3$ , and volute base circle  $D_3$  (Fig. 7.3). The selection of these elements is governed by theoretical considerations given below, but their actual values have been established experimentally for best hydraulic performance.

(a) **Volute Areas.** Reference to Fig. 7.3 will show that the total pump capacity passes through the volute throat AB, Section 8; only part of pump capacity passes at any other section, the amount depending on the location of the section from the dividing wall. Thus, volute areas are gradually increased from a point A, called the volute tongue or cut-water, toward the volute nozzle to accommodate the discharge along the impeller periphery. A certain amount of liquid will be recircu-

lated between the cut-water and the impeller diameter and also between the impeller shrouds and casing side walls. The velocity in the volute varies with the pump capacity; therefore the analysis will be confined to the best efficiency point, or design capacity only. The capacity through the volute is lower than that discharged from the impeller by the amount of leakage, but the latter will be disregarded and taken care of later by an experimental factor.

The velocity distribution across any volute section is not uniform. This is easy to visualize by having in mind the flow pattern in a pipe under the most favorable conditions. There the mean velocity of flow is from 0.78 to 0.92 of the maximum velocity at the center of the pipe. With small pipe diameters still lower ratios are possible. In a volute



FIG. 7.4.  
Spiral flow in  
volute cas-  
ing.

the maximum velocity is at the impeller periphery but is not uniform across the width of the impeller as shown on Fig. 3.20. Also, the velocity decreases toward the volute walls. In contrast with pipe flow, the high velocity core in the volute is driven by the impeller and, under such circumstances, the ratio of mean velocity to the maximum discharge velocity from the impeller is lower than that which can be expected in straight pipe flow. This ratio has been found to vary from 0.56 to 0.82 for pumps covering a wide range of sizes and specific speeds. The flow pattern is complicated further by the radial outward component of the absolute velocity which causes a spiral motion along the volute.

This motion is outward in the middle and inward near the walls of the volute (Fig. 7.4). Such a velocity distribution and spiral motion in the volute were visually observed by Kranz.<sup>2</sup>

In view of the complicated pattern of flow in the volute, a theoretical determination of the velocity distribution along the volute in terms of the tangential component of the impeller discharge velocity is impossible. Several attempts in that direction presented volute design methods which proved to be inferior in performance to volute designs based entirely on experimental study. Pfeleiderer<sup>3</sup> assumes the flow in the volute to follow the law

$$c_u r = \text{constant} = c_{u3} r_2 \quad (7.1)$$

where  $c_u$  is the velocity in the volute at radius  $r$  and  $c_{u3}$  is the tangential velocity in the volute at the impeller periphery. This results in volute areas giving higher average velocities at the small sections of volute than those near the discharge nozzle. But even the largest sections result in velocities which are too high to obtain the optimum

pump efficiency.\* The best modern pumps are designed for a constant average velocity for all sections of the volute; this means that volute areas are increased in proportion to their angular advancement from the cut-water. The average volute velocity  $c_3$  is determined experimentally from the relationship

$$c_3 = K_3 \sqrt{2gH} \quad (7.2)$$

where  $K_3$  is an experimental design factor. This varies with the specific speed. Figure 7.5 shows values of  $K_3$  for volute pumps. Considerable deviations from these average values are possible and take place when

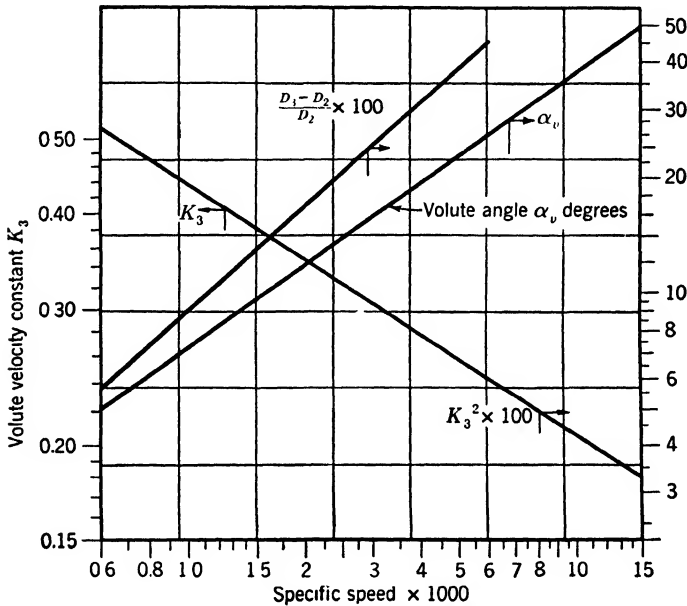


FIG. 7.5. Volute constants.

the impeller diameter is cut, or when several impellers are used with the same casing. However, if volute areas are too small in comparison to the optimum values, the peak efficiency will decrease slightly and move toward a lower capacity, or if volute areas are too large the peak efficiency may increase but will move toward a higher capacity. The efficiency at partial capacities will be lower in the latter case.

\* Tests on centrifugal fans by Polikovskiy and Abramovitch of the Central Aero-Hydrodynamical Institute, U.S.S.R., reveal that "the measured tangential velocity components did not follow the law of constant angular momentum. Instead of this, the measurements showed an almost constant value for the tangential velocity component." Review by A. Nekrassov, *Mech. Eng.*, Aug. 1937, p. 628.

In laying out volute areas it is immaterial whether they are measured from the base circle ( $D_3$  in Fig. 7.3) or from the inside edge of the cut-water at  $D_v$ . In both cases the area increment from one section to the next will be the same for the same angular displacement, and the last section, Section 8, may be at either  $AB$  or  $CD$ , which are always very nearly equal.

When volute areas are measured from the cut-water, starting with identical areas at Section 8, areas of other volute sections are very slightly smaller than when volute areas are measured from the base circle  $D_3$ . Thus, referring to Fig. 7.3, in the first case Section 4, with half of the total area, is at  $EF$  whereas in the second case it is at  $GH$ . Section heights  $EF$  and  $GH$  are very nearly equal.

**(b) Volute Angle.** Considering the volute casing as a one-vane diffusion casing, the volute angle  $\alpha_v$  (Fig. 7.3) should correspond to the angle between the absolute velocity and the peripheral velocity. In practice this is true only approximately because the effect of variation of the angle  $\alpha_v$  cannot be detected. In the first place, it cannot be expected that one vane can have much guiding effect on the total impeller capacity; secondly, no loss is incurred where there is a small angle of attack between the actual liquid direction and the shape of the cut-water. But in general  $\alpha_v$  follows the trend of variation of the angle  $\alpha_2'$  on the input discharge velocity triangles for different specific speeds. The volute angle  $\alpha_v$  increases for higher specific speeds; see Fig. 3.12 (b). The average values of  $\alpha_v$  for different specific speeds are given in Fig. 7.5. A more accurate method of determination of the volute angle is given in Chapter 9, Fig. 9.16.

**(c) Volute Width.** Volute width  $b_3$ , Fig. 7.3, is determined by the following considerations.

(1) In view of the flow pattern in the volute as presented above, less loss is incurred at the impeller outlet if the high velocity flow is discharged into a body of rotating liquid rather than against stationary walls. (2) The volute casing should be able to accommodate impellers of different diameters and widths. (3) In multistage pumps, a liberal clearance is necessary between the impeller shrouds and casing walls to take care of possible inaccuracies of castings and shrinkage. With small pumps of 6 or 8 stages this becomes a problem. For pumps of medium specific speeds,  $b_3 = 1.75b_2$  where  $b_2$  is the impeller width at discharge. For small pumps of lower specific speeds ( $b_2$  is small), including multistage pumps,  $b_3 = 2.0b_2$ . For high specific speed pumps ( $n_s > 3000$  double suction)  $b_3$  can be reduced to  $b_3 = 1.6b_2$ .

**(d) Base Circle.** The base circle is used for drawing the volute layout, and the cut-water diameter  $D_v$ , fixed by the base circle diameter,

determines the physical limitations of the maximum impeller diameter. If a certain minimum gap between the casing and the impeller outside diameter is not maintained the pump may become noisy and the efficiency may be impaired. Figure 7.5 shows the minimum diametrical gap at the cut-water expressed as a fraction of the impeller diameter, or

$$\rho = \frac{D_3 - D_2}{D_2} \quad (7.3)$$

which is plotted against specific speed. These values increase when the impeller diameter is cut. It has been found by special tests that an unnecessarily large base circle for a given impeller diameter reduces the pump optimum efficiency as extra power is required to circulate liquid through the gap between the cut-water and the impeller.

**(e) Volute Areas versus Specific Speed.** Referring to the chart in Fig. 7.5, it will be noticed that for a given head  $H$  and capacity  $Q$ , the volute velocity decreases for higher specific speeds. This has been indicated from considerations of Euler's velocity triangles in Chapter 3, Fig. 3.12 (b), and is shown in Fig. 9.16, Chapter 9, for "actual" velocity triangles. *This means that if a higher specific speed is selected the volute areas will be increased irrespective of the actual rotative speed, as*

$$c_3 = K_3 \sqrt{2gH} \quad \text{and} \quad A_8 = \frac{Q}{c_3}$$

The kinetic energy contained in the flow in the volute, expressed as a ratio of the velocity head,  $c_3^2/2g$ , to the pump total head is also decreased. This follows from

$$K_3 = \frac{c_3}{\sqrt{2gH}} \quad \text{and} \quad \frac{c_3^2}{2g} \cdot \frac{1}{H} = K_3^2 \quad (7.4)$$

and is shown in Fig. 7.5. The average pressure in the volute casing above the suction pressure at b.e.p. is equal to  $H(1 - K_3^2)$ , disregarding the loss of head due to friction in the volute casing and the velocity head in the suction nozzle.

The physical overall dimensions of the pump casing are determined by the size of the volute areas and the diameter of the base circle. For a given head and capacity, the areas increase as the specific speed is increased, but the base circle and the impeller diameter decrease. At a certain specific speed the two will balance each other and a further increase in specific speed will not reduce the size and weight of the casing.

### 7.3 PRESSURE DISTRIBUTION AND RADIAL THRUST IN THE VOLUTE CASING

**(a) Radial Thrust.** *That a constant average velocity in the volute casing is the most favorable for the pump performance is shown by the fact that in actual pumps, at and near the best efficiency point, the pressure is the same in all volute sections around the impeller. Evidently this is the most desirable condition for the impeller discharge. However, on both sides of the best efficiency point this equilibrium of volute pressure is destroyed.*

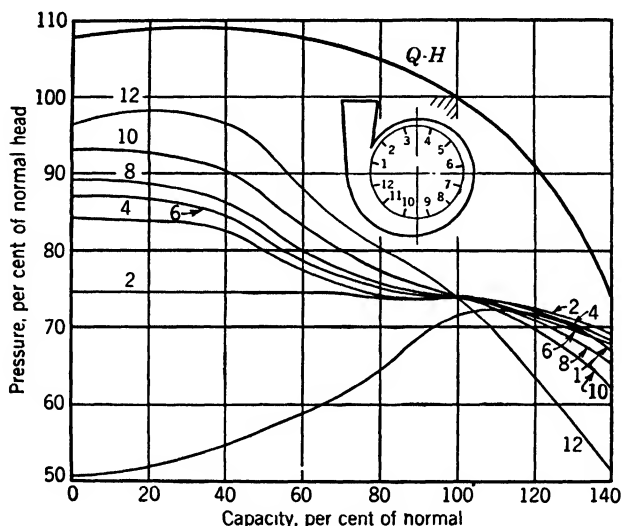


FIG. 7.6. Volute pressure distribution, 6-in. single-suction pump.  $n_s = 1700$ .

Figure 7.6 shows a typical volute pressure distribution. Figure 7.7 (a) shows results of radial thrust measurements on a 4-in. pump. The magnitude of the forces was determined by measuring the shaft deflections and calibrating the shaft by dead weights. The radial thrust can be expressed by a formula

$$P = \frac{KHD_2B_2}{2.31} \quad (7.5)$$

where  $P$  = radial resultant force, in pounds

$H$  = head, in feet

$D_2$  = impeller diameter, in inches

$B_2$  = impeller overall width including shrouds, in inches

$K$  = a constant which varies with capacity as given by the following formula arrived at experimentally.

$$K = 0.36 \left[ 1 - \left( \frac{Q}{Q_n} \right)^2 \right] \quad (7.6)$$

where  $Q$  is any capacity and  $Q_n$  is the normal capacity. This formula gives zero radial thrust at normal capacity and maximum radial thrust at zero capacity when  $K = 0.36$ . The value of  $K$  depends on the pump

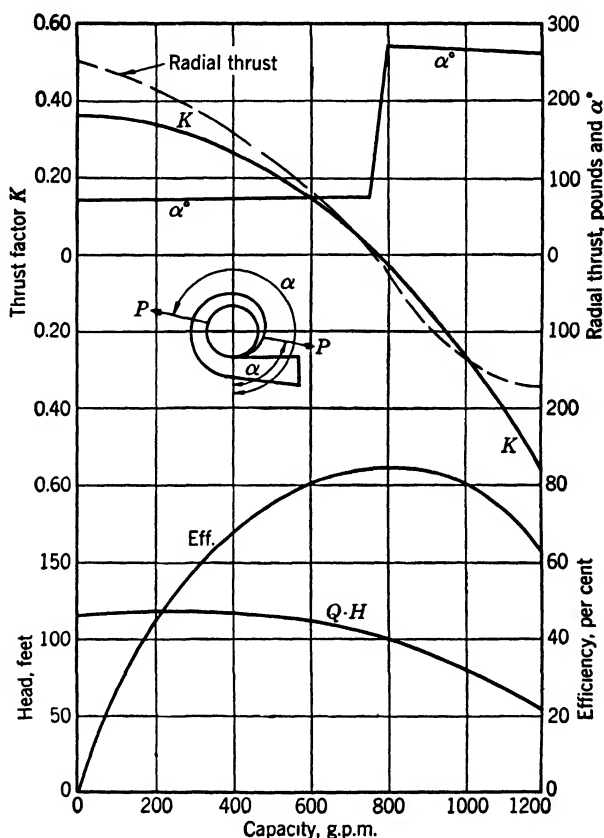


FIG. 7.7 (a). Radial thrust in a single-volute 4-in. pump.  $D_2 = 10\frac{1}{2}$  in.,  $B_2 = 1\frac{1}{4}$ ; 1760 r.p.m.

type. Higher values than that given by equation 7.6 have been observed ( $K = 0.6$  at zero capacity).

The immediate effect of radial forces in the volute casing is excessive shaft deflection, which results in the rapid wear of the wearing rings and shaft breakage due to fatigue failure of the shaft material. Shaft failures mostly occur in double-suction pumps having a large bearing



span. One peculiar feature of shaft failures due to this cause is that, in a great majority of cases, the shafts fail immediately beyond the impeller on the outboard side where torque stresses do not exist. The break usually starts either at the key seat on the shaft or at threads for

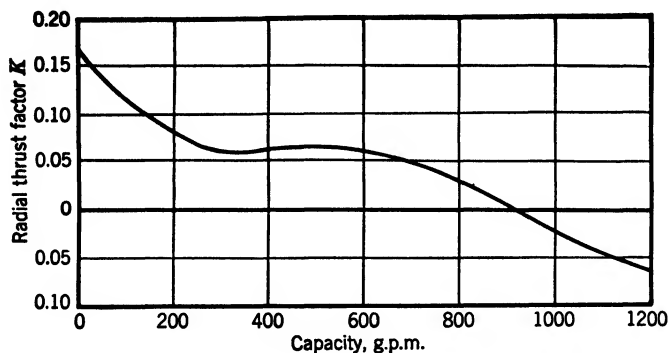


FIG. 7.7 (b). Radial thrust in a double-volute 4-in. pump at 1760 r.p.m. The impeller is the same as that in Fig. 7.7 (a).

the impeller nut or shaft sleeves. This location of the break puzzled pump engineers for a long time until recently when an explanation was advanced by H. F. Moore † who pointed out that the weight of the coupling (Fig. 7.8) sets up a negative bending moment at the inboard bearing  $B$ , which results in a greater bending moment and flexural stress in the plane  $GH$  than in the plane  $EF$ . In every case of shaft failure in

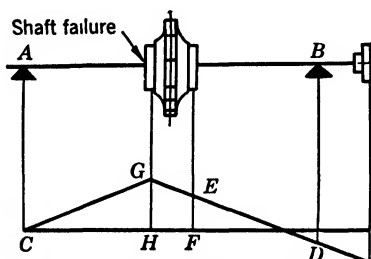


FIG. 7.8. Moment diagram of a pump shaft.

the manner described it has been found that the pump was operating at partial capacities. The increase in operating speeds of modern pumps has aggravated the conditions as heads and the frequency of flexure reversals have increased. For long life, a shaft material with a high endurance limit should be used; also, threads should be removed from the middle portion of the shaft, and the

key seat should be milled out with a proper fillet. Note that shrinking the impeller on the shaft reduces the endurance limit.<sup>4</sup>

**(b) Double Volute.** To eliminate radial thrust, double volute casings have been introduced. In such a casing the flow is divided into two

† H. F. Moore, Professor at University of Illinois, in private correspondence with the author, August 1941.

equal streams by two cut-waters 180 degrees apart (Fig. 7.9). Although the volute pressure inequalities remain as in a single-volute casing, owing to symmetry there are two resultants of radial forces opposing each other.

Actual measurements of pressure distribution along the volutes of a double-volute casing by Knapp<sup>5</sup> and *direct measurements of radial forces by Ingersoll-Rand Company (1936, not published)* show that a complete elimination of the radial thrust is not accomplished by the double volute.

Figure 7.7 (b) shows the values of radial thrust factors for a 4-in. single-suction pump with a double-volute casing. It will be noticed that for a double-volute casing the radial thrust variation for different capacities is of the same type, but on a reduced scale, as that for a single-volute pump, as shown in Fig. 7.7 (a). *The direction of the radial thrust in a double-volute casing is approximately the same as it is in a single-volute casing.* The same impeller was used in both cases.

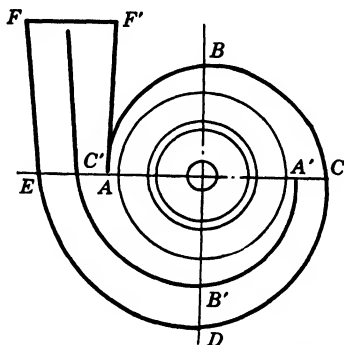


FIG. 7.9. Double-volute casing reduces but does not eliminate radial thrust.

The reason radial thrust exists in a double-volute casing is that the outlets from the two volutes are not identical. The outer volute path, *ABCDEF* (Fig. 7.9), is approximately twice as long as that of the inner volute *A'B'C'D'*. *The energy gradient drop along the first volute is greater than that along the second. But, since the final pressures and velocities at the discharge flange are the same, the pressure in the volute ABC is lower than that in the volute A'B'C'.* Variation of radial thrust with the capacity is better understood from the study of the energy gradient in the volute casing given later in this chapter.

For a complete symmetry of impeller discharge pressure distribution the suction impeller approach should be also symmetrical. Any deviation from symmetry at the impeller eye results in different heads produced by different portions of the impeller periphery. There are cases on the record of shaft failures in large, high speed, double-suction pumps with double-volute casings.

The efficiency of the double-volute casing pumps approaches within one point that of single-volute pumps. But for optimum performance, double-volute pumps require more work in matching passages of split casing pumps, and cleaning of double-volute passages is very difficult. The efficiency curve of double-volute pumps is flatter and the improve-

ment over single-volute pumps appears more at capacities over the normal than at partial capacities. The reason for such an improvement of pump efficiency on both sides of the peak efficiency point lies in the fact that the impeller is discharging against a more uniform pressure in a double volute than in a single volute.

(c) **Circular Casing.** Figure 7.10 shows the performance and radial thrust of a 4-in. pump with a circular casing having constant volute areas. Such designs have been used in the past for small pumps. The

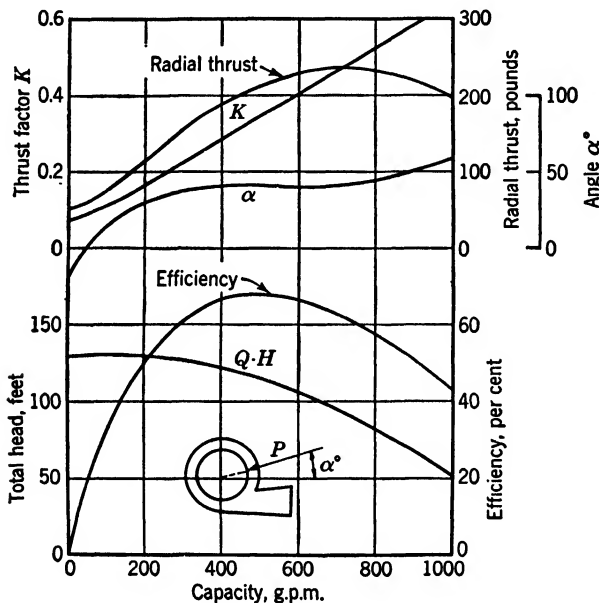


FIG. 7.10. Radial thrust in a circular casing.  $D_2 = 10\frac{1}{2}$  in.,  $B_2 = 1\frac{1}{4}$  in., 1760 r.p.m.

maximum radial forces are developed at the best efficiency point and the radial thrust is always directed away from the cut-water. The factor  $K$  in formula 7.5 for the circular casing, as determined experimentally, can be expressed by

$$K = 0.36 \frac{Q}{Q_n} \quad (7.6a)$$

Pumps with circular casings, besides being larger, were inferior in efficiency to pumps with constant velocity volute casings and were discontinued.

(d) **Radial Thrust in Volute Casing.** *The pressure distribution in the volute casing, the location of the resultant of all radial forces acting on the*

impeller, and reversal of its direction can be explained by the energy gradient variation along the liquid path from the impeller periphery to the casing discharge nozzle. In a volute casing designed for a constant velocity, the pressure gradient will parallel the energy gradient. On Fig. 7.11, line  $AF$  represents the static pressure gradient along the periphery of the impeller for zero flow and developed on a straight line. Point  $A$  is at or near the cut-water. Pressure rises steadily toward the discharge flange. This can be easily visualized because, with the discharge blocked, liquid is crowded toward the discharge nozzle and cut off by the cut-water; or, the conditions in the casing can be looked upon as an eccentric forced vortex, in which particles on a larger radius develop higher

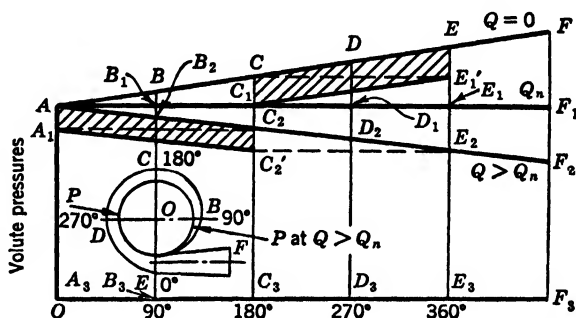


FIG. 7.11. Energy gradient and radial thrust in a single-volute casing.

pressure. Pressures along  $AC$  oppose those along  $CE$  because they are 180 degrees apart. The resultant pressure forces are proportional to the areas on the diagram. The pressure area  $AA_3CC_3$  will balance the area  $C_1C_3E_1'E_3$ . The unbalanced radial forces will be represented by the area  $CC_1EE_1'$ . The direction of the resultant is along a radial line toward the center and 270 degrees from the cut-water.

When flow starts in the volute, the hydraulic gradient drops below  $AF$  and at normal capacity it reaches a position  $AF_1$ , where pressures are equal all around the impeller. The hydraulic gradient drop increases along the volute from zero at  $A$  to  $BB_1$ ,  $CC_1$ , and so on. At normal capacity the resultant of all radial forces is zero.

As the flow increases further to  $Q > Q_n$  the hydraulic gradient continues to drop from  $BB_1$  to  $BB_2$ ; from  $CC_1$  to  $CC_2$ , and so on. Now pressures are higher along  $AC$  than along  $CE$ . Pressure area  $A_1A_3C_2'C_3$  balances area  $C_2C_3E_2E_3$  and the unbalanced radial forces are represented by the area  $AA_1C_2C_2'$ . The direction of the resultant of these forces is from smaller volute sections toward larger sections. Note that pressure at the nozzle  $F_2$  is lower than at any point in the volute.

Figure 7.7 (a) shows that the directions of the resultant radial force vary slightly from those arrived at on the diagram in Fig. 7.11. In Fig. 7.12 is shown a pressure distribution for three capacities of an 8-in. pump at 2500 r.p.m. tested at the California Institute of Technology.<sup>6</sup> From this it is seen that the pressure distribution along the volute deviates from the straight line assumed on Fig. 7.11, particularly at and near the cut-water where two regions with different pressures meet. The general trend of the pressure curves, however, substantiates the reasoning underlying the construction of Fig. 7.11.

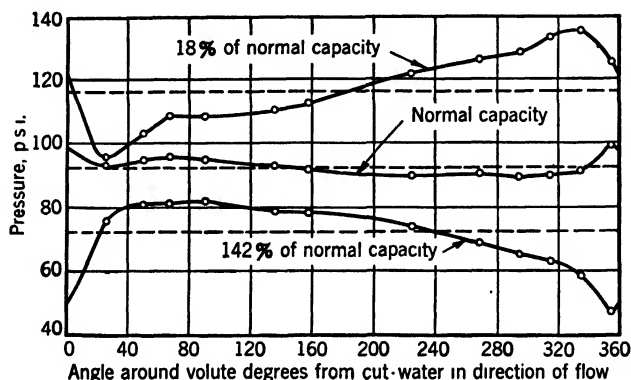


FIG. 7.12. Pressure distribution around the volute casing; 8-in. pump, 2500 r.p.m. (California Institute of Technology).

The energy gradient diagram for the double volute would have the same appearance as that for the single volute in Fig. 7.11. By referring to Fig. 7.9, it will be seen that pressures in the two volutes are equalized beyond the discharge flange. They are also equal just ahead of the inner volute cut-water  $A'$ . At all intermediate points the pressures will be indicated by the direction of the energy gradient drop giving, a diagram similar to Fig. 7.11. Therefore, variation of the radial thrust and its direction in the double volute are of the same nature as they are in the single volute, Fig. 7.7 (b).

**(e) Circular Casing Radial Thrust Diagram.** Figure 7.13 represents a diagram of the pressure gradient in a circular casing. At no flow a forced symmetrical vortex, maintained by the impeller, produces a uniform pressure around the impeller, line  $AF$ . When flow starts, the gradient line will be below  $AF$  for all capacities. At each capacity, pressure area  $C_1C_2E'E_2$  will balance the area  $A_1'A_2C_1'C_2$  and area  $AA_1'C_1C_1'$  will represent the unbalanced forces directed from  $AC$  toward the  $CE$  portion of the volute (Fig. 7.10).

It is interesting to note that the radial thrust factor  $K$  in formula 7.5 for a volute casing at zero capacity is equal to the thrust factor  $K$  for the circular casing at the best efficiency point. This factor is an index of the volute pressure distribution. The above fact suggests that the pressure distribution at zero capacity in a volute casing is similar to that at the best efficiency point in a circular casing. The impeller is

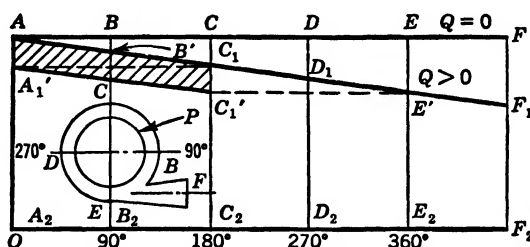


FIG. 7.13. Energy gradient and radial thrust in a circular casing.

discharging approximately uniformly around its periphery. Then the flow in the circular casing can be resolved into two parts, one of which is an active part carrying the impeller discharge out through the nozzle (Fig. 7.14, shaded part). This part will form a volute body of liquid inside the casing. The second or inactive part will be circulated in the casing, filling the remaining portions of the casing sections. This part will also be in the shape of a volute supplementing the first, the section areas increasing in a direction opposite to the first. It is the second part that contributes to the radial force, which in this case is an eccentric forced vortex similar to the one in the volute casing at zero discharge. The active volute body of liquid with constant velocity is similar to that in the volute casing at the best efficiency point, giving no radial forces. Note that Fig. 7.14 shows that the inactive casing areas increase in a direction opposite to that of a volute casing, and thus the radial thrust direction is opposite to that of a volute casing at zero discharge.

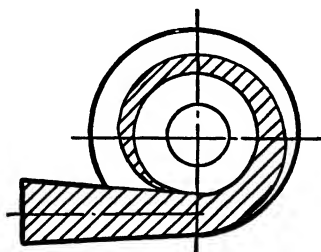


FIG. 7.14. Flow pattern in a circular casing.

In comparing the pressure distribution and radial forces of the volute casing with those of the circular casing it can be concluded that: (1) if the casing sections are steadily increased in area from the cut-water toward the discharge nozzle, but at a lower rate than in a constant velocity volute, the point of zero radial thrust will be at some partial capacity between zero and normal; (2) if casing sections are steadily

increased in area from the cut-water toward the nozzle, so that the velocities are generally decreased (Pfleiderer method of volute design), the point of zero thrust will be at a capacity beyond the normal. In both cases there will be a radial thrust at the best efficiency point. *The constant velocity volute is the only one giving zero radial thrust at or near the best efficiency point.*

#### 7.4 CROSSOVER

In multistage pumps, the channel leading from the discharge volute of one stage to the impeller eye of the next stage is called a crossover. This channel must perform several important functions:

- (1) Convert high velocity energy prevailing in the volute into pressure by reducing the velocity sufficiently to perform the next function with a minimum loss.
- (2) Make a 180-degree turn to direct the flow into the eye of the next impeller. (Depending on the stage arrangement this flow may travel axially through one or more stage spacings.)
- (3) Change the shape of the channel so that it will distribute the flow uniformly around the eye of the next impeller (Fig. 7.15).

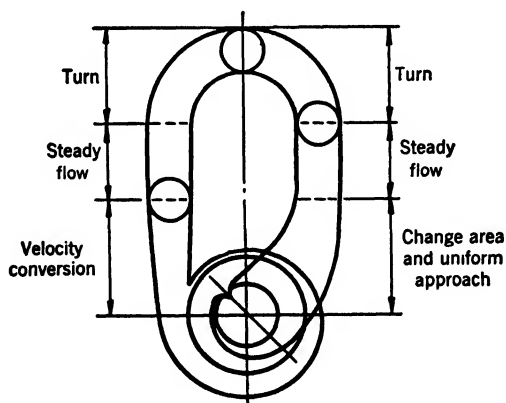


FIG. 7.15. Diagram of a crossover.

For efficient operation, each of these functions should be completed independently or one at a time. Velocity cannot be converted efficiently by diffusing and making a turn simultaneously because, during the turn, higher velocities are shifted to the outer side of the elbow and no conversion will result. Also, while changing the shape of the passage equal areas will not result in uniform velocity if a change in direction of flow is made at the same time. In each plane the diffusion rate must be

kept within permissible limits. When the channel is being shifted from one stage to the other, turns are not in one plane; therefore there will be a spiral motion set up in the flow. A circular section is best suited

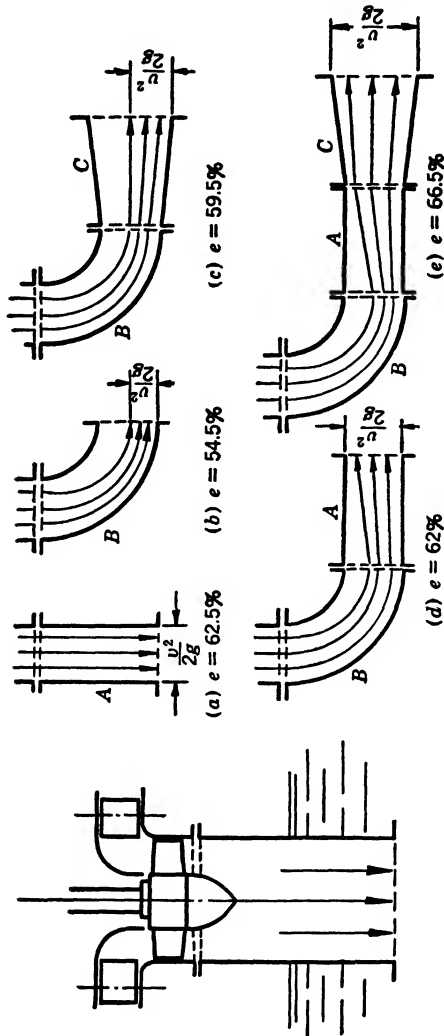


FIG. 7.16. Efficiency of a Kaplan water turbine with different draft tube pieces.

for such turns. Figure 7.15 shows a diagram of an ideal crossover. The immediate approach to the impeller eye is developed in the same manner as the first-stage suction discussed in Art. 7.1.

Kaplan<sup>7</sup> gives a very instructive illustration showing that turning and diffusing cannot be performed efficiently at the same time. He



tested a model of a low head propeller turbine having a  $7\frac{1}{4}$ -in. impeller diameter with different forms of draft tubes. Figure 7.16 shows several of the combinations tried. The efficiency of the model turbine reflects the efficiency of the conversion of velocity head at the discharge, because the rest of the conditions were identical in every set-up. The loss in every case is equal to the velocity head, but in different arrangements only part of the channel is utilized, and high local velocities result. The beneficial effect of a straight piece between the elbow and the diffuser is of particular interest. The friction loss is apparently negligible in all combinations because the longest combination, Fig. 7.16 (e) is the most efficient.

### 7.5 DIFFUSION CASING

A diffusion casing, used mostly in multistage pumps, combines the functions of the volute and of the crossover. The mechanical arrangement of diffusion casings for horizontal pumps differs greatly from that of vertical pumps of the turbine type, and will be discussed separately.

**(a) Horizontal Pumps.** Figures 11.8 and 17.10 show two types of high pressure multistage pumps with diffusion vane casings. Hydraulically both are equivalent, but the first one is assembled in a horizontally split casing whereas the latter is assembled within a cylindrical shell, each stage having a separate casing including the diffuser ring and return passages. The latter design is used for higher pressures.

Selection of diffusion casing areas ( $AB$ , Fig. 7.17) is made in the same manner as for volute pumps. Since the outlet from the impeller is spread all around the periphery, the width of the diffusion ring  $b_3$  cannot be made as wide, in comparison with the impeller, as in the volute casing. Usually  $b_3 = 1.1 \times b_2$ . Limitation in the diffuser ring width imposes several restrictions on the design: (1) only small impeller cuts are possible, otherwise the expanding flow from the impeller will hit the corners of the diffuser ring; (2) an accurate assembly of the rotor, and rotor setting in the casing, is required to match the impeller passage with those of the diffusion rings; (3) only a small gap is allowed between the diffusion vanes and the impeller and, for better performance, accurate tapering of both impeller vane ends and diffusion vane tips are necessary for quiet operation.

The diffusion vane angle  $\alpha_3$  is selected from the same consideration as the volute angle  $\alpha_v$ , but experience has shown that the area of the diffusion ring is of much greater importance than the angle. The diffusion ring depth  $D_4 - D_3$  is an important factor in developing a satisfactory conversion of velocities which should be completed before a turn is made into the eye of the impeller of the next stage. A larger ring

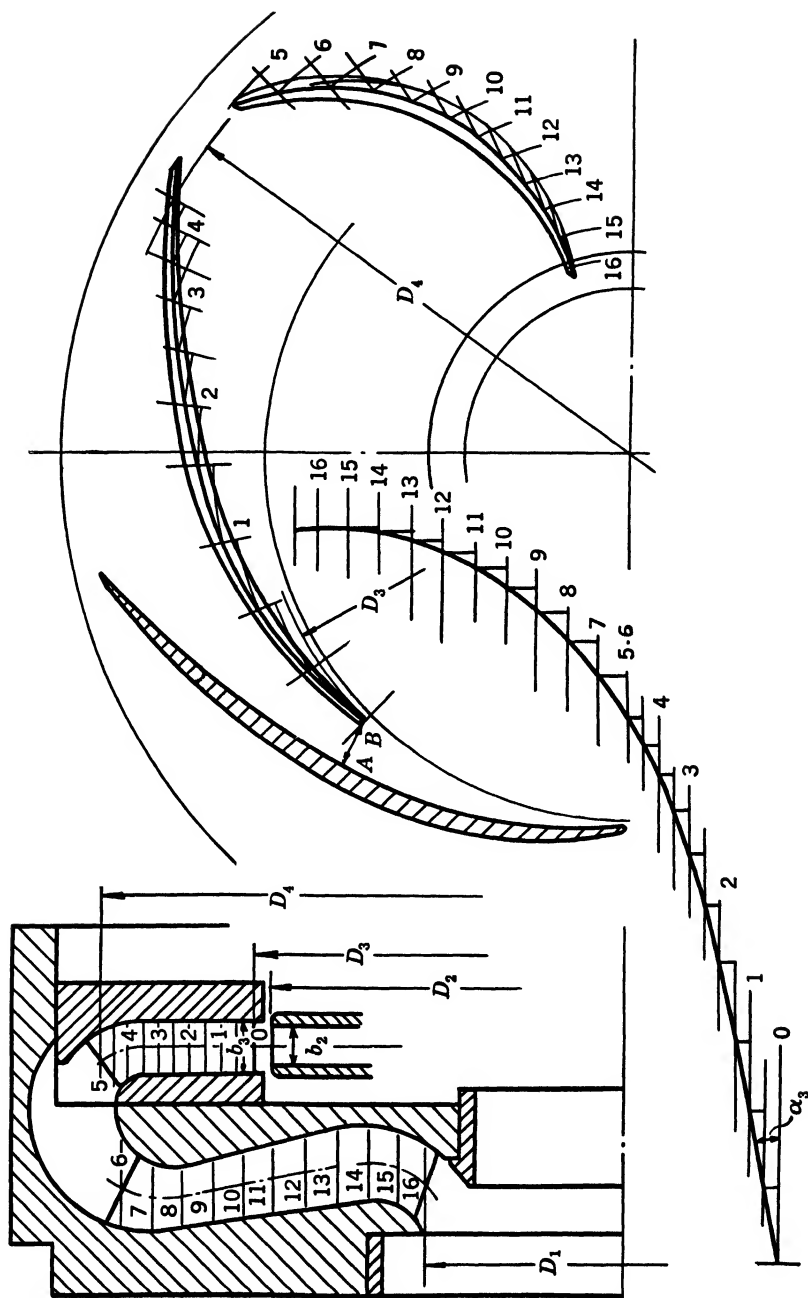


Fig. 7.17. Diffusion and return vanes layout.

means a larger casing. As a rule a spacious casing is more efficient, but in the outer barrel design, in order to reduce the cost of the barrel, some efficiency is sacrificed for a more compact design. The ratio of  $D_4/D_2$  varies from 1.25 to 1.50. A greater number of diffusion vanes is used with the lower ratio  $D_4/D_2$ . The number of vanes is selected from the following considerations. (1) The number of vanes should have no common factor with the number of vanes of the impeller; for example 8 diffuser vanes, 7 impeller vanes, or 9 diffuser vanes, 8 impeller vanes. But with good tapering of vanes the consideration is not important. (2) A greater number of vanes gives a better diffuser channel with greater overlapping of vanes, but increases the friction loss and cost of vane polishing. (3) The most favorable shape of the channel at  $D_3$  is a square; therefore vane number, ring radial depth and vane angle  $\alpha_3$  ought to be adjusted to get that form of vane opening.

The vane layout is prepared better by using the "error triangle" method (Chapter 6), putting part of the vane in the ring and the remainder into the return channels. After the shape of the vanes is drawn it is sometimes possible to duplicate the curve, plotted point by point, with one or two sections of circular arcs by trial. The profile of the return passage is laid out, the precautions given for the crossover design being observed. As a rule wide stage spacing results in a more efficient diffusion casing. This has been fully demonstrated in the design and performance of vertical turbine pumps.

**(b) Radial Forces with Diffusion Casings.** In horizontal pumps of this type, radial forces may appear in the following cases. (1) The first-

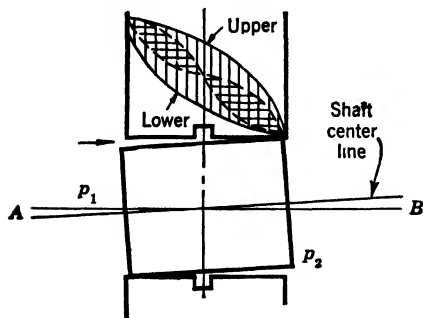


Fig. 7.18. Radial forces on the balancing drum due to uneven radial clearance.

stage impeller may experience radial forces as a result of uneven head generation by the impeller caused by an unsymmetrical suction approach. (2) Any eccentricity between the diffusion ring and the impeller will result in radial unbalanced forces. (3) The majority of multistage high pressure pumps have long balancing drums on the high pressure end to eliminate the axial thrust.

Because of the shaft deflection the flow through the clearance around the drum is not uniform, and an uneven pressure distribution results. As a result, radial force appears, as shown on the diagram in Fig. 7.18. In the upper part of the clearance space the pressure drop will follow the upper curve, and on the lower half it will be as shown by the lower curve. The area enclosed

between the two will indicate the unbalanced forces directed downward. This is greatly reduced if an equalizing groove is cut either on the drum or in the stationary piece. Then the unbalanced area, shown by horizontal cross-hatching, is greatly reduced.

(c) **Diffusion Casing of Vertical Turbine Pumps.** To this class belong all vertical pumps of a wide range of specific speeds (1000 to

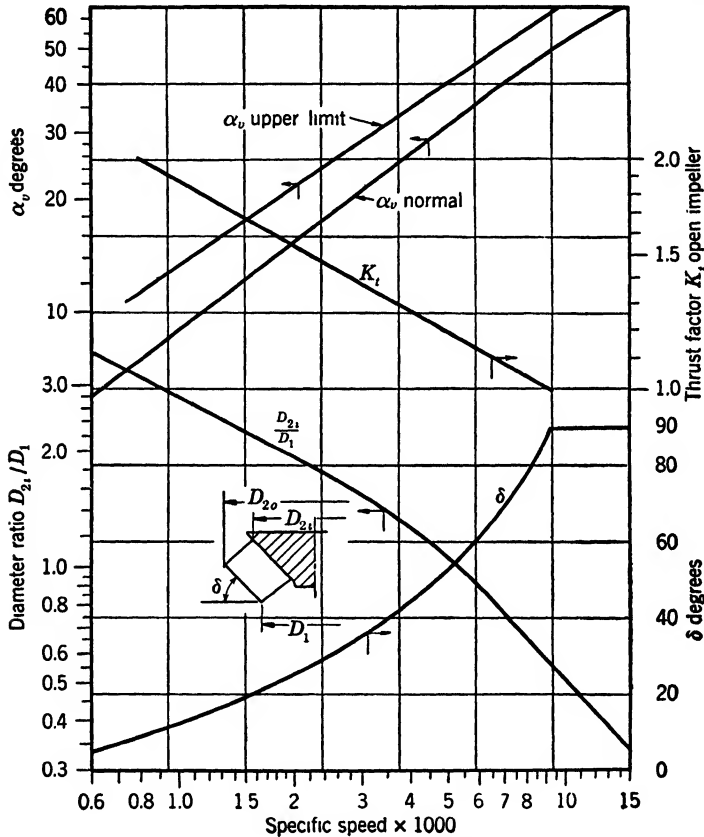


FIG. 7.19. Vertical turbine pump constants.

15,000). In smaller sizes and in low and medium specific speeds (1500 to 4500), these pumps have been used mostly on irrigation projects in West Coast states for pumping from drilled wells. They have been perfected to a high degree and at the present represent the most efficient type of multistage centrifugal pump. Laboratory pump efficiencies up to 90 per cent for 1200-g.p.m. pumps at 1760 r.p.m. are on the record. Several factors contributed to this progress: (1) selection of favorable specific speeds of 2500 to 4000, not used in any other multistage pumps;

(2) use of open impellers, which reduce the disk friction loss and permit better cleaning and polishing of the impeller vanes; (3) improved hydraulic design of the casing with a liberal stage spacing; (4) keen competition of a score of companies, simple, cheap patterns, and large sales volume, which permit continuous improvements and change in design; (5) owing to the stage arrangement, absence of (a) interstage leakage, (b) leakage for balancing devices, as hydraulic thrust is taken up by the motor thrust bearing, (c) high pressure stuffing boxes in open shaft designs.

Hydraulically, the casing design involves several features resulting from the vertical arrangement: (a) the diffusion vanes are arranged more in an axial direction; (b) the diffusion vanes are developed in one piece and without sharp turns (Fig. 16.27), thus allowing more space between the impeller and the diffusion vanes; (c) it is possible to use impellers of different diameters and widths. With increasing specific speed the impeller profile gradually changes from a straight radial to a conical mixed flow, and finally to a straight axial flow (Fig. 7.19).

Selection of diffusion vane angles and velocities follows the same guiding considerations. Much higher velocities through the diffuser are possible with vertical pumps than with volute pumps of the same specific speed, particularly in the high specific speed range, because all turns are gradual and in axial and mixed flow types little or no turns in the meridional velocities are present.

In order to obtain a maximum capacity for a given diameter of pump casing, considerably higher diffusion vane angles  $\alpha_v$  are used in vertical turbine pumps than in horizontal volute pumps.

Figure 7.19 gives limits of  $\alpha_v$  values for turbine pumps.

## REFERENCES

1. R. W. ALLEN, "Some Experiences of the Use of Scale Models in General Engineering, *Engineering*, Sept. 9, 1938, p. 313.
2. H. KRANZ, "Stromung in Spiralgehäusen," *Verein deutscher Ingenieure, Bulletin* 370, 1935.
3. C. PFLEIDERER, *Die Kreiselpumpen*, Berlin, Julius Springer, 1932, p. 161.
4. BATTELLE MEMORIAL INSTITUTE, *Prevention of the Failure of Metals under Repeated Stress*, New York, John Wiley & Sons, 1941, p. 44.
5. R. T. KNAPP, "Centrifugal Pump Performance as Affected by Design Features," *Trans. A.S.M.E.*, Vol. 63, No. 3, April, 1941, p. 254.
6. R. C. BINDER and R. T. KNAPP, "Experimental Determination of the Flow Characteristics in the Volute of Centrifugal Pumps, *Trans. A.S.M.E.*, Vol. 58, No. 8, Nov. 1936, p. 659.
7. VICTOR KAPLAN and ALFRED LECHNER, *Theorie und Bau von Turbinen-Schnellläufern*, Munich, R. Oldenbourg, 1931, p. 219.

## CHAPTER 8

### AXIAL FLOW PUMPS

In studying and following up the development of straight axial flow pumps, it is very profitable for a centrifugal pump engineer to be familiar with the progress in the two related fields: axial flow water turbines of the Kaplan type and axial blowers. In these fields trends of theoretical thought and practical design have very much in common with axial flow pumps, and several references will be made in this chapter to water turbine and axial blower experience to illustrate some points when similar pump examples are not available. Test results on water turbine or axial blowers are not always directly applicable to axial pumps, but their educational value should not be overlooked.

#### 8.1 RANGE OF SPECIFIC SPEEDS

The useful range of specific speeds covered by axial flow pumps extends from 10,000 to 15,000. Axial flow pumps having specific speeds lower than 10,000 have been designed but they cannot compete with mixed flow impeller design in efficiency.<sup>1</sup> Besides they lead to very high values of shut-off brake horsepower and undesirable cavitation characteristics. Specific speeds above 15,000 are possible but the peak efficiency will not be higher than that of pumps with a specific speed of 15,000 operating at capacities above the normal. Axial flow air blowers are designed for specific speeds as low as 5000, but they are built as multistage units to obtain a maximum possible pressure to compete with centrifugal compressors in price, size, and efficiency. Multistage axial flow pumps, however, would not be commercially valuable.

Axial flow Kaplan water turbines of specific speeds below 10,000 are built to utilize the adjustable impeller vane feature possible with a cylindrical impeller hub. It is possible that axial flow pumps with adjustable impeller vanes will find a wider application in the future. Then their range may be extended to higher heads and lower specific speeds.

#### 8.2 FACTORS AFFECTING SPECIFIC SPEED

Variation of specific speed within the above range is obtained by a suitable combination of several elements of design; and the selection of these elements for optimum peak efficiency and the best shape of

head-capacity and efficiency curves depends on the skill of the designer. These elements of design will now be considered at some detail.

✱ (a) **Impeller Hub Ratio.** The ratio of the impeller hub diameter to the impeller outside diameter is directly connected with the specific speed of axial flow pumps. This ratio is established experimentally. Higher specific speed pumps have smaller hubs, which give a greater

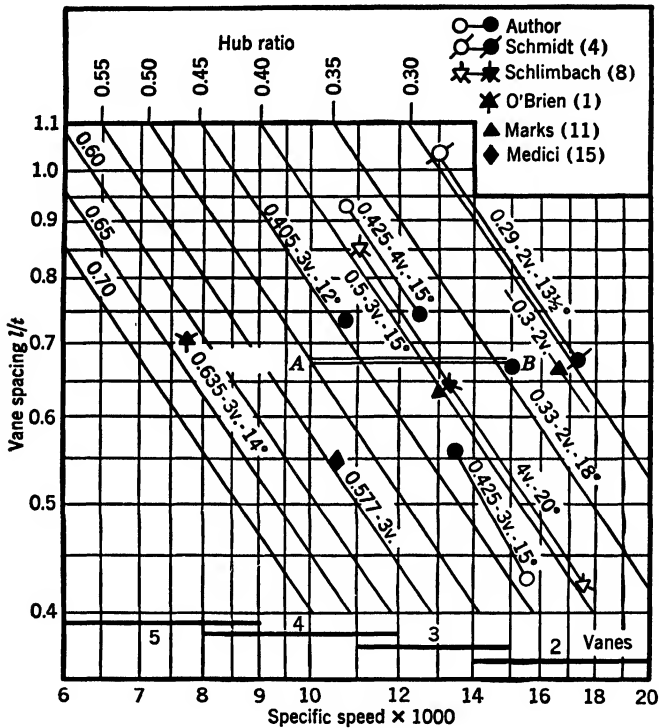


FIG. 8.1. Hub ratio, number of vanes, and  $l/t$  ratio for axial flow pumps.

free area for the flow and a smaller diameter to the average streamline, resulting in a greater capacity and a lower head. Figure 8.1 gives hub ratios for various specific speeds compiled from a number of modern axial flow pumps and blowers. Note that the ratio  $D_{2i}/D_1$  (in Fig. 7.19) becomes the hub ratio for axial flow pumps above  $n_s = 9350$ . This is shown in Fig. 8.1 by the line  $AB$  and can be used as a guide. The scatter of the points contributed by the author resulted from the attempt to use several impellers in the same pump casing. When more than one point is shown at the same hub ratio a black mark indicates the better point of this group.

**(b) Vane Area.** The vane area or vane length is one of the important factors affecting the head and the specific speed of axial flow pumps. The ratio of the vane area (true area, not a plan view) to the free area between the casing outer wall and the hub is referred to as solidity.<sup>2</sup> However, the ratio  $l/t$  of the vane length  $l$  to the vane spacing  $t = \pi D/z$ , where  $z$  is the number of vanes and  $D$  is the diameter of the vane section (Fig. 8.2), is used more frequently for the same purpose. The latter factor may serve as a characteristic of the vane profile at any radius, while solidity is a characteristic of the whole vane. For axial flow pumps of specific speeds of 10,000 and higher, the ratio  $l/t$  is less than unity.

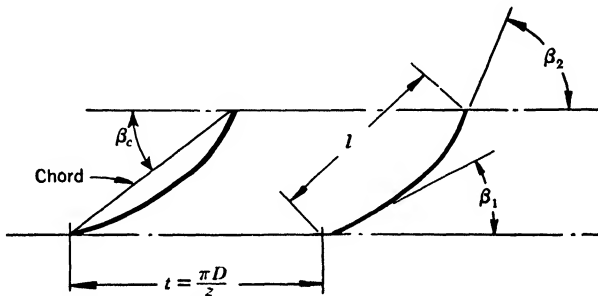


FIG. 8.2. Vane spacing  $l/t$  and vane angles.

For impellers cast in one piece, non-overlapping vanes are mostly used, as they require a very simple molding procedure without any core work. The ratio  $l/t$  varies along the radius, increasing toward the hub. This increase in  $l/t$  at the hub is desirable for mechanical reasons.

Figure 8.1 shows values of the  $l/t$  ratio for the section at the periphery of the impeller for various hub ratios. The value of  $l/t$  at the hub is 1.25 to 1.30 times that at the outside diameter of the impeller, depending on the hub ratios. Higher  $l/t$  ratios at hub have been used but are less suitable for the adjustable vane design, and may complicate the molding method for a one-piece casting.<sup>15</sup> It is possible to obtain the same values of  $l/t$  with a different number of vanes. The actual hub ratios, number of vanes, and the chord angle of the periphery are marked for each point on Fig. 8.1.

**(c) Number of Vanes.** Basing his opinion on the extensive tests with hydraulic turbines, Kaplan<sup>3</sup> has found that for a given wetted area of the vane ( $l/t$ ) the number of vanes should be a minimum. This was also confirmed by Schmidt's tests<sup>4</sup> which showed that a two-vane impeller is most efficient with a projected vane area of about 63 per cent. Figure 8.3 is reproduced from Schmidt's results. For a given vane curvature,  $\beta_2 - \beta_1$ , there is a definite vane length, or  $l/t$  ratio, which



will perform the water deflection most efficiently. Extending the vane beyond this would only increase the friction loss and add nothing to the head produced.

It has been found that for low specific speed pumps, 3, 4, or even 5 vanes may be necessary to apply power to water efficiently. With two vanes the difference between the maximum and minimum local pressures and velocities becomes too great. Adding extra vanes results in a more uniform power application and pressure and velocity distribution. A greater number of vanes also has a beneficial effect upon the cavitation characteristics of the impeller. Figure 8.1 also indicates the

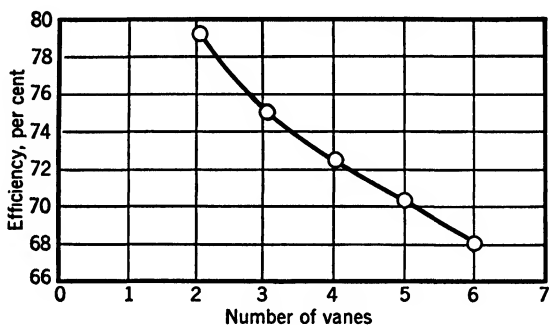


FIG. 8.3. Pump efficiency with different number of vanes and the projected vane area of 63 per cent (Schmidt).

number of vanes for different specific speed ranges. In water turbines of the Kaplan type, the maximum number of vanes employed experimentally was 8 at a specific speed of about 6000<sup>5,6</sup> and heads over 150 ft.

**(d) Vane Characteristics; Airfoils.** To describe the vane curvature and vane angle variation at various radii, the following terms are used: For a very thin vane of uniform thickness,

$\beta_1$  is the entrance angle.

$\beta_2$  is the discharge angle (Fig. 8.2). The line joining ends of vane  $AB$  is called a chord.

$\beta_c$  is the chord angle.

All angles are measured from the direction of peripheral velocity. The maximum distance from the chord to the vane is called camber and is usually expressed in per cent of the chord length (Fig. 8.4). If the vane thickness is varied and the vane is streamlined to the extreme by making the entrance edge heavy and the discharge end sharp, the

camber is referred to the mean line. The maximum vane thickness  $2y_t$  is also expressed in per cent of the chord length. Such streamlined airfoil profiles are classified by the N.A.C.A.\* according to the camber and vane thickness. Each profile is assigned a four-digit number such as 4312, the first digit 4 indicating the camber of the mean line in per cent of the chord and the second the location of the camber from the leading edge in tenths of the chord length. The last two digits indicate the vane thickness in per cent of the chord. *All good airfoil sections have nearly the same thickness variation along the line, the maximum thickness being different for different profiles.*

The *angle of attack* is the acute angle between the vane chord of the section and the direction of the relative velocity of the flow. The *aspect*

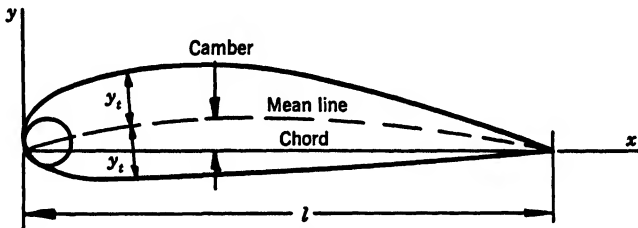


FIG. 8.4. Airfoil nomenclature.

*ratio* is the ratio of the length of the airfoil span to the length of the chord of the section. All N.A.C.A. sections were tested with an aspect ratio of 6:1, but results were also recalculated for an infinite aspect ratio. Since, in a pump, liquid cannot escape along the sides and is confined by the hub and casing side walls, the data for infinite aspect ratio are used for the selection of the vane sections for impellers. When a number of identical airfoils are arranged in a row or a cascade, the ratio of the chord length to the vane spacing  $l/t$  is an important characteristic. In a pump, if the vanes are sectioned by a cylinder, the development of the latter will give a vane cascade or a lattice. *To apply power to liquid efficiently, the vane angle should increase from the inlet to the outlet, otherwise all the deflection of the water path will occur at the inlet portion of the vane, the discharge end contributing nothing to the head except for increasing the friction loss.*

**(e) Vane Curvature.** The vane curvature can be expressed as  $\beta_2 - \beta_1$ , the difference in the vane discharge and entrance angles. The angles are taken for the mean camber line. Evidently if  $\beta_2 - \beta_1$  has a higher value, a higher camber of the vane results. If vane sections are selected from the N.A.C.A. airfoil profiles, the camber is given

\* National Advisory Committee for Aeronautics, Report 460, 1935.

rather than angle  $\beta_2$  or  $\beta_1$ . Equation 8.13 gives vane curvature  $\beta_2 - \beta_1$  in terms of the camber and its location. *The vane thickness does not change the vane curvature or camber and has no immediate effect on the head produced by the vane.*

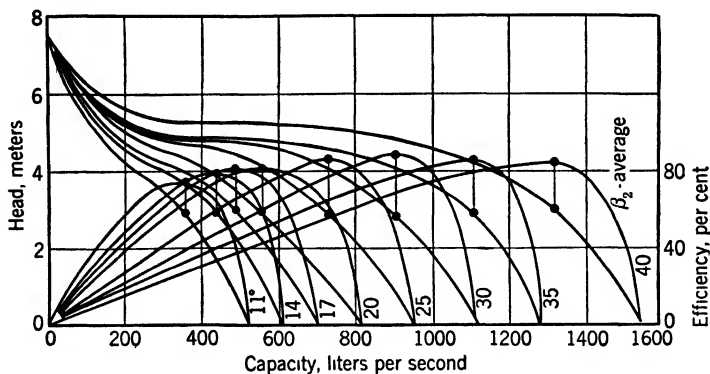


FIG. 8.5. Performance 4-vane impeller, 500-mm. diameter, at different vane angles, 650 r.p.m. (Schlmbach).

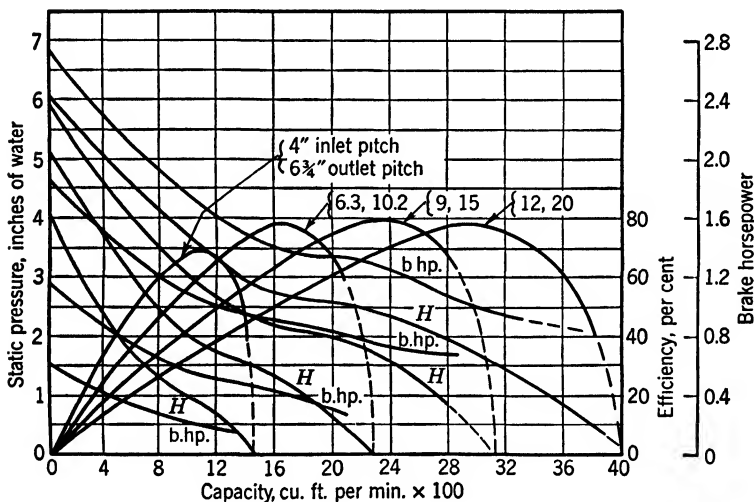


FIG. 8.6. Performance of 4 impellers each of 63.5 per cent projected area and pitch ratio 1.67, 4000 r.p.m., 12-in. diameter, pumping air (Schmidt).

The usable vane curvature is closely related to the number of vanes. With larger  $l/t$  ratios, a greater deflection of the liquid is possible since  $\beta_2 - \beta_1$  can also be increased. It has been found experimentally by several investigators,<sup>8</sup> including the author, that *if the vane is turned*

as a whole in the hub or all vane angles are increased by the same amount the head at the b.e.p. stays approximately the same, indicating that  $\beta_2 - \beta_1$  is a criterion of the head produced.†

When all the vanes are turned through the same angle, the capacity increases approximately directly as the inlet pitch, or  $\beta_1$ . Figure 8.5 is reproduced from Schlimbach's<sup>8</sup> paper to illustrate this point. Figure 8.6 shows Schmidt's<sup>4</sup> results for impeller vanes of the same projected area; the vane angles varied so that a pitch ratio  $\tan \beta_2 / \tan \beta_1 = 1.67$  was maintained. The capacity increased as  $\tan \beta_1$ ; the head also increased because  $\beta_2 - \beta_1$  was increased even though  $\tan \beta_2 / \tan \beta_1$  was kept constant.

Good efficiency is possible for a wide variation of vane angles; thus, the selection of the vane setting (chord angle  $\beta_c$ ) is not a deciding factor, but the vane curvature  $\beta_2 - \beta_1$  is.

(f) **Vane Twist.** This expression is frequently used to denote the difference between the chord angles at the hub and at the periphery of the impellers.

$$\beta_{ch} - \beta_{co} = \text{vane twist} \quad (8.1)$$

Since vane curvature and performance may vary greatly for the same chord angle the vane twist is not a deciding factor. The vane curvature  $\beta_2 - \beta_1$  determines the hydraulic characteristics of a vane section. The ratio of the vane curvature at the hub to that at the periphery varies within a narrow range.

$$\frac{\beta_{2h} - \beta_{1h}}{\beta_{2o} - \beta_{1o}} = 1.85 \text{ to } 2.2 \quad (8.2)$$

The terms and ratios presented here are only means of describing the individual vane profiles and their arrangement along the radius. But actual determination of vane angles for several radii follows from Euler's velocity triangles as outlined in Chapter 4.

### 8.3 SUMMARY OF TEST RESULTS

The effect of various design elements upon the pump performance has been established almost entirely by experiment. In every case the theory indicates the general direction of variation of the head capacity or the efficiency of the pump, but quantitative connection between the variables involved is furnished by tests.

† Using airfoil terminology,  $\beta_2 - \beta_1$  fixes the vane profile camber and its location and, hence, its hydrodynamic properties as described later in this chapter, Fig. 8.16.

(a) **Number of Vanes.** Figure 8.7 shows a test of a pump with identical vanes numbered from 2 to 5. Note that

(1) The capacities at normal and zero head are the same for the several impellers. This is determined mainly by the vane entrance angle.

(2) The heads increase with the number of vanes. This is entirely due to the increase in the  $l/t$  ratio.

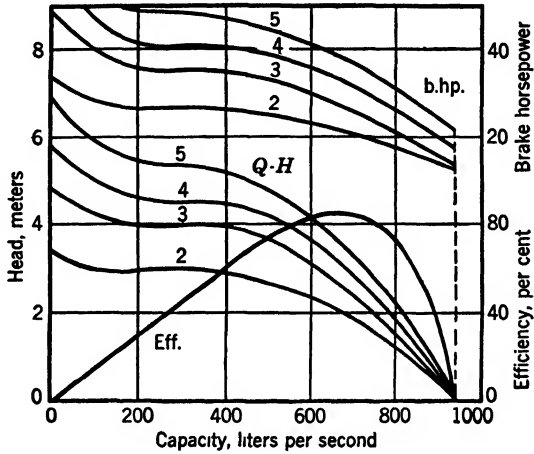


FIG. 8.7. Effect of number of vanes on performance (Schlimbach).

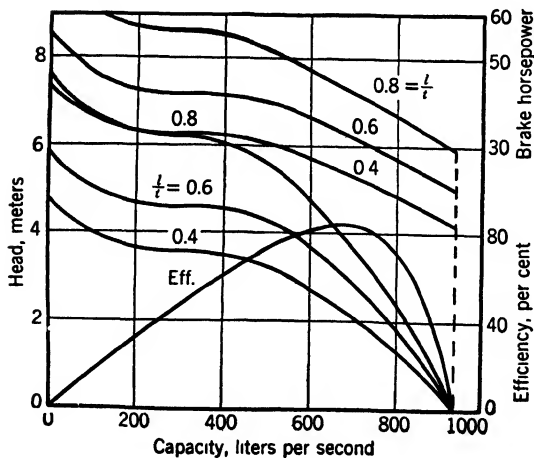


FIG. 8.8. Effect of  $l/t$  on performance; 730 r.p.m.;  $\beta_2 = 20^\circ$  average (Schlimbach).

With heavy vanes and a low chord angle, the maximum number of vanes is almost fixed since adding vanes will restrict the free area of the flow. The normal capacity will decrease and efficiency will drop. In one example a good performance was obtained with 3 and 4 vanes only. With 2 vanes, the ratio  $l/t$  was too low for good efficiency and with 5 vanes both head capacity and efficiency dropped. (Schmidt has shown that the minimum projected area for two vanes is 63 per cent.)

**(b) Chord-Vane Spacing Ratio.** Figure 8.8 shows tests of 3 impellers having 4 vanes each, but with  $l/t$  ratios of 0.4, 0.6, and 0.8. The curves are similar to the ones shown in Fig. 8.7, as in both cases  $l/t$  was varied.

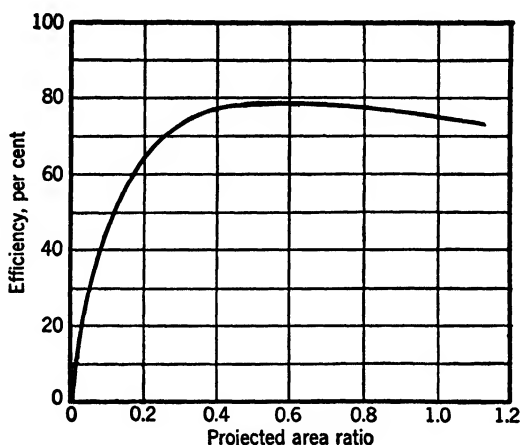


FIG. 8.9. Effect of the projected area on the impeller efficiency (Schmidt).

Figure 8.9 shows results of Schmidt's tests for 2-vane impellers of the same inlet and outlet angles and of different projected area. Note that there is an optimum vane area, on both sides of which the efficiency drops. This is to be expected, although it does not appear on Schlimbach's tests<sup>8</sup> (Fig. 8.8).

**(c) Adjustable Vanes.** Figure 8.5 shows the performance of a 4-vane impeller with different vane settings. The points of interest are:

- (1) The shut-off head is the same for all vane settings.
- (2) The normal head is essentially the same, since  $\beta_2 - \beta_1$  is constant although the pitch ratio varies.
- (3) There is an optimum vane setting, but the efficiency remains good, within one point from optimum, for 10 degrees of vane turn.
- (4) The specific speed increases with higher vane angles, because the normal capacity increases the head remaining the same.

(5) Since turning the vane through a few degrees (not over  $\pm 5$  degrees) does not change the head and affects the efficiency only slightly, it would appear that vane twist should not affect the head or efficiency appreciably, as any twist can be considered as turning several portions of vane through different degrees. A different angular velocity of the absolute flow at discharge will result and a different type of vortex will be produced, which will be stable, as outlined in Art. 1.7, Chapter 1.

(d) **Effect of Camber.** A greater difference in  $\beta_2 - \beta_1$  means a more curved vane and higher camber. Tests show that for the same entrance

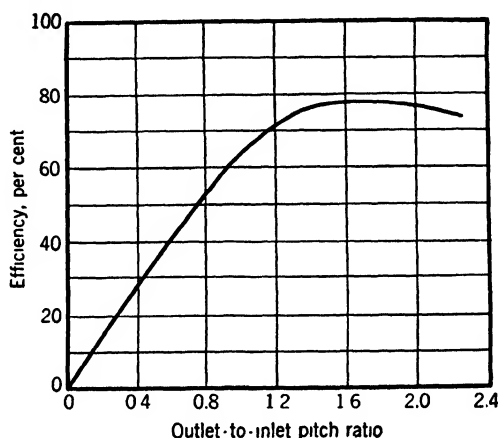


FIG. 8.10. Effect of vane curvature on impeller efficiency; 2 vanes, 63 per cent projected area, entrance angle  $\beta_1 = 9^\circ$ . Outlet-to-inlet pitch ratio  $= \tan \beta_2 / \tan \beta_1$ .

angle, if the discharge angle is increased, both the head and the capacity increase, as they do in centrifugal pumps, and the specific speed decreases. For two vanes with 63 per cent projected area, the best efficiency is obtained at a pitch ratio,  $\tan \beta_2 / \tan \beta_1$ , of about 1.70. It decreases rapidly, however, for lower ratios and rather slowly at a higher pitch ratio (Fig. 8.10).

(e) **Number of Vanes for Same  $l/t$ .** Schmidt has shown by means of tests of impellers with thin vanes, all having an  $l/t$  ratio of 0.66 and the same pitch ratio— $\tan \beta_2 / \tan \beta_1 = 1.67$ —that the head and capacity remain essentially the same, and efficiency is maximum with 2 vanes (Fig. 8.3). This is true for a pump of  $n_s = 16,000$ . For lower specific speeds 3, 4, or 5 vanes give better performance.

(f) **Vane Thickness.** Tests of an airblower by Eckert,<sup>17</sup> reproduced in Fig. 8.11, show that a *thin vane* and an *airfoil vane* with the same mean camber line and vane twist perform identically as far as the head-capacity

and efficiency are concerned. A similar conclusion was reached by several investigators of pumps who are quoted later in this chapter. Thus the advantages of airfoil sections lie in the fact that they permit the desired mechanical strength with a minimum sacrifice of efficiency.†

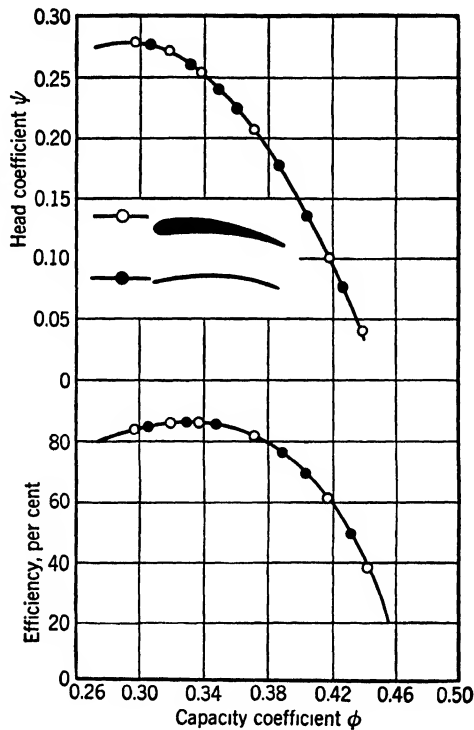


FIG. 8.11. Performance of a thin vane and an airfoil (Eckert).

(g) **Ratios of Brake Horsepower and Head at Zero Capacity to Those at Best Efficiency Point.** Steep head capacity curves and brake-horsepower curves rising toward zero capacity are characteristic of all axial flow pumps. Variation of design elements affect these ratios very little.

(1) Increasing the number of vanes from 2 to 5 (Fig. 8.7) increased the head ratio from 1.85 to 1.97 and the brake-horsepower ratio from 1.62 to 1.90.

† N.A.C.A. Report 460 makes a very clear statement to that effect on p. 3: "The thickness form is of particular importance from a structural standpoint. On the other hand, the form of the mean line determines almost independently some of the most important aerodynamic properties of the airfoil section."



(2) Changing  $l/t$  from 0.4 to 0.8 with 4 vanes changed the head ratio from 2.2 to 1.93 and the brake-horsepower ratio from 1.9 to 1.7 (Fig. 8.8).

(3) Turning the vane from an average angle of  $25^\circ$  to  $41^\circ$  did not change the head ratio as the shut-off head and head at the best efficiency point stayed approximately the same. The brake-horsepower ratio is about 2.30 for all vane settings (Fig. 8.5).

(4) Changing the number of vanes while keeping the vane projected area constant did not change the shut-off head ratio or the brake-horsepower ratio (Schmidt tests).

(5) Increasing the vane curvature  $\beta_2 - \beta_1$ , pitch ratios from 1.0 to 2.0, decreased the brake-horsepower ratio from 3.4 to 2.5 (Schmidt tests).

#### 8.4 DESIGN PROCEDURE FOR AN AXIAL FLOW IMPELLER

From the preceding discussion it follows that previous experience and experimental data based on successful designs are essential for the impeller design of axial flow pumps. A knowledge of the theory of impeller vane action and the relationship among several design elements is essential in the selection of the design constants necessary to achieve the desired performance with best possible efficiency. The design procedure involves the following steps.

(1) To meet a given set of head-capacity requirements, the speed (r.p.m.) is selected; thus the specific speed of the impeller is fixed. Due consideration should be given to the head range the proposed pump should cover in future applications under the most adverse suction conditions.

(2) For the specific speed thus obtained, the hub ratio and vane spacing  $l/t$  are selected, Fig. 8.1 being used as a guide. The number of vanes is assumed at the same time.

(3) The speed constant and the capacity constants are chosen next. The chart in Fig. 5.9 gives these constants for an average impeller discharge angle of approximately  $22\frac{1}{2}^\circ$ . For values at different discharge angles the diagram in Fig. 9.16 can be used (see Chapter 9). These constants having been established, the meridional velocity and impeller diameter can be calculated and the impeller profile can be drawn.

(4) The impeller vane profiles, both vane curvature and vane twist, are drawn after the entrance and discharge vane angles for several streamlines are established from Euler's entrance and exit velocity triangles. Chapter 4 gives guiding principles for the drawing of these triangles. The diagram in Fig. 9.16, in Chapter 9, establishes the im-

PELLING RATIOS IN TERMS OF SPECIFIC SPEED. In drawing the vane profiles for several streamlines, airfoil shapes are good examples to follow, but the vane thickness should be kept to a minimum consistent with the vane mechanical strength and good foundry practice.

The design procedure as outlined is applicable to mixed flow and radial impellers. When used for extreme mixed flow and axial flow impeller design, Euler's entrance and exit velocity triangles determine completely the impeller vane profile sections for all radii. The impelling ratio becomes an all-important factor in constructing Euler's velocity triangles for high specific speed impellers. For radial flow and mixed flow impellers having the same vane discharge angle for several streamlines the impelling ratio is of secondary importance, as the discharge vane angle can be selected on the basis of other considerations.

### 8.5 USE OF AIRFOIL DATA FOR IMPELLER DESIGN

A lack of reliable test and design data on axial flow pumps in the early stage of development is responsible for the attempts of several investigators to make use of the extensive test data on airplane airfoil profiles for axial pump design. The *airfoil theory* of axial flow pumps establishes a connection between the lift coefficients of airfoil test data and the pump head. The design procedure itself consists of the selection of suitable airfoil profiles for several radii of the pump impeller and the determination of the vane chord angles at the respective radii. A constant head for several streamlines is usually assumed in this method even though other assumptions are possible. The other impeller design elements, as (1) hub ratio, (2)  $l/t$  ratio for several radii, (3) revolutions per minute or specific speed, (4) axial velocity, and (5) impeller diameter, are selected from data based on previous experience. There is nothing in the airfoil theory to help or guide in making such selections. Thus the impeller design is still entirely experimental, airfoil experimental data being used for selecting vane curvature only. Evidently, as soon as sufficient data are accumulated on good axial flow pumps, the airfoil theory will become a matter of academic interest only.

**(a) Airfoil Properties.** Knowledge of airfoil properties is helpful in discussing the impeller vane profiles of axial flow pumps. A great many airfoil sections have been tested in several countries for the last twenty-five years in order to determine the airfoil profile which, when applied to airplane wing design, will support a maximum load with a minimum expenditure of power. In N.A.C.A. Report 460, all useful airfoil sections have been classified according to their curvature and thickness.

For this purpose airfoil profiles are considered as made up of certain profile thickness forms disposed about certain mean lines. *The form of the mean line determines completely most of the important hydraulic properties of the airfoil profile, whereas thickness is dictated by the structural or mechanical requirements. The same thickness variation along the mean line was used for the whole family of these airfoils.*

**(b) Lift and Drag; Gliding Angle.** If an airfoil is exposed to an air flow, the forces acting upon it can be resolved into two components: one,  $L$  normal to the direction of the approaching undisturbed flow

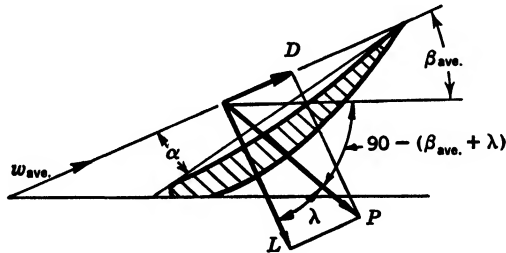


FIG. 8.12. Forces acting on an airfoil.

which is called the lift, and the other, component  $D$  in the direction of the air flow which is called resistance or the drag (Fig. 8.12). The magnitude of these forces can be represented with the following formulas.

$$L = C_L b l \rho \frac{w_{ave.}^2}{2} \quad (8.3)$$

and

$$D = C_D b l \rho \frac{w_{ave.}^2}{2} \quad (8.4)$$

where  $C_L$  and  $C_D$  are experimental coefficients of lift and drag

$b$  is the width of the airfoil

$l$  is the length of the chord of the airfoil

$w_{ave.}$  is the undisturbed relative air velocity

$\rho$  is the density of the fluid.

Both  $C_L$  and  $C_D$  depend on the profile of the airfoil, the angle of attack  $\alpha$ , and the aspect ratio. Their values have been experimentally deter-

§ In the early German tests of airfoils (Göttingen University 1920, N.A.C.A. Report 315) the aerodynamic properties of airfoils were connected with the vane thickness (measured above the chord drawn tangent to the under side of the airfoil) rather than the camber of the mean line. This resulted in an erroneous impression that the vane thickness was an important factor contributing to the lift and vane efficiency. The same method is still used by the ship propeller designers.<sup>18</sup>

mined for a great number of profiles of airfoils.  $C_D$  is very small in comparison with  $C_L$ . The ratio  $C_D/C_L$  defines  $\lambda$  which is called the gliding angle. At this angle an airplane can perform a steady gliding flight. The drag force  $D$  includes (1) the skin friction, which depends greatly on the smoothness of the surface and (2) losses due to eddies in the wake behind the wing. This part of the drag is greater for thick profiles. A well-rounded front nose and a sharp tail edge reduce this part of the drag.

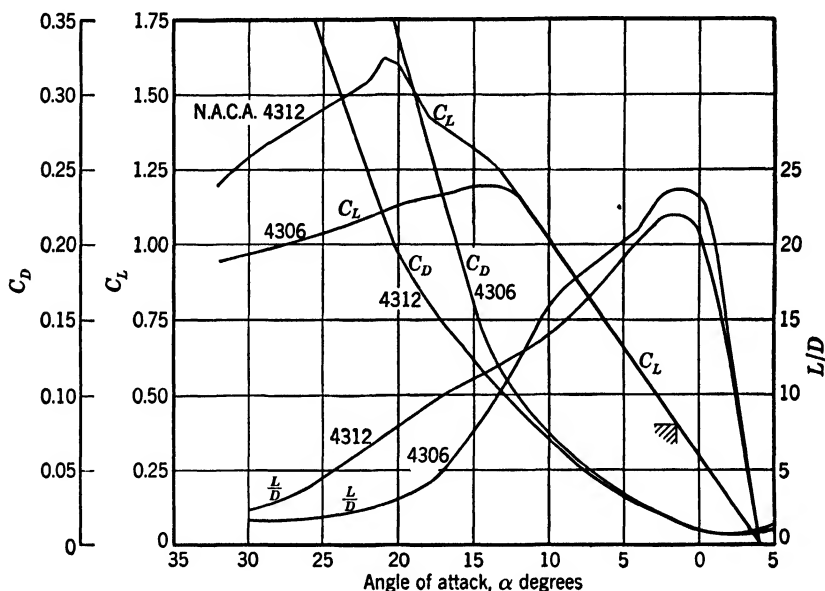


FIG. 8.13. Effect of vane thickness on airfoil performance (N.A.C.A. Report 460).

Figure 8.13 shows performance of airfoils 4306 and 4312 replotted from N.A.C.A. Report 460 to show the effect of the airfoil thickness upon the lift and drag coefficient  $C_L$  and  $C_D$  respectively. For the useful range,  $C_L$  is identical for both airfoils. The ratio  $L/D$  serves as an index of the airfoil efficiency. This is better for a thin airfoil. The maximum value of the lift coefficient  $C_L$  is obtained with 12 per cent airfoil thickness. Airfoils 4315, 4318, and 4321 have a lower maximum lift.

For this plot the scale for the angle of attack  $\alpha$  was deliberately reversed from that of Report 460 to show the resemblance of the  $C_L$  vs.  $\alpha$  curve to the ordinary head-capacity curve of axial flow pumps,  $C_L$  standing for head, the angle of attack  $\alpha$  for capacity, and the ratio  $L/D$  representing efficiency.

Figure 8.14, plotted in the same manner, shows the effect of the vane camber. Higher lifts at a lower angle of attack are obtained with 6 per cent camber than with 2 per cent camber at the optimum  $L/D$  ratio.

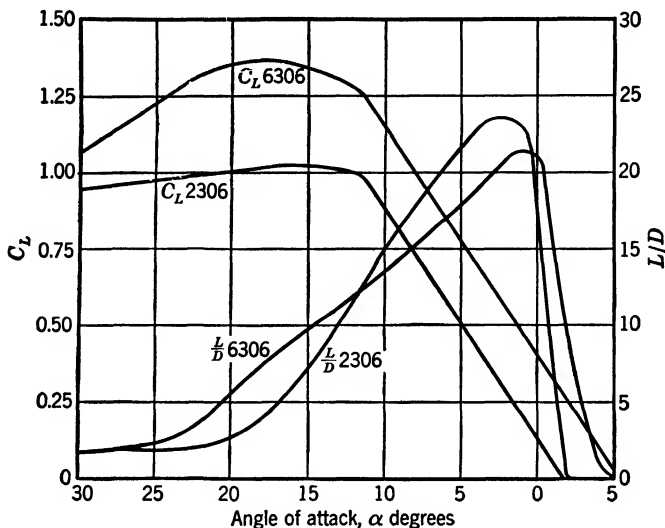


FIG. 8.14. Effect of vane camber (curvature) on airfoil performance (N.A.C.A. Report 460).

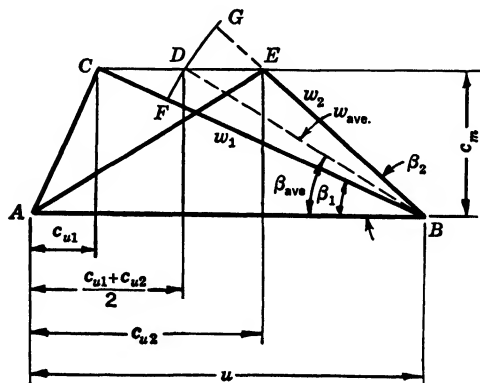


FIG. 8.15. Velocity diagrams of flow ahead of and past the airfoil.

(c) **Total Head Equation.** If a cylindrical cut is made through an axial flow pump impeller and the cylinder is developed onto a plane, a row of vane profiles will result. The action of water on the profile can be considered similar to that taking place on an airfoil in a wind tunnel,

provided the relative velocity  $w_{ave.}$  is an average value of the relative velocity of approach  $w_1$  and at discharge  $w_2$  which exist before and after the vane at a distance where the effect of the flow through the row of vanes is equalized (Fig. 8.12). The effect of the cascade arrangement of vanes on the lift coefficient  $C_L$  is little known and has been neglected by several advocates of the airfoil theory of the axial flow impeller.<sup>11</sup>

The total force  $P$  exerted by the liquid per unit of vane length is a resultant of lift  $L$  and drag  $D$  and makes an angle  $\lambda$  with  $L$  (Fig. 8.12).  $P$  forms an angle  $90^\circ - (\beta_{ave.} + \lambda)$  with the peripheral velocity of the impeller. The tangential component of  $P$  is

$$P \cos [90^\circ - (\beta_{ave.} + \lambda)] = P \sin (\beta_{ave.} + \lambda) \quad (8.5)$$

The work per second is

$$E = Pu \sin (\beta_{ave.} + \lambda) \quad (8.6)$$

Considering a slice of vane between two concentric cylindrical surfaces of radius  $r$  and  $r + dr$  the corresponding work per second for  $z$  vanes is

$$zdE = zPdr \sin (\beta_{ave.} + \lambda) \quad (8.7)$$

If  $dQ$  denotes the volume of liquid included between the two cylindrical surfaces, the work per pound of water is

$$H_t = \frac{zdE}{dQ\gamma} = \frac{Pu \sin (\beta_{ave.} + \lambda)z}{dQ\gamma} dr \quad (8.8)$$

But  $dQ = ztdrc_m$ ,  $P = L/\cos \lambda$ , and  $L = C_L(\gamma w_{ave.}^2 F)/2g$  where  $F = l \times 1 = l$ , area per unit length. Then

$$P = C_L \frac{\gamma l w_{ave.}^2}{2g \cos \lambda} \quad (8.9)$$

and equation 8.8 becomes

$$H_t = C_L \cdot \frac{l}{t} \cdot \frac{u}{c_m} \cdot \frac{w_{ave.}^2}{2g} \cdot \frac{\sin (\beta_{ave.} + \lambda)}{\cos \lambda} \quad (8.10)$$

or

$$C_L \frac{l}{t} = H_t \frac{2g}{w_{ave.}^2} \cdot \frac{c_m}{u} \cdot \frac{\cos \lambda}{\sin (\beta_{ave.} + \lambda)} \quad (8.11)$$

The theoretical head  $H_t$  is obtained from  $H_t = H/e_h$ , where  $e_h$  is hydraulic efficiency, which has to be assumed.

$w_{ave.}$  and  $\beta_{ave.}$  are obtained from the velocity diagram (Fig. 8.15) constructed for an average tangential component,  $(c_{u2} + c_{u1})/2$ . The

value of  $c_{u2}$  is obtained from

$$c_{u2} - c_{u1} = \frac{gH_t}{u} \quad (8.12)$$

Usually  $c_{u1}$  is assumed to be equal to zero. ||

From equation 8.11 it is seen that for greater  $u$  and  $w_{ave}$ , the value of  $C_L(l/t)$  is lower; that is, at larger radii  $l/t$  and  $C_L$  are lower than at the hub. Equation 8.11 includes the  $l/t$  ratio, and does not give any indication of the number of vanes. For higher heads, higher values of  $C_L$  and  $l/t$  are required; or, more vane area and a higher cambered profile are required.

Equation 8.11 is used for the calculation of  $C_L(l/t)$  for several radii of the impeller. It is assumed that  $H_t$  and  $c_m$  are constant along a radius. Next  $l/t$  is assumed. For a fixed hub ratio,  $l/t$  can vary only within narrow limits for a given specific speed, and vane profiles are selected for a chosen  $l/t$  ratio. Experience is necessary to select proper values of  $l/t$  to obtain  $C_L$  and the vane profile in order to produce an efficient impeller and head-capacity and efficiency curves of good shape.

|| The development of equation 8.11 follows that given by Pfeleiderer in his book.<sup>7</sup> It has been further simplified by the following approximations.

$$\cos \lambda \approx 1 \quad \frac{c_m}{w_{ave}} \approx \sin \beta_{ave}.$$

since  $\lambda$  is of the order of 1 degree. Substituting  $H_t = uc_{u2}/g$  into equation 8.11 we obtain

$$C_L \frac{l}{t} = \frac{2c_{u2}}{w_{ave}} \quad (8.11a)$$

(F. Weinig, *Strömung um die Schaufeln von Turbomaschinen*, Leipzig, 1935, p. 6.)

The left-hand side of equation 8.11 (a) can be expressed easily in terms of vane curvature  $(\beta_2 - \beta_1)$ . In Fig. 8.15 area of triangle  $CEB = \frac{1}{2}c_m(c_{u2} - c_{u1}) = \frac{1}{2}c_m c_{u2}$  if  $c_{u1} = 0$ . This is approximately but very closely equal to the area of the sector  $FGB = \frac{1}{2}w_{ave}^2(\beta_2 - \beta_1)$ . Hence

$$c_m c_{u2} = w_{ave}^2(\beta_2 - \beta_1) \quad \text{or} \quad \frac{c_{u2}}{w_{ave}} = \frac{\beta_2 - \beta_1}{c_m} w_{ave}.$$

and

$$C_L \frac{l}{t} = \frac{2(\beta_2 - \beta_1)}{\sin \beta_{ave}} \quad (8.11b)$$

If use is made of equation 8.13, developed later, equation 8.11 (b) takes the form

$$C_L \frac{l}{t} = \frac{4c}{l_c(1 - l_c) \sin \beta_{ave}} \quad (8.11c)$$

where  $c$  is the airfoil camber and  $l_c$  is its location relative to the leading edge of the airfoil.

Note that  $w_{ave}$ , as defined in Fig. 8.15 is only approximately equal to the average of  $w_1$  and  $w_2$ ; similarly  $\beta_{ave}$ , is not an exact average of  $\beta_1$  and  $\beta_2$ .

## 8.6 DISCUSSION OF AIRFOIL THEORY

The airfoil data used for the vane selection for axial flow pumps were obtained experimentally for conditions vastly different from those existing in a pump. A great number of simplifying assumptions are necessary to make possible a comparison of the flow of the two. Thus, the effect of mutual vane interference is not sufficiently known. S. Ober<sup>11</sup> has found that the lift coefficients of a single airfoil should be multiplied by a factor which varies from 0.70 to 0.20 for values of  $l/t$  from 0.40 to 2.0, respectively. These data are strongly at variance with the theoretical values of Numachi<sup>12</sup> quoted by Pfeleiderer. Again, a series of airfoils of variable pitch in circular motion will not perform in the same manner as a single airfoil in the straight flow of a wind tunnel. In this connection, statements by Spannhake<sup>10</sup> are very significant: "*It will be thus appreciated that there are many unknown factors in the direct application of airfoil theory and experimental knowledge to the design of turbines and pumps. Laboratory experience with such runners must certainly be called upon to check the results of the use of such a theory, and therefore it may be questioned whether or not the airfoil theory is, after all, the best one upon which to base our ideas.*"

Spannhake<sup>10</sup> points out the difference in the action of airfoils in air and water: "Profiles advantageously applied to airfoil design often show comparatively thick forms of the leading edges, which, in the flow of a compressible medium, do not do any harm so long as the local surplus of velocity does not approach the velocity of sound, whereas in an incompressible fluid they very soon may create local cavitation. The author prefers forms of leading noses like hatchets with edges rounded only a little." There are serious practical limitations to the use of the airfoil theory for the axial flow impeller design. (1) N.A.C.A. data are limited to cambers of 0, 2, 4, and 6 per cent. For impeller design much higher cambers (9 per cent) are quite common, and any intermediate camber may be required. (2) The method becomes less accurate and workable for lower specific speed axial flow pumps (below 10,000) and fails entirely for extreme mixed flow types.¶ The continuity of mental pattern of flow, theoretical reasoning, and geometrical procedure for vane layout is indispensable for a pump designer.

¶ Limitations of the airfoil theory became apparent to the high pressure axial flow compressor designers. The so-called stream filament or lattice blading of the axial flow compressor impeller is based on Euler's velocity triangles, exaggerated angles or overcurvature of vanes being used to bring the calculated and actual heads to some agreement. (Minutes of Axial Flow Compressor Meeting of June 26, 1946, on German Articles, primarily by Bruno Eckert and Group. Published by Navy Dept., Code 445A, Bureau of Ships, pp. 27, 40, Washington, D. C., 1946.)



By the time reliable and ample airfoil test data were published, Kaplan water turbine impellers had attained a high degree of perfection. This development proceeded entirely experimentally by use of actual impellers in a suitable water turbine casing. It is only natural that axial pump development should follow the same path, that is, experimentation with impellers in a suitable pump casing.

Max M. Munk has shown<sup>13</sup> that the mean camber lines of the N.A.C.A. four-digit airfoil profiles and their aerodynamic properties are completely defined by two tangents with their points of contact at the leading and trailing edges of the mean line ( $AC$  and  $BC$  in Fig.

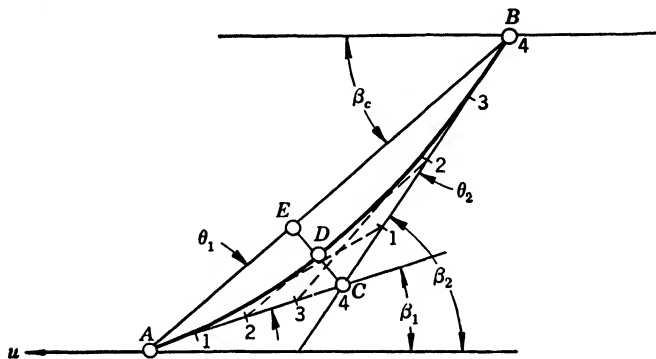


FIG. 8.16. Airfoil characteristics in terms of curvature  $\beta_2 - \beta_1 = \theta_2 + \theta_1$ .

8.16). This follows from the properties of parabolic curves comprising the mean camber lines of this family of the airfoils. Tangents  $AC$  and  $BC$  may be given by specifying angles  $\theta_1$  and  $\theta_2$  between the chord and the tangents. Additional tangents can be drawn by dividing the tangents  $AC$  and  $BC$  into a number of equal parts and joining the corresponding points (1, 2, 3, and 4). The point  $C$  of intersection of two tangents determines the location of the maximum camber station, and the value of the camber  $ED$  is equal to one half of the distance  $EC$ . It is evident that Munk's method of geometrical drawing of the mean camber line of airfoils parallels the procedure of drawing the axial flow impeller sections presented by the author, and based on the inlet and discharge angles  $\beta_1$  and  $\beta_2$  established from Euler's velocity triangles. From Fig. 8.16 the following relationships between angles  $\beta_1$ ,  $\beta_2$ ,  $\theta_1$ , and  $\theta_2$  are evident.

$$\beta_1 = \beta_c - \theta_1 \quad \text{and} \quad \beta_2 = \beta_c + \theta_2$$

Hence

$$\beta_2 - \beta_1 = \theta_2 + \theta_1$$

The vane curvature ( $\beta_2 - \beta_1$ ) can be expressed easily in terms of camber and its location of the mean line. From Fig. 8.16  $\tan \theta_1 = 2ED/AE$

$= 2c/l_c$  and  $\tan \theta_2 = 2ED/EB = 2c/(1 - l_c)$  where  $c$  is the camber and  $l_c$  is its location relative to the leading edge, both expressed as fractions of the airfoil chord length. Since angles  $\theta_1$  and  $\theta_2$  are usually small, the values of the angles in radians are approximately equal to their tangents. Then the vane curvature becomes

$$\beta_2 - \beta_1 = \frac{2c}{l_c} + \frac{2c}{1 - l_c} = \frac{2c}{l_c(1 - l_c)} \quad (8.13)$$

Equation 8.13 shows that the vane curvature ( $\beta_2 - \beta_1$ ) establishes the hydrodynamic properties of airfoil just as completely as the camber and its location in the N.A.C.A. classification.

### 8.7 GUIDE VANES AHEAD OF THE IMPELLER

An arrangement universally adopted for axial flow pumps is one in which the diffusion casing is beyond the impeller. In this arrangement, the fluid approaches the impeller axially and is given a tangential com-

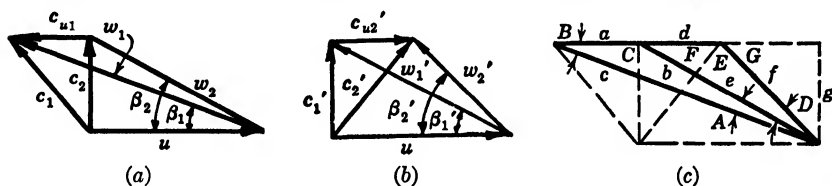


FIG. 8.17. Velocity diagrams for axial flow pumps with diffusion casing ahead of and beyond the impeller.

ponent by the impeller. After that the flow is restored to an axial direction by the diffusion casing. In multistage axial blowers, guide vanes precede the impeller. With this arrangement, the guide vanes give the air a tangential component in a direction opposite to that of the rotation of the impeller, and consequently reduce the pressure ahead of the impeller. The impeller in turn imparts a tangential component to the flow in the direction of rotation, thus restoring the flow to the axial direction. A pump engineer should be familiar with the effect of guide vanes in the impeller suction on the performance of the impeller as in the future the range of axial flow pumps may be extended to higher heads and the use of guide vanes in the impeller suction may be one of the means to accomplish this. Theoretically the problem does not present anything new. The actual velocity diagram for a pump with guide vanes ahead of the impeller is shown in Fig. 8.17 (a) and Fig. 8.17 (b) shows a velocity diagram for a pump with the diffusion casing past the impeller.

A comparison of the two will show that with guide vanes ahead of the impeller the same head (tangential component  $c_{u2}$ ) is obtained with a

smaller difference of the vane angles  $(\beta_2 - \beta_1)$ . It can be shown that

$$\frac{\sin(\beta_2 - \beta_1)}{\sin(\beta_2' - \beta_1')} = \frac{w_2'}{w_1} \quad (8.14)$$

Drawing a composite diagram Fig. 8.17 (c) and using for brevity a notation

$$\begin{aligned} c_{u1} &= a & w_1 &= c & w_1' &= w_2 = e \\ c_{u2}' &= d & w_2 &= b & w_2' &= f \end{aligned}$$

The proof of equation 8.14 follows. For the triangle  $ABC$ ,

$$\frac{a}{\sin A} = \frac{b}{\sin B} = \frac{c}{\sin C}$$

Hence

$$a = b \frac{\sin A}{\sin B}$$

From triangle  $FED$

$$\frac{d}{\sin D} = \frac{e}{\sin E} = \frac{f}{\sin F}$$

Hence

$$d = e \frac{\sin D}{\sin E}$$

but  $a = d$  and  $b = e$ . Then

$$\frac{\sin A}{\sin D} = \frac{\sin B}{\sin E} = \frac{\sin B}{\sin G} = \frac{g}{c} \cdot \frac{f}{g} = \frac{f}{c}$$

Substituting the following values

$$\begin{aligned} A &= \beta_2 - \beta_1 & D &= \beta_2' - \beta_1' & c &= w_1 & f &= w_2' \\ \frac{\sin(\beta_2 - \beta_1)}{\sin(\beta_2' - \beta_1')} &= \frac{w_2'}{w_1} < 1 \end{aligned} \quad (8.14)$$

*For the same impeller vane, higher heads are obtained with guide vanes ahead of the impeller.* This has been confirmed by the author's tests. By referring to Figs. 8.17 (a) and 8.17 (b) it will be noticed that with guide vanes ahead of the impeller the average relative velocities are higher than with the diffusion casing past the impeller. It is expected that higher relative velocities will affect adversely the cavitation characteristics of the pump and increase the friction loss. It is possible that a final design of a high head axial flow pump will be a compromise between the two arrangements; that is, the pump will have guide vanes in the impeller approach, and a diffusion vane beyond the impeller.

Figure 8.18 (a) shows the entrance velocity triangle with guide vanes ahead of the impeller and a forced vortex pattern of flow for two points, one at the periphery and the other near the hub of the impeller. The tangential velocities of prerotation  $c_{u0}$  and  $c_{uh}$  are proportional to their

respective peripheral velocities  $u_o$  and  $u_h$ . Figure 8.18 (b) shows in dotted lines Euler's discharge velocity diagram for the same arrangement with the "actual" velocities shown by solid lines. The ratio  $P_{2s}/c_m$  is the impelling ratio. The requirement for a forced vortex, given by equation 4.16, is satisfied because

$$u_o \tan \beta_{2o} = u_h \tan \beta_{2h}$$

Axial flow pumps with the guide vanes ahead of the impeller have a flatter brake-horsepower curve with a lower ratio of shut-off brake horsepower to the normal brake horsepower than pumps with the diffusion casing beyond the impeller. For example, an axial flow pump

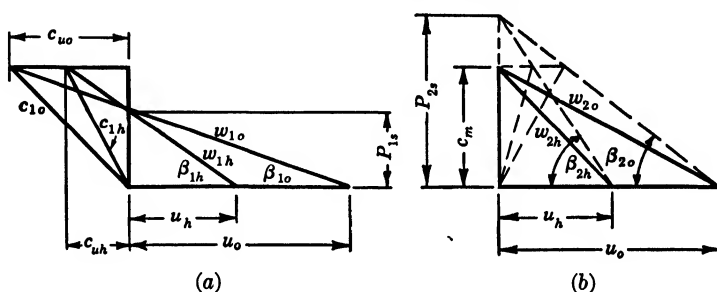


FIG. 8.18. Velocity diagrams for diffusion vanes ahead of the impeller arrangement.

of  $n_s = 9500$  had a brake horsepower not exceeding the normal down to 35 per cent of the normal capacity. This advantage alone may be sufficient inducement for a study of this arrangement and a search for the best design incorporating a maximum of the desirable features.

It should be noted that when impeller vanes are turned in an axial flow pump with the guide vanes ahead of the impeller, the head increases for higher vane angle setting,<sup>14</sup> whereas with the diffusion vanes beyond the impeller the head remains constant. This is because with guide vanes ahead of the impeller the liquid entrance angle is fixed by the guide vanes, and therefore variation of the vane setting has the effect of the increase of the discharge angle only. Without guide vanes in the impeller approach liquid is free to adjust itself to the vane entrance angle, and the head is determined by the vane curvature ( $\beta_2 - \beta_1$ ) and remains unchanged.

### 8.8 THE AXIAL FLOW PUMP CASING

The purpose of the diffusion casing of an axial flow pump is to convert into pressure the tangential component of the absolute velocity leaving the impeller. This is accomplished by "straightening" the flow as it leaves the impeller and reducing the velocity.

The diffusion vane curvature is selected so that the liquid enters the diffusion vanes with a minimum loss and leaves the casing axially. With an impeller designed for a forced vortex pattern of flow, the angular velocity of the flow leaving the impeller is constant. The diffusion vane angularity is adjusted so that the flow continues with the constant angular velocity, the value of which is decreased until all the tangential component is taken out of the flow. To accomplish this the diffusion vane entrance angles should be laid out for a constant pitch  $P_{3s}$  (Fig. 8.19).

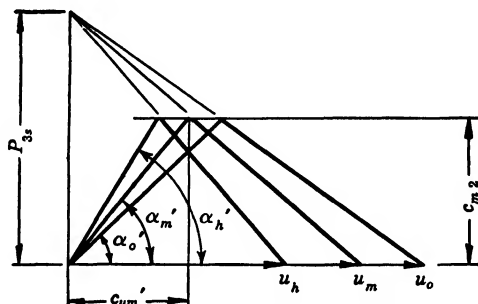


FIG. 8.19. Velocity diagram at entrance to diffusion casing.

The design of the casing involves the following steps.

(a) **Mean Effective Impeller Diameter.** First, the direction of the absolute velocity at the impeller exit, at least at one point, is determined. *It is advantageous to select this point at the mean effective diameter, which is defined as*

$$D_m = \sqrt{\frac{D_o^2 + D_h^2}{2}} \quad (8.15)$$

*It will be shown that the head produced at this diameter is equal to the total integrated head.* In Chapter 4, equation 4.10 and Fig. 4.6, it has been shown that the integrated head is equal to the arithmetical average of the heads generated at the hub and at the periphery, and

$$H_e = \frac{u_o c_{uo} + u_h c_{uh}}{2g} = \frac{u_m c_{um}}{g} \quad (8.16)$$

Where  $u_m$  is the peripheral velocity at diameter  $D_m$  and  $c_{um}$  is the tangential component at the same diameter. From equation 8.16

$$2 = \frac{u_o c_{uo}}{u_m c_{um}} + \frac{u_h c_{uh}}{u_m c_{um}} \quad (8.17)$$

In a forced vortex peripheral and tangential velocities vary as the diameters; therefore

$$2 = \frac{D_o^2}{D_m^2} + \frac{D_h^2}{D_m^2}$$

or

$$D_m = \sqrt{\frac{D_o^2 + D_h^2}{2}} \quad (8.18)$$

*Note that the mean effective diameter as defined by equation 8.18 is directly connected with the forced vortex pattern of head generation in the axial flow pump.*

**(b) Head at Impeller Exit.** Next, the head at the impeller exit is estimated. The total head  $H$  and the pump gross efficiency  $e$  are considered as known. Taking the hydraulic efficiency as  $e_h = \sqrt{e}$ , the input head  $H_i$  is determined from

$$H_i = \frac{H}{\sqrt{e}} \quad (8.19)$$

The head at the impeller exit is less than  $H_i$  by the amount of the hydraulic losses in the impeller. If the casing losses are equal to those of the impeller (each part represents a set of vanes) the head at the impeller exit  $H_d$  is

$$H_d = \frac{H_i + H}{2} = \frac{\frac{H}{\sqrt{e}} + H}{2} \quad (8.20)$$

This head can be expressed as

$$H_d = \frac{u_m c_{um}'}{g} \quad (8.21)$$

hence  $c_{um}'$  can be determined giving the direction of flow at the diameter  $D_m$ . The direction of flow at any other diameter is found from

$$\frac{c_{uo}'}{D_o} = \frac{c_{uh}'}{D_h} = \frac{c_{um}'}{D_m} = \frac{\omega'}{2} \quad (8.22)$$

or may be found graphically as shown on Fig. 8.19 where the absolute velocity angles  $\alpha_o'$ ,  $\alpha_h'$ , and  $\alpha_m'$  are indicated.

To deflect liquid from these directions the diffusion vane angles should be greater by a few degrees, or an angle of attack should be allowed. Without this the vane tips would be inactive. To maintain a forced vortex pattern of flow the vane should be of constant pitch. The angle of attack can be allowed by reducing pitch per second,  $P_{3s}$ .

In addition to the reduction obtained by converting the tangential velocity component into pressure, the axial velocity is also reduced by increasing the diffuser diameter at the discharge. A small divergence angle of the diffuser cone ( $8^\circ$  total) is essential for an effective conversion.

The number of vanes in the diffuser casing varies from 5 to 8, a smaller number of vanes being used for smaller pumps. The vane length at the hub can be reduced ( $DC < AB$ , Fig. 8.20) because the vane spacing is closer at the hub than it is at the outside diameter. The axial dis-

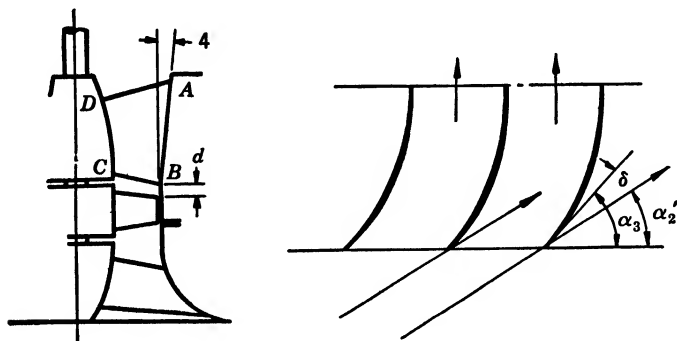


FIG. 8.20. Axial flow pump diffusion casing.

tance  $d$  between the impeller vanes and the diffusion vanes has some bearing on the performance, and the most favorable value of the ratio  $d/D_o$  is about 0.05. When the value of  $d$  is being selected, provision should be made for accommodating an impeller with a higher vane angle setting, which requires more axial space. The impeller hub length should be fixed with this idea in mind.

The value of the diffusion vane angle is not very critical, and variations as great as  $\pm 5$  degrees from the optimum value have hardly any noticeable effect on the pump performance. This is rather fortunate as usually one pump casing is used with several impellers requiring different diffusion vane angles. When the diffusion angle is reduced, the b.e.p. is moved toward a lower capacity. Figure 7.19 gives the average values of the diffusion vane angle  $\alpha_v$  based on the mean effective diameter  $D_m$  for different specific speeds. In Chapter 9, a new method of the graphical determination of the diffusion vane angle or volute angle is given (in Fig. 9.16).

It is also possible to straighten the flow beyond the impeller by using another impeller of opposite rotation. Experimental axial blowers have been built (N.A.C.A., 1942) with two opposing impellers. It is inter-

esting to note that (1) with two impellers alike the second impeller takes more power and contributes more to the total head than the first impeller; (2) the total head is more than double that of a single impeller with a stationary diffusion casing; (3) efficiency is essentially the same as that of a single impeller with a stationary diffusion casing. For a commercial application the arrangement with twin opposing impellers is impractical for pumps or blowers. However, it is used successfully for airplane counter-rotating propellers; in this application it improves efficiency and doubles the axial thrust without increasing the propeller diameter.

## REFERENCES

1. MORROUGH P. O'BRIEN and RICHARD G. FOLSOM, "The Design of Propeller Pumps and Fans," Univ. of Calif. Publ., Vol. 4, No. 1, pp. 1-18.
2. E. BARTON BELL, "Test of a Single Stage Axial-flow Fan," N.A.C.A. Report 729.
3. VICTOR KAPLAN and ALFRED LECHNER, *Theorie und Bau von Turbinen-Schnelllaufern*, Munich, R. Oldenbourg, 1931, p. 145.
4. HENRY F. SCHMIDT, "Some Screw Propeller Experiments with Particular Reference to Pumps and Blowers," *Jour. Am. Soc. Nav. Eng.*, Vol. XL, No. 1, Feb. 1928.
5. J. M. MOUSSON, "Cavitation Problems and Their Effects upon the Design of Hydraulic Turbines," State Univ. of Iowa, Proceedings of the Second Hydraulic Conference, p. 147.
6. C. KELLER and H. BLEULER, "A Method for Determining the Cavitation Factor by Air Tests," *Escher-Wyss News*, No. 1-2, 1939, pp. 23, 27.
7. C. PFLEIDERER, *Die Kreiselpumpen*, Berlin, Julius Springer, 1932, p. 326.
8. A. SCHLIMBACH, "Der Man-Schraubenschaufler," *Mill. Forsch. Anst. GHH-Konzern*, Oct. 1935, p. 54 (Maschinenfabric Augsburg-Nürnberg).
9. G. F. WISLICENUS, "A Study of the Theory of Axial Flow Pumps," *Trans. A.S.M.E.*, Vol. 67, No. 6, Aug. 1945, p. 451.
10. WILHELM SPANNHAKE, "Problems of Modern Pump and Turbine Design," *Trans. A.S.M.E.*, April 1934, Vol. 56, No. 4, pp. 229, 232, 248.
11. L. S. MARKS and J. R. WESKE, "The Design and Performance of an Axial Flow Fan," *Trans. A.S.M.E.*, Vol. 56, No. 11, pp. 807, 812.
12. F. NUMACHI, "Aerofoil Theory of Propeller-Turbines and Pumps," *Technol. Report Tohoku Univ.*, Vol. 8, 1929, p. 411.
13. MAX M. MUNK, "On the Geometry of Streamlining," Theodore von Kármán Anniversary Volume, Calif. Inst. of Tech., Pasadena, 1941, p. 8.
14. A. PFENNIGER, "Research on Scale Effect," *Escher-Wyss News*, No. 1-2, 1939, p. 42.
15. M. MEDICI, "Versuche an Propeller- und Kaplanpumpen," Verein deutscher Ingenieure, Bulletin 87, No. 21/22, May 29, 1943.
16. CURT KELLER, *The Theory and Performance of Axial Flow Fans*, New York, McGraw-Hill, 1937, p. 21.
17. B. ECKERT, "Neuere Erfahrungen an Überdruck-Axialgelbläsen," Verein deutscher Ingenieure, Bulletin 88, No. 37/38, Sept. 16, 1944, p. 516.
18. D. W. TAYLOR, *The Speed and Power of Ships*, revised by U. S. Shipping Board Washington, D. C., 1935, p. 108.



## CHAPTER 9

### HYDRAULIC PERFORMANCE OF CENTRIFUGAL PUMPS

A study of losses in centrifugal pumps may be undertaken for one of the following reasons: (1) information about the nature and magnitude of losses may indicate the way to reduce these losses; (2) if the losses are known, it is possible to predetermine the head-capacity curve of a new pump by first assuming or establishing in some other manner the head-capacity curve of an idealized pump; (3) since the  $Q$ - $H$  curve of an idealized pump is a straight line, the shape of the head-capacity curve of an actual pump is determined by the hydraulic losses. Thus it would seem possible, when something is known about the losses, to change the shape of the head-capacity curve to suit some special requirement.

*Considering the high degree of perfection of modern pumps, as demonstrated by pump gross efficiencies of over 90 per cent, it is remarkable that so little exact knowledge is available on the losses of centrifugal pumps.* None of the three above objectives has been achieved to any appreciable degree because of the present lack of knowledge of losses.

The progress in pump design has been accomplished mostly in an experimental way, the pump gross efficiency being the only criterion of improvement in performance. In this book all losses are grouped under the headings: hydraulic, leakage, mechanical, and disk friction losses. Only hydraulic losses will be discussed in this chapter.

#### 9.1 HYDRAULIC LOSSES

These are the least known of all the losses in pumps, and at the same time they are the most essential ones for the attainment of the three objectives set forth above. The reason for this is that there are so many factors contributing to the hydraulic losses. Even the combined effect of these factors cannot be ascertained accurately. In general it can be said that hydraulic losses are caused by: (1) skin friction and (2) eddy and separation losses due to changes in direction and magnitude of the velocity of flow. The latter group includes the so-called shock loss and diffusion loss.

In the channels from the suction to the discharge nozzle, there is not a single stretch of the path where either the direction of flow or the area and shape of the channel is constant; besides, part of the channel is rotating, thus upsetting the velocity distribution and further complicating the study of hydraulic losses. Under such conditions it is impossible to calculate the friction loss through the pump with a degree of accuracy sufficient to serve any useful purpose.

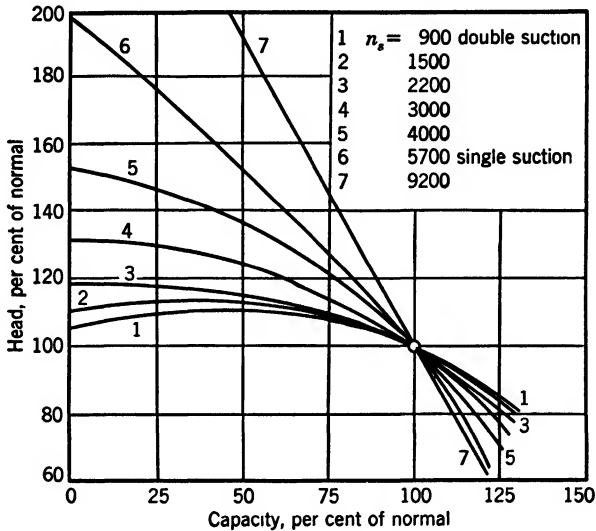


FIG. 9.1. Head-capacity curves for several specific speeds.

Note that the error in calculations of straight pipe friction losses is  $\pm 10$  per cent, according to Richter,<sup>1</sup> or even greater, according to Gibson.<sup>2</sup>

In the following discussion no attempt will be made to give formulas or methods for calculating hydraulic losses in various parts of centrifugal pumps. The need for prediction of head-capacity characteristics of a pump has long passed because, when new types are contemplated, sufficient data are available for designers to estimate the characteristics from existing types.

Figure 9.1 shows typical head-capacity curves, Fig. 9.2 shows efficiency curves, and Fig. 9.3 shows brake-horsepower curves for several specific speeds. The head-capacity, efficiency, and brake-horsepower curves are so interrelated that a change in the form of one is followed by a change in the form of the other two. The responsibility for the change in the pump characteristics to incorporate a maximum of desirable

features with a minimum sacrifice in efficiency rests upon the skill of the designer. This phase of the subject is treated in Chapter 14. However, a general discussion of hydraulic losses, without any attempt to

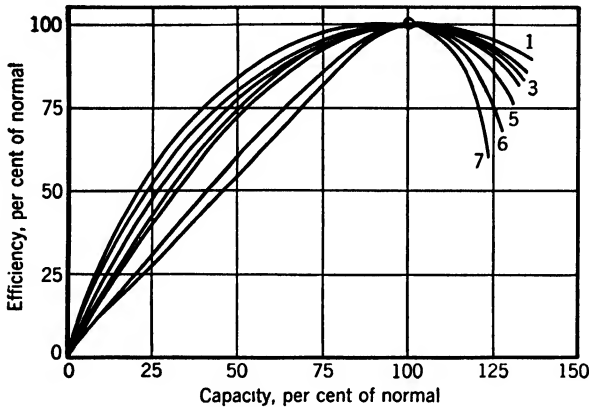


FIG. 9.2. Efficiency curves for different specific speeds.

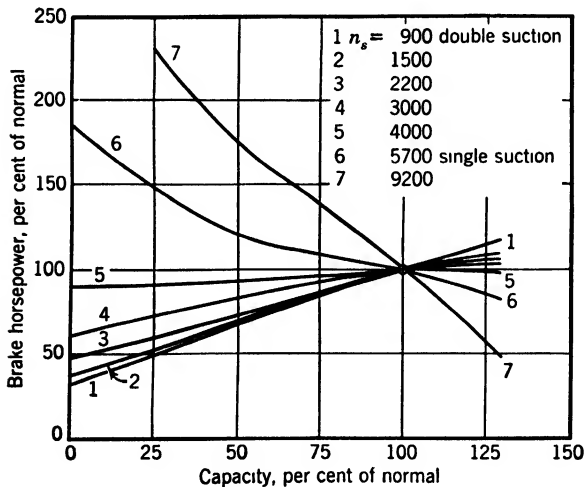


FIG. 9.3. Brake horsepower curves for different specific speeds.

evaluate individual losses, will show the relation between the characteristics of an actual and those of an idealized pump, and will illustrate the manner in which different types of characteristics are obtained.

(a) **Friction and Diffusion Losses.** The general formula for friction loss is

$$h_f = f \frac{L}{4m} \frac{v^2}{2g} \quad (9.1)$$

where  $f$  is a friction coefficient

$L$  is the length of the channel

$m$  is the hydraulic radius of the channel section

$v$  is the velocity at the section with the hydraulic radius  $m$ .

This could be applied to the several parts of the total path, as the suction nozzle, impeller channel, volute, and discharge nozzle. However, actual measurements of the length  $L$ , and the hydraulic radius  $m$  may present difficulty in many cases (extreme mixed flow impeller or suction nozzle of a double suction pump, for instance). The selection of a suitable friction coefficient is a problem in itself. For these reasons several investigators combine all the friction losses in one term, expressing it by a simplified formula:

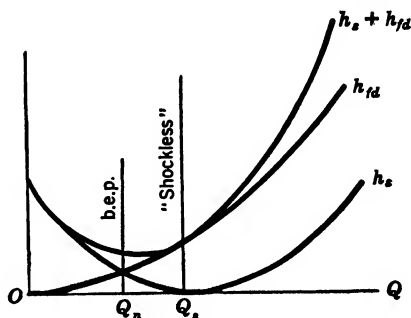


FIG. 9.4. Hydraulic losses.

$$h_f = K_1 \frac{v_1^2}{2g} = K_1 Q^2 \quad (9.2)$$

where  $K_1$  is a constant for a given pump and includes all lengths, areas and area ratios, and friction coefficients. Thus  $K_1$  covers all the unknown factors and also any errors caused by the inability to find a better expression for the several items contributing to the friction losses. Similarly an expression can be set up for the diffusion loss in the impeller channel or discharge nozzle and stated by

$$h_d = f_2 \frac{v_2^2}{2g} \quad (9.3)$$

Again, selection of the coefficient  $f_2$  for the impeller channel presents difficulty. Therefore, for simplicity it is customary to express all diffusion losses by a formula

$$h_d = K_2 \frac{v_2^2}{2g} = K_2 Q^2 \quad (9.4)$$

where  $K_2$  is a constant for a given pump.

Since the losses expressed by equations 9.2 and 9.4 both vary as the square of the capacity they can be combined into one formula:

$$h_{fd} = h_f + h_d = K_3 Q^2 \quad (9.5)$$

which is a square parabola with its axis on the axis of heads (Fig. 9.4).

**(b) Eddy and Separation Losses.** Losses at the impeller entrance and exit are usually called shock losses. *The author accepts this term very reluctantly because in mechanics "shock" or impact does not necessarily mean a loss, and in hydraulics, if impact is in the direction of flow, most of the energy of impact is recoverable (impulse action). Liquid flow*

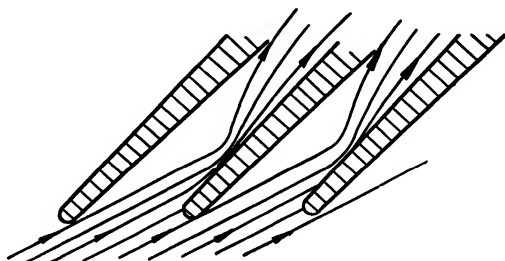


FIG. 9.5. Shock loss is a diffusion loss.

*in a pump tends to avoid shock by acquiring prerotation at the impeller inlet and by establishing a velocity gradient in the volute casing at the impeller discharge, thus cushioning the shock. The nature of the hydraulic loss at the impeller entrance, when liquid approaches at a high angle of attack, is that due to a sudden expansion or diffusion after separation (Fig. 9.5). At the impeller discharge the loss is mostly caused by a high rate of shear due to a low average velocity in the volute and high velocity at the impeller discharge. It should be noted that even at the b.e.p., the average volute velocity is considerably lower than the tangential component of the absolute velocity at the impeller discharge ( $c_{u2}'$ ), and since this is the optimum condition it cannot be improved by changing the volute area (Chapter 7). Besides this, there is a shock loss at the cut-water of a volute pump and at the entrance of diffusion vanes when a diffusion vane casing is used. These losses are of the same nature as shock loss at the entrance to the impeller; that is, they are diffusion losses.*

If we assume that the impeller design is such that at a capacity  $Q_s$  (shockless) the direction of flow agrees with the vane angles at both entrance and discharge, thus incurring no additional losses at these points, then at capacities above and below  $Q_s$  there will be a sudden

change in the direction and magnitude of the velocity of flow. This change results in losses which can be expressed as

$$h_{s1} = K_4 \frac{\Delta c_{u1}^2}{2g} \quad (9.6)$$

for the entrance, and

$$h_{s2} = K_5 \frac{\Delta c_{u2}^2}{2g} \quad (9.7)$$

for the exit of the impeller.

In Fig. 9.6 at capacity  $Q_s$  the meridional velocity at impeller entrance is  $c_{m1}$ , the flow is approaching the impeller under an angle  $\alpha_1$  with a

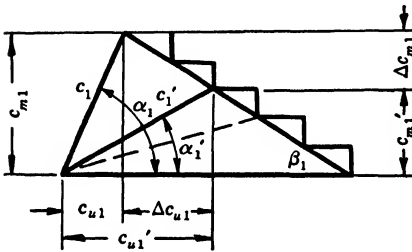


FIG. 9.6. Shock component of peripheral velocity at entrance to impeller.

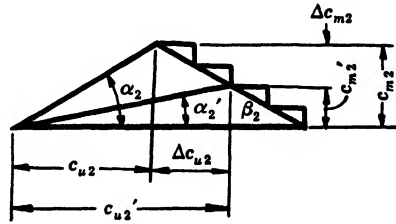


FIG. 9.7. Shock component of velocities at discharge.

tangential component of the absolute velocity  $c_{u1}$ . When the capacity is reduced ( $c_{m1}' < c_{m1}$ ) the liquid should have a tangential component  $c_{u1}'$  to enter the vanes at an angle  $\beta_1$ , and

$$\Delta c_{u1} = c_{u1}' - c_{u1}$$

Similarly, at the discharge (Fig. 9.7) at capacity  $Q_s$  the meridional velocity is  $c_{m2}$ , the tangential component of the absolute velocity is  $c_{u2}$ . At a reduced capacity, the tangential component will increase to  $c_{u2}'$ , and the increment of the tangential component is the difference between the two:  $\Delta c_{u2} = c_{u2}' - c_{u2}$ . At capacities greater than  $Q_s$ , both  $\Delta c_{u1}$  and  $\Delta c_{u2}$  are negative. Note that, in Figs. 9.6 and 9.7, for equal increments of  $c_{m1}$  or capacity,  $\Delta c_{u1}$  increases the same amount. Similarly, for the same steps in  $c_{m2}$  the value of  $\Delta c_{u2}$  increases by an equal amount. Thus both items increase on both sides of  $Q_s$  as the square of the capacity. In this way it is possible to combine both equations 9.6 and 9.7 into one expression, or

$$h_s = K_6(Q - Q_s)^2 \quad (9.8)$$

This represents a square parabola with its apex at  $Q_s$  (Fig. 9.4).

## 9.2 TOTAL HEAD-CAPACITY CURVE

(a) **The Head-Capacity Curve Equation.** The head-capacity curve of an idealized pump is a straight line. For a given discharge vane angle, a single line will represent the characteristics of pumps of all specific speeds when plotted to dimensionless scales. When the essential design elements are selected, the location of the best efficiency point, and hence the specific speed, are fixed. Hydraulic losses for the selected proportions of essential passages will determine the head-capacity curve of the actual pump. In general, for a constant speed,

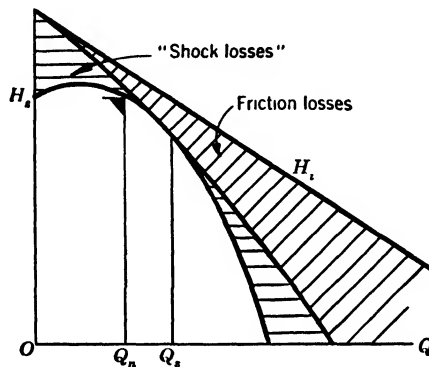


FIG. 9.8.  $Q$ - $H$  curve is obtained by subtraction of hydraulic losses from input head.

the head-capacity curve can be obtained by subtracting losses from the input head of an idealized pump. For a given capacity the actual head may be expressed by

$$H = H_i - K_3 Q^2 - K_6 (Q - Q_s)^2 \quad (9.9)$$

To draw the  $H_i$  line the knowledge of one point only on this line is necessary since, at zero head,  $H_i$  and  $H_e$  lines intersect at a capacity given by  $\phi = c_{m2}/u_2 = \tan \beta_2$ . Such a point is shown in Fig. 9.16 (point  $B$ ) and is discussed later. The procedure for the determination of one point on the  $H_i$  line is outlined in Chapter 10.

Constants  $K_3$  and  $K_6$  are determined from an actual  $Q$ - $H$  curve by selecting several points on the head-capacity curve, substituting the values of  $Q$  and  $H$  into equation 9.9, and obtaining any desired number of simultaneous equations which can be solved for  $K_3$  and  $K_6$ . As should be expected, the value of the constants thus found are different from pump to pump and are inconsistent along the same curve. For that reason there has been no serious attempt to establish such constants.

Graphically the total head-capacity curve is obtained by subtracting the friction and shock losses, as shown in Fig. 9.4 from the  $H_i$  curve (Fig. 9.8). By referring to Fig. 9.4 it will be noticed that *the b.e.p. will always occur at a capacity lower than the shockless capacity  $Q_s$  because the sum of the friction and shock losses determines the location of the peak efficiency. The impeller vane entrance angle at the b.e.p. is exaggerated, or laid out for a meridional inlet (without prerotation) for a capacity greater than the normal capacity; this means that at the b.e.p. prerotation is allowed.*

The  $Q$ - $H$  curve on Fig. 9.8 is a parabola with its apex displaced to the right of the axis of heads. Such curves are observed on low and medium specific speed pumps. But, when found objectionable, the droop of the  $Q$ - $H$  curve at shut-off can be eliminated by special design, as discussed in Chapter 14. On medium and high specific speed pumps the  $Q$ - $H$  curve rises constantly toward zero capacity, thus indicating the inaccuracy of the method outlined for establishing the total head-capacity curve from the input head-capacity characteristics.

**(b) Hydraulic Efficiency at Zero Capacity.** In Chapter 5 it was shown that the shut-off head of actual pumps, expressed in dimensionless coordinates, is essentially constant for pumps of all specific speeds. This is expressed by the fact that the speed constant at shut-off,  $K_{us}$  is constant for all specific speeds. *This in turn means that the hydraulic efficiency at shut-off is constant for all specific speeds and all angles  $\beta_2$ .*

$$\frac{H_s}{H_{is}} = e_{hs} = \text{constant}$$

$$H_s = \frac{u_2^2}{2g} \cdot \frac{1}{K_{us}^2}$$

from Fig. 5.9,

$$K_{us} = 0.925$$

$$H_s = 1.17 \frac{u_2^2}{2g} = 0.585 \frac{u_2^2}{g} \quad (9.10)$$

From Fig. 9.16,

$$e_{hs} = \frac{DO}{BO} = \frac{0.585}{0.725} = 0.808$$

**(c) General Pump Characteristics.** By expressing the constants  $K_3$  and  $K_6$  of equation 9.9 in terms of the pump physical dimensions (ratios) and angles it is possible to transform equation 9.9 to the form

$$H = An^2 + BnQ + CQ^2 \quad (9.11)$$



where  $A$ ,  $B$ , and  $C$  are constants depending on the pump design. For a constant speed  $n$ , this is an equation of the head-capacity curve. Since equation 9.11 has no practical application and its development does not reveal anything new or instructive, it is omitted from this discussion.\*

In Chapter 13 a more detailed study of complete pump characteristics is made. Figures 13.1 and 13.2 give charts showing the actual pump characteristics plotted for constant  $n$ ,  $Q$ , or  $H$ .

### 9.3 HYDRAULIC EFFICIENCY

(a) **Hydraulic Efficiency versus Specific Speed.** On Fig. 9.9  $AD$  is the input head line,  $NEPFV$  is the actual total head-capacity curve, and  $UKV$  is the hydraulic efficiency curve. If a line  $CD$  is drawn through  $D$  intersecting the total head-capacity curve at two points,  $E$  and  $F$ , these points will be found to be points of equal hydraulic efficiency since

$$\frac{EM}{SM} = \frac{FL}{TL}$$

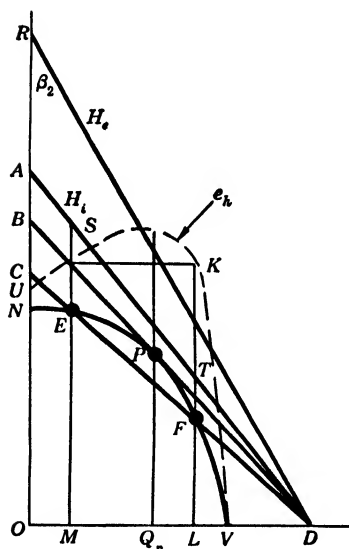


FIG. 9.9. Hydraulic efficiency.

This follows from the relation of the two sets of similar triangles,  $EMD$  and  $FLD$ , and  $SMD$  and  $TLD$ . As line  $CD$  is moved toward line  $AD$  it will always cut the total head-capacity curve at two points of equal hydraulic efficiency and, in the limiting case, line  $CD$  will become tangent to the total head-capacity curve at the point of maximum hydraulic efficiency.†

If several total head-capacity curves for pumps of different specific speeds are intersected by a line  $CD$  (Fig. 9.10) all the points of intersection,  $P$ ,  $R$ ,  $S$ ,  $T$ ,  $U$ ,  $V$ , will be points of the same hydraulic efficiency. Now, if line  $CD$  is moved toward line  $AD$  it will become tangent to the several total head-capacity curves at the points of best hydraulic efficiency.

\* The development of equation 9.11 is given by Pfeleiderer,<sup>3</sup> Spannake,<sup>4</sup> LeConte,<sup>5</sup> and others.

† Lichtenstein<sup>6</sup> has proved analytically that a tangent to the total head-capacity curve at the point of best hydraulic efficiency will pass through the point  $D$ , intersection of the input head line with the axis of capacities.

*Experimental evidence indicates that all head-capacity curves for a continuous row of pumps within the useful range of specific speeds will have a common tangent BD at the point of best hydraulic efficiency.*

In Fig. 9.11 are plotted several head-capacity points representing the best efficiency points of pumps of different specific speeds. These pumps are of consistent design, the same impeller discharge angle, about  $22\frac{1}{2}^\circ$ , being used. The points show a definite trend to align themselves along the line passing through the point of zero input head ( $c_{m2}/u_2 = \tan 22\frac{1}{2}^\circ$ ). Now, if it is assumed that all total head-

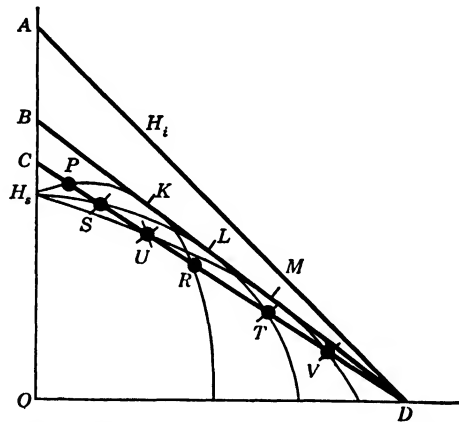


FIG. 9.10. Hydraulic efficiency is the same for impellers of all specific speeds.

capacity curves have a common tangent, *the optimum peak hydraulic efficiency is the same for pumps of all specific speeds.* Such a conclusion can be justified by the following reasoning and qualifications.

(1) It is assumed that all pumps are of such sizes that the scale effect can be disregarded.

(2) For a continuous and consistent row of pumps of different specific speeds it will be assumed that the hydraulic losses are divided between the impeller and casing in the same ratio. Then, confining discussion to the impeller only, it can be stated with more confidence that the impeller hydraulic efficiency is the same for all specific speeds. *At the b.e.p. hydraulic losses are almost entirely friction losses. These are proportional to the number of impeller channels and their lengths, but the head produced also increases with the number of channels and length. If both maintain the same ratio the optimum hydraulic efficiency of the impeller will remain constant for all specific speeds. At zero capacity hydraulic friction losses are zero and the hydraulic efficiency is determined by the shock losses only. These bear a constant ratio to the total head for several*

*specific speeds, and a constant pump hydraulic efficiency at shut-off results. This has been proved experimentally.*

(3) The total head measurements of a pump always include some of the hydraulic losses in the casing and, to be consistent, the design of the casing should be similar and such that hydraulic losses in the casing

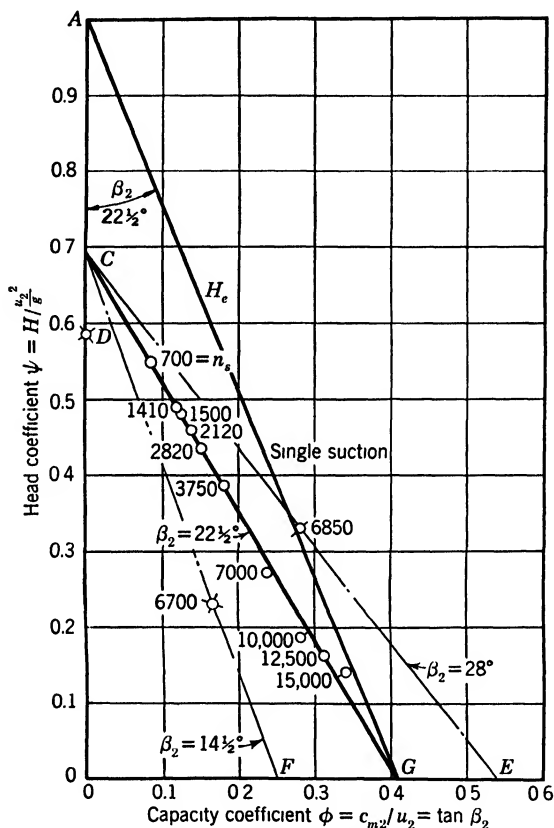


FIG. 9.11. Best efficiency points of pumps of different specific speeds on  $\phi$ - $\psi$  chart.

bear the same ratio to the total head. This cannot be accomplished in practice over a wide range of specific speeds. The total head as measured is affected by the casing design, testing procedure, and scale effect. The gross efficiency is not a reliable indication of the hydraulic efficiency of the pump and it is an even less reliable indication of the hydraulic efficiency of the impeller for the reasons given below.

(a) Low specific speed pumps are usually built in small sizes, scale effect reducing the total measured head and hydraulic efficiency. The

gross efficiency drops off rapidly with decreasing specific speed on account of increasing disk friction and leakage losses (Fig. 9.12).

(b) Reduction in the gross efficiency (and measured head) of double-suction pumps of specific speeds 4000 to 6000 (Fig. 9.12) shows the bad effect of a 90-degree turn in the impeller approach. End suction pumps and vertical turbine and propeller pumps with a straight impeller approach show an appreciable gain in efficiency over double-suction pumps in the same range of specific speeds.

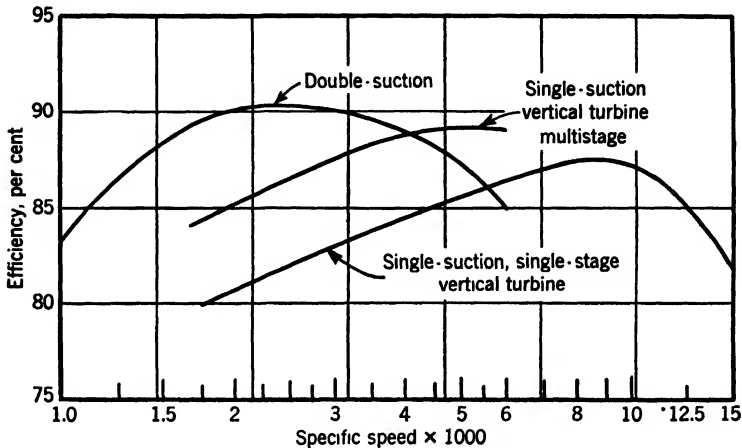


FIG. 9.12. Pump efficiency is affected by the casing design.

(c) Measurements of total head differ for horizontal pumps and vertical turbine and propeller pumps. The latter are charged with the suction entrance and discharge column and elbow losses, whereas in horizontal pumps the head is measured between the suction and discharge flanges. The difference in efficiency between single-stage and multistage turbine pumps is explained by the fact that the entrances and column losses are a smaller fraction of the total head of a multistage pump than of a single-stage pump.

Decrease in efficiency of high specific speed propeller pumps again can be charged to the casing as casing losses become an increasingly greater fraction of the total head. Figures 10.9 and 16.15 provide a good illustration of this point.

(4) For axial flow and mixed flow pumps angle  $\beta_2$  for Fig. 9.11 is taken at the mean effective diameter  $D_m = \sqrt{(D_{2o}^2 + D_{2i}^2)}/2$ . The peripheral velocity  $u_2$  for the dimensionless head and capacity coefficients is based on the mean effective diameter. For straight axial flow pumps  $\beta_2$  is the discharge angle of the mean line and not a chord angle.

(b) **Effect of Discharge Angle  $\beta_2$  on Impeller Hydraulic Efficiency.** Figure 9.13 shows Euler's head  $H_e$ , and input head  $H_i$  lines  $AD$  and  $BD$  respectively, for a given discharge angle  $\beta_2$ . Line  $CD$  is the locus of the best hydraulic efficiency points of actual total head curves for all specific speeds. The point  $H_s$ , the actual shut-off head, is common for all total head-capacity curves.† Location of the maximum capacity point  $D$  is fixed by the angle  $\beta_2$  as  $OD = \tan \beta_2$ . The optimum hydraulic efficiency of the impellers of all specific speeds is  $CO/BO$ .

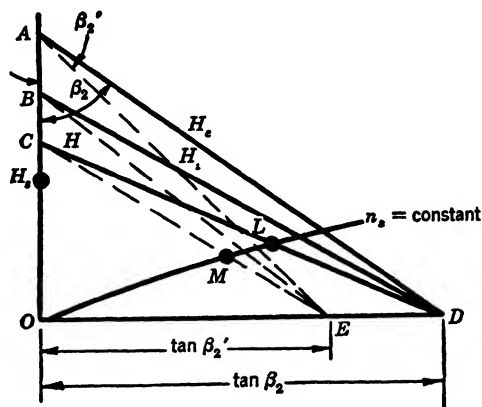


FIG. 9.13. Hydraulic and vane efficiency are constant for all values of impeller discharge angle  $\beta_2$ .

If the impeller discharge angle is changed from  $\beta_2$  to  $\beta_2'$  the maximum capacity point  $E$  will be given by the relationship  $OE = \tan \beta_2'$ . Points  $A$ ,  $B$ ,  $C$ , and  $H_s$  remain the same, and  $H_e$ ,  $H_i$ , and  $H$  lines can be drawn as shown by dotted lines. The line  $CE$  now becomes the locus of heads for the optimum hydraulic efficiency of the impeller. The hydraulic efficiency itself stays unchanged and is still equal to  $CO/BO$ . Thus *the optimum impeller hydraulic efficiency is constant for all specific speeds and does not depend on the discharge vane angle  $\beta_2$ .*

It is believed that there is sufficient experimental evidence to corroborate this conclusion, the gross pump efficiency being taken in every case as a basis of comparison of impeller and pump hydraulic efficiency. Figure 9.14 reproduces a series of tests by Schröter<sup>7</sup> of a pump operated with impellers having a discharge angle  $\beta_2 = 12^\circ$  to  $90^\circ$ . The scatter of gross efficiency points is remarkably small, since no other changes were made to accommodate the widely varied discharge angle.

† Variation of shut-off head from its average value  $H_s$  is discussed in Chapter 5 (Art. 5.5).

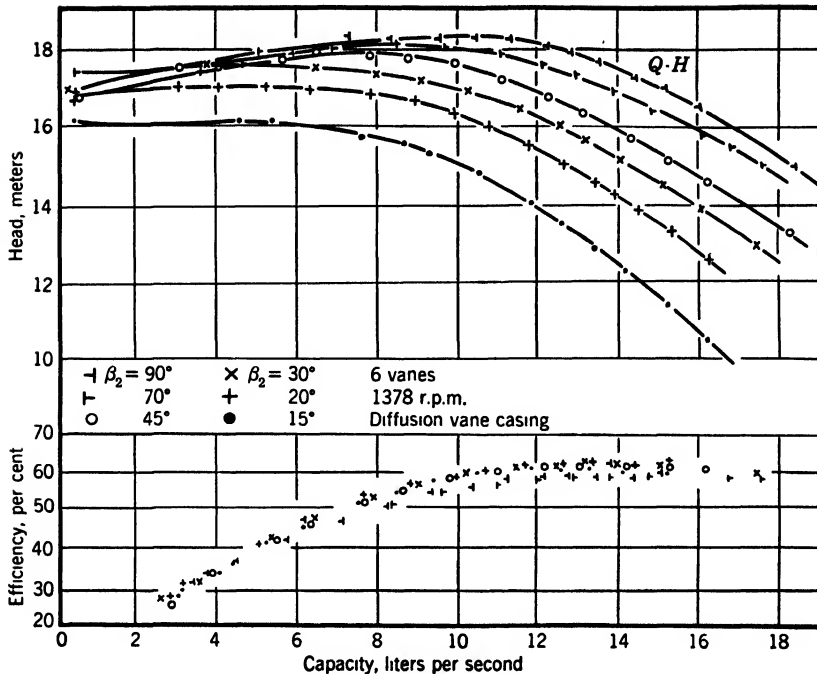


FIG. 9.14. Performance of a pump with impellers of different discharge angles.

Figure 9.15 shows an impeller of a 3-in. pump with discharge angle  $\beta_2 = 8^\circ$ . The number of vanes had to be reduced to a minimum. At 1750 r.p.m., 360 g.p.m., at 122-ft. head ( $n_s = 900$ ), this pump has shown 75 per cent efficiency. This compares favorably with the performance of pumps of the same size and specific speed using more common values of  $\beta_2$ . Referring to Fig. 9.13, it will be noticed that the vane efficiency,  $e_{va} = BO/AO$ , being constant for impellers of all specific speeds and at all capacities, does not change when the discharge angle  $\beta_2$  is varied. It has been found that when the discharge angle is varied, the head and capacity change in such a way that the specific speed remains constant.

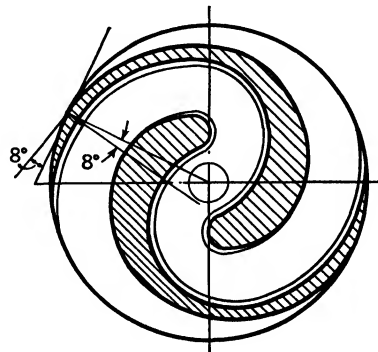


FIG. 9.15. Low angle two-vane impeller.

$$\omega_s = \frac{\sqrt{\phi}}{\psi^{3/4}} = \text{constant} \quad (9.12)$$

**9.4 AUTHOR'S DIAGRAM OF CENTRIFUGAL PUMP CHARACTERISTICS**

The head and capacity coefficients  $\psi$  and  $\phi$  used in Fig. 9.11 have a fixed relationship to the speed constant  $K_u$  and capacity constant  $K_{m2}$  established in Chapter 5 (equations 5.34 and 5.37), or

$$\phi = \frac{K_{m2}}{K_u} \quad \text{and} \quad \psi = \frac{1}{2K_u^2}$$

Therefore the points plotted on Fig. 9.11 represent the same design information connecting the head and capacity constants with the specific speed as that given in Fig. 5.9 but expressed in different units and confined to one value of  $\beta_2 = 22\frac{1}{2}^\circ$ . To use Fig. 9.11 for the selection of the design constants, a specific speed scale must be plotted on line  $CE$  which will permit entrance to the chart to read off the head and capacity coefficients. The fact that the points line up along a straight line on Fig. 9.11 for one value of  $\beta_2$  strongly suggests that the test points for a different value of  $\beta_2$  will also fall on a line connecting the point  $C$  with a point on the capacity axis fixed by the corresponding value of  $\tan \beta_2$ .

The author has checked a great number of head and capacity coefficients of good pumps of normal design for several vane angles other than  $22\frac{1}{2}^\circ$  and has found that these points never fail to follow the line determined by the point  $C$  on the axis of  $\psi$  and  $\tan \beta_2$  on the axis of  $\phi$ . Two such lines are shown in Fig. 9.11 by  $CE$  and  $CF$ .§

**(a) Construction of Diagram.** In Fig. 9.16 the author has prepared a master diagram which covers all essential design and performance features of pumps of all specific speeds on basis of the optimum b.e.p. for any practical value of the impeller discharge angle  $\beta_2$ . The construction of the diagram and its use follows.

The diagram is an extension of Fig. 9.11, made by adding a series of lines radiating from the point  $C$  to intersect the axis of  $\phi$  at various values of  $\tan \beta_2$ . These lines represent loci of the b.e.p. of head-capacity curves of actual pumps for different values of  $\beta_2$ .

The point  $C$  was determined by the plot of actual b.e.p. head-capacity coefficients of 12- to 16-in. pumps of good commercial manufacture. With custom-built pumps of larger sizes, point  $C$  may be located 1 or 2 per cent higher.

§ Two examples are of special interest: (1) high head axial flow pump with guide vanes in the impeller approach and  $\beta_2 = 35^\circ$  and (2) centrifugal single-stage air blower with a deep vaneless diffusion ring and  $\beta_2 = 55^\circ$ . Both have furnished points in Fig. 9.16 falling accurately on their respective lines. Both casing designs deviate materially from the normal pump design. These examples illustrate that if the pump casing (taking no part in head generation) does not incur undue losses of head it does not affect the impeller characteristics, as shown in Fig. 9.16.

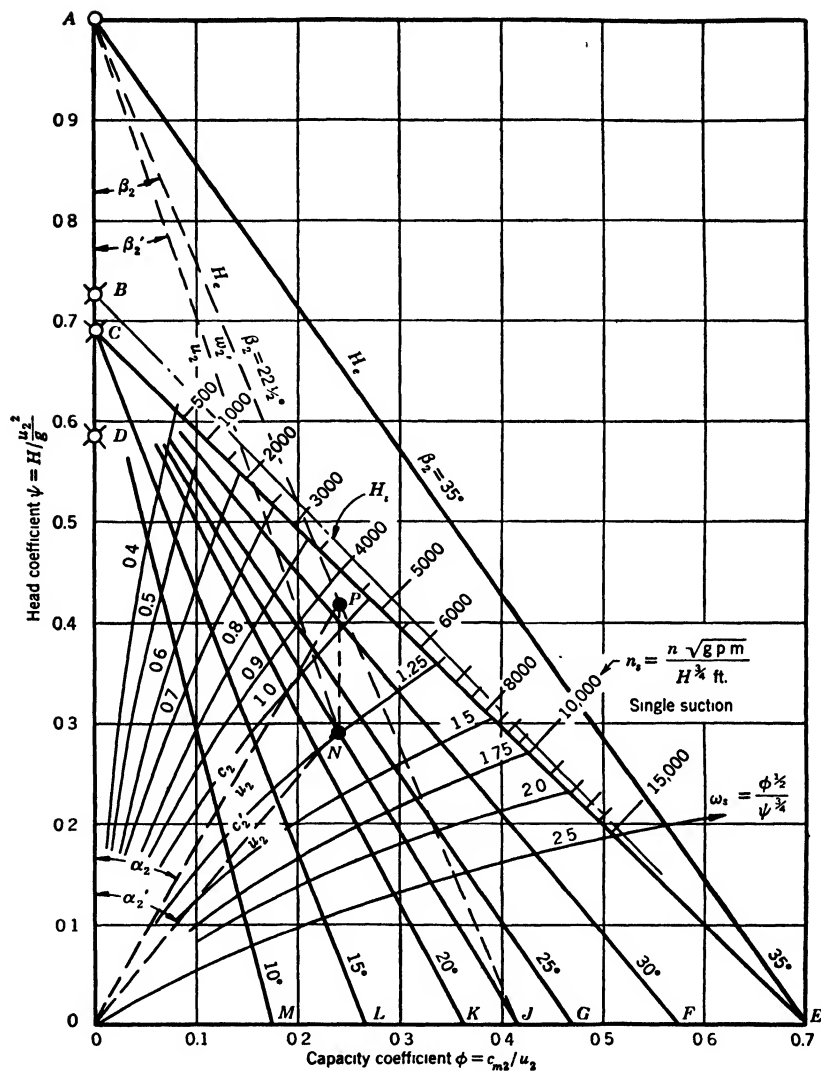


FIG. 9.16. Author's diagram of centrifugal pump characteristics for water.

Point *B* is added to the diagram (Fig. 9.16) which was obtained by estimating the hydraulic efficiency  $CO/BO$  as shown in Chapter 10. In addition, lines of constant specific speed

$$\omega_s = \frac{\phi^{1/2}}{\psi^{3/4}}$$

are shown. To convert specific speed  $\omega_s$  to  $n_s$  expressed in terms of



gallons per minute and  $H$  in feet, the specific speed should be multiplied by a numerical factor.

$$n_s = \frac{n\sqrt{\text{g.p.m.}}}{H^{3/4} \text{ ft.}} = C \left( \frac{b_2}{D_m} \right)^{1/2} \left( \frac{D_{\text{ave.}}}{D_m} \right)^{1/2} \frac{\phi^{1/2}}{\psi^{3/4}} \quad (9.13)$$

where  $C = 9675$  is a numerical constant,  $D_{\text{ave.}} = (D_{2o} + D_{2i})/2$  is the average impeller diameter, and  $b_2/D_m$  varies with the specific speed. The scale of  $n_s$  in terms of gallons per minute and feet is also given on the diagram.

It is important to realize that two pumps of the same specific speed  $n_s$  based on the hydraulic performance at the b.e.p. but of different design will have different dimensionless specific speed  $\omega_s$  depending on the actual impeller profile as it affects the ratios  $b_2/D_m$  and  $D_{\text{ave.}}/D_m$  in the expression for the conversion factor given by equation 9.13. The scale of specific speed  $n_s$  in Fig. 9.16 applies to a continuous row of pumps of one particular design upon which it is based. If the diagram in Fig. 9.16 is entered using the dimensionless specific speed  $\omega_s$  scale, which is absolute, the points will plot on the lines corresponding to the impeller discharge angle  $\beta_2$  irrespective of the variation in the impeller design. Thus the dimensionless specific speed  $\omega_s$  is closely associated with the impeller physical proportions fixing the hydraulic performance at the same time. On the other hand, specific speed  $n_s$  based on the hydraulic performance can be met with impellers of different design.

Figure 9.16 contains the essential elements of design and performance of all centrifugal pumps with any discharge angle  $\beta_2$  and includes (1) Euler's, input, and "actual" velocity triangles for the b.e.p.; (2) design constants to establish the leading physical dimensions of the pump; (3) actual performance data; (4) functional relationship between all the variables involved. Each of these four properties of the diagram will be discussed in detail.

**(b) Velocity Triangles.** In Chapter 3 it has been shown that Euler's head-capacity diagram, if drawn on suitable scales (the head and capacity coefficients being used), will represent Euler's velocity triangles to a scale where all velocities are expressed as ratios to the impeller peripheral velocity  $u_2$ . The same chapter has also shown how the input discharge velocity triangle is obtained if the vane efficiency is known; Figs. 3.12 (a) and 3.12 (b).

Following the same procedure, the "actual" velocity triangles for the b.e.p. can be drawn as shown on Fig. 9.17 for one value of the angle  $\beta_2$ . Points  $O$ ,  $C$ ,  $A$ , and  $J$  in Fig. 9.17 represent the same points in Fig. 9.16.

For a certain capacity and specific speed,  $OPA$  represents Euler's discharge velocity triangle;  $ONA$  is an "actual" velocity triangle, velocities  $c_2'$  and  $w_2'$  and angle  $\beta_2'$  being "actual" values at the discharge. The "actual" velocity triangle  $ONA$  gives only approximate values of velocities and angles at the impeller discharge, however. The error is introduced by the fact that the line  $JC$  on Figs. 9.16 and 9.17 shows the b.e.p. head-capacity with head measured at the pump discharge. This is less than the head at the impeller discharge by the amount of the hydraulic losses in the pump casing. Disregarding this difference for

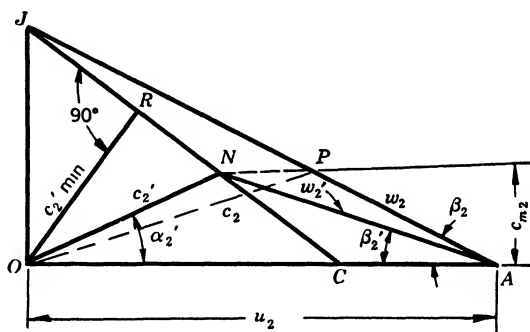


FIG. 9.17. Actual discharge velocity triangle.

optimum conditions introduces a slight error in the velocity diagrams (not over 2 per cent) and an error in angles  $\alpha_2'$  and  $\beta_2'$  of not over 1 degree.

Note that the value of the absolute velocity  $c_2'$  decreases as the specific speed increases (higher  $c_{m2}$ ) until a point  $R$  is reached where  $c_2'$  is normal to the line  $JC$ . After that the absolute velocity  $c_2'$  begins to increase. For the useful range of specific speeds the absolute velocity  $c_2'$  decreases with the specific speed. The average volute velocity is lower than  $c_2'$  obtained from the actual velocity triangle for reasons given in Chapter 7.

In Fig. 9.16 the whole field represents the b.e.p. of pumps. Thus by connecting any point ( $N$ ) on the chart with points  $O$  and  $A$ , the "actual" discharge velocity triangle is obtained; it gives the values of the relative and absolute velocities ( $c_2'$  and  $w_2'$ ) to scale, and the magnitude of the angles  $\alpha_2'$  and  $\beta_2'$ . Angle  $\alpha_2'$  determines the volute angle  $\alpha_v$  or the diffusion vane angle  $\alpha_3$ .

The experimental values of the diffusion vane angle  $\alpha_v$  at the mean effective diameter  $D_m$  and of the discharge angle  $\beta_2 = 22\frac{1}{2}^\circ$  for vertical turbine pumps, in Fig. 7.19, are in agreement with the values of the angle  $\alpha_2'$  determined from Fig. 9.16. Those marked "upper limit"

(in Fig. 7.19) are used with higher discharge angles  $\beta_2$  to obtain a maximum output from a given size of the pump casing. The practical values of the volute angle  $\alpha_v$  are appreciably lower than those for the vertical turbine pumps of the same specific speed. In a great many existing designs the high angle portion of the volute cut-water has been removed to accommodate oversize impellers without an appreciable effect on the pump efficiency.

Knowledge of the value of the relative velocity  $w_2'$  permits a check of the area normal to the relative velocity. This is important as it is possible to lay out an impeller for given values of  $c_{m2}$  and  $\beta_2$  and at the same time not to provide a sufficient area for the relative velocity  $w_2'$ . This usually happens when short cuts, such as the use of an arc of circle to draw a vane, or the development of the vane tips on a cone and the drawing of the rest of the vane by eye, are used in laying out the impeller vanes.

**(c) Design Constants.** *To enter the chart for a selection of design constants the specific speed  $n_s$  should be known. This means that the rotative speed should be selected for a given set of head-capacity conditions. The b.e.p. is located for an established specific speed and chosen angle  $\beta_2$ . The value of  $\phi$  and  $\psi$  give the capacity and speed coefficients. The peripheral velocity  $u_2$  and impeller mean effective diameter  $D_m$  are found from the head constant  $\psi$ ; the meridional velocity  $c_{m2}$  is obtained from the capacity constant  $\phi$ .*

For axial flow impellers outside diameter  $D_o$  is obtained from

$$D_o^2 = \frac{2D_m^2}{1 - \rho^2} \quad (9.14)$$

where  $\rho = D_h/D_o$  is the assumed hub ratio.

*The ratio of  $(\tan \beta_2)/\phi$ , both being read from the diagram, is simply the impelling ratio, a useful factor for the determination of vane discharge angles for several streamlines when that for the mean effective diameter is known.*

*The value of the head coefficient gives, at the same time, the value of the vane spacing  $l/t$  to a certain scale.*

$$\frac{l}{t} = C_H \psi \quad (9.15)$$

where  $t = \pi D_m/z$ , and  $z$  is the number of vanes. The constant can be established experimentally if the optimum value of  $l/t$  at one set of values of  $\phi$  and  $\psi$  is available.

From Schmidt's tests of a two-vane impeller of an axial flow pump, it has been found that  $l/t = 0.665$  (63 per cent of projected area) and the value of  $\psi = 0.14$ , thus giving  $C_t = 4.75$ .

*The value of  $l/t$  gives the vane length for axial flow impellers and number of vanes for mixed flow and centrifugal impellers, the vane length for these pumps being fixed by the impeller profile and vane angles.*

**(d) Performance Data.** Euler's and input head-capacity lines can be drawn for any discharge vane angle by connecting points  $A$  and  $B$  respectively with the  $\tan \beta_2$  points on the  $\phi$  axis for a selected value of  $\beta_2$ . For the actual performance two points are available, the b.e.p. and the shut-off head  $\psi_s$ . The b.e.p. is obtained from the intersection of the specific speed curve  $n_s$  (or  $\omega_s$ ) with the  $\psi$  lines radiating from point  $C$ . The shut-off head  $\psi_s = 0.585$  (point  $D$ ) is common for pumps of all specific speeds. The ratio  $\psi_s/\psi$  determines the steepness of the head-capacity curve. The complete curve is drawn from the typical curve for the selected specific speed and two known points  $\psi_s$  and b.e.p.

The hydraulic efficiency  $e_h = CO/BO$  and the vane efficiency  $e_{va} = BO/AO$  are constant for all specific speeds and are independent of the impeller discharge angle  $\beta_2$ .

It has been shown in Chapter 3 that areas on the head-capacity and velocity diagrams represent work to scale. The input diagram will give the input energy; the "actual" velocity or head-capacity diagrams will give the output of the pump. This property of the diagram has little practical importance.

**(e) The Functional Relationships.** The functional relationship of the variables represented in Fig. 9.16 is shown by the fact that every point on the chart represents the b.e.p. for a certain specific speed and at the same time reveals the main design features to obtain such performance. A definite pattern of flow was followed, and a number of deductions were necessary to establish the basic principles for the construction of the diagram. These are reviewed briefly below.

(a) *Consideration was limited to pump sizes where the scale effect could be disregarded, and the performance approached its "optimum" value.*

(b) *The discussion was confined to best efficiency points only. The effect of the casing is reduced to a minimum, and all the hydraulic losses are essentially friction losses.*

(c) *One value of the discharge angle was selected for all theoretical deductions and the results were applied to any value of the discharge angle.*

(d) *The mean effective discharge diameter  $D_m$  was used to represent the characteristics of all pumps. It is only on this basis that all pumps—centrifugal, mixed flow, and axial flow—fall into one continuous row.*

(e) *The conception of the mean effective diameter has meaning only when the forced vortex pattern of head generation at different diameters is accepted.*

(f) In order to accept the forced vortex mode of action in the impeller it is necessary to refute the prevailing conception that the free vortex pattern of flow is the only one giving a stable condition without "cross flows."

(g) *To introduce the forced vortex pattern of flow it was necessary to introduce the concepts of integrated head and conduction of pressure to explain the action of the pump diffusion casing.*

(h) *To obtain the forced vortex component of flow, the meridional flow needed the use of "energy gradient" to explain the flow.*

(i) *The geometrical procedure for the construction of the diagram is based on the vane efficiency and hydraulic efficiency being constant for all specific speeds and independent of the discharge vane angle.*

(j) Use of consistent dimensionless head and capacity coefficients  $\psi$  and  $\phi$  reduced the head-capacity and discharge velocity diagrams to the same scale (in fact made them identical), thus combining in one chart both essential features of design and performance.

The diagram as it appears in Fig. 9.16 involves only the essential elements of the discharge velocity triangle. The experimental speed and capacity constants are based on designs where some prerotation was allowed. It has been shown in Fig. 9.4 that prerotation is unavoidable at the b.e.p. This affects the selection of the vane entrance angle  $\beta_1$ . A few guiding thoughts were given for its selection in Chapter 5. For a normal design, no provision should be made for prerotation when the author's diagram is being used. However, if for some reason prerotation exceeding the normal is allowed, it could be taken care of by adding to the required total head a value equal to the subtractive term of the complete Euler's equation and calculating the head coefficient for the new head  $H'$  thus obtained, or

$$H' = \frac{u_2 c_{u2}'}{g} = H + \frac{u_1 c_{u1}}{g} \quad (9.15)$$

where  $c_{u1}$  is the estimated tangential component of the absolute velocity at entrance.

There are a number of design elements in addition to those represented in the diagram of Fig. 9.16 which have a bearing upon the pump performance, such as the hub ratio and the profile cone angle of propeller pumps. If these deviate considerably from the normal average

values, the points of  $\psi$  and  $\phi$  values will not fall on their proper places in Fig. 9.16.

It is impossible to define what constitutes a "continuous and consistent row" of specific speed types, even for the impellers alone, without discussing every detail of a line of good representative types. The effect of the pump casing (even the suction sump in the case of propeller pumps) introduces additional uncertainties. It is left to the designer's judgment to recognize such deviations from normal designs and anticipate their effect on the pump performance.

**(f) Author's Diagram of Centrifugal Pump Characteristics for Viscous Liquids.** Location of point  $C$  in Fig. 9.16 determines the optimum hydraulic efficiency for pumps pumping water. When viscous liquids are being handled, the optimum hydraulic efficiency of pumps will be lower and the point  $C$  will be placed below its position in Fig. 9.16, depending on the viscosity of the liquid. If position of the point  $C$  on the diagram is connected with the Reynolds number rather than with the viscosity of the liquid, the hydraulic efficiency  $CO/BO$  will express the effect of the pump size in addition to the effect of viscosity. In fact it is possible to construct a scale of Reynolds numbers along the axis of  $\psi$  in Fig. 9.16; this will permit drawing the hydraulic characteristics for any liquid and size of pump, the procedure outlined in this chapter being used.

However, there are a number of difficulties in construction of such a "universal" diagram: (1) when viscous liquids are being pumped the affinity laws become approximate only, deviation increasing with viscosity (Fig. 14.14), and affinity laws are the basis of the diagram in Fig. 9.16; (2) the difference between the input and total head is a hydraulic loss. At high viscosity or low Reynolds numbers hydraulic losses may follow different laws for different specific speeds, and there is no assurance that line joining the b.e.p. for a given impeller discharge angle and the Reynolds number will fall on a straight line. There is no experimental data covering a wide range of specific speeds to plot such lines experimentally. In any case, such a "universal" diagram would be of academic interest only, as design of centrifugal pumps is always referred to water performance. Characteristics of pumps handling viscous liquids are estimated by applying correction factors to water head, capacity, and efficiency as presented in Chapter 14.

#### REFERENCES

1. HUGO RICHTER, *Rohrhydraulic*, Berlin, Julius Springer, 1934, p. 201.
2. A. H. GIBSON, *Hydraulics and Its Applications*, New York, D. Van Nostrand, 1935, p. 200.

3. C. PFLEIDERER, *Die Kreiselpumpen*, Berlin, Julius Springer, 1932, p. 199.
4. WILHELM SPANNHAKE, *Centrifugal Pumps*, Cambridge, Mass. Inst. of Tech. 1934, p. 152 (translation).
5. JOSEPH N. LECONTE, *Hydraulics*, New York, McGraw-Hill, 1926, p. 314.
6. JOSEPH LICHTENSTEIN, "Method of Analyzing the Performance Curves of Centrifugal Pumps," *Trans. A.S.M.E.*, Vol. 50, No. 3, 1928, p. 3.
7. ERICH SCHRÖDER, *Das Förderhohenverhältnis einer radialen Kreiselpumpe*, doctoral dissertation, Tech. Hochschule Braunschweig, 1933, p. 26.

## CHAPTER 10

### LEAKAGE, DISK FRICTION, AND MECHANICAL LOSSES

#### 10.1 LEAKAGE LOSS

(a) **Volumetric Efficiency.** Leakage loss is a loss of capacity through the running clearances between the rotating element and the stationary casing parts. Leakage can take place in one or several of the following places, according to the type of pump: (1) between the casing and the impeller at the impeller eye; (2) between two adjacent stages in multistage pumps; (3) through the stuffing box; (4) through axial thrust balancing devices; (5) through bleed-off bushings when used to reduce the pressure on the stuffing box; (6) past vanes in open impeller pumps; (7) at any bleed-off used for bearing and stuffing box cooling.

The capacity through the impeller is greater than the measured capacity of the pump by the amount of leakage, and the ratio of the measured capacity  $Q$  to the impeller capacity  $Q + Q_L$  is the volumetric efficiency.

$$\frac{Q}{(Q + Q_L)} = e_v \quad (10.1)$$

Usually the volumetric efficiency takes into account only the leakage between the impeller and casing at the impeller eye for multistage and single-stage pumps. The interstage leakage in multistage pumps and leakage through the balancing devices or any other point should be treated separately. In each case the amount of such leakage should be multiplied by the pressure drop across the clearance to obtain the power loss due to leakage. Although the actual pressure at the clearance may be reduced as a result of the vortex action of the impeller, the full-stage pressure, or a multiple of the stage-pressure, depending on the stage at which the loss occurs, should be used to calculate the loss of power due to leakage since the amount of leakage is given full input head when it passes through the impeller. Thus  $(hp.)_L = Q_L H / e_h$  is the power loss due to leakage.

Figure 10.1 shows several popular designs of impeller and casing rings. These may be modified by including a step instead of one continuous throttling surface. The bleed-off devices consist of long throttling sur-



faces (Fig. 10.2), continuous or interrupted by steps, grooves, or arranged as a labyrinth, in which case there are really several throttling surfaces in series.

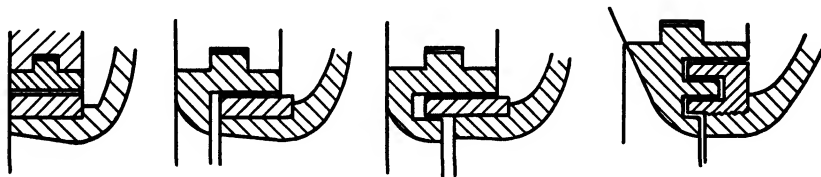


FIG. 10.1. Wearing-ring types.

For a known pressure drop across the clearance, the amount of leakage can be calculated by the following formula.

$$H_L = f \frac{L}{d} \frac{v^2}{2g} + 0.5 \frac{v^2}{2g} + \frac{v^2}{2g} = \left( f \frac{L}{d} + 1.5 \right) \frac{v^2}{2g} \quad (10.2)$$

where  $H_L$  is the head across the clearance, in feet

$f$  is a friction coefficient—dimensionless

$v$  is velocity through the clearance, in feet per second

$L$  is the length of the throttling surface, or width of the wearing ring, in feet

$d$  is the diameter of a circular pipe, in feet, having the same hydraulic radius  $m$  as the annular channel of the clearance.

Hydraulic radius is defined as

$$m = \frac{d}{4} = \frac{\text{area of clearance}}{\text{wetted perimeter}} = \frac{\pi Da}{2\pi D \times 2} = \frac{a}{4} \quad (10.3)$$

where  $D$  is the average diameter of the throttling surfaces and  $a$  is the diametrical clearance, both in feet. Note from the above that  $d = a$ .

The first term in equation 10.2 represents the friction loss, the second the entrance loss, and the last the velocity head at discharge from the clearance. The diameter  $d$  of a circular pipe having the same hydraulic

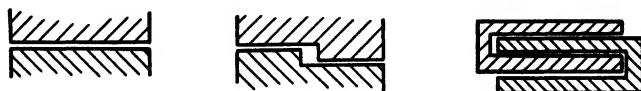


FIG. 10.2. High pressure sealing arrangements.

radius as the annular channel of the clearance is introduced to make possible comparisons of friction coefficients found on special tests for close annular clearances with those for circular pipes. Figure 10.3 shows the values of  $f$  calculated by formula 10.2 from test results of

several investigations. The values of  $f$  are plotted against the Reynolds number  $R = vd/\nu$ , where  $\nu$  is the kinematic viscosity of liquid in square feet per second.

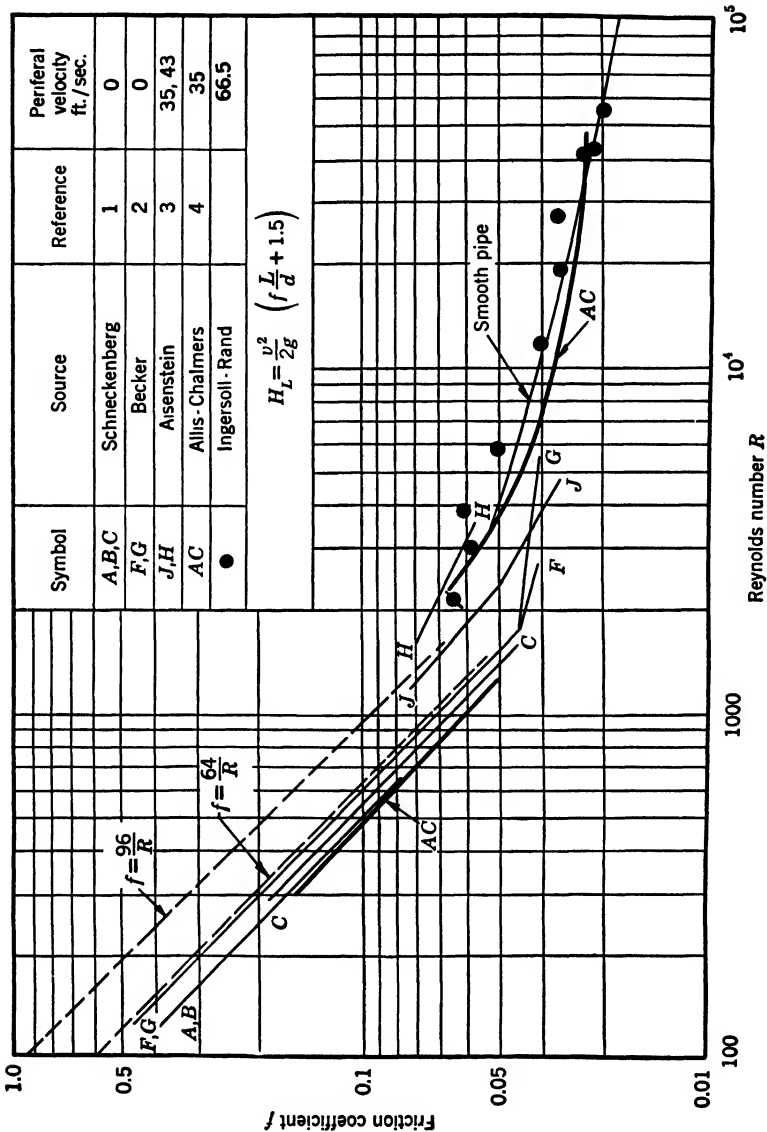


Fig. 10.3. Friction coefficient for flow through annular clearances.

In the turbulent flow region, ( $R > 2500$ ) the values of  $f$  for small annular channels with revolving rings follow the curve for smooth round pipes.<sup>10</sup> This is merely a coincidence, because there is no geo-

metrical similarity of the channels or velocity distribution between the two patterns of flow. In the turbulent region of flow the amount of flow does not depend on the shaft speed (Ingersoll-Rand tests with  $4\frac{1}{4}$ -in. shaft at 0 to 3600 r.p.m.).

In the laminar region, the experimental points for both a stationary and revolving ring arrange themselves nearer the line  $f = 64/R$  (determined theoretically for circular pipes) than the line  $f = 96/R$  for the annular channels. The value of  $f$  for laminar flow is affected by the speed of rotation, and will be found to increase with the speed. It is also sensitive to the eccentricity of the clearance. Thus, according to Schneckenberg<sup>1</sup> maximum eccentricity may increase the amount of leakage to 2.5 times the amount for a concentric annular channel. In the turbulent region of flow the increase of flow due to eccentricity is only about 30 per cent.

Values of  $f$  for narrow rings in the viscous flow regime will be found to be higher than those on Fig. 10.3 as there is not sufficient time for the flow to assume its final velocity distribution. According to Nikuradse<sup>5</sup> it takes a length of 30 to 40 pipe diameters for the flow to develop its steady pattern of velocity distribution. The matter is further complicated by the effect of heat (produced by friction) on the viscosity of the liquid. This becomes an important factor for viscous liquids where long throttling surfaces and small clearances are involved. Calculation of the amount of leakage under such conditions becomes very uncertain. The author has run very extensive tests on leakage through rings of different designs under actual operating conditions of the pump. The chart in Fig. 10.4 is compiled from the original report,<sup>6</sup> and the comparative merits of different designs are evident from this tabulation. Blackwell and Murdock's tests<sup>4</sup> show that the amount of leakage is reduced 20 to 25 per cent when either the stationary bushing or the revolving sleeve is grooved.

**(b) Pressure at the Wearing Rings.** The pressure  $H_L$  across the clearance at the impeller eye is lower than the pressure in the volute casing  $H_p$ . The reduction in pressure at the wearing ring is caused by rotation of the liquid in the space between the impeller and casing walls. It is usually assumed that the liquid in this space rotates at half the impeller angular velocity. The pressure in the volute can be obtained by subtracting from the pump total head the kinetic energy of flow in the volute (the loss of head due to friction in the volute casing and the velocity head in the suction nozzle being disregarded).

$$H_v = H - \frac{c_3^2}{2g} = H(1 - K_3^2) \quad (10.4)$$

where  $c_3$  is the volute velocity and  $K_3$  is determined from  $c_3 = K_3\sqrt{2gH}$ ,


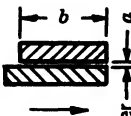





		a in.	b in.	Leakage per cent at r.p.m.			
				1400	1700	2000	2500
1		0.012	$1\frac{1}{16}$	1.52	1.80	2.00	2.18
2	 On diameter	0.012	$1\frac{1}{16}$	2.85	3.32	3.52	3.70
3		0.012	$1\frac{1}{16}$	3.52	4.03	4.33	4.50
4		0.017	$1\frac{1}{16}$	6.06	6.65	6.70	6.70
5		0.020	$1\frac{1}{16}$	7.92	8.62	8.86	8.60
6		0.029	$1\frac{1}{16}$	13.2	13.9	14.0	14.0
7		0.039	$1\frac{1}{16}$	18.7	19.6	19.8	20.0
8	 Circular groove $\frac{1}{16} \times \frac{1}{16}$ $\frac{1}{8}$ apart	0.017	$1\frac{1}{16}$	4.83	5.38	5.58	5.52
9		0.029	$1\frac{1}{16}$	12.7	13.5	13.7	13.6
10		0.011	$1\frac{1}{16}$	3.18	3.68	3.94	4.08
11		0.021	$1\frac{1}{16}$	8.53	9.04	9.15	9.19
12		0.011	$1\frac{1}{16}$	2.52	2.88	2.92	2.98
13	$\frac{1}{16} \times \frac{1}{16}$ spiral groove	0.021	$1\frac{1}{16}$	6.24	6.68	6.89	6.82
14		0.010	$1\frac{1}{16}$	2.55	3.03	3.28	3.44
15		0.010	$1\frac{1}{16}$	2.07	2.34	2.45	2.52

FIG. 10.4. Leakage loss in per cent of normal capacity at several speeds; 3-in. pump,  $n_s = 1090$ ,  $D_2 = 10\frac{1}{8}$  in., ring diameter =  $4\frac{1}{8}$  in.

one of the design constants. The pressure at the wearing rings is given by

$$H_L = H(1 - K_3^2) - \frac{1}{4} \frac{u_2^2 - u_r^2}{2g} \quad (10.5)$$

where  $u_r$  is the peripheral velocity of the impeller ring. From actual pressure measurements on one pump of  $n_s = 1090$ , using two impeller diameters, the author has developed an empirical formula for the pressure at the ring for b.e.p. The equation is

$$H_L = \frac{3}{4} \frac{u_2^2 - u_1^2}{2g} \quad (10.6)$$

where  $u_1$  is the peripheral velocity of the vane entrance tip. The development of this formula is given in the original report.<sup>6</sup>

(c) **Leakage Loss versus Specific Speed.** Using coefficients from Fig. 10.3, the author has calculated the leakage loss for a number of

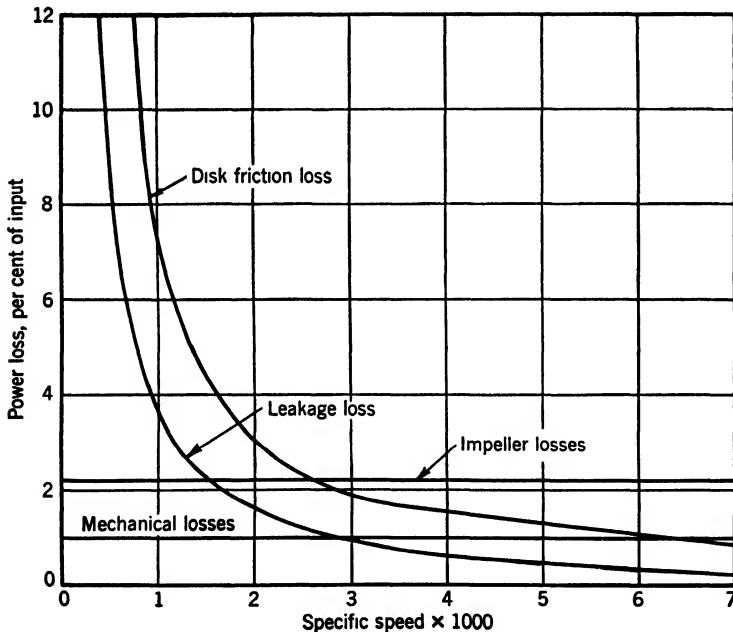


FIG. 10.5. Losses versus specific speed for double-suction pumps.

double-suction horizontally split pumps of different specific speeds, and the results are shown in Fig. 10.5. In all cases actual clearances and wearing-ring widths for plain flat rings were used. It will be observed that leakage loss decreases rapidly with increasing specific speed.

For the purpose of further discussion it is important to establish some general relationships between leakage loss and specific speed. It will be shown that the power loss due to leakage is constant for pumps of the same specific speed, irrespective of pump size and speed. Equation 10.2 will be used for calculation of the amount of leakage.

$$Q_L = CA\sqrt{2gH_L} \quad (10.7)$$

where

$$C = \frac{1}{\sqrt{f\frac{L}{d} + 1.5}}$$

$$A = \frac{a\pi D}{2}, \text{ the clearance area}$$

$$H_L = K_r H$$

The coefficient of discharge  $C$  and the factor  $K_r$ , expressing  $H_L$  as a fraction of the pump total head, are assumed to be constant for similar pumps. The power lost because of the back-flow through the clearance is

$$(\text{hp.})_L = \frac{Q_L \gamma H}{e_h 550} \quad (10.8)$$

where  $\gamma$  is the weight of 1 cu. ft. of water. The ratio of power lost due to leakage of two pumps is equal to

$$\frac{(\text{hp.})_{L1}}{(\text{hp.})_{L2}} = \frac{a_1 D_1 H_1^{3/2}}{a_2 D_2 H_2^{3/2}} \quad (10.9)$$

If similarity of the two pumps is extended to the wearing-ring diameters and clearances,

$$\frac{a_1 D_1}{a_2 D_2} = \frac{D_{1o}^2}{D_{2o}^2} \quad (10.10)$$

where  $D_{1o}$  and  $D_{2o}$  are the outside impeller diameters of the two pumps. Substituting this into equation 10.9 we obtain

$$\frac{(\text{hp.})_{L1}}{(\text{hp.})_{L2}} = \frac{D_{1o}^2 H_1^{3/2}}{D_{2o}^2 H_2^{3/2}} \quad (10.11)$$

Making use of equation 10.12, which gives the type-unit-capacity relationships for similar pumps, we can change equation 10.11 to 10.13.

$$\frac{Q_1}{\sqrt{H_1 D_{1o}^2}} = \frac{Q_2}{\sqrt{H_2 D_{2o}^2}} = \text{constant} \quad (10.12)$$

$$\frac{(\text{hp.})_{L1}}{(\text{hp.})_{L2}} = \frac{Q_1 H_1}{Q_2 H_2} = \text{constant} \quad (10.13)$$

This equation states that *the power lost in leakage is proportional to the pump output. Hence, if expressed as a percentage of the pump output, this loss is constant for all similar pumps.\** In practice, however, the leakage loss is greater for smaller pumps, because the clearances cannot be reduced below a certain minimum; also because the wearing rings of larger pumps are wider, and the coefficient of discharge  $C$  is smaller.

In order to compare the leakage loss horsepower for pumps of the same output but of different specific speed, revolutions per minute, and size, we may write equation 10.9 as before:

$$\frac{(\text{hp.})_{L1}}{(\text{hp.})_{L2}} = \frac{a_1 D_1 H_1^{3/2}}{a_2 D_2 H_2^{3/2}} = \frac{D_1^2 H_1^{3/2}}{D_2^2 H_2^{3/2}} \quad (10.14)$$

assuming that the width of the wearing rings and the coefficient  $C$  have the same value, and that the clearances vary in the same ratio as the impeller wearing-ring diameters. The radial velocity at the impeller eye varies with the impeller type and speed, and a ratio of radial velocities may be expressed in terms of the head as follows.

$$\frac{c_{m1}}{c_{m2}} = \frac{K_{m1} H_1^{1/2}}{K_{m2} H_2^{1/2}} \quad (10.15)$$

Assuming that the full impeller eye area  $= \pi D^2/4$  is available for the flow, that is, the pump is of the overhung impeller construction, or that the effect of the presence of the shaft in the impeller eye upon the ratio of the impeller eye areas may be neglected, we can write

$$\frac{Q_1}{Q_2} = \frac{c_{m1} D_1^2}{c_{m2} D_2^2} = \frac{K_{m1} H_1^{1/2} D_1^2}{K_{m2} H_2^{1/2} D_2^2} \quad (10.16)$$

Combining this equation with equation 10.14 we obtain

$$\frac{(\text{hp.})_{L1}}{(\text{hp.})_{L2}} = \frac{Q_1 H_1 K_{m1}}{Q_2 H_2 K_{m2}} = \frac{K_{m2}}{K_{m1}} \quad (10.17)$$

Since the water horsepower (w.hp.) is the same for both pumps, the ratio of the leakage loss horsepower, expressed in per cent of water horsepower, will be given by equation 10.17. The value of factor  $K_m$  increases with an increase of specific speed; hence for the same pump output the leakage loss is higher for the lower specific speed pump.

\* The relationship represented by equation 10.13 (and later by equation 10.17) is approximate only and is intended to show the trend of variation of the leakage loss with specific speed, pump size, and speed. In addition to depending on the physical dimensions of the throttling surfaces, the amount of leakage also depends on the Reynolds number, as shown by Fig. 10.3. The same applies to equations 10.24 and 10.28, which deal with the disk friction loss.

For example, for  $n_s = 1000$  the factor  $K_{m1} = 0.138$ , and for  $n_s = 2000$  the factor  $K_{m2} = 0.188$ , and the ratio of the leakage loss horsepower is equal to

$$\frac{(\text{hp.})_{L1}}{(\text{hp.})_{L2}} = \frac{0.188}{0.138} = 1.35$$

## 10.2 DISK FRICTION LOSS

**(a) Disk Friction Loss Formulas.** Of all external mechanical losses the disk friction is by far the most important. Considerable test data are available on the disk friction loss for cold water, and several formulas are in use. All of these stem from one fundamental formula:

$$(\text{hp.})_d = Kn^3D^5 \quad (10.18)$$

where  $(\text{hp.})_d$  is the power absorbed by disk friction

$K$  is an experimental factor which also takes care of the units used

$n$  is the revolutions per minute

$D$  is the disk diameter in feet.

Several formulas use fractional exponents for  $n$  and  $D$ , the authors claiming that only in that case is  $K$  a real constant. The derivation of the formula 10.18 follows. Referring to Fig. 10.6, a disk of diameter  $D$ , or radius  $r$ , is revolved at an angular speed of  $\omega$ . Assuming turbulent flow at the disk surface, the friction force at radius  $r$  exerted on a ring having width  $dr$  can be expressed as

$$F = KAv^2 = K2\pi v^2 r dr$$

The power required to overcome this resisting force is found by multiplying it by the velocity  $v$ , or

$$(\text{hp.})_d = K2\pi \int_0^r v^3 r dr = K2\pi \omega^3 \int_0^r r^4 dr = \frac{K2\pi \omega^3 r^5}{5}$$

If we combine all constants into one, include the power loss for both sides of the disk, use  $n = \text{r.p.m.}$  instead of angular velocity  $\omega$ , and diameter  $D$  instead of the radius, we obtain the formula

$$(\text{hp.})_d = Kn^3D^5 \quad (10.18)$$

The particles of liquid in the space between the disk and stationary walls acquire a rotary motion. As a result of centrifugal forces, particles start moving outward in the immediate neighborhood of the disk and

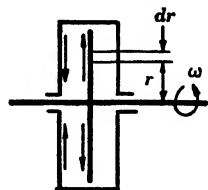


FIG. 10.6. Disk friction loss.



new particles approach the disk near the center. Thus a circulation is established. If the path of circulation is short, or the volume of the liquid surrounding the disk is small, particles approaching the disk will retain part of their rotary motion, thus requiring less power from the disk. Gibson and Ryan<sup>7</sup> and LeConte<sup>8</sup> have found experimentally that the power to drive a disk increases as the clearance between the disk and walls is increased. For instance, when the clearance was increased from 1.03 to 17.7 per cent of the disk diameter, the power increased by 4 to 12 per cent. The same investigators have also established that: (a) painting a rough cast iron casing reduces disk friction power by 16 to 20 per cent; (b) polishing the disk reduces the loss by 13 to 20 per cent; (c) badly rusted cast iron disks take 30 per cent more power than the same disks newly machined; (d) increase of water temperature from 65°F. to 150°F. decreased the disk friction power by 7 to 19 per cent, depending on the combination of the disk and casing finish.

The formulas by Gibson and LeConte have fractional exponents and are not convenient for use. Pfeiderer<sup>11</sup> gives the following formula for disk friction horsepower for water.

$$(\text{hp.})_d = \frac{0.375n^3D^5}{10^9} \quad (10.18a)$$

where  $D$  is the disk diameter in feet. This formula gives values of  $(\text{hp.})_d$  in close agreement with those obtained by using the Gibson and LeConte formulas.†

When viscous liquids are being pumped the disk friction loss becomes of increased importance. von Kármán<sup>12</sup> has developed analytically a formula for disk friction loss for *one side of the disk only* which is for the laminar flow:

$$M = \frac{1.84}{\sqrt{R}} \gamma r^3 \frac{u^2}{2g} \quad (10.19)$$

For the turbulent flow

$$M = \frac{0.073}{\sqrt[5]{R}} \gamma r^3 \frac{u^2}{2g} \quad (10.20)$$

where  $M$  is the resisting moment, in foot-pounds

$R$  is Reynolds' number, dimensionless

$r$  is the disk radius, in feet

$u$  is the peripheral velocity at radius  $r$ , in feet per second

$\gamma$  is the liquid density, in pounds per cubic foot (62.3 for water).

† In the second edition (1932) of his book, *Die Kreiselpumpen*, pp. 47 and 221, Pfeiderer increased the numerical constant in formula 10.18a from 0.375 to 0.41, which is believed to be on the high side.

Kármán's formulas were developed for a disk revolving on the surface of unlimited liquid space, and was substantiated in tests by Schmidt and Kempf.<sup>12</sup> When applied to calculation of disk friction losses for a disk running in a housing, the calculated loss is too high in comparison with other formulas based on experimental data.

Ippen,<sup>18</sup> applying Kármán's method of analysis for a disk revolving in a casing, has arrived at numerical coefficients in formulas 10.19 and 10.20 considerably smaller than those in Kármán's formulas. Thus for the laminar flow and one side of the disk

$$M = \frac{1.30}{\sqrt{R}} \gamma r^3 \frac{u^2}{2g} \quad (10.19a)$$

and for the turbulent flow

$$M = \frac{0.0418}{\sqrt[5]{R}} \gamma r^3 \frac{u^2}{2g} \quad (10.20a)$$

These formulas agree satisfactorily with the Schultz-Grunow<sup>9</sup> and Zumbusch experimental results for disks revolving in housings.

At the critical Reynolds number both formulas should give the same result; hence, for the critical conditions

$$\frac{1.30}{\sqrt{R}} = \frac{0.0418}{\sqrt[5]{R}}$$

and the critical Reynolds number is found to be  $R = 10^5$ .

Schultz-Grunow<sup>9</sup> also has confirmed experimentally what has been a common assumption, that the liquid confined between the disk and the casing walls rotates bodily with one half of the angular velocity of the disk.

**(b) Disk Friction of Pumps of Same Specific Speed but of Different Size and Speed.** Consider two pumps of the same specific speed having impeller diameters  $D_1$  and  $D_2$ , heads  $H_1$  and  $H_2$ , capacities  $Q_1$  and  $Q_2$ , and speeds  $n_1$  and  $n_2$  respectively. The power consumed by disk friction is

$$(\text{hp.})_d = Kn^3 D^5 \quad (10.21)$$

The ratio of the disk friction horsepower of the two pumps is

$$\frac{(\text{hp.})_d)_1}{(\text{hp.})_d)_2} = \frac{(D_1 n_1)^3 D_1^2}{(D_2 n_2)^3 D_2^2} \quad (10.22)$$

Combining this equation with those for the type-unit-capacities (equation 10.12) and the type unit speed equation 10.23,

$$\frac{n_1 D_{10}}{\sqrt{H_1}} = \frac{n_2 D_{20}}{\sqrt{H_2}} \quad (10.23)$$

we obtain

$$\frac{(\text{hp}.d)_1}{(\text{hp}.d)_2} = \frac{Q_1 H_1}{Q_2 H_2} \quad (10.24)$$

which states that the disk friction horsepower varies as the pump output. This could be expected from an inspection of the formula for disk friction loss because both the disk friction power loss and the pump output (water horsepower) vary as the cube of the speed and the fifth power of the impeller diameter. *From equation 10.24 it follows that the ratio of the disk friction horsepower to the water horsepower is constant for the same specific speed irrespective of the size and speed of the pump.*

**(c) Disk Friction of Pumps of Same Output but of Different Specific Speed, Size, and Revolutions per Minute.** For two pumps of the same water horsepower, the ratio of specific speeds is

$$\frac{n_{s1}}{n_{s2}} = \frac{n_1 Q_1^{1/2} H_2^{3/4}}{n_2 Q_2^{1/2} H_1^{3/4}} = \frac{n_1 H_2^{5/4}}{n_2 H_1^{5/4}} \quad (10.25)$$

Ratio of heads may be obtained from

$$\frac{u_1}{u_2} = \frac{K_{u1} \sqrt{H_1}}{K_{u2} \sqrt{H_2}} = \frac{D_1 n_1}{D_2 n_2} \quad (10.26)$$

where  $u_1$  and  $u_2$  are the peripheral velocities of the two impellers at the outlet and  $K_{u1}$  and  $K_{u2}$  are the speed factors from

$$u = K_u \sqrt{2gH} \quad (10.27)$$

Combining equations 10.25 and 10.26 with equation 10.21 we get for the ratio of the horsepower consumed by the disk friction of the two pumps

$$\frac{(\text{hp}.d)_1}{(\text{hp}.d)_2} = \frac{n_{s2}^2 K_{u1}^5}{n_{s1}^2 K_{u2}^5} \quad (10.28)$$

For example, for  $n_{s1} = 1000$ ,  $K_{u1} = 0.98$ ; for  $n_{s2} = 2000$ ,  $K_{u2} = 1.04$ ; Thus

$$\frac{(\text{hp}.d)_1}{(\text{hp}.d)_2} = \frac{(2000)^2 (0.98)^5}{(1000)^2 (1.04)^5} = 4 \times 0.735 = 2.94$$

**(d) Actual Disk Friction Loss versus Specific Speed.** By using Pfleiderer's formula (10.18a) the disk friction loss was computed for a number of double-suction pumps of different specific speeds. This loss expressed as percentage of pump brake horsepower is plotted in Fig. 10.5. Attention is called to the rapid rise of disk friction loss at specific

speeds below 2000. It is interesting to note that, almost throughout the entire range of specific speeds, leakage loss is approximately equal to one half of the disk friction loss.

### 10.3 MECHANICAL LOSSES

**(a) Stuffing Box and Bearing Losses.** Although the nature of mechanical losses in the bearings and stuffing boxes is well understood, very little actual data on the values of these losses are available. The difficulty lies in their being small and difficult to measure with ordinary testing facilities. On the other hand, it is felt that such tests will be of only slight value to pump manufacturers in so far as improvement of pump performance is concerned. Both stuffing box and bearing designs are governed by requirements for satisfactory mechanical performance. The matter of friction loss in both is of secondary importance. Besides, friction loss in the stuffing boxes is affected by a number of factors, for example, size and depth of stuffing box, pump speed, pressure, and method of packing and lubrication, so that any actual values will be illustrative of a certain type of stuffing box application only.

Although ball bearing sizes are well standardized, the friction loss in the ball bearings varies for the same size and load for different makes of bearings. Also, the method of lubrication affects the losses in ball bearing, as shown by bearing running temperatures. It has been found that the type of coupling between the pump and driver affects the bearing behavior and, hence, losses, as some couplings impose an axial load on the thrust-type ball bearings.

Figures 10.7 and 10.8 show stuffing box friction power loss obtained by Mockridge.<sup>13</sup> Note that the frictional torque is very high with a tight gland and small leakage, but decreases rapidly as the gland is loosened and the leakage increases. A slight increase in torque follows on further loosening of glands, as packing pulls away from the bottom of the stuffing box. In Fig. 10.8 the power loss varies approximately as the square of the speed. Assuming that the shaft as tested is good for 1250 hp. at 3000 r.p.m., the loss at the stuffing boxes at that speed will be only 0.22 per cent. At 1500 r.p.m. the same pump would require only 156 hp., and the stuffing box loss will be 0.48 per cent. Allowing an equal loss for the bearings, the mechanical losses for both items will be only about 1 per cent in the last example. However, in small pumps, under unfavorable conditions, mechanical losses may be 2 or 3 per cent or more of the brake horsepower.

Recently tests were run by Ingersoll-Rand Company on a special rotor equipped with two stuffing boxes having nine  $\frac{1}{2} \times \frac{1}{2}$  rings of

packing,  $4\frac{7}{8}$  in. outside diameter of shaft sleeves, two sleeve bearings, and a Kingsbury thrust bearing. When the boxes were sealed against 300 p.s.i. of water at  $350^{\circ}\text{F}$ ., and allowing about half a gallon of leakage

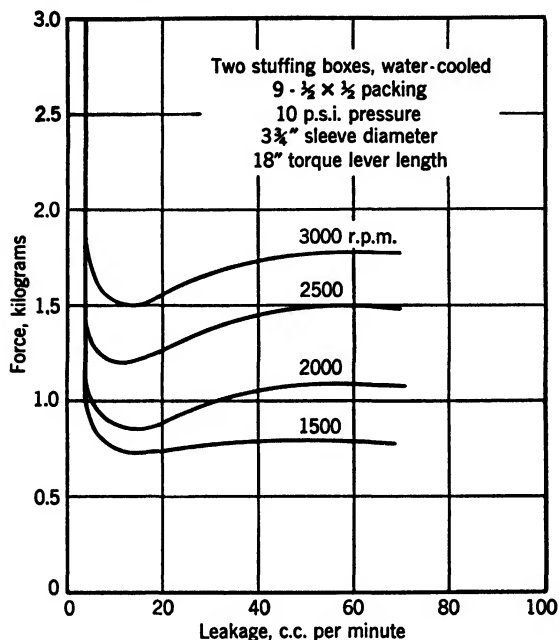


FIG. 10.7. Stuffing box friction loss (Mockridge).

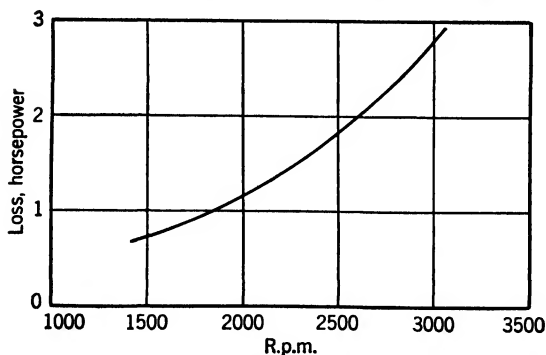


FIG. 10.8. Stuffing box friction loss. Data from Fig. 10.7 (Mockridge).

per minute from two stuffing boxes at 3500 r.p.m., the stuffing box friction horsepower was found to vary from 7.5 at the start of run to 2.5 after several hundred hours of operation. The bearing friction horsepower, with no thrust load on the bearing, was found to be 1.5. This

size of shaft was used for high pressure boiler feed pumps requiring up to 1500 hp. Thus the stuffing box friction for such a pump would vary from 0.5 to 0.2 per cent of the brake horsepower and the bearing loss would be probably 0.2 per cent, which is double the loss actually measured in the tests to allow for some axial thrust load on the thrust bearing. In the above tests the sleeves were new, the packing was properly adjusted, the stuffing boxes were water-cooled, and glands were quenched. On the basis of the above figures, a 1 per cent loss for bearings and stuffing boxes of high speed pumps would appear to be a good estimated average value. For the purpose of this discussion it will be assumed that the stuffing box and bearing friction will be equal to 1 per cent of the brake horsepower and will be independent of the specific speed. This is also shown in Fig. 10.5.

**(b) Power Balance versus Specific Speed.** If the mechanical, disk, and leakage losses for the b.e.p. for different specific speeds are known, it is possible to determine the hydraulic losses for the same points. Double-suction pumps will be considered here with their optimum efficiencies for different specific speeds as given in Fig. 9.12. Taking the lowest specific speed at which a maximum efficiency of over 90 per cent is reached ( $n_s = 2000$ ), the known losses from Fig. 10.5 are: disk friction 3.0 per cent, leakage 1.5 per cent, and mechanical loss 1.0 per cent, making a total of 5.5 per cent of the power input. Since the pump output is 90 per cent this leaves 4.5 per cent for all hydraulic losses. The hydraulic losses are essentially all friction losses and will be assumed to be equally divided between the impeller and the casing. Impeller hydraulic losses of 2.25 per cent will be assumed constant for all specific speeds.

In Fig. 10.9, a power balance is drawn for double-suction pumps of different specific speeds. The casing hydraulic losses are obtained by subtraction from the pump input of all known losses and the pump output. For specific speeds below 2000 the casing hydraulic losses remain constant and equal to the impeller losses by assumption. For higher specific speeds the casing losses increase. In Fig. 10.9 the pump output is numerically equal to the pump gross efficiency, as all values are percentages of the pump input. The output of vertical pumps is shown by a broken line. The difference between the casing losses of the two types of pumps is ascribed to the effect of the suction approach in double-suction pumps. This does not necessarily mean extra hydraulic losses in the suction nozzle as the loss also includes the detrimental effect of the 90-degree turn ahead of the impeller eye on the impeller efficiency. This effect is also evidenced by the impaired cavitation characteristics as compared with pumps of the same specific speed having a straight suction approach.

The hydraulic efficiency in terms of power is expressed as

$$e_h = \frac{Q\gamma H}{Q\gamma H + \frac{Q\gamma h_l}{e_v}} = \frac{H}{H + \frac{h_l}{e_v}} \quad (10.29)$$

where  $h_l$  is the sum of all hydraulic losses and  $e_v$  is the volumetric efficiency. The hydraulic efficiency of pumps of specific speeds below 2000 is approximately constant. Although the hydraulic losses in

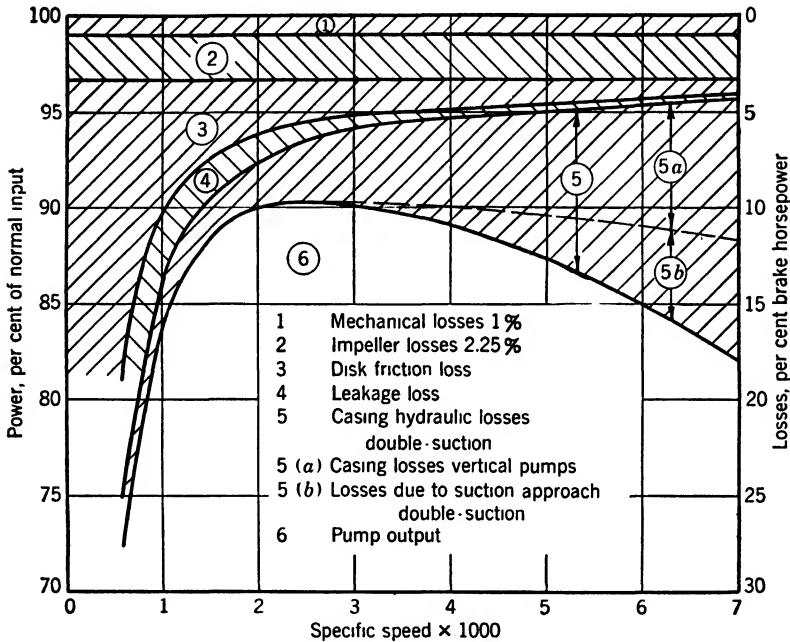


FIG. 10.9. Power balance for double-suction pumps at best efficiency points.

percent of power input are constant for pumps of specific speeds below 2000, the volumetric efficiency decreases with the specific speed and the hydraulic efficiency will also decrease, as equation 10.29 shows.

At specific speed  $n_s = 2000$ , the hydraulic efficiency as calculated from the data in Fig. 10.9 is equal to  $e_h = 95.3$  per cent. This is taken as an optimum hydraulic efficiency for all specific speeds and is marked as point *B* on the author's diagram, Fig. 9.16. *It follows from Fig. 10.9 that the hydraulic efficiency decreases for specific speeds above 2000, and this is entirely due to the increased pump casing hydraulic losses. At lower specific speeds the reduction of the gross efficiency is caused by the increased disk friction and leakage losses.*

## 10.4 LOSSES VERSUS CAPACITY AT CONSTANT SPEED

A power balance for a pump operating at a constant speed and variable capacities can be drawn, as shown in Fig. 10.10, in the following manner. This will be done for a 12-in. double-suction pump of

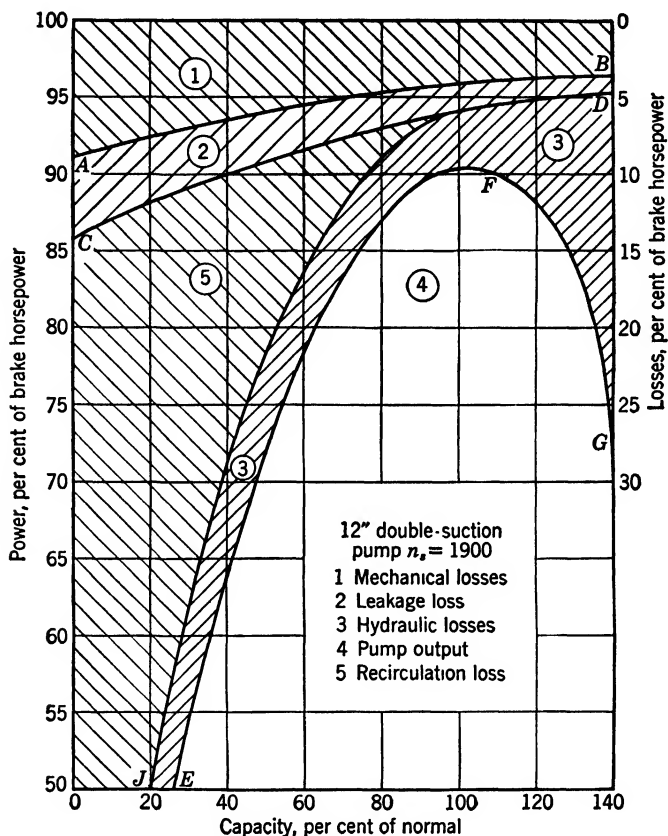


Fig. 10.10. Power balance versus capacity at constant speed.

$n_s = 1900$ , performance for which is shown in Fig. 10.11. In the same figure, the hydraulic efficiency curve is drawn. For this three points are known. For the b.e.p. the hydraulic efficiency was estimated above to be 95.3 per cent. At shut-off the hydraulic efficiency is obtained from Fig. 9.16 and is equal to

$$e_h = \frac{DO}{BO} = \frac{58.5}{72.5} = 0.808 \quad (10.30)$$



The third point is the zero efficiency point which is zero head point on the head-capacity curve. The hydraulic efficiency for two points *A* and *B* being known, the input head line *DE* can be drawn, and hydraulic efficiency  $e_h = H/H_i$  can be plotted for every point. To

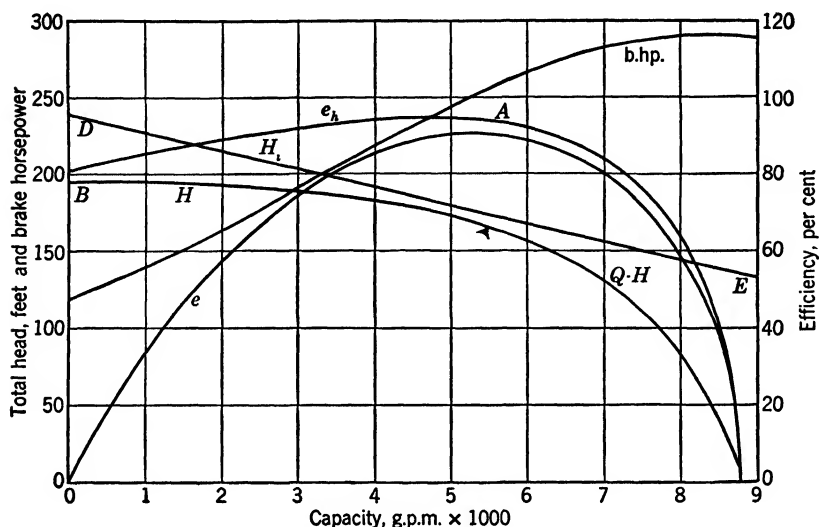


FIG. 10.11. Performance of 12-in. double-suction pump, 1180 r.p.m.;  $n_s = 1900$ .

draw the input head line, the zero input head point can be used as one of the points. The capacity for this point can be obtained from

$$\phi = \frac{c_{m2}}{u_2} = \tan \beta_2$$

The points of equal hydraulic efficiency on the head-capacity curve should fall on a straight line joining these points and the point of zero input head, as shown in Fig. 9.9.

The difference between  $H_i$  and  $H$  curves represents hydraulic losses  $h_l$ . The power loss due to hydraulic losses can be calculated from

$$(\text{hp.})_h = (Q + Q_L)\gamma h_l = \frac{Q\gamma h_l}{e_v} \quad (10.31)$$

The pump output in Fig. 10.10 is represented by the curve *EFG*, which is the gross efficiency curve, since

$$e = \frac{Q\gamma H}{\text{b.hp.}} \quad (10.32)$$

Although mechanical losses, including the disk friction loss, are constant for any capacity in Fig. 10.10, when expressed as a percentage of the brake horsepower the percentage will increase for lower capacities since the brake horsepower decreases toward zero capacity. Also the percentage of leakage loss horsepower increases for the same reason. Besides, leakage in gallons per minute increases as the capacity decreases on account of the increasing head toward shut-off.

$$(\text{hp.})_L = Q_L \gamma H_i = \frac{Q_L \gamma H}{e_h} \quad (10.33)$$

All known losses and the output of the pump having been drawn on Fig. 10.10, a considerable loss of power remains unaccounted for at capacities lower than normal. These power losses cannot be hydraulic

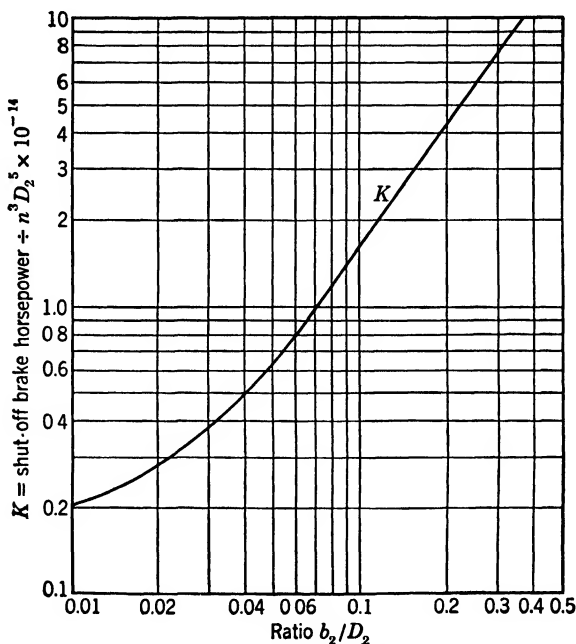


FIG. 10.12. Shut-off b.hp. versus  $b_2/D_2$  (Mockridge).

losses because then the hydraulic efficiency would be too low, or the input head  $H_i$  too high; in fact  $H_i$  would be higher than  $u_2^2/g$ , which is an absurdity. These unaccounted-for losses of power could not be an error in calculation of disk, mechanical, or leakage losses, as they would be out of proportion. *Thus it is necessary to assume another loss*

of power which is zero at the b.e.p. and increases toward zero capacity. This loss of power is caused by the exchange of momentum of liquid particles in the impeller passages at the periphery with those in the volute casing moving with much lower velocities. It is somewhat similar to the disk friction losses. It is believed that a major part of this loss is caused by recirculation of the high pressure liquid from the leading face of the vane into the low pressure zone near the underside of the vane, thus again absorbing energy from the impeller and losing it on the next drop from the high pressure face of the vane into the low pressure zone. Wide impellers and a small number of vanes waste more power by recirculation, thus increasing the brake horsepower near zero capacity. Mockridge<sup>13</sup> has plotted

$$\frac{\text{b.hp. at shut-off} \times 10^{14}}{n^3 D_2^5} \text{ vs. } \frac{b_2}{D_2}$$

to study the trend of variation of brake horsepower at zero capacity as a function of specific speed or  $b_2/D_2$  (Fig. 10.12). As the specific speed approaches zero the brake horsepower is approaching the disk friction loss.

Existence of a recirculation loss was realized by Daugherty<sup>15</sup> and called a churning loss. Pfeleiderer also mentions the recirculation loss in his book.<sup>16</sup> No formulas have been offered to express the recirculation loss in terms of known variables.

**Remarks on Losses in Centrifugal Pumps.** In reviewing the progress in design and improvements in efficiencies of centrifugal pumps in the course of the last two decades, the following factors can be pointed out, in the order of their importance, as being responsible for the improvements in performance.

(1) Use of more favorable specific speed types to meet a given set of conditions. Factors contributing to this step were the use of high speed motors (3600 r.p.m. or higher), an increasing demand for higher capacities in every field, and the splitting up of the head into a greater number of stages. Increased size and brake horsepower of pumps increased the importance of efficiency, thus permitting more expensive patterns and manufacturing procedure.

(2) A general perfection of the hydraulic design of all types of pumps, accomplished primarily through better streamlining of all parts taking part in the generation of head (this becomes apparent by a comparison of catalog cuts of twenty years ago with modern sectional drawings), and secondly through establishing optimum proportions of various pump passages, or velocity ratios, to obtain a maximum efficiency at

the desired point. Elimination of cavitation by better design is an important factor contributing to a better initial and sustained efficiency.

(3) Increased competition and importance of high efficiency, which demanded better manufacturing methods.

To obtain optimum efficiency, clean and smooth liquid passages are absolutely essential. Since a part of the casing and most of the impeller passages are not accessible for cleaning, the importance of a good quality of castings cannot be overemphasized. In small sizes, cleaning of the volute passages alone may show a difference of 2 to 4 points in efficiency. In the more competitive line of vertical deep-well turbine pumps, porcelain enameling on the cases and impellers (cast iron) is in wide use. The gain in efficiency due to porcelain enameling of cases varies from 2 to 3 points and is dependent on the size and the specific speed. Porcelain coating of open impellers has little advantage over polishing as all surfaces are accessible for cleaning. But with closed impellers, particularly of low specific speed (say 1500), the efficiency gain is about 2 points. Porcelain enameling is less advantageous with volute casings than with diffusion casings of vertical turbine pumps because of the accessibility for cleaning and relatively greater areas of passages. On a 3- or 4-in. pump this gain in efficiency may be about 1 point. Enameling of volute cases is not practiced commercially.

### 10.5 OPEN IMPELLER DESIGN

The introduction of open impeller construction in recent years was one of the major design features contributing to the improvement of performance of medium and high specific speed pumps. In addition to having hydraulic advantages, open impellers are capable of handling suspended matter with a minimum of clogging, and they permit restoration of the running clearance between the impeller vanes and the stationary casing, thus maintaining the original efficiency. The impeller passages are accessible for cleaning, and the manufacturing cost is lower.

The improvement in efficiency of the open impeller design results from reduction of disk friction loss by elimination of the front shroud. Hydraulic friction loss through an open impeller changes little or not at all. In a closed impeller there is friction loss due to the flow relative to the inner side of the outer shroud proportional to  $w_2^2/2g$  where  $w_2$  is the relative velocity through the impeller. In open impellers this loss is absent but instead there appears a hydraulic friction loss against a stationary casing wall while liquid is passing the impeller channel en-

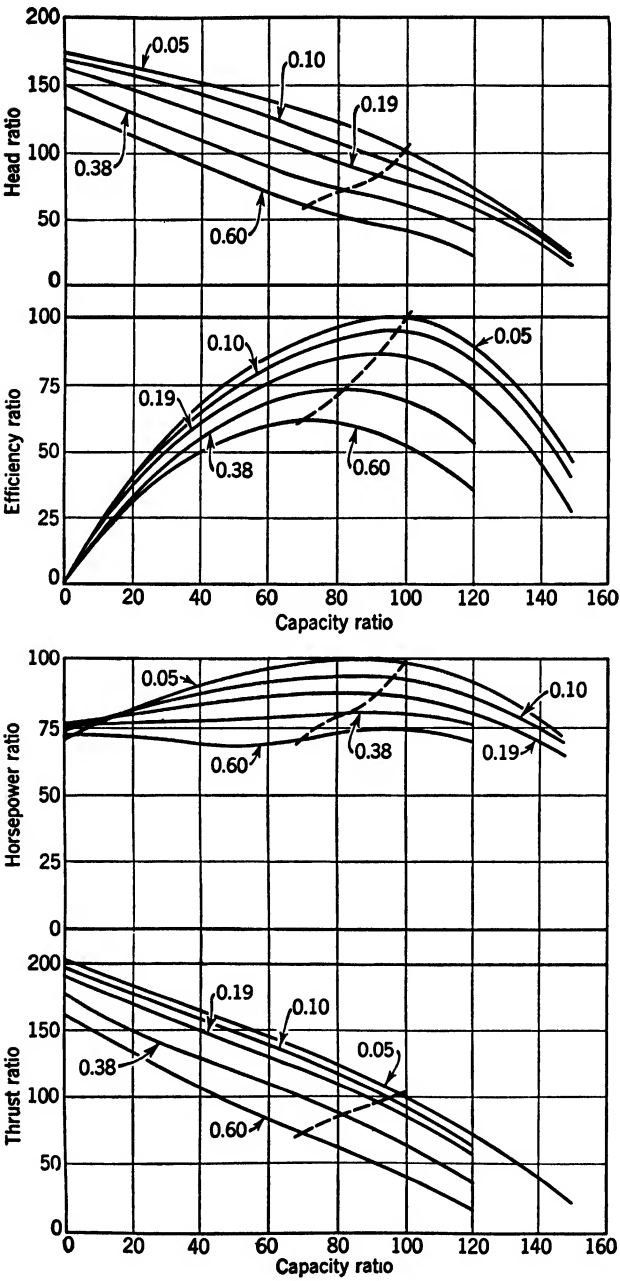


FIG. 10.13. Effect of clearance on the performance of open impeller vertical turbine pumps (Folsom).

closed between two adjacent vanes. This loss is proportional to  $c_2^2/2g$  where  $c_2$  is the absolute velocity of flow through the impeller. For high specific speed pumps these two items approximately balance each other; thus the reduction in disk friction loss is a net gain. Omission of the front shroud improves the gross efficiency about 2 points for medium specific speed pumps (2500 to 6000). Kaplan<sup>14</sup> gives a gain in efficiency for axial propeller turbines with shrouds removed 5 to 10 points. By

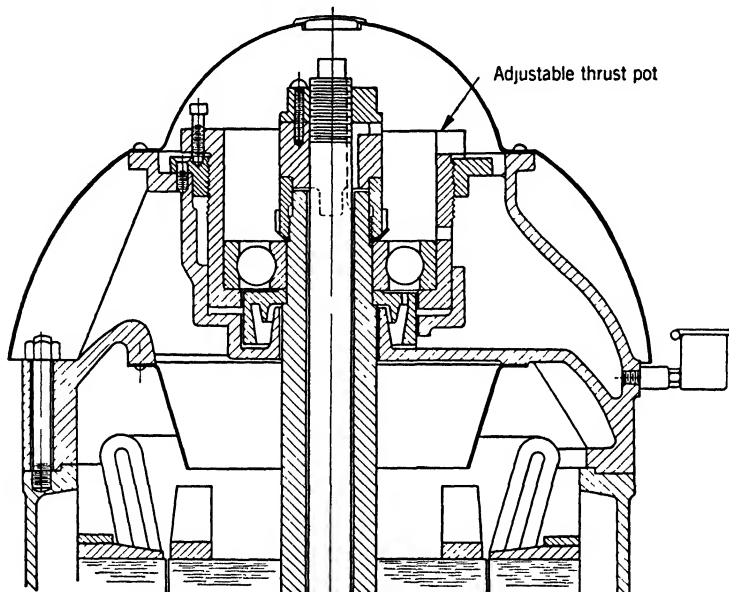


FIG. 10.14. Vertical hollow shaft rotor provided with adjustment of clearance while running vertical turbine pump (Byron Jackson).

removing the front shroud the leakage through the wearing rings is eliminated, but instead leakage from the front side to the back side of impeller vanes is introduced. It is believed that the latter loss is no higher than the normal leakage loss of closed impellers, provided a minimum running clearance is maintained. If clearance is increased the head, capacity, efficiency, and brake horsepower are reduced. Figure 10.13, obtained by Folsom,<sup>17</sup> shows the effect of the clearance on the pump performance. The clearances are given as ratios of clearance to the impeller width  $b_2$ . The rest of variables are given as percentages of the values at b.e.p. The decrease of brake horsepower obtained with increased clearance indicates that the impeller vanes at the open edge are not fully loaded. Note that the minimum clearance shown in Fig. 10.13 is about 0.020 in., which is excessive for normal operation.

Maintaining a minimum running clearance in high head vertical turbine pumps become a problem with long units. The shaft extension due to hydraulic thrust and rotor weight becomes appreciable. For instance, in a pump 200 ft. long and designed for a 200-ft. head, a  $1\frac{1}{2}$ -in. shaft will extend about  $\frac{1}{8}$  in. This shaft extension should be allowed for when the impeller clearance is set. There have been attempts to develop vertical motors which would permit an adjustment of the pump shaft while running. Figure 10.14 shows one example of such a design. As a further refinement to obtain an optimum performance from a vertical turbine pump, the difference in shaft extension between the stages can be provided for by inserting shims between the pump casings during assembly when impeller position on the shaft is being fixed. The shims are removed when the assembly of the pumping element is completed and casing bolts are tightened up. With long multistage pumps of low specific speed a gain in efficiency as high as 2 points has been obtained in this way. Impellers adjusted for a minimum running clearance may rub against the casing if operated at a reduced capacity owing to the higher hydraulic thrust.

The disadvantages of open impellers are (1) much higher axial thrust than with the closed impeller and (2) need of mechanical means to adjust running clearances. No satisfactory method has been devised to make horizontal multistage pumps with open impellers.

#### REFERENCES

1. E. SCHECKENBERG, "Der Durchfluss durch Drosselspalte," *Z. Ver. deut. Ing.*, Vol. 74, 1930, p. 485.
2. E. BECKER, "Strömungsvorgänge in ringförmigen Spalten," *Z. Ver. deut. Ing.*, Vol. 51, 1907, pp. 1133-1141.
3. M. D. AISENSTEIN, "Construction Details Need to be Considered in Choosing Suitable Centrifugal Hot Oil Pumps," *Oil and Gas Jour.*, Vol. 32, April 5, 1934, pp. 49-50.
4. E. J. BLACKWELL and M. L. MURDOCK, "Leakage in High Pressure Centrifugal Boiler Feed Pumps," *Current Trends* No. 6, *Allis-Chalmers Eng. Bul.*, B-6158, 1941.
5. J. NIKURADSE, "Strömungsgesetze in rauhen Röhren," *Forschungsheft*, No. 361.
6. A. J. STEPANOFF, "Leakage Loss and Axial Thrust in Centrifugal Pumps," *Trans. A.S.M.E.*, Aug. 15, 1932, p. 65.
7. A. H. GIBSON, *Hydraulics and Its Application*, New York, D. Van Nostrand, 1925, p. 186.
8. JOSEPH N. LECONTE, *Hydraulics*, New York, McGraw-Hill, 1934, p. 332.
9. F. SCHULTZ-GRUNOW, "Der Reibungswiderstand rotierender Scheiben in Gehäusen," *Z. angew. Math. Mech.*, *Bull.* 4, July 1935, pp. 194-204, Berlin, Verein deutscher Ingenieure.

10. L. F. MOODY, "Friction Factors for Pipe Flow," *Trans. A.S.M.E.*, Vol. 66, No. 8, Nov. 1944, p. 671.
11. C. PFLEIDERER, *Die Kreiselpumpen*, Berlin, Julius Springer, 1924, p. 39.
12. TH. VON KÁRMÁN and T. LEVI-CIVITA, *Vorträge aus dem Gebiete der Hydro- und Aerodynamic*, Berlin, Julius Springer, 1924, pp. 152-170.
13. C. R. MOCKRIDGE, discussion of "Centrifugal Pump Performance as a Function of Specific Speed," by A. J. Stepanoff, *Trans. A.S.M.E.*, Aug. 1943, p. 642.
14. VICTOR KAPLAN and ALFRED LECHNER, *Theorie und Bau von Turbinen-Schnellläufern*, Berlin, R. Oldenbourg, 1931, p. 142.
15. R. L. DAUGHERTY, *Centrifugal Pumps*, New York, McGraw-Hill, 1915, p. 76.
16. C. PFLEIDERER, *Die Kreiselpumpen*, Berlin, Julius Springer, 1932, p. 70.
17. R. G. FOLSOM, "Some Performance Characteristics of Deep-Well Turbine Pumps," *Trans. A.S.M.E.*, Vol. 63, No. 3, April 1941, p. 245.
18. ARTHUR T. IPFEN, "The Influence of Viscosity on Centrifugal Pump Performance," *Trans. A.S.M.E.*, Vol. 68, No. 8, 1946, p. 823.



## CHAPTER 11

### AXIAL THRUST

#### 11.1 SINGLE-STAGE PUMPS

(a) **Balancing Axial Thrust.** A double-suction impeller is balanced for axial thrust due to symmetry. If this balance is not destroyed by an unsymmetrical impeller approach, there really is no need for a thrust bearing. Older-type, slow speed, low head pumps were fitted with only a thrust collar to locate the rotating element axially. All modern double-suction pumps have a small thrust bearing to take care of any possible accidental thrust.

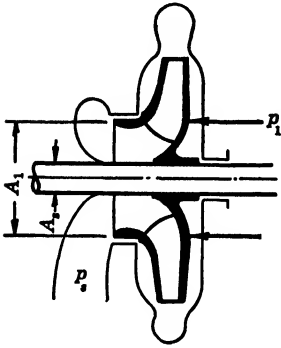


FIG. 11.1. Axial thrust on a single-suction impeller.

Single-suction impellers (Fig. 11.1) are subjected to an axial thrust because the area opposite the impeller eye is under suction pressure at the front of the back shroud and under discharge pressure at the rear of the back shroud. The magnitude of the

axial thrust can be calculated from

$$T = (A_1 - A_s)(p_1 - p_s) \quad (11.1)$$

where  $T$  is the axial thrust, in pounds

$A_1$  is the area corresponding to the diameter  $D_r$  of the impeller wearing ring, in square inches

$A_s$  is the area of the shaft sleeve through the stuffing box, in square inches

$p_s$  is the suction pressure, in pounds per square inch

$p_1$  is the pressure on the back shroud at diameter  $D_r$ , in pounds per square inch.

The pressure difference  $(p_1 - p_s)$  is less than the total head of the pump because the liquid behind the impeller is in rotation. It is more accurately expressed as  $H_L/2.31$  where  $H_L$  is determined as shown in Chapter 10, equation 10.5. This can be assumed to be uniform over

the whole unbalanced area. The actual thrust is somewhat less than the value given by equation 11.1, the reduction being caused by the change in momentum of the flow through the impeller eye, which in a straight centrifugal pump makes a 90-degree turn at this point. The opposing force is equal to

$$F = \frac{W}{g} c_1 = A_e c_1^2 \frac{\gamma}{g} = 2A_e \gamma \frac{c_1^2}{2g} \quad (11.2)$$

where  $A_e$  is the net impeller eye area, and  $c_1$  is the meridional velocity through the impeller eye. When the axial thrust can be safely carried by a thrust bearing, this is the most efficient way to take care of it.

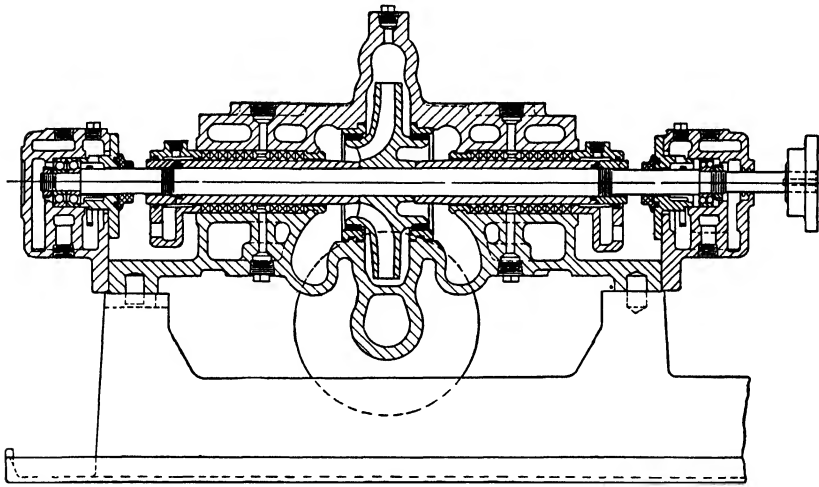


FIG. 11.2. Single-suction impeller in a double-suction casing is balanced for axial thrust (Ingersoll-Rand).

Otherwise some means should be provided to reduce the thrust on the bearing. This can be done only at the expense of the pump efficiency.

One of two methods is usually employed to reduce or eliminate axial thrust in single-stage pumps. In the first a chamber on the back of the impeller is provided with a closely fitted set of wearing rings, and suction pressure is admitted to this chamber either by drilling holes through the impeller back shroud into the eye (Fig. 2.2) or by providing a special channel connecting the balancing chamber to the suction nozzle (Fig. 2.1). Figure 11.2 shows a single-suction pump with a balance chamber on the back of the impeller. A symmetrical double-suction casing is used on this pump, one half of the suction nozzle serving to connect the balancing chamber to the suction nozzle.

In the second method, radial ribs are used on the back shroud to reduce the pressure in the space between the impeller and the pump casing. *It is evident that the first method doubles the leakage loss of the pump, which in turn increases as wearing rings are worn. The second method requires some additional power which, however, does not change with time. In addition it is cheaper and more effective than the first method. It will be shown later that this method requires no more power than is lost through leakage under normal conditions.*

The use of drilled holes through the impeller shroud to the balancing chamber is inferior to the arrangement using a special channel to con-

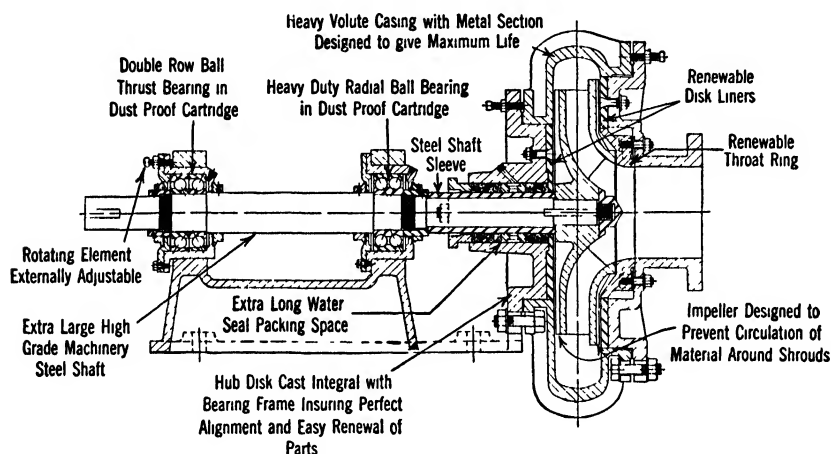


FIG. 11.3. Morris slurry pump.

nect the balancing chamber with the suction nozzle because leakage through the holes is directed against the flow in the impeller eye causing disturbances. *The balance by this method is never complete. From 10 to 25 per cent of the axial thrust always remains, depending on the size of the holes.<sup>1</sup> For a complete balance the diameter of the wearing rings of the balancing chamber should be greater than that at the impeller eye.*

The axial thrust depends on the pressure distribution in the space between the impeller shrouds and the stationary casing walls. The pressure distribution depends in turn on the clearance between the shrouds and the casing walls. These clearances are made small in special pumps handling solids in suspension, such as dredge pumps, to keep solids from these spaces. To promote circulation between the shrouds and casing, radial ribs are attached to both front and back shrouds. The axial thrust can be reduced or reversed by reducing the clearances between the back shroud and the casing and increasing the

clearance between the front shroud and the casing.<sup>2</sup> On some dredge pumps, in order to reduce the thrust, the back shroud is made smaller in diameter than the front shroud (Fig. 11.3).

Modern pumps are made with ample clearance between the casing and the impeller so that if the impeller is placed  $\frac{1}{8}$  or  $\frac{1}{4}$  in. from the plane of symmetry of the casing no appreciable axial thrust appears.

The author has run extensive tests covering axial thrust measurements on horizontal single-stage and multistage pumps, a complete

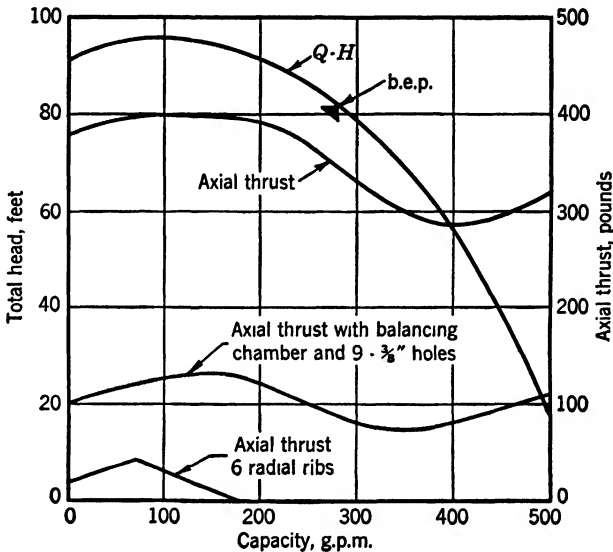


FIG. 11.4. Axial thrust, 3-in. pump, 2000 r.p.m.,  $8\frac{1}{2}$ -in. impeller,  $4\frac{1}{8}$ -in. diameter of wearing ring.

report of which is given in Reference 1. Figure 11.4 shows one typical test curve giving values of axial thrust for an unbalanced impeller, for an impeller with a balancing chamber on the back shroud using nine  $\frac{3}{8}$ -in. holes through the impeller web, and for an impeller with radial ribs on the back of the impeller. In the latter case the thrust was reversed before the b.e.p. was reached.

The reason for the increase of axial thrust at capacities above normal is not entirely clear. Similar thrust curves were obtained by several investigators.<sup>3</sup> It is likely that at high capacities the heads produced along the outer and inner shrouds are not equal, and this inequality produces different pressures in the volute and between the impeller shrouds and the casing walls. High velocities through the 90-degree turn in the impeller eye may also cause such conditions. Local cavi-

tation at the impeller entrance may be another contributing factor. Vertical turbine pumps, with open or closed impellers, never show an increase of axial thrust at high capacities.

(b) **Balancing with Radial Ribs.** Figure 11.5 shows the pressure distribution between the impeller shrouds and the casing walls for an impeller with radial back ribs. All pressures are taken above the suction pressure. The axial forces on the impeller shrouds are represented by volumes enclosed by the surfaces of revolution  $ABCD$  on the front

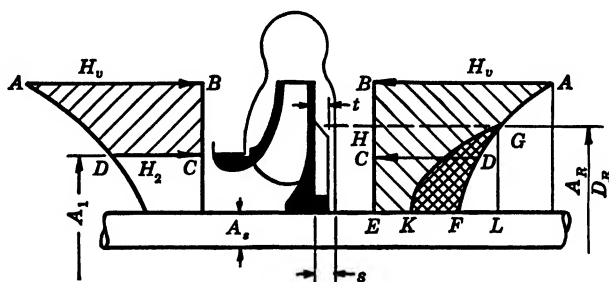


FIG. 11.5. Balancing axial thrust with radial ribs.

shroud and  $ABEF$  on the back shroud. The unbalanced axial thrust on the back shroud  $T_b$  is equal to the volume  $CDEF$ , which is expressed by

$$T_b = (A_1 - A_s) \left( H_L - \frac{1}{8} \frac{u_r^2 - u_s^2}{2g} \right) \gamma \approx (A_1 - A_s) \gamma H_L \quad (11.3)$$

where  $u_r$  is the peripheral velocity at the impeller wearing ring diameter, and  $u_s$  is the peripheral velocity at the shaft sleeve diameter. For practical purposes the head  $H_L$  can be assumed to act over the whole unbalanced area  $(A_1 - A_s)$ . The pressure distribution in the space between the impeller shrouds is based on the assumption that the angular velocity of rotation of the liquid in this space is equal to the one-half that of the impeller. This has been confirmed by Schultz-Grunow (Reference 9, Chapter 10) and the author's own tests.<sup>1</sup> To balance the axial thrust  $T_b$  (equation 11.3) radial ribs are provided on the back shroud. With these ribs closely fitted to the casing walls the liquid will rotate approximately with full impeller angular velocity. This will further reduce the pressure on the impeller back shroud over the area  $A_R$ , determined by the diameter of the radial ribs  $D_R$ . The reduction of the axial forces on the back shroud is given by the volume  $GFKG$  (Fig. 11.5, double cross-hatched) which is the difference of volumes of the two paraboloids  $GKL$  and  $GFL$ . Note that the volume of a parab-

olid is equal to one-half the volume of a cylinder of the same base and height.

$$\begin{aligned}
 T_{bR} &= (A_R - A_s) \left( \frac{HG + EF}{2} - \frac{HG + EK}{2} \right) \gamma \\
 &= (A_R - A_s) \left( \frac{EF - EK}{2} \right) \gamma \\
 &= \frac{A_R - A_s}{2} \left[ \left( H_v - \frac{1}{4} \frac{u_2^2 - u_s^2}{2g} \right) \right. \\
 &\quad \left. - \left( H_v - \frac{u_2^2 - u_R^2}{8g} - \frac{u_R^2 - u_s^2}{2g} \right) \right] \gamma \\
 T_{bR} &= \frac{3}{8} (A_R - A_s) \left( \frac{u_R^2 - u_s^2}{2g} \right) \gamma \quad (11.4)
 \end{aligned}$$

For a complete balance,  $T_b = T_{bR}$ . From this relationship the diameter of radial ribs can be determined. If radial ribs do not fit closely to the casing wall the angular velocity of the liquid in the space between the back impeller shroud and the casing will be lower than the impeller angular velocity  $\omega$ , but higher than  $\omega/2$ . It can be assumed, approximately, that the angular velocity of the liquid can be represented by the relationship

$$\omega' = \frac{\omega}{2} \left( 1 + \frac{t}{s} \right) \quad (11.5)$$

where  $s$  is the average distance between the casing wall and the impeller back shroud and  $t$  is the height or thickness of the radial ribs (Fig. 11.5). The number of ribs varies from 4 for small pumps to 6 for large pumps.

For overhung impeller pumps there is an additional thrust component in a direction opposite to the impeller suction equal to the suction pressure  $p_s$  times the area of the sleeve through the stuffing box ( $A_s$ ).

$$T_s = p_s A_s \quad (11.6)$$

*Thus for overhung impeller pumps the diameter of the balancing ribs depends on the suction pressure.*

## 11.2 MULTISTAGE PUMPS

**(a) Balancing Axial Thrust.** The problem of axial thrust becomes more important when dealing with multistage pumps because of the

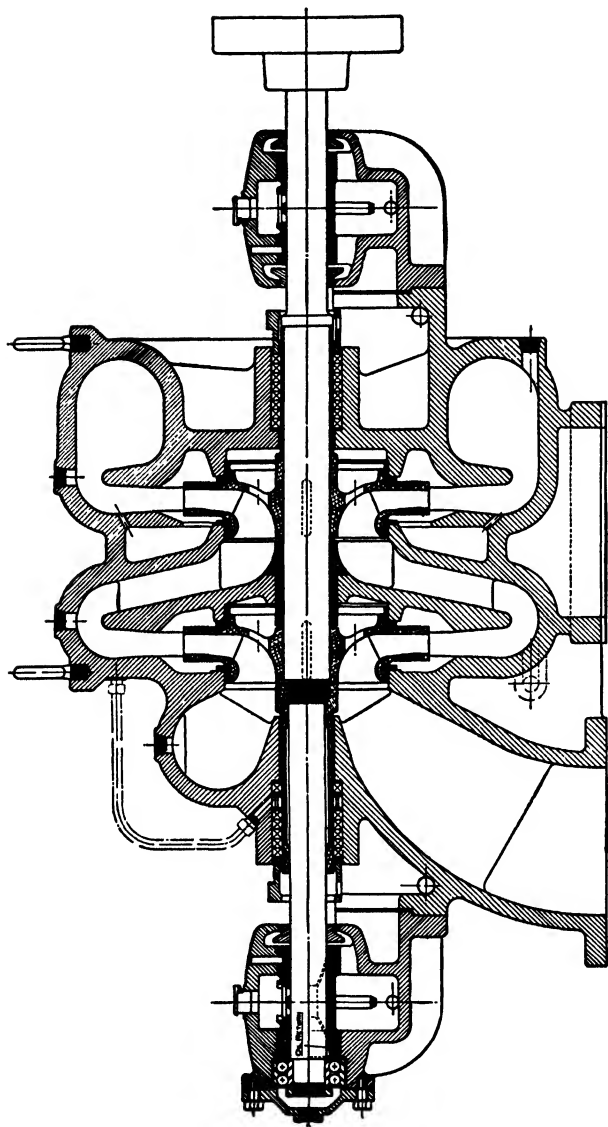


FIG. 11.6. Gould's multistage pump with individually balanced impellers.

higher pressures involved and the combined thrust of several stages. Several methods are used to balance axial thrust in multistage pumps: (1) impellers with even numbers of stages may be arranged in two opposing groups (Fig. 11.11); (2) individual stages may be balanced by providing balancing chambers on the back of each impeller (Fig. 11.6) but this method is seldom used for modern pumps; (3) double-suction impellers may be used in all stages (Fig. 11.7); (4) special balancing devices such as the automatic balancing disk and balancing drum may be used.

The automatic balancing disk operates on the following principle. All impellers are faced in the same direction (Fig. 11.8). On the back of the last stage impeller a balancing chamber, connected through a throttle *A* to the first-stage suction, is formed. The balancing disk *C* is of larger diameter than the impeller wearing rings. The rotating element is free to move axially. Axial thrust tends to move the disk to the left, thus closing the gap between the disk and a stationary face *B*. This reduces the pressure in the balancing chamber behind disk *C*. At the same time the full pump pressure will move disk *C* to the right until a perfect balance is reached. The amount of leakage is controlled by the throttle *A*. When this is worn the gap between the disk *C* and the face *B* increases in order to maintain the required pressure on the back of the disk.

To protect the disk *C* and face *B* from damage under any possible condition a spring-loaded bearing keeps the faces apart about  $\frac{1}{32}$  in. when the pump does not develop full pressure. Under normal conditions the spring permits the rotating element to float freely with only a slight increase in pressure to overcome the spring tension. The calculation of the amount of leakage past the balancing disk is complicated by the uncertainty of actual clearances and pressures controlling the leakage. However, the leakage can easily be measured.

Figure 17.10 shows a combination of a balancing drum and an automatic balancing disk. It works on the same principle as the one described except that the fixed throttle is arranged ahead of the automatic disk throttle. *The pressure ahead of the disk is fixed by the amount of unbalanced axial thrust, and when the auxiliary throttle becomes worn the disk gap increases in order to maintain the required pressure at the disk, thus increasing the amount of leakage. In every case the total pressure through the balancing device is split up by automatic throttle in the same ratio to balance the same axial thrust.*

When a balancing drum alone is used the axial thrust is eliminated or reduced to the extent that it can be safely carried by the thrust bearing by means of a low pressure balancing chamber on the high pressure



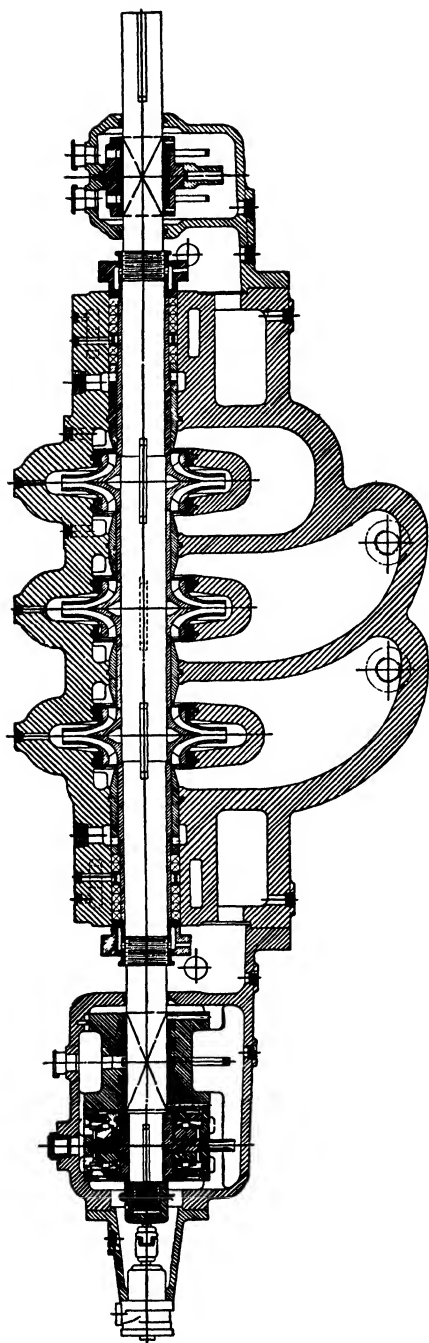


FIG. 11.7. Allis-Chalmers boiler feed pump; for high pressure, built in seven stages.

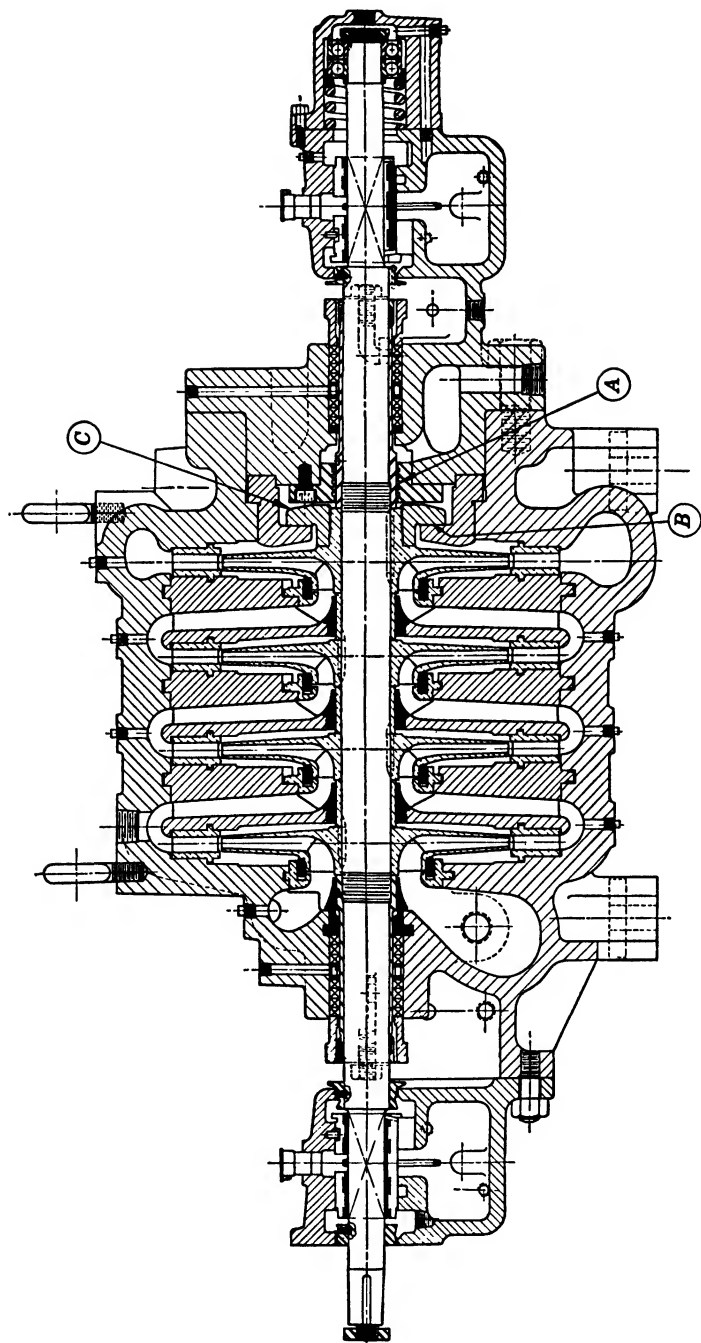


Fig. 11.8. DeLaval boiler feed pump with automatic balancing disk.

end of the pump (Fig. 11.9). This is separated from the last stage casing by a drum closely fitted into the stationary casing bushing. Full pump pressure acts on the drum and gives a force essentially equal to the axial thrust of all the impellers. The amount of leakage through the drum increases with drum and bushing wear. Normal leakage is 2 to 3 per cent. The balancing drum alone is seldom used on modern pumps.

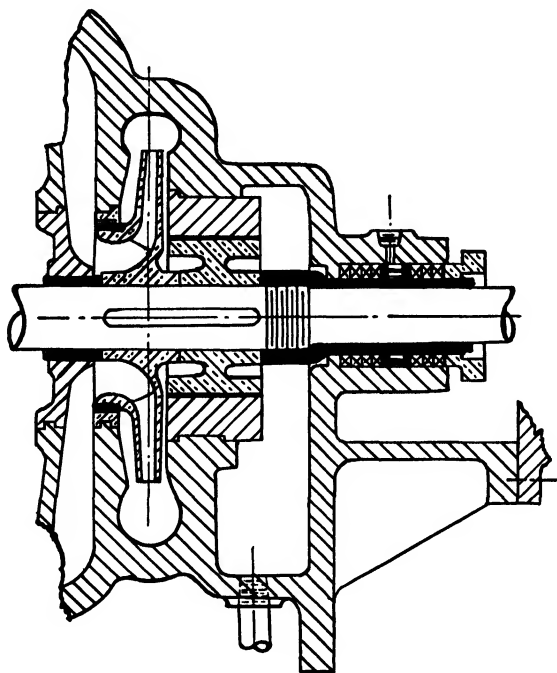


FIG. 11.9. Balancing drum, not used on modern pumps.

**(b) Thrust Due to Shaft Shoulders and Impeller Hubs.** *Multistage pumps having impellers arranged in two opposing groups are balanced for axial thrust only if the pumps have two stuffing boxes, if the shaft is of a constant diameter throughout the pump, and if the impeller hubs do not extend through the casing walls separating two adjacent stages.* Modern high pressure, high speed pumps usually have shafts which are heavier in the middle portion, and the impeller hubs frequently extend through the casing walls of two adjacent stages. This produces considerable axial thrust. Figure 11.10 shows diagrammatically the principle involved. The thrust direction is indicated on this figure as well as the method of calculating the thrust.

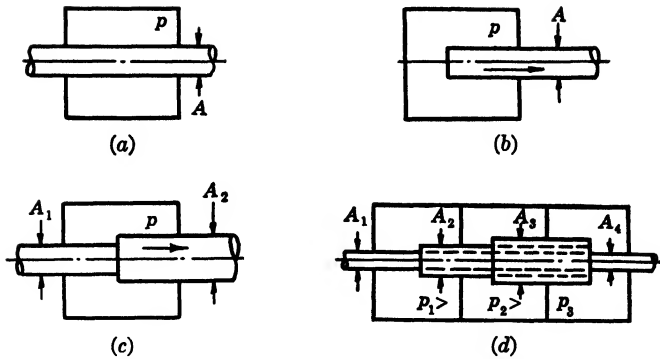


Fig. 11.10. (a) Axial force  $T = 0$ ; (b)  $T = pA$ ; (c)  $T = p(A_2 - A_1)$ ; (d)  $T = (p_1 - p_3)(A_2 - A_1) + (p_2 - p_3)(A_3 - A_2)$ ; direction of  $T$  is to the right.

Now consider as an example a four-stage pump with impellers arranged as in Fig. 11.11. The following notation will be used in this discussion.

$p_s$  = suction pressure

$p_1$  = volute pressure in the first stage =  $p_s + p$  where  $p$  is the pressure produced by one stage

$p_2$  = volute pressure in the second stage =  $2p + p_s$

$p_3$  = volute pressure in the third stage =  $3p + p_s$

$p_4$  = volute pressure in the fourth stage =  $4p + p_s$

$D_s$  = diameter of shaft or shaft sleeve at the stuffing box, equal on both sides

$D_h$  = impeller hub diameter

$D_c$  = shaft diameter at the center

$D_1$  = impeller wearing ring diameter

$A_1, A_s, A_h, A_c$  = areas of the circles corresponding to diameters  $D_1, D_s, D_h$ , and  $D_c$

All pressures are in pounds per square inch and areas are in square inches.

Assume that the pressures in the clearances between the pump case and the impeller shrouds are uniform and equal to that of the corresponding volute pressure. Assume also that the suction pressure of the third stage is the same as the discharge pressure of the second, and so on. These assumptions do not affect the final result, since there is always a one-stage pressure difference  $p$  between two similar points in two successive stages.

It is evident that the pressures on both sides of the impeller shrouds from diameter  $D_2$  to diameter  $D_1$  are equal and balanced. Consider

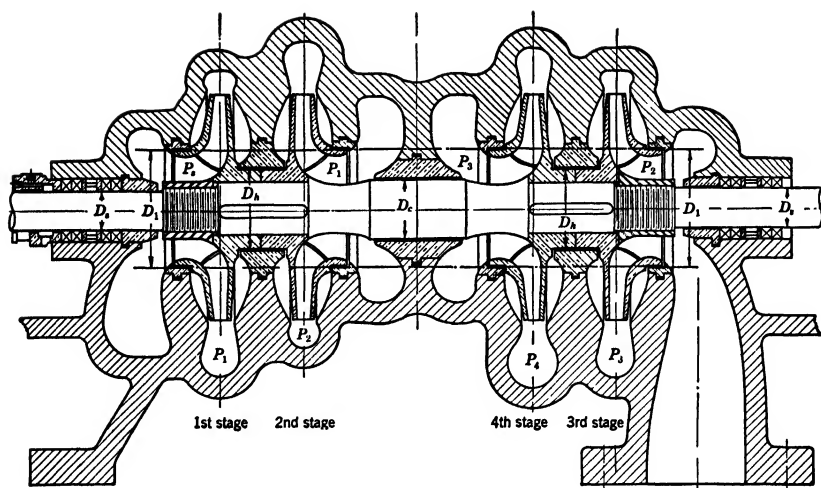


FIG. 11.11. Four-stage pump. Axial thrust due to shaft shoulders and impeller hubs.

now the pressures on each impeller after exclusion of the areas between  $D_2$  and  $D_1$ . Call pressures to the left positive, those to the right negative. Then the forces on the rotating element are

$$(A_1 - A_h)p_1 - (A_1 - A_s)p_s = \text{first-stage thrust}$$

$$(A_1 - A_c)p_1 - (A_1 - A_h)p_2 = \text{second-stage thrust}$$

$$(A_1 - A_h)p_4 - (A_1 - A_c)p_3 = \text{fourth-stage thrust}$$

$$(A_1 - A_s)p_2 - (A_1 - A_h)p_3 = \text{third-stage thrust}$$

The axial thrust is equal to the sum of these forces. Adding and rearranging,

$$T = A_1(2p_1 + p_2 + p_4 - p_s - p_2 - 2p_3) + A_h(p_2 + p_3 - p_4 - p_1) + A_s(p_s - p_2) + A_c(p_3 - p_1)$$

Substituting for  $p_1$ ,  $p_2$ ,  $p_3$ , and  $p_4$  their values ( $p + p_s$ , and so on) and reducing,

$$T = 2p(A_c - A_s) = 2p(D_c^2 - D_s^2)0.785 \quad (11.7)$$

It is seen that, owing to symmetry,  $D_1$  and  $D_h$  do not appear in the final result. The whole system can be represented diagrammatically as equivalent to the simple case shown in Fig. 11.12. This result holds for the arrangement of stages as shown (1, 2, 4, 3) which gives a minimum thrust.

To obtain an idea of the magnitude of the thrust produced in this way, take a numerical example. A 4-in. four-stage pump with an arrangement of stages like that in Fig. 11.11 and developing 100 p.s.i. per stage has the dimensions:  $D_s = 1\frac{3}{4}$  in.,  $D_h = 3\frac{1}{4}$  in., and  $D_c = 2\frac{5}{8}$  in. Substituting these values in formula 11.7 we get

$$T = 2 \times 100 \times 0.785[(2.625)^2 - (1.75)^2] = 597 \text{ lb.}$$

*In a multistage pump with one stuffing box and one internal bearing there is a thrust due to the pressure acting on the end of the closed shaft. This should be added to the thrust due to shoulders on the shaft and impeller hubs. Suppose that, in the pump shown in Fig. 11.11, the*

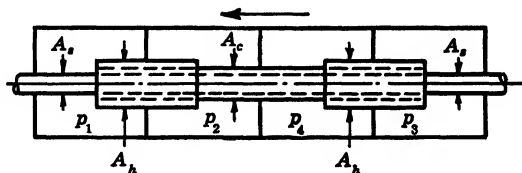


FIG. 11.12. Diagram of a 4-stage pump. Axial thrust  $T = (p_3 - p_1)(A_c - A_s)$ .

right-hand stuffing box is replaced by a closed bearing. The pressure on this end of the shaft is  $2p$ , the area is  $A_s$ , and the additional thrust is

$$T' = p_2 \cdot A_s = A_s(2p + p_s) \quad (11.8)$$

When  $p_s$  is equal to atmospheric pressure,

$$T_1 = 200 \times 0.785 \times (1.75)^2 = 480 \text{ lb.}$$

*From expression 11.8 it is seen that the thrust due to an internal bearing depends on the suction pressure on the first stage. The thrust increases as the suction pressure increases, and it may reach a high value if the pump is operating under a considerable positive head (for instance, if two pumps are working in series). The main object of pumps with one stuffing box is elimination of the high pressure stuffing box. The thrust due to this cause is always toward the first-stage suction, or in the same direction as the thrust due to shoulders on the shaft. The thrust on the enclosed shaft end may be reduced or eliminated by using an uneven number of stages and grouping them so that the thrust due to one stage will balance that due to the enclosed bearing.*

*Thrust due to shaft shoulders and impeller hubs can be balanced by making the hubs of different diameters and such that the resulting force opposes the axial thrust of the impellers. Thus, for example, if we assume that the impeller hubs on stages 3 and 4 are made larger than those on stages 1 and 2 (Fig. 11.11), and if we let  $D_{h1}$  denote the diameter of the im-*

PELLER hubs for stages 1 and 2 and  $D_{h2}$  the diameter of the impeller hubs for stages 3 and 4 ( $A_{h1}$  and  $A_{h2}$  denoting the corresponding areas) we can repeat the calculations with these changes, and the following expression is obtained for the axial thrust.

$$T = 2p(A_c - A_s) - p(A_{h2} - A_{h1}) \quad (11.9)$$

By equating the thrust to zero we get:

$$2(A_c - A_s) = A_{h2} - A_{h1} \quad (11.10)$$

For the same values of  $A_c$  and  $A_s$ ,  $D_{h1} = 3\frac{1}{4}$  in.,  $A_{h2}$  is equal to 14.3 sq. in., or  $D_{h2} = 4.27$  in.

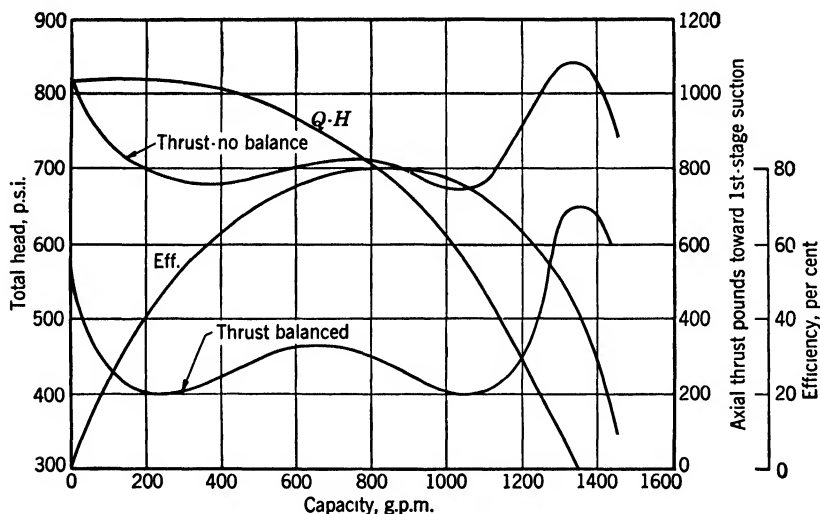


FIG. 11.13. Four-inch 4-stage pump, 3560 r.p.m., suction pressure 60 p.s.i.

AXIAL thrust due to shaft shoulders and impeller hubs can be eliminated by making impeller ring diameters  $D_r$ , or impeller diameters  $D_2$  (and stage pressure  $p$ ) different for several stages, but both of these methods have several objections from a practical point of view.

Figures 11.13 and 11.14 show tests run by the author on a 4-in. four-stage pump, described in the above examples. The test proves the effectiveness of the described balancing method.

Equation 11.7 is based on the assumption that each stage develops the same pressure and that the balance should hold at all capacities. Figures 11.13 and 11.14 show that this is not true in practice. The discrepancy is caused by the inequality of stage pressures for different stages; apparently the difference varies with capacity.

*Interstage leakage is the principal cause of the difference in stage pressures in multistage pumps; it results in axial thrust with the opposed impeller arrangement.* In general, with increasing leakage (worn wearing rings) the head drops for a given capacity. Owing to interstage leakage across two adjacent stages, the head produced by the high pressure stage is lower than that produced by the low pressure stage. This follows from the fact that, for a measured pump capacity  $Q$ , the low pressure stage impeller capacity is  $Q_1 = Q + Q_L$ , where  $Q_L$  is the leakage

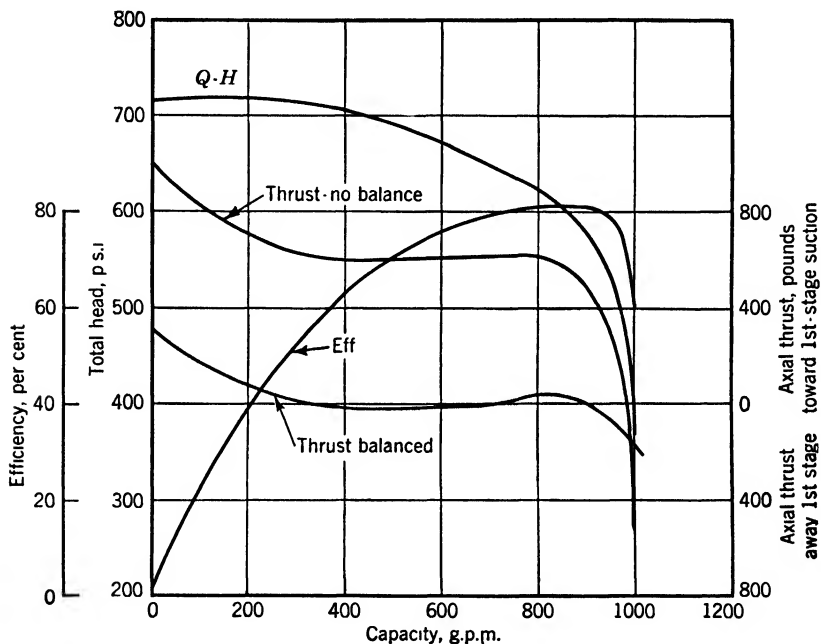


FIG. 11.14. Four-inch 4-stage pump, 3560 r.p.m., suction lift 10 ft.

through the wearing rings. At the same time the high pressure stage impeller capacity is  $Q_2 = Q + Q_L + Q_i$ , where  $Q_i$  is the interstage leakage circulating between the high pressure and the low pressure casings. But since both impellers have identical head-capacity characteristics, the high pressure impeller working at a higher capacity will produce a lower head than the low pressure impeller.

Figure 11.15 shows a test of a 2-in. two-stage pump with normal and worn interstage clearances. The axial thrust increased about six times because of the increased interstage leakage.

Any difference in the leakage through the wearing rings at the impeller eye leads to a difference in head of individual stages and, hence,



unbalance of axial thrust. When the pump handles capacities above normal under limited suction head, cavitation may set in at the first-stage impeller, and thus reduce the head produced by this stage and

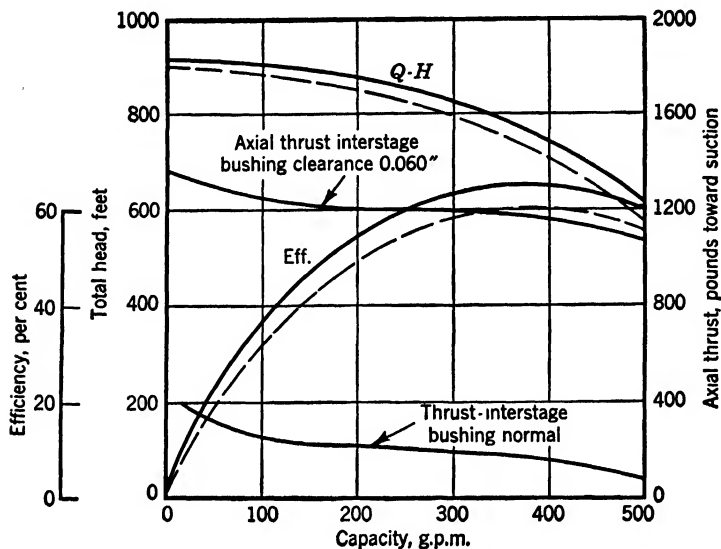


FIG. 11.15. Axial thrust due to interstage leakage; 2-in. 2-stage pump, 3500 r.p.m. Back-to-back impellers.

upset the axial thrust balance. A displacement of impellers from the central position in their respective volute cases may be a contributing factor to the unaccounted-for axial thrust of multistage pumps with opposed impellers. Because none of the above causes of hydraulic thrust can be determined with certainty a thrust bearing is always provided in multistage pumps with opposed impellers.

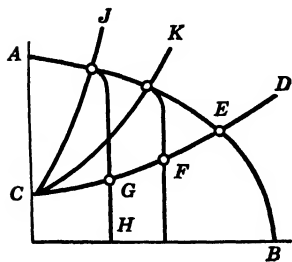


FIG. 11.16. Diagram of condensate pump performance.

(c) **Condensate Pumps.** Pumps working under very low submergence, such as hot-well or condensate pumps, may be required to operate under a head considerably lower than normal, depending on the amount of liquid coming into the pump and the characteristics of the discharge system. In Fig. 11.16, assume that  $AB$  is the normal head-capacity characteristic and that  $CD$  is the discharge system curve. Point  $E$  is the normal operating point when sufficient submergence is available. When the

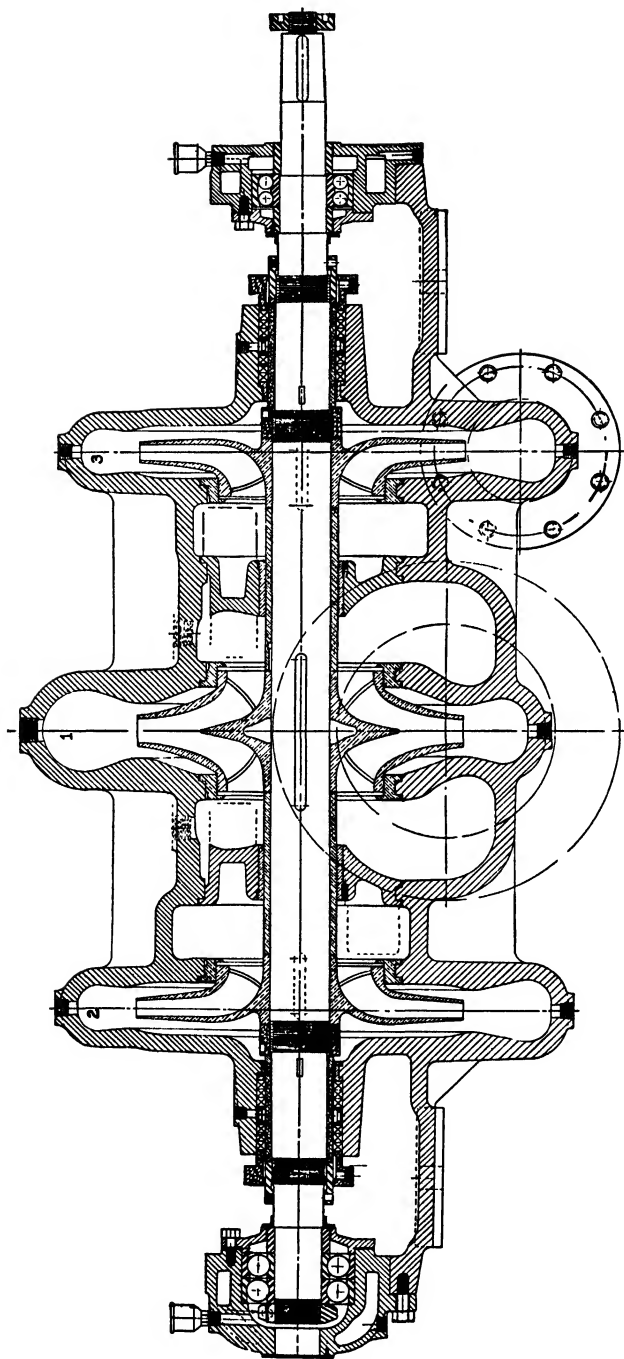


FIG. 11.17. Worthington 3-stage condensate pump.

rate of flow to the pump suction is reduced the submergence will fall, cavitation will set in, and the head-capacity curve will break off suddenly. The operating points will remain on curve  $CD$ . At point  $G$  the pump total head is less than the normal head for this capacity. *If the pump is a two-stage pump with two opposing single-suction impellers, the entire head  $GH$  will be produced by the second stage, as this stage is under discharge pressure from the system and is capable of maintaining this pressure alone without the aid of the first stage.* The first stage will produce no head. Therefore the axial balance will be destroyed. Since most condensate pumps are low speed with the large impellers, this unbalance may ruin the thrust bearing selected for normal operating conditions. Automatic liquid level controls will overcome this by maintaining the operating point on the normal characteristic. In this set-up the discharge valve is controlled by a float in the suction receiver which causes the valve to throttle as the liquid level tends to lower, thus changing the system characteristic to  $CJ$  or  $CK$ . The pump will operate at the intersection of such curves with the normal pump head-capacity curve. If both stages have double-suction impellers, no undue thrust develops under cavitation. Figure 11.17 shows a three-stage horizontal condensate pump with a double-suction first-stage impeller and two single-suction impellers for the second and third stages. These pumps are free from undue axial thrust under all load conditions. Two-stage condensate pumps are built with a double-suction first-stage impeller and two single-suction impellers in parallel for the second stage. In Chapter 16, condensate pumps of the vertical turbine type are described which have marked advantages over horizontal condensate pumps.

### 11.3 OPEN IMPELLERS

**(a) Axial Thrust.** Open impellers produce higher axial thrust than closed impellers. The thrust on the back shroud is only partly balanced by the pressure inside the impeller (Fig. 11.18). The thrust on the back shroud is given by equation 11.11.

$$T_b = (A_2 - A_s) \left[ H_v - \frac{1}{8} \frac{(u_2^2 - u_s^2)}{2g} \right] \gamma \quad (11.11)$$

The pressure inside the impeller is  $H_v$  at the periphery and the suction pressure at the diameter is  $D_1$ . The thrust on the inside of the back shroud is

$$T_{bi} = (A_2 - A_1) \frac{H_v}{2} \gamma \quad (11.12)$$

The net axial thrust is the difference between  $T_b$  and  $T_{bi}$  or

$$\begin{aligned} T &= T_b - T_{bi} \\ &= (A_2 - A_s) \left[ H_v - \frac{1}{8} \frac{(u_2^2 - u_s^2)}{2g} \right] \gamma - (A_2 - A_1) \frac{H_v}{2} \gamma \quad (11.13) \end{aligned}$$

Radial ribs on the back shroud are the only practical means for the reduction of the axial thrust of open impellers. Multistage pumps with open impellers are always of the vertical turbine type, having impellers facing the same direction and the axial thrust taken up by the thrust bearing. Radial ribs are used to reduce the axial thrust if it is beyond the bearing capacity. However, this reduces the pump gross efficiency. No accurate information is available on the power loss due to radial ribs. On tests of several vertical turbine pumps the author found that the pump gross efficiency dropped approximately 2 points when ribs were added on the back shrouds and the axial thrust was reduced to one-half its normal value. The power loss due to ribs increases rapidly with the diameter of the ribs. Therefore, the rib diameter should be no greater than necessary to reduce the thrust by the desired amount. Single-

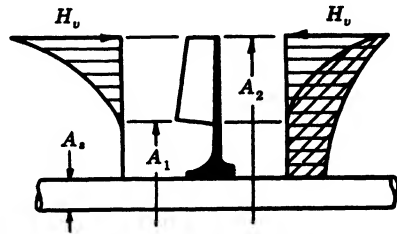


FIG. 11.18. Open impeller axial thrust.

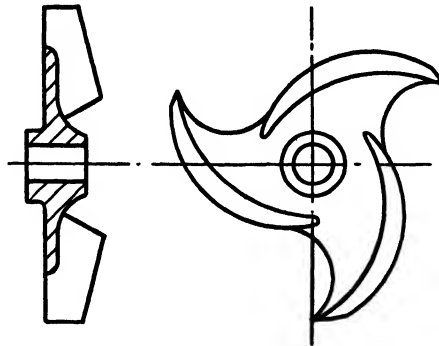


FIG. 11.19. Open impeller with back shrouds removed.

stage pumps handling suspended material such as paper stock have impellers with part of the back shroud removed (Fig. 11.19). These impellers reduce the axial thrust and help impellers to clear themselves of stringy matters.

**(b) Axial Thrust in Axial Flow Pumps.** In radial impellers, open or closed, the axial thrust is produced by static pressure on the impeller shrouds, which do not take part in the generation of head. The flow takes place in a plane normal to the axis and the difference of pressure on the faces of impeller vanes does not contribute to the axial thrust. In axial impellers there are no shrouds, and the flow is in the axial direction; any difference in pressure on the two faces of the vanes register as axial thrust on the rotating element. There is also a small axial force due to the difference in pressure on the two faces of the impeller hub. The axial thrust of an axial flow impeller is equal to  $T = A_e \gamma H / e_h$ , where  $A_e$  is area of the annulus between the impeller hub and the casing,  $H$  is the total head of the pump in feet,  $\gamma$  is the specific weight of liquid, and  $e_h$  is the hydraulic efficiency. This expression can be obtained from the following consideration. The work per unit time done in lifting liquid by an axial impeller can be represented as  $Tc_1$ , where  $c_1$  is the axial velocity and  $T$  is an axial force. This force is a liquid reaction on the impeller vanes and is equal to the axial thrust. On the other hand the same work per second is equal to the impeller input  $Q\gamma H / e_h$ . By equating the two we obtain the expression sought, or

$$Tc_1 = \frac{Q\gamma H}{e_h}$$

hence

$$T = \frac{Q}{c_1} \frac{\gamma H}{e_h} = \frac{A_e \gamma H}{e_h} \quad (11.14)$$

To this thrust  $T$  must be added a force due to the static difference in pressure on the two faces of the hub.

**(c) Axial Thrust in a Mixed Flow Pump.** Mixed flow impellers have axial thrust due to both vane dynamic action and static pressure on the impeller hub. The method of calculation thrust for axial flow pumps can be applied here also, but instead of the axial velocity  $c_1$ , the axial component of the meridional velocity  $c_1 \cos \theta$  (Fig. 11.20) is used. The axial thrust due to static pressure on the impeller hub is greater than that in the axial flow pump. Note that there is an upward component of thrust due to pressure on the conical part of the hub. This is variable and is applied on area  $(A_{h2} - A_{h1})$ .

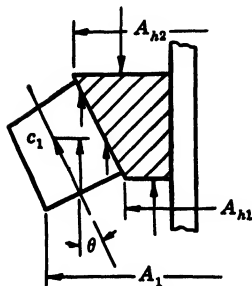


FIG. 11.20. Axial thrust on a mixed flow impeller.

For practical purposes great accuracy of thrust calculations is seldom required as there is always a thrust bearing to take care of the unbal-

anced thrust. For that reason simple experimental formulas are in use which permit quick thrust calculations. One of these has the form

$$T = A_e p K_t$$

where  $T$  is thrust in pounds,  $A_e$  is the impeller eye area in square inches,  $p$  is the total head in pounds per square inch, and  $K_t$  is an experimental

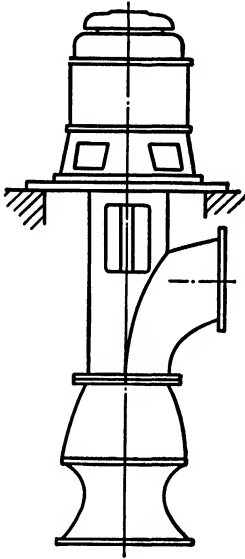


FIG. 11.21. Motor support does not carry impeller axial thrust.

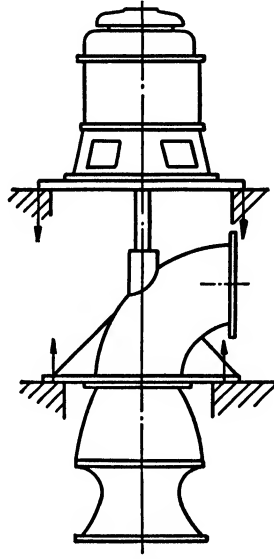


FIG. 11.22. Motor support carries full axial thrust.

factor which is equal to 1.0 for axial flow pumps and increases for mixed flow and radial impellers. The value of  $K_t$  for different specific speeds is given in Fig. 7.19.

In a vertical pump of the propeller or turbine type, when the hydraulic thrust is carried by the motor bearing, the thrust does not impose any load on the motor support in addition to the dead weight of the pump and the liquid in the column if the motor support is integral with the pump discharge column (Fig. 11.21). This is because the thrust is an internal force in a self-contained system comprising the pumping element, the discharge column, and the motor. The hydraulic thrust imposes

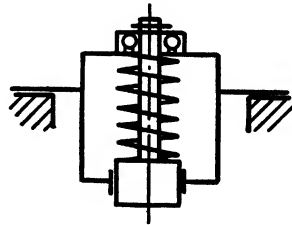


FIG. 11.23. Supports do not carry spring load.

some internal stresses on certain parts of the system and can be compared to a spring in a box (Fig. 11.23). However, if the pump and motor have independent supports (Fig. 11.22) then the motor support carries full downward hydraulic thrust in addition to the weight of the rotating element, and the pump support carries an equal upward casing hydraulic reaction.<sup>4</sup>

**(d) Thrust Bearing Lock.** *In horizontal pumps having no axial thrust, the outer race of the thrust bearing should be prevented from rotating (Fig. 17.17). Otherwise, while floating within the available axial clearance, the outer race may acquire sufficient momentum to hit and grind the end stops of the ball bearing. Large high speed thrust bearings have been damaged in this way.*

#### REFERENCES

1. A. J. STEPANOFF, "Leakage Loss and Axial Thrust in Centrifugal Pumps," *Trans. A.S.M.E.*, Vol. 54, No. 15, Aug. 15, 1932, pp. 100, 101.
2. J. H. POLHEMUS and J. HENLY, "Dredge Pump Pressures and Thrust Loads," *Trans. A.S.M.E.*, Vol. 51, No. 6, Jan.-Apr. 1929, p. 33.
3. F. G. SWITZER, discussion in reference 1, p. 104.
4. A. J. STEPANOFF, "Propeller Pumps for Circulation of Molten Salt," *Refiner and Natural Gasoline Manufacturer*, Vol. 19, No. 12, Dec. 1940, p. 474.

## CHAPTER 12

### CAVITATION IN CENTRIFUGAL PUMPS

#### 12.1 INTRODUCTION AND DEFINITION

In the last decade no other phase of hydraulic machinery design and operation has been given so much attention in technical literature as cavitation. The reason for this was the use of higher specific speeds, for both hydraulic turbines and centrifugal pumps, with the increased danger of cavitation. To cope with the problem, experimental and theoretical studies of cavitation were made on hydraulic turbines, centrifugal pumps, and apparatus without moving parts, such as venturi-shaped water conduits. As a result of the study and accumulated experience, pumps now operate at higher speeds and are safer against cavitation damage than they used to be.

The term cavitation refers to conditions within the pump where, owing to a local pressure drop, cavities filled with water vapor are formed; these cavities collapse as soon as the vapor bubbles reach regions of higher pressure on their way through the pump. In order to form such vapor cavities, the pressure first has to drop to the vapor pressure corresponding to the prevailing water temperature. The liberation of air or the formation of air- or gas-filled cavities, however, is not sufficient to produce cavitation because the effect of air bubbles on the performance and behavior of the pump is different.

Cavitation should be distinguished from separation, which is a separation of the streamlines from the low pressure side of the vane and the formation of a turbulent wake behind the vane. Separation is possible only with real viscous fluids, whereas cavitation is possible with hypothetical perfect liquids too. Experimentally, separation has been found to exist without cavitation, and cavitation without separation. Although centrifugal fans work on the same principle as centrifugal pumps, the former can have separation whereas the latter can have both separation and cavitation. Cavitation can appear along stationary parts of a hydraulic machine or along a moving vane, as in centrifugal pump impellers.

The reduction of the absolute pressure to that of vapor tension may be either general for the whole system or merely local; the latter may



be realized without a change of the average pressure. A general pressure drop may be produced by one of the following means: (1) an increase in the static lift of the centrifugal pump; (2) a decrease in the atmospheric pressure with a rise in the altitude; (3) a decrease in the absolute pressure on the system, as in the case of pumping from vessels under vacuum; and (4) an increase in the temperature of the pumping liquid, which has the same effect as a decrease in the absolute pressure of the system.

A local decrease in pressure is produced by one of the following dynamic means: (1) an increase in velocity by speeding up the pump; (2) a result of separation and contraction of flow (viscosity); and (3) a deviation of streamlines from their normal trajectory, such as takes place in a turn or in a passing obstruction to the flow.

Low absolute pressures and cavitation may also be caused by a sudden starting and stopping and recoil of the water column, such as occurs during water hammer phenomena. This type of cavitation is transient in character and is of little importance in centrifugal pump practice.

## 12.2 SIGNS OF CAVITATION

Cavitation is manifested by one or several of the following signs, all of which adversely affect the pump performance and may damage pump parts in severe cases.

**(a) Noise and Vibration.** This is caused by the sudden collapse of vapor bubbles as soon as they reach the high pressure zones within the pump; the bigger the pump, the greater the noise and vibration. Although these signs of cavitation may appear in the normal operating range of the pump only if the suction head is not sufficient to suppress cavitation, noise and accompanying vibration are present in all pumps to a varying degree when they are operated at points far removed from the best efficiency point because of a bad angle of attack at the entrance to the impeller. By admitting small amounts of air into the pump suction noise can be almost completely eliminated. In this way the air serves as a cushion when the vapor bubbles collapse. This method, however, is not often used to eliminate noises in centrifugal pumps, although it is an established procedure with water turbines and large butterfly valves where air is admitted automatically at partial loads.<sup>1, 2, 29</sup> The beneficial effect of air admission to the pump suction under cavitation conditions is not limited to the elimination of noise and mechanical vibration, for the impeller vane pitting is also reduced if not entirely eliminated, as it is caused by the mechanical shock accompanying the collapse of the vapor bubbles.

(b) **Drop in Head-Capacity and Efficiency Curves.** This appears in varying degrees with pumps of different specific speeds. With low specific speed pumps (up to 1500), the head-capacity, the efficiency, and the

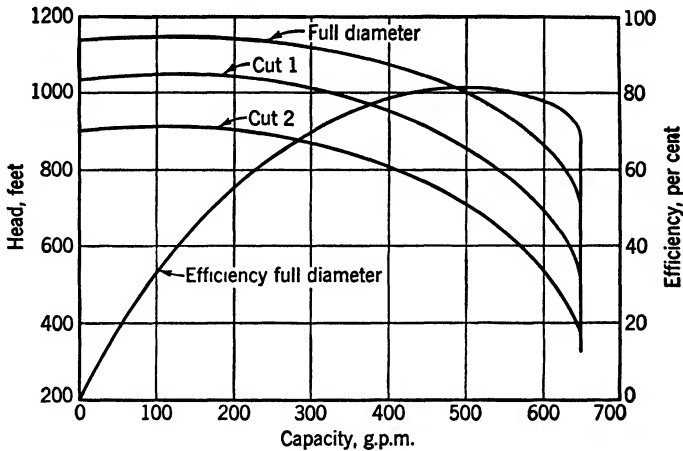


FIG. 12.1. Effect of impeller diameter on cavitation; 4-in. 4-stage pump, 3550 r.p.m.  
 $n_s = 1200$ .

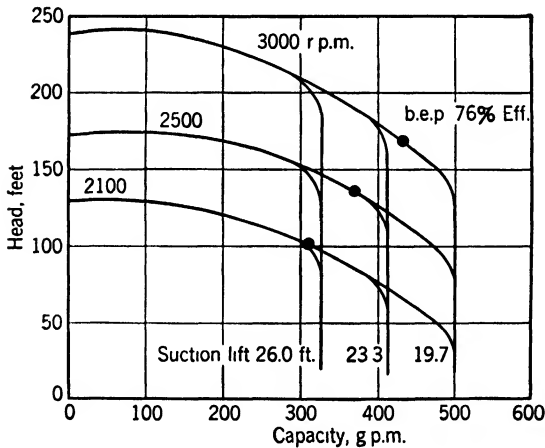


FIG. 12.2. Effect of speed and suction lift on cavitation; 3-in. single-suction pump,  
 $n_s = 1000$ .

brake-horsepower curves drop off suddenly when  $Q$  is increased to the point where cavitation is reached (Figs. 12.1 and 12.2). With higher specific speed pumps (1500–5000), however, the head-capacity and the efficiency curves begin to drop along the whole range gradually before

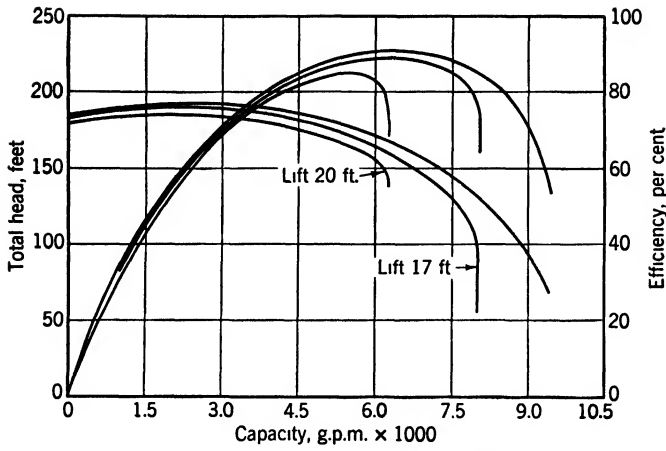


FIG. 12.3. Twelve-inch double-suction pump, 1200 r.p.m.,  $n_s = 2100$ .

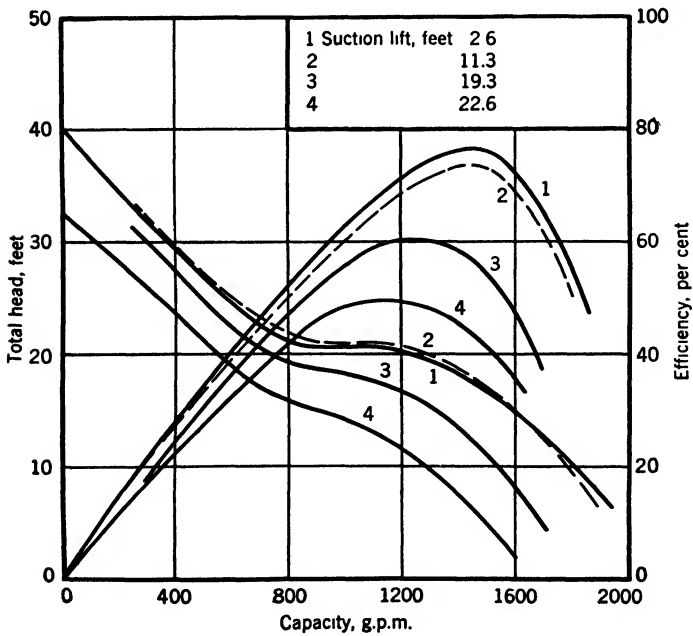


FIG. 12.4. Axial flow pump performance,  $6\frac{1}{2}$ -in. impeller diameter, 2250 r.p.m.  $n_s = 9750$  (Tenot).

the point of sudden break-off is reached (Fig. 12.3). The degree of drop in the head-capacity and efficiency curves depends on the specific speed and on the suction pressure, increasing for higher specific speed and lower suction pressure.

With very high specific speed pumps (above 6000) of the propeller type, there is no definite break-off point on the curves (Fig. 12.4); instead, there is a gradual drop in the head-capacity and the efficiency curves along the whole range. In this type of pump, the drop in the efficiency appears before there is a perceptible drop in the head-capacity curve. Therefore, a drop in the efficiency is a more reliable criterion of approaching cavitation conditions. Even the objectionable noise may not appear until cavitation has progressed beyond the point where the efficiency becomes unsuited commercially.

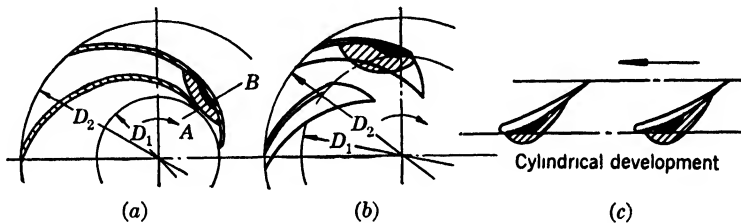


FIG. 12.5. Low pressure zones on back side of impeller vanes: (a) low specific speed; (b) medium specific speed; (c) propeller pump.

The difference in the behavior of pumps of different specific speeds results from the difference in the impeller design. Low specific speed impeller vanes form a definite channel, the length of which depends on the vane angles, the number of vanes, and the ratio of the impeller eye diameter  $D_1$  to the impeller outside diameter  $D_2$  (Fig. 12.5). When the pressure at the impeller eye reaches the vapor pressure, usually on the back side of the vane entrance tips, it extends very rapidly across the whole width of the channel, A-B, Fig. 12.5 (a)—with a small increase in capacity and decrease in head. A further drop in the discharge pressure does not produce any more flow because the pressure differential moving water to the impeller eye cannot be increased any more. This differential is fixed by the suction pressure outside the pump, and the vapor pressure across the whole channel between any two vanes at the impeller entrance.

With high specific speed impellers, the channel between two vanes is wider and shorter; see Fig. 12.5 (b). More drop in head and a greater increase in capacity are required to extend the vapor pressure zone across the whole channel. Therefore, the drop in the head-capacity curve extends through a wider range before the sudden break-off occurs.

With propeller pumps the vanes do not overlap; see Fig. 12.5 (c). Therefore, although the low pressure zone extends when the pump head is reduced, there are always parts of the channel which remain at pressures higher than vapor pressure, and the flow through the impeller will steadily increase even though cavitation has definitely set in.

With low and medium specific speed pumps, a reduction in capacity, instead of an increase, is frequently observed at reduced discharge pressure under cavitation conditions (Fig. 12.6). This is caused by a further increase of the low pressure zone along the impeller channel and the expansion of air in the vacuous pockets.

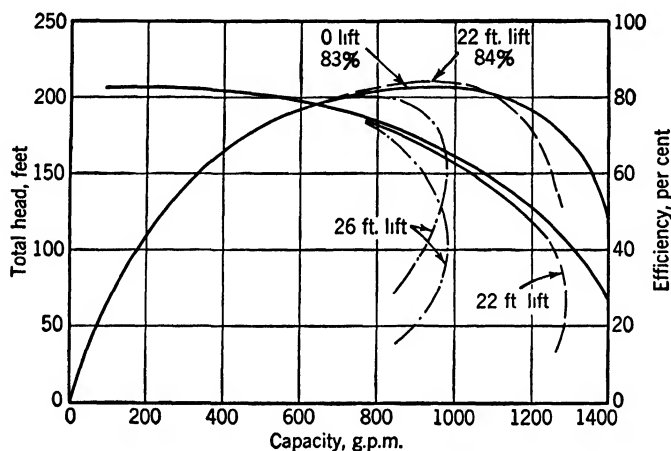


FIG. 12.6. Decrease of capacity at reduced discharge pressures; 5-in. double-suction pump, 1760 r.p.m.,  $n_s = 1200$ .

In multistage pumps cavitation affects only the first stage; therefore the drop in head-capacity and efficiency is less pronounced than in a single-stage pump. The cut-off capacity is determined by the first stage.

The drop in the head-capacity and the efficiency curves may begin before the vapor pressure is reached in certain parts of the impeller suction. This is caused by the liberation of air or light fractions in petroleum oils at reduced pressures in the impeller eye. The absolute pressure in the vacuous pockets is the sum of all the partial pressures of the gases occupying this space, in accordance with Dalton's law of partial pressures.

The drop in the head-capacity and the efficiency curves due to liberation of free air in the water is followed by a reduction in the brake horsepower also. This method has been suggested<sup>3</sup> as a means of reducing the head and at the same time saving power instead of throttling the

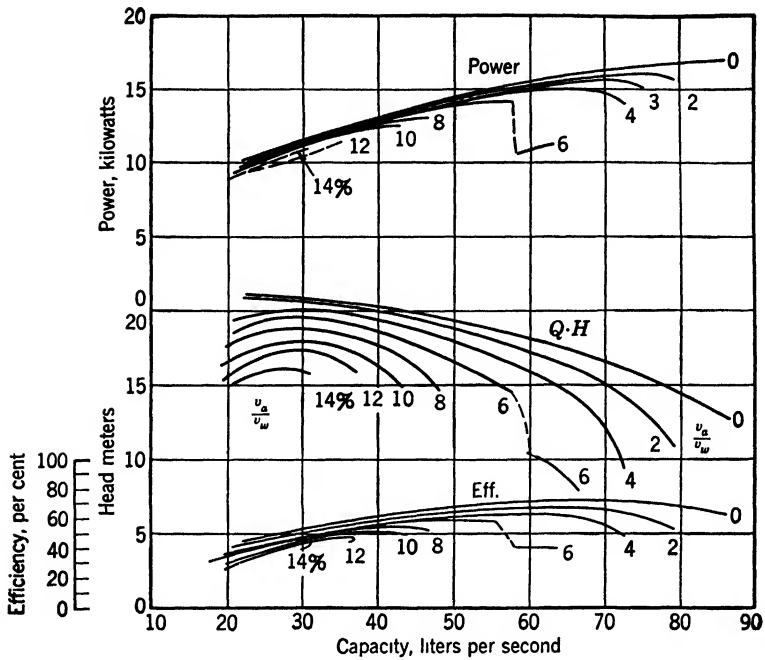


FIG. 12.7. Effect of admission of air into pump suction (Siebrecht).

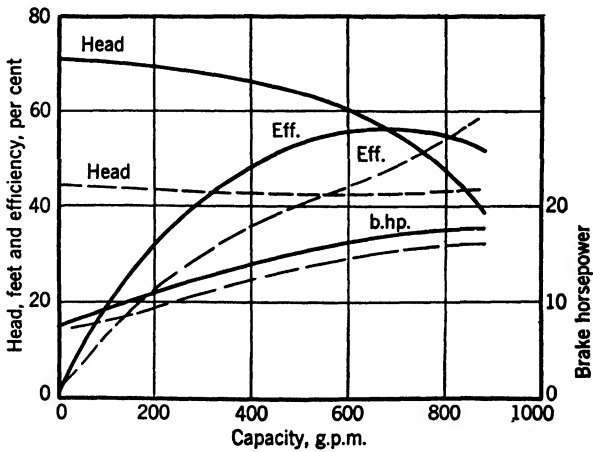


FIG. 12.8. Throttling of pump suction instead of discharge to save power may be a dangerous procedure; 5-in. pump, 1160 r.p.m.,  $\eta_s = 1500$  (Van Leer).

pump discharge, as done ordinarily. Figure 12.7 shows test results obtained by Siebrecht, namely, the head-capacity, efficiency, and brake-horsepower curves of a pump with different volumes of air admitted to the pump. The author does not know of any case where this method was employed in actual installations, but a modification of this method, whereby the pump suction is throttled instead of the discharge to reduce the head, is frequently employed. At reduced suction pressures, air or gases begin to be liberated from the liquid, producing a lower head-capacity curve and lower brake-horsepower. However, this method is not recommended because, if suction throttling is carried too far, cavitation will start with all its bad effects—noise, pitting, and vibration. Figure 12.8 shows a test of a 5-in. pump with the suction and the discharge throttled. A comparison of the brake-horsepower curves shows the power saved by suction throttling.<sup>4</sup>

On several occasions it has been found by careful tests on centrifugal pumps and water turbines that the efficiency may show a slight increase shortly before cavitation sets in (Fig. 12.6). This is explained by a reduction of friction at the beginning of separation, just before the disturbing water hammering begins.<sup>5, 9, 12, 22</sup>

**(c) Impeller Vane Pitting and Corrosion Fatigue Failure of Metals.**

If a pump is operated under cavitation conditions for a sufficient length of time, impeller vane pitting appears, the amount of metal lost depending on the material in the impeller and the degree of cavitation. *Foettinger<sup>5</sup> showed very conclusively that vane pitting is caused solely by the mechanical (water hammer) action of collapsing vapor bubbles, and that electrolytic and chemical action is entirely insignificant in this process.* He proved this by producing cavitation in a venturi-shaped channel made of neutral glass which was pitted in the same manner as the metal in a centrifugal pump or water turbine impeller vanes. *If electrolytic or chemical reaction is active, it should affect all the parts of the same material and not only the spots subject to cavitation water hammer.*

The fact that air or gases may be more active at the instant of liberation has been stated in the past. However, the places affected by pitting are always beyond the low pressure points where the vapor bubbles are formed. Another corroboration of the mechanical nature of the metal destruction has been shown by the damage of a lead plate without any loss of weight.<sup>6</sup>

By experience it has been found that the collapse of vapor bubbles is harmless when it takes place entirely surrounded by the stream of liquid.<sup>6</sup> *In addition to metal destruction due to the fatigue of the metal surface as a result of repeated water hammer blows, Poulter<sup>7</sup> has shown that metal particles can be torn off and carried away by liquid penetrating*

*into and escaping from the pores of the metal under successive pressure waves.* In that case, more porous materials are most readily affected by such destruction. The degree of destruction depends on the length of time the specimen is under pressure, or the time between two successive pressure waves.

There seems to be no correlation between the hardness and the cavitation erosion of metals, but apparently the molecular size and the viscosity of liquids play an important part in cavitation pitting.

Cavitation pitting should be distinguished from corrosion and erosion. The first is caused exclusively by chemical and electrolytic action of the pumped liquids; the second is the wearing away of the metal parts in a pump by foreign bodies carried by the pumped liquids, such as sand, grit, coke, and coal. There is no difficulty in distinguishing these three kinds of pitting by the appearance of the attacked parts and their location in the water passages of the pump.

Frequencies of hammering were recorded from 600 to 1000 cycles per second by Hunsaker and up to 25,000 cycles per second by de Haller.<sup>8</sup> The intensity of hammering depends on the velocity. Pressures of 300 atm. were measured by de Haller. Local pressures confined to very small areas (the piston area of de Haller's pressure-measuring device was 1.5 mm.) may be considerably higher than those recorded. A satisfactory explanation of how such high pressures may arise in the case of cavitation has been lacking.

*In the light of Poultier's investigation,<sup>7</sup> it may appear possible that high destructive pressures are derived from the elastic forces of metal parts extending over areas larger than those actually attacked by cavitation. These parts are under fluctuating forces of large magnitude, so large that often the whole foundation supporting the pump is set in vibration under cavitation conditions. Under fluctuating stresses liquid is drawn in and squeezed from the pores, and it is during this squeezing phase that tremendous pressures may be produced in small restricted areas.*

*A similar process may be a partial explanation of what is known as corrosion fatigue of metals, or metal failure under repeated stresses in presence of liquids. The corrosive effect of water as compared with oils in the case of corrosion fatigue is due to the fact that water molecules are smaller than those of oil; therefore, water penetration of metals would be deeper than that of oil; hence the destructive effect on the metal is greater where it is subjected to rapidly fluctuating stresses. This will explain the failure by corrosion fatigue of non-corrosive high chromium steels in the presence of water. Another illustration and proof that the penetration of metals by liquid plays an important part in metal destruction by corrosion fatigue is furnished by results of laboratory tests*



by McKay and Worthington.<sup>30</sup> They have found that the endurance limit depends not only on the stress level and the total number of cycles, but also on the frequency of stress reversals. For the same total number of cycles, the low frequency gives a much lower endurance limit because more time is allowed for liquid penetration of metal with consequently higher destructive pressures developed in the metal pores when the liquid is compressed on the stress reversal.

### 12.3 MATERIALS TO RESIST CAVITATION PITTING

(a) **Experimental Study.** Different materials resist cavitation pitting in varying degrees. In addition to the chemical composition, the heat treatment of metals and also the surface conditions control the amount

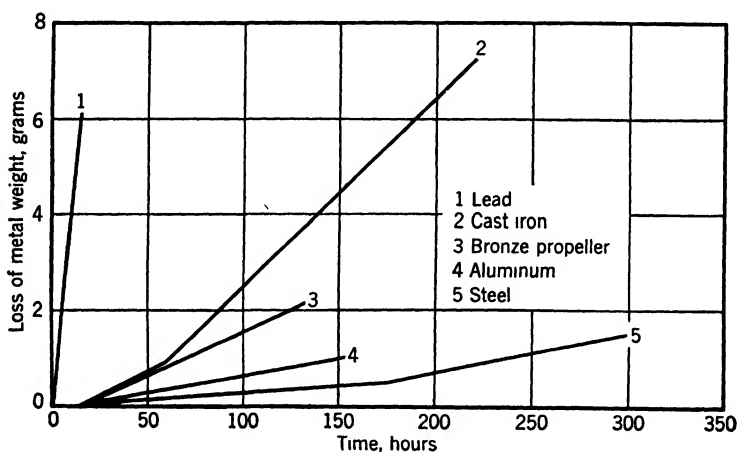


FIG. 12.9. Loss of metal due to cavitation (Schroeter).

of material destroyed by cavitation. The behavior of metals under cavitation parallels that under corrosion fatigue conditions. Any notches, nicks, scratches, flaws, or sharp corners on the surface of metals attacked by cavitation accelerate the beginning of pitting. Protective coats do not improve the resistance of metals to cavitation pitting.

Schroeter<sup>10</sup> has run tests on different materials under cavitation in a venturi-shaped conduit built for the purpose. A velocity of 197 ft. per sec. was maintained throughout these tests. Figure 12.9 shows some materials tested by Schroeter.

Hardening decreases the rate of metal destruction although the hardness alone (for different materials) is not a determining factor as far as resistance to cavitation is concerned.

To prolong the life of runners of large Kaplan turbines working under high heads (over 50 ft.), the turbine manufacturers protect with welded stainless steel the places subject to cavitation pitting.<sup>11</sup> Propeller pumps of the same type are not built in sizes justifying such procedure, nor are they operated at such high heads.

Although covering the surface of metals with rubber helps them to resist the impact of water hammering very well, its bond to the metal fails after a short time. No practical method of rubber protection of

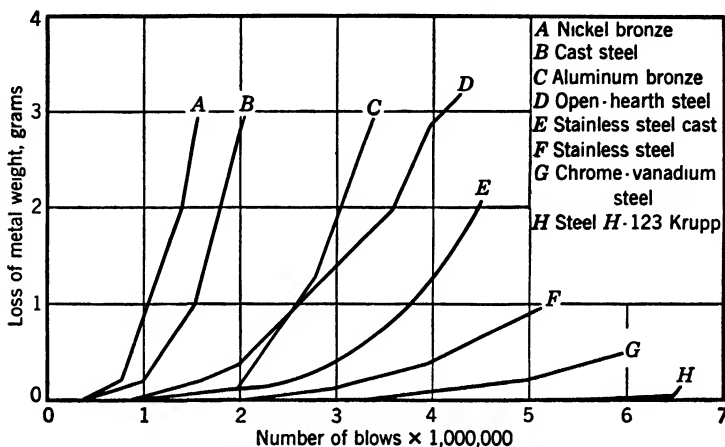


FIG. 12.10. Loss of metal by jet drop-impact (de Haller).

metals against cavitation has yet been developed. Tests with rubber again corroborate the mechanical nature of the destruction of materials by cavitation.<sup>10</sup>

Schroeter's tests have definitely established the fact that the beginning of cavitation and its extent depend on the velocity of the flow. This must be expected as all the destructive blows by water hammer derive their energy from the kinetic energy of the flow.

De Haller<sup>8</sup> has found that the behavior of various metals is analogous during tests with direct drop-impact and with cavitation. In both cases the metal destruction is caused by water hammering. Although the mechanism of water blows against metals is different, their result is quite similar. In a special apparatus resembling a steam turbine wheel, de Haller ran erosion tests on a number of materials, and his results, reproduced in Fig. 12.10, are in agreement with Schroeter's. De Haller's method of testing materials for cavitation resistance requires only a short time to produce cavitation pitting.

Kerr<sup>21</sup> has tested 80 materials for cavitation in sea water in a special vibratory apparatus developed by the Massachusetts Institute of Tech-

nology. These tests show that cavitation damage was slightly greater by sea water than by fresh water. It has been found also that the temperature of water has a marked effect upon the metal loss by cavitation, the loss increasing with temperature. *At higher temperatures the amount of air dissolved in water is reduced, and thus the cushioning effect of water hammer blows is reduced, while at the same time the increased vapor pressure tends to increase the vapor bubble formation.*

Mousson<sup>32</sup> has found that loss of metal by cavitation is approximately proportional to vapor pressure. He also demonstrated the beneficial effect of admission of small amounts of air upon the metal damage by cavitation. Mousson and Kerr give extensive test data which are very useful in the selection of materials when cavitation is expected.

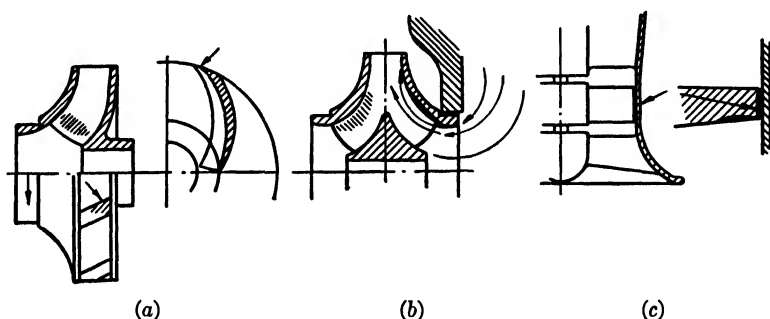


FIG. 12.11. Examples of impeller cavitation.

**(b) Examples of Metal Attack by Cavitation.** In pumps of normal design, the lowest pressure occurs on the back side of the impeller vane slightly beyond the suction edge. The cavitation pitting appears somewhat farther downstream where the vapor bubbles collapse; Figs. 12.11 (a), 12.12 (a), and 12.12 (b). However, if the pump is operating continuously at a capacity considerably higher than normal, the pitting may appear on the front side of the vane at the suction vane tips; Fig. 12.13 (a). Cavitation in this case accompanies separation resulting from a bad angle of attack.

Figure 12.11 (b) shows vane and shroud pitting near the outer shroud due to lack of streamlining.

Figure 12.11 (a) shows vane pitting at the impeller discharge caused by the vane's blunt discharge tips.

Figure 12.11 (c) shows a marginal cavitation observed on propeller pumps and also on centrifugal pumps with open impellers. Local high velocity through the clearance and separation due to a sudden change in direction produced the marginal cavitation and pitting. Rounding off of

the high pressure side corners of vanes eliminates the marginal pitting at the expense of increased leakage through the clearance.<sup>12</sup>

Figure 12.12 (a) shows pitting of the volute casing of a propeller pump caused by a lack of streamlining.

Figure 12.12 (b) shows a diffusion casing vane pitting due to a discrepancy between angles of incoming flow and diffusion vane.

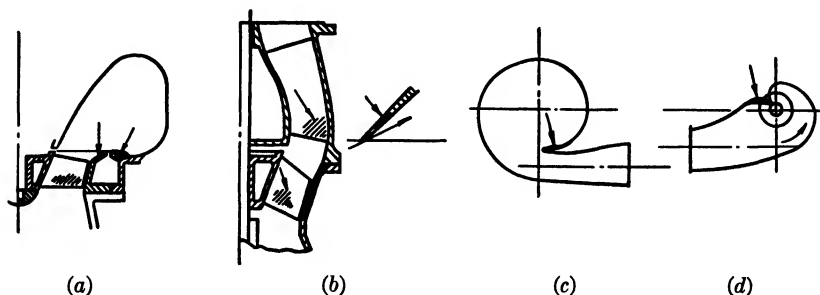


FIG. 12.12. Examples of casing cavitation.

Figure 12.12 (c) shows pitting of the tongue of a volute casing observed when a pump is operated continuously at capacities above normal.

Figure 12.12 (d) is an example of pitting of the baffle in the suction nozzle, which permits excessive prerotation of the flow before it enters the impeller eye.

In general, sudden change in direction, sudden increase in area, and lack of streamlining are responsible for local pitting of pump parts. This may appear only if the suction pressure is reduced below a certain minimum. On the other hand, pitting of pump parts on the discharge side of the pump has been observed when the pump pressure is not high enough to suppress cavitation.

**(c) Cavitation Due to Vibration.** Destruction of metal parts by cavitation can take place when there is no apparent local drop in pressure due to high velocity flow. It is possible for cavitation conditions to appear as a result of vibration of parts in contact with water. Water is unable to follow the frequency of a vibrating body, and at each reversal of the deflection vapor-filled cavities are formed between the water and the vibrating body and these collapse upon each reversal of the deflection. This principle has been used in the building of material-testing machines for cavitation studies.<sup>31</sup> Pitting of metal parts, typical of cavitation and caused by vibration, has been observed on such parts as diesel engine cylinder liners on the water jacket side, or locally on ship hulls in spots which respond to the vibration of the machinery inside the hull. In centrifugal pumps, evidence of cavitation due to

vibration of parts was never definitely established. However, it may be responsible for, or contribute to, the pitting of parts on which cavitation is difficult to explain from the standpoint of local dynamic depression or lack of streamlining.

(d) **"Air Impingement Attack of Metals."** In literature dealing with corrosion of condenser tubes another method of metal destruction is frequently mentioned, that of "impingement of air bubbles" on the tube surface. This conception contradicts the theory and test results of metal destruction by cavitation in hydraulic machinery as described by many authentic reports quoted in this chapter. The physical side of the air impingement attack of metals is not easy to visualize when it is borne in mind that air bubbles in a condenser tube move at the same velocity as the water, and particles of air are 800 times lighter than particles of water.

Air bubbles do not carry sufficient energy to make any appreciable effect by impingement on the stationary boundary layer of liquid attached to the tube walls. The effect of such attack would be somewhat similar to the hitting of the bottom of a swimming pool with a toy balloon or a tennis ball. The experimental proof of the metal damage by air impingement, such as that carried out by May,<sup>24</sup> lacks conclusiveness, because in every case when samples of metal were subjected to a jet of air-water mixture the sample was free to vibrate. The fact that metal destruction could be accomplished only with a fixed air-water ratio and with a certain size of air bubbles suggests that, apparently, those were the necessary conditions for exciting vibration of the sample. It is believed that in the de Haller tests,<sup>8</sup> which were performed with a water jet impact against revolving plates, vibration of the samples was an important factor in producing the cavitation effect.

Where conditions are favorable to chemical corrosion, cavitation may accelerate the damage because the products of corrosion and protective films are removed more rapidly and new and fresh surfaces are exposed to action.

#### 12.4 THEORETICAL RELATIONSHIP AT CAVITATION CONDITIONS

The flow to the impeller of a centrifugal pump following the energy gradient is determined by the existing pressure difference between the suction pressure and the pressure established by the flow at the impeller eye. The latter is not uniform at any section of the impeller passages, and even determination of the average pressure inside the impeller presents difficulties. For that reason, the theoretical relationship for the flow through the impeller eye, although easy to establish, does not give

a reliable tool for an accurate predetermination of cavitation conditions. An examination of the theoretical formulas for the flow through the impeller eye, however, enables one to learn the effect of several factors upon cavitation. A study of theoretical relationship has also resulted in the introduction of simplified formulas incorporating experimental coefficients which permit prediction of a pump's behavior with regard to cavitation if experimental data are available on similar pumps.

Let

$H_a$  be the absolute pressure prevailing at the surface of the pump suction supply. This will be atmospheric pressure if the suction vessel is open to the atmosphere. If the suction is taken from an enclosed vessel  $H_a$  is the absolute pressure in this vessel.

$h_s$  be the static head in the suction vessel above the pump center line. If it is suction lift, it is negative.

$h_v$  be the vapor pressure at the prevailing water temperature.

$h_l$  be the head loss in the suction pipe and impeller approach.

$c_1$  be the average absolute velocity through the impeller eye; Fig. 12.13 (b).

$\lambda w_1^2/2g$  be the local pressure drop below the average at the point of cavitation. Here  $w_1$  is the average relative velocity at entrance, and  $\lambda$  is an experimental coefficient.

This local pressure drop is caused by the difference in pressure on the leading and trailing sides of the vane. When pressure is applied by the

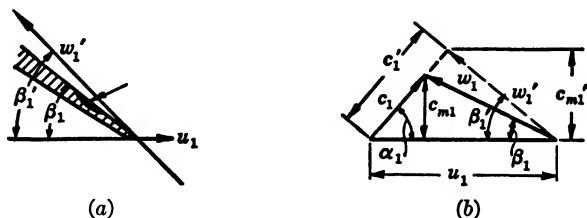


FIG. 12.13. (a) Entrance vane pitting at capacities above normal; (b) entrance velocity triangle at capacity above normal.

vane on water, the water exerts an equal reaction in the opposite direction, which exists as a pressure difference on the two faces of vanes. This is frequently referred to as a dynamic depression. Figure 3.21 shows a typical pressure distribution inside an impeller channel obtained by Uchamaru<sup>28</sup> under actual operating conditions.

Evidently cavitation starts when

$$H_a + h_s = h_l + h_v + \frac{c_1^2}{2g} + \lambda \frac{w_1^2}{2g} \quad (12.1)$$

When liquid in the suction vessel is boiling, the pressure in the vessel  $H_a$  is equal to the vapor pressure, or  $H_a = h_v$ , and equation 12.1 becomes

$$h_s = h_t + \frac{c_1^2}{2g} + \lambda \frac{w_1^2}{2g} \quad (12.1a)$$

meaning that a positive suction head  $h_s$  is necessary to produce the flow. To prevent vaporization, an excess of suction head is necessary above  $h_s$ .

Equation 12.1 is not suitable for determining the maximum permissible suction lift for a given pump capacity ( $c_1$  and  $w_1$ ), because the true

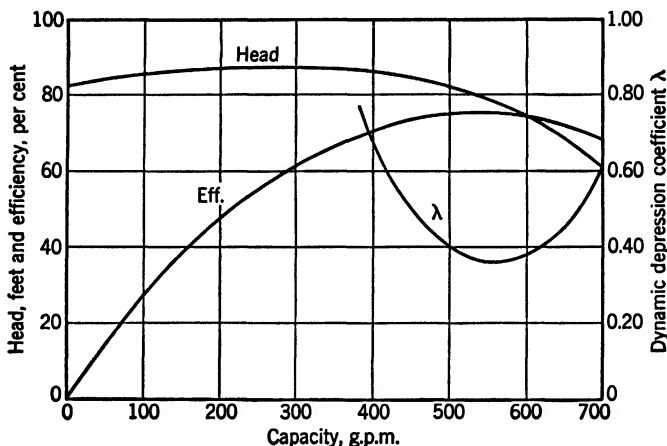


FIG. 12.14. Dynamic depression coefficient  $\lambda$  (Krisam).

value of maximum  $c_1$  is not known, and also because the value of  $\lambda$  varies for pumps of different specific speed.\* Even for a given pump at constant speed,  $\lambda$  varies with capacity, being a minimum near the best efficiency point and increasing on both sides of this point. Figure 12.14 shows a typical curve of  $\lambda$  variation obtained by Krisam.<sup>13</sup> Similar curves were published by von Widdern.<sup>14</sup> The increase of  $\lambda$  on both sides of the best efficiency point shows the effect of the angle of attack [see Fig. 12.13 (a)] between the direction of relative velocity and the vane angle at the impeller entrance.

\* Equation 12.1 is Bernoulli's equation applied between two points, one at the suction nozzle and the other somewhere in the impeller channel. Every limitation to its validity discussed in Art. 1.1, Chapter 1, is in evidence here: the flow is not steady; vapors and air are liberated; part of the channel is curved, divergent, and moving, with power applied to it. Therefore it is not surprising that equation 12.1 is not suitable for a quantitative determination of approaching cavitation conditions, although the qualitative deductions hold in practice.

## 12.5 FACTORS AFFECTING CAVITATION

A study of equation 12.1 permits a number of conclusions which hold in practice for, at cavitation conditions, a change in one term of the equation is always followed by a change in another to satisfy the relationship. Thus

(a) If atmospheric pressure is decreased because of an increased elevation (about 1 ft. per 1000 ft. of elevation), the pump maximum capacity will decrease ( $c_1$  and  $w_1$  will decrease).

(b) If suction lift is increased ( $-h_s$  greater), or if vapor pressure rises as a result of the higher temperature of water, pump maximum capacity will decrease.

(c) Higher suction lifts may be possible with low velocities ( $c_1$  and  $w_1$ ) or with a minimum loss  $h_l$  in the suction pipe.

(d) Note that  $H_a$  expressed in feet of liquid depends on the specific gravity of the liquid. Thus, when molten salt (used as a heating medium in the petroleum refinery process) of specific gravity 1.75 is being pumped and the suction vessel is under atmospheric pressure,  $H_a = 19.4$  ft. Therefore the danger of cavitation is much greater with heavier liquids.<sup>15</sup> Vapor pressure should not be overlooked with liquids other than water.

(e) For given average velocities,  $c_1$  and  $w_1$ , the approach of cavitation is affected by the casing and impeller design because they affect the velocity distribution. Thus, pump suction design permitting more prerotation in the impeller eye will decrease the maximum capacity for a fixed suction pressure. Any lack of streamlining in the suction passages of the pump and impellers results in the formation of dead water pockets (separation), which increase local velocities beyond the average or those obtained from the velocity triangle.

(f) With pumps of high specific speed of the axial flow type, the beginning of cavitation is indicated by a gradual drop of pump efficiency without any sudden drop in the head-capacity curve. In this case a further reduction in the suction pressure extends to the region affected by cavitation and equation 12.1 does not apply, as the vapor pressure is reached locally only; the impeller vanes do not form an entirely enclosed channel, and Bernoulli's equation (12.1) cannot be used.

(g) The presence of gases in the liquid does not affect the validity of equation 12.1 except that, according to Dalton's law of partial pressures, the vapor will behave as if it occupied the voids alone, and vaporization will begin at an absolute pressure higher than its normal boiling point and corresponding to the existing temperature. Petroleum oils represent the most complicated example of this. Being mixtures of different individual hydrocarbons, each of which has its own vapor pressure,



light fractions will vaporize at pressures far above their normal boiling points, but the vaporization will affect only a small portion of the total flowing volume. As a result, the drop in the  $Q$ - $H$  curve is more gradual with oils than with water, and the mechanical disturbance is not so violent. The fact that vaporization and condensation during cavitation require a heat exchange tends to slow down the bubble formation in oils as compared with water on account of the lower heat conductivity of oil.

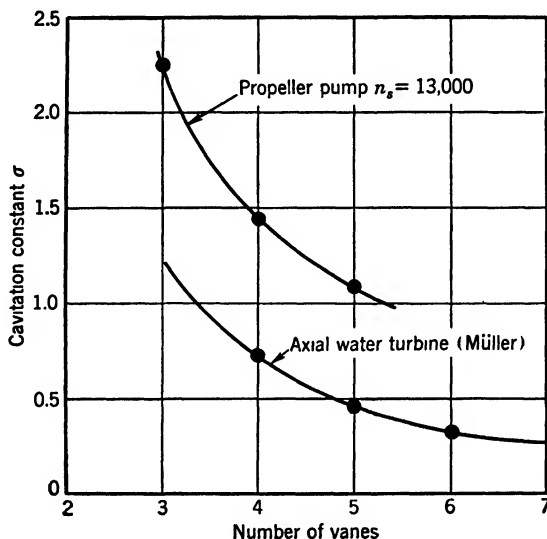


FIG. 12.15. Effect of number of vanes on sigma.

In dealing with petroleum products the “bubble point” pressure should be used and not Reid vapor pressure, as the latter gives a summary pressure of several fractions and not the beginning of vaporization of the lighter fraction.<sup>33</sup>

(h) In the study of cavitation, the suction pressure should be specified or measured at the pump suction nozzle. In this way the loss in the suction pipe and the entrance loss are eliminated. The loss in the suction nozzle is negligibly small, owing to a low velocity, a short distance, and accelerated flow in a normal nozzle design.

(i) In small pumps of low specific speed, the term  $c_1^2/2g$  is predominant in setting up cavitation conditions, and the term  $\lambda(w_1^2/2g)$  is of little significance. In high specific speed pumps approaching propeller pump type the term  $\lambda(w_1^2/2g)$  is the controlling factor, and  $c_1^2/2g$  is of secondary importance.  $\lambda(w_1^2/2g)$  depends on the pump head (and

hence speed) and the number of impeller vanes, and it decreases with a smaller head or a lesser speed and a greater number of vanes.

With low specific speed pumps the maximum capacity for a given suction head can be increased by cutting away part of the vane in the impeller eye and filing the vane tips, thus increasing the available area for  $c_1$  and making  $c_1$  smaller. On the other hand, with propeller pumps, increasing the number of vanes will lower the vane loading and will im-

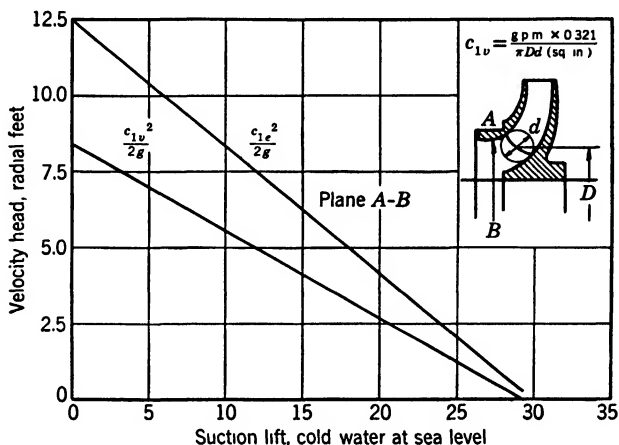


FIG. 12.16. Meridional velocity versus suction lift at cavitation conditions.

prove the cavitation conditions of the pump (Fig. 12.15) for a given submergence, and thus permit higher head without noise or drop in efficiency.

(j) With low specific pumps the maximum absolute velocity  $c_1$  may be reached either at the impeller eye (plane A-B, Fig. 12.16), or at the vane entrance. The actual effective area of both sections is greatly affected by the impeller approach design. In the study of cavitation test data, both sections should be investigated.

## 12.6 PREDETERMINATION OF CAVITATION CONDITIONS FROM VELOCITY CONSIDERATIONS

From a great number of observations on pumps of low and medium specific speeds (up to 1500), the author has found that for cold water (70°F.), equation 12.1 can be simplified to

$$30 - h_s = 2.4 \frac{c_{1e}^2}{2g} \quad (12.2)$$

where  $c_{1e}$  is the meridional velocity through the impeller eye at cut-off capacity (plane *A-B*, Fig. 12.16) at suction lift  $h_s$  taken at the suction nozzle and referred to the pump shaft center line. The same relationship is represented by a curve on Fig. 12.16.

A similar curve, plotted for meridional velocities at the vane entrance tips, is shown in Fig. 12.16.<sup>16</sup> This curve can be expressed by

$$30 - h_s = 3.5 \frac{c_{1v}^2}{2g} \quad (12.3)$$

A comparison of equations 12.2 and 12.3 with equation 12.1 leads to the following conclusions.

(a) The difference between atmospheric pressure  $H_a = 34$  and  $H_a = 30$  in equations 12.2 and 12.3, or 4 ft., includes: a vapor pressure of 0.85 ft. at 70°F. water temperature; the loss of head ( $h_l$ ) in the suction nozzle, a local drop in pressure due to uneven velocity distribution in the impeller approach and a small margin of safety.

(b) The right-hand term in equation 12.2 can be expanded as follows.

$$2.4 \frac{c_{1e}^2}{2g} = \frac{c_1^2}{2g} + \lambda \frac{w_1^2}{2g} = \frac{c_{1e}^2}{2g} \left[ \frac{1}{(\sin \alpha_1)^2} + \frac{\lambda}{(\sin \beta_1)^2} \right] \quad (12.4)$$

where  $\alpha_1$  is the absolute velocity angle and  $\beta_1$  is the vane angle at the entrance; Fig. 12.13 (b). Similarly, in equation 12.3 the right-hand terms can be represented as follows.

$$3.5 \frac{c_{1v}^2}{2g} = \frac{c_1^2}{2g} + \lambda \frac{w_1^2}{2g} = \frac{c_{1v}^2}{2g} \left[ \frac{1}{(\sin \alpha_1)^2} + \frac{\lambda}{(\sin \beta_1)^2} \right] \frac{1}{\delta^2} \quad (12.5)$$

$\delta$  is a contraction coefficient to account for the vane thickness because this was disregarded when  $c_{1v}$  was calculated.

(c) Since curves on Fig. 12.16 have been plotted for low specific speed pumps where the term  $\lambda(w_1^2/2g)$  is of secondary importance, the cut-off capacity is determined by the impeller eye velocity,  $c_{1e}$  or  $c_{1v}$ , and is independent of the impeller diameter or pump speed as long as the cut-off capacity occurs at or near the best efficiency point, as shown on Figs. 12.1 and 12.2. (Similar tests were published by von Widern.<sup>14</sup>) Within the range specified for a fixed suction head, the cut-off capacity is independent of the specific speed and is governed by the absolute velocity through the impeller eye. Either the term  $\lambda(w_1^2/2g)$  is small or it varies little with the specific speed and bears an approximately constant ratio to  $c_1^2/2g$ , thus leaving the experimental numerical constant in the right-hand terms of equations 12.2 and 12.3 essentially constant.

With pumps of medium and high specific speed (1500 to 4000), the cut-off capacity will increase somewhat with the speed if the cut-off takes place to the right of the best efficiency point. The cut-off capacity will decrease at higher speeds if the cut-off takes place at capacities smaller than normal (Fig. 12.17). The reason for this is the variation of the coefficient  $\lambda$  in the term  $\lambda(w_1^2/2g)$ . Figure 12.14 shows that this is a minimum near the best efficiency point. When the cut-off takes place at capacities above normal, the best efficiency point moves nearer to the cut-off capacity at a higher speed where  $\lambda$  is smaller, and thus  $\lambda(w_1^2/2g)$  is smaller; hence  $c_1^2/2g$  or pump capacity will increase. At partial

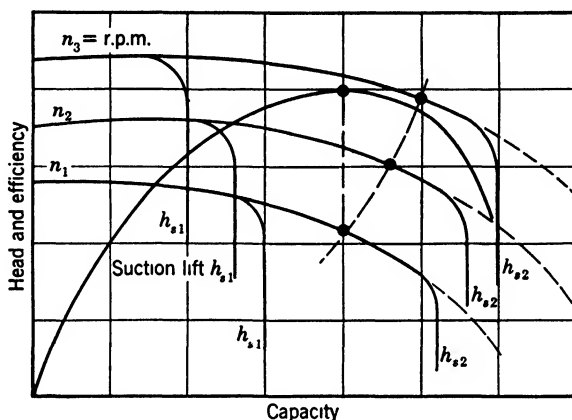


FIG. 12.17. Cut-off capacities at several speeds.

capacities the peak efficiency moves away from the cut-off capacity at higher speeds, while  $\lambda$  is increasing and the cut-off capacity is decreasing.

Looking at the same phenomena from a different point of view, it will be noticed that where the cut-off capacity is nearer the peak efficiency at higher speed, the angle of attack of the incoming flow at the impeller entrance is smaller, the extent of separation is reduced at the vane tips, and the effective area available for the flow is increased. Thus, at the same suction pressure, a higher capacity is possible at a higher speed. When the cut-off takes place at partial capacity and the best efficiency point is moving farther at a higher speed, the angle of attack is increasing, separation is more pronounced, the effective area is reduced, and the cut-off capacity is lower at a higher speed.

Since the best angle of attack may not coincide with the point of best efficiency, the effect of the angle of attack upon the maximum capacity at several speeds may not be apparent if the cut-off capacity is not sufficiently removed from the best efficiency point.

## 12.7 THOMA'S CAVITATION CONSTANT

The experimental relationship between the impeller eye velocity at cut-off capacity and the suction pressure gives a satisfactory means for predicting cavitation for low specific speed pumps.

For higher specific speed pumps this connection becomes inaccurate and, moreover, with high specific speed pumps, the drop in efficiency may appear much sooner than the pump capacity cut-off. There is no simple way to predict the beginning of cavitation in high specific speed pumps.

Thoma<sup>17,23</sup> has suggested that the dynamic depression, including the velocity head at the impeller eye, can be expressed as a fraction of the total head, or

$$\frac{c_1^2}{2g} + \lambda \frac{w_1^2}{2g} = \Delta h = \sigma H \quad (12.6)$$

The coefficient  $\sigma$  is determined experimentally. If, for the dynamic depression, its value in terms of  $\sigma$  and  $H$  are substituted, equation 12.1 takes the form

$$H_a + h_s - h_v = \sigma H \quad (12.7)$$

or

$$\sigma = \frac{H_a + h_s - h_v}{H} \quad (12.8)$$

The use of the cavitation coefficient  $\sigma$  became quite general among water turbine designers and is coming into wide use among centrifugal pump builders.

The use of the cavitation constant  $\sigma$  is subject to a number of considerations:

(a) For the same pump at different speeds or similar pumps operated at the corresponding points (the same specific speed), all velocities vary as  $\sqrt{H}$ , and hence

$$\sigma = \frac{\Delta h}{H} = \text{constant} \quad (12.9)$$

This presupposes that  $\lambda$  in equation 12.6 remains constant. This relationship is the basis of all model testing for cavitation. If  $\sigma$  is determined by test for a certain design, equation 12.8 or equation 12.9 can be used to determine the required suction head for a given pump total head.

(b) *Equation 12.9 holds only at conditions approaching cavitation while the affinity laws still hold. When cavitation sets in, the laws of similarity*

are not fulfilled and the relationship,  $\sigma = \text{constant}$ , expressing similarity of conditions regarding cavitation, becomes approximate only.

(c) Tenot<sup>10</sup> gives the following relationship for the similarity regarding cavitation when it has progressed beyond the incipient stage.

$$\frac{\sigma_1 - \sigma_c}{\sigma_2 - \sigma_c} = \frac{H_2}{H_1} \quad (12.10)$$

where  $\sigma_c$  is the critical sigma coefficient which is constant for both model and prototype,  $\sigma_c = \sigma_{c1} = \sigma_{c2}$ .

$$\begin{aligned} \sigma_1 &= \frac{\Delta h_1}{H_1} && \text{is sigma for the model} \\ \sigma_2 &= \frac{\Delta h_2}{H_2} && \text{is sigma for the prototype} \end{aligned}$$

$H_1$  and  $H_2$  are the operating heads of the model and prototype respectively.

Tenot has demonstrated the validity of this relationship by high speed (1/1,000,000 sec.) photography of a small propeller pump, operated at several speeds with different suction heads.

Equation 12.10 can be transformed as follows. Multiply both sides by  $H_2 H_1$ :

$$\begin{aligned} \frac{\sigma_1 - \sigma_{c1}}{H_2} &= \frac{\sigma_2 - \sigma_{c2}}{H_1} \\ (\sigma_1 - \sigma_{c1})H_1 &= (\sigma_2 - \sigma_{c2})H_2 \\ \Delta h_1 - \Delta h_{c1} &= \Delta h_2 - \Delta h_{c2} \end{aligned} \quad (12.11)$$

Equation 12.11 shows that, for cavitation similarity in two pumps, the absolute pressure at the points of minimum pressure in the impellers are equally removed from the critical pressures (vapor pressure) existing at the incipient cavitation conditions. This means that if two pumps operate at different heads ( $H_1 \neq H_2$ ) but if the suction pressures are such that  $\sigma_1 = \sigma_2$ , the pump with the higher head will have cavitation developed to a smaller degree than that prevailing in the low head pump.

If both model and prototype are tested at the same head, ( $H_1 = H_2$ ),

$$\frac{\sigma_1 - \sigma_c}{\sigma_2 - \sigma_c} = 1 \quad \text{and} \quad \sigma_1 = \sigma_2 \quad (12.12)$$

and consequently, if equation 12.10 holds and  $H_1 \neq H_2$ ,  $\sigma_1 \neq \sigma_2$ .

(d) It has been pointed out already that it is very difficult to detect incipient cavitation, and any  $\sigma_c$  determined as a sigma for the critical cavitation conditions really may represent the state of cavitation progressed sufficiently to be measured by the available testing equipment. Therefore the relationships discussed under (c) are of particular importance.

Again, with wider use of high specific speed water turbines and pumps, it frequently becomes uneconomical to provide sufficient submergence to suppress cavitation completely under all operating conditions; therefore, unless the heads are reproduced in the model testing the conditions,  $\sigma_1 = \sigma_2$  will only approximately represent the cavitation similarity. In water turbine practice, when it is impossible to provide a proper submergence due to the high cost of excavation, the runner vanes are protected with stainless steel in the places subject to cavitation pitting.<sup>20</sup>

(e) *To make the discussion of cavitation more definite, the criterion of incipient cavitation should be stated—whether it is the breaking off of the head-capacity curve, or the drop in efficiency, or noise and vibration, or the pitting of the impeller vane. The drop in efficiency is more general because it applies to pumps irrespective of the specific speed and may be found while other signs of cavitation are not yet apparent.* Depending on the testing facilities and requirements, a drop of 1 per cent or even just a fraction of a point in the efficiency may be taken to indicate that cavitation has already set in.

During cavitation tests,  $\sigma$  variation is obtained either by changing the suction pressure (mostly by throttling), or by changing the pump speed and hence the head at the same static suction pressure.

Although the first method is simpler to arrange, better results are obtained with the variable head tests. For laboratory testing a special testing equipment has been used to a limited extent. With this method the pump suction is taken from a vessel which can be kept under different pressures. With a variable speed drive this procedure is ideal for accurate  $\sigma$  determination.<sup>18</sup>

Although the same  $\sigma$  value may be obtained either with low head and low suction pressure (high suction lift), or with high head and correspondingly higher suction head (large pump or higher speed), the physical aspect of the phenomenon as far as cavitation is concerned is not exactly the same. In the first case the whole suction pipe is under suction lift and, with low velocities, ample time may be available for air or gases to liberate and accumulate in quantities sufficient to impair the pump's efficiency and reduce the head-capacity before actual formation of vapor bubbles starts. In the second case the pressure drop is mostly dynamic and is limited to a small part of the impeller passages.

In addition, with high velocities through the impeller the time required for the water particles to cross the low pressure zone is shorter and, since in all thermodynamic changes time is an essential factor, the relative volume of vaporization and its effect on the pump performance is smaller for high head pumps.<sup>14</sup>

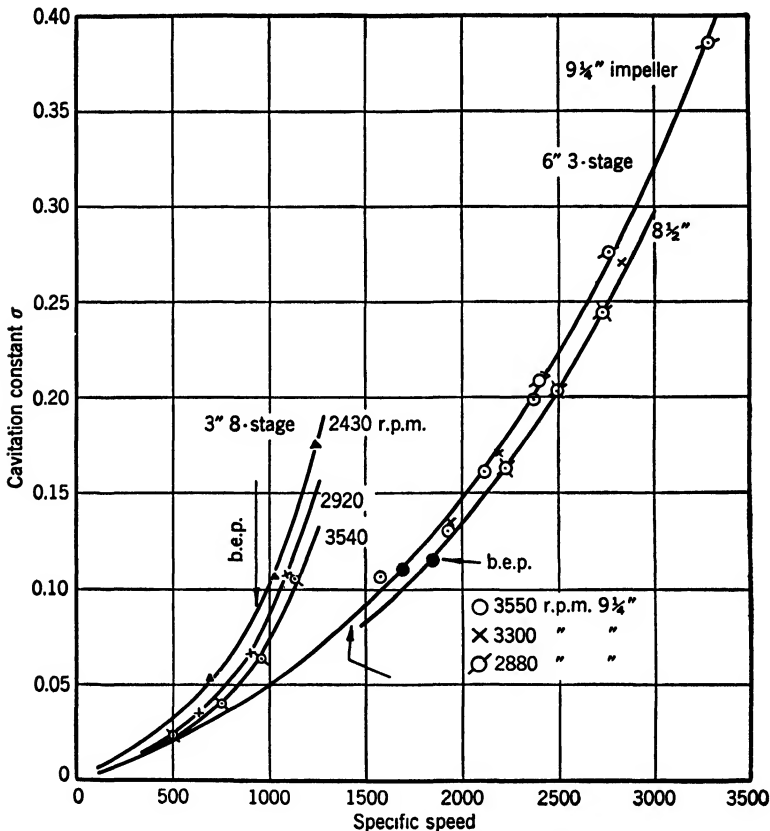


FIG. 12.18. Cavitation constant  $\sigma$  versus specific speed for a constant speed head-capacity curve.

Even for two similar pumps of different sizes operating at the same head and the same  $\sigma$  value (which in this case means the same suction pressure), the extent of cavitation is not in proportion to the pump size, and the bad effects of cavitation will be less pronounced in the large unit.<sup>21</sup>

Although the velocities at similar points in the impellers are the same in both pumps under such conditions, the effect of the curvature of the impeller profile or suction approach upon the velocity distribution (the maximum local velocity) is not the same in the small model and the



large prototype because the Reynolds numbers are different. The centrifugal forces which are instrumental in the distortion of the velocity distribution along the curved path are inversely proportional to the radius of curvature; therefore, negotiating the curves through the impeller eye and suction approach in a large pump results in lower maximum local velocities, as compared with the average, than in a small model.

(f) There are several ways to represent graphically the results of cavitation tests. In one of them  $\sigma$  is determined for several points on the head-capacity curve and plotted versus specific speed of the same points. Figure 12.18 shows curves for two pumps plotted on this basis. These curves give complete cavitation characteristics of the pump irrespective of size and speed.

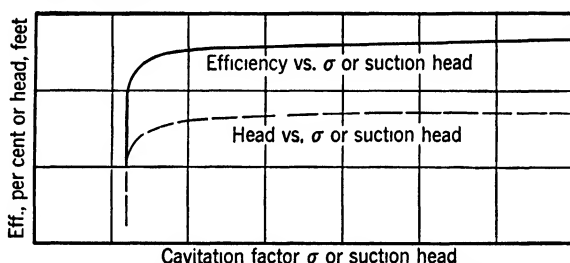


FIG. 12.19. Cavitation characteristics at constant speed and capacity.

In another method, efficiency or head is plotted against  $\sigma$  or suction head, at a constant speed and capacity, the drop in efficiency and head curves indicating the beginning of cavitation (Fig. 12.19). These curves give cavitation information for one point on the head-capacity curve, and this method is used mostly for model testing when head-capacity conditions are fixed and safe suction head is determined from model testing.

The general trend of  $\sigma$  variation for the best efficiency points of pumps of different specific speeds is shown in Fig. 12.20 and is discussed further under (g) below.

When the plant's pumping capacity, head, and suction head are given, the plant's  $\sigma$  is fixed. By selecting the proper pump speed, pumps of different specific speed may be used to meet the plant's requirements with a desired degree of protection from cavitation. Frequently, the speed is also fixed by the specifications. In that case the specific speed of the plant is fixed. Only a slight variation in pump design is possible in such a case by placing the operating point to the right or left of the best efficiency point. The pump's rated normal specific speed at the best efficiency point will be different from the plant's specific speed, but

special designs may be resorted to to obtain the desired degree of protection against cavitation. With pumps of high specific speed, where the dynamic depression  $\lambda(w_1^2/2g)$  plays an important part in setting up cavitation conditions, the number of impeller vanes is a very effective

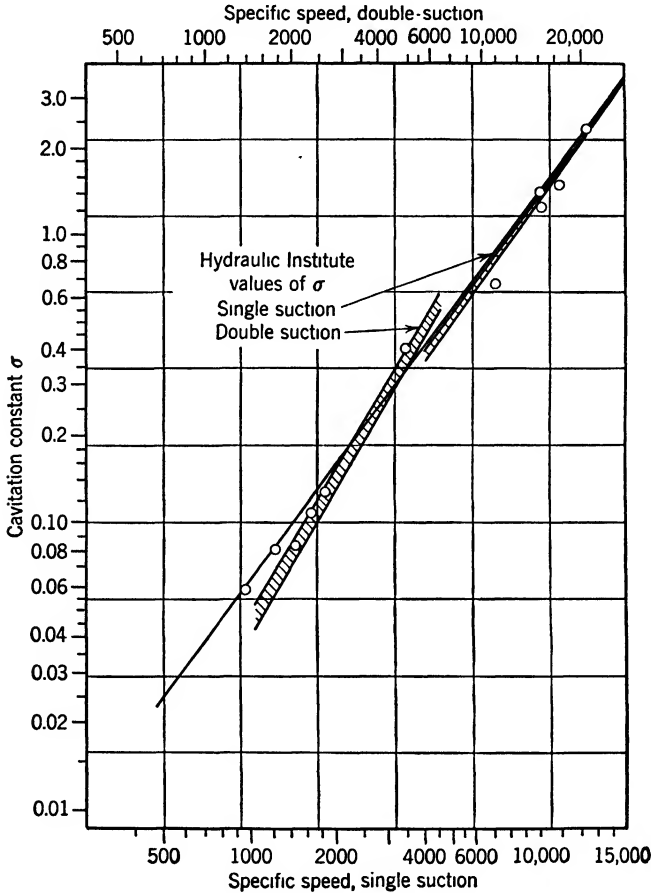


FIG. 12.20. Cavitation constant  $\sigma$  versus specific speed for best efficiency points.

means of reducing the critical  $\sigma$  value without changing the specific speed materially (Fig. 12.15).

(g) From theoretical consideration, it is possible to establish a relationship between the  $\sigma$  factors and specific speed for best efficiency points.<sup>14, 25</sup>

$$\frac{\sigma_2}{\sigma_1} = \left( \frac{n_{s2}}{n_{s1}} \right)^{5/4} \quad (12.13)$$

The general trend of  $\sigma$  variation as a function of specific speed as found by actually plotting experimental results agrees very well with formula 12.13, as evidenced, for instance, by the curve published by Wislicenus, Watson, and Karassik,<sup>26</sup> which follows exactly equation 12.13. For a series of pumps of consistent design, a continuous curve of  $\sigma$  values versus specific speed should be obtained, as all design factors governing cavitation (eye area, number of vanes, and so on) are continuous functions of specific speed. The  $\sigma$  curve on Fig. 12.20 can be expressed by the following equations.

$$\sigma = \frac{6.3n_s^{4/3}}{10^6} \quad \text{for single-suction pumps} \quad (12.14)$$

$$\sigma = \frac{4.0n_s^{4/3}}{10^6} \quad \text{for double-suction pumps} \quad (12.15)$$

Figure 12.20 also shows  $\sigma$  values obtained from the Hydraulic Institute charts of the upper limits of specific speeds for double-suction and single-suction pumps. This chart gives a belt of  $\sigma$  values for several specific speeds rather than a single curve, higher values of sigma applying to lower head pumps. Such arrangement resulted from the superimposition of performances of pumps of different makes.

(h) Attempts have been made to introduce another cavitation criterion in addition to the generally accepted  $\sigma$ . It is called suction specific speed,<sup>26, 27</sup> and is defined as

$$S = \frac{\text{r.p.m.} \sqrt{\text{g.p.m.}}}{\Delta h^{3/4}} \quad (12.16)$$

The development of this equation is based on the use of similarity relations (affinity laws) at conditions approaching cavitation, and it does not establish any new relationship between the variables entering into this expression which cannot be determined from the affinity laws or  $\sigma$  consideration. There is a fixed connection between the factor  $S$ ,  $\sigma$ , and specific speed.

$$\frac{n_s}{S} = \sigma^{3/4} \quad (12.17)$$

Substituting the values of  $\sigma$  from equations 12.14 and 12.15 into equation 12.17 shows that

$$S = 7900 = \text{constant} \quad \text{for single-stage pumps} \quad (12.18)$$

$$S = 11,200 = \text{constant} \quad \text{for double-suction pumps} \quad (12.19)$$

(i) *When using a model for testing performance and cavitation conditions, the similarity of the model and the prototype should be extended to the suction approach to the impeller and the discharge piping.*

### 12.8 MEANS OF AVOIDING OR REDUCING CAVITATION

(a) *A knowledge of the cavitation characteristics of pumps is the most important prerequisite of any cavitation problem study.*

(b) *Second in importance is the knowledge of existing suction conditions of the plant at the time the pump selection is made.*

(c) An increase of suction pipe size, reduction of suction pipe length, elimination of turns, provision of a good suction bell—in other words, reduction of losses in the suction pipe—improve the suction conditions of a pump with regard to cavitation.

(d) An increase in the number of vanes in high specific speed pumps, or the removal of parts of the vanes and opening the passages in the impeller eye of low specific speed pumps will reduce the minimum suction head to meet fixed head-capacity conditions.

(e) An ample suction approach area without excessive prerotation and a better streamlining of impeller approach are essential to obtain optimum cavitation characteristics of a pump.

(f) Special materials may be used to reduce the pitting of pump parts due to cavitation, when justified, or when it is impossible to eliminate cavitation by any other means.

(g) The noise and vibration caused by cavitation can be reduced or eliminated by the admission of a small amount of air to the pump suction.

(h) The impeller velocities, impeller vane load, and head per stage should be low for minimum suction head. All these factors lead to a bigger pump operated at a low speed, and possibly to location of the operating point to the left of the best efficiency point.

### REFERENCES

1. I. A. WINTER, "Hydraulic Turbine Development," *Proc. A.S.C.E.*, Vol. 65, 1939, pp. 1553–1589; abstracted in *Mech. Eng.*, Vol. 62, 1940, p. 27.
2. R. L. MAHON, "Hydraulic Butterfly Valves," *Trans. A.S.M.E.*, Vol. 54; *Hydraulics*, 54–2, 1932.
3. W. SIEBRECHT, "Untersuchungen über Regelung von Kreiselpumpen," *Z. Ver. deut. Ing.*, Vol. 74, 1930, p. 87.
4. B. R. VAN LEER, "Throttling Suction Changes Pump Characteristic," *Power Plant Eng.*, Vol. 31, 1927, p. 1133.
5. H. FOETTINGER, "Untersuchungen über Kavitation und Korrosion," *Hydraulische Probleme*, Berlin, Verein deutscher Ingenieure, 1926, p. 14.
6. J. C. HUNSAKER, "Cavitation Research," *Mech. Eng.*, Vol. 57, 1935, p. 211.
7. T. C. POULTER, "The Mechanism of Cavitation Erosion," *Trans. A.S.M.E.*, Vol. 9, 1942, pp. A-31–A-37.
8. P. DE HALLER, "Investigation of Corrosion Phenomena in Water Turbines," *Escher-Wyss News*, May–June 1933, p. 77.

9. A. J. STEPANOFF, "Leakage Loss and Axial Thrust in Centrifugal Pumps," *Trans. A.S.M.E.*, Vol. 54, *Hydraulics*, 54-5, 1932.
10. H. SCHROETER, "Versuche zur Frage der Werkstoffanfraßung durch Kavitation," Munich, R. Oldenbourg, 1935.
11. E. B. SHARP, "Cavitation of Hydraulic Turbine Runners," *Trans. A.S.M.E.*, Vol. 62, 1940, p. 569.
12. HANS MUELLER, "Spalt Kavitation an Schnellaufenden Turbomachinen," *Z. Ver. deut. Ing.*, Vol. 79, 1935, p. 1165.
13. FRITZ KRISAM, "Versuche und Rechnungen zum Kavitations Problem der Kreiselpumpen," Mitt. Inst. Stromungsmaschinen Tech. Hochschule, Karlsruhe, Feb. 1930.
14. H. CARDINAL VON WIDDERN, "On Cavitation in Centrifugal Pumps," *Escher-Wyss News*, Jan.-March, 1936, p. 15.
15. A. J. STEPANOFF, "Propeller Pumps for Circulation of Molten Salt," *Refiner and Natural Gasoline Manufacturer*, Vol. 19, 1940, pp. 474-476.
16. RAYMOND DEFELD, "A Practical Treatise on Single and Double Suction Pumps," London, Chapman and Hall, 1930, p. 35.
17. D. THOMA, "Bericht zur Weltkraftkonferenz, London, 1924," *Z. Ver. deut. Ing.*, Vol. 79, 1935, p. 329.
18. G. F. WISLICENUS, "Test Stand for Centrifugal and Propeller Pumps," *Trans. A.S.M.E.*, Vol. 64, No. 6, 1942, p. 619.
19. M. A. TENOT, "Phénomènes de la Cavitation," Mém. Soc. Ing. Civ., May and June, Paris, *Bull.* 1934, pp. 377-480.
20. R. E. B. SHARP, "Cavitation of Hydraulic Turbine Runners," *Trans. A.S.M.E.*, Vol. 62, 1940, p. 569.
21. F. H. ROGERS, *Trans. A.S.M.E.*, Vol. 58, 1936, p. 317.
22. C. PFLEIDERER, *Die Kreiselpumpen*, Berlin, Julius Springer, 1932, p. 241.
23. D. THOMA, "Verhalten einer Kreiselpumpe beim Betrieb im Hohlzug Bereich," *Z. Ver. deut. Ing.*, Vol. 81, 1937, p. 972.
24. "Eighth Report to the Corrosion Research Committee," *Jour. Inst. Metals*, Vol. XL, No. 2, 1928.
25. A. J. STEPANOFF, *Trans. A.S.M.E.*, Vol. 62, 1940, pp. 158, 164.
26. G. F. WISLICENUS, R. M. WATSON, and I. J. KARASSIK, "Cavitation Characteristics of Centrifugal Pumps," *Trans. A.S.M.E.*, Vol. 61, 1939, p. 17.
27. PAUL BERGERON, *Trans. A.S.M.E.*, Vol. 62, 1940, p. 162.
28. SAICHIRO UCHIMARU, "Experimental Research on the Distribution of Water Pressure in a Centrifugal Pump Impeller," *Jour. Faculty Eng., Tokyo Imp. Univ.*, Vol. 16, 1925.
29. R. V. TERRY, "Development of the Automatic Adjustable Blade-Type Propeller Turbine," *Trans. A.S.M.E.*, Vol. 63, 1941, pp. 394-409.
30. BATTELLE MEMORIAL INSTITUTE, *Prevention of the Failure of Metals under Repeated Stress*, New York, John Wiley & Sons, 1941, p. 164.
31. S. L. KERR, "Determination of the Relative Resistance to Cavitation Erosion by the Vibratory Method," *Trans. A.S.M.E.*, Vol. 59, 1937, p. 373.
32. J. M. MOUSSON, "Pitting Resistance of Metals under Cavitation Conditions," *Trans. A.S.M.E.*, Vol. 59, 1937, p. 399.
33. C. D. BOWER and P. H. BROWN, "Prediction of Suction Limitations when Pumping Volatile Liquids," *Calif. Oil World and Petr. Industry*, April 1943, p. 15.

## CHAPTER 13

### SPECIAL OPERATING CONDITIONS OF CENTRIFUGAL PUMPS

#### 13.1 INTRODUCTION

This chapter deals with operating conditions of centrifugal pumps beyond their normal head-capacity and speed range. If head-capacity and speed are assumed as positive for normal pump operation, the head-capacity characteristics are confined to one quadrant on the head-capacity coordinates. All the unusual head-capacity characteristics occupy the remaining three quadrants for a positive rotation, and all four quadrants for a negative rotation. Some of the special operating conditions are unavoidable; others occur accidentally; and still others can be reproduced only in the laboratory or they develop during a transient period while changing from one state to another. Operation of a centrifugal pump as a hydraulic turbine, behavior of a pump in the event of power failure, or starting a pump running in reverse are examples of unusual operating conditions.

In Fig. 13.1 (*a*), quadrant *A* shows normal head-capacity curves at several speeds. These are expressed as percentage of the normal head-capacity (at best efficiency point) for a certain speed selected as normal. It is possible to extend the head-capacity curves beyond zero head and zero capacity lines. In the first case—Fig. 13.1 (*a*), quadrants *G* and *H*—water has to be forced through the pump, or the head is higher at the suction nozzle than at the discharge. Such a head is defined as negative. In the second case—Fig. 13.1 (*a*), quadrant *B*—a head higher than the pump shut-off head is applied to the discharge nozzle and the flow through the pump is reversed, thus the flow becomes negative.

Figure 13.1 (*c*) shows similar head-capacity curves with the pump speed reversed, or negative. Figure 13.1 (*b*) shows the torque curves for all possible conditions appearing on Figs. 13.1 (*a*) and 13.1 (*c*). Obtained experimentally, such curves represent complete pump characteristics. A considerable interest has been aroused in the study of such complete pump characteristics by several articles published in Germany by Thoma,<sup>1</sup> Engel,<sup>2</sup> and Kittredge.<sup>3</sup> In the United States, several investigations conducted at the California Institute of Technology have been reported by Knapp.<sup>4</sup>

Prediction of pump behavior from theoretical considerations alone is impossible. Therefore, for solutions of such problems one has to rely on experimental results or complete pump characteristics covering all possible cases or combinations of head, capacity, torque, and speed.

### 13.2 COMPLETE PUMP CHARACTERISTICS; REPRESENTATION OF TEST RESULTS

This discussion is based on test results appearing in the publications listed as references and is supplemented with some test data by the author. To make the data applicable to all similar pumps, irrespective of pump size and speed, the head, capacity, torque, and speed are expressed in percentages of those values at the best efficiency point, a certain speed being selected as normal.

To show all test values of the four variables involved, that is, head  $H$ , capacity  $Q$ , torque  $T$ , and speed  $n$ , on one chart, two of these can be taken as independent coordinates and the remaining two as parameters. Evidently, six combinations of pairs of independent variables are possible. By actual trial it has been found that speed versus capacity gives the best chart; Fig. 13.2 shows one such chart, based on data by Knapp. This chart will be used in the solution of several typical problems dealing with some unusual pump operating conditions.

### 13.3 MECHANICAL PROBLEMS CONNECTED WITH PUMP OPERATION OUTSIDE THE NORMAL HEAD-CAPACITY AND ROTATION RANGE

**(a) Mechanical Damage.** Opinions have been expressed <sup>1, 2, 3</sup> that, should power suddenly fail on a pump and reverse flow develop (no check valve in the discharge line), dangerous pressure surges may develop or the pump may reach a dangerous runaway speed in the reverse direction. These dangers are not founded when pumping cold water or any liquid far removed from the boiling point. *Although pressure surges do result from a sudden reversal of the flow and the motor may reach a speed exceeding the normal motor speed, the magnitude of both is such that no dangerous stresses develop in any standard part normally used for pumps or motors.*

It should be noted that at the time the studies of the complete pump characteristics were launched (about 1930), thousands of vertical pumps of the deep-well type had already been installed and were subjected to reverse rotation under maximum heads approaching the pump total head every time they were stopped. The maximum reverse speeds recorded were in excess of 120 per cent of the normal pump speed. No





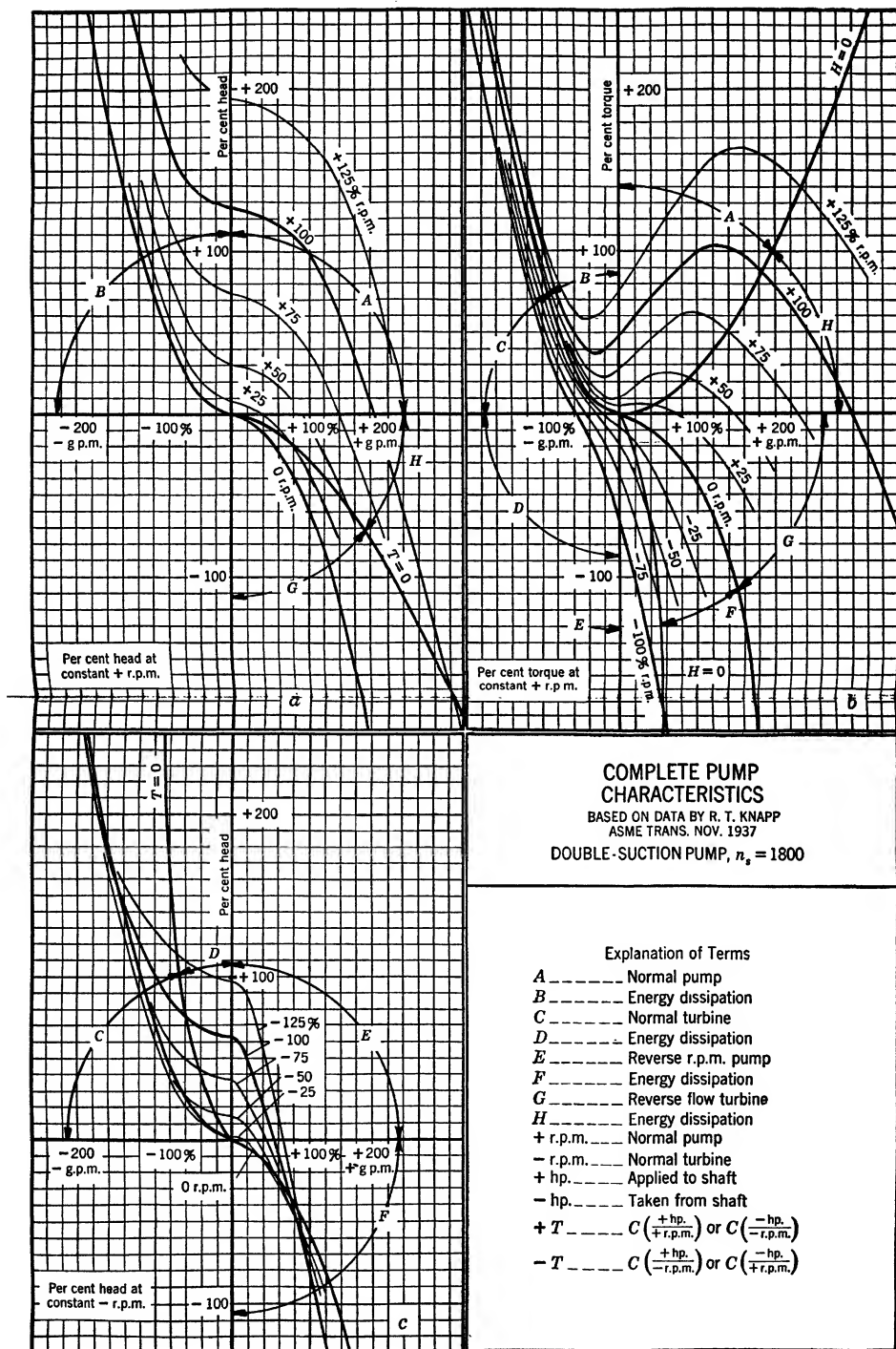


FIG. 13.1. Complete pump characteristics, double-suction pump;  $n_s = 1800$ .

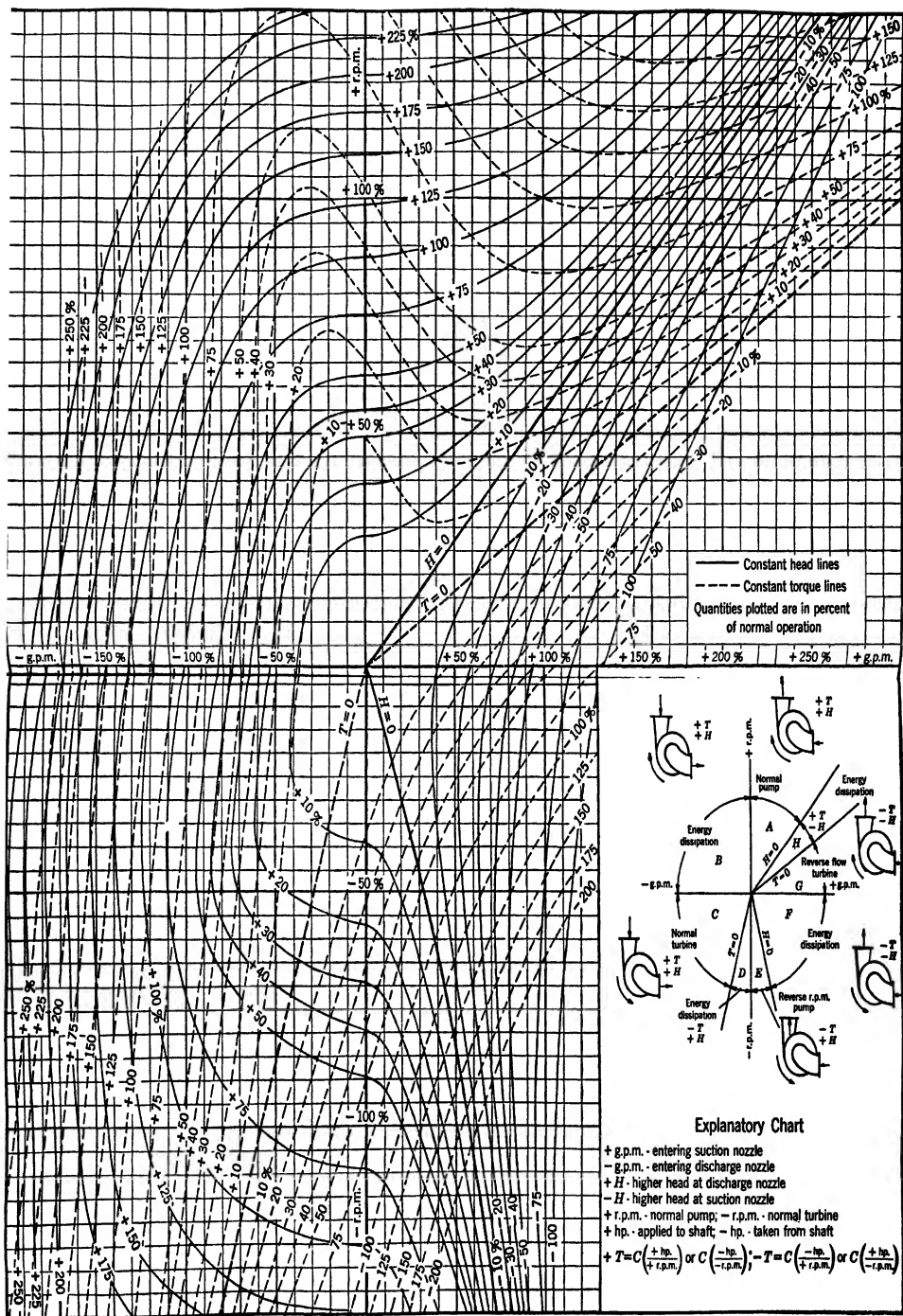


FIG. 13.2. Complete pump characteristics, double-suction pump;  $n_s = 1800$ .



dangerous speeds, pressure rise, or stresses in the pump shafts were observed.

*When liquids approaching their boiling points, such as light hydrocarbons or boiler feed water, are being pumped, if the check valve fails (mechanical obstruction) in a sudden power failure, the liquid flowing from the discharge pipe will flash into vapor because of the sudden drop in*

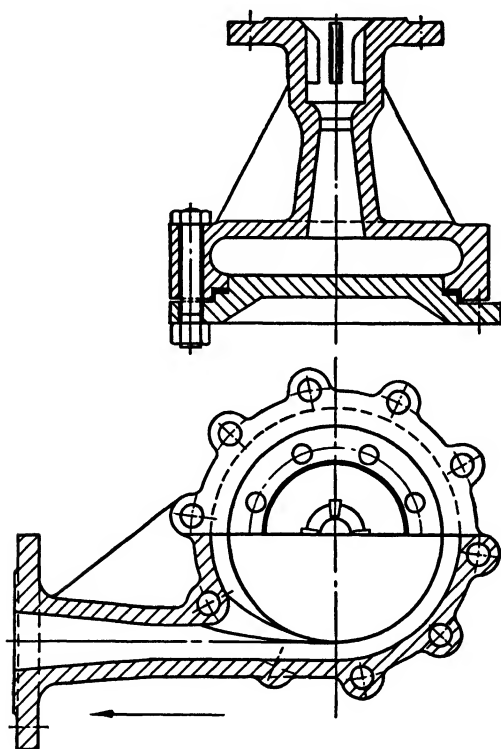


FIG. 13.3. "Non-reversing elbow." Resistance to the flow in reverse direction is 100 times that for the normal flow (Zobel).

*pressure through the check valve. The reverse gas flow under the full discharge pressure in pounds per square inch will correspond to that under a head several hundred times the pump operating head expressed in feet of flowing gas. Under such conditions the pump reverse speed may exceed the normal speed a great many times, if not prevented by mechanical damage to the pump or driver. If only a small fraction of the total back-flow flashes into vapor it may be sufficient to ruin the pump or driver. Two cases of motor damage under such conditions have been called to the author's attention recently (1944).*

It is possible to keep the flow below the safe limit by installing in the discharge line a device which presents little resistance in the normal direction and greatly increased resistance in the reverse direction. Zobel <sup>5</sup> has tested an apparatus which in effect is a "non-reversing elbow" shown in Fig. 13.3. It resembles the volute casing of an ordinary single-stage pump. Normally the flow enters through the suction nozzle and leaves through the discharge nozzle, with a loss of a few feet of head. But when the flow is reversed the coefficient of resistance increases about one hundred times. If the liquid is flashed into vapor all velocities will increase as the square root of the head in feet, and resistance will increase as the square of velocities, or directly as the head, thus limiting the flow to a safe rate.

**(b) Reverse Speed.** Deep-well pumps have presented a number of problems connected with reverse rotation from the very early stages of their introduction; through the use of complete pump characteristics charts, solution of several problems has been simplified. Figure 16.27 shows a typical deep-well pump. In a great majority of cases the deep-well pumps used for irrigation lift water to the surface, and thus work against all static head. Every time the power is shut off the pump is subjected to a full pump head and works as a turbine in a reverse direction at runaway speed or zero torque.

The experience of many years shows that no dangerous speed develops under these conditions and no mechanical damage results. By following the 100 per cent head line of Fig. 13.2 from the first quadrant through the second and to the intersection with the zero torque line in the third quadrant, it is found that this particular pump will develop 117 per cent reverse speed and 68 per cent capacity.

If part of the pump total head is friction then the head on the pump when operating as a turbine at the runaway speed will be static head less friction head. If the speed and capacity are known at one head the speed and capacity at any other head can be found by applying the affinity laws, that is, the speed and capacity vary directly as the square root of the head.

**(c) Shaft Couplings.** The screwed type of couplings is universally adopted for the column shaft deep-well pumps in this country. The hand of the threads is such that in normal pump operation the torque exerted by the motor tightens the threads in the shaft couplings (Fig. 16.27). When the flow and speed are reversed, the pump becomes a driver and, although the direction of rotation is changed, the torque developed by the pump tends again to tighten the threads of the shaft couplings. For that reason no special means are employed to lock the threaded couplings on the shafts on vertical pumps. When power is

applied to the shaft coupling, threads are tightened until the applied torque is equal the friction torque in the threads. The latter increases as the compression of the two shaft ends increases. To unscrew the coupling an equal torque is required. With large shafts this may present some difficulty.

**(d) Motor-Disengaging Clutch.** If the motor of a deep-well pump is not wired to the power lines correctly and the pump is started in the wrong direction, the column shaft will unscrew in one of the couplings. Motor-disengaging clutches are used to prevent damage to the pump shaft or motor in such a case. Figure 13.4 shows a disengaging clutch.

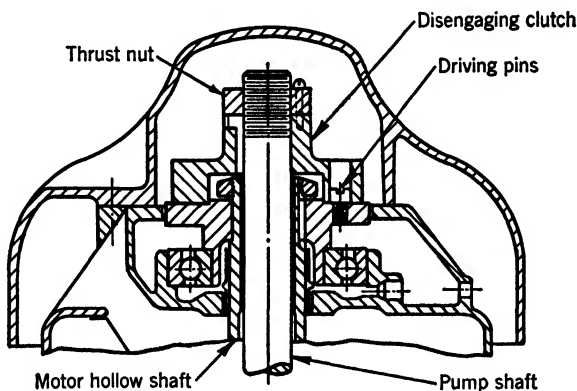


FIG. 13.4. Disengaging clutch (General Electric).

The pump column shaft is keyed to the upper half of the clutch. The nut carries the axial thrust of the pump and the weight of the rotating element. The upper half of the clutch engages the lower half by means of screwed pins, and the lower half of the clutch is rigidly connected to the motor hollow shaft. If the motor starts in the wrong direction the column shaft will unscrew in one of the couplings. The lower part of the shaft will drop until the pump impellers will rest on the casing. The upper sections of the shaft will continue to unscrew and rise until the upper half of the clutch is disengaged from the lower half and the motor hollow shaft. Disengaging of the clutch prevents complete unscrewing of the shaft in the coupling. However, the clutch will not engage automatically upon reversal of the motor and it is necessary to take the clutch apart and screw the shaft back before the motor can be started in the right direction.

Without the clutch the shaft would unscrew entirely and damage the threaded shaft ends, and would require the removal of the pump until the loose joint is discovered.

The disengaging clutch is now a standard part of all hollow shaft motors. Evidently, to avoid trouble, the motor rotation should be checked before it is connected to the pump. The possibility of reversal of rotation due to power phase crossing on the power lines is very remote and can be disregarded.

**(e) Wrong Rotation of Horizontal Pumps.** Use of locking devices (such as lock nuts and set screws) on deep-well shafts proved to be im-

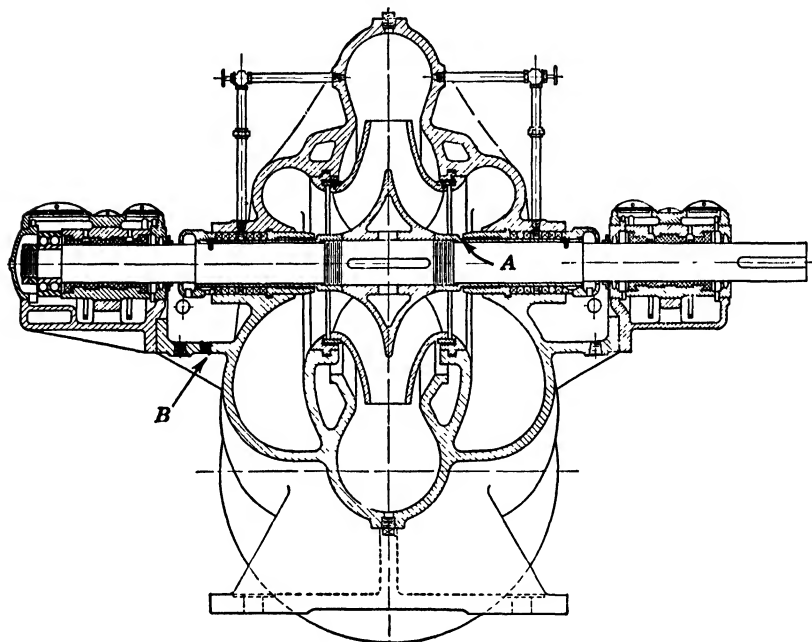


FIG. 13.5. Broken bearing bracket resulted from wrong rotation.

practical. They increase the cost of parts and delay in assembly of deep-well pumps, without providing foolproof protection. However, on horizontal pumps, locking devices for parts mounted on the shaft are considered a necessity. Although checking of the motor rotation before it is coupled to the pump is prescribed by all pump manufacturers, all pumps are built so that no damage occurs if a pump is started in the wrong direction. What happens if these precautionary measures are neglected will be seen from the following illustration.

A 16-in. double-suction pump of conventional design, shown in Fig. 13.5, was installed at an industrial plant. Before starting the pump it was decided to test the whole piping system hydrostatically, including the pump. During this process leakage was observed from the stuffing

box and from under the shaft sleeves. Accordingly, the set screws were removed from the shaft sleeves, and the sleeves and the stuffing box glands were tightened. After the completion of the hydrostatic test, the pump was started and after a few seconds the bracket supporting the outboard bearing was broken off. The motor rotation happened to be wrong and, since the stuffing boxes had been tightened, one of the sleeves started to unscrew until the shoulder on the inboard sleeve butted against the stuffing box bushing at *A*. Then the rotating element started to move outward, breaking off the thrust bearing support at *B*.

**(f) Motor Rotation.** There is no way to determine the rotation of a three-phase induction motor except by trial and observation of the exposed shaft end of the motor. The motor rotation should be ascertained before the motor is connected to the pump. However, in special designs the motor may be enclosed into a common cell with the pump so that no moving part of the pump or motor can be observed (submersible motor pumps). In that case all parts mounted on the pump shaft should be securely locked. The correct rotation of such units can be found by observing the pump head developed by the pump with discharge valve closed. By referring to Figs. 13.1 (*a*) and 13.1 (*c*) it will be noticed that at the same speed (say 100 per cent) the pump shut-off head under correct rotation is in excess of the pump rated head (125 per cent), whereas at reversed speed the shut-off head is only about 60 per cent of the pump rated head. In every case when the motor rotation is checked with the pump coupled to the driver the pump should be filled with liquid before the motor trial to avoid seizure in closely fitted parts.

**(g) Non-Reversing Ratchets.** A great number of deep-well pumps are driven by tractor engines through a power take-off and a quarter-turn belt. It has been found that the driving belt has a tendency to slip off the pulleys when the pump rotation is reversed after stopping. All deep-well belt-drive heads are equipped now with non-reversing ratchets. These permit the pump pulley to be driven in only one direction. Figure 13.6 shows a belt-drive deep-well head. In this the upper half of the clutch carries several loose vertical pins. These are pushed up and held in their position by centrifugal force when the pump starts rotating in the right direction. When the power is cut off and the pump pulley slows down to almost zero speed the pins drop down and engage the teeth of the stationary ratchet. Evidently, the ratchet will prevent the pump rotation if the belt quarter-turn is made in the wrong direction.

**(h) Pressure Surges during Reverse Rotation.** *With the introduction of the open impeller construction into the deep-well pump field it was dis-*



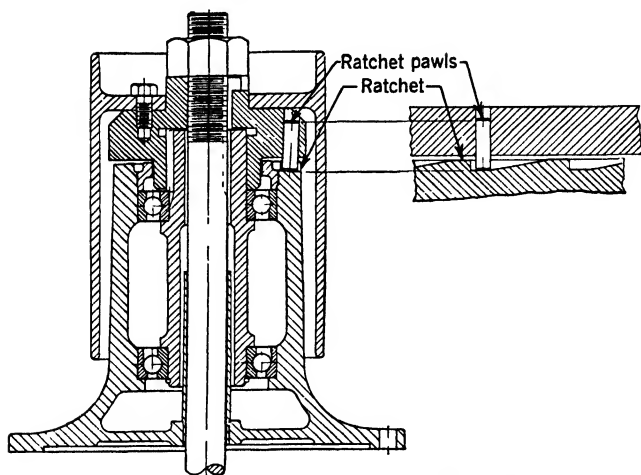


FIG. 13.6. Deep-well belt-drive head with non-reverse ratchet (Peerless Pumps).

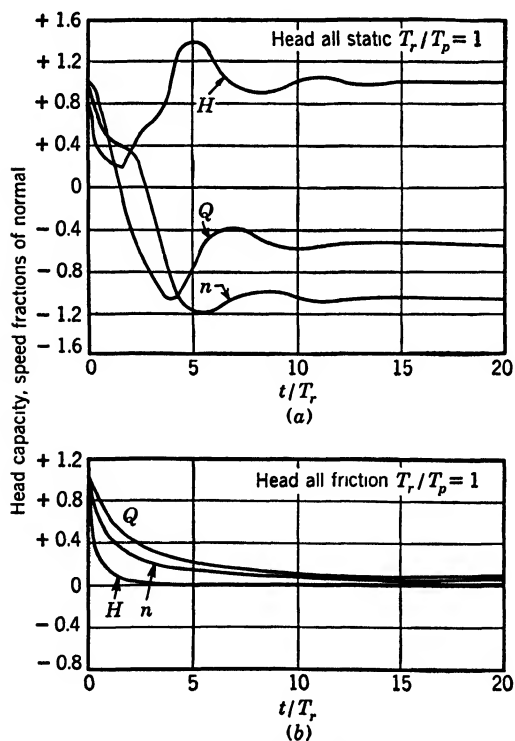


FIG. 13.7. Head, capacity, and speed variation after a sudden power failure under 100 per cent head (Kittredge).  $t$  = time, multiple of  $T_r$ ;  $T_r$  = time to accelerate pipe water column to normal velocity;  $T_p$  = starting time of pump.

*covered that with long settings pressure waves developed in the discharge column when the flow is reversed which caused impeller hammering against their seats. With closed impellers such pressure waves did no harm and passed unnoticed because there was sufficient axial clearance between the rotating element and the stationary pump casing to prevent interference between the two. However, with open impellers, the axial thrust was greater than with the closed impellers, and the running axial clearance was reduced to a minimum to obtain a maximum efficiency. The impeller pounding against the casing while revolving in the reverse direction resulted in the impeller vane grinding to such an extent that it was impossible to maintain normal pump efficiency. It should be borne in mind that the pump shaft extension due to the hydraulic thrust in average deep-well pumps with over 200 ft. setting is of the order of  $\frac{1}{4}$  or  $\frac{1}{2}$  in. Pressure waves cause variation in the shaft extension. This could be observed on the surface by a violent vibration of the pump support.*

Kittredge<sup>3</sup> has made calculations of the pressure, capacity, and speed variation from the moment the power is cut off to the moment of final equilibrium under the 100 per cent total head, differently divided between the static and friction heads. Figures 13.7 (a) and 13.7 (b) show one set of Kittredge's results. Actually the phenomenon is much more complicated than it appears on the figure as the elastic forces of the water column, the discharge pipe and the column shaft come into play. Kittredge's calculations take into consideration only the variation of the head, capacity, and speed during the transient period, and inertia forces of the water column and the pump rotating element. Peabody<sup>6</sup> made similar calculations for one of the pumps of the Colorado River Aqueduct, where the pipe friction could be neglected.

To eliminate the wear of the impeller vanes and reduce the mechanical disturbance during reverse flow of water through the pump, some of the deep-well motors are provided with non-reversing ratchets similar to that shown in Fig. 13.6. These prevent rotation of the shaft in the reverse direction, although they do not eliminate the pressure waves or mechanical vibration during the reverse flow of water through the pump. Figure 13.8 shows a non-reversing ratchet developed by General Electric Company.

In all non-reversing ratchets, the ratchet is engaged when the pump speed is approaching zero, but the torque developed by the pump is not zero, as can be seen from Fig. 13.2. The torque is applied suddenly and, therefore, all parts subject to stress due to this torque, such as keys and pins, should be able to stand the imposed stresses under such conditions.

Several pump manufacturers used check valves in the discharge column to prevent or reduce the bad effects of the pressure surges during reverse flow but with a limited degree of success.

The bad effects of the pressure surges in a deep-well pump with open impellers are pronounced with high head pumps, long discharge columns, and relatively small shafts. However, the advantages of open impel-

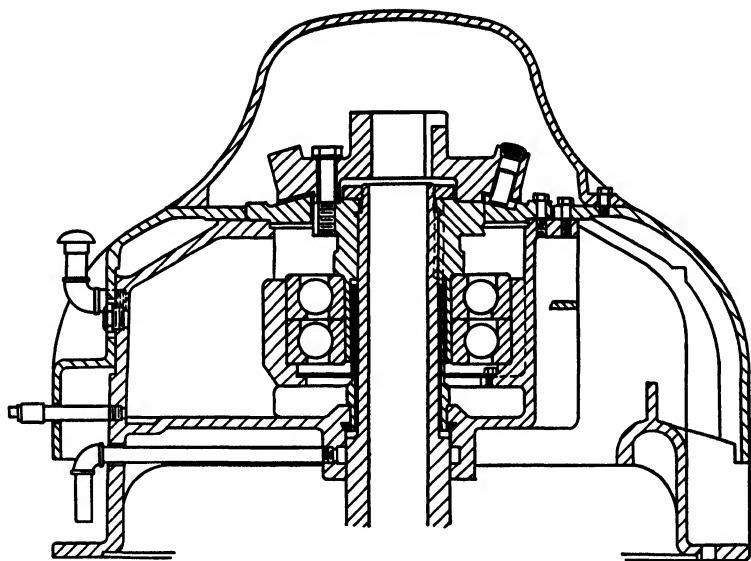


FIG. 13.8. Vertical hollow shaft motor thrust bearing with a non-reversing ratchet (General Electric).

lers (better hydraulic efficiency, possibility of adjusting for wear, freedom from sand locking, and accessibility for cleaning) make this construction more popular than the closed impeller design.

### 13.4 HYDRAULIC PROBLEMS ARISING DURING UNUSUAL PUMP OPERATING CONDITIONS

**(a) Centrifugal Pumps Operating as Turbines.** When the flow in a centrifugal pump is reversed by applying head to the discharge nozzle, the pump becomes a hydraulic turbine. In centrifugal pump practice this may happen unintentionally when the motor is stopped and no means are used to prevent the reverse flow. Since no power is being utilized from the shaft, the pump is operated as a turbine at what is known as runaway speed. The question of speed and capacity under such conditions has been discussed already.

Special tests conducted to operate centrifugal pumps as hydraulic turbines throughout the head-capacity-speed range <sup>3, 4, 7</sup> show that a good centrifugal pump makes an efficient hydraulic turbine. To establish the relationship between the head and capacity (at the best efficiency point) of a unit when operated as a hydraulic turbine at the same speed in terms of the head and capacity when it is operated as a pump is of interest and practical importance. From the theoretical considerations <sup>2</sup> it is possible to state that at the same speed

$$H_t = \frac{H_p}{e_{ht}e_{hp}} = \frac{H_p}{e_h^2} \quad (13.1)$$

$$Q_t = \frac{Q_p}{e_h} \quad (13.2)$$

$$n_{st} = n_{sp}e_h \quad (13.3)$$

where  $H$  is the total head at the best efficiency point

$Q$  is the capacity

$n_s$  is the specific speed

$e_h$  is hydraulic efficiency, taken the same for the turbine and the pump.

Subscripts  $t$  and  $p$  refer to operation as a turbine and a pump respectively. Since the exact value of the hydraulic efficiency is never known  $\sqrt{e}$  can be taken as an approximation, where  $e$  is the gross pump efficiency. These relationships hold approximately in practice.

If torque, head, capacity, and speed values are taken from the turbine section,  $C$  in Fig. 13.2, the calculated turbine efficiency is considerably lower than the pump efficiency, which is not a true turbine efficiency. To obtain the latter the first should be divided by the pump efficiency or

$$\text{True } e_t = \frac{e_t \text{ (from chart)}}{e_p \text{ (true)}} \quad (13.4)$$

This is because all variables for the turbine are expressed in terms of those for the pump. Thus

$$\text{True turbine efficiency } e_t = \frac{T_t n_t}{Q_t H_t} \times \frac{3960}{5250} \quad (13.5)$$

$$\text{True pump efficiency } e_p = \frac{Q_p H_p}{T_p n_p} \times \frac{5250}{3960} \quad (13.6)$$

By multiplying the two and rearranging we get

$$e_t e_p = \frac{\frac{T_t}{T_p} \times \frac{n_t}{n_p}}{\frac{Q_t}{Q_p} \times \frac{H_t}{H_p}} = e_t' = \text{turbine efficiency in terms of pump variables} \quad (13.7)$$

Hence

$$e_t = \frac{e_t'}{e_p} \quad (13.8)$$

The idea of a combined hydraulic machine used as a turbine and pump has attracted considerable attention in connection with pumped storage plants, particularly in Europe.\* However, there are difficulties which make such machines impractical. The first plant of this type was built in Europe in 1933 at Baldeney in Germany. The majority of pumped storage plants have separate units for pump and turbine, the same electric machine being used as generator and motor,<sup>8</sup> and others used two entirely independent generating and pumping sets.

The difficulty in using the same hydraulic machine for both a turbine and a pump lies in the fact that for the same speed (fixed by electric machine design) the pump will deliver only a portion of its rated turbine capacity at a reduced efficiency when pumping against a head equal to the turbine head. This follows from equation 13.1 and shows that at the same speed the pump total head at the best efficiency point is considerably below that of a turbine. This is the reason why the electric machine of the Baldeney plant is of the induction type with two speed windings. It is interesting to mention that on the acceptance test of the Baldeney plant the turbine showed 90 per cent efficiency whereas the pump test efficiency was only 78 per cent.<sup>9</sup> This serves as an illustration of the fact observed on several occasions that, although a good pump always makes a good turbine, a great many good turbines show much lower efficiency when operated as pumps. The reason for this is that in a water turbine the flow toward the impeller and the relative flow through the impeller are accelerated. A high rate of acceleration does not entail any losses but, when the flow

\* There is only one pumped storage plant for the power generation in this country, that of the Connecticut Light and Power Company at Rocky River. This is independent of any other hydroelectric plant and is using the off-peak power generated at one of the company's steam stations. The plant consists of two vertical single-suction pumps, 8100 hp. each, and one water turbine for power generation. (*Engineering*, Jan. 10, 1930, pp. 33-38, and Jan. 24, 1930, pp. 97-100.)

is reversed, the high rate of deceleration is followed by a considerable diffusion loss. In a good pump the rate of deceleration is small, making it equally efficient for flow in both directions.

Multistage pumps operated as turbines behave in the same manner as single-stage pumps. Vertical multistage pumps of the deep-well type show the same efficiency when operated either as turbines or as pumps (unpublished tests by University of California).

Figure 13.2, Section *G*, shows that power is generated by the pump (torque is negative), although the flow direction is opposite to that of a normal turbine; that is, it is outward. The efficiency of such a turbine is very low. A 4-in. pump with pump efficiency over 80 per cent has shown only about 10 per cent efficiency as an outward flow turbine. It might be mentioned here that the pump, when operated in a reverse direction (negative r.p.m., Section *E* of Fig. 13.2), is also very inefficient. The pump referred to above has showed only about 8 per cent with r.p.m. reversed.

**(b) Two Pumps in Parallel; Power of One Cut-Off.** When two pumps operate in parallel and power of one of them fails while the other continues to operate, the flow in the first will be reversed and it will operate as a turbine at runaway speed. The following questions arise under these conditions: (1) What portion of the pump capacity will go into the discharge system and what portion will go back to the suction sump through the idle pump? (2) What will be the reverse speed of the idle pump? (3) What can be accomplished by preventing the reverse rotation of the idle pump?

To show the method of attack in solving this problem, an illustration will be taken of two propeller pumps circulating cooling water through a condenser. The total pump head is used to overcome the friction of the system. Figure 13.9 shows the head-capacity curves of one and two pumps in parallel each delivering 100 per cent of their rated capacities when in parallel. The condenser resistance curve *AB* is also shown. To answer the above three questions the pump characteristics under reversed flow should be known. This is shown in Fig. 13.9 for a free rotor. To determine how the capacity of one pump will be divided between the condenser and the idle pump, a combined (total) resistance of both should be plotted. This is done by adding capacities for the same heads. The intersection of this curve with the head-capacity curve of a single pump (point *C*) will give the pump operating point. From this it is seen that with the rotor free (Fig. 13.9) the active pump will operate at 129 per cent of its normal capacity, delivering 96.5 of its normal capacity per cent to the system; the rest will be wasted through the idle pump. By similar procedure it has been found that,

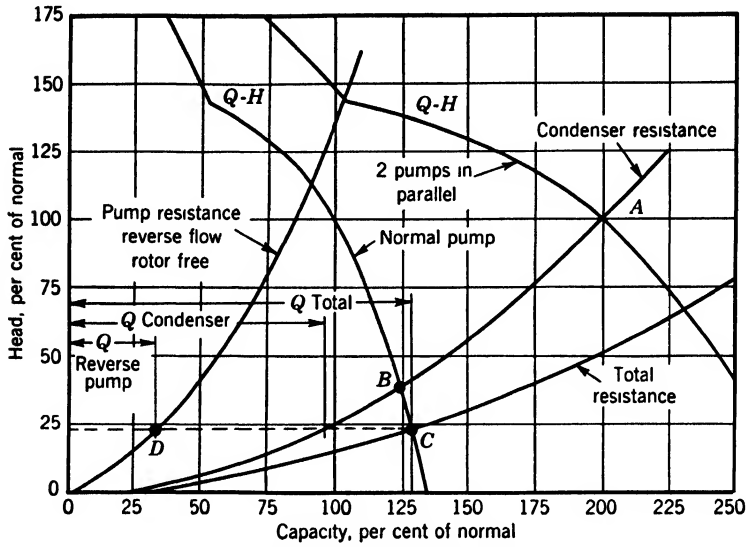


FIG. 13.9. Two pumps in parallel, power failure on one pump.

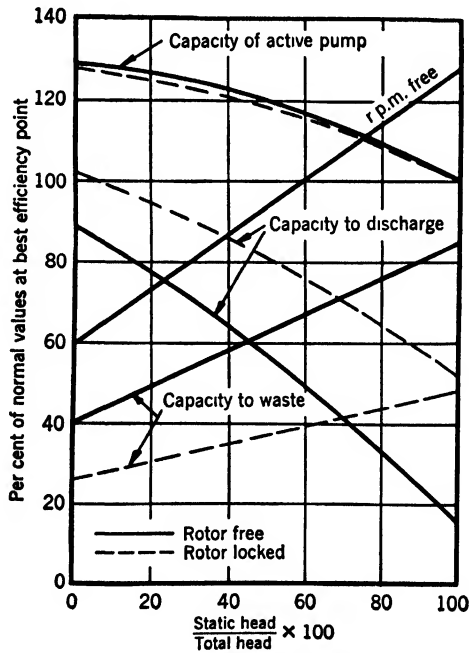


FIG. 13.10. Two pumps in parallel, power failed in one;  $n_s = 1800$ , double-suction pumps.

with the rotor locked, the pump will deliver 127.5 per cent of its normal capacity, 108 per cent being delivered to the system and the rest being returned to the suction through the idle pump.

Figure 13.9 shows that, when the rotor is free, the idle pump operates at 23 per cent of its normal head (point *D*). Its reverse speed under 100 per cent head is 128 per cent (see Table 1), and at 23 per cent head the speed is 61 per cent of normal speed. The pump characteristics under reversed flow have to be determined experimentally at least for one point and the curve then has to be plotted by applying affinity laws.

Note that both with free and locked rotor the operative pump works at 129 and 127.5 per cent of its rated capacity. With propeller pumps, the brake horsepower at these points is lower than at the normal capacity; therefore, the motor will be unloaded. With pumps of lower specific speed the brake-horsepower curve rises with increasing capacity, and under such conditions the motor may be overloaded beyond the safe limit.

Figure 13.10 shows the capacity division between the useful discharge and the waste through the idle pump for a centrifugal pump at different ratios of static head to total pump head with both free and locked rotor. This curve was calculated in the same manner as that in Fig. 13.9. *For a given head a greater portion of the capacity goes to waste with the rotor locked. This is similar to the induction motor, which draws more current with the rotor locked than with the rotor free. A motor generates counter-electromotive force which reduces the current through the rotor. In centrifugal pumps with the rotor free, part of the applied head is used to overcome the head generated by the pump, and the remaining part produces the reverse flow which is less than with the rotor locked.*

Figure 13.11 shows similar curves for a propeller pump. *Note that here a greater capacity is returned to the suction sump with the rotor free than with the rotor locked. In propeller pumps no centrifugal head is generated by rotation; on the other hand, rotation permits the impeller to move enough to reduce the absolute path of the water, and thus to increase the flow.*

**(c) Two Pumps in Series.** Frequently, in order to increase the capacity during extremely low river level, booster pumps of the propeller type are installed in series with pumps taking their suction from a river. To simplify the piping these pumps are left in line when not in operation. In this connection it is important to know what the pump resistance will be with the rotor free and with the rotor locked; also at what speed the idle pump will rotate. In this case the capacity is positive and the head is negative. Using the chart in Fig. 13.2 ( $n_s = 1800$ ) for convenience, at 100 per cent capacity and zero torque the speed is 33 per cent of normal, the head is 25 per cent. This falls into section *G*,



and the pump is operated as a turbine with reversed flow and at runaway speed. *If the rotor is locked the same chart shows that at 100 per cent capacity and zero speed the head is 56 per cent, thus showing that the pump resistance is greater with a locked rotor when full capacity is drawn through the pump.*

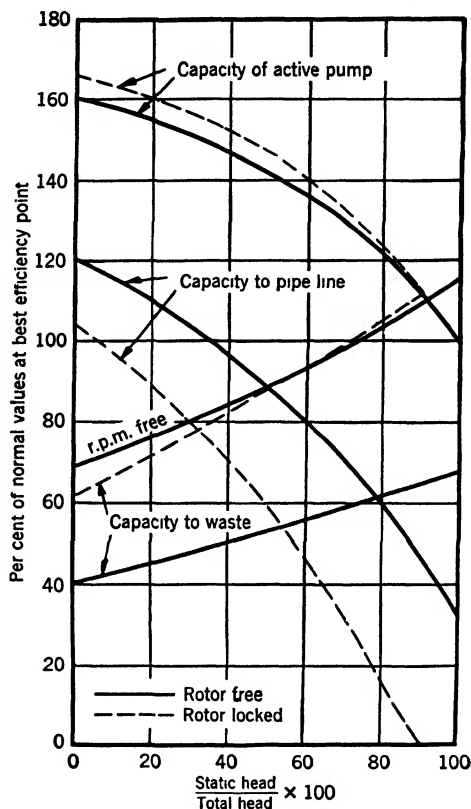


FIG. 13.11. Two pumps in parallel, power failed in one;  $n_s = 7500$ , propeller pumps.

For a propeller booster pump of 7200 specific speed operating with a free rotor and at full capacity the resistance is 34 per cent and the speed is 65 per cent of normal (Table 1). With the rotor locked the resistance is 310 per cent of the pump normal head. The difference in behavior of the two types of pumps running as a turbine at runaway speed and under reversed flow is quite apparent.

When two pumps are operated in series, if the power should fail on the high pressure pump and the flow reverse (all or part of the total head static and no check valve in the pipe line), the booster pump will operate as shown in the second quadrant, *B* on Figs. 13.1 (a), 13.1 (b),

and 13.2; that is, the speed is positive, the flow is negative, and the head is positive and higher than the booster shut-off head. If the head applied from the pipe line, through the idle main pump, is high in comparison with the booster's own head, dangerous overload will develop on the booster pump motor, and it probably will be cut off by the overload protection relays.

**(d) Pump Operation under Negative Head, Section H, Fig. 13.1 (a).**

In this section the flow is positive, rotation is positive, and head is negative. If two pumps are operated in series and the booster pump is of much larger capacity than the high pressure pump, the discharge valve on the latter can be opened until the differential pressure across the pump will reach zero and then become negative. The capacity will increase beyond the maximum capacity at zero head. Evidently, under such conditions the pump not only does not generate any head, but it also absorbs some of the head produced by the booster pump.

The author knows of a case where similar conditions prevailed with one pump taking its suction from a high pressure oil well. When the valve was opened wide the pump discharge pressure gradually fell below that on the suction. The pump happened to be of the double-casing type. In this kind of pump the outer barrel is under full discharge pressure, which keeps the inner casing halves tight. Only small bolts hold the inner casing halves when assembled. When the discharge pressure fell below the suction pressure, these bolts were not strong enough to keep the pump halves together, and mechanical damage to the rotating element resulted. The cause of the damage was not easily established at that time as the conceptions about the pump operation outside its normal head-capacity range were only beginning to attract the attention of pump engineers.

### 13.5 STARTING OF CENTRIFUGAL PUMPS

A knowledge of complete pump characteristics is very helpful for solving some problems connected with starting centrifugal pumps. In general the torque requirements of centrifugal pumps during the starting period are easily met with standard motors, induction or synchronous. However, conditions may arise, depending on the pumping arrangement, which impose severe requirements on the motor during the starting period, calling for high motor starting and pull-in torques. In special cases, a definite starting procedure is prescribed to permit the motor to pull in into its normal operating speed. Several typical cases will be considered, including the most difficult ones. In every instance it will be assumed that the same relationship exists between the head-

capacity and the speed during the transient period of acceleration as that at the same speed with a steady established flow. Knapp<sup>4</sup> has shown that this assumption gives results in close agreement with an actual test in his calculations of the time-speed relation during the reverse rotation after the power failure of a pump.

(a) **Speed-Torque Curve.** When a centrifugal pump of low and medium specific speed (below 3500) is started, the power at shut-off, or zero capacity, is lower than the normal brake horsepower. Figure 13.12 shows constant speed head-capacity and torque curves for  $n_s = 1800$ . If started against the shut-off head the torque-speed curve for

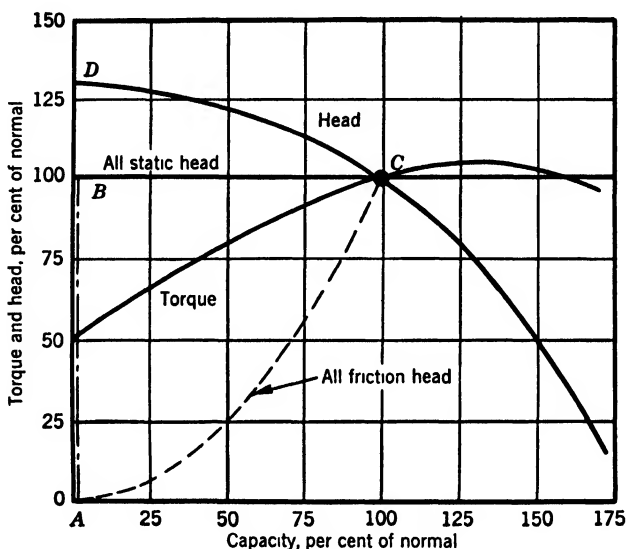


FIG. 13.12. Constant speed pump characteristics.

such pumps is a square parabola as torque varies as the square of the speed  $A'B'D'$  (Fig. 13.13). While pumping torque is zero at zero speed, the starting torque of the motor should overcome the static mechanical friction in the bearings and stuffing boxes. This varies greatly with the size and speed of the pump, and also with the stuffing box size and pressure.

A horizontal pump with two stuffing boxes packed to hold 250 lb. with a 3.375-in. shaft sleeve, two sleeve bearings, and a ball thrust bearing requires 430 lb.-in. starting torque. This constitutes 1.25 per cent of the pump normal torque at 3600 r.p.m., 5.0 per cent at 1800 r.p.m., and 11.25 per cent at 1200 r.p.m. The portion  $EF$  of the speed-torque curve in Fig. 13.13 near zero speed is drawn arbitrarily and its exact

form is not important. From this example it is seen that the starting torque is higher for low speed pumps, but is low enough to be met by any standard motor.

If a centrifugal pump is started with the discharge valve open the speed-torque curve depends on the head-capacity characteristics of the system into which the pump is delivering. Suppose a pump with head-capacity and torque characteristics as shown on Fig. 13.12 is pumping against a static head only. The system characteristic will be  $ABC$ . In this case, when started the pump will work near the shut-off head until the total static head is reached at  $B$ ; then the pump will begin to

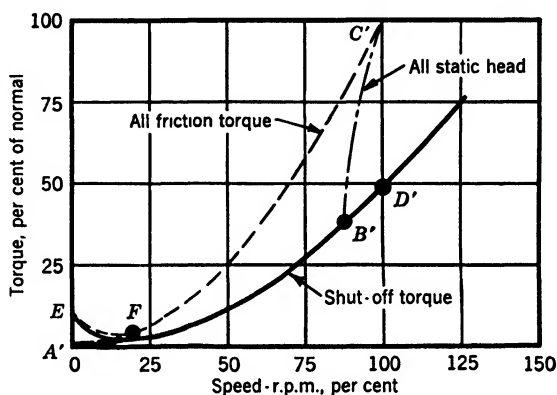


FIG. 13.13. Speed-torque curves.

discharge into the system along the constant head line  $BC$ . The speed-torque curve is plotted by finding the speed to obtain head-capacity points along  $BC$  and reducing the torque for the same points from the constant speed torque curve.

As another example consider the case when the total head is all friction head,  $AC$  in Fig. 13.12, and the pipe length is short, as with a condenser circulating pump. The head-capacity point during the starting period will move along the system characteristic curve  $AC$  and, when the corresponding points (of the same specific speed) on the constant head-capacity curve are located the speed and torque can be determined and plotted,  $A'C'$  in Fig. 13.13, the procedure outlined above being followed.

If the pipe line is long (several miles) the mass of the liquid to be moved becomes so great that the time required to accelerate the liquid in the pipe line is much greater than the time required to bring the motor up to speed, and the pump behavior during the starting period will approach that when operating against a closed discharge valve.

Cases intermediate between these two extremes will have their speed-torque curves lying between  $A'C'$  and  $A'D'$  in Fig. 13.13. Similarly, if the total head consists partly of static and partly of friction, curves similar to  $A'C'$  and  $A'B'C'$  can be plotted; if the pipe line is long, the speed-torque curve will approach that with shut-off discharge.

(b) **Starting a Pump Running Backwards.** For centrifugal pumps having brake-horsepower curves either flat or decreasing toward zero capacity, the torque never exceeds 100 per cent of normal with any possible method of starting and any system characteristics so long as

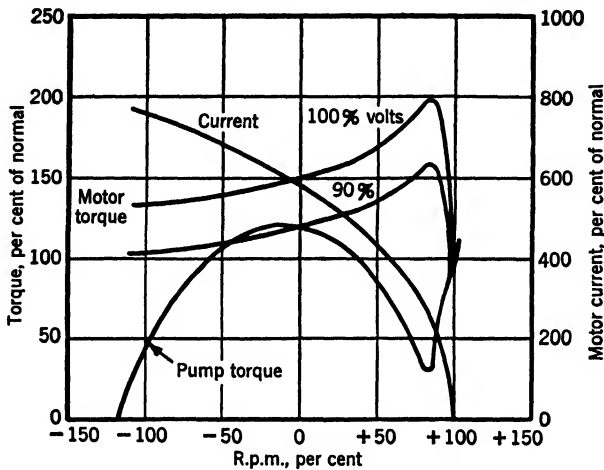


FIG. 13.14. Speed-torque curves; pump  $n_s = 1800$ ; 4-pole motor.

the pump is not allowed to run backwards under the head from the system. But, if a part or all of the total head is static and if there is no provision to prevent back-flow through the pump, the opposing torque may exceed the normal torque when starting with the discharge valve open and it depends on the head applied to the pump. Assume a case when the pump is running backwards under 100 per cent head from the system. As long as an equilibrium is reached the pump is operating at runaway speed and generating no torque. However, if the motor is put on the line and the reverse speed of the unit begins to drop, the pump will develop opposing torque, as can be seen from Fig. 13.2 when following the 100 per cent head line from the zero torque line through sections  $C$  and  $B$ , to  $A$ . Figure 13.14 shows the torque-speed curve plotted from Fig. 13.2 for 100 per cent head from full reverse speed to 100 per cent forward speed. Prevention of reverse rotation by mechanical means, such as a non-reversing ratchet (a spring solenoid-operated brake applied to the coupling between motor and pump has been used

on condenser circulating pumps to prevent reverse rotation) does not change the speed-torque curve from zero speed to full positive speed, thus high motor starting torque is required to overcome pump torque at zero speed, which is 120 per cent in Fig. 13.14. Attention is called to the fact that, for cases where the pump may be started while running backwards, the motor speed-torque curve should be known for a negative rotation, that is, the positive torque developed by the motor when put on the line while rotating in the opposite direction.

Figure 13.14 shows motor torque-speed curves for a typical 4-pole induction motor. *It will be noticed that although a standard motor will be able to accelerate the pump from 120 per cent reverse speed, the starting time will increase, and the starting current will increase, and this may result in excessive heating of the motor. At a slightly reduced voltage the motor may not be able to pull into full speed, and may be cut out of the line by the overload relays.* Evidently, it is impossible to establish a general rule on pump and motor behavior under such conditions and each case should be studied individually.

**(c) Starting Propeller Pumps.** The peculiar feature of these pumps is that they have a brake-horsepower curve rising toward zero capacity. The brake horsepower at shut-off may be twice (or more) that of the normal for the higher specific speed pumps of this group.

Evidently, if started with the discharge valve shut these pumps will require a pull-in torque twice (or more) the normal. Standard motors cannot develop such pull-in torque. Instead of going to special motor design several schemes have been devised to start propeller pumps with standard motors.<sup>10</sup> These include

- (1) Using a check valve in addition to a gate valve in the discharge line. With the gate valve open the pump is started against static head only.

- (2) A small by-pass back to the suction sump, open during the starting period; locating the by-pass as close as possible to the pumping element will increase the by-passed capacity for a given size of by-pass.

- (3) Starting with discharge valve partially open, allowing the pump to rotate backwards.

- (4) Placing the impeller above the suction level and starting the pump dry, then priming the pump after the motor pulls into step.<sup>11</sup> A similar effect is obtained by depressing the water level in the pump below the impeller by compressed air during the starting period.

With a variable speed driver the pump can be started at a reduced speed to produce a head slightly above the normal, when the discharge valve can be opened and the pump brought up to normal speed.

The torque-speed curves for propeller pumps are plotted in the same manner as those for centrifugal pumps, particular attention being given to the peculiarities of the brake-horsepower curves.

Frequently propeller pumps are used for lifting water from one level to another over the crest of a levee (drainage or irrigation plants). The discharge pipe of such pumps forms a siphon. To start a siphon the pump has to fill it with water, and this requires a static head higher than the pump normal head. The torque requirements during the starting period of the pump should be studied, the pump being considered as working at or near the shut-off point until the siphon is primed, whereupon the pump head will fall suddenly to its normal static head.

Priming the siphon by extracting air with a special primer may lead to complications during starting because, as soon as the siphon is primed, a reverse flow through the pump starts under full pump head and starting conditions become similar to those with pumps running in reverse direction as described above.

In addition to torque requirements for pumping during the starting period shown on speed-torque curves, the motor has to furnish the torque for accelerating the mass of the rotating element of the pump. Although the impellers are filled with water, the acceleration of the latter is already taken care of by the pumping speed-torque curve, as pumping is produced by water acceleration.

Starting large pumps, even with a flat brake-horsepower curve, against a closed valve and with the pipe empty has been found undesirable as the shock of the water column against the valve may cause mechanical damage to the pump or column parts. This has been actually observed on pumps circulating molten salt in catalytic oil-cracking processes. The high specific gravity of this material (1.75 to 1.90) increases the intensity of the shock during the starting period.

### **13.6 EFFECT OF SPECIFIC SPEED UPON THE BEHAVIOR OF CENTRIFUGAL PUMPS UNDER SPECIAL OPERATING CONDITIONS**

When complete pump characteristics are available, questions connected with any possible operating conditions outside the normal head-capacity and speed range can be easily answered. Unfortunately, experimental determination of complete pump characteristics requires equipment usually not found among commercial testing facilities of the pump manufacturers. As a result, only a few complete pump characteristics are available. These fall into a low or medium specific speed group not exceeding 2100 for a single-suction pump. To study the effect

of the specific speed upon the pump behavior under unusual operating conditions the author has tested four pumps, extending the range of specific speeds up to 13,500.

The author had no means of absorbing the power developed by the pumps when operated as hydraulic turbines; therefore, only tests with zero torque (at runaway speed) and at zero speed (with the rotor locked) were made both for positive and negative flow.

*In the course of these tests it has been found that propeller pumps (items 11, 12, and 13, Table 1) with the rotor locked do not follow the affinity laws for both positive and negative flows. The values given in Table 1 for these*

TABLE 1. SPECIAL OPERATING CONDITIONS OF PUMPS OF DIFFERENT SPECIFIC SPEEDS

Operation		Negative Flow				Positive Flow				Remarks		
No.	Specific speed, single-suction	Rotor-free		Locked		Rotor-free		Locked		Values of head ( $H$ ), capacity ( $Q$ ), and torque ( $T$ ) are percentages of normal pump operation		
		$H = +100$ $T = 0$		$H = +100$ r p m. = 0		$Q = +100$ $T = 0$		$H = -100$ r p m. = 0				
		$-Q$	$-$ r p m	$-Q$	$+T$	$-H$	$+$ r.p.m.	$+Q$	$-T$	Size	Type of pump	Source
1	1,190	85	104	104						1½	Multistage	Stepanoff
2	1,220	76	108	117	96					2	Multistage	Stepanoff
3	1,270	68	117	118	120	25	32	133	80	4	Double-suction	Knapp
4	1,285		117							4	Four-stage	Stepanoff
5	1,700	58	125	115	146					8	Single-suction	Knapp
6	1,760	52	106	103	110	37	30	117	73	2	Single-suction	Kittredge
7	1,940	75	125	108	130	40	30	105	60	8	Single-suction	Kittredge
8	2,140	60	123	95	125					8	Single-suction single-volute	Knapp
9	2,140	50	123	108	140					8	Single-suction double-volute	Knapp
10	3,500	80	125	84	116	40	50	84	93	12	Double-suction	Stepanoff
11	6,700	112	126	79	88	33	66	55	67	16	Propeller	Stepanoff
12	7,200	85	128	37	74	34	65	50	68	16	Propeller	Stepanoff
13	13,500	121	128	66	37	40	70	72	54	16	Propeller	Stepanoff

NOTES. To find operating conditions other than those shown apply affinity laws except for propeller pumps with rotors locked.

Pumps 8 and 9 have the same impeller.

Pumps 11 and 12 have the same casing but the impellers are different.

conditions were either actually taken at 100 per cent head and capacity or, when these values could not be reached, 100 per cent values were obtained by extrapolating the curves rather than by applying the affinity laws. The reason for such shape of head and torque curves is not clear. *With the rotor free, all pumps did follow the affinity laws very accurately.*



The condensed results are presented in Table 1, together with other available data. The following remarks will be made from the examination of tabulated results.

(1) The table gives two points for the normal and two points for the reverse flow: one at zero torque or runaway speed and the other at zero speed or rotor locked.

(2) With a negative flow and 100 per cent head applied to the discharge nozzle (normal turbine operation) the runaway speed for all pumps with efficiency over 80 per cent is approximately 125 per cent of the normal pump speed irrespective of specific speed.† Items 1, 2, and 6 are small, low efficiency pumps and show a lower runaway speed. Capacity under the above conditions stays below 100 per cent, except for propeller pumps (items 12 and 13).

(3) With a negative flow and the rotor locked under 100 per cent head, pumps of high specific speed show a lower capacity and torque than low specific speed pumps; therefore they will produce a speed-torque curve considerably below that shown in Fig. 13.14, good for a single-suction pump with  $n_s = 1270$ . Three points are available for construction of speed-torque curves for a negative flow for specific speeds much different from that on which Fig. 13.2 is based: (1) speed at zero torque, (2) torque at zero speed (both from data in Table 1); and (3) the normal torque at normal speed.

(4) With a negative flow under the same head low specific speed pumps show lower capacity with the rotor free than with the rotor locked, whereas the reverse is true for high specific speed pumps.

(5) With a positive flow at runaway speed (abnormal outward flow turbine) the pressure drop for a given capacity (100 per cent) is about 40 per cent, irrespective of specific speed. The r.p.m. at the same conditions shows a tendency to increase for higher specific speed pumps. With a positive flow and rotor locked for a given pressure drop ( $H = 100$  per cent) high specific speed pumps put through less water than low specific speed pumps, whereas no definite tendency can be established regarding the torque variation under these conditions in terms of specific speed.

† The maximum runaway speed of high specific speed water turbines of the Kaplan type may exceed 2.5 times the normal speed. This occurs at high gate opening with the runner vanes nearly closed. When vanes are allowed to open fully the runaway speed is held to 1.8 to 2.0 times normal, for which overspeed generators are usually designed.<sup>12</sup> Normally 10 to 15 per cent of the gate opening is sufficient to bring the unit to synchronous speed with runner vanes flat. In propeller pumps the impeller vane angle is fixed at or near the maximum whereas the fixed diffusion vane angle is far from the maximum possible, that is the reason why the propeller pump runaway speed under 100 per cent head is relatively low in comparison with the maximum runaway speed of propeller water turbines.

(6) With a positive flow at a fixed capacity ( $Q = 100$  per cent) the head loss through the pump is lower with the rotor free than with the rotor locked; this difference increases rapidly with the specific speed.

## REFERENCES

1. D. THOMA, "Vorgänge beim Ausfallen des Antriebes von Kreiselpumpen," Mitt. Hyd. Inst. Tech. Hochschule, München, Vol. 4, 1931, pp. 102-104, Munich, R. Oldenbourg; also in English translation: C. P. KITTREDGE and D. THOMA, "Centrifugal Pumps Operated under Abnormal Conditions," *Power*, June 2, 1931, pp. 881-884.
2. LUDOLF ENGEL, "Die Rucklaufdrehzahlen der Kreiselpumpen," doctoral dissertation, Tech. Hochschule zu Braunschweig.
3. CLIFFORD P. KITTREDGE, "Vorgänge bei Zentrifugalpumpenanlagen nach plötzlichem Ausfallen des Antriebes," Munich, R. Oldenbourg, 1933.
4. R. T. KNAPP, "Complete Characteristics of Centrifugal Pumps and Their Use in the Prediction of Transient Behavior," *Trans. A.S.M.E.*, Nov. 1937, pp. 683-689.
5. ROBERT ZOBEL, "Versuche an der hydraulischen Rückstromdrossel," Mitt. Hyd. Inst. Tech. Hochschule, München, Vol. 8, pp. 1-47, Munich, R. Oldenbourg.
6. R. M. PEABODY, "Typical Analysis of Water Hammer in a Pumping Plant of the Colorado River Aqueduct," *Trans. A.S.M.E.*, Feb. 1939, p. 117.
7. R. T. KNAPP, "Centrifugal Pump Performance as Affected by Design Features," *Trans. A.S.M.E.*, April 1941, Vol. 63, No. 3.
8. R. W. ANGUS, *Trans. A.S.M.E.*, Vol. 64, No. 8, Nov. 1942.
9. OSKAR SPETZLER, "Die Turbinenpumpe im Stauwerk Baldeney," *Z. Ver. deut. Ing.*, Vol. 78, No. 41, Oct. 13, 1934, p. 1183.
10. C. B. TULEY, "Propeller Pumps in Parallel," *Power*, April 1934, p. 187.
11. M. F. WAGNITZ, "Stormwater Pumping Station at Detroit," *Eng. News-Record*, July 30, 1931.
12. R. V. TERRY, "Development of the Automatic Adjustable Blade-Type Propeller Turbine," *Trans. A.S.M.E.*, July 1941, pp. 398, 405, 406.

## CHAPTER 14

### SPECIAL PROBLEMS OF PUMP DESIGN AND APPLICATION

#### 14.1 UNSTABLE HEAD-CAPACITY CHARACTERISTICS OF CENTRIFUGAL PUMPS

A theoretical investigation has shown that the actual head-capacity curve is a parabola with its apex displaced to the right of the zero capacity axis (Fig. 14.1). The shut-off head is lower than the maximum head ( $H_s < H_{\max}$ ). Actual test curves of low specific speed pumps ( $n_s \approx 1000$ ) approach this form. Under certain operating conditions part  $AB$  of the head-capacity curve is unstable, and this instability results in head-capacity fluctuations or failure to pump entirely.

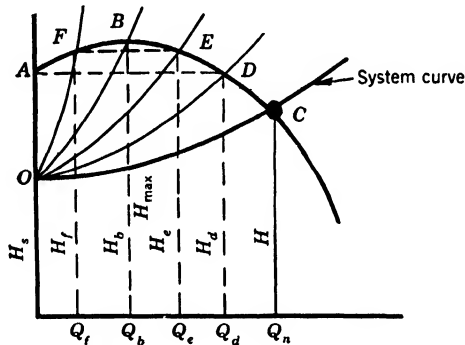


FIG. 14.1. Unstable  $Q$ - $H$  characteristic.

This happens if the capacity is reduced to  $Q_b$  or less. At certain conditions, such as when two pumps work in parallel, head-capacity swings may start at capacity  $Q_d$ . Fluctuations of head-capacity are followed by fluctuations in the power and speed of the unit and, if the frequency of such swings coincides with that of the adjoining piping system, severe mechanical vibrations of the piping are induced.

**(a) Conditions for Head-Capacity Swings.** *The following conditions must exist to develop head-capacity and power swings in a system including a pump.*

(1) *The mass of water must be free to oscillate.* This condition exists when the water mass is suspended between two free surfaces, as in

boiler-feed and condensate pumping cycles. In both, the suction is taken from a vessel that has a free surface, and the water is discharged into another vessel with a free surface.

(2) *There must be a member in the system which can store and give back the pressure energy or act as a spring in a water system.* The static water column in a water system, having two free surfaces, serves this purpose. In a boiler-feed pump cycle, the elastic steam cushion in the boiler also serves the same purpose. Long piping, with or without a vessel having a vapor or air cushion, may provide the necessary spring effect to produce oscillations. When compressible fluids, air, or gases are being pumped, the fluid itself serves as an elastic member of the system. As a result, air blowers with unstable head-capacity characteristics cannot be operated near the maximum head point. The blower head-capacity swings produce a peculiar pulsating sound similar to that of plunger pumps and is referred to as pumping.

(3) *There must be some member that will provide impulses at regular intervals to start the swings.* When the head-capacity curve is unstable, such conditions appear when the capacity is as low as, or lower than, that corresponding to the maximum head or that at capacity  $Q_b$ . Even with stable head-capacity curves, capacity surges may be induced by excessive rotation in the impeller approach.

**(b) Analogy to Water Turbine Experience.** It should be pointed out that hydraulic water turbine installations contain all the conditions necessary for head-capacity and power swings, and surges have been observed on a great many installations during part-load operation. These conditions are aggravated by the fact that power swings of such magnitude are induced in the electrical system that some of the units cannot be kept in parallel operation with other units on the line. An investigation by Rheingans<sup>1</sup> and several discussions of his original article on the subject have shown that the power swings originate in the water turbine draft tube (corresponding to the pump suction). At partial loads, the residual component of the tangential velocity sets up a whirl in the draft tube which, because it is not symmetrical about the axis of rotation, causes the runner to discharge against a fluctuating head. When the fluctuation frequency equals that of the system, the swings appear at their maximum value.

The whirl occurring in the draft tube of a water turbine at partial loads appears also in centrifugal pumps to a different degree, depending on the suction and impeller design, provided the rest of the conditions necessary for oscillation are existent. Power swings in water turbines may be eliminated or reduced to the point that they do no harm by providing baffles in the draft tubes and by changing the runner design

so that rotation of water in the draft tube is reduced. Similar means are used in pump design to achieve the same goal. More specifically, *the suction nozzle should provide a gradually accelerated flow and have proper baffling to suppress the prerotation in the impeller approach, and the impeller should have plain vanes in preference to the extreme Francis type to reduce churning in the impeller eye.*

**(c) Stable Curves for Boiler-Feed Service.** All modern boiler-feed pumps are designed with a stable head-capacity curve, that is, the head is constantly increasing toward zero capacity. Frequently the shut-off head is specified to be not lower than a certain minimum as, for example, 117 per cent of the normal operating head. Such limitation in itself does not guarantee a stable head-capacity curve. In many instances a maximum shut-off head instead of a minimum is stipulated. Such a request is usually inspired by considerations of power saving, presuming that a flatter head-capacity curve will result in less loss due to throttling at partial capacities. This is not necessarily true because: (1) *the slope of the brake-horsepower curve is affected by the shape of the efficiency curve and* (2) *if the shut-off head limit is too low (110 per cent) the requirement must be met by locating the full-load condition to the left of the best efficiency capacity of the pump, thus defeating the purpose of reducing power over a wide range.* Furthermore, setting the minimum shut-off head too low reduces the margin of safety against surges in discharge lines.

The ratio of  $H_s/H$  is in general a measure of stability of the head-capacity curve and is an important factor in reducing the hunting of governing devices.<sup>2</sup>

**(d) Cause of Surges.** During each cycle of the swinging conditions the pump goes through the following steps. When the pump capacity is reduced from the normal  $Q_n$  (Fig. 14.1) by throttling the pump discharge, new system curves,  $OD$ ,  $OE$ , and  $OB$ , are produced by additional resistance in the throttle valve requiring higher heads at each capacity  $Q_d$ ,  $Q_e$ ,  $Q_b$ . Until capacity  $Q_b$  is reached, the pump is able to furnish increasing head demand. At the instant the capacity is reduced below  $Q_b$ , the pump head  $H_f$  will be lower than the pressure in the system and there will be a tendency for the flow to reverse with the operating point moving from  $B$  to  $F$  and  $A$ . But as soon as the flow is reduced the pressure in the system begins to drop and the pump will again begin to discharge into the system until the pressure is built up to  $H_b$  at capacity  $Q_b$ . Since the demand from the system is only for a capacity  $Q_f$ , there will again be a tendency to reverse the flow and the cycle will be repeated. Fluctuations in head and capacity are accompanied by power and speed oscillations. This makes the phenomenon more complicated. However, *the origin of the pressure variation lies in*

*the fact that, at certain times, the pressure in the discharge line is higher than the pump head and a tendency to reverse flow appears.*

The compressibility of a column of high temperature water is an important factor in the swinging systems of a boiler-feed pump. *If the throttle valve is placed next to the pump discharge nozzle, the oscillations do not appear as the water column is too short to provide the necessary compressibility, and the turbulence set up by the throttle valve destroys the regularity of impulses from the pump.*

It may be mentioned here that if a pump is operating under cavitation conditions, such as self-regulating condensate pumps (points *F* and *G*, Fig. 11.16), oscillations do not appear because the irregular water hammer blows resulting from cavitation destroy the regularity of impulses which may be present otherwise.

In the majority of applications, the friction head is a major portion of the total head and the capacity is varied by throttling a valve next to the discharge flange. Under such conditions no swings appear, even with unstable head-capacity characteristics.

**(e) Parallel Operation.** A stable head-capacity characteristic is essential for parallel operation of several boiler-feed pumps. If a set of pumps have unstable head-capacity curves and the operating pressure happens to be at a point *E* (Fig. 14.1) which is higher than the shut-off head  $H_s$ , a pump cannot be put on the line as the zero capacity head  $H_s$  is not sufficient to open the check valve in a common discharge manifold. Also, if several pumps work at a head  $H_e$  some pumps may be working at a point *F* beyond the maximum head  $H_b$ , while others are working at point *E* on the rising part of the head-capacity curve. If the throttle valve is opened under such conditions, a pump working at point *E* will increase their capacity and those working at *F* will decrease their capacity. The latter group of pumps may cease to deliver entirely. Fluctuations in capacity and pressure will result. When one of a group of pumps working on the same boiler begins to surge, the rest of the pumps respond immediately with swings of the same frequency, thereby increasing the total oscillating mass. The swings stop immediately when the faulty pump is stopped.

**(f) Rising Characteristics.** A rising head-capacity curve is essential for boiler-feed service and other applications where conditions for setting up pressure surges exist. Theory gives only one hint of how to produce a rising head-capacity curve, that is, making the discharge angle  $\beta_2$  smaller. In actual pumps this condition is not sufficient, as the number of vanes, the vane angle at entrance  $\beta_1$ , and the vane development between  $\beta_1$  and  $\beta_2$  have a marked effect on the shape of the head-capacity curve near shut-off.

By referring to Fig. 9.16 it will be noticed that lower impeller discharge vane angles  $\beta_2$  and higher specific speeds produce a steeper head-capacity curve. Usually specific speed is selected from economic and mechanical considerations by fixing the number of stages for a specified head. For a given specific speed and a selected vane angle  $\beta_2$  the number of vanes is obtained from Fig. 9.16 and equation 9.15. For a known true vane length  $l$ , the ratio  $l/t$  gives the number of vanes. In practice the number of vanes varies from 5 to 7, as shown also by Fig. 14.2.

Schröder<sup>3</sup> has studied the form of the head-capacity curve as a function of the vane angle  $\beta_2$ , and the number of vanes. Figure 14.2 shows

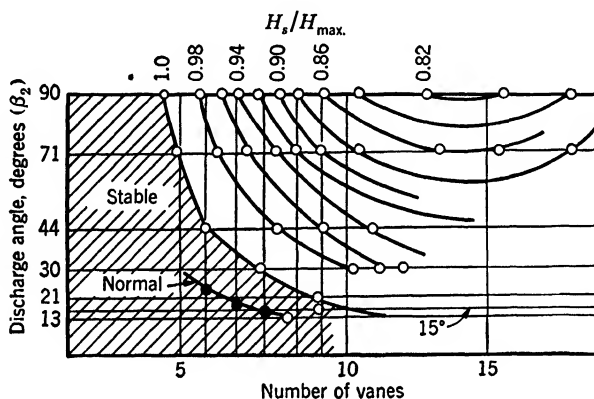


FIG. 14.2. Conditions for a stable  $Q$ - $H$  curve (Schröder).

a summary of his results. The shape of the head-capacity curve near zero capacity is represented by the ratio  $H_s/H_{max.}$ . For a ratio less than unity the curve is unstable. Lower angles and fewer vanes tend to produce a more stable curve. Points marked "normal" added by the author.

**(g) Means to Reduce or Stop Head-Capacity Swings.** (1) Bypassing part of the capacity to the suction supply tank. This step is also recommended as a precautionary measure to protect the pump from overheating in case the discharge is shut off.

(2) With the automatic capacity governor near the boiler, very slight throttling at the pump will stop head-capacity swings.

(3) All piping to and from the pump should be braced except for a provision for heat expansion. The mechanical vibration can be checked in this way.

(4) Operation near the critical point should be avoided. In large stations the total capacity is split between several pumps. Units are put on and off the steam to meet the load instead of depending entirely on the governor for the capacity variations.

Dzialis<sup>4</sup> has studied swings of head-capacity curves of centrifugal pumps with unstable characteristics experimentally. His testing arrangement included an air chamber for an elastic member in the systems. These tests have definitely connected the swings in the systems to the unstable form of the head-capacity characteristics of the pump.

#### 14.2 DETERMINING OPERATING POINTS OF CENTRIFUGAL PUMPS WORKING ON PIPE LINES

When a pump has to overcome the pipe line resistance in addition to a static head, the head against which the pump has to work varies with the capacity, pipe line resistance increasing with the capacity. The operating conditions of the pump in that case are best determined graphically by plotting, on the same sheet and to the same scale, both the pump head-capacity curve and the pipe line resistance curve. The operating point is obtained by the intersection of the two. The procedure is very simple when only one pump and one pipe line of a constant diameter are involved. However, when more than one pump is used to produce the total head or when the pipe line consists of several sections of different diameters going through points at different elevations, or when the flow from a main pipe line is divided, the plotting of the pipe line resistance curve becomes more complicated.

In every case, the operating point is obtained as an intersection of the pump head-capacity curve and the pipe line characteristics curve. When the total head is produced by more than one pump operating in series, the pump head-capacity curve is obtained by adding the heads for a given capacity. Figure 14.3 shows the head-capacity curve for two pumps in series. When the total capacity is divided between the two pumps, the combined head-capacity curve is obtained by doubling the capacities for given heads. Figure 14.3 also shows the head-capacity curve for two pumps in parallel. The same procedure is followed if the pumps are not alike. When two pumps are available and are to operate against pipe line resistance, it is not always possible to say off-hand whether the maximum capacity will be obtained when the pumps are being operated in series or parallel. This depends on the characteristics of the pumps and pipe line. Only by plotting head-capacity curves for series and parallel operation and determining the points of intersection of these with the pipe line resistance curve is the correct answer obtained.

**(a) Pipe Line Resistance Curve.** It is the plotting of the pipe line resistance curve that may present difficulties in some complicated cases.



In every case the problem is broken up into several simple ones, and the final pipe line resistance curve is plotted by combining the pipe line resistance curves of the several elements comprising the given pipe line. Several cases will be considered, starting from the simple and working up to more complicated cases.

When a pump is working against the static head  $H_s$  only, the pipe line resistance curve is a horizontal line drawn at a distance equal to the static head  $H_s$  from the zero head on the head-capacity scales (Fig. 14.3). When the pump is discharging into a pipe line laid out on a perfectly flat surface, the pump total head is used to overcome the pipe line

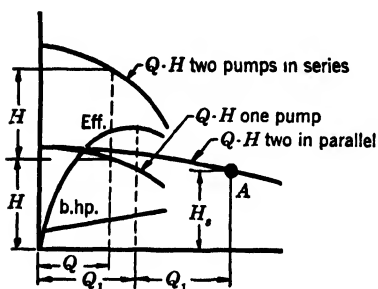


FIG. 14.3. Characteristics of two pumps in series and in parallel.

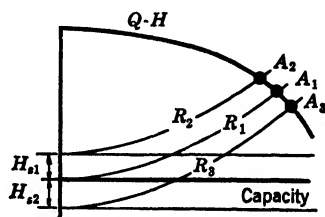


FIG. 14.4. Characteristics of a single pipe line.

friction. The pipe line friction increases with the capacity going through the pipe line approximately as the square of the capacity, and the pipe line characteristics curve is a parabola with the apex going through the zero head point of the head-capacity curve. In Fig. 14.4 curve  $R_1$  represents the pipe line resistance curve for such a case. Operating point  $A_1$  is obtained as the intersection of the pipe line resistance curve and the pump head-capacity curve. When, in addition to pipe line resistance, the pump has to overcome a static head  $H_{s1}$ , the combined pipe line characteristics curve is obtained by plotting the pipe line resistance curve ( $R_2$ , Fig. 14.4) as the sum of the static head and the pipe line resistance curve. When the final point of destination is located below the pumping station, the pump total head required to force the liquid through the pipe line is less by the difference in elevation, as this would assist the flow, and at small capacities the flow will take place by gravity. The pipe line characteristics curve in that case is obtained by subtraction of the difference in elevation between the pumping station and the end of the pipe line, which results in shifting the pipe line resistance curve ( $R_3$ , Fig. 14.4) by the static head  $H_{s2}$  below the zero head line. The pump operating point in every case is obtained as an

intersection of the pipe line resistance curve, and the pump head-capacity curve (points  $A_1, A_2, A_3$ , Fig. 14.4).

When the pipe line consists of two sections of different diameters, the combined pipe line resistance curve is obtained by adding the pipe line resistance for a given capacity of the component parts of the pipe line. In Fig. 14.5 (a), suppose pumping takes place from point  $B$  to point  $D$ , point  $D$  being higher than point  $B$  by  $H_s$  feet. The pipe line from  $B$  to  $C$  is of diameter  $d_1$  and from  $C$  to  $D$  is of diameter  $d_2$ . In Fig. 14.5 (b), curve  $R_1$ , the pipe line resistance curve is plotted for section  $BC$ , and curve  $R_2$  is plotted for section  $CD$ . The combined pipe

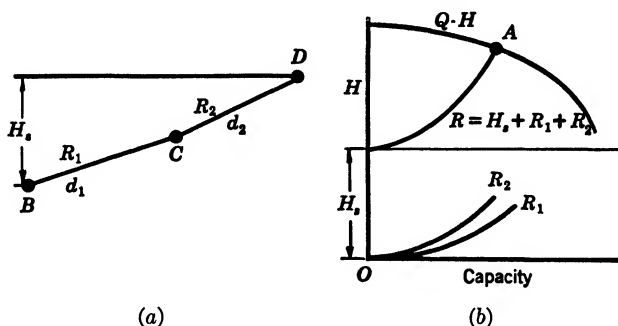


FIG. 14.5. Two pipe lines in series.

line resistance curve  $R$  is obtained by adding the ordinates for curves  $R_1$  and  $R_2$  and the static head  $H_s$ . The operating point  $A$  is obtained as an intersection of the combined pipe line resistance curve  $R$  and the pump head-capacity curve  $Q-H$ .

**(b) Two Parallel Lines.** When the pump is working on two pipe lines discharging either at two different points or at the same point, the operating point is obtained as an intersection of the pump  $Q-H$  curve and the pipe line resistance curve, which is obtained by adding the capacities for given heads of the individual pipe lines. In Fig. 14.6 (a), suppose pump is at point  $B$  and pumping into two pipe lines to points  $C$  and  $D$ , located at the same elevation as point  $B$ . In Fig. 14.6 (b),  $R_1$  is a pipe line characteristic for the line  $BC$ ;  $R_2$  is a pipe line resistance curve for the line  $BD$ . The combined pipe line resistance curve  $R$  is obtained by adding capacities for the same head. The operating point  $A$  is obtained as an intersection of pipe line resistance curve  $R$  and pump head-capacity curve  $Q-H$ . The pump capacity  $Q$  will be a sum of the capacities  $Q_1$  and  $Q_2$  going through the lines  $BC$  and  $BD$ , respectively, which are obtained by reference to the curves  $R_1$  and  $R_2$  for a given head  $H$ .

In Figs. 14.7 (a) and 14.7 (b) an example similar to the one shown in Figs. 14.6 (a) and 14.6 (b) is presented, but points  $C$  and  $D$  are located higher than point  $B$  by  $H_{s1}$  and  $H_{s2}$  feet respectively. The procedure is the same. In Fig. 14.7 (b) curve  $R_1$  is the pipe line resistance for line  $BC$ . Curve  $R_2$  is the pipe line resistance for line  $BD$ , plotted in the

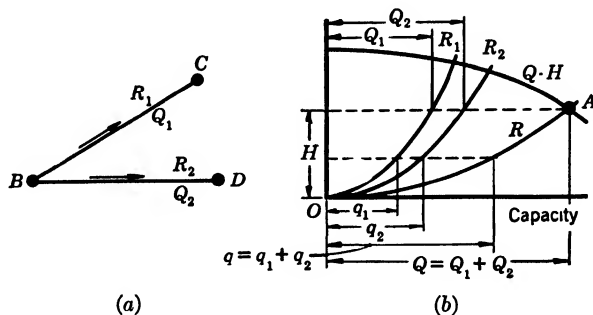


FIG. 14.6. Two pipe lines in parallel.

manner previously explained. The combined pipe line resistance curve  $R$  is obtained by adding the capacities for given heads from the curves  $R_1$  and  $R_2$ . The pump-operating point  $A$  is obtained as an intersection of the combined pipe line resistance curve  $R$  and the pump head-capacity curve  $Q-H$ . Of the total capacity  $Q$ ,  $Q_1$  would go to point  $C$ ,  $Q_2$  to point  $D$ , which are read off from the curves  $R_1$  and  $R_2$  at the head  $H$ .

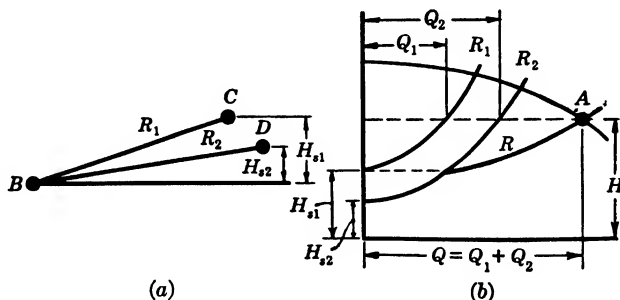


FIG. 14.7. Two pipe lines in parallel at different elevations.

As another example, suppose we are to pump from point  $B$  to point  $D$ , Fig. 14.8 (a). At point  $C$  a constant quantity of liquid  $Q_3$  is taken off. To find the operating point of the pump, proceed as follows. The pipe line resistance for the section of pipe line  $BC$  is plotted in the regular way, curve  $R_1$ , Fig. 14.8 (b). The pipe line resistance for section  $CD$  is plotted with the zero point displaced with respect to head-capacity

zero point by the capacity  $Q_3$ , which is going through pipe section  $BC$  but is not going through pipe section  $CD$ , curve  $R_2$ , Fig. 14.8 (b). The resistance of the complete pipe line  $BD$  is obtained by adding the pipe line resistances for the same capacity from curves  $R_1$  and  $R_2$ ; curve  $R$ , Fig. 14.8 (b). Operating point  $A$  is obtained as the intersection of curve  $Q-H$ , with curve  $R$  in Fig. 14.8 (b). Of the total quantity,  $Q_1$  going through section  $BC$ ,  $Q_3$  is discharged at point  $C$  and  $Q_2$  is going through section  $CD$ .

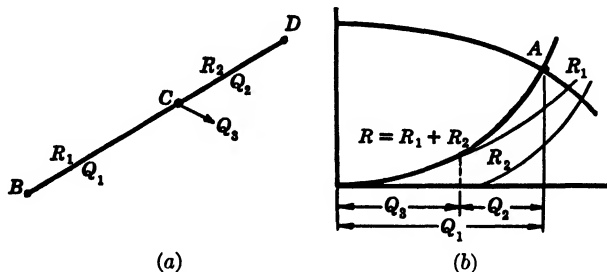


FIG. 14.8. Two pipe lines in series with a side outlet.

**(c) Pipe Line Throttling.** The determination of the operating point of centrifugal pumps working on pipe lines as treated in this article gives the maximum capacity possible with the existing pipe line and selected pumps. Very often this maximum capacity is not available when the pipe line is put in operation, and the flow must be throttled to reduce the throughput of the pipe line. When several stations are working in series, the throttling of the pumps requires great care. Thus, if all the throttling is done at the last station, the pipe line pressure at this station may exceed the safe limits for the pipe line or the pump itself. Therefore, the throttling is divided uniformly among the stations in such a way that the suction pressures at each station are kept at the required minimum. If too much throttling is done at some intermediate station, the suction pressure at the next station may drop below the safe minimum and the pump may start cavitating, reducing the flow below the required capacity. This may also result in some abnormal operating conditions at some stations above the one causing the trouble. This case is illustrated in one example taken from actual experience.<sup>5</sup>

Three pumps with head-capacity characteristics as shown in Fig. 14.9 were installed to operate in series on a pipe line with pipe line characteristics as shown in the same figure. The expected capacity obtained by intersection of the combined head-capacity curve of the three pumps in series and the pipe line resistance curve was 1110 g.p.m. The first pump took suction from a tank, and several feet of static

liquid head were available above the pump center line. The last pump discharged into a tank located 240 ft. above the location of the first pump. The liquid pumped was gasoline, of specific gravity 0.73. The following readings were obtained when all three pumps were operating in series.

	Suction Pressure	Discharge Pressure (lb.)	Differential Pressure (lb.)
First pump, A	7 in. Hg	60	64
Second pump, B	46 lb.	33	-13
Third pump, C	23 lb.	87	64

The capacity going through the pipe line was 770 g.p.m. instead of the expected 1110 g.p.m.

Attention is called to the behavior of the second pump B, which not only did not produce any head, but also wasted 13 lb. of the head produced by the first station. However, the trouble was caused not by

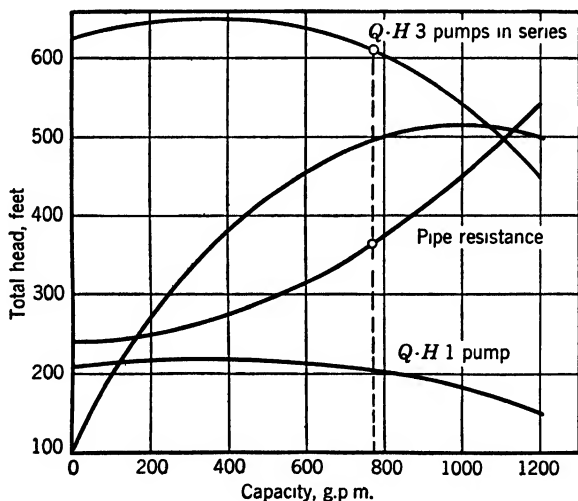


FIG. 14.9. Performance of 5-in. double-suction pump at 1760 r.p.m., efficiency 83 per cent.

the second pump, but by the first pump, which by all appearances and by comparison with pump C gave the impression of normal operation. However, 7 in. of vacuum on the first pump, when it was pumping gasoline, caused this pump to cut off at 770 g.p.m., thus fixing the capacity for the whole pipe line at 770 g.p.m. With this capacity the pipe line resistance is only 364 ft., including the 240 ft. of static head, and

two pumps were more than enough to produce this head. Thus, there was no work to be done by the second pump. Just why this pump and not the third pump had to loaf can be seen from Fig. 14.10, which gives the hydraulic gradient of the pipe line. The slope of the hydraulic gradient is given by line *ED*. The first and third pumps produced 202 ft. of head. Pump C had 154 ft. of static head to overcome in addition to 48 ft. of pipe line friction. The first pump produced 202 ft. of head, corresponding to 770 g.p.m. capacity. By drawing the hydraulic gradient lines from points *C* and *F*, points *G* and *H* are obtained, indi-

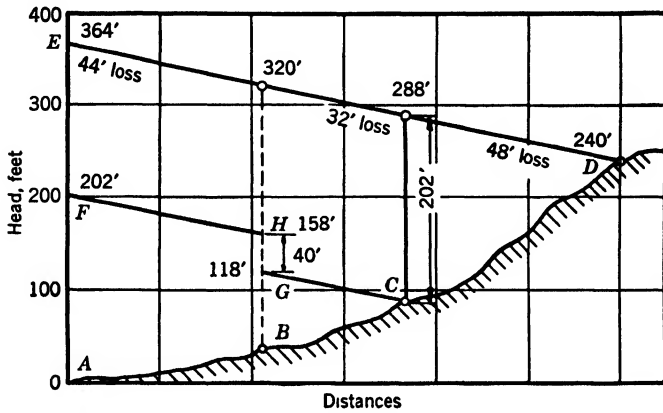


FIG. 14.10. Hydraulic gradient of the system represented in Fig. 14.9.

cating that the pressure available at station *B* was more than required to overcome the pipe line friction and static head without the operation of station *B*.

If the profile of the pipe line were such that the major portion of the static head was between stations *B* and *C*, then station *B* would have to overcome this static head and there would be an excess of head available at station *C* which would have to be destroyed by the third pump.

### 14.3 VARIABLE SPEED ENGINE DRIVE

With the engine throttle wide open or in a fixed position the engine output (brake horsepower) increases with the speed. If the head of an engine-driven centrifugal pump is changed so that the brake horsepower is increased the engine will slow down. This will cause the pump brake horsepower to drop; this brake horsepower decreases much faster than the engine brake horsepower, and the unit will operate at a point where both engine and pump brake horsepower meet. If the head on the

pump is changed so that the brake horsepower is decreased, the engine will speed up, until at a certain speed again the pump brake horsepower becomes equal to the engine brake horsepower.

If the engine has sufficient power to meet any brake-horsepower requirement at a constant speed, a constant speed governor may take care of any possible variation of the brake-horsepower requirement by changing the engine throttle opening. However, in practice, it is frequently desired to utilize all the power available from the engine at any speed; for example, with fire engines. Then the determination of the variation of capacity with head becomes more complicated, as a change in head will result in a speed change, which in turn will change the head

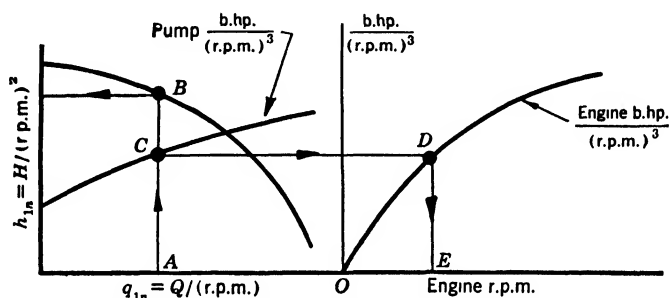


FIG. 14.11. Determination of the operating point of an engine-driven pump.

and capacity. Determination of the operating point by trial and error is a tedious and slow procedure. Below is offered a direct and simple method of plotting the variable speed head-capacity curves of engine-driven centrifugal pumps for a given engine rating.

Use is made of the unit head  $h_{1n}$  and unit capacity  $q_{1n}$ , defined in Chapter 5, Art. 5.2 (k). The unit brake horsepower can be defined in a similar manner:  $(b.hp.)_{1n} = b.hp./n^3$ , where  $n$  is r.p.m. In Fig. 14.11 the performance of a given pump is plotted in terms of the unit capacity, unit head, and unit brake horsepower. Suppose the engine is directly coupled to the pump; then the engine horsepower can also be reduced to the unit speed by dividing the engine output by the corresponding  $(r.p.m.)^3$ . This is plotted in Fig. 14.11 to the right of the pump curve, a common scale for the unit brake horsepower being used.

The operating points of the pump are determined by the condition that the unit brake horsepower of the pump is equal to the unit brake horsepower of the engine. Then, for any unit capacity  $A$ , the unit head is  $B$ , the pump unit brake horsepower is  $C$  and is equal to that of the engine (point  $D$ ), and the engine speed at which this unit brake horsepower is available is given by point  $E$ , which is the pump speed.

To find the capacity in gallons per minute multiply the unit capacity by the speed; the head is obtained by multiplying the unit head by  $n^2$ .

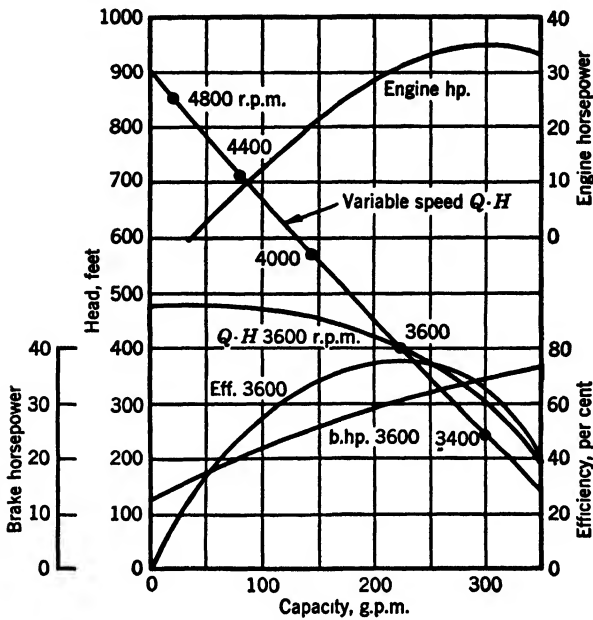


FIG. 14.12. Three-inch 2-stage engine-driven pump with throttle wide open.

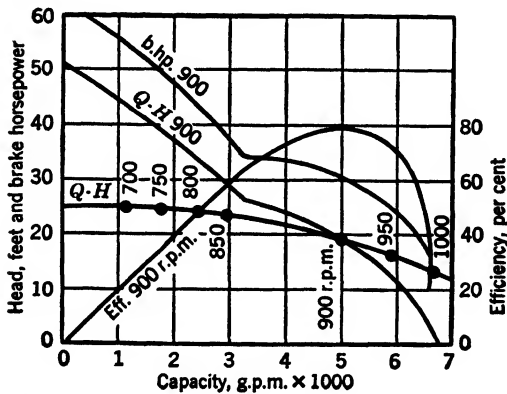


FIG. 14.13. Sixteen-inch propeller pump, engine-driven, with throttle wide open.

If the engine speed differs from that of the pump because of a gear reducer or increaser between the pump and the engine, the pump speeds are used for plotting the engine unit brake-horsepower curve. In other



words, the gear reducer or increaser is considered a part of the engine, with a power output at the pump speed.

Figure 14.12 shows the performance of a 3-in. two-stage pump of  $n_s = 1000$ , engine-driven, with the throttle wide open. Constant speed head-capacity and brake-horsepower curves are also shown. The variable speed head-capacity curve is much steeper than the constant speed characteristic. Pumps having increasing brake horsepower toward shut-off, when engine-driven, have a flatter variable speed head-capacity curve than the constant speed curve. Figure 14.13 shows a variable speed 16-in. propeller pump of  $n_s = 7000$ , engine-driven through a right-angle geared head. Constant speed head-capacity and brake-horsepower curves are also shown for comparison.\*

#### 14.4 PUMPING VISCOUS LIQUIDS WITH CENTRIFUGAL PUMPS

(a) **Pump Characteristics.** Pumping petroleum products is next in importance to pumping water. In general, in pumping viscous liquids the head and capacity at the b.e.p. are reduced by additional frictional losses and the brake horsepower increases, owing primarily to increased disk friction loss. The performance of a pump handling viscous oils is generally estimated by means of corrections applied to the water performance, because test facilities of the pump manufacturers provide only for water tests and most of the accumulated data and experience refer to water performance.

It is impossible to establish the performance of a pump handling viscous oil by purely theoretical deductions, even when the water performance is known. An analysis of the problem with the aid of dimensional analysis (Chapter 5) makes it evident that the relationship between head and capacity at constant speed is an experimental one, each viscosity producing a different head-capacity curve. However, the same analysis establishes certain relationships between variables describing the operation of centrifugal pumps which are confirmed by experiments. These constitute important guides in correlating the experimental test data for liquids of various viscosities and provide means for predicting pump performance for viscous liquids when water performance data are available. The following deductions suggested by the theory have been proven experimentally.

(1) *The affinity laws hold for all viscosities but with less accuracy than those for water. This means that when speed varies the capacity varies*

\* A direct method of determining the performance of engine-driven centrifugal pumps without the use of unit capacity, unit head, and unit brake-horsepower is described in the author's article, Reference 6.

directly as the speed, and the head varies directly as the square of the speed. Usually the efficiency is better at higher speeds; therefore when the speed is increased the brake horsepower increases less than the cube of the speed and the head increases more than the square of the speed (Fig. 14.14).† When speed is varied the specific speed at b.e.p. remains unchanged when viscous liquids are being pumped, irrespective of the deviation from the affinity laws stated above.

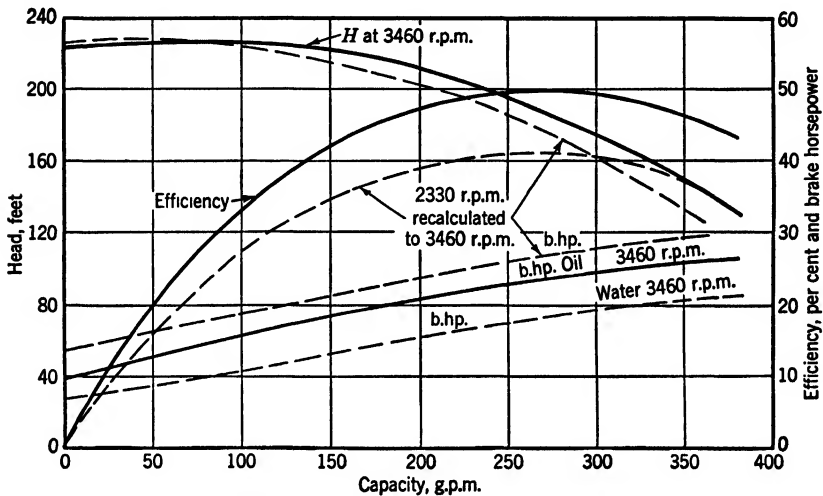


FIG. 14.14. Performance of 2-in. pump at two speeds pumping oil 825 S.S.U. ( $\nu \times 10^6 = 195$ ),  $D_2 = 7\frac{1}{4}$  in.,  $n_s = 1160$  (Ingersoll-Rand).

(2) At a constant speed the head-capacity decreases, as the viscosity increases, in such a way that the specific speed at b.e.p. remains constant (Fig. 14.15).

$$n_s = \frac{n\sqrt{Q_1}}{H_1^{3/4}} = \frac{n\sqrt{Q_2}}{H_2^{3/4}} \quad (14.1)$$

where  $Q_1$  and  $H_1$  are the capacity and head at one viscosity and  $Q_2$  and  $H_2$  the same at another viscosity. From equation 14.1 it follows that

$$\frac{Q_1}{Q_2} = \left(\frac{H_1}{H_2}\right)^{3/2} \quad (14.2)$$

This is an important relationship. Thus to estimate the b.e.p. when viscous oil is being pumped, only one experimental correction factor is necessary, either that for the head or that for the capacity; the other will follow from the relationship of equation 14.2.

† From unpublished tests by Lehigh University for Ingersoll-Rand Company.

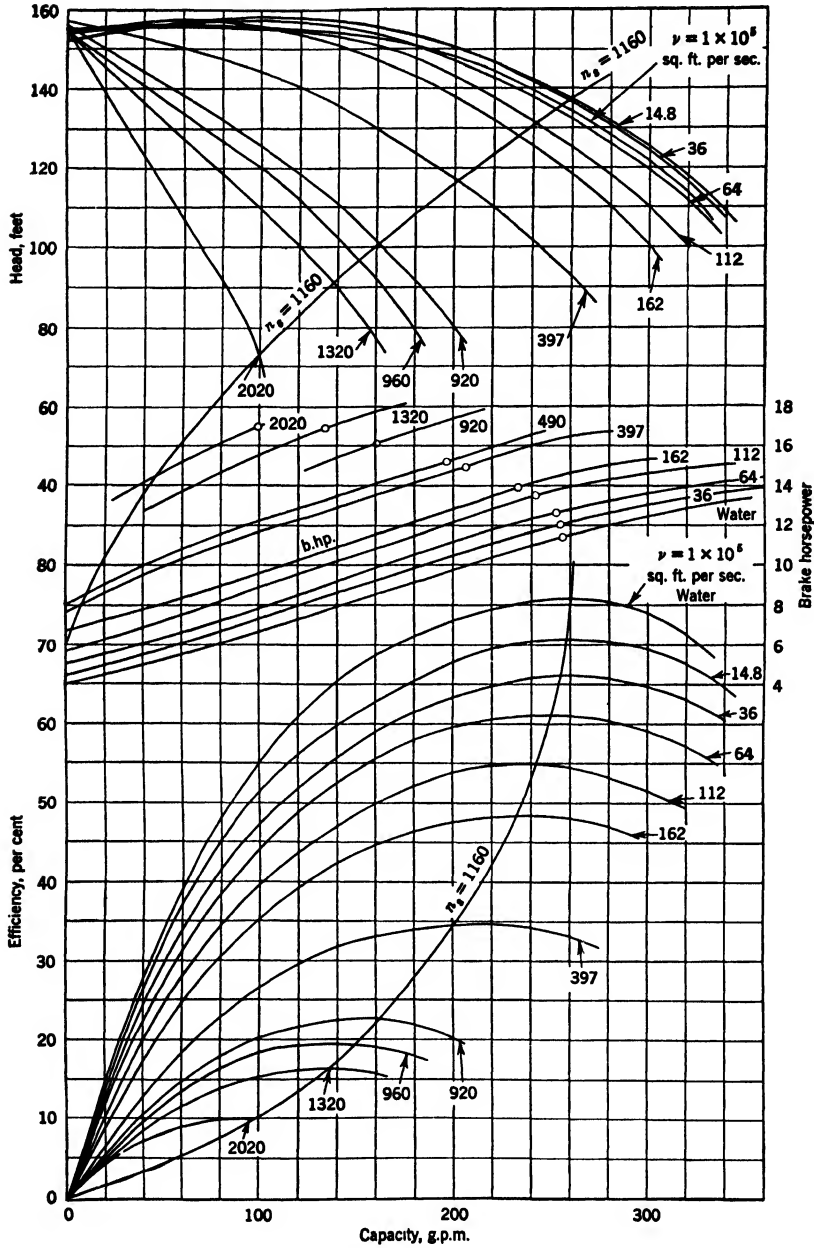


FIG. 14.15. Performance of 2-in. pump, pumping oil at 2875 r.p.m. (Ingersoll-Rand)

The following formulas are used for conversion of the oil viscosities from S.S.U. to kinematic viscosity in square feet per second.

$$\text{For S.S.U.} > 100 \quad \nu \times 10^5 = 0.237 \text{ S.S.U.} - (145/\text{S.S.U.}) \quad (14.3)$$

$$\text{For S.S.U.} < 100 \quad \nu \times 10^5 = 0.244 \text{ S.S.U.} - (210/\text{S.S.U.}) \quad (14.4)$$

To convert the kinematic viscosity from metric units in stokes (square centimeters per second) to English units (square feet per second) divide the value in stokes by  $929.03 = (2.54 \times 12)^2$ . Note that in metric units the kinematic viscosity of water at  $68^\circ\text{F.} = 1$  centistoke. In English units the kinematic viscosity of water at  $75^\circ\text{F.} = 1/10^5$  sq. ft. per sec.

(3) *At constant speed and variable viscosity the head-capacity decreases as the viscosity increases, but the head at zero capacity remains essentially the same, thus resulting in steeper head-capacity curves for higher viscosities. Therefore, it can be generalized that the shut-off head does not depend on the impeller discharge angle and viscosity of the liquid.* However, it is affected appreciably by the pump casing, more so when pumping viscous liquids than when pumping water. *For instance, if the impeller diameter is too small for the pump casing (cut impeller diameter) and there is a large gap between the impeller periphery and the volute casing cut-water, the shut-off head will be lower for higher viscosities, and the head drop at b.e.p. will be greater than for the same impeller in a normal casing.* This is due to the fact that the impeller cannot maintain a normal velocity distribution in the pump casing, because most of the shear takes place at the impeller periphery and a lower generated head results. *On the other hand, if an impeller pumping a viscous liquid is fitted too closely to the cut-water in the casing it will build up excess head—higher than with water at low capacities—because of the viscous drag.*

*It has been observed on lower specific speed pumps with closed impellers that the head, even at the b.e.p., will increase above that for water upon a slight increase of viscosity before the head begins to drop upon a further increase of viscosity. This is caused by the fact that a slight increase in viscosity suppresses the relative circulation within the impeller channels, Fig. 3.15, sufficiently to increase the generated head more than is necessary to compensate for the increased hydraulic losses through the pump.* With open impellers, owing to the absence of one of the shrouds, no such effects have been noticed. Also, in high specific speed impellers, the shrouds are relatively small and the impellers wide, and the effect of the shrouds on the head is negligible.

(4) *For a constant viscosity and variable speed, efficiency at the b.e.p. is higher at higher rotative speeds (Figs. 14.16 and 14.14).* The reason

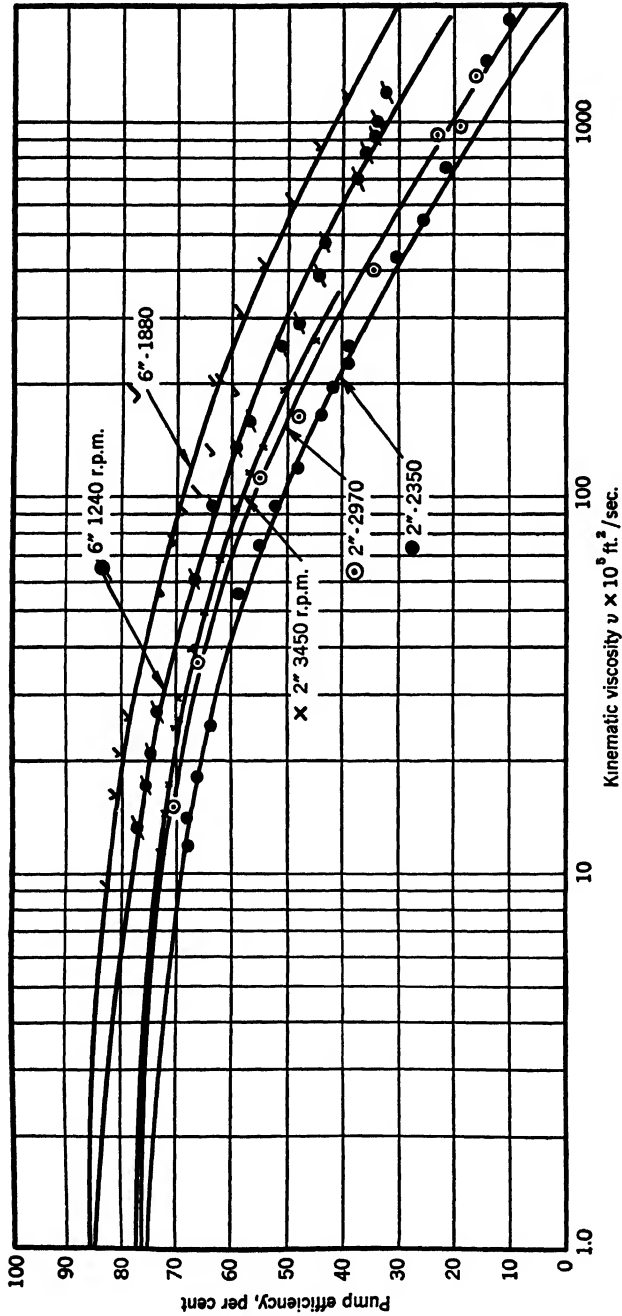


Fig. 14.16. Effect of viscosity and speed on pump efficiency at b.e.p.; 2-in. pump,  $n_s = 1160$ ; 6-in. double-suction pump,  $n_s = 2000$  (Ingersoll-Rand).

for this is that when the speed is varied the disk friction increases as the 2.5 power of the speed for viscous flow and the 2.8 power for turbulent flow, equations 10.19a and 10.20a,† while the pump output varies directly as the cube of the speed. It will be noticed in Fig. 14.14 that the reduction in brake horsepower at 3460 r.p.m. is constant for all capacities. Hydraulic losses expressed as a percentage of the total head are also lower at higher speeds; thus a higher head than would follow from the affinity laws results. This contributes to the higher efficiency at higher speeds.

(5) *From Figs. 14.14 and 14.15 it will be noticed that when viscous oils are being pumped the brake horsepower increases the same amount for a wide capacity range, the increase being the increase in disk friction loss. A slight reduction in the disk friction loss power is observed near and at the shut-off and at capacities over normal. The first is caused by a reduction of viscosity due to the temperature rise of the liquid at low capacities. The reduction of the power at capacities above normal shows the approach of cavitation at the higher rates of flow. With increasing viscosity the friction in the closely fitted running clearances between the rotating element and the stationary parts becomes increasingly important. But even an approximate determination of this loss is difficult on account of the uncertain temperature of the oil in the clearance. Since leakage through the running clearances becomes negligible at high viscosities, liquid confined between the impeller shrouds and casing walls and adjacent to the running clearances may be at a higher temperature than the pumped liquid.*

*Also, it is important to note that the brake horsepower at b.e.p. increases with viscosity. This means that, although the head and capacity drop with viscosity, the efficiency decreases more rapidly than the product of the head and capacity, as seen from the simple relationships below.*

For water

$$\frac{QH}{3960 \times e} = \text{b.hp.} \quad (14.5)$$

For an oil of specific gravity  $s_1$  and viscosity  $\nu_1$ ,

$$\frac{Q_1 H_1 s_1}{3960 \times e_1} = (\text{b.hp.})_1 \quad (14.6)$$

Then

$$\frac{QH}{e} < \frac{Q_1 H_1 s_1}{e_1} \quad (14.7)$$

† These exponents are obtained from equations 10.19a and 10.20a by multiplying both sides of these equations by the angular velocity to obtain the disk friction loss power and substituting for the Reynolds number its value  $R = ru/\nu$ .

Hence

$$\frac{Q_1}{Q} \times \frac{H_1}{H} \times s_1 > \frac{e_1}{e} \quad (14.8)$$

Letting the ratio  $Q_1/Q = F_Q$  denote the capacity correction factor, and  $H_1/H = F_H$  the head correction factor, and  $e_1/e = F_e$  the efficiency correction factor, from equation 14.8 we find

$$F_Q F_H s_1 > F_e \quad (14.9)$$

Or, utilizing the relationship from equation 14.2,

$$F_H^{5/2} s_1 > F_e \quad (14.10)$$

Equations 14.2 and 14.10 give the relative values of the correction factors for head, capacity, and efficiency, when viscous liquids are being pumped, in term of those when pumping water. The absolute values of these factors have to be determined experimentally.

**(b) Estimating Performance for Viscous Liquids.** Performance of centrifugal pumps for viscous liquids is usually estimated only for the b.e.p., correction factors based on test data being used. Two such factors are sufficient, one for the head and one for the efficiency. The capacity correction factor is determined from equation 14.2. The head and capacity for the b.e.p. having been established, the head-capacity curve is drawn by eye through the shut-off head point, which remains the same irrespective of viscosity. To complete the efficiency curve, the brake horsepower is calculated for the b.e.p., then the brake-horsepower curve is drawn by eye, the general slope of the brake-horsepower curve for water being followed. The efficiency curve is calculated from the brake-horsepower and head-capacity curves.

Figure 14.17 shows the head correction factor and efficiency (not a factor) plotted against the Reynolds number  $R = QD_2/D_2^2\nu = Q/D_2\nu$ , which is the expression given in equation 5.10 and discussed in Chapter 5. § Note that  $Q/D_2^2$  in the expression for the Reynolds number represents the velocity of flow. Numerically this quantity differs by a constant from any velocity of flow through the pump for similar

§ All variables in the expression for Reynolds' number are measured in the fundamental units: capacity  $Q$  in cubic feet per second;  $D_2$  in feet; and the kinematic viscosity  $\nu$  in square feet per second. For viscosities above 100 S.S.U., omitting the subtractive term in equation 14.3, a formula for Reynolds' number in terms of capacity in gallons per minute, the impeller diameter in inches, and viscosity in S.S.U. is obtained which is more convenient for practical use.

$$\frac{\text{g.p.m.}}{D_2 \text{ in.} \times \text{S.S.U.}} \times 11,300 = R \text{ (dimensionless)}$$

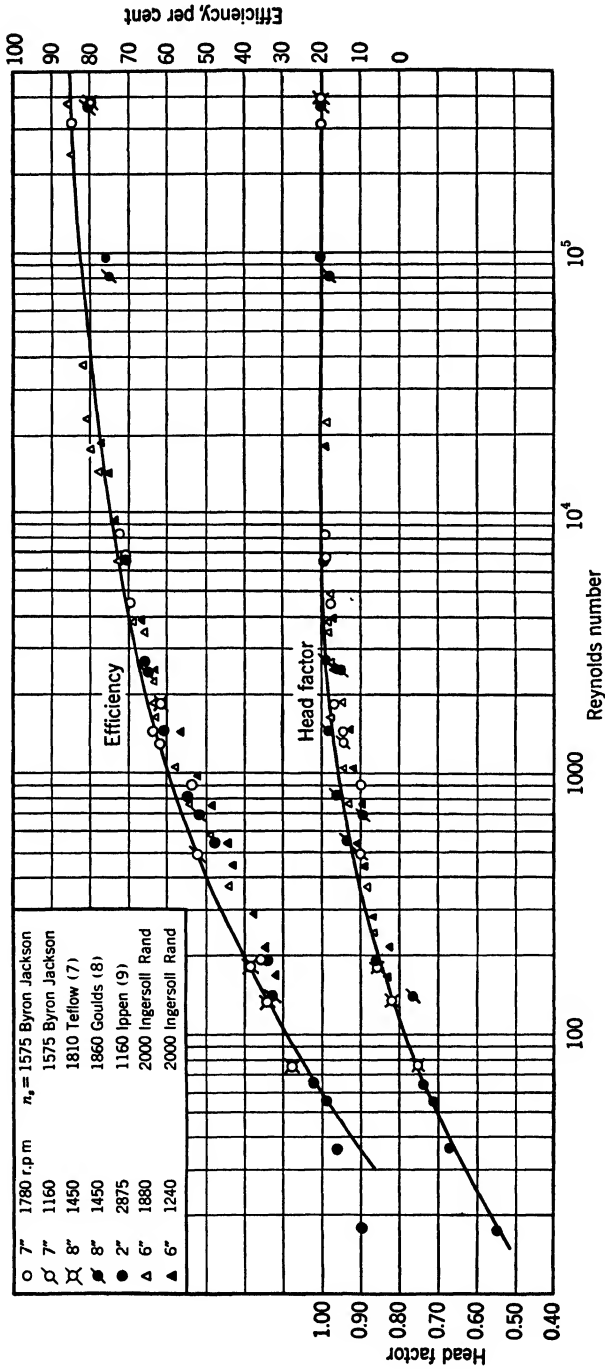


Fig. 14.17. Head and efficiency corrections for viscosity.



pumps. Use of a velocity through a definite section of the impeller or the casing passages would result only in shifting the Reynolds number scale. This would have no advantage and would not justify the complications necessary to calculate such velocities. Only recent test data on modern pumps are included in Fig. 14.17. Some older tests on pumps of obsolete design were considered but discarded.|| Efficiencies on these pumps were below par by 5 to 10 points, so it hardly could be expected that their head and efficiency variation with viscosity would be indicative of that of the average modern pump.

*It is important to realize that the Reynolds number as defined above, or any other of several Reynolds numbers possible for several sections of the channels comprising a centrifugal pump, does not possess the properties of a criterion of flow through the pump usually associated with the Reynolds number for pipe flow.* Thus the same Reynolds number does not assure the same pattern of velocity distribution or the same regime; therefore scattering of points in Fig. 14.17 must be expected. The change from laminar to turbulent flow may take place at different Reynolds numbers for different parts of the pump. Therefore there is no definite change in curvature in the curves of the head correction factors and efficiency in Fig. 14.17. It should be pointed out that Reynolds' number as used in Fig. 14.17 expresses indirectly the effect of specific speed on the head correction factor and efficiency; for a given impeller diameter, if capacity is varied, different Reynolds numbers are obtained which correspond to different specific speeds.

Several factors contribute to the inconsistency of the test data on pumping viscous liquids and scatter of points in Fig. 14.17, even for selected pumps:

(1) Variation of design elements which constitute the deviation from a "continuous row," because tested pumps are of different make and mechanical arrangement; some are of the single-suction overhung type, others are double-suction pumps.

|| A low gross efficiency of obsolete or "bad" pumps is caused by the excessive eddy losses as a result of a faulty hydraulic design. The mechanical and volumetric efficiencies and also the hydraulic skin friction loss of such pumps are essentially the same as those for modern pumps. When pumping viscous oils with obsolete pumps, pump efficiency points plot on Fig. 14.17 below those for modern pumps, the difference remaining approximately constant for all Reynolds numbers. The head correction factor curve for obsolete pumps shows a more rapid drop with decreasing Reynolds numbers than for normal pumps. It is pointed out elsewhere in this chapter that for the same Reynolds number there is no similarity of the flow pattern in centrifugal pumps. Therefore the deviation of the head correction factor from the general trend shown in Fig. 14.17 for bad pumps, with eddy losses predominant, is to be expected.

(2) In a study of losses in pipes in the turbulent region introduction of "roughness scale" was necessary to correlate satisfactorily the test data. Establishment of a similar roughness scale for pump channels is hardly possible with the available knowledge of the flow through the pump.

(3) Extreme difficulty of accurate testing of pumps handling very viscous liquids, coupled with the difference in procedure and apparatus used by different experimenters.

For a given capacity the input head  $H_i$  and Euler's head  $H_e$  are the same for all viscosities, and they depend on the impeller discharge angle only. This means that for a given capacity (for instance, the b.e.p. at a given viscosity) the impeller power input does not depend on the viscosity, and the increase in power, as compared to the power at the same capacity when pumping water, is caused solely by the increased external friction of the rotating element. If the latter could be calculated the brake horsepower and the efficiency, when viscous liquids are being pumped, could be obtained. In this way only one correction factor for the head would be necessary to predict the performance. However, accurate calculation of the disk friction and ring friction losses presents great difficulties, as temperature of the liquid in the ring and the space between the impeller shrouds and the casing walls may differ considerably from that of the pumped liquid. Therefore, in practice, estimation of the pump efficiency when pumping viscous liquids are being pumped will depend on experimental data such as shown in Fig. 14.17.

Attention is called to the fact that when viscous liquids are being pumped for a given capacity, Euler's and the input velocity triangles remain the same as for water. However, for b.e.p. both Euler's and the input triangles are different for each viscosity although specific speed  $n_s$  remains the same. Thus a complete dynamic similarity is not possible under these conditions because  $n_s = \text{constant}$  and  $R = \text{constant}$  cannot both be satisfied at the same time. When pumping water the effect of Reynolds' number is negligible, and the laws of similarity hold; but when pumping viscous liquids Reynolds' number becomes a predominant factor and dynamic similarity is impaired as viscosity is increased.

#### 14.5 REGULATION OF CAPACITY OF CENTRIFUGAL PUMPS

Pump capacity may vary for one of the following reasons: (1) change in total head, which is quite common with low head pumps taking their suction from, or discharging into, rivers, lakes, or oceans; (2) variation

in the demand, such as in boiler-feed systems; and (3) variation in supply at the pump suction, as on condensate pump service.

In the first case, particularly with low and medium specific speed pumps, there is a danger of the motor overloading if the head decreases since the b.h.p. increases with the capacity. Throttling of the pump discharge is necessary to protect the motor. On propeller pumps, the brake horsepower increases as the head is increased; therefore the motor should be selected to handle the load at the highest possible head. On the other hand, a decrease in operating head on a propeller pump will result in decreased power, and throttling will not be necessary to protect the motor.

When the demand is variable, throttling of the discharge is used to adjust the capacity to meet the demand. With low and medium specific speed pumps power is saved when the discharge is throttled. With propeller pumps, reduction of the pump capacity by throttling will increase the load on the motor and evidently it will be more economical to by-pass the excess capacity back to the suction sump. Some power can be saved by throttling the pump suction instead of the pump discharge, but the danger of cavitation makes this method unpractical.

When the supply on the pump suction is limited there is always a danger that the pump will lose prime or cavitate. Therefore it is advisable to throttle the discharge so that a minimum submergence is maintained on the pump suction. Vertical condensate pumps of the turbine type (Fig. 16.28) can operate without control of the discharge and without bad effects of cavitation.

Variable speed drives, such as steam turbines or gasoline engines, permit capacity variation by changing speed. This entails very little or no power loss, whereas throttling always wastes power. A number of means have been developed to vary pump capacity with a power saving as compared with throttling. These will be briefly described here.

Siebrecht<sup>10</sup> has studied a number of methods of varying the pump capacity, all of which proved to be unpractical for various reasons, although some of them had shown some power saving as compared with discharge throttling. The schemes tested by Siebrecht included the following.

(1) *Adjustable Diffusion Casing Vanes.* This arrangement shows an appreciable gain in efficiency at reduced capacity. The saving in power, however, is not in proportion to the gain in efficiency, as the head increases at partial capacities and the discharge must be throttled. The mechanical complications make this method unpractical in the United States. However, there are several large installations of this type in

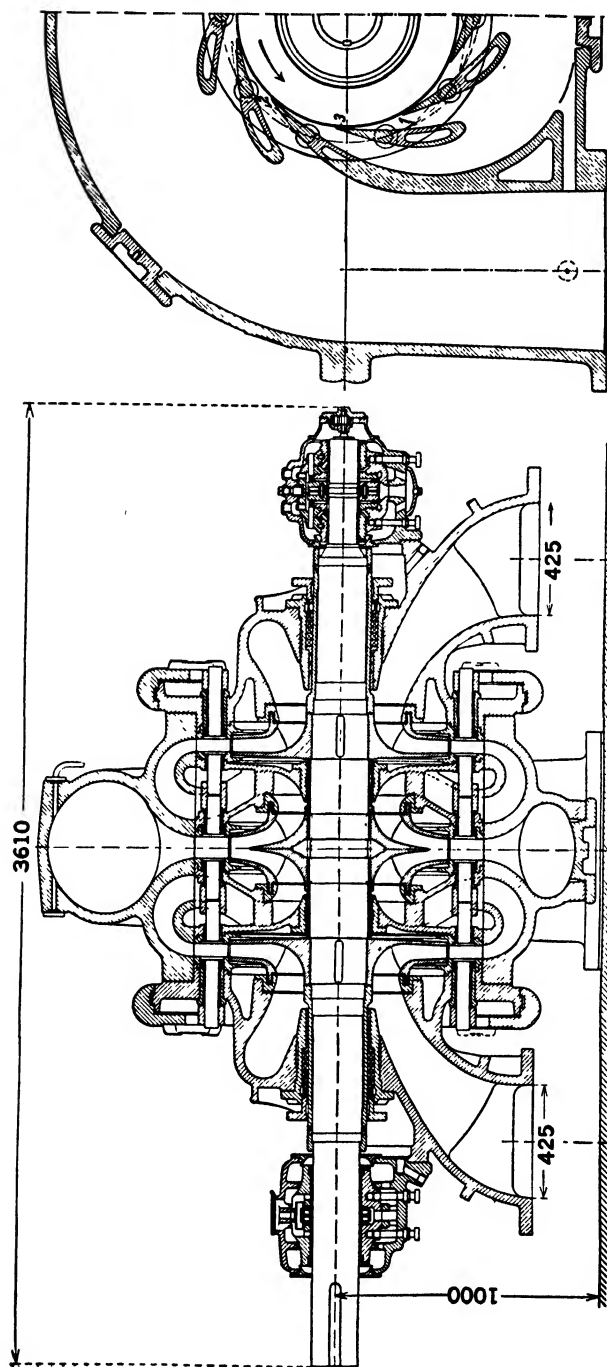


FIG. 14.18. Seventeen-inch 2-stage pump with adjustable diffuser vanes; 17,400 g.p.m., 755 ft., 1000 r.p.m.,  $n_s = 1540$ . Storage pump—ing at Schwarzenbachwerks (Escher, Wyss). (Dimensions in millimeters.)

Europe. Figures 14.18 and 14.19 show the sectional drawing and performance of one unit of this type.

(2) *Throttle between the Impeller and Diffusion Vanes.* The impeller discharge was throttled in this scheme by a cylindrical throttle inserted between the impeller discharge and the diffusion casing vane. There was no improvement in efficiency with the impeller throttled at any

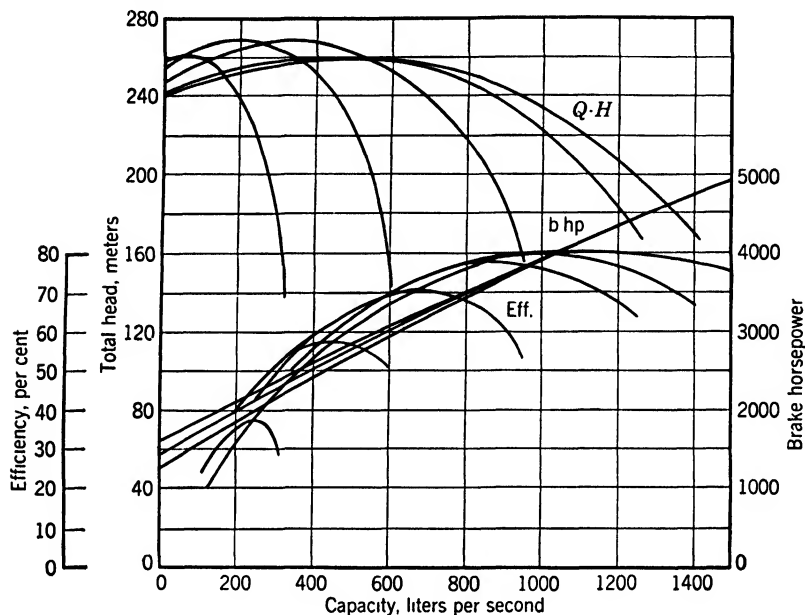


FIG. 14.19. Performance of pump shown in Fig. 14.18.

capacity. However, a small saving of power was effected by this method as the head at partial capacities was reduced more than the efficiency. This method was never tried on commercial pumps.

(3) *Admission of Air to Pump Suction.* Figure 12.7 reproduces Siebrecht's tests wherein small amounts of air were admitted to the pump suction. Danger of losing prime and objection to air in the system make this method undesirable. The author knows of isolated cases where automatic admission of air into the suction bell of vertical pumps was used to maintain the submergence as the supply to the suction sump was decreased.

(a) **Capacity Regulation at Constant Speed.** Variable capacity demand at constant motor speed can be met in one of the following ways:

(1) By providing a storage capacity and by intermittent pump operation.

(2) By dividing the maximum capacity demand among several units, and operating one or more units at a time.

(3) By throttling the pump discharge or by-passing part of the capacity. The latter method is used in preference to throttling to protect the pump when capacity varies from zero to a maximum.

Pump throttling is by far the most frequently used means to vary the pump capacity. With large units a considerable power saving can be effected by a proper selection of the pump characteristic to suit the existing requirements of the plant. Depending on whether the head on the pump varies with the capacity, and on the amount of time the pump has to operate at several capacities, location of the best efficiency point and selection of the proper slope of the head-capacity curve may make an appreciable difference in the total power cost. In the majority of cases the best characteristics can be determined only by trial calculations.

**(b) Variable Speed Drive.** This can be realized by the use of one of the following arrangements:

- (1) Steam turbine or engine drive.
- (2) Variable speed electric motors.
- (3) Constant speed electric motors with variable speed coupling.

The first method is the best as it does not involve any waste of power. Since the driver and pump efficiency vary with the speed and location of the operating point, selection of the best speed for the driver and location of the pump b.e.p. requires consideration to obtain a minimum yearly power expenditure to meet the variable capacity demand. Speed increasers or reducers between the driver and the pump frequently provide the best solution.

The direct-current electric motor is the most efficient electric drive for variable speed conditions and is widely used for marine service. Direct-current motors are not available at high speed owing to commutation difficulties.

The wound-rotor induction motor is the most common and the simplest of the electric variable speed drives. Its efficiency varies approximately directly as the speed, but since the pump output varies directly as the cube of the speed a considerable power saving can be effected with this type of drive. The shape of the head-capacity curve has some bearing on the power demand at reduced speeds as a flat  $Q-H$  curve requires less reduction in speed to meet the reduced capacity.

Speed variation of wound-rotor motors is not continuous but in steps, usually six for large motors. By selecting the speed steps to suit the requirements some saving in power can be realized.

Variable speed couplings can be of the magnetic or the hydraulic type. The economy of both types is approximately the same. The magnetic coupling needs direct current for excitation, requiring either a synchronous motor with an oversize exciter for a drive, or special excitation equipment. The hydraulic coupling speed reduction is not over 20 per cent and is less efficient than the wound-rotor induction motor.

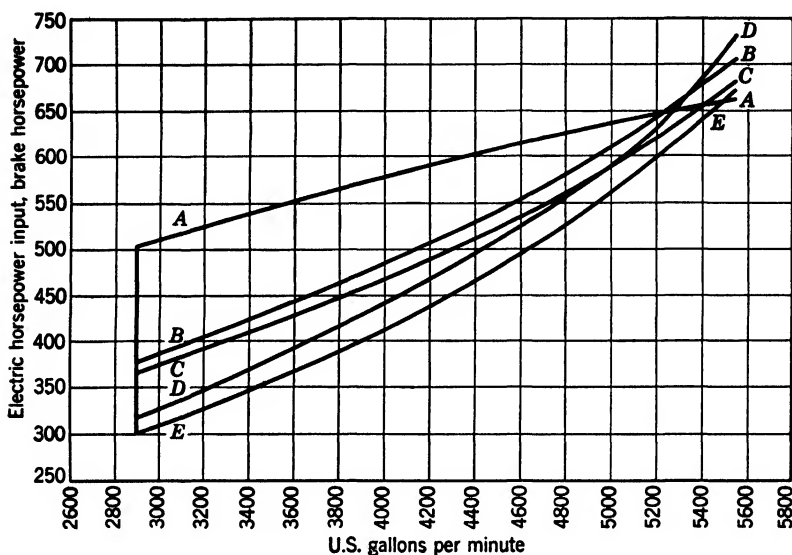


Fig. 14.20. Two double-suction pumps in series; 382 ft. total head at 1800 r.p.m.; variable capacity; constant head. Comparison of adjusting pump speed with throttling discharge. Curve A, horsepower input constant speed, throttling for reduced capacity; B, horsepower input variable speed, synchronous motor hydraulic coupling both pumps; C, horsepower input variable speed, wound-rotor induction motor; D, horsepower input variable speed, d-c. motor and rectifier using shunt field control; E, horsepower input variable speed, synchronous motor with variable speed, constant efficiency mechanical speed reducer.

Richardson<sup>11</sup> has made a study of comparative costs and relative power savings with constant and variable speed electric motor-driven units for variable capacity. Figure 14.20 is reproduced from his article. Note that curve D represents a direct-current motor drive through a rectifier from an alternating-current power source. When direct-current power is available, direct-current motors provide the most efficient variable speed drive. Curve B shows the electric horsepower input with a synchronous motor drive through a hydraulic coupling, both pumps operating at a reduced speed. However, a cheaper and more efficient arrangement is obtained by operating one pump at constant speed and

the second pump at variable speed through a coupling between the pumps. The power input will be almost exactly as shown by curve *B*, the power saving resulting from the smaller initial slip loss of a smaller coupling.

Variation of capacity of axial flow pumps with a variable pitch impeller is discussed in Chapter 16.

#### 14.6 MODEL TESTING

Models of pumps are built to obtain the desired information about the hydraulic performance of a given type of pump with a minimum expense of time and money. Model testing is resorted to in the following cases.

(a) As part of the general development of a new type of pump to be built in different sizes.

(b) To determine the pump behavior under special conditions, reproducing those existing in a new proposed plant, such as the cavitation characteristics of the pump and the effect of different arrangements of several pumps within the pumping station.

(c) For use on acceptance tests where tests on the full-size pump are impossible owing to physical limitations of the plant or economic considerations.

In general, laboratory testing of a model is more accurate than field tests on a large pump because measuring large quantities of water accurately presents some difficulties. To arrive at the head and capacity of the prototype from the model tests, affinity laws are used. It has been pointed out that the cavitation conditions are best approached by the model if the pump is tested at the same head and submergence as the prototype. If this is impossible then the model can be operated at any head and the submergence is so adjusted as to obtain the same value of the cavitation constant  $\sigma$ . Where a model is operated at the same head as the prototype, capacity varies as the square of the multiplier (ratio of impeller diameters of the model and prototype) and the speed varies inversely as the multiplier, or

$$\frac{Q_m}{Q} = F^2 \quad \text{and} \quad \frac{n_m}{n} = \frac{1}{F}$$

where  $Q_m$  and  $n_m$  are model capacity and speed, and  $F$  is a multiplier.

For accurate results, field suction and discharge conditions should be reproduced for the model testing. When this is impossible the suction and discharge should be so arranged as to make their effect negligible on the pump performance.



Experience has shown that the efficiency of large units is higher than that of their models, but there are no set rules to predict the efficiency of the prototype from the model efficiency. The Hydraulic Institute recommends that the efficiency guarantee should be made on the basis of a model acceptance test. In that case the estimated efficiency of the full-size pump may be used for estimating the motor size only.

Moody's formula<sup>12</sup>

$$\frac{1 - E}{1 - e} = \left(\frac{d}{D}\right)^{1/4} \left(\frac{h}{H}\right)^{1/10} \quad (14.11)$$

is in use in water turbine practice to estimate efficiency of a large unit from the model efficiency, and it is used occasionally by pump engineers. If the model is tested at the same head as the prototype Moody's formula reduces to

$$\frac{1 - E}{1 - e} = \left(\frac{d}{D}\right)^{1/4} \quad (14.12)$$

where  $E$  is the efficiency,  $D$  is the impeller diameter, and  $H$  is the head of the prototype, and  $e$ ,  $d$ , and  $h$  are the same variables for the model. The same formula can be used for estimating efficiency from a reduced speed test of the full-size pump, in which case  $d/D = 1$ . Although a good agreement between efficiencies obtained with Moody's formula and actual field tests were observed on many occasions, there are cases on record when the discrepancy between the two efficiencies was 1.4 points.<sup>13</sup> On one recent installation of a large centrifugal pump the prototype efficiency determined by the field test did not exceed that of the 8-in. model, which was more than 6 times smaller than the prototype.

## REFERENCES

1. W. J. RHEINGANS, "Power Swings in Hydraulic Power Plants," *Trans. A.S.M.E.*, April 1940, p. 171.
2. KARL GRÜN, *Dampfkessel-Speisepumpen*, Vienna, Julius Springer, 1934, p. 77.
3. ERICH SCHRÖDER, "Das Förderhohenverhältnis einer radialen Kreiselpumpe," Tech. Hochschule Braunschweig, doctoral dissertation, 1933; chart plotted by C. PFLEIDERER and published in *Z. Ver. deut. Ing.*, Vol. 82, No. 9, Feb. 26, 1938, p. 263.
4. R. DZIALAS, "Schwingungen bei Kreiselpumpen mit labiler Kennlinie," *Arch. Wärmewirtschaft und Dampfkesselwesen*, Vol. 22, Bull. 3, March 1941, p. 63.
5. A. J. STEPANOFF, "Determining Operating Points of Centrifugal Pumps Working on Pipe Lines," *Oil and Gas Jour.*, Dec. 4, 1941.
6. A. J. STEPANOFF, "How to Determine Performance of Engine Driven Pumps," *Power*, Nov. 1940, p. 84.
7. N. TETLOW, "A Survey of Modern Centrifugal Pump Practice," *Inst. Mech. Eng.*, 1942, pp. 121-134.

8. "A Further Investigation of the Performance of Centrifugal Pumps when Pumping Oils," Goulds Pump Inc., Bulletin 130, 1926.
9. ARTHUR T. IPPEN, "The Influence of Viscosity on Centrifugal Pump Performance," *Trans. A.S.M.E.*, Vol. 68, No. 8, 1946, p. 823.
10. WILHELM SIEBRECHT, "Beitrag zur Regelung der Kreiselpumpen," Berlin, Verein deutscher Ingenieure, 1929, Bulletin 321.
11. C. A. RICHARDSON, "Economics of Electric Power Pumping," *Allis-Chalmers Elec. Rev.*, June 1944, p. 20.
12. L. F. MOODY, "The Propeller Type Turbine," *Trans. A.S.C.E.*, Vol. 89, 1926, pp. 625, 690.
13. F. H. ROGERS and R. E. B. SHARP, "45,000 HP Propeller Turbine for Wheeler Dam," *Mech. Eng.*, Vol. 57, Aug. 1935, p. 500.

## CHAPTER 15

### SHAFT DESIGN FOR CRITICAL SPEEDS

#### 15.1 THEORETICAL RELATIONSHIPS

The pump shaft is designed to transmit the required power without vibration. Besides the torque and rotor's own weight, axial thrust and side thrust from the single-volute casing must be considered.

Theoretically, the shaft deflection should always be less than the radial clearance between the closely fitted parts of the rotating element and the stationary casing parts. In practice, however, owing to the inevitable eccentricity of the several running fits inside the pump, this condition is never fulfilled and some of the closely fitted parts serve as internal bearings. *In pumps having proper selection of materials, it has been found that when liquids such as water and hot petroleum products are being pumped, they serve as a lubricating and cooling medium for such internal bearings.*

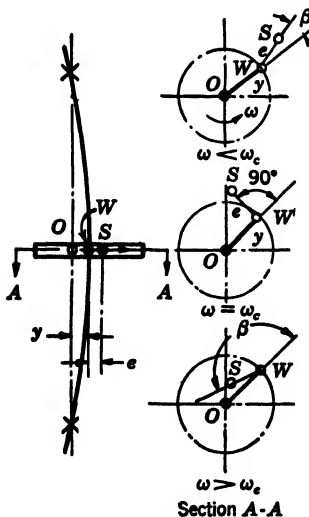


FIG. 15.1. Single load on a vertical weightless shaft.

Shaft vibration usually appears as a result of dynamic deflections which reach their maximum value at critical speeds. Even with carefully balanced rotors, there is always a residual unbalance which develops a centrifugal force, and the latter causes a dynamic shaft deflection in addition to the static deflection due to the rotor's own weight. The centrifugal force increases with the increase of deflection at higher speeds until some internal parts are damaged or the shaft fails.

**(a) Critical Speed of a Single Impeller on a Weightless Shaft.** A disk of weight  $W$  and mass  $m = W/g$  is fastened on a weightless shaft so that its center of gravity  $S$  is displaced a distance  $e$  from the axis of the vertical shaft (Fig. 15.1). If the center of the disk is deflected a distance  $y$  from the axis of rotation, then the center of gravity of the disk is displaced a distance

$y + e$  from the axis of rotation, and the centrifugal force is

$$P = m(y + e)\omega^2 \quad (15.1)$$

where  $\omega$  is the angular velocity in radians per second.

Since there is proportionality between the force and the deflection,

$$P = Ky \quad (15.2)$$

where  $K$  is a constant for a given type of load and support and is defined as a force to give a unit deflection.

Substituting equation 15.2 into equation 15.1 we get

$$m(y + e)\omega^2 = Ky \quad (15.3)$$

and

$$y = \frac{me\omega^2}{K - m\omega^2} \quad (15.4)$$

If  $\omega$  is increased so that the denominator becomes equal to zero or

$$K - m\omega^2 = 0 \quad \text{and} \quad \omega_c = \sqrt{\frac{K}{m}} \quad (15.5)$$

then  $y$  becomes infinite,  $y = \infty$ , and the shaft should theoretically break. In practice, violent vibration is observed only as the value of  $y$  is limited by the close internal fits inside the pump. *Even in machines having no closely fitted internal parts, the shaft deflection at the critical speed stays limited because (a) the critical speed, mathematically, is a point on both sides of which the shaft regains rapidly its ability to resist deflection; (b) time is necessary for the shaft to develop its maximum deflection, which may not be available when the critical speed is passed rapidly; (c) the surrounding medium causes external friction and damping; (d) internal friction of shaft material causes energy dissipation.*

$\omega_c$  is called the critical angular velocity to which a critical speed in revolutions per minute corresponds:

$$n = \frac{30\omega_c}{\pi} = \frac{30}{\pi} \sqrt{\frac{K}{m}} \quad (15.6)$$

The value of  $K$  depends on the shaft dimensions, its material, method of support, and load distribution. Thus, if  $I$  is the moment of inertia of the shaft,  $a$  and  $b$  are the distance of the disk from support, and  $E$  is the modulus of elasticity of the shaft material: then, for a freely supported shaft,

$$y = \frac{Pa^2b^2}{3EI(a + b)} \quad (15.7)$$

and

$$K = \frac{3EI(a+b)}{a^2b^2} \quad (15.7a)$$

Combining equations 15.4 and 15.5

$$y = \left( \frac{\omega^2}{\omega_c^2 - \omega^2} \right) e = \left( \frac{n^2}{n_c^2 - n^2} \right) e \quad (15.8)$$

If the operating speed  $n$  is above  $n_c$ ,  $y$  becomes negative and its value decreases. In other words, the shaft again approaches the straight line joining the two points of support. At  $n = \infty$ ,  $y = e$ , or the center of

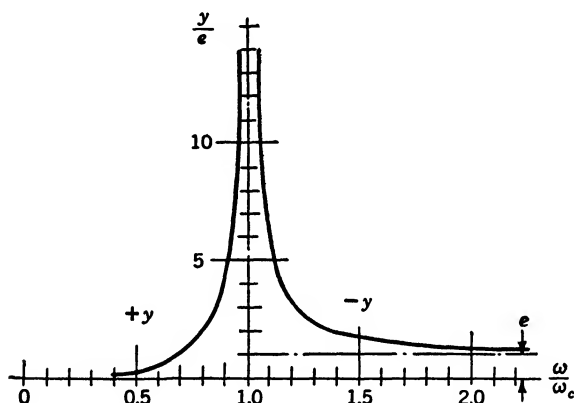


FIG. 15.2. Shaft deflections at different speeds.

gravity  $S$  is on the axis of rotation (Fig. 15.1). The location of the point of disk fastening and the center of gravity have exchanged their positions. Thus the mass  $m$  has a tendency to balance itself in the sense that above critical speed the rotating body tends to rotate about the center of gravity.

Note that equation 15.8 gives for critical speed ( $y = \infty$  or large) not a point but a belt. This is confirmed by the actual behavior of pump shafts near the critical speed (Fig. 15.2). Vibration-free operation of pumps is possible on both sides of the critical speed. A great majority of multistage pumps with mechanical seals (no support at stuffing boxes), operating at 3000 or 3600 r.p.m., operate above the critical speed.

**(b) Effect of Disk's Weight.** With a horizontal shaft, there is always a deflection  $y_0$  due to the disk's weight  $W$  directed downward (Fig. 15.3). The center of gravity  $S$  of the disk describes now a circle with a center  $O'$  below the line connecting the two shaft supports by

$y_0$ . The radius of the circle is  $y + e$ , and the result of the above deductions remains the same. Thus, a given shaft has the same critical speed when operated horizontally, vertically, or at any angle. The dynamic deflection due to centrifugal force is superimposed upon the static deflection of a horizontal shaft.

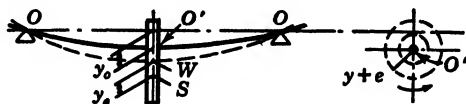


FIG. 15.3. Single load on a horizontal shaft.

**(c) Connection between the Shaft Deflection Due to the Disk Weight and the Critical Speed.** The deflection due to the disk's weight can be found from equation 15.2.

$$W = Ky_0 \quad (15.9)$$

From this the value of the shaft constant  $K$  can be found.

$$K = \frac{W}{y_0} \quad (15.10)$$

By substituting this value of  $K$  in equation 15.5 we obtain

$$\omega_c = \sqrt{\frac{W}{y_0 m}} = \sqrt{\frac{g}{y_0}} \quad (15.11)$$

where  $W$  is the disk weight, and  $m$  is the disk mass,  $m = W/g$ . Note that the value of the shaft's static deflection  $y_0$  due to the weight of the disk is a measure of the shaft elastic properties only. The actual value of the shaft's static deflection under operating conditions may be different, but the critical speed remains the same. Thus, if the same shaft is operated vertically,  $y_0 = 0$ . There may be an additional deflection due to belt pull or, if the shaft is operated submerged, as in a centrifugal pump, there is a force of buoyancy directed upward reducing the actual shaft deflection, but in all cases the critical speed is the same as that given by equation 15.11. Also, if the actual deflection of the shaft is limited inside the pump by the internal running clearances to less than  $y_0$ , the critical speed remains the same, unless the clearance is so small that it becomes an internal bearing.

In a centrifugal pump there is a number of factors which reduce the amplitude of vibration at the critical speed. A number of closely fitted running clearances act as dampers. If the clearance of one of them, say at the middle of the shaft, is gradually reduced, the amplitude of vibration will be reduced

further until it disappears entirely. At this point, this part becomes an internal bearing, and the critical speed is found as in the case of a three-bearing shaft.

**(d) A Perfectly Balanced Shaft.** In a perfectly balanced shaft the center of gravity of the rotor coincides with the axis of rotation; thus  $e = 0$ . Then equation 15.3 becomes

$$m\omega^2 = Ky \quad (15.12)$$

Conditions represented by equation 15.12 show that the shaft is in indifferent equilibrium, a state in which the centrifugal force developed is balanced by the elastic forces at any value of  $y$ , or the smallest force may, if allowed sufficient time, deflect the shaft to infinity or break it. The deflecting force is usually supplied by the unavoidable deviation of the centers of gravity of the various loads from the center line of the shaft. Conditions of indifferent equilibrium represented by equation 15.12 can occur only at the critical speed, because equation 15.12, when  $y \neq 0$  reduces to

$$m\omega^2 = K \quad (15.13)$$

which is the same as equation 15.5 defining the critical speed.

**(e) The Period of Natural Vibration and the Critical Speed.** From equation 15.5 the number of revolutions per second at the critical speed is

$$n_c = \frac{1}{2\pi} \sqrt{\frac{K}{m}} \quad (15.14)$$

This is also the formula for the period of natural transverse vibration of the same rotor. Thus, at the critical speed, the shaft vibrations are synchronized with the natural period of vibration of the shaft.

It is possible to determine the critical speed of a rotor by observing the natural period of transverse vibration of the rotor with some vibration indicating device, and setting up vibration by a hammer blow.

**(f) Several Disks on a Weightless Shaft.** The following simple case will be considered (Fig. 15.4).

A shaft of length  $4l$  carries two disks each a distance  $l$  from the nearest bearing. Apparently both forms of the elastic curve,  $A$  and  $B$ , are possible. For the first critical speed, the rotating masses arrange themselves so that the deflection is a maximum

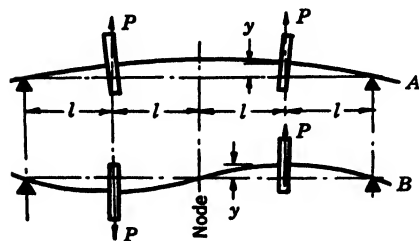


FIG. 15.4. Elastic curves with two loads.

(curve A). The points of zero deflection can occur only at the bearings. In other words there are no nodes (points of zero deflection, curve B) between the bearings at the first critical speed. These are dynamic deflections due to centrifugal forces which are superimposed upon the static deflection of the shaft. Evidently centrifugal forces are different in two cases, and the values of  $K$  are different for the two deflection curves. Owing to symmetry, equations developed for a single disk can be applied.

Case A:

$$y = \frac{4 Pl^3}{3 EI} \quad K_1 = \frac{3 EI}{4 l^3} \quad \omega_{c1}^2 = \frac{K_1}{m} \quad (15.15)$$

Case B:

$$y = \frac{1 Pl^3}{6 EI} \quad K_2 = \frac{6 EI}{l^3} \quad \omega_{c2}^2 = \frac{K_2}{m} \quad (15.16)$$

$$\frac{\omega_{c1}^2}{\omega_{c2}^2} = \frac{K_1}{K_2} = \frac{1}{8} \quad (15.17)$$

Thus with two loads two critical speeds are possible. Their ratio is  $1:\sqrt{8}$  for load locations, as in Fig. 15.4.

The result is not changed provided eccentricity of the center of gravity of the loads is provided for, if the eccentricity is small in comparison with the shaft deflection.

In the case of two disks of different weights and mounted in any possible way, the numerical values will change, but in every case there will be two critical speeds, the first and the second with deflection curves similar to A and B on Fig. 15.4. Similarly, with three loads there will be three critical speeds and with twelve loads, twelve critical speeds. In multistage pumps, if the weight of the shaft is considered in addition to the impellers, an unlimited number of critical speeds is possible. In practice it is possible to observe only a few.

*In general, irrespective of the number of loads on the shaft and their distribution, the first critical speed always corresponds to the period of natural transverse vibration of the rotating element. At speeds above the first critical speed, the center of gravity of the rotor approaches the axis of rotation, and thus the shaft tends to straighten itself. Also, at the first critical speed, the shaft's dynamic deflection is a maximum and there are no nodes between the two supports of the shaft.*

With several loads the value of the critical speed does not depend on the magnitude and on the location of the eccentricities of the individual loads (Stodola<sup>1</sup>).



### 15.2 MAIN FACTORS AFFECTING THE CRITICAL SPEED

**(a) Effect of Liquid.** Practically all textbooks and treatises on critical speeds deal with steam turbine or gas blower rotors. The operation of centrifugal pumps differs from that of these machines in that (1) the pumped liquid exerts a definite damping effect on the shaft vibrations; (2) there are a number of closely fitted parts inside the pump which reduce, or limit, the amplitude of vibrations or serve as bearings; (3) *stuffing boxes of modern pumps serve as perfect bearings, and thus reduce the span of the shaft between the supports.* Everyday experience has shown that a great many pumps which vibrate when the running clearances are worn stop vibrating when the clearances are restored.

**(b) Force of Buoyancy.** Although the weight of the rotating element when submerged in water is reduced by the amount of the displaced water, its mass is not changed. Therefore, the critical speed (equation 15.5) stays the same. The force of buoyancy should be considered an external force, like belt pull, which does not change the properties of the revolving mass or the shaft elastic constant.

**(c) Damping Effect of Liquid.** The liquid in the pump casing presents some resistance to the vibration of the rotating element. Part of the kinetic energy of the vibrating shaft is continuously absorbed by the surrounding liquid. As a result, the amplitude of vibrations is reduced. The closely fitted parts, if they do not serve as bearings, tend to dampen the vibrations since at each cycle liquid is squeezed from one side and drawn in at the other. Special tests run by Stodola<sup>1</sup> have shown that a shaft having appreciable vibration at the three observed critical speeds had its amplitude reduced as soon as the flume containing the shaft was gradually filled with water, and finally vibration could hardly be detected.

**(d) Stuffing Boxes.** By far the greatest effect on the critical speed of pumps is due to stuffing boxes. A number of pumps which vibrated at the critical speeds when operated with mechanical seals (no shaft support at stuffing box) stopped vibrating entirely when operated with the stuffing boxes packed. If the stuffing boxes are considered as bearings, the calculated critical speeds are usually found to be above the operating speeds in the majority of cases (above 3600 r.p.m.) and no other vibrations appear.

As a result of the factors just discussed, centrifugal pumps are essentially trouble-free from critical speeds or vibrations; however, introduction of mechanical seals, increase of operating speeds (6000 r.p.m. and over), reduction of shaft sizes, and the like may create conditions in which critical speeds may appear. *Sometimes these critical speeds are of*





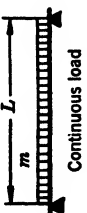
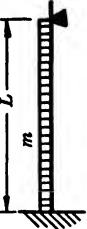
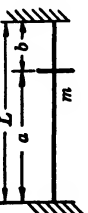
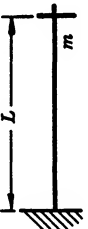
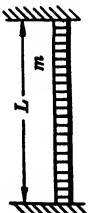
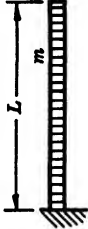
	$\omega_{c1}^2 = \frac{3EI}{ma^3b^3}$		$\omega_{c1}^2 = \frac{3EI}{ma^2L}$
	$\omega_{c1}^2 = \frac{6EI}{ma^3(3L-4a)}$ $\frac{\omega_{c1}^2}{\omega_{c2}^2} = \frac{(L-2a)^2}{L(3L-4a)}$		$\omega_{c1}^2 = \frac{12EI}{ma^3b^2(3L+b)}$
	$\omega_{c1}^2 = \frac{98EI}{mL^3}$ $\omega_{c1} : \omega_{c2} : \omega_{c3} = 1 : 4 : 9$		$\omega_{c1}^2 = \frac{237EI}{mL^3}$ $\omega_{c1} : \omega_{c2} : \omega_{c3} = 1 : 3.24 : 6.76$
	$\omega_{c1}^2 = \frac{3L^3EI}{ma^3b^3}$		$\omega_{c1}^2 = \frac{3EI}{mL^3}$
	$\omega_{c1}^2 = \frac{502EI}{mL^3}$ $\omega_{c1} : \omega_{c2} : \omega_{c3} = 1 : 2.78 : 5.45$		$\omega_{c1}^2 = \frac{12.4EI}{mL^3}$ $\omega_{c1} : \omega_{c2} : \omega_{c3} = 1 : 6.3 : 17.5$

FIG. 15.5. Critical speeds for simple loadings.

*secondary nature and are induced by a number of factors not entering into calculation of the first or higher critical speeds and, therefore, they are difficult to predict. Solutions of such cases present some difficulties, as there is no easy way to identify some of the causes and some of them are not easily removed. Some of the factors causing secondary vibrations are discussed later.*

### 15.3 CALCULATION OF CRITICAL SPEEDS

**(a) The First Critical Speed.** The first critical speed can be calculated by using equation 15.5.

$$\omega_c^2 = \frac{K}{m} \quad (15.18)$$

where  $m$  is the mass of the rotating element and  $K$  is the shaft elastic constant which depends on the shaft dimensions, material, and method of support and loading. From equation 15.2

$$K = \frac{P}{y}$$

For concentrated loads on a weightless shaft,  $K$  can be found by substituting for  $P$  the weight of the rotating masses and for  $y$  the static deflection  $y_0$  under these weights. By substituting the value of  $K$  thus found, equation 15.5 becomes

$$\omega_c^2 = \frac{g}{y} \quad (15.19)$$

*With uniformly distributed loads (shaft weight) the load on the shaft due to centrifugal forces is different from the static load distribution; therefore, the value of  $K$  is different, and is higher than for static loads only. Also, with a two-bearing shaft, an overhung load, such as a coupling, increases the dynamic deflection whereas the static deflection is reduced by the overhung load.*

*These cases demonstrate that the static deflection is used for determination of the shaft elastic constant only for concentrated loads and has nothing to do with the critical speeds. With distributed loads, the dynamic deflection is used only for calculating the shaft elastic constant. Its absolute value varies with the speed as shown by equation 15.4 and Fig. 15.2, whereas the shaft constant  $K$  and the critical speed are fixed quantities. Formula*

15.19 can be used for any kind of loading with an experimental factor, the maximum static deflection  $y_0$  being used.

$$\omega_c = \sqrt{C \frac{g}{y_0}} \quad (15.20)$$

For a two-bearing supported shaft the coefficient  $C$  is

$$1 < C < 1.2685 \quad (15.21)$$

The higher value applied to a uniformly loaded shaft (shaft's own weight), and  $C = 1$  for concentrated loads, a maximum value of the shaft deflection being used. For multistage centrifugal pumps,  $C = 1.08$  according to Bauman (Holba,<sup>3</sup> p. 19). The factor  $C$  accounts for the difference between the static and dynamic load distribution resulting from the fact that near the bearings centrifugal forces have a smaller effect on the shaft deflection.

Static deflections can be determined by methods found in the textbooks on strength of materials. Solution of simple cases is given in Fig. 15.5. *With one or two impellers and a symmetrical shaft of uniform section, the maximum deflections due to shaft weight and impellers occur in the middle of the shaft. Therefore,  $y_0$  can be found separately for the shaft and impellers and added to obtain the maximum static shaft deflection.*

When shafts are of variable diameter and the load distribution is not uniform, it is very laborious to calculate the static deflection of the shaft. Graphical methods developed by strength of material studies are used. However, for a general case, the use of maximum static deflection is not accurate for critical speed calculation, and the constant  $K$  is determined for dynamic loading at an arbitrary speed, the static shaft deflection for calculation of centrifugal forces being used as a first approximation.

**(b) Dunkerley's Formula.** Dunkerley in England has found by extensive experiments that for several concentrated loads and a shaft freely supported on two bearings the critical speed is very accurately expressed by the following formula (15.22).

$$\frac{1}{\omega_c^2} = \frac{1}{\omega_s^2} + \frac{1}{\omega_1^2} + \frac{1}{\omega_2^2} + \text{etc.} \quad (15.22)$$

where  $\omega_c$  is the critical speed of the system

$\omega_s$  is the critical speed of the shaft alone

$\omega_1$  is the critical speed of the weight (1) on a weightless shaft

$\omega_2$  is the critical speed for the disk (2), and so on.

By using formula 15.19 for the individual loads and dividing the shaft into several concentrated loads, Dunkerley's formula reduces to

$$\omega_c^2 = \frac{g}{\Sigma y} \quad (15.23)$$

Evidently, the critical speed of the system is lower than the critical speed due to individual loads.

If the shaft diameter is variable, Dunkerley's formula is applied either by substituting a shaft of uniform section (which will reduce the accuracy of the results) or by dividing the shaft into a number of parts and substituting concentrated loads for the several sections of the shaft.

#### 15.4 EXAMPLE OF GRAPHICAL DETERMINATION OF THE CRITICAL SPEED

When the problem involves several concentrated loads and a stepped shaft freely supported on two bearings, a general solution is possible by a graphical method employing successive approximations.

Use is made of the conditions prevailing at the critical speed, namely, that in a balanced shaft centrifugal forces balance the shaft elastic forces at all deflections. This equilibrium is reached for a definite elastic curve. It is also maintained when the deflections for all points are either increased or reduced in the same ratio, as internal stresses and centrifugal forces are proportional to the deflections.

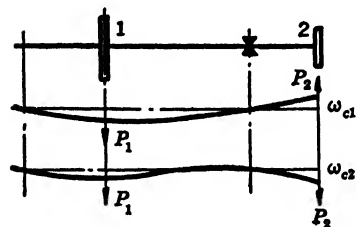


FIG. 15.6. Elastic curves with overhanging load.

The static shaft deflection curve is used as a first approximation for the calculation of centrifugal forces. However, the static deflection curve, as obtained by graphical statics methods, should be modified if there is an overhanging load such as a coupling.

For the first critical speed calculations the zero deflections (nodes) can occur only at the bearings, so that, with a two-bearing shaft, if there is an overhanging load (a heavy coupling on a long shaft extension) it must be replaced with one acting in an opposite direction from the loads between the bearings. Figure 15.6 shows the dynamic deflection curves for two loads. The first one, corresponding to the first critical speed  $\omega_{c1}$ , shows a greater deflection than the second curve which occurs at the second critical speed  $\omega_{c2}$ . At the first critical speed, the dynamic deflection due to loads between the bearings and overhung loads are

180 degrees apart. This curve prevails between the first and second critical speeds.

The graphical determination of the first critical speed includes the following steps.

(a) A moment diagram is drawn by Mohr's method, used in graphical statics. For this, several concentrated loads are substituted for the shaft's weight.

(b) The moment diagram is corrected for variation of the shaft diameter.

(c) The static deflection curve is drawn, the corrected moment diagram being used.

(d) Centrifugal forces are calculated on the basis of an assumed arbitrary speed; with these centrifugal forces being used as concentrated loads, the dynamic deflections are found by following the same procedure.

(e) The critical speed is calculated by making use of the equilibrium conditions between the centrifugal forces and the shaft elastic forces for a balanced shaft at the critical speed.

**(a) Static Curve-Moment Diagram (Fig. 15.7).** Choose a suitable scale for drawing the essential features of the shaft. In the example, 1 in. = 4 in. is used. Vectors are used to represent the loads and reactions as shown. If the weight of the shaft is to be included, it is subdivided into sections and the weights of these sections are considered as concentrated loads located at their respective centers of gravity. The direction of the vectors representing overhung loads are reversed to get the maximum shaft deflection used for calculation of the first critical speed. The loads are lettered *BA*, *BC*, *CD*, and so on, starting from the left and proceeding in a clockwise direction until the extreme right end load is labeled. Next the reactions are lettered in a similar fashion, the clockwise direction around the length of the shaft (*AR* and *RQ*) being maintained.

Beneath the shaft and to the right, locate a vertical line (*AQ*) on which to place the load vectors. Using a force scale that will give a conveniently sized diagram (1 in. = 100 lb.), the loads are scaled off on the vertical line (*AQ*) in alphabetical order and labeled. The diagram is completed by measuring a pole distance to the right of *AQ* (pole distance = 5 in.) and drawing the rays *AO*, *BO*, *CO*, and so on. The pole distance may be any convenient length that will give a convenient scale for the moment diagram which follows. The moment scale is equal to the shaft scale times the force scale times the pole distance (moment scale 1 in. =  $4 \times 100 \times 5 = 2000$  lb.-in.).

From the loads and the reactions on the shaft drawing, vertical lines

are extended down. Then starting with ray  $AO$ , a line parallel to it ( $A'$ ) is drawn between reaction  $AR$  and load  $BA$ . Next  $BO$  is transferred and placed between  $AB$  and  $BC$  and adjoining  $A'$ . Following the clockwise rotation, the rest of the rays are transferred until  $QO$  is drawn between load  $PQ$  and reaction  $QR$ . The figure is now closed by drawing a line between reactions  $AR$  and  $RQ$  to the ends of the exposed rays.

The value of the moment at any point on the shaft is the vertical distance between the boundaries to the scale as determined before.

**(b)  $M/EI$  Diagram.** The moment diagram is revised by dividing the moment values by the moment of inertia at the point and by the modulus of elasticity of the shaft (steel,  $E = 30 \times 10^6$ ). A tabular arrangement as shown is helpful.

At all the points where a change in cross section takes place, and at in-between points where necessary, the moments are scaled and tabulated. These are then divided by the moment of inertia at the point and by  $E$ , and the resulting  $M/EI$  values are also listed.

In the example, the moment at point 1 is 600 lb.-in., and  $EI$  is  $27.5 \times 10^6$  and  $57.6 \times 10^6$ . This gives two  $M/EI$  values for the point,  $16.0/10^6$  and  $10.3/10^6$ .

To draw the diagram, a horizontal line is located under the moment diagram and the various values for  $M/EI$  are plotted to any scale upwards from their respective points. The figure is closed by connecting the tips of the vectors in the proper order. (1 in. =  $10/10^6$  in.)

With a uniform shaft, the  $M/EI$  diagram has the same shape as the moment diagram, but the vertical distances have a slightly different meaning.

**(c) Slope Diagram.** In order to get the slope curve, it is first necessary to get the midpoints of the subdivisions used in the  $M/EI$  diagram. These points ( $a$ ,  $b$ ,  $c$ , and so on) are then projected horizontally to the right until they meet  $AQ$  extended. After locating another pole distance or using the same one as before, rays  $a'O'$ ,  $b'O'$ ,  $c'O'$ , and so on, are drawn. Following the same procedure used in getting the moment diagram, the slope curve is obtained by transferring the rays over to their respective divisions, ray  $a'O'$  to  $a''$ ,  $b'O'$  to  $b''$ , and so on.

The scale is the product of the drawing scale times the pole distance times the  $M/EI$  scale. (Example: slope scale, 1 in. =  $4 \times 7.5 \times 10/10^6 = 3/10^4$ .)

**(d) Static Deflection Diagram.** The subdivision midpoints used in getting the slope curve are extended down until they meet the slope curve ( $aa''$ ,  $bb''$ ,  $cc''$ , and so on). Following the method used before, the points are next projected horizontally to the right to  $AQ$  extended







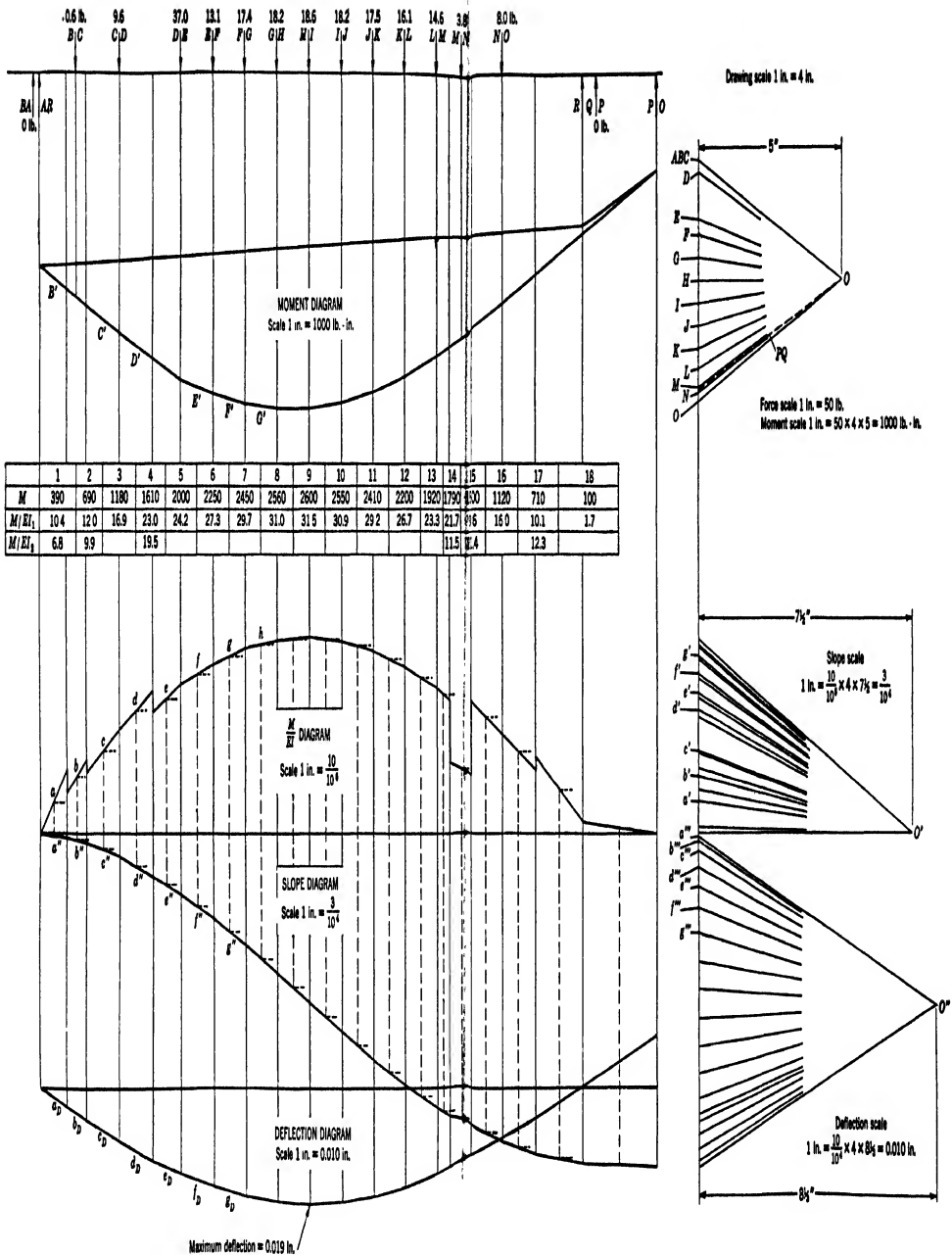


FIG. 15.8. Dynamic deflection curve due to centrifugal forces.



( $a'''$ ,  $b'''$ ,  $c'''$ ). The polygon is closed by locating an appropriate pole distance to the right and drawing the rays  $a'''O''$ ,  $b'''O''$ , and so on. This fixes the deflection scale which is now equal to the drawing scale times the pole distance times the slope scale (deflection scale,  $1 \text{ in.} = 4 \times 8.33 \times (3/10^4) = 0.010''$ ). The deflection curve itself is obtained by transferring the rays  $a'''O''$ ,  $b'''O''$ , and so on, over to their proper subdivisions as lines  $a$ ,  $b$ ,  $c$ , and so on.

Since the shaft deflection is zero at the bearings, a line is drawn through them to represent the straight shaft. The vertical distance between this line and the curve is the deflection at the point to the scale determined by the pole distance.

(e) **Dynamic Deflection (Fig. 15.8).** The dynamic deflection curve is caused by the centrifugal forces developed by the various loads instead of the load itself. Therefore the loads are replaced by the new values which are calculated with

$$P = \frac{W}{g} \omega_0^2 y_0 \quad (15.24)$$

where  $W$  = weight

$\omega_0$  = any assumed angular velocity

$y_0$  = static deflection at  $W$ .

For instance, with load  $BC$ ,  $W = 3.8$ ,  $y_0 = .00573 \text{ in.}$ ,  $\omega_0 = 100 \text{ rad per sec.}$ ,  $g = 386 \text{ in. per sec. per sec.}$

$$P = 0.6 \text{ lb.}$$

By using centrifugal forces a new deflection curve is obtained graphically in the same manner in which the static curve was derived. The only difference that may be encountered is that because the old scales may be too small to accommodate the smaller weight, new scales may have to be used.

The new dynamic deflections  $y$  will not agree with the deflections on the static curve taken as a first approximation for the calculation of centrifugal forces, because  $\omega_0$  was assumed arbitrarily and is not a critical angular velocity. But if the angular velocity is increased to  $\omega_c$  selected so that

$$\frac{\omega_c^2}{\omega_0^2} = \frac{y_0}{y} \quad (15.25)$$

then  $\omega_c$  will be the critical speed.

$$\omega_c = \omega_0 \sqrt{\frac{y_0}{y}} \quad (15.26)$$

Equation 15.25 is true because at the critical speed the centrifugal forces are proportional to the square of the speed and are balanced by elastic forces at any deflection.  $\omega_c$  should be constant for all corresponding points on the static and dynamic deflection curves. Should the discrepancy be too great, the procedure should be repeated, this time using the  $y$  curve for calculating the centrifugal forces. The second approximation is very seldom justified.

The critical speed in the example is calculated by using equation 15.26.

$$\omega_c = 100 \sqrt{\frac{0.0297}{0.019}} = 125 \text{ rad. per sec.} \quad \text{or} \quad 1195 \text{ r.p.m.}$$

Experimentally the critical speed was observed to be about 1300 r.p.m.

The discrepancy between the observed and calculated critical speeds is explained by the stiffening effect of the shaft sleeves and the impeller hubs although the shaft nuts were loose during these tests.

**(f) The Same Example Using Dunkerley's Formula.** The weight of the shaft is distributed among the loads in the same manner as for the graphical solution. An average diameter is found for calculations by

$$d = \frac{d_1 l_1 + d_2 l_2 + \cdots}{L} \quad (15.27)$$

where  $d$  and  $l$  are diameter and length of shaft sections with constant diameter.

$d$	$l$	$dl$
$2\frac{1}{4}$	$3\frac{3}{4}$	8.44
$2\frac{1}{2}$	$2\frac{3}{4}$	6.87
$2\frac{5}{8}$	$9\frac{1}{4}$	24.25
$2\frac{3}{4}$	$41\frac{3}{4}$	115.0
$3\frac{1}{8}$	$3\frac{1}{2}$	10.93
$2\frac{5}{8}$	$9\frac{1}{8}$	23.95
$2\frac{1}{2}$	$6\frac{5}{8}$	16.55
$L$	$76\frac{7}{8}$	205.99

$$d = \frac{206}{76\frac{7}{8}} = 2.68$$

To get the individual deflections use the formula from the first example in Fig. 15.5:

$$y = \frac{Wa^2b^2}{3EIL} \quad (15.28)$$

The critical speed is obtained from formula 15.23. Calculations of  $\Sigma y$  are tabulated below.

$W$	$a$	$b$	$(ab)^2$	$W(ab)^2$
3.8	5	$71\frac{7}{8}$	129,000	$0.50 \times 10^6$
27.9	$11\frac{1}{8}$	$65\frac{3}{4}$	535,000	15.0
64.9	$19\frac{3}{4}$	$57\frac{1}{8}$	1,270,000	82.5
20.1	$24\frac{3}{4}$	$52\frac{1}{2}$	1,540,000	30.9
24.2	$28\frac{7}{8}$	48	1,920,000	46.5
24.2	$33\frac{3}{8}$	$43\frac{1}{2}$	2,110,000	51.1
24.2	$37\frac{7}{8}$	39	2,190,000	53.0
24.2	$42\frac{3}{8}$	$34\frac{1}{2}$	2,140,000	51.8
24.2	$46\frac{7}{8}$	30	1,980,000	48.0
24.2	$51\frac{3}{8}$	$25\frac{1}{2}$	1,650,000	40.0
25.2	$55\frac{7}{8}$	21	1,380,000	34.8
7.6	$59\frac{3}{8}$	$17\frac{1}{2}$	1,080,000	8.2
23.3	$65\frac{5}{8}$	$11\frac{1}{4}$	544,000	12.7
348.0	$76\frac{7}{8}$	$76\frac{7}{8}$		$475.0 \times 10^6$

$$I = \frac{\pi}{64} \times (2.68)^4 = 2.53$$

$$\Sigma y = \frac{\Sigma W a^2 b^2}{3 E I L} = \frac{475 \times 10^6}{3 \times 30 \times 10^6 \times 2.53 \times 76.875} = 0.0271 \text{ in.}$$

$$\omega_c = \sqrt{\frac{386}{\Sigma y}} = 119 \text{ rad. per sec.} \quad \text{or} \quad 1140 \text{ r.p.m.}$$

**(g) Approximate Formula for Pump Shafts.** When the method of support, load distribution, and the shaft diameter varies little, as in a multistage pump, it is possible to obtain a quick approximation of the first critical speed by using a formula with an experimental factor of the type

$$y = \frac{W L^3}{C E I} \quad \text{and} \quad \omega_{c1} = \sqrt{\frac{g}{y}} \quad (15.29)$$

where  $W$  is total weight of the rotating element, in pounds

$L$  is the bearing span of the freely supported shaft, in inches

$E$  is 30,000,000 lb. per sq. in. for steel

$I$  is the average moment of inertia of shaft section, in in.<sup>4</sup>

$C$  is a numerical constant to account for the method of support, load distributions, and so on.

For a single load,  $C = 48$  (from Fig. 15.5); for a uniformly loaded shaft,  $C = 98$ ; for all intermediate cases values of  $C$  lie between these

limits. Figure 15.9 shows values of  $C$  calculated for a different ratio of the weights of the shaft and the impellers, and for different impeller spacings ( $L_1$ , the distance between two extreme impellers) and the shaft span. The weight of all impellers is assumed to be uniformly distributed

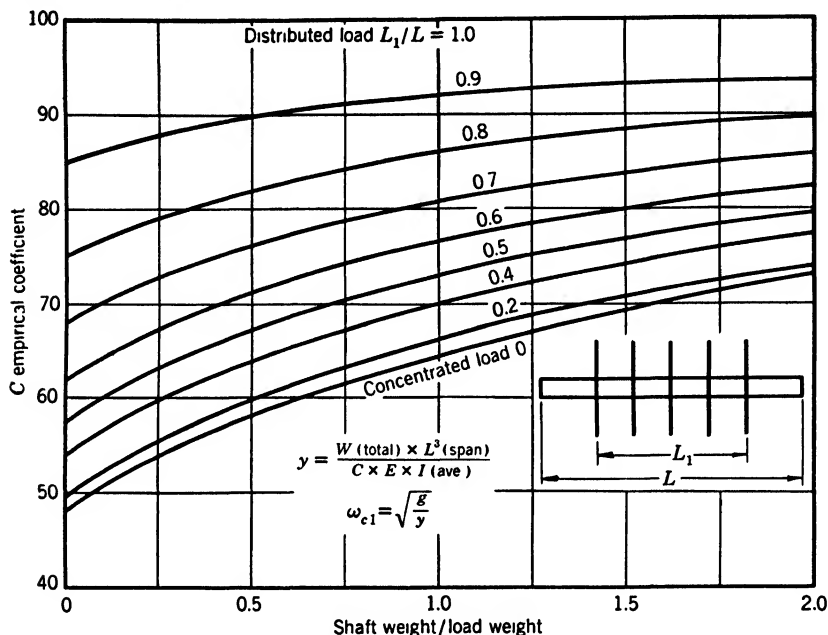


FIG. 15.9. Dynamic deflection coefficient for symmetrical rotors.

along  $L_1$ . Evidently the more impellers there are on the shaft, the more accurate are the results obtained from the chart. The chart cannot be used for pumps with packed stuffing boxes.

### 15.5 CRITICAL SPEED TESTS

To check the first critical speed with stuffing boxes packed, a special light shaft and heavy dummy impellers were built for a 2-in. six-stage pump. With this shaft the first critical speed was brought within the range of pump operating speeds. Tests with this rotor and also with a standard pump rotating element revealed the following.

(1) *With stuffing boxes packed the first critical speed took place at a speed corresponding to that for a shaft with shaft ends fixed at the middle of the stuffing boxes.*

(2) When the pump rotating element operated in air and without packing in stuffing boxes, it vibrated through a wide range of speeds

above the first critical speed. When assembled with mechanical seals and pumping water the rotor operated satisfactorily.

(3) With the light shaft, vibrations were observed above the first critical speed with stuffing boxes packed. *It was found that the driver's vibrations, including the coupling, increasing gear, and dynamometer, superimpose their amplitudes of vibration upon the shaft's own.* By eliminating the gear box and using a smaller driver and coupling, these vibrations were reduced, but not entirely eliminated. *When operated in water and with closely fitted casing rings, no objectionable vibrations were observed.*

Note that the power to drive the dummy rotor was negligibly small; therefore the coupling and gear box were not properly loaded. Also, the mass of the rotor was very small in comparison with that of the large test drivers. Under these conditions the effect of driver vibrations on the light rotor were exaggerated.

### 15.6 THE THREE-BEARING SHAFT

A three-bearing, freely supported shaft is seldom, if ever, used in centrifugal pumps. Occasionally three-bearing systems are encountered when the pump and the driver use a common shaft and one intermediate bearing is omitted. In this case, the driver manufacturers should check the shaft for critical speeds because they usually furnish the shaft and have more experience in dealing with critical speeds. With closely fitted internal parts, conditions may arise when the pump shaft may be considered as having three or more supports.

A few remarks will be made on the three-bearing shaft. Figure 15.10 shows the deflection curves for the first three critical speeds of a uniform shaft supported at three bearings.

In this case the first critical speed is the same as for a two-bearing set of half the length of the three-bearing set, as though the shaft were cut at the middle (Kimball,<sup>2</sup> p. 75).

The second critical speed is a direct result of the presence of the middle bearing, which supports a vibration reaction and at which there is a point of maximum flexure. The third critical speed corresponds exactly to the second critical speed for a single span of half the length. Like the first critical speed, the frequency of the third would not be altered

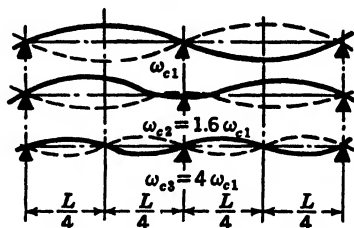


FIG. 15.10. Elastic curve with uniform shaft and three bearings.



if the shaft were cut at the middle bearing. Thus, the frequency of the third critical is four times that of the first, but that of the second is about 1.6 times the first. With three-bearing sets it is very seldom that second or higher critical speeds are observed. Determination of the first critical speed as outlined above gives quite accurate results if the shaft and loading are symmetrical about the middle bearing.

In general, the critical speed of the three-bearing shaft is higher than the individual critical speed of the shaft part obtained by bisecting the shaft at the middle bearing. These individual critical speeds of shaft parts never appear; neither does the critical speed of the whole shaft with the middle bearing removed. Higher critical speeds for the whole shaft as compared with two halves is explained by the stiffening effect of one part upon the other (Holba,<sup>3</sup> p. 131).

### 15.7 HIGHER CRITICAL SPEEDS

With a weightless shaft there may appear as many critical speeds as there are individual loads on the shaft. To each critical speed corresponds a different form of the elastic curve and a different value of  $K$  in equation 15.5. With a distributed load an infinite number of critical speeds are possible, theoretically. However, in pump design critical speeds of higher order very seldom come into consideration. The graphical method of critical speed determination previously described cannot be applied for calculation of the second critical speed, because it is not convergent. Instead of approaching a certain limit, the deflection lines move farther apart with each successive approximation. Other methods are more complicated and will not be discussed here. *However, in a great many cases when the pump shaft is approximately symmetrical about its middle, the second critical speed can be determined by using the first critical for one-half of the shaft obtained by bisecting the shaft in the middle and replacing the node (zero deflection point) with a free supporting bearing. This is the same method that was used in the determination of the first critical speed of a three-bearing shaft.* The method is quite general; that is, if the location of the node is known, substitution of a third bearing at this point reduces the problem to the finding of the first critical speed for a three-bearing shaft (Hohenemser method, in Holba,<sup>3</sup> p. 129). *In some simpler cases the second critical speed can be approximated by comparing the shaft loading and support with some cases for which solutions are known, such as those given in Fig. 15.5, where ratios of critical speeds of higher order to the first critical speed are given.* It will be noticed that the second critical speed is at least about three times the first critical speed.

### 15.8 SECONDARY CRITICAL SPEEDS

Under this heading will be considered critical speeds caused by forces other than centrifugal. A number of these have been observed and studied. All of them occur seldom and for that reason are difficult to recognize as there are not sufficient signs to identify each, and some of them are not easy to remove.

**(a) Weight Disturbances.** The alternate rise and fall of the center of gravity in respect to the center of rotation induces speed variation and minute disturbances of the circular path. Under some critical conditions this may produce a "secondary" critical speed at half of the first critical speed. Noticeable disturbances are possible only with a considerable eccentricity of the center of gravity, or if the rotor is badly out of balance.

According to Föppl, a similar secondary critical speed appears as a result of the fluctuation of rotative speed caused by the type of drive.

**(b) Friction between the Shaft Sleeves, the Impeller Hubs, and the Shaft.** At the critical speed centrifugal forces are balanced by the shaft stresses at all deflections and a vertical shaft is whirled bodily as though it had a permanent set with the same side out. Thus, there is no relative slipping of the impeller hubs on the shaft. At speeds higher than the critical, even if there is whirling of the shaft, the shaft sides are alternately extended and compressed. Thus there is relative motion between the shaft and the shaft sleeves or impeller hubs, resisted by whatever friction develops during such slipping. It has been proved (Kimball,<sup>2</sup> p. 126) that as result of such friction a component of frictional forces develops which tends to whirl the shaft in the same direction as the shaft revolves when operated above the first critical speed. This whirling speed may reach the critical speed at which condition vibration due to synchronism between the whirling speed and the natural period of vibration develops. Thus the frequency of vibration is the same as the first critical speed, and operating speed is higher than the latter.

Vibration of this type was obtained experimentally. With horizontal shafts, extension and compression of the outer filaments occur every revolution and, when impellers and sleeves are shrunk on the shaft, such shafts may develop vibration due to friction between the shaft and the impeller hubs, if operated above the critical speed.

It may be of interest to mention that the shaft's own internal friction during the process of extension and compression of its outer filaments of material will develop similar tangential components contributing to the whirling of the shaft. But, with steel shafts, tests show that such

internal friction forces alone are unable to build up and maintain such a whirl.

This cause of vibration of the rotors caused manufacturers of centrifugal compressors and steam turbines to mount their disks with a narrow ring contact between the disks and the shaft. Long flexible laminated rotors of electric motors may vibrate as a result of internal friction between laminations regardless of a careful dynamic balance of the rotors.

**(c) Oil Whip.** It has been found experimentally and was observed on actual machines that with oil-lubricated sleeve bearings, the oil wedge travels around at half the shaft speed. If this speed falls near the shaft's first critical speed, the shaft whirling produces vibration, which does not die down even when the shaft speed is increased more than twice the critical speed. The oil wedge continues to stay at the same speed, having all the encouragement from the shaft. With horizontal shafts the weight of the rotor is not sufficient to suppress the oil whip vibrations. In general these vibrations are not easily eliminated. The following steps have been tried with different degree of success: (1) change to ball bearing; (2) decrease bearing length to increase the load on the oil film; (3) deliberately put bearing out of line with the shaft.

The best way to avoid vibrations due to oil whip is not to run the pump above twice the critical speed.

**(d) Reverse Synchronous Precession.** Stodola has studied and shown experimentally that under certain conditions disturbing moments can arise which produce reverse synchronous precession. This may result in vibrations at an operating speed twice the first critical speed. To eliminate vibration of this nature the impeller positions on the shaft can be changed and the rotor rebalanced (Holba,<sup>3</sup> p. 46).

**(e) Sleeve Bearings versus Ball Bearings.** *With sleeve bearings small disturbances from the coupling, the driver, or any other cause easily produce secondary vibrations of the pump shaft, as the weight of the shaft is not sufficient to maintain a continuous contact between the shaft and the bearings.* During tests of the 2-in. six-stage pump shaft referred to previously the shaft ran smoothly with stuffing boxes packed and with no water in the pump casing. Replacing the packing with a closely fitted bushing with normal bearing clearances, grease-lubricated, produced vibration. Ball bearings provide a positive support for the shaft, and have an advantage over sleeve bearings in this respect. Grün<sup>5</sup> advocates ball bearings in preference to sleeve bearings to reduce a tendency to vibration for boiler feed pumps. Stodola<sup>1</sup> (p. 956) states that on several

occasions vibration disappeared when sleeve bearing clearances were reduced below normal, thus indicating that the sleeve bearing was not functioning properly. Note that shaft vibration due to oil whip, described above, also is characteristic of sleeve bearings and cannot occur with ball bearings.

**(f) Effect of the Coupling on Secondary Vibrations.** The disturbing effect of the coupling comes as a result of either misalignment or transmission of disturbance from the driver. Even with elastic couplings if the shaft runs above the first critical speed a slight misalignment between the pump and driver shafts produces periodic disturbing forces which may induce secondary vibrations (Holba,<sup>3</sup> p. 168). Vibrations induced or transmitted by the coupling are not easily eliminated. If no other means are available a substitution of a rigid coupling may either remove secondary vibrations or bring them outside the operating speed range. Rigid couplings are universally used with vertical propeller or turbine pumps, and also on horizontal turbo-generating units.

**(g) Summary of Secondary Critical Speeds.** *A general conclusion from the study of secondary critical speeds is that operation of the pump should be avoided at speeds which are even fractions ( $\omega_c/2$ ;  $\omega_c/3$ ) or multiples of the first critical speed. Considering that the first critical speed is not a point but a belt and that its calculations are more or less approximate, the above rule imposes a great limitation on the speed selection.*

*In spite of the vast experience and knowledge accumulated on critical speeds, some puzzling cases of shaft vibration are encountered which do not fall into any of the above descriptions. (Stodola,<sup>1</sup> p. 956.) Fortunately, such examples are rare in centrifugal pump practice.*

## 15.9 SECONDARY FACTORS AFFECTING CRITICAL SPEED

Under this heading a number of factors which affect the critical speed in general will be considered, although in the case of centrifugal pumps their effect may be neglected.

**(a) Axial Forces.** In some designs of multistage pumps and in all vertical pumps, besides transmitting torque, the shafts carry a considerable axial force due to axial thrust. It has been found that axial forces tend to increase the critical speed. This tendency is more pronounced in shafts having a low critical speed. This is in agreement with experience with strings used for musical instruments, where tension determines the frequency of vibration of the string (tone). However, axial forces encountered in centrifugal pump shafts are too small to produce any appreciable differences in the critical speed (Holba,<sup>3</sup> p. 27).

**(b) Torque.** Theoretically, a shaft transmitting higher torque should have a lower critical speed, as shaft stiffness decreases when the torque increases. However, this effect is negligible in general (Holba,<sup>3</sup> p. 31).

**(c) Friction.** Mechanical friction of the impellers and the shaft tends to reduce the amplitude of vibration without any effect on its frequency. This, in addition to the internal molecular friction of the shaft, results in a finite shaft deflection at the critical speed. The time element is also a contributing factor in limiting the amplitude of the shaft at and near the critical speed.

**(d) Shaft Moment of Inertia.** If the shaft moment of inertia about two axes is different, for instance if it is a result of keyways in the shaft, there will be two critical speeds of the first order. The region between the two is unstable. The author does not know one case where two critical speeds due to keyways being in one plane were observed.

**(e) Gyroscopic Action.** When there are several impellers on the shaft, all impellers except the middle ones revolve in planes not normal to the line joining two bearings. Under such conditions gyroscopic action causes a restoring force in addition to the shaft elastic stiffness. This results in increasing the frequency of vibration. However, in centrifugal pumps the mass of the impellers is too small to have any noticeable gyroscopic effects. In large steam turbines gyroscopic action may increase the critical speed 2 to 3 per cent (Kimball,<sup>2</sup> p. 25).

**(f) Elasticity of Bearings.** All critical speed calculations are based on the assumption of perfectly rigid bearing supports. In horizontal pumps this condition is approached practically in every case. In vertical pumps with long shafts, bearings are either supported by the inner tubing enclosing the shaft or mounted on horizontal beams. Both have a marked degree of flexibility. Under such conditions, reduction of as much as 25 per cent in the first critical speed is possible; under extreme conditions reduction to below one-half the critical speed with rigid bearings is possible. With long vertical pumps of the deep-well type, it is common practice to provide spiders to steady the inner tube and bearings.

**(g) Elasticity and Mass of the Foundation.** If a pump is mounted on a support which in itself is not sufficiently rigid, a compound vibrating system results with two or more critical speeds, depending on the degree of freedom of the support. With only up-and-down motion of the base-plate two critical speeds will appear, one when the shaft and the support frequencies of vibration are in phase, and the other when they are 180 degrees out of phase. There is no way to calculate the critical speeds under such conditions. A solid foundation is the main prerequisite for vibration-free operation of pumps.

**(h) Stiffening by Impeller Hubs and Shaft Sleeves.** When impellers are individually mounted without spacer sleeves between them, the stiffening effect of the hubs on the shaft can be disregarded. However, if all impellers are assembled on the shaft with spacers between the hubs and nuts on both ends outside the stuffing box shaft sleeves, the stiffening effect of the parts mounted on the shaft is appreciable. A considerable difference in the critical speed was observed experimentally (1800 versus 1400 in one case), by running the shaft with nuts tight and loose. To calculate the critical speed, only part (50 to 65 per cent) of the moment of inertia of sections of impeller hubs or sleeves should be added to the shaft moment of inertia to account for the stiffening effect of all parts mounted on the shaft.

**(i) Effect of Temperature.** Centrifugal pumps are employed at present for liquids at temperatures up to 850°F. At such temperatures the modulus of elasticity  $E$  drops considerably, as shown by the tabulation below for low-carbon steels; it is given in millions of pounds per square inch.

$E = 30$	0 to 300°F.
28	480
25	750
20	930
13	1100

Shaft deflection is inversely proportional to the modulus of elasticity,<sup>4</sup> and hence the critical speed will be lower at high temperatures.

Another effect of temperature on critical speeds is observed when the degree of stiffening of the shaft by the impeller hubs and sleeves changes as a result of difference in the heat expansion of the shaft and parts mounted on the shaft.

**(j) Wear.** On several occasions it has been found that pumps begin to vibrate after being in service for some time. Several causes may contribute to such conditions: (1) worn internal closely fitted parts which acted as bearings or provided enough damping effect for quiet operation when new; (2) loss of balance by rotor owing to clogging of one of impeller passages; or (3) wearing out of bearings.

**(k) Torsional Vibrations.** Special tests run by Stodola<sup>1</sup> (p. 470) failed to show any effect of torsional vibrations on the first critical speed of the shaft.

## 15.10 SELECTION OF CRITICAL SPEED

Extensive experiments by several investigators have proved a very satisfactory agreement between the calculated and the observed values of critical speeds. Therefore, it is possible to select shaft dimensions in

such a way as to reduce the possibility of shaft vibration to a minimum. Operation below the critical speed gives a maximum assurance of vibration-free operation. However, this frequently leads to designs impractical from a commercial point of view.

From the considerations discussed in previous articles, the selection of the shaft sizes for critical speed should be guided by the following considerations.

(a) The operating speed should not be an even fraction ( $\frac{1}{2}$ ,  $\frac{1}{3}$ ,  $\frac{1}{4}$ ) or multiple (2, 3, 4, ...) of the first critical speed.

(b) The operating speed should not be too close to the critical speeds, first or second.

$$n < 0.8 n_{c1} \text{ where } n = \text{operating speed}$$

$$n > 1.3 n_{c1} \quad n_{c1} = \text{first critical speed}$$

$$n < 0.7 n_{c2} \quad n_{c2} = \text{second critical speed.}$$

(c) Satisfactory operation above the second critical speed is impossible according to Eck (Holba,<sup>3</sup> p. 169).

At high speed and especially above the critical speed, the deflection of the shaft may have a considerable effect on balancing. As a result of this, the rotor can be balanced only for one definite speed, and under certain conditions it cannot be balanced at all (Holba,<sup>3</sup> p. 179). This can be seen from the following simple example (Fig. 15.11). Consider a shaft of uniform cross section with a single unbalance  $m$  in the middle. This can be balanced by adding corrective weights  $m_1$  and  $m_2$  in any two balancing planes at the first critical speed. However, at the second critical speed the unbalance happens to be at a node, and the corrective weights  $m_1$  and  $m_2$  become unbalanced.<sup>6</sup>

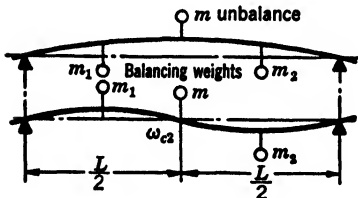


FIG. 15.11. Flexible shaft is dynamically balanced at one speed only.

Owing to the simplicity of mass distribution, static balancing of the individual impellers of a multistage pump is sufficient for an average job, but in doubtful cases complete rotors should be checked on the dynamic balancing machine at the operating speed.

## REFERENCES

1. A. STODOLA, "Steam and Gas Turbines," New York, McGraw-Hill, 1927 (translation of the sixth German edition).
2. ARTHUR L. KIMBALL, "Vibration Prevention in Engineering," New York, John Wiley & Sons, 1932.

3. J. J. HOLBA, "Berechnungsverfahren zur Bestimmung der kritischen Drehzahlen von geraden Wellen," Vienna, Julius Springer, 1936.
4. S. TIMOSHENKO and J. M. LESSELLS, *Applied Elasticity*, Westinghouse Tech. Night School Press, 1925.
5. KARL GRÜN, *Dampfkessel-Speisepumpen*, Vienna, Julius Springer, 1934, p. 68.
6. R. P. KROON, "Balancing of Rotating Apparatus," *Trans. A.S.M.E.*, Vol. 10, No. 4, p. 228.



## CHAPTER 16

### SPECIAL PROBLEMS AND APPLICATIONS OF VERTICAL TURBINE AND AXIAL FLOW PUMPS

#### 16.1 BRAKE HORSEPOWER AT ZERO CAPACITY

The most desirable form of brake-horsepower curve for any application is one which has a maximum value at the best efficiency point. Such a curve eliminates the danger of overloading the motor at any point on the head-capacity curve. Pumps of medium specific speeds (3000 to 4000, single-suction) have brake-horsepower characteristics of this type. At lower specific speeds the brake horsepower continues to increase at capacities greater than that at the best efficiency point, the minimum being at zero capacity. Such brake-horsepower curves are satisfactory for a great majority of applications as they permit the starting of pumps under minimum load with the discharge valve closed, and it is not often that such pumps have to operate at capacities much in excess of normal.

High specific speed pumps, particularly of the axial flow type, have brake-horsepower curves which rise sharply toward zero capacity. The brake horsepower at shut-off may be twice (or more) that at the best efficiency point. This is a very undesirable feature because, as a rule, the head on propeller pumps varies with water level variations in the suction or discharge reservoirs, and thus require an oversize motor to permit operation at higher heads than the normal. Also, to permit starting of the pump with the discharge valve closed, an oversize motor and starting equipment are required. Attention of designers has been directed toward developing types of propeller pumps having a lower value of horsepower at shut-off. In high specific speed pumps of the axial flow type, very little has been accomplished to date (1947) and prospects are not bright. In the range of specific speeds from 6000 to 8000, pumps have been produced which have a value of shut-off horsepower lower, or only slightly higher, than that of the power at the b.e.p. Such a shut-off horsepower permits operation of the pump at any point on the head-capacity curve without overloading the motor. The best of these new types of pumps show efficiencies equal to those of "standard" older design. In some cases, the efficiency at part loads

has been improved, and in all cases the head-capacity curve is flatter. Figure 16.1 shows representative curves of normal and special designs at the same specific speed.

**(a) Number of Vanes.** The shape of a brake-horsepower curve can best be described by a ratio of the brake horsepower at zero capacity to the brake horsepower at the best efficiency point. *Reduction of this ratio has been accomplished by a reduction of the brake horsepower at shut-off, and by an increase of the brake horsepower at the rated head and capacity*

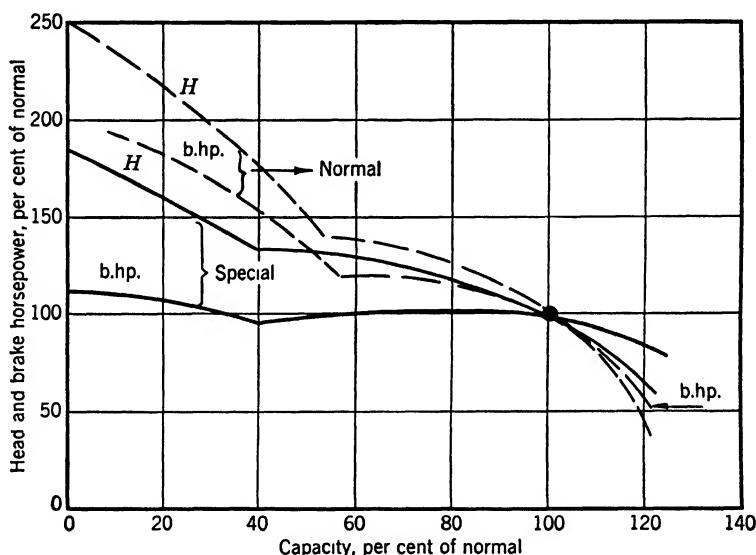


FIG. 16.1. Reduction of brake horsepower at zero capacity of propeller pumps of  $n_s = 7500$ .

*ity. The first is accomplished by reducing the shut-off head and improving the pump efficiency at partial capacities by reduction of wasteful recirculation of liquid from vane to vane. A steep head-capacity curve is a necessary attribute of high specific speed pumps; therefore the several means of reducing the shut-off head would tend to reduce specific speed too. This tendency should be counteracted by some other means to maintain the specific speed within the desired range. To increase the brake horsepower at the normal head and capacity means increasing the pump output. To reduce the brake horsepower ratio this should be done without affecting the head and the brake horsepower at shut-off. The effect of several design elements upon the brake horsepower ratio will be discussed below.*

In mixed flow impellers, the meridional velocity at normal capacity is approximately uniform and is determined by the pitch of the impeller

vane conical screw surface. At partial capacities, this velocity is reduced by the amount of slip in the same manner as in straight axial flow

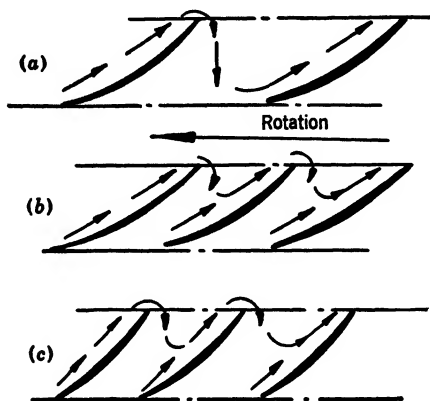


FIG. 16.2. Flow pattern at shut-off of propeller pumps.

pumps. This slip can be visualized not only as a reduction of the true meridional velocity, but also as an actual climb of liquid segments along the vane and subsequent drop from one vane to the other at the impeller exit (Fig. 16.2). This results in a loss of pressure and velocity energy, all taken from the impeller vane.

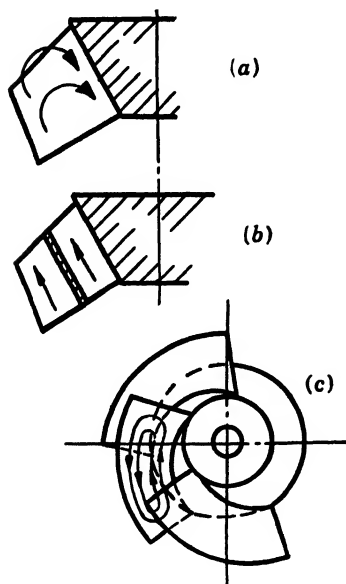


FIG. 16.3. Flow pattern in mixed flow impellers.

At and near shut-off, circulation from the periphery of the impeller toward the hub, or vice versa (Fig. 16.3) is not an important factor in absorbing power, as tests of an impeller with a shroud added to divide it into two partial impellers show a very slight increase in brake-horsepower ratio and a higher head near shut-off. The increase in head is caused by a reduction of the relative circulation in the impeller channel.

A comparison of the pattern of flow of Fig. 16.2 (a) with that of Fig. 16.2 (b) shows that a greater number of vanes results in less drop in pressure and a smaller volume of water between two adjacent vanes. Therefore waste of power near shut-off is smaller. The combined effect of the number of vanes and the vane angle may be expressed

as vane lap, or the degree of vane overlapping. Greater vane lap produces a flatter brake-horsepower curve. Vane lap also includes the effect of the impeller meridional depth (Fig. 16.4) discussed below. However, increase in skin friction and decrease in efficiency imposes practical limitations on the number of vanes. Eight vanes is probably the upper limit for the number of vanes in propeller pump impellers. For a given impeller profile, a maximum number of vanes is possible only with higher vane angles, as the total vane area is lower with high vane angles.

(b) **Vane Angles.** Vane angles, entrance and discharge, have a predominant effect on the pump characteristics. At zero capacity, the head is independent of the discharge vane angle, as in centrifugal pumps.

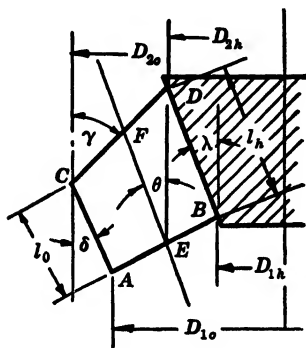


FIG. 16.4. Mixed flow impeller profile.

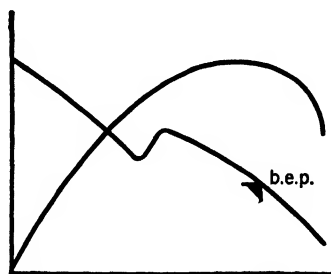


FIG. 16.5. Discontinuity in  $Q$ - $H$  curve.

The shut-off brake horsepower increases with higher discharge vane angles. This can be visualized by having in mind the flow pattern of Fig. 16.2. For a given number of vanes, the drop from vane to vane is greater with higher vane angles, Fig. 16.2 (c); therefore, waste of energy is greater and shut-off brake horsepower is higher.

*With higher vane angles, the normal head capacity increases, as does the normal brake horsepower, so that the shut-off brake-horsepower ratio decreases.* For a given impeller profile and number of vanes, there is an optimum maximum vane angle beyond which the efficiency begins to drop rapidly and discontinuity in head-capacity curves appears (Fig. 16.5).

(c) **Impeller Profile.** The maximum vane angle is different for different impeller profiles and number of vanes. *The more the impeller profile deviates from that of the straight axial flow pump (Fig. 16.4) (angles  $\delta$  and  $\lambda$  higher) the lower become the brake horsepower at shut-off and the shut-off brake-horsepower ratio.* A greater difference between the maximum outside impeller diameter  $D_{2o}$  and the impeller eye diameter  $D_{1o}$

indicates that a greater portion of the total head is a centrifugal head. The shut-off head is reduced as the average profile angle  $\theta$  is increased. The ratio of shut-off head to normal also becomes lower. This is true for all flow lines, including the one following the hub profile. For a comparison of the total effect of the vane profile on the shut-off brake-horsepower ratio, the slope of the mean streamline can be taken as determined by the angle  $\theta = (\delta + \lambda)/2$ . However, the slope of the outer edge  $AC$  has more effect on the slope of the pump characteristics than the slope of the hub  $BD$ .

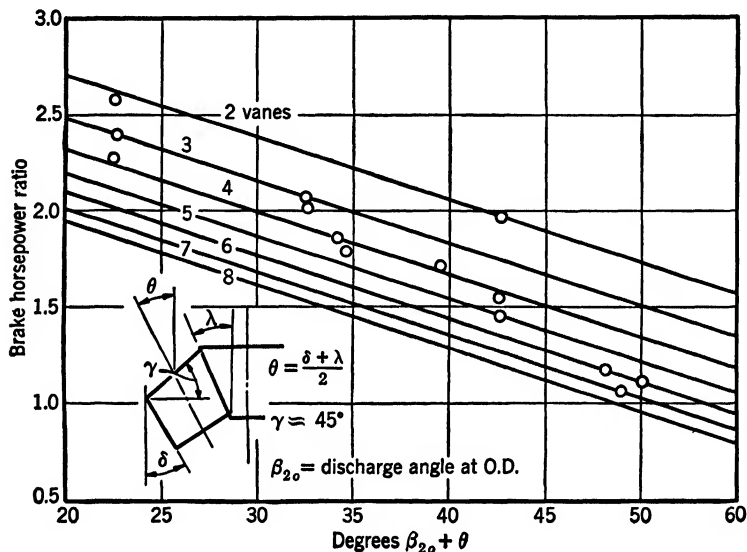


FIG. 16.6. Brake-horsepower ratio in terms of design elements.

Figure 16.6 shows a general trend of the shut-off brake-horsepower ratio variation in terms of number of vanes, discharge angle  $\beta_{2o}$ , and the average profile angle  $\theta$ . The latter two angles were combined for the purpose of this chart, as their effect is in the same direction and for small angle increments it is approximately equal. For a given profile angle, Fig. 16.6 shows the effect of discharge angle  $\beta_{2o}$  on the brake-horsepower ratio. For a given  $\beta_{2o}$  the same chart represents the effect of the profile angle on the brake-horsepower ratio. With both  $\beta_2$  and  $\theta$  fixed, the result of variation of the number of vanes on the brake-horsepower ratio can be determined.

The vane meridional length on the circular projection ( $l_o$ , Fig. 16.4) has an important effect on the shut-off brake-horsepower ratio. For the same number of vanes and vane angles, a greater vane length  $l$

means a lower pressure differential on two sides of the vane; hence there will be less waste of power at shut-off because of liquid slipping from vane to vane. *Therefore, a lower brake-horsepower ratio is obtained with longer vanes on the profile view. In addition, the vane length has an important effect upon the stability of the head-capacity curve at partial capacity. Vane meridional length contributes to the vane lap, by increasing the true combined vane area. Until an optimum vane area is reached, greater vane areas result in a lower brake-horsepower ratio.* A normal ratio of the profile vane length at the hub to that at the periphery  $l_h/l_o$  varies from 1.25 to 1.35, the higher ratio referring to high vane angles and giving a lower brake-horsepower ratio.

The discharge edge of the vanes ( $CD$ , Fig. 16.4) contributes to the shape of the head-capacity and brake-horsepower curves. Assuming that the vane suction edge  $AB$  and the vane meridional length  $l_o$  at the periphery are fixed on the profile, lower discharge edge angles  $\gamma$  result in a longer vane length at the hub. Besides, the difference between the  $D_{2o}$  and  $D_{2h}$  is reduced; thus the discharge becomes more radial. All this tends to reduce the brake-horsepower ratio and specific speed at the same time. The discharge edge angle affects the profile of the diffusion casing, low angles requiring a large casing diameter. Probably  $\gamma = 45^\circ$  represents a good compromise between several factors connected with the discharge edge angle.

**(d) Casing.** The effect of the casing design on the brake-horsepower ratio is indirect. A greater number of diffusion vanes and lower diffusion vane angles tend to reduce the brake-horsepower ratio, but result in a reduction of specific speed, since the best efficiency point moves toward lower capacities while no appreciable change takes place in the shape of the brake-horsepower or head-capacity curves. A reduction of space between the impellers and the diffusion vanes of the casing also tends to reduce the brake-horsepower ratio as the volume of liquid involved in the energy waste at shut-off is reduced.

It is left to the skill of the designer to manipulate the various design elements in the sense indicated above to obtain a flat brake-horsepower characteristic and to stay within the prescribed specific speed range without undue sacrifice in efficiency and shape of the head-capacity curve. The best combination of the several design elements to meet all these conditions can be determined only experimentally.

In straight axial flow pumps or mixed flow pumps with high shut-off brake horsepower, several methods have been devised to start the pumps without overloading the motors. On a great many installations, pumps can be started with the discharge wide open; in such cases the advantages of a flat brake-horsepower curve are minimized.

## 16.2 VERTICAL PROPELLER PUMPS VERSUS HORIZONTAL PUMPS

(a) **Hydraulic Performance.** By referring to Fig. 9.12 it will be noticed that, at specific speeds above 5000, vertical mixed flow and axial flow pumps have a better efficiency than horizontal pumps. It has been pointed out that the difference is caused mostly by the adverse effect of the suction approach on the impeller performance. The relative performance of vertical pumps is even better than it appears from this chart as the entrance loss and loss in the discharge column, including the elbow, are charged against the pump, whereas in horizontal pumps

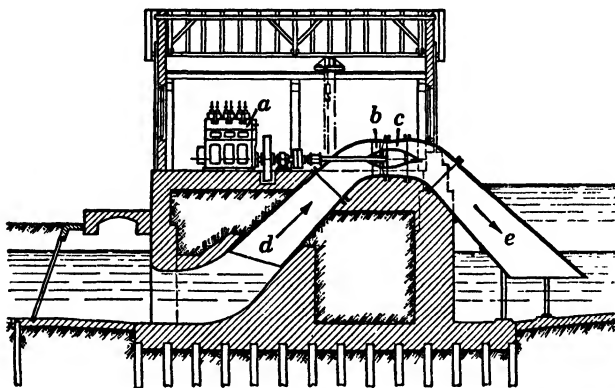


FIG. 16.7 (a). Axial flow pump, engine-driven (Maschinenfabric Augsburg-Nurnberg).

the head is measured between the suction and discharge flanges, and the loss in the suction pipe should be charged to the pump to put the comparison on the same basis.

Moreover, horizontal pumps usually require an increaser on the discharge nozzle, thus incurring additional loss of head, whereas in propeller pump discharge elbow velocities are already reduced to what they are in the discharge pipe.

*Horizontal propeller pumps lose part of their advantages if there is an elbow on the suction or if the pump has to work under a suction lift. In the past, horizontal propeller pumps were invariably used for engine-driven jobs; Figs. 16.7 (a) and 16.7 (b). This resulted in a slow speed pump operating under suction lift, and required a deep excavation to reduce the static lift of the pump. The recent trend is to use vertical submerged pumps driven through a right-angle geared head. This permits freedom of speed selection for the pump, and gives all the advantages of vertical pumps as to submergence and impeller approach. The engine floor can be located*

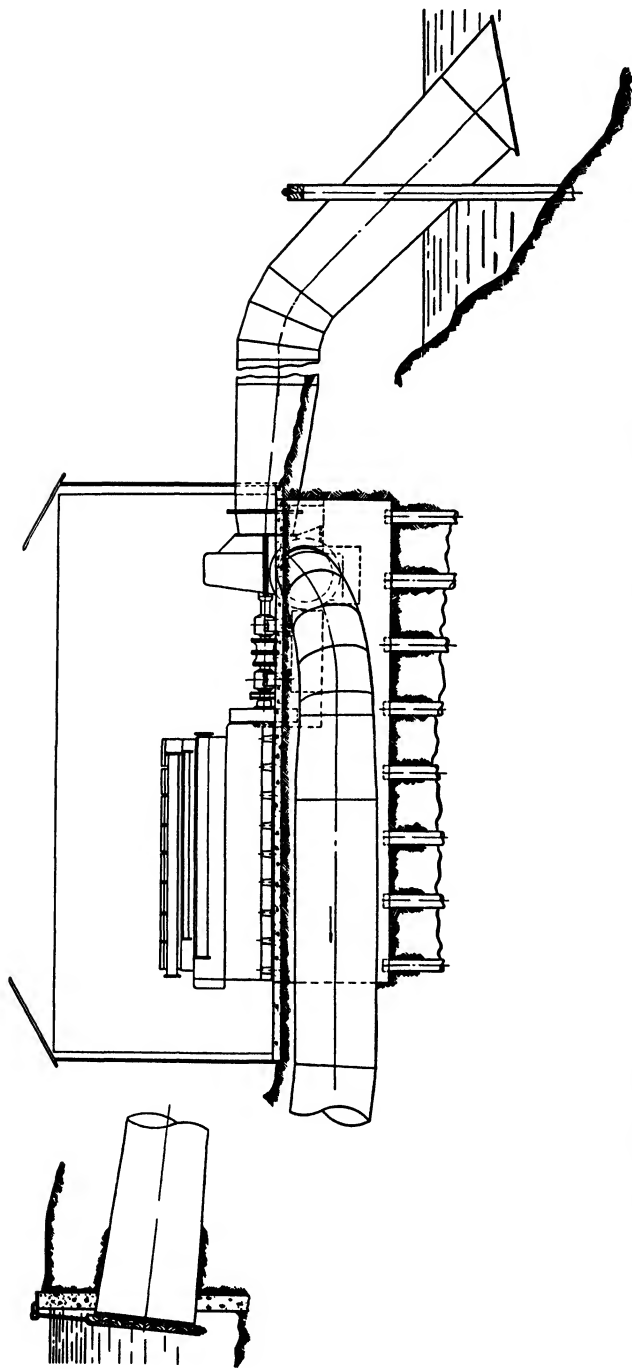


FIG. 16.7 (b). Worthington 48-in. horizontal volute propeller pump, diesel-engine-driven; 72,000 g.p.m., 28 ft. head, 350 r.p.m., 646 b.hp.



at any convenient level, and the overall cost of the pumping station is lower. Figure 16.8 shows one example of such an arrangement.

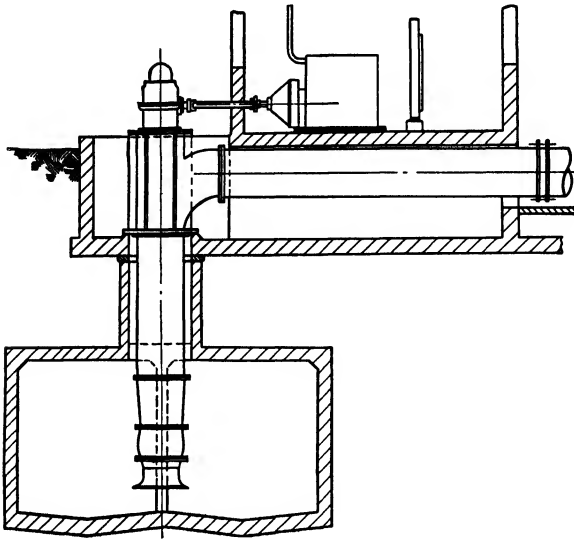


FIG. 16.8. Ingersoll-Rand 24-in. propeller pump engine-driven through a right angle geared head (Fairfax Drainage District, Kansas City, Kansas).

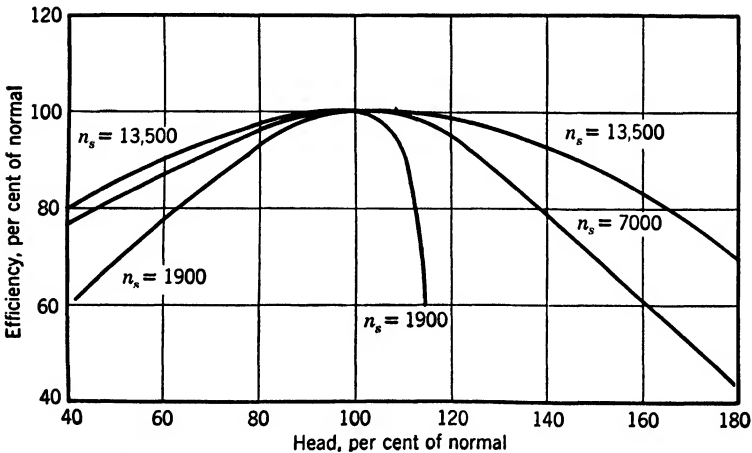


FIG. 16.9. Efficiency versus head of one centrifugal and two propeller pumps.

**(b) Variable Head-Capacity Performance.** The efficiency curve of a low specific speed centrifugal pump, when plotted against capacity, is flatter than that of propeller pumps. When capacity is varied by throt-

ting this has a definite advantage. But low head pumps are used mostly where head varies as a result of suction level variation (tide, seasonal change in river levels, and so on) and maximum capacity is wanted at any head. In this case propeller pumps with a steep head-capacity curve have a definite advantage and they will deliver more water within a given head range, and at a better efficiency, than the centrifugal pump. The fact that the efficiency is better is more evident if the efficiency of both centrifugal and propeller pumps are plotted against the head (Fig. 16.9). On this basis the propeller pump efficiency curve is flatter than that of the centrifugal pump.

### 16.3 SUCTION SUMP DESIGN

Owing to the features of propeller pumps—high relative velocities, short impeller passages, few vanes, and little guiding action from the suction bell—their performance is affected markedly by the flow in the suction sump. Therefore particular attention should be paid to the sump design in order to obtain optimum performance of propeller pumps. The sump design is frequently beyond the control of the pump designer. Although it is impossible to foresee all the possible field conditions which would adversely affect pump performance, several well-established principles cover the minimum requirements which should be met in laying out a pumping station to assure normal pump performance. These include: (1) submergence; (2) clearances from the floor and walls; (3) sump intake, or flow distribution in the sump; (4) spacing of several units; (5) strainers and trash racks.

Only vertical turbine pumps, or diffusion-casing-type propeller pumps, will be considered here, as these have replaced entirely the volute-type vertical pumps used in the past. Also, wet-pit construction is now used universally, the dry-pit station layout having been used mostly in connection with volute propeller pumps.

**(a) Submergence.** Submergence is selected with due regard for cavitation limits. Hydraulic Institute Standards give the recommended submergence in terms of pump head and specific speed for an average design. Individual designs of several manufacturers may require different submergences. Another point in setting a minimum submergence is the prevention of vortices in the suction sump which may permit air to be drawn into the pump suction. This depends on the sump layout, velocity of approach, suction bell design, effect of adjacent pumps, and the like. For these reasons the submergence on an average job should not be less than 5 ft. above the suction bell edge. With low suction bell velocity (2 to 3 ft. per sec.) and small units, this can be

reduced to  $D/2$  where  $D$  is the suction bell diameter, which on an average pump should be not less than twice the diameter of the impeller eye. When vortices appear in an existing station they can be checked by providing wooden floats around the pump discharge pipe, or baffles in the suction sump. All vortices originate from the impeller; for that reason pumps having a bottom bearing with radial supporting baffles in the suction bell are less likely to set up vortices in the suction sump. Submergence also has an important bearing on the velocity distribution in the suction bell approach, particularly if there are several pumps in the same sump. With ample submergence, water can approach the suction bell from all directions with a uniform velocity and with a minimum of disturbance from the flow toward several units in the same pit.

**(b) Floor Clearance.** The free area between the suction bell and the sump floor should be at least equal to the area of the bell itself. This requires a distance between the bell and the floor equal to  $D/4$  where

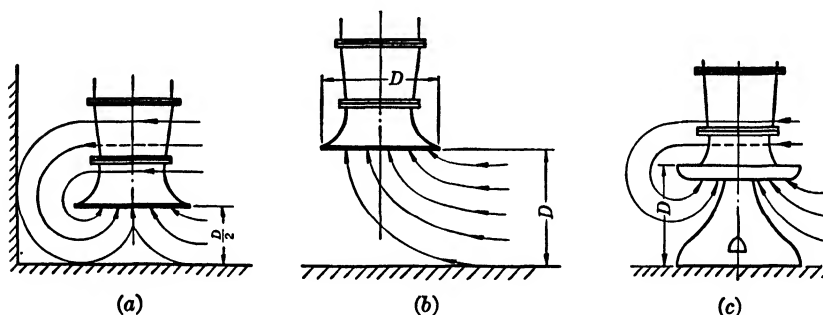


FIG. 16.10. Pattern of flow with suction bell distance to floor  $D/2$  and  $D$ .

$D$  is the bell outside diameter. But this will cause the water to make a sharp turn inside the bell. It has been found that a distance  $D/2$  between the bottom of the pit and the suction bell is ample for normal pump performance. A further increase in this distance may even impair, rather than improve, the velocity distribution in the suction bell approach. Tests at the University of California<sup>1</sup> have shown that the best performance is obtained with a clearance of  $D/2$ . An increase of the clearance to  $D$  reduced the gross pump efficiency about 1 point. This has been confirmed by later tests by Kerr and Moyer.<sup>2</sup> The possible patterns of flow are shown in Fig. 16.10. When the bottom clearance is  $D/2$ , a more uniform velocity distribution in the suction bell is obtained. With the distance between the suction bell and the floor  $D$  or more, a guide cone on the floor and suction bell design as shown in Fig. 16.10 (c) will improve velocity distribution in the impeller approach. Guide cones

have been found beneficial also when pumping from high velocity channels.<sup>11</sup> The wall clearances for normal performance should be at least  $D/2$ . If the sump intake is such that the flow is equally divided among several units, the minimum spacing between the units should be  $2D$  (Fig. 16.11).

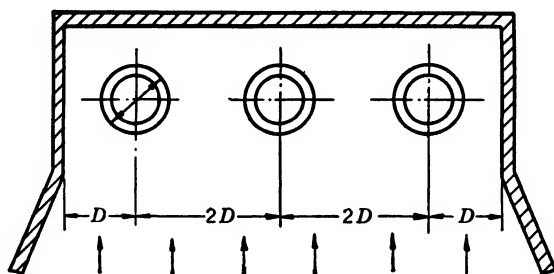


FIG. 16.11. Pump spacing with a uniform approach—best.

**(c) Sump Design.** When water is brought to the suction sump by means of a tunnel, equal distribution of the flow among several units becomes very important. Baffling may be necessary to assure minimum interference between the flow to several units (Fig. 16.12).

Cases are on record<sup>3</sup> where normal pump performance in the field could not be realized on account of a suction sump design which did not permit equal distribution of flow among three pumps. However, after proper baffling and change in the inlet tunnel, all determined by model testing, normal performance of all pumps was restored.

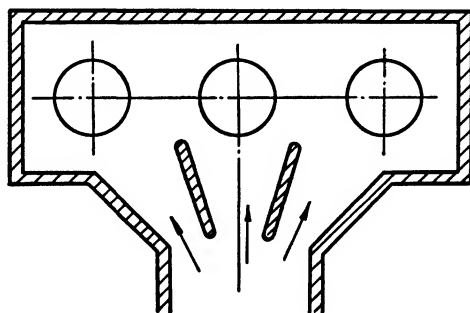


FIG. 16.12. Tunnel inlet to a suction sump—satisfactory.

The sump plan arrangement shown in Fig. 16.13, where the sump intake is at one end of the sump, will inevitably result in an uneven flow distribution and mutual interference of the several units. The units nearest to the intake will be affected most. The example shown in Fig. 16.14 was called to the author's attention. Each pump, *A* and *B*,

worked satisfactorily when operating alone. When both were operating, *A* would run normally while *B* would develop mechanical vibration and drop in capacity (and possibly in efficiency). When local conditions do not permit a favorable station layout to assure an equal distribution of flow among several pumps, the adverse effects of inadequate sump design

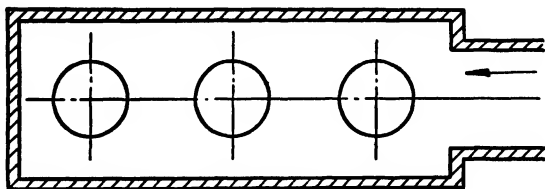


FIG. 16.13. A suction sump arrangement to be avoided.

are minimized if the velocity of approach to each pump is kept as low as possible, and if spacing between the pumps is increased above the minimum stated above.

All modern pumping stations are provided either with manually cleaned trash racks or moving screens. These are preferred to the individual suction strainers as the latter, even when clean, result in an appreciable loss of head. When clogged up with trash, the resistance may increase to the extent that cavitation may appear. The velocity through the trash rack should not exceed one foot per second.

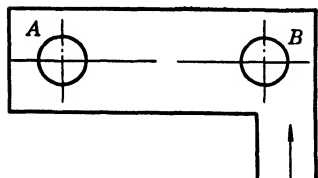


FIG. 16.14. A suction sump and pump arrangement proved unsatisfactory.

**(d) Design of Discharge Column.** Although the discharge columns of propeller pumps are usually short, the loss in the column should be kept to a minimum for low head pumps. All high speed propeller

pumps need an increaser next to the pump diffusion casing. The total angle of the increaser should be about 8 degrees for efficient conversion of velocity into pressure. Fabricated steel elbows should be laid out with at least five sections, and a minimum radius of curvature of at least  $1.25d$ , where  $d$  is the pipe diameter. In no case should a tee be substituted for an elbow. (Refer to the Fig. 1.14 for relative losses of several elbow designs and tees.) The size of the discharge column is selected so that the velocity head in the column does not exceed 4 to 5 per cent of the pump total head. Medici<sup>4</sup> has shown that pump efficiency can be improved 6 points by reducing velocity in the discharge columns (Fig. 16.15). When discharging into an open canal or lake, the discharge pipe outlet should be submerged, and velocity at the discharge should

be reduced to a minimum. When there is no valve on the discharge pipe, a flap valve will serve the same purpose. Nagler<sup>5</sup> has found that resistance of freely suspended flap valves does not exceed 0.10 ft. if their weight is light or if the weight is balanced.

In irrigation and drainage plants the discharge pipe is frequently put over a levee. To recover the extra lift over the levee a siphon action is provided by submerging the discharge end of the pipe, Figs. 16.7 (a) and 16.7 (b). In that case no valve is necessary on the discharge pipe, but an automatic vacuum breaking valve should be provided in the discharge pipe to prevent back-flow through the siphon. When the pump

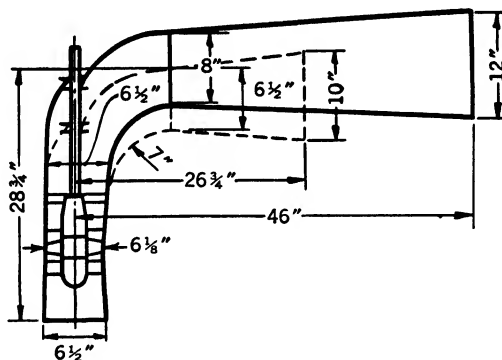


FIG. 16.15. Increase of size of discharge elbow improved efficiency 6 points (Medici).

is started, to prime the siphon the pump should be able to lift water over the hump. With rising brake-horsepower curve and synchronous motor drive the pull-in torque of the motor should be sufficient to produce the head necessary to prime the siphon.

#### 16.4 ADJUSTABLE IMPELLER VANE AXIAL FLOW PUMPS

When adjustable impeller vanes are provided on axial flow pumps it is possible to vary the head and capacity over a wide range with good efficiency by changing the position of the impeller vanes in the hub. This type of construction is widely used in Kaplan water turbines, but has been applied to pumps only recently. As used in water turbines, the cost of this design was prohibitive considering the size of pumps. Early pumps with adjustable impeller vanes were built in accordance with the water turbine practice.<sup>6,7</sup> In these the rod operating the mechanism inside the impeller hub was brought out through hollow pump and motor shafts. The author has designed an adjustable vane axial flow pump in which the adjusting mechanism was arranged externally

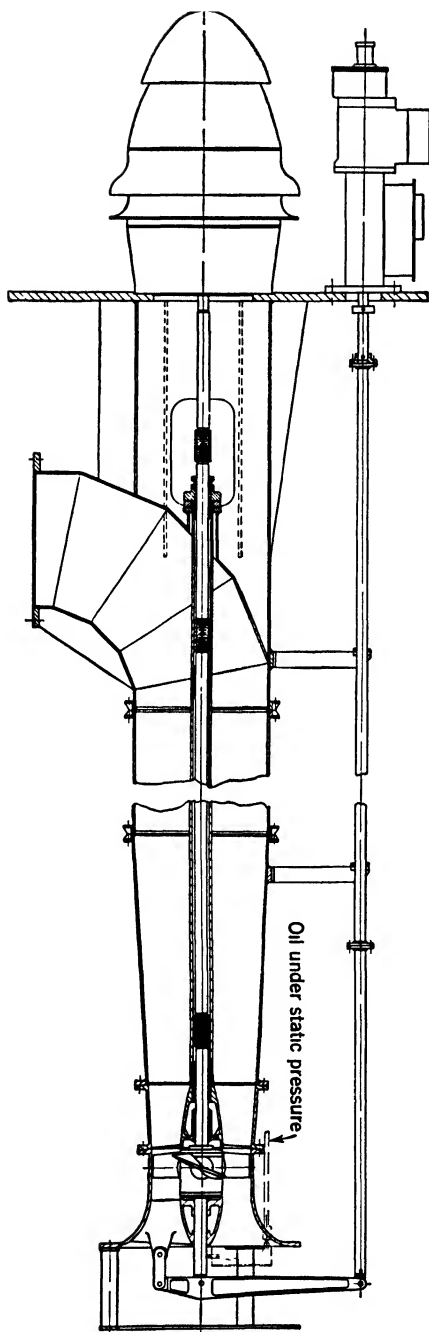


FIG. 16.16. Twenty-four-inch Ingersoll-Rand adjustable impeller vane axial flow pump at Central Illinois Electric and Gas Company; 22,000 g.p.m., 24 8 ft. head, 880 r.p.m.

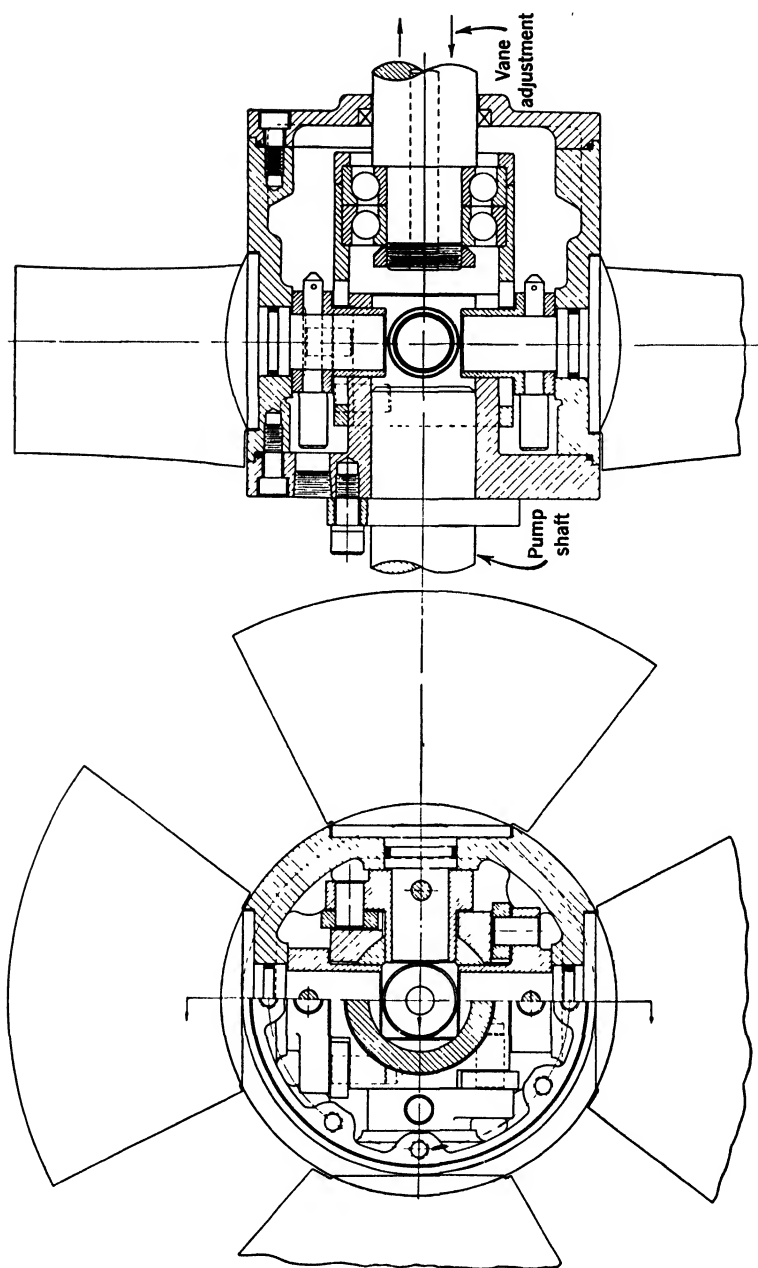


Fig. 16.17. Impeller hub detail of pump in Fig. 16.16 (Ingersoll-Rand).



to the pump, as shown in Fig. 16.16. The details of the impeller hub design are shown in Fig. 16.17.\*

Except for the impeller the rest of the pump parts are the same as those of pumps which have one-piece standard impellers. The mechanism is operated electrically by remote control from a switchboard. The

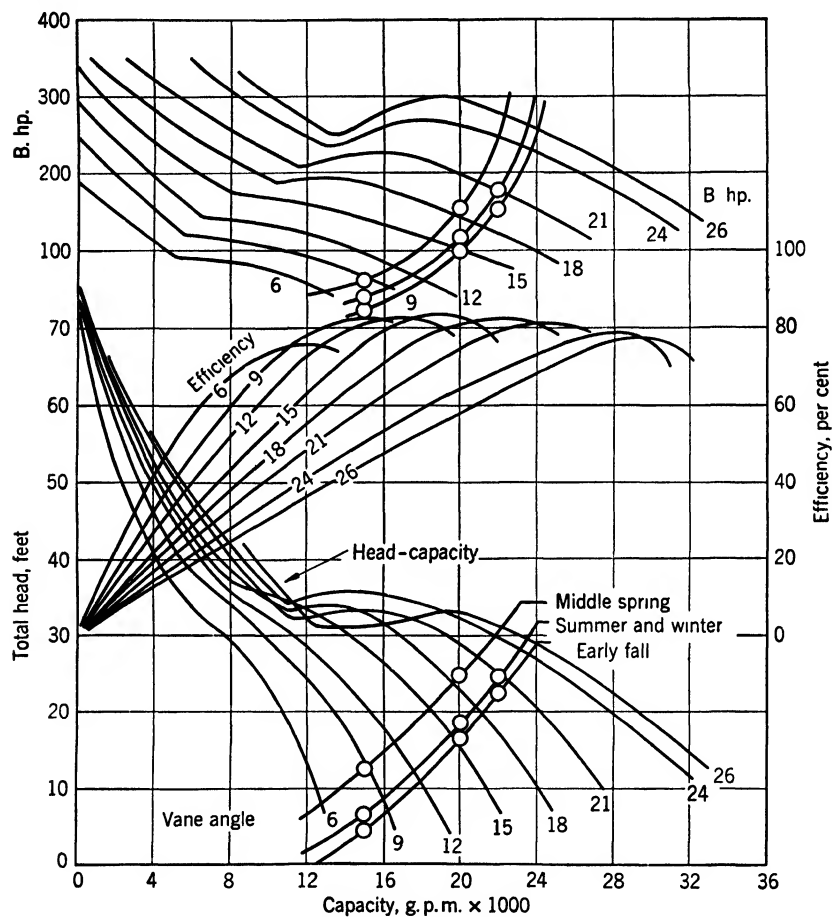


Fig. 16.18. Test curve of pump shown in Fig. 16.16.

performance of this pump is shown in Fig. 16.18. The system characteristics of the plant varies with the season of the year. Note that a 25 per cent reduction in capacity results in over 50 per cent saving in power. The pump can be started with the discharge valve closed, and when the impeller vanes are flat the pump requires about 25 per cent of the maxi-

\* U. S. patents 2,324,650, 2,357,914, and 2,379,839.

*imum rated brake horsepower. In condenser circulating service the variation in capacity is caused not only by the load on the condenser but also by the water temperature. By adjusting the pump capacity to the actual needs of the installation, the life of condenser tubes is appreciably prolonged as minimum velocities through the condenser are maintained at all loads.*

For manual control of the vanes, particularly where the change in the vane setting is not frequent and the pump can be stopped for the change (irrigation, drainage), this design becomes particularly simple. All the external leverage is omitted and vanes are moved by reversing the procedure; that is, by moving the pump shaft and holding the lower stub shaft rigidly attached to the suction bell. A hollow shaft motor is employed and the pump shaft is moved by means of the adjusting nut on top of the motor in the same manner as for the adjustment of running clearance of regular vertical turbine pumps with open impellers.

Ingersoll-Rand Company has built a 16-in. mixed flow pump of  $n_s = 7000$  with adjustable diffusion casing vanes to be used with a standard impeller. This has shown marked improvement in efficiency at reduced capacities. However, the head increased at the same time and there was little or no reduction in brake horsepower.

## 16.5 EXAMPLES OF PROPELLER AND VERTICAL TURBINE PUMPS

(a) **Axial Flow and Mixed Flow Propeller Pumps.** Figure 16.19 shows a mixed flow pump of specific speed 6000 to 7500. The points of interest are bottom bearing (grease-packed or water-lubricated) enclosed shaft for oil or clean water lubrication, and adjustable coupling for sizes for which hollow shaft motors are not available. A great majority of pumps of this type are built with water-lubricated rubber bearings since oil lubrication is not effective with short units and variable suction level. Hollow shaft motors are primarily designed for deep-well turbine pump service and are widely used for propeller pumps. Their range of ratings is constantly increasing.

Figure 16.20 shows an axial flow propeller pump of specific speed 12,500 to 13,500. The mechanical design of this pump is similar to the one in Fig. 16.19. Figure 16.21 shows an installation of three 48-in. mixed flow pumps with close spacing, which has been performing satisfactorily.

Figure 16.22 shows an installation of an axial flow pump for very low heads as used for rice irrigation. This arrangement, omitting the discharge column and valves, gives the simplest station layout for low head pumping.

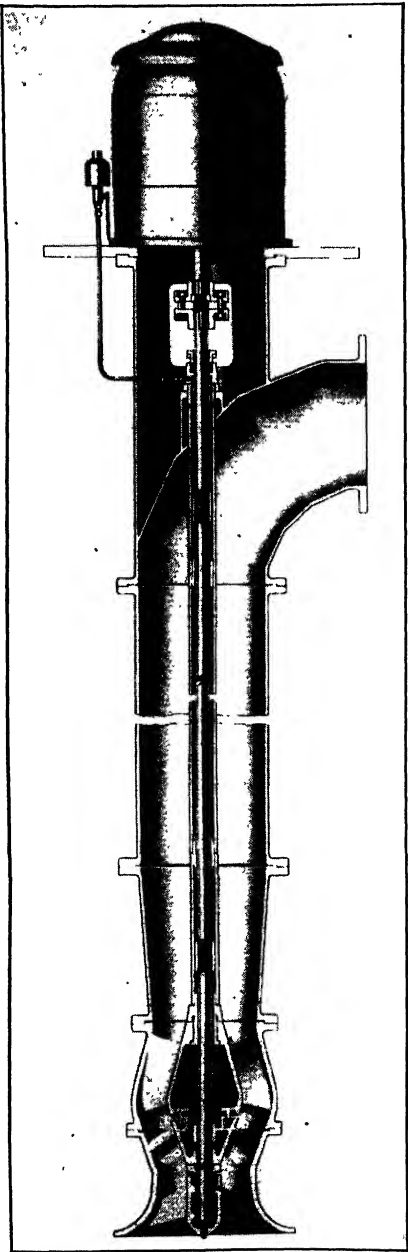


FIG. 16.19. Ingersoll-Rand mixed flow propeller pump.

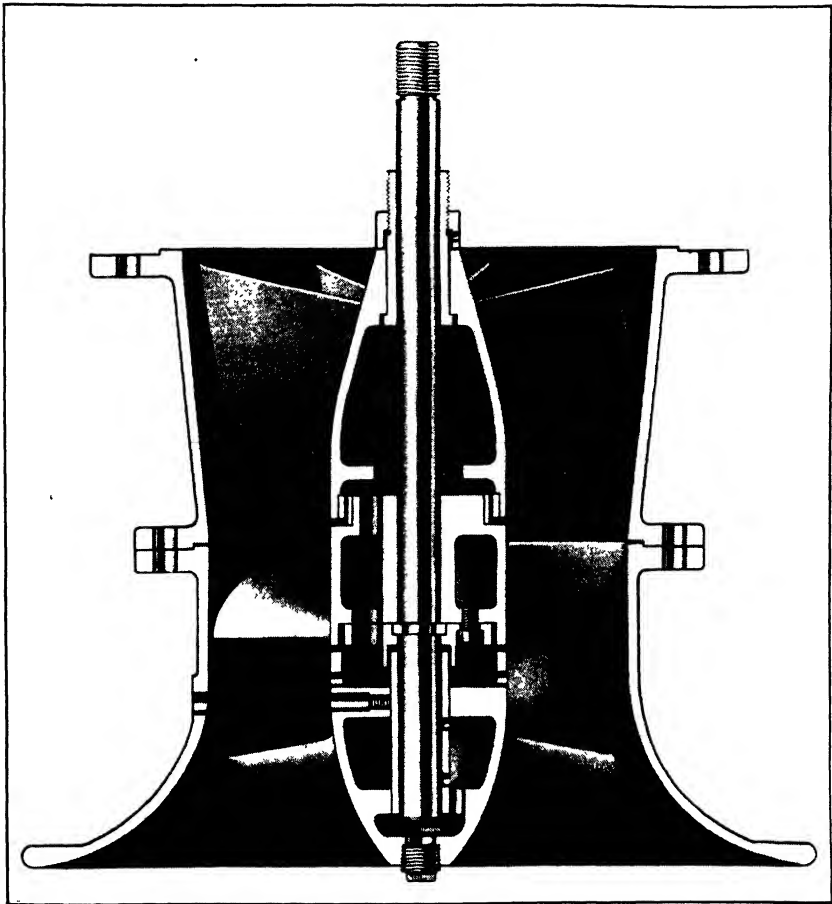


FIG. 16.20. Ingersoll-Rand axial flow pump.

Figure 16.23 shows a horizontal mixed flow volute pump. In small sizes (up to 24 in.) such pumps find a wide application in industrial plants where the head-capacity requirements fall outside the range of double-suction pumps. For very low heads, axial flow pumps are available for similar service (Fig. 16.24). On paper stock applications the diffusion casing is often dispensed with at some sacrifice in efficiency.

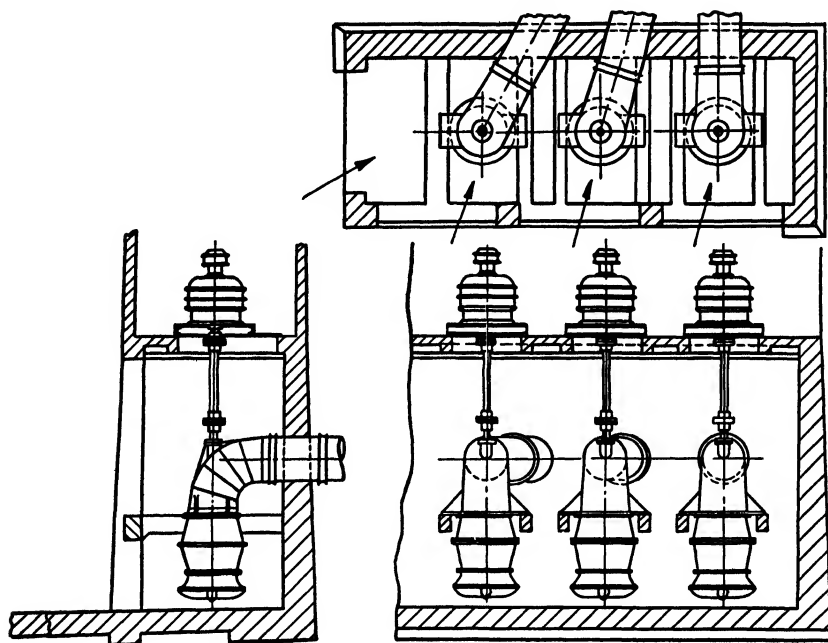


FIG. 16.21. Three 48-in. Byron Jackson propeller pumps rated 45,000 g.p.m. at 8 ft. head, 277 r.p.m., 200-hp. motors (Reclamation District 1500, Woodland, Calif.).

Figure 16.25 shows a horizontal mixed flow pump with diffusion casing. The design of this pump does not differ from that of vertical turbine pumps but, owing to the addition of the short radius elbow, the pump efficiency is appreciably below that of vertical turbine pumps in the ideal setting.

Figure 16.26 shows a small propeller pump used for circulation in a low pressure hot water heating system.

**(b) Vertical Turbine Pumps.** Originally developed on the West Coast in small sizes for irrigation service, vertical turbine pumps soon became an independent industry. According to the United States Census of 1940 there are 78,500 deep-well pumps, for irrigation service,

in 19 states, 52,000 of which are in California with a total horsepower of 1,762,000. The average capacity of these pumps is 1000 g.p.m., at an average head of 52 ft. The same census reveals there are 1284 drainage plants, and of this number 125 plants use propeller pumps having an average capacity of 28,500 g.p.m. The relatively low capacity of the average deep-well pump is governed by the productivity of deep

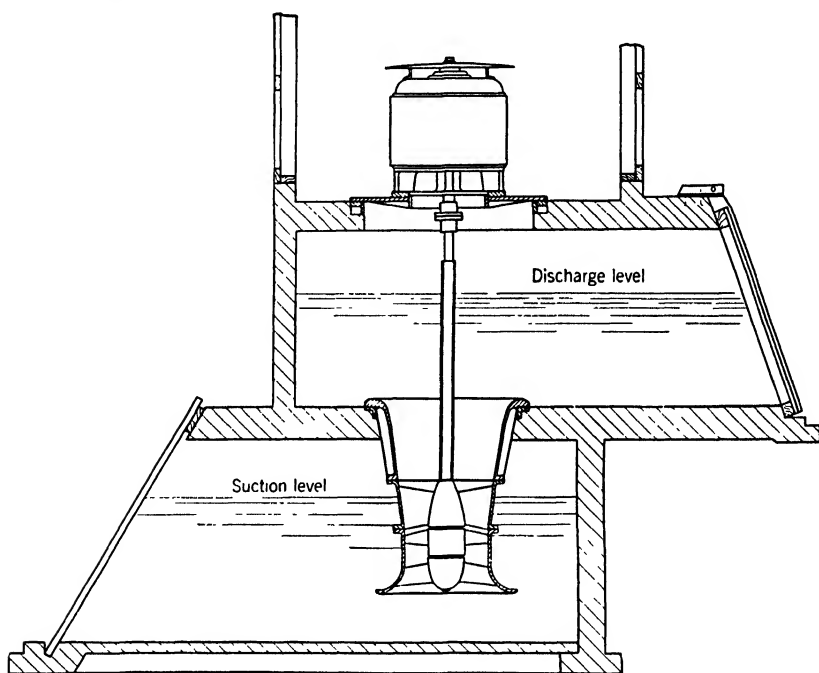


FIG. 16.22. Byron Jackson 30-in. axial flow pump, 32,500 g.p.m., 3 to 5 ft. head (Gulf Coast Water Co., Bay City, Texas).

wells, which falls off very rapidly for sizes above 12 in. in diameter. Thus, if the productivity of a 12-in. well is taken as 100 per cent, the same draw-down on a 24-in. well will produce only 108 per cent capacity; a 6-in. well capacity is 86 per cent. Increasing the draw-down increases the cost of pumping. Considering the cost of drilling, a 12-in. well becomes the most economical size. At the present time the field of application of vertical turbine pumps includes the following services: cooling tower, mine dewatering, condensate, petroleum refinery products, oil well, sump drainage, and many others. High efficiency and simple construction are responsible for such a wide use of vertical turbine pumps.

The design of these pumps is standardized for the entire industry in the United States. Figure 16.27 shows an open shaft water-lubricated open impeller pump. This is a later development than the oil-lubricated columns and its use is constantly increasing. Hollow shaft motors are standard equipment with vertical turbine pumps. Although it has been stated that the contamination of water with oil is the main objec-

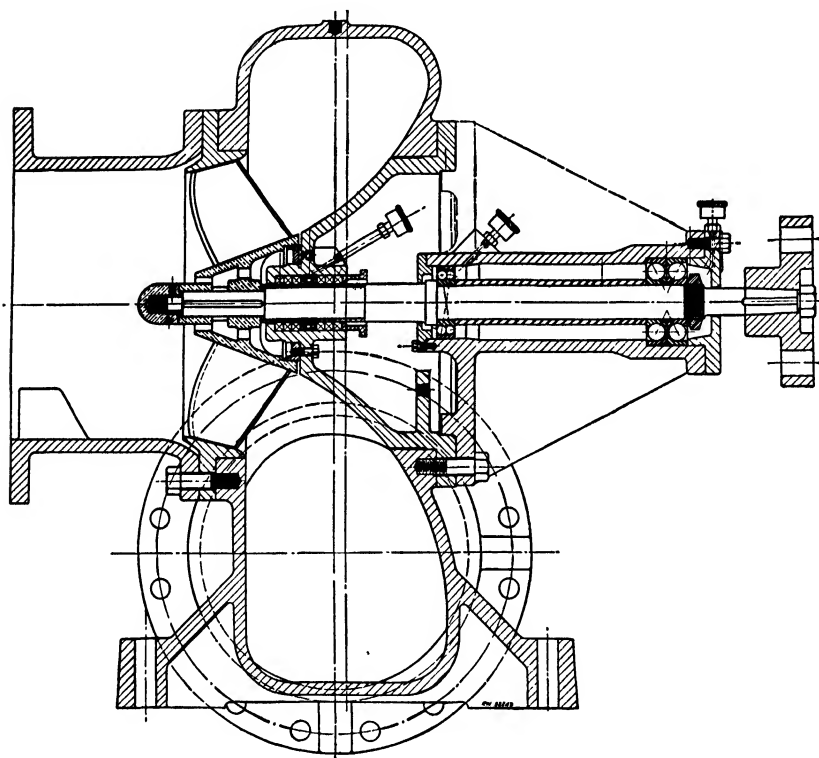


FIG. 16.23. Worthington horizontal mixed flow propeller pump.

tion to oil-lubricated column bearings on deep-well pumps, the real advantages of the open column design (water-lubricated column shaft and open impellers) were lower cost and higher sustained efficiency.<sup>†</sup>

Only the most efficient specific speeds 2500 to 4500 were used for deep-well pumps;  $n_s = 1800$  was used only on small sizes to increase the generated head per stage.

<sup>†</sup> It so happened that the water-lubricated column shaft and open impellers appeared at about the same time and were promoted by the same pump manufacturers.

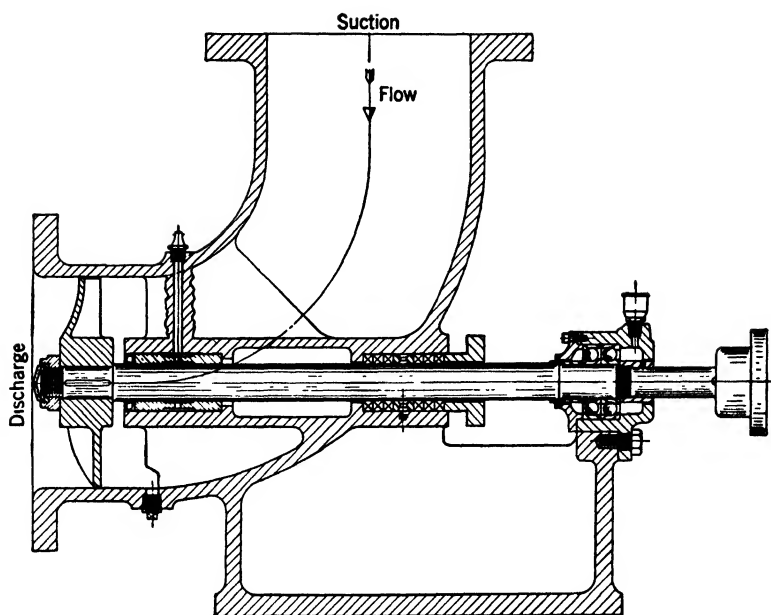


FIG. 16.24. Worthington horizontal axial flow pump, elbow type.

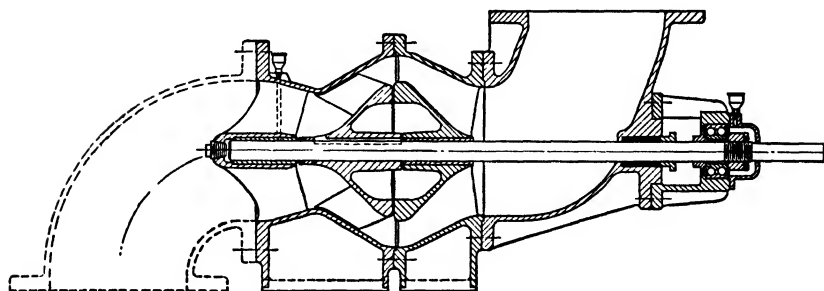


FIG. 16.25. Aurora horizontal mixed flow pump with diffusion casing.



**(c) Vertical Turbine Condensate Pumps.** Figure 16.28 shows a vertical turbine pump arranged for condensate pumping. The pump is mounted as close as possible to the discharge head, and the pumping element proper is placed in a barrel which is long enough to provide the necessary submergence for normal operation at the rated capacity.

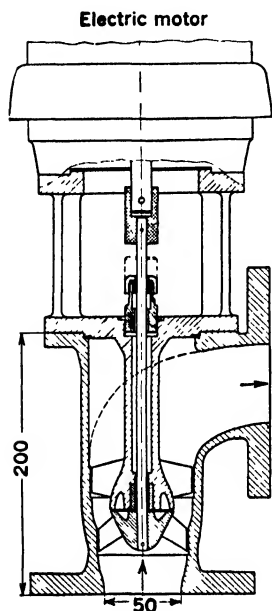


FIG. 16.26. Klein, Schanzlin and Becker small propeller circulating pump for hot water heating system; dimensions in millimeters.

Placing the pump barrel in the basement floor hole does not complicate the construction problem; on the contrary it permits bringing the basement floor closer to the condenser hot-well, thus reducing the size of the building. The hydraulic advantages of the vertical turbine condensate pumps can be summarized as follows: (1) freedom from cavitation at the rated capacity; (2) minimum adverse effects from cavitation at reduced rates of flow; (3) no excess axial thrust, noise, or vibration when operated without governing of the pump discharge; (4) better gross efficiency resulting from a better hydraulic type with less head per stage. As a rule all horizontal pumps are selected oversize because of a limited available submergence. Figure 16.29 shows a general arrangement of a condenser installation with vertical propeller circulating pumps and vertical turbine condensate pumps. Vertical pumps, in addition to better hydraulic and mechanical performance (as compared to horizontal pumps), reduce the floor space and head room requirements, thus materially reducing the cost of the power station building. With proper

materials vertical turbine condensate pumps are used for pumping oil distillates at high temperatures.

**(d) Submersible Motor Deep-Well Pumps.** The last ten or fifteen years have witnessed the development here and in Europe, of submersible motors which are intended primarily for deep-well pump service. In all these designs, the motor is close-coupled to the pump and lowered into the well as one unit. In this way the long column shaft is entirely eliminated. Such designs are particularly suited for very deep or crooked wells where long column shafts are likely to cause mechanical difficulties. The special design features of submersible motors are centered around the problems of (1) keeping the motor windings and power cable dry, (2) designing motors to fit a given size of well without sacri-

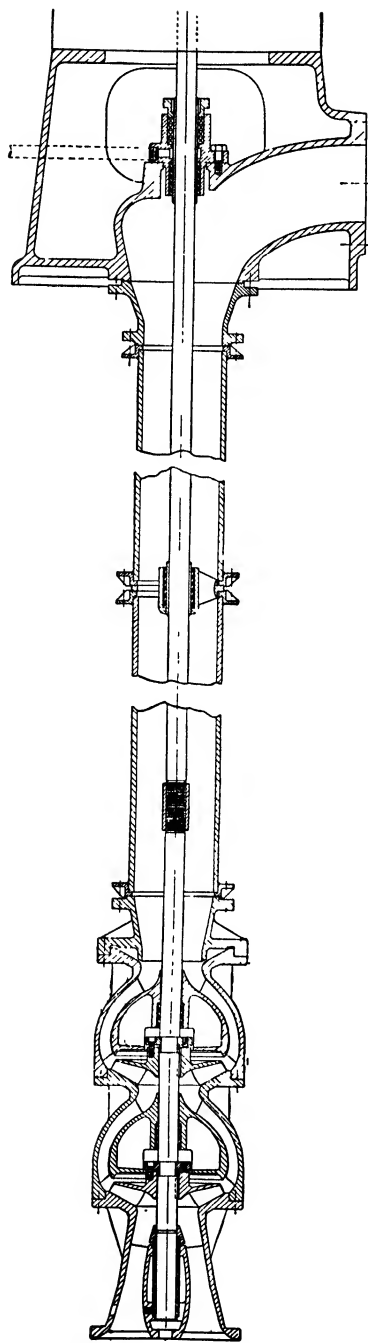


FIG. 16.27. Ingersoll-Rand vertical turbine pump with water-lubricated bearings.

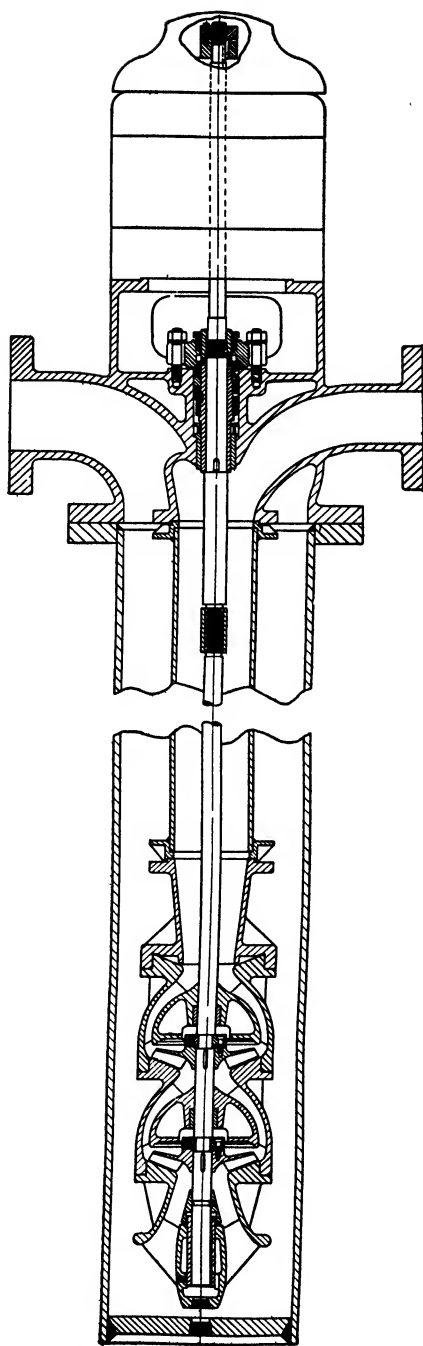


FIG. 16.28. Ingersoll-Rand vertical turbine condensate pump.

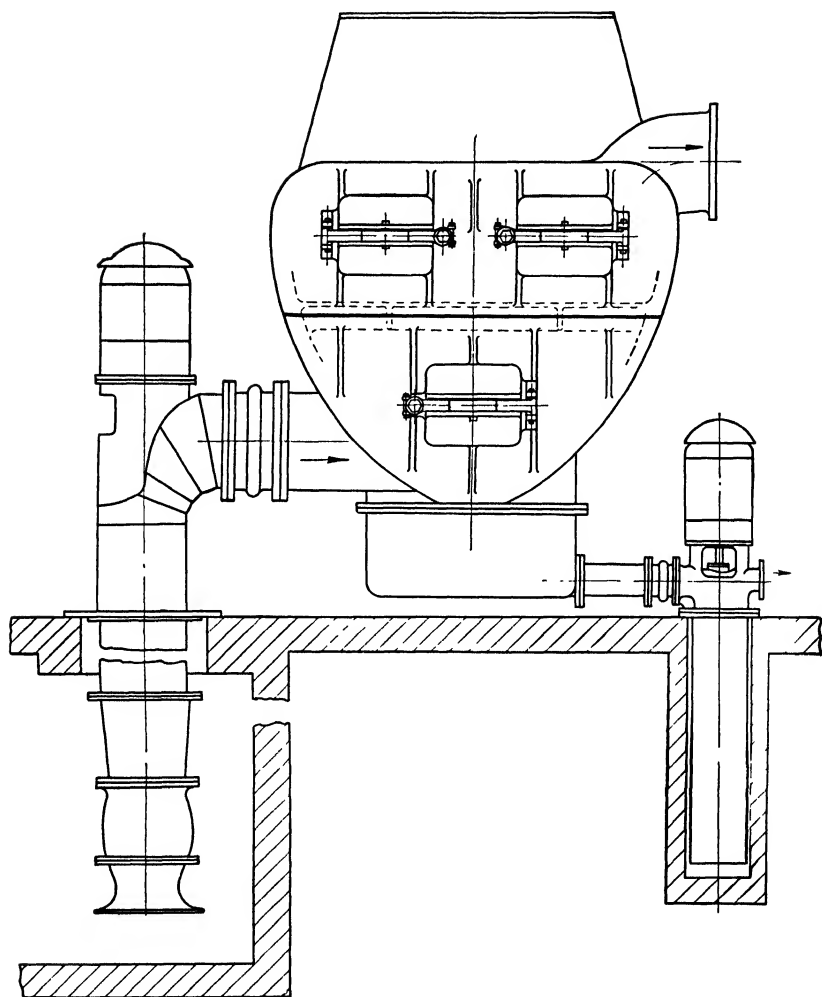


FIG. 16.29. Ingersoll-Rand condenser with vertical propeller circulating and vertical turbine condensate pumps.

ficing motor efficiency, and (3) radial and thrust bearing design. The pumping element does not differ much from a regular deep-well design.

Figure 16.30 shows a submersible motor deep-well pump built up to 350 hp. at 1750 r.p.m. The motor is oil-filled and separated from the water by means of a mercury seal. The lower end of the motor is open to the well pressure, thus allowing oil expansion in the motor shell. Figure 16.31 shows a special application of the same motor for a "stuffing box-less" pump. A complete unit comprising pump and motor are enclosed in a barrel which serves as a suction chamber. There are no other openings from the barrel except the suction and discharge nozzles and cable connection. This design is intended for pumping light hydrocarbons under high suction pressures, where stuffing box difficulties may be anticipated.

Figure 16.32 shows a submersible motor with the stator windings protected by a stainless sleeve mounted between the rotor and stator. The rotor operates in water. The thrust bearing is of the plate type. The pumping element is of the straight centrifugal type with diffusion vane casing.

Figure 16.33 shows a submersible motor pump designed specifically for oil-well pumping. The motor of this unit is oil-filled and kept under a pressure above the well pressure by a spring-loaded grease protector.<sup>8</sup> The major design features of this motor are listed below.

All motors are two-pole, 3600 r.p.m., 440 to 910 volts. Overall plant efficiency 33 to 45 per cent for small capacity, 40 to 55 per cent for large capacity.

Small-diameter motors fit  $4\frac{1}{2}$ -in. well casing, rated up to 52.5 hp.

Large motors fit  $8\frac{5}{8}$ -in. casing, rated up to 240 hp.

Capacities from 1 g.p.m. to 400 ( $8\frac{5}{8}$ -in. casing).

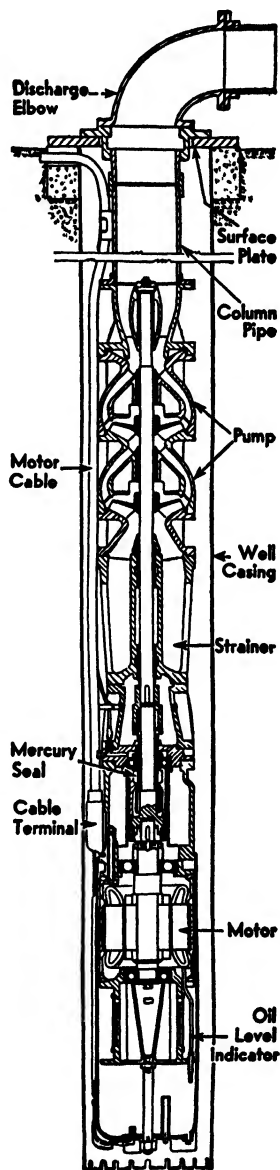


FIG. 16.30. Byron Jackson submersible pump.

Lifts up to 12,000 ft.; at 270°F. bottom hole temperature.

Maximum number of stages 317.

Continuous operation from 200 to 348 days.

Owing to the small diameter and high horsepower ratings these motors are very long. The motor rotor is built up of several sections with a ball bearing in between.

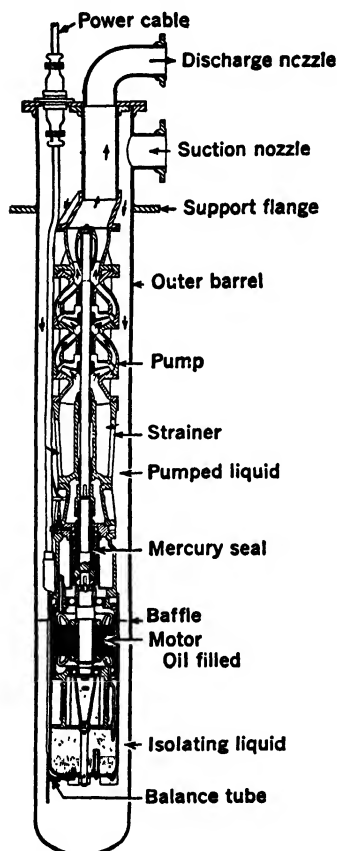


Fig. 16.31. Byron Jackson stuffing-boxless pump.

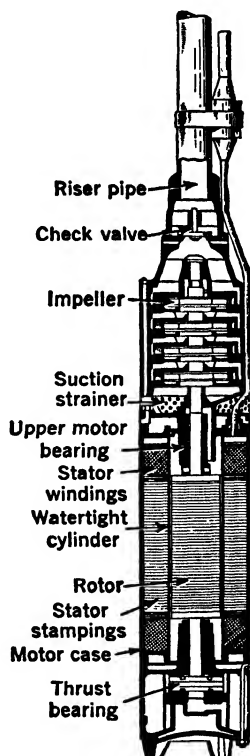


FIG. 16.32. American-Marsh submersible pump.

In European designs of submersible motors the following means are in use to protect the motor from moisture.

- (1) Motor windings are rubber insulated; the rotor runs in water.
- (2) The motor is air-filled, with an air compressor on the surface of the ground, or built into the pump.
- (3) A stainless liner between the stator and rotor as described above<sup>9</sup> is used.

Figure 16.34 shows a submersible portable pump with a centrifugal pumping element. The motor is air-filled and the space between the pump and the motor is oil-filled. There are mechanical seals to keep water out of the oil, and oil out of the motor. The pump is not intended for continuous operation. After 12 hours of operation the oil in the stuffing box compartment is replaced with fresh oil. The motor is water cooled, it is direct-current motor, with 230 volts for use on ships. The pumping element is rated 180 g.p.m. at 50 ft. of head. The complete unit weighs 98 lb. and its outside diameter is  $6\frac{1}{2}$  in.

#### 16.6 MEASURING LARGE VOLUMES OF WATER IN THE FIELD

A large number of propeller pumps are built in sizes which are beyond the testing facilities of the pump manufacturers. Field testing of large pumps presents some difficulties not encountered in testing water turbines. The Allen Salt Velocity and Gibson Methods developed for testing water turbines require a considerable length of discharge pipe which is seldom available in propeller pump installations.†

When the discharge goes into an open flume, weirs constructed across the canal have been found satisfactory for measuring pump capacity. On the Pacific Coast an instrument, known as the Collins Flow Gage,<sup>10</sup> has been used with good results. This works on the pitot tube principle, but is much simpler to use in the field. Fig. 16.35 shows the gage installed in a pipe. It consists of a  $\frac{1}{4}$ - or  $\frac{3}{8}$ -in. tube inserted across the pipe. Two small holes are drilled in the tube diametrically opposite each other, and separated by a short plug. One hole is facing the flow, the other is facing downstream. Owing to the suction effect of the downstream hole the differential pressure across the two ends of the tube is twice the dynamic head of the flow. The originator of

† A further discussion of the methods of measuring large volumes of water is given in Art. 17.5.

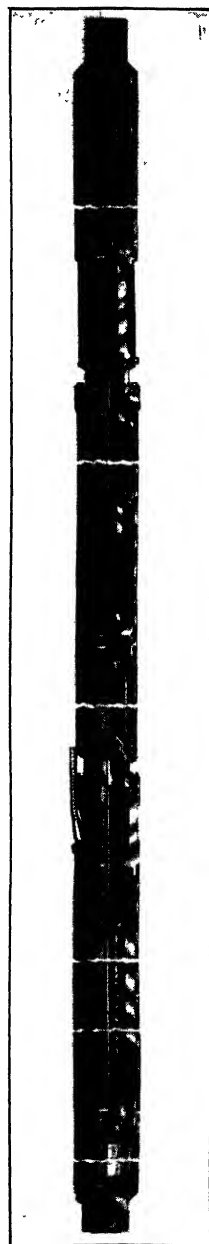


FIG. 16.33. Reda submersible electric pump for oil-well pumping.

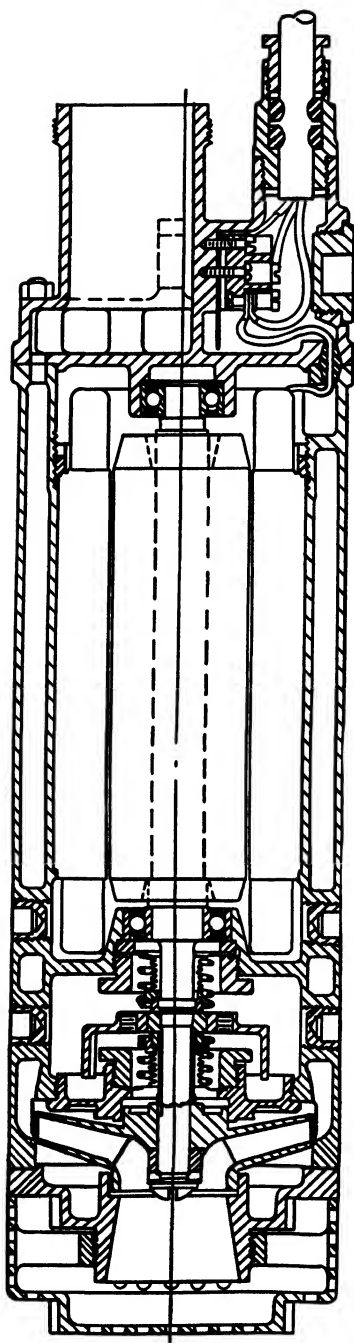


FIG. 16.34. Sawyer portable submersible pump (A. O. Smith Corp.).

this instrument gives the following experimental coefficient for this gage:

$$v = 1.638\sqrt{h}$$

where  $v$  is velocity in feet, and  $h$  is the differential pressure in inches of water. Any desired number of points can be taken in a traverse of a pipe section. For a greater accuracy two traverses 90 degrees apart can be taken simultaneously.

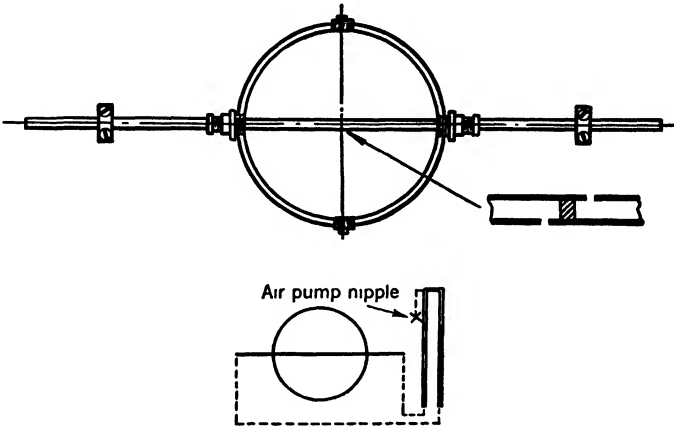


FIG. 16.35. Collins pitot tube.

16.7 FIELD PERFORMANCE OF VERTICAL TURBINE PUMPS

The field performance of vertical pumps with a long discharge column may differ materially from the laboratory or shop performance. Since the motor is selected to meet the field brake-horsepower requirement and the user of the pump is mostly interested in the field performance of the pump, it is important to be able to estimate the field performance of the vertical turbine pump from the shop test or pump rating.

Calculation of the field performance involves the following steps and is better arranged in a tabular form with column headings as shown below.

1	2	3	4	5	6	7	8
Capacity g.p.m.	Field Head ft.	Hydrau- lic Loss ft.	Shop Total Head ft.	Shop Effi- ciency %	Shop b.hp.	Field b.hp.	Field Effi- ciency %



(1) Specified capacity is entered in column 1, to be followed by other capacities to complete the performance curve.

(2) Field head is equal to the static head plus the specified discharge nozzle pressure plus the discharge nozzle velocity head.

(3) Hydraulic friction loss for the total length of discharge column (excluding the discharge elbow) is calculated by using Hydraulic Institute Standards, Charts E-3 or E-4.

(4) Shop total head equals field head (2 above) plus hydraulic friction loss (3 above). The pump is selected to meet the shop head at the specified capacity. Next, columns 1, 4, and 5 are filled out for several capacities from the selected rating curve. Also column 3 is filled out by assuming that the friction loss varies directly as the square of capacity. Column 2 is then filled in by subtracting column 3 from column 4.

(5) Shop rated efficiency is obtained from the rating curves.

(6) Shop brake horsepower

$$= \frac{\text{g.p.m.} \times \text{shop total head}}{3960 \times \text{shop efficiency}} = \frac{(1) \times (4)}{3960 \times (5)}$$

(7) Field brake horsepower = shop brake horsepower plus column shaft friction loss, from Hydraulic Institute Standards, Chart E-5.

$$(8) \text{ Field efficiency} = \frac{(1) \times (2)}{3960 \times (7)}$$

When testing or estimating the performance of vertical turbine pumps used for irrigation service it is customary to charge the discharge velocity head as a loss against the pump. Thus the velocity head is not included in calculating the field head. However, when used for industrial installations, vertical turbine pumps are credited with the velocity head at discharge according to the A.S.M.E. test code.

## REFERENCES

1. *Univ. of Calif. Tech. Memo.* VI, HP-14, 1940.
2. S. LOGAN KERR and STANLEY MOYER, "Hydraulic Engineering Problems at Southwark Generating Stations," *Trans. A.S.M.E.*, Vol. 64, No. 6, Aug. 1942, p. 539.
3. RICHARD W. ALLEN, "Some Experiences of the Use of Scale Models in General Engineering," *Engineering*, Sept. 9, 1938.
4. M. MEDICI, "Versuche an Propeller- und Kaplanpumpen," *Z. Ver. deut. Ing.*, Vol. 87, No. 21/22, May 29, 1943, p. 331.
5. FLOYD A. NAGLER, "Hydraulic Tests of Flap Valves on Drainage Pipe Outlets," *Eng. News-Record*, Vol. 91, No. 26.
6. L. N. REEVE and J. D. SCOVILLE, "Adjustable-Blade Axial-Flow Pumps for Circulating Water," *Combustion*, May 1943, pp. 30-37.

7. J. D. SCOVILLE, "Comparative Characteristics of Fixed and Adjustable-Blade Axial-Flow Pumps," *Trans. A.S.M.E.*, Vol. 64, No. 6, Aug. 1942, pp. 599-605.
8. J. ZABA, "Characteristics of the Submersible Electric Pumps," *Oil and Gas Jour.*, June 3, 1944.
9. C. PFLEIDERER, "Der Entwicklungsstand der Tauchpumpen," *Z. Ver. deut. Ing.*, Vol. 80, No. 9, Feb. 29, 1936, pp. 253-256.
10. U. S. Patent 1,374,359, 1921; by Arthur L. Collins, Berkeley, Calif.
11. J. W. McNULTY, "Propeller-Type Pump Shows High Efficiency," *Power*, Jan. 13, 1931, p. 63.

## CHAPTER 17

### SPECIAL PROBLEMS AND APPLICATIONS OF CENTRIFUGAL PUMPS

#### 17.1 HOT-OIL PUMPS

The application of centrifugal pumps to the pumping of petroleum oils under high pressures and temperatures presented several very difficult problems, some of which took many years to solve. The development of modern hot-oil pumps depended on a satisfactory solution of the following problems.

(a) A suitable stuffing box design capable of sealing such pumps operating at high rotative speeds with minimum attention and maximum packing life.

(b) The selection of materials to withstand high pressures, temperatures, and the corrosive action of petroleum oils.

(c) A suitable mechanical design to counteract uneven heat absorption and radiation by the pump casing and to prevent seizure and scoring of internal parts.

Experience has shown that good metallic packing, hard rustless shaft sleeves, and freedom from vibration are the prerequisites for successful stuffing box operation. Water-jacketing of the stuffing boxes is universal on hot-oil pumps.

The application of centrifugal pumps to the pumping of light hydrocarbons presented somewhat different stuffing box problems. In this case, the liquid is cold while the stuffing box pressures are high, and the liquid flashes into gas at atmospheric pressure; thus, it is impossible to lubricate stuffing boxes with the pumped liquid. In most cases, the stuffing boxes are sealed with a heavier oil at a pressure slightly above the vapor pressure of the pumped liquid. In many cases, the stuffing boxes are heated through the jackets to counterbalance the refrigerating effect of the escaping gas.

In recent years mechanical seals have been used successfully for sealing high pressure stuffing boxes up to 600 p.s.i. and at temperatures above 250°F.<sup>1, 2</sup>

To reduce the possibility of internal seizure of rotating parts, a vertical construction was adopted on the first hot-oil pumps. This design had one stuffing box and a blind outboard bearing. However, it was later learned that, with a proper selection of materials and provision for heat expansion of different materials, seizures were practically eliminated. The vertical design proved to be unpractical for several reasons, one being the axial thrust problem created by the blind bearing construction.

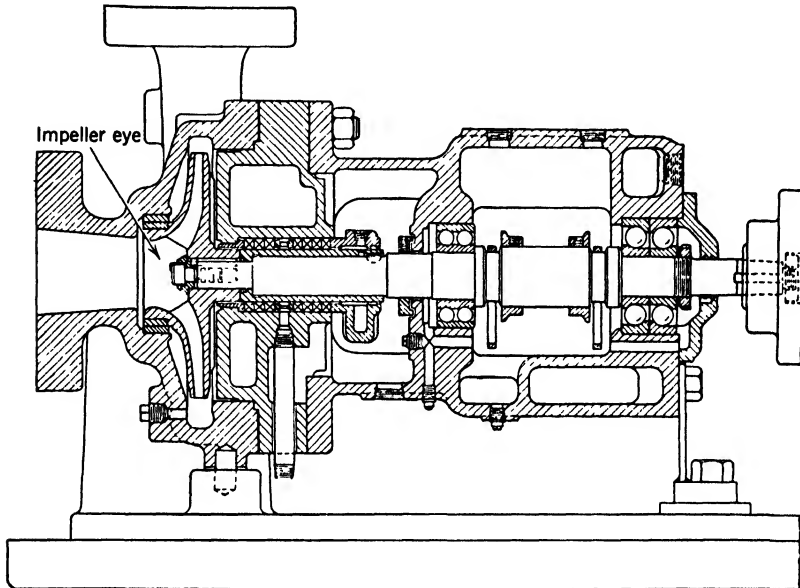


FIG. 17.1. Ingersoll-Rand single-stage hot-oil pump.

In order to withstand high pressures at high temperatures, hot-oil casings are designed so that the case openings have circular confined gaskets. Figure 17.1 shows the design of a single-stage pump. The spacer-type coupling used with this construction permits removal of the rotating element, including the ball bearing bracket, without disturbing the piping or alignment of the units. Pumps with more than two stages are designed with an internal casing placed inside a cylindrical shell having one or two end covers (Fig. 17.2). The inner casing is split vertically or horizontally and is under compression due to full discharge pressure existing between the shell and the inner casing. The design of the outer shell is made in the same manner as that for any unfired pressure vessel, except that the stresses are kept low because any deflection of the casing affects the alignment of the rotating element with

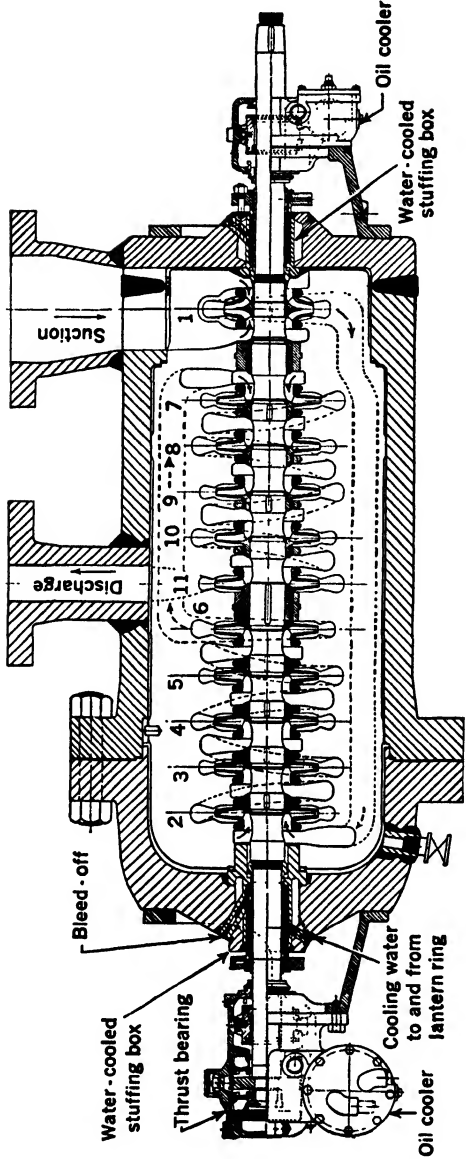


FIG. 17.2. Byron Jackson hot-oil charging pump.

respect to the stationary parts. As a rule, the pump casing carries the bearing supports; thus any distortion of the outer shell is reflected in the location of the rotating element. Pumps having independent bearing supports proved impractical. The vertical construction is still used on the small capacity, high head pumps having a great number of stages. In these, the pumping element is enclosed in a barrel, under full discharge pressure, which is mounted below the floor level (Fig. 17.3).

The inner casing is made up of one-stage sections and can be assembled in any number of stages. Stages can be added or removed if the head requirements change. To obtain a complete balance of radial forces on the rotating element, adjacent stages are turned through 180 degrees. Axial balance is obtained by dividing the total number of stages into two groups, the impellers of each group facing in opposite directions. The number of stages in each group may or may not be equal.

The problem of corrosion is most effectively taken care of by using special materials which will resist the corrosive action of chemicals carried by the pumped oil. The practice of lining pump barrels with stainless steel sheets or bars, and use of stainless welding, has been used to a limited extent. In all other cases a corrosion allowance is made for the decrease of metal thickness to assure the required years of service. For the majority of pumps (single-stage and two-stage) this allowance requires no excess of metal thickness over that necessary to obtain a satisfactory steel casting.

The heat expansion of pump parts can affect the mechanical performance of the pump in several ways:

(a) If the parts of the rotating element are of different materials than the pump casing, the running clearances may be reduced below a safe minimum owing to a difference in the coefficients of expansion and a difference in temperature.

(b) Such parts as shaft sleeves, impeller rings, and casing wearing rings, which are tightly fitted when cold, may become loose when hot owing to a difference in temperature or coefficient of expansion. For example, *if the impeller expands more than the impeller wearing ring, the latter may be stretched beyond the elastic limit when hot, and become loose on the impeller when cold; also, if the casing wearing ring expands more than the casing, the ring may be compressed beyond the elastic limit when hot, and become loose in the casing when cold.* In both cases the running clearance is reduced below the original when the pump is cold.

(c) The rotating element, in perfect alignment when cold, may get out of alignment when the casing is hot owing to heat distortion of the

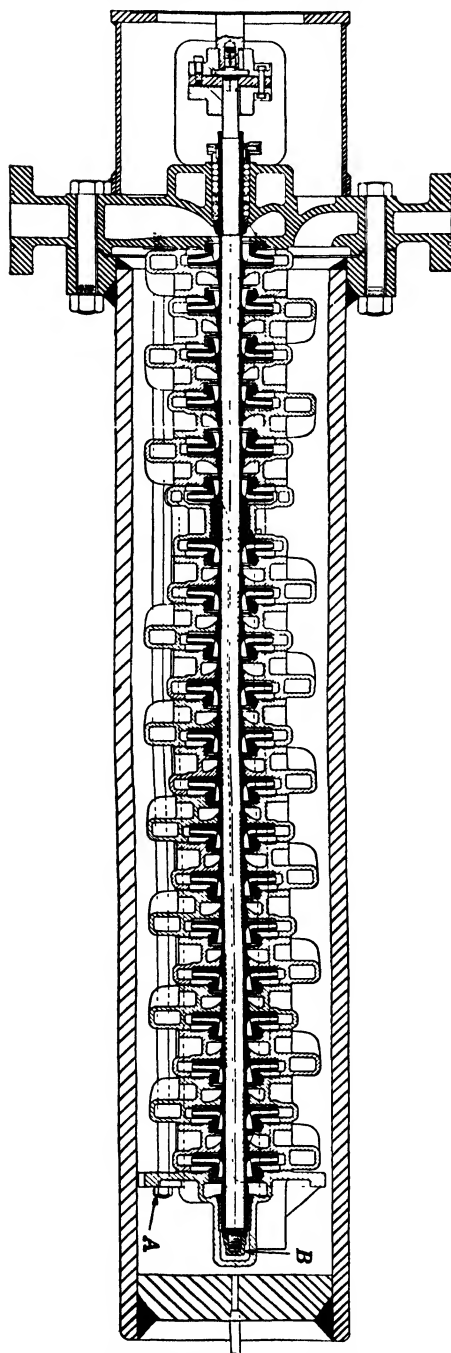


FIG. 17.3. Ingersoll-Rand vertical multistage pump.

casing. To prevent misalignment the pump casings are supported near the center plane of the rotating element and are keyed to the baseplate in the vertical central plane (Fig. 17.4). *However, this is not sufficient to assure freedom from casing distortion caused by a difference in the rate of heat absorption by different parts of the casing during the starting period and a difference in the heat dissipation when thermal equilibrium of all the pump parts is reached.*

*Water cooling of the pump bases or supporting pedestals, as used on the early pumps, can do more harm than good under certain conditions, as the following considerations show. Without water cooling, the pedestals are seldom hotter than 120° to 140°F. Motors and most steam turbines*

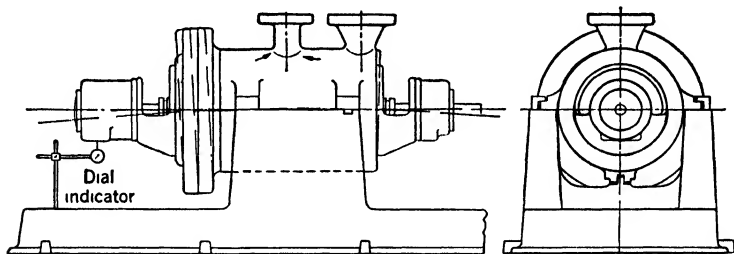


FIG. 17.4. Casing distortion when starting cold pump on hot oil.

are bottom-mounted, and their frames reach about the same temperature as the pump pedestals. Steam turbines, even when center-mounted, are never provided with water-cooled supports. Thus it is evident that if the pump and the driver are aligned when cold they will maintain the alignment better without water cooling of the pump supports.

Uneven heat expansion of the pump casing is the most serious cause of mechanical failures. This is more pronounced in large multistage pumps of the double-case type, such as used for charging service (Fig. 17.4). If the pump is put on stream cold when starting a run and is brought up to temperature gradually during several hours, there is sufficient time for all parts to reach the same temperature, and no casing distortion results. However, if hot oil is charged to the pump suddenly the various pump parts do not reach the same temperature at the same time. Usually, the upper part of the outer casing reaches its highest temperature an hour or more before the bottom. This is because both the suction and discharge nozzles, which carry hot liquid, are on top, whereas at the bottom there are dead spaces filled with cold oil (between the inner and outer pump casings). Under these circumstances the pump casing is distorted as shown in Fig. 17.4. The amount of distortion actually observed on a pump with a bearing span of 80 in.



was in excess of  $\frac{3}{16}$  in. This was measured with a dial indicator at the outboard bearing. Calculations indicate a difference in temperature, between the top and the bottom of the outer casing, of about 350°F. Even after thermal equilibrium is reached there is an appreciable temperature difference and, hence, the casing distorts if special means are not provided to prevent it.

There are several ways to eliminate or reduce casing distortion:

(a) Hot oil is circulated through the casing of a spare pump to keep it ready for starting on hot oil in case of an emergency.

(b) Oil circulation is provided through the bottom of the barrel during the starting period even when starting on cold oil, by means of by-passes from the bottom of the barrel to the pump suction.

(c) The discharge from the inner casing is divided so that one half of it is directed upward and the other half downward.

(d) The pump casing is well insulated to reduce and equalize loss of heat from the outer casing to the atmosphere.

Evidently heat distortion imposes a severe strain on a pump shaft and bearings and usually results in permanent damage. A self-aligning radial bearing reduces the chances for shaft damage under such conditions.

Still another example damaging a pump mechanically will be presented.<sup>3</sup> The cause in this case may affect even small single-stage pumps; it lies in the temperature difference between the internal parts and the outside casing when the latter is not insulated. Figure 17.5 shows a single-stage, hot-oil pump with a vertically split casing sealed with a circular confined gasket. The diaphragm separating the suction chamber from the discharge casing is closely fitted into the casing. In a pump of this type, when oils are being pumped at a temperature of about 800°F. with the casing uninsulated, the temperature of the diaphragm will be equal to that of the hot oil, and that of the casing will be several hundred degrees lower. The expansion of the diaphragm, being restricted by the cooler casing, may result in compression of the diaphragm and tension in the casing beyond the elastic limit, and both will receive a permanent deformation. When cold, the diaphragm will be loose in the casing. If the joint between the volute casing and suction chamber is made without a gasket (metal-to-metal fit), loss of capacity will result when the pump is operated at a temperature lower than the maximum to which the casing was subjected. The magnitude of stresses developed under such conditions can be judged by the fact that steel casings made from perfectly sound steel castings of normal wall thickness were found cracked under such conditions.

Calculations show that if a steel bar is heated and its expansion is prevented by an outside force a temperature of only 100°F. is required

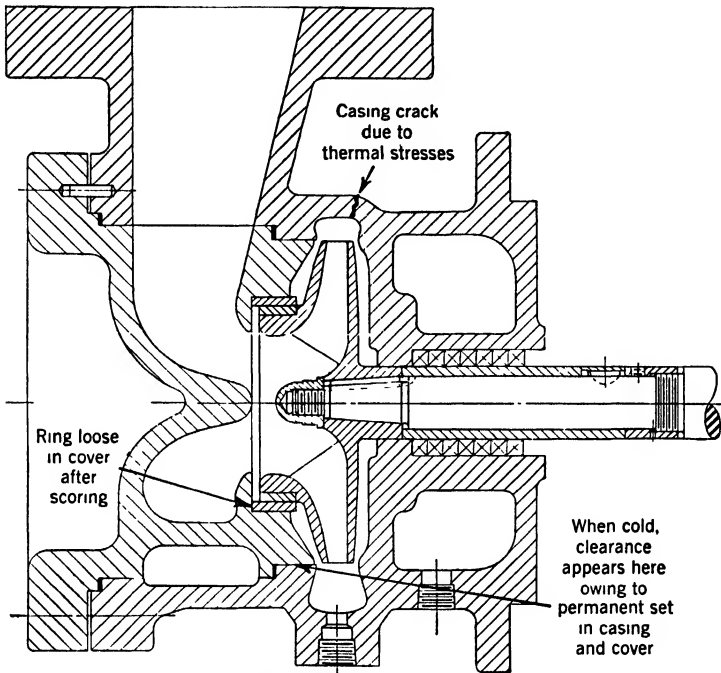


FIG. 17.5. Effect of temperature difference inside and outside of pump.

for the bar to reach its elastic limit of 50,000 per square inch. If heating is continued the bar will get a permanent deformation and will be crushed (Fig. 17.6). Upon cooling, the bar will contract in a regular manner but will be shorter than it was originally. This is independent of bar section or length.

These examples emphasize again the importance of insulation on hot-oil pumps, not to conserve heat, but to assure satisfactory mechanical operation of the pump.

It is well to mention here that scored casing wearing rings of pumps handling cold liquids are frequently found loose in the casing although they were originally tightly fitted. The reason for this is that the ring is subjected to heat expansion from the heat generated by rubbing or scoring and, since the

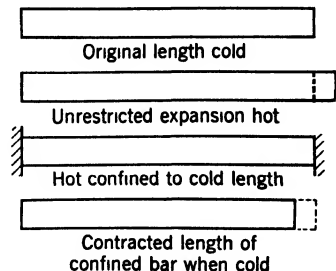


FIG. 17.6. Steel bar crushed by restricted heat expansion.

ring is held in a confined space, it receives at permanent set in a manner similar to that of the diaphragm described in the preceding example.

It can be stated that modern hot-oil centrifugal pumps are just as simple, efficient, and reliable as cold-water pumps. Their higher cost is governed by special materials and the design necessary to meet the service requirements of the refinery.

## 17.2 FIELD TESTING OF HOT-OIL PUMPS

Owing to high pressures and temperatures the testing of hot-oil pumps under actual operating conditions in the field requires a somewhat different procedure from that established for testing water pumps. The complication results from the fact that oil cannot be considered incompressible at the temperatures and pressures involved, and the specific gravity and volume measurements at suction pressure are different from those taken at the pump discharge. At the pressures and temperatures encountered with hot-oil charging pumps, the compressibility of the oil as it passes through the pump becomes appreciable as can be seen from the following examples:

At 680°F.	Atmospheric Pressure	400 p.s.i.	800 p.s.i.
Specific gravity of oil	0.598	0.620	0.638

The variation of specific gravity affects calculation of the pump output. Depending on the formula used for the pump output specific gravity enters in either measurements of head in feet or capacity. Thus, taking the formula

$$\text{Pump output} = \frac{Q\gamma H}{550} = \frac{WH}{550} \text{ hp.} \quad (17.1)$$

where  $W$  = weight of liquid pumped per second, measured either at pump suction or discharge

$H$  = head in feet determined from

$$H = \frac{(p_d - p_s)2.31}{s} \quad (17.2)$$

where  $p_d$  = pump discharge pressure in pounds per square inch

$p_s$  = suction pressure in pounds per square inch

$s$  = specific gravity of pumped oil.

If pump output is calculated by using the formula

$$\text{Pump output} = \frac{\text{g.p.m. } (p_d - p_s)}{1714} \text{ hp.} \quad (17.3)$$

the net head in pounds is obtained directly from the pressure gage readings, but capacity measurements depend on the specific gravity.

The author has shown<sup>4</sup> that the true pump output is obtained very accurately if, in formula 17.2, the average of the specific gravities at suction and discharge pressures is used; also that the same result is obtained if, in formula 17.3, the average capacity of those measured at the suction and discharge pressures is used.

The question can be looked upon from a different point of view. As long as the liquid cannot be considered incompressible the pump should be credited not only with the work of lifting the liquid from one level to the other but also with the work of compressing the liquid. The work of compression of the liquid can be calculated with formulas of thermodynamics when the law of the variation of volume with pressure is known. This is not the case with petroleum oils. The work of pumping incompressible liquids can be represented by a rectangle  $ABCD$  on the  $pV$  diagram, Fig. 17.7. If the liquid is compressible the work done on the liquid will be represented by an area  $ABCE$  where  $BE$  represents the compression line from the suction pressure  $p_s$  and volume  $V_s$  to the discharge pressure  $p_d$  and volume  $V_d$ .

Using average capacity in formula 17.3 is equivalent to substituting the rectangle  $AFGC$  for area  $ABCE$  or assuming a straight line variation of volume with pressure. For the range of pressures and volume changes dealt with in hot-oil pumping this approximation results in an error considerably smaller than the accuracy of the observation and calculating involved. The capacity of hot-oil pumps is measured in the field with flowmeters, usually provided with recording mechanisms, and calculations of capacity from flowmeter observations involve several steps not encountered in calculations of capacities of incompressible liquids at normal temperatures. The procedure is outlined in the author's article.<sup>4</sup>

### 17.3 BOILER FEED PUMPS

**(a) Requirements.** Application of centrifugal pumps to boiler feed service presented a number of problems not encountered in any other field of application involving high pressure and high temperature pumps. These may be listed as follows.

(1) Requirement of a stable head-capacity characteristic throughout the whole range of capacities (see discussion in Chapter 14).

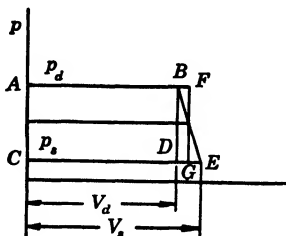


FIG. 17.7. Work diagram pumping compressible liquids.

(2) The NPSH requirements are in excess of those given by the cavitation constant  $\sigma$  to prevent vapor binding as a result of sudden reduction of electric load, or sudden increase of pump capacity.

(3) Protection against overheating when operating at zero or low capacities.

(4) Material selection to suit the feed water composition to assure normal life of pump parts.

Hydraulic and mechanical problems connected with high pressures and temperatures are not different from those of hot-oil charging pumps described above.

**(b) Minimum NPSH.** In Chapter 12 it has been shown that the NPSH above the vapor pressure does not depend on the temperature or pressure of the liquid if the liquid is in the boiling state. However, in boiler feed service it has been found by experience that there is a danger of flashing in the pump suction whenever the load on the steam turbine is dropped suddenly. The sequence of events in this case is as follows. As the electric load on the generator is reduced, the steam turbine tends to speed up. The constant speed controls act to throttle the steam supply to the steam turbine; as a result the pressure drops in all stages of the steam turbine, including the stage feeding steam to the direct contact heater. The water in the storage space of the heater and suction piping is then at a higher temperature than that corresponding to the reduced pressure, and violent vaporization of the water will take place until the pressure-temperature equilibrium is established. A sudden "dynamic" pressure drop may occur in the suction pipe when the throttle on the discharge pipe is opened suddenly. This action requires that the mass of water in all piping be accelerated in a short interval of time. The pressure differential in the suction line may not provide sufficient force to accelerate the liquid in the suction line as rapidly as that of the discharge system, and a severe pressure drop results.<sup>5, 6</sup>

The Hydraulic Institute Standards give NPSH recommendations in terms of pump capacity and speed for water at 212°F. (see chart B-24 in Reference 7). The additional suction head required for water of higher temperature is given in chart B-26. These values do not represent absolute minimum values of NPSH fixed by the pump design, but are safe values derived from successful practice in power plant design.

**(c) Minimum Flow.** In order to protect boiler feed pumps from overheating (vapor binding and scoring may follow) when the capacity is reduced below a safe limit, provision is made to by-pass a small portion of the pump capacity back to the water heater. The amount of

water by-passed varies from 5 to 10 per cent of the normal capacity. The minimum volume of water to be by-passed is determined by the NPSH available on the pump suction, which determines the permissible water temperature rise. If this limit is exceeded, flashing will take place at the throttling surfaces of balancing devices. Such by-passes are either operated manually or automatically from the feed water flowmeter. In some cases they are left open continuously. The leak-off from the balancing devices can be used as a portion of by-passed capacity; in every case the leak-off is piped to the heater storage space rather than to the pump suction.

(d) **Selection of Materials.** This selection is governed by the following factors: pressure, temperature, water treatment, and cost of

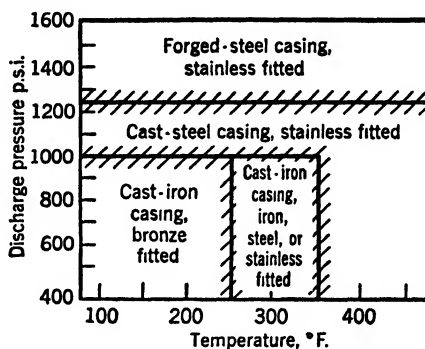


FIG. 17.8. Boiler feed pump materials in terms of pressure and temperature.

material. Figure 17.8 shows materials for boiler feed pumps in terms of pressure and temperature alone. Final selection depends on the nature of the boiler feed water.

The activity of water in attacking materials is represented by *pH* values. *pH* stands for potential of hydrogen, and the *pH* number represents the hydrogen-ion concentration. The *pH* numbers are the logarithms of the concentration with the sign reversed (or logarithms of the reciprocal of concentrations); thus the concentration of pure water is 1/1,000,000; its *pH* number is 7.0. An increase of one in the *pH* number denotes a concentration decrease of ten times. On the *pH* scale, 7.0 represents a neutral solution; decreasing values below 7.0 show increasing acidity, and increasing values above 7.0 denote increasing alkalinity. The *pH* value of water varies with the temperature. Pure water is susceptible to *pH* fluctuations. Figure 17.9 gives material selections based on *pH* values of boiler feed water.<sup>8</sup> When feed water is pure condensate, the *pH* value does not accurately describe the cor-

rosiveness of water, and corrosion-resisting materials (stainless steel) should be used.<sup>9</sup>

Although the speed of 60-cycle motor-driven boiler feed pumps is limited to 3600 r.p.m., steam turbine-driven pumps in smaller sizes are operated at speeds up to 7500 r.p.m. Higher speeds permit the use of centrifugal boiler feed pumps for low capacities and high heads because the resulting specific speed produces more efficient types than those possible at 3600 r.p.m.

Figure 17.10 shows a double-case, high pressure, boiler feed pump. The inner casing consists of diffusion casing sections with all impellers

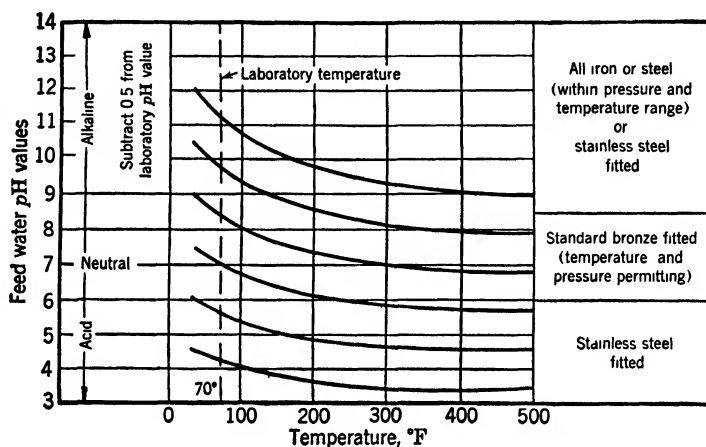


FIG. 17.9. Boiler feed pump materials based on pH values of feed water (Karassik).

facing in one direction. The axial thrust is balanced by means of a balancing disk with a throttle ahead of the disk. Pumps of this type are in service with the discharge pressure up to 2800 p.s.i.

Figure 17.2 shows a high pressure, double-case, boiler feed pump with an inner casing of the horizontally split volute type. Figures 11.7 and 11.8 show boiler feed pumps with horizontally split casings. The first one is of the volute type, and all the impellers are of the double-suction type. The second is of the diffusion vane casing type with the automatic balancing disk. Both pumps are built in seven stages for high pressure boiler feed.

Figure 17.11 shows a single-stage, high speed, boiler feed pump built integral with the steam turbine, intended primarily for locomotive and marine service. These pumps are built for capacities up to 300 g.p.m., pressures up to 750 p.s.i. or 1800 ft. of head, water temperatures up to 300°F., and speeds of 7400 r.p.m.

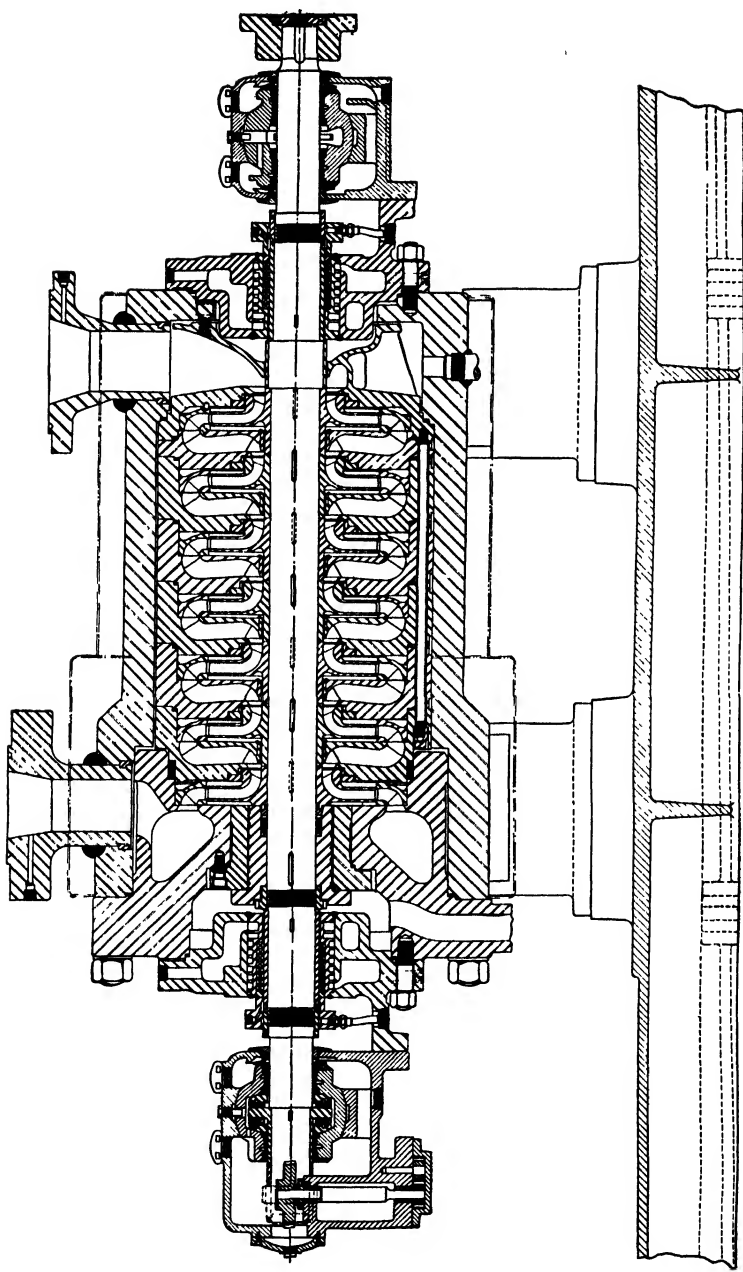


Fig. 17.10. Ingersoll-Rand boiler feed pump.



Figure 17.12 shows a small eight-stage pump with a horizontally split casing and opposed impellers. In four and six stages, this pump was widely used for boiler feed service, within its pressure and temperature range, at speeds up to 6000 r.p.m.

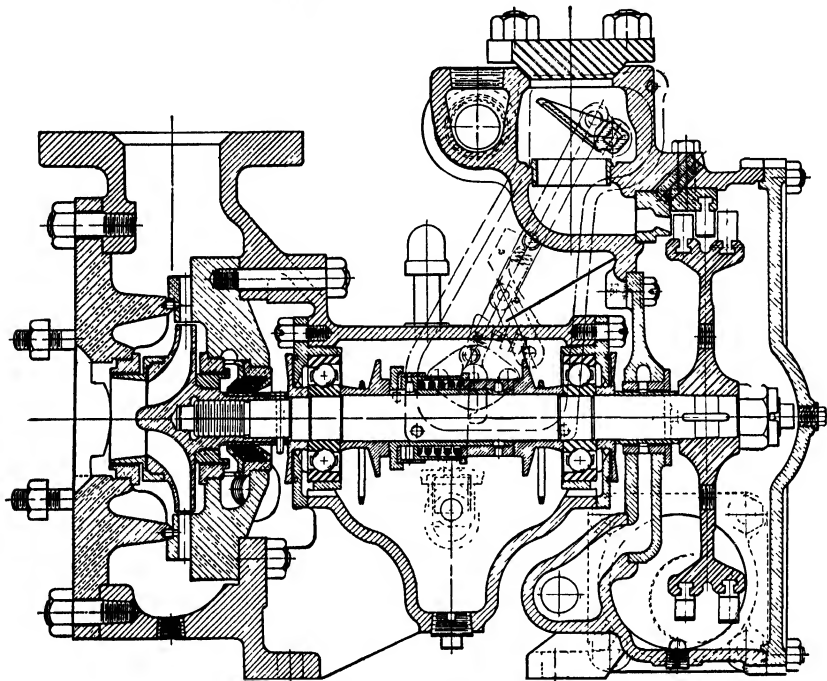


FIG. 17.11. Coffin boiler feed pump.

#### 17.4 BOILER FORCED CIRCULATION PUMPS

Although used widely in Europe, boilers with forced circulation are new and few in the United States.<sup>10</sup> The circulation cycle consists in withdrawing a certain quantity of water from the boiler drum and forcing it through the evaporating section of the boiler. The head on the circulating pump is relatively low (50 to 60 lb.) and represents only the friction through the boiler evaporator section. The pump capacity is equal to about three times the full load evaporation rate of the boiler. The overhung single-suction type of pump is universally used for this service. Since the suction pressure is equal to full boiler pressure, the overhung construction produces a very high axial thrust equal to the shaft sleeve area or shaft area through the stuffing box times the suction pressure in pounds per square inch. Sealing the stuffing box presents a

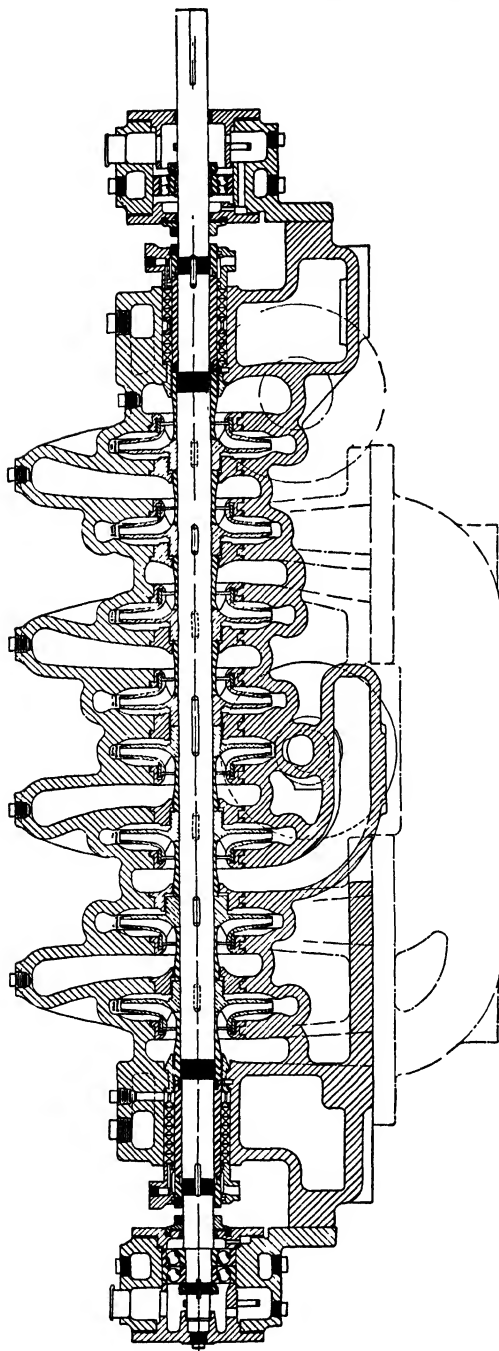


FIG. 17.12. Ingersoll-Rand 8-stage pump.

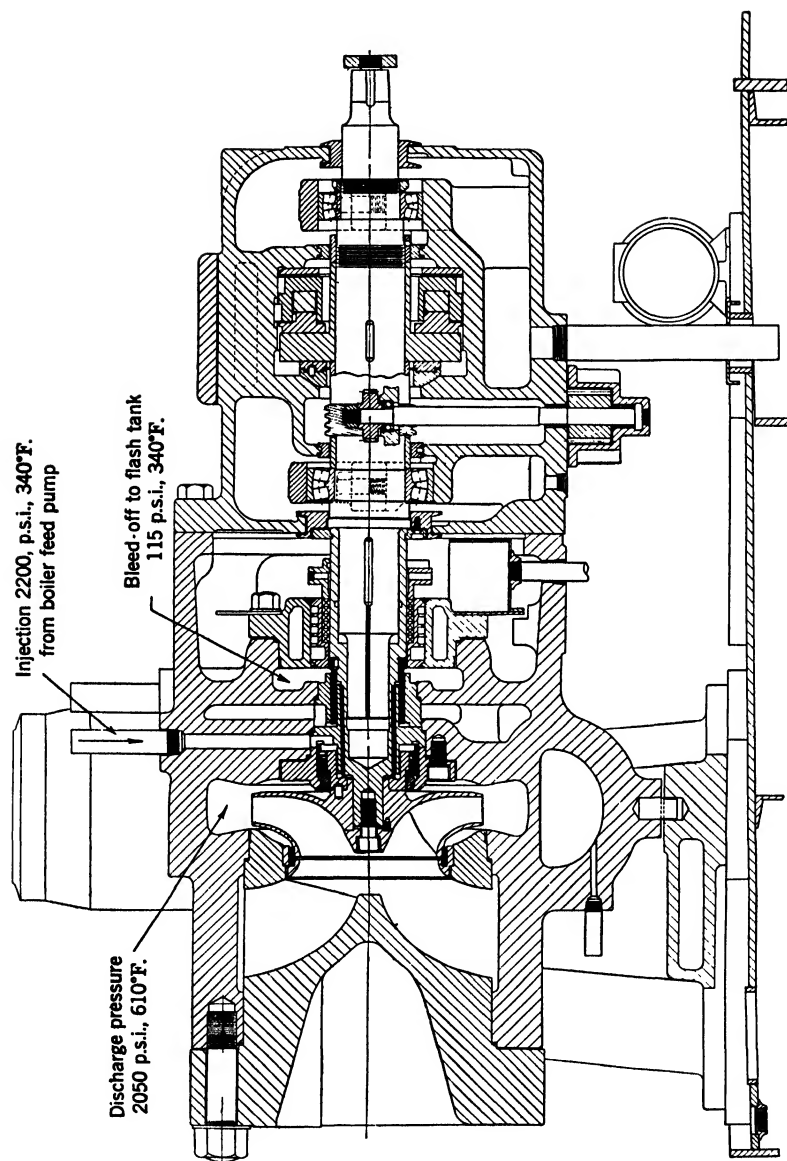


FIG. 17.13. Ingersoll-Rand boiler circulating pump, 3500 g.p.m., 50 p.s.i. head, 1760 r.p.m., suction pressure 2000 p.s.i., water temperature 690°F. (at Montaup Electric Company).

problem. To reduce the axial thrust and stuffing box bleed-off leakage, some European designs<sup>11</sup> taper off the impeller end of the shaft and eliminate the shaft sleeves.

Figure 17.13 shows a 12-in., 3500 g.p.m., 50-p.s.i., 1760-r.p.m. circulating pump. The suction pressure is 2000 p.s.i. and the water temperature is 690°F. Boiler feed water at 340°F. is injected at the inner end of the stuffing box, and the box pressure is reduced from 2200 p.s.i. to 115 p.s.i. by means of a labyrinth bleed-off. In Europe, circulating pumps have been built for pressures up to 3500 p.s.i. for Benson boilers.

### 17.5 EXAMPLES OF CENTRIFUGAL PUMPS AND INSTALLATIONS

Figure 17.14 shows the design of the largest of the group of pumps of the Colorado River Aqueduct. The rating of this pump is 90,000 g.p.m., 444 ft. of head, at 450 r.p.m., and it requires 12,500 hp. The specific speed is 1400. Efficiencies over 90 per cent were obtained with an 8-in. model of this pump.<sup>12</sup> These are the largest pumps in the United States at the present time, but they will be dwarfed by the proposed Grand Coulee project calling for pumps rated at 607,000 g.p.m. and 310 ft. of head at 200 r.p.m. These will have a specific speed of 2110 and will require 65,000-hp. drivers.

Figure 17.15 shows the general arrangement of the intake pumping plant of the Colorado River Aqueduct which is typical of the five plants of the project.<sup>13</sup> The field test covering pumps of three different makes (for different head but same capacity) failed to show any gain in efficiency over that of their models. There are several reasons for this: (1) the model pump impellers and casings were highly polished so there was hardly any decrease in the relative roughness in the full-sized pumps; (2) neither suction nor discharge piping, including their valves, were reproduced in the model testing; (3) inaccuracy of the field testing methods.\*

All methods used for measuring large volumes of flow in pipes were developed for water turbine application. The accepted tolerances favorable for the water turbines are unfavorable for the pumps. Very extensive tests<sup>14</sup> have shown that weir measurements (Rehbock formula), flowmeters of the Ott type, and salt-velocity methods all show capacities too low as compared with volumetric measurements on a large scale. In addition, the last method has shown that the results depend appreciably on the distance between the point of salt injection

\* In Art. 3.5 it was pointed out that suction head measurements were adversely affected by the forced vortex in the suction pipe.

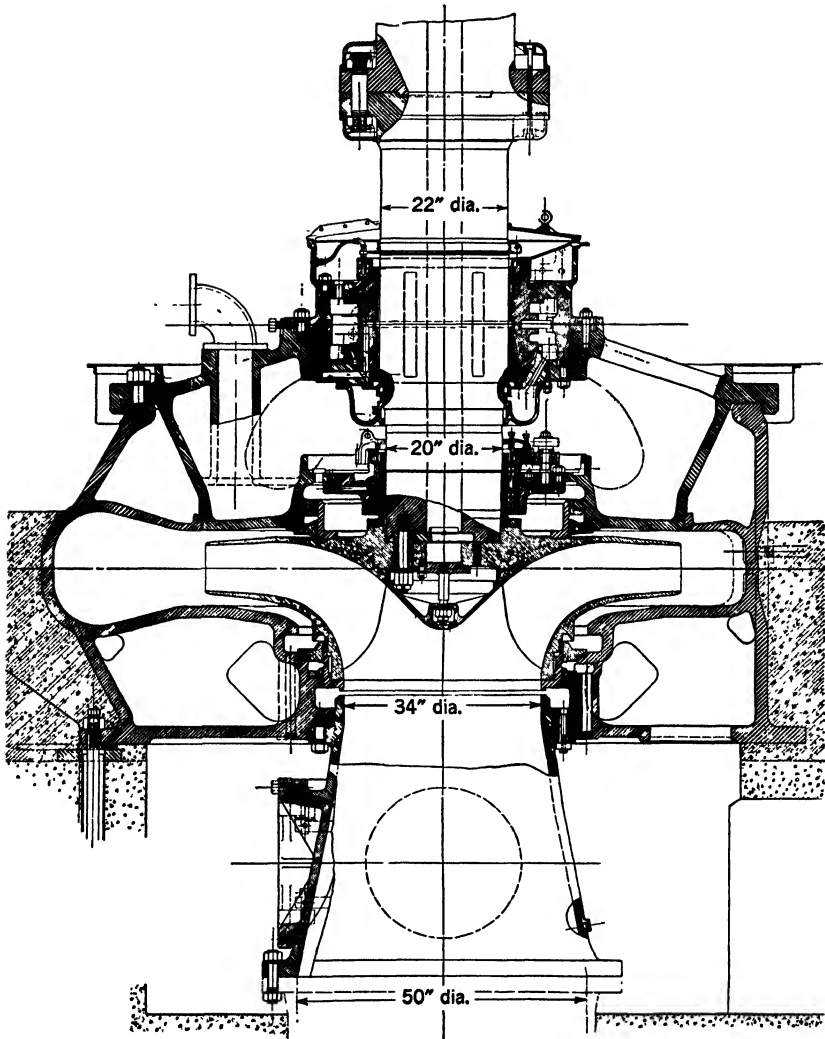


FIG. 17.14. Worthington 42-in. pump, 90,000 g.p.m., 444 ft. head, 450 r.p.m., 12,500 hp.,  $n_s = 1400$  (Eagle Mountain and Hayfield Stations, Colorado River Aqueduct).

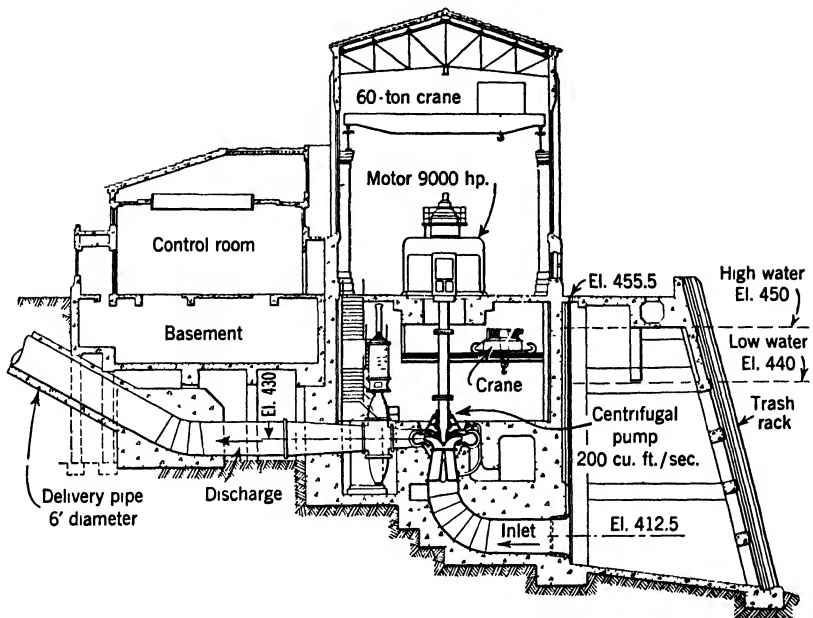


FIG. 17.15. The Intake Station of the Colorado River Aqueduct.

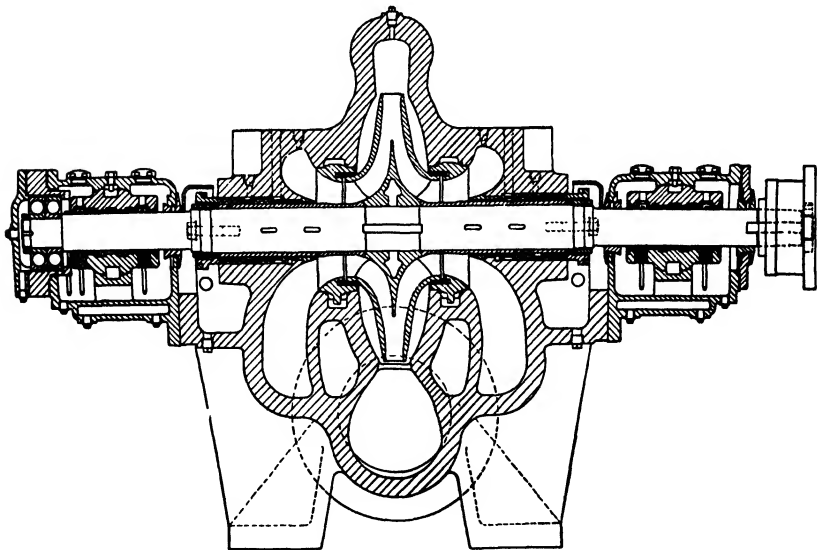


FIG. 17.16. Ingersoll-Rand 12-in. double-suction, double-volute pump; 8750 g.p.m., 707 ft. head, 1780 r.p.m.,  $n_s = 1210$ .

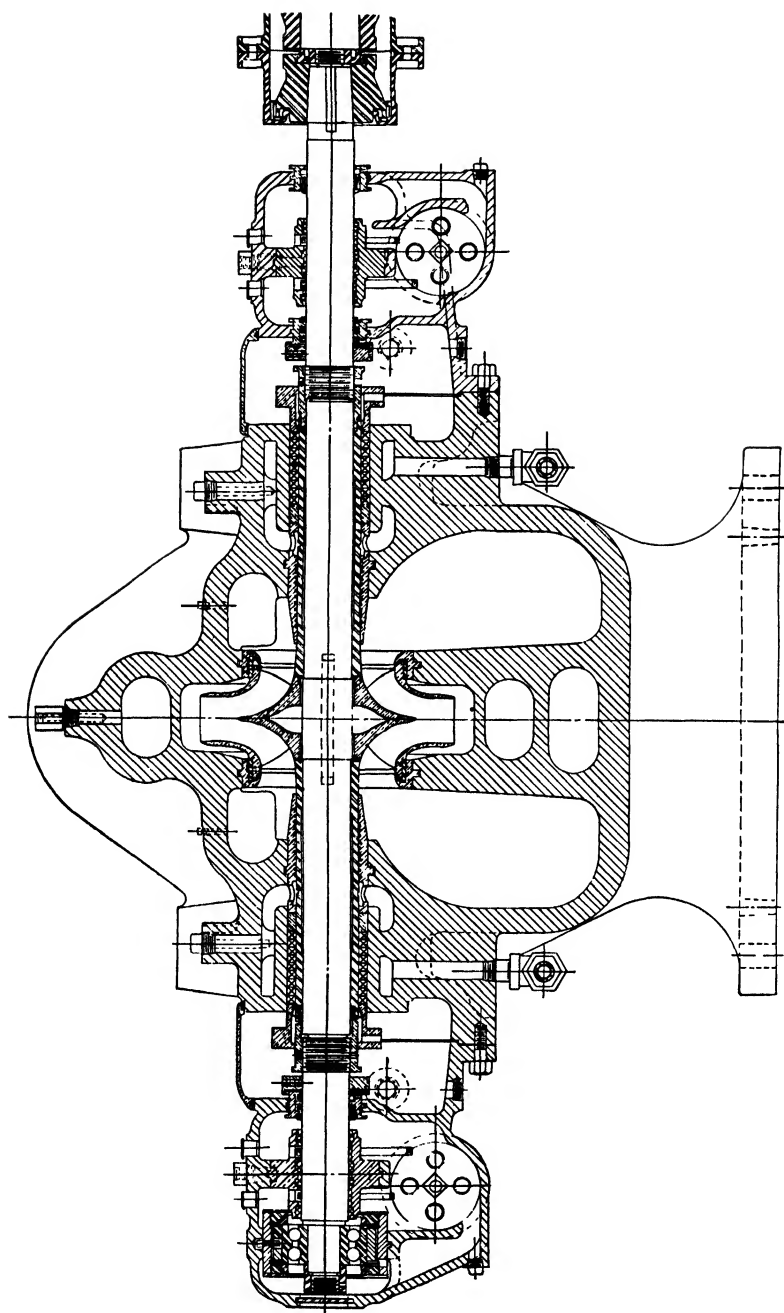


FIG. 17.17. Allis-Chalmers 12-in. double-suction, double-volute pump, 6875 g.p.m., 828 ft. head, 3550 r.p.m.,  $n_s = 1920$ .





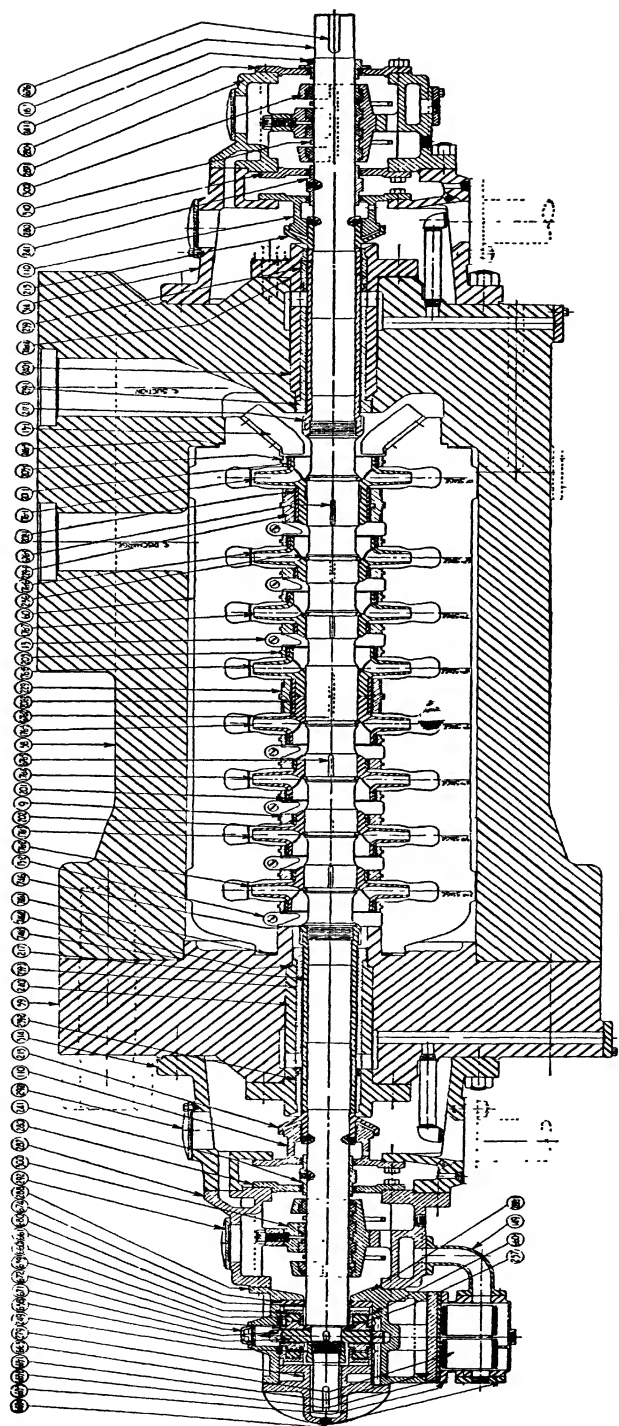


FIG. 17.18. Byron Jackson high pressure pump, 1500 g.p.m., 1800 p.s.i. head, at 3600 r.p.m., 2000 hp. Three pumps in series produce 5400 p.s.i. pressure for hydraulic forging press.  
(At Mesta Machine Works.)



and the location of the recording electrode stations, the error increasing with shorter distance.

The same tests have shown that the salt-solution or chemical method (titration) is the most accurate and consistent of the four tested. The average value of the numerous runs coincided exactly with the volumetric capacity.†

Figure 17.16 shows a 12-in. double-suction pump designed for 8750 g.p.m., 707 ft. of head, at 1780 r.p.m. The specific speed is 1210 and

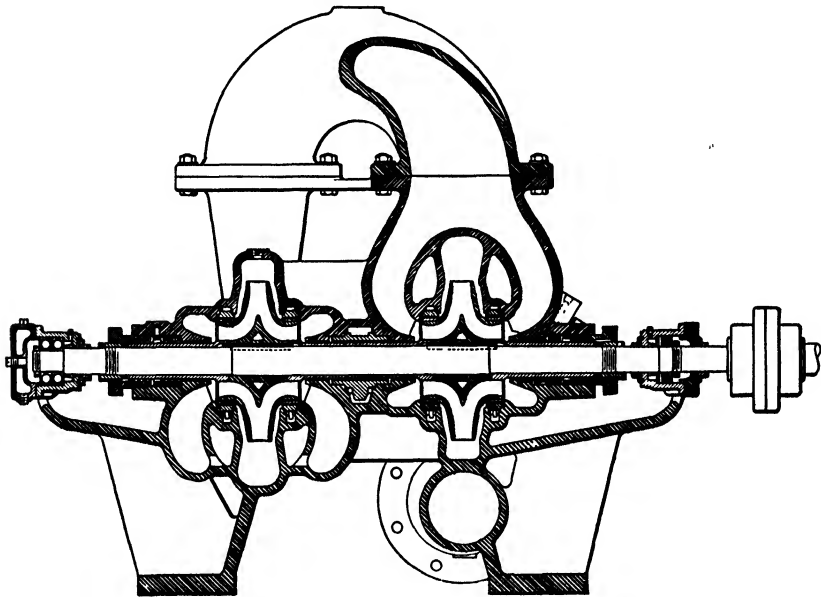


FIG. 17.19. Ingersoll-Rand 6-in. two-stage pump.

the efficiency 86.5 per cent. Three of these pumps in series were used in each of a number of stations for pumping oil from Texas to the New York area through the so-called Big Inch pipe line. Figure 17.17 shows a 12-in. pump designed for 6875 g.p.m., 828 ft. of head, 3550 r.p.m., with a specific speed of 1920 and efficiency of 85 per cent. Three of these in series were used in each station for pumping gasoline on the same project. Both pumps have double volutes, and use bleed-offs to reduce the pressures on the stuffing boxes of the high pressure pumps. For the

† The salt-solution method of capacity measurements is particularly adaptable to centrifugal pumps because it insures a thorough mixing and thus does not require a long discharge pipe. The method is described in *Hydraulics*, by Joseph N. LeConte. McGraw-Hill, 1926, p. 199.

size and type, these pumps generate the highest head per stage up to date.

Figure 17.18 shows a high pressure pump used for a hydraulic forging press. Three such pumps in series produce 5400 p.s.i. working pressure with 6600 p.s.i. shut-off head. This is the highest pressure ever produced by centrifugal pumps. Each pump is driven by 2000-hp. motors

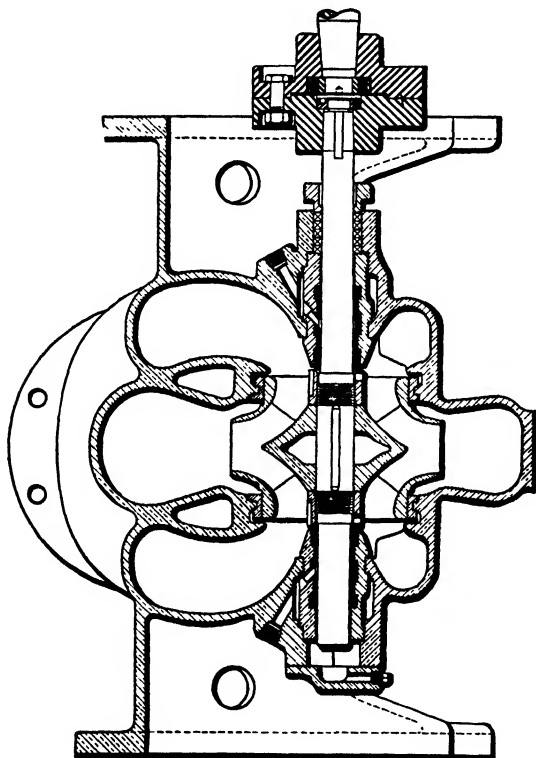


FIG. 17.20. Ingersoll-Rand vertical condenser circulating pumps for marine service.

at 3600 r.p.m.; capacity is 1500 g.p.m. There are no packed stuffing boxes in these pumps. The stuffing box pressure, at times 3600 p.s.i., is bled off to atmosphere through the closely fitted long throttle bushings.

Figure 17.19 shows a two-stage double-suction pump. This type of pump has proved the most efficient for large capacities and heads within the range of two-stage pumps.

Figure 17.20 shows a vertical double-suction pump widely used for condenser circulating service on ships. In smaller sizes and with higher speeds such pumps are built with independent ball bearings (Fig. 17.21) and have been used as cargo pumps on ships.

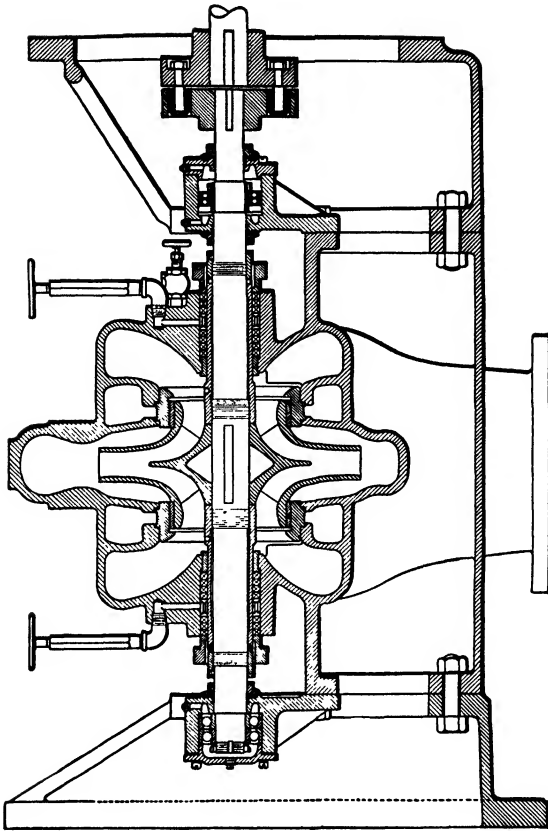


FIG. 17.21. Ingersoll-Rand vertical cargo pump for marine service.

## REFERENCES

1. A. HOLLANDER, "Stuffing Box for Refinery Pumps," *Calif. Oil World and Petroleum Industry*, March 1944.
2. HANS HORNSCHUCH, "Why Mechanical Seals Improve Centrifugal Pump Operation," *Power*, Aug. 1943.
3. A. J. STEPANOFF, "Mechanical Performance of Hot Oil Centrifugal Pumps," *Petroleum Refiner*, Dec. 1942.
4. A. J. STEPANOFF, "Testing Hot Oil Pumps under Actual Operating Conditions," *Oil and Gas Jour.*, Oct. 31, 1940.
5. KARL GRÜN, *Dampfkessel-Speisepumpen*, Vienna, Julius Springer, 1934, pp. 75, 126.
6. A. H. RICHARDS, "High-Pressure Centrifugal Boiler Feed Pumps," *Combustion*, April 1938; reprinted by Ingersoll-Rand Company.
7. *Standards of the Hydraulic Institute*, New York, Figs. B-24, B-25, B-26.

8. IGOR KARASSIK, "So You Are Going to Buy a Boiler Feed Pump," *Southern Power & Industry*, April 1942 to July 1943, pp. 55, 57 (a series of twelve articles distributed by Worthington Pump and Machinery Corporation).
9. J. W. GODSHALL, "Prevention of Feed-Pump Corrosion," *Edison Electric Institute Report*, 1941-1942, New York; reprinted by Ingersoll-Rand Company.
10. F. S. CLARK, F. H. ROSENCRANTS, and W. H. ARMACOST, "1825 Lb. Pressure Topping Unit with Special Reference to Forced Circulation Boiler," *Trans. A.S.M.E.*, Vol. 65, July 1943, p. 461.
11. F. FLATT, "Steam Circulating Pumps for High Pressure," *Escher-Wyss News*, May-June 1932.
12. R. L. DAUGHERTY, "Centrifugal Pumps for the Colorado River Aqueduct," *Mech. Eng.*, April 1938, pp. 295-299.
13. R. M. PEABODY, "Pump Discharge Valves on the Colorado River Aqueduct," *Trans. A.S.M.E.*, Vol. 62, No. 7, Oct. 1940, p. 555.
14. O. KIRSCHMER and B. ESTERER, "Die Genauigkeit einiger Wassermessverfahren," *Z. Ver. deut. Ing.*, Vol. 74, No. 44, Nov. 1, 1930, p. 1499.

## CHAPTER 18

### CENTRIFUGAL-JET PUMP WATER SYSTEMS

#### 18.1 GENERAL ARRANGEMENT

For small capacities and low lifts (up to 125 ft.) a special type of pumping unit has been developed which consists of a combination of a centrifugal pump and a jet pump or ejector. The first is mounted next to the motor at the ground surface and furnishes the driving head and capacity for the jet pump placed in the well below the water surface (Fig. 18.1). For shallow wells up to 25 ft. the jet pump can be placed on the surface of the ground or built into the centrifugal pump casing.<sup>1</sup> The mechanical advantage of this arrangement is evident as there are no moving parts in the well, and the centrifugal pump, with its motor, can be placed at some convenient point. The hydraulic advantages are: steep head-capacity characteristics with operating head about 50 per cent higher than that of the centrifugal pump alone and a brake-horsepower curve which is non-overloading. The peak efficiency of the combination is equal to or better than that of the jet pump but is lower than that of centrifugal or vertical turbine pumps.

However, at the operating capacity the efficiency is equal to or better than that of the centrifugal pump at the same capacity. In small sizes, this type of pumping unit is widely used for the domestic water supply. According to U. S. Department of Commerce Census ("Facts for

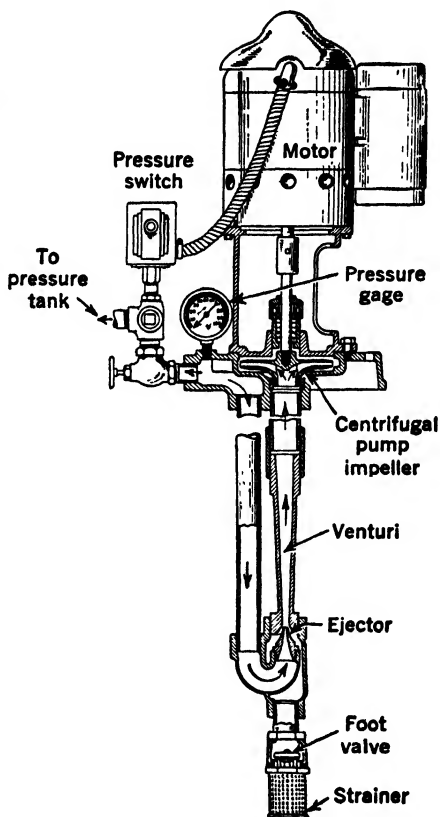


FIG. 18.1. Jacuzzi jet pump water system.

Industry," Series M31B-116) 318,758 jet-type water systems were sold in 1946, representing a value of \$24,136,614. A great majority of units are for capacities from 5 to 10 g.p.m.

## 18.2 JET PUMPS

Figure 18.2 shows a diagram of the jet-centrifugal combination and the notation for several terms used for discussion. Figure 18.3 shows

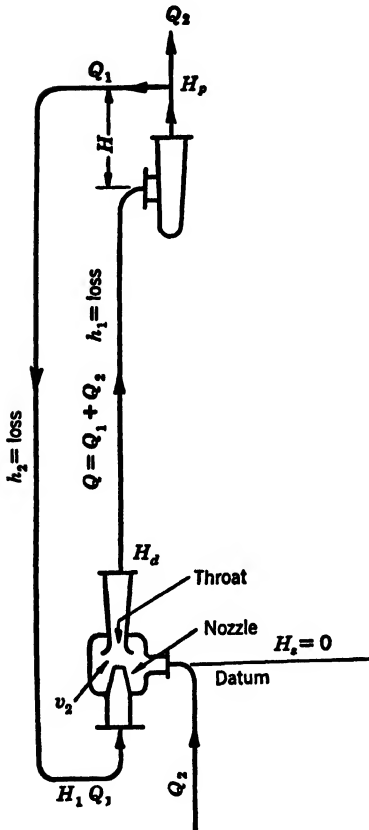


FIG. 18.2. Jet-centrifugal pump combination.

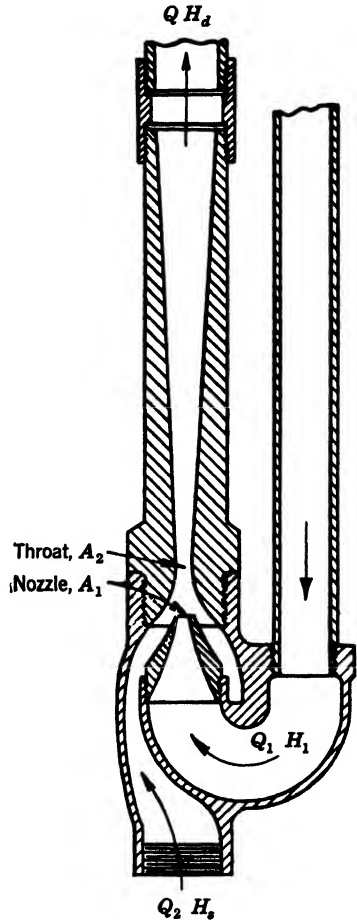


FIG. 18.3. Jet pump.

an enlarged view of the jet pump, and Fig. 18.4 gives the performance of a jet pump under several driving heads, kept constant for each head-capacity curve. Note the resemblance of these curves to centrifugal



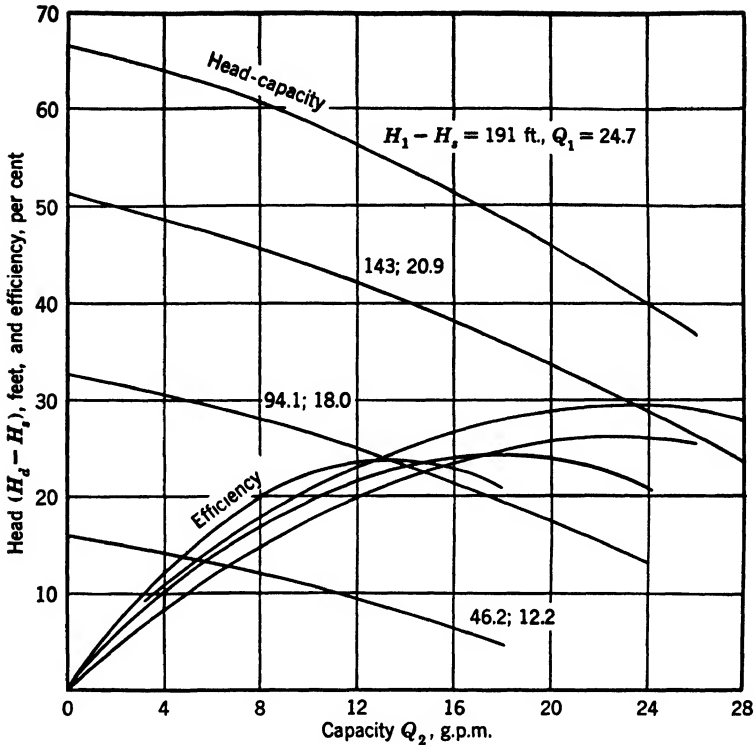


FIG. 18.4. Jet pump performance (Gosline and O'Brien).

pump characteristics at several speeds. According to Gosline and O'Brien<sup>2</sup> the characteristics of jet pumps can be described by three ratios:

$$(1) \quad R = \frac{A_1}{A_2} = \frac{\text{nozzle area}}{\text{throat area}} \quad (18.1)$$

$$(2) \quad M = \frac{Q_2}{Q_1} = \frac{\text{pumped capacity}}{\text{driving capacity}} \quad (18.2)$$

$$(3) \quad N = \frac{H_d - H_s}{H_1 - H_d} = \frac{\text{net jet pump head}}{\text{net driving head}} \quad (18.3)$$

The driving head  $H_1$  and the driving capacity  $Q_1$  are furnished from the outside source. Capacity  $Q_2$  enters the jet pump suction under the head  $H_s$ . The capacity leaving the jet pump discharge equals the sum of the driving capacity and the jet pump capacity:

$$Q = Q_1 + Q_2 \quad (18.4)$$

Figure 18.5 shows several typical characteristics of jet pumps in terms of  $M$  and  $N$  for four values of  $R$ . Except for the extreme values of  $R$

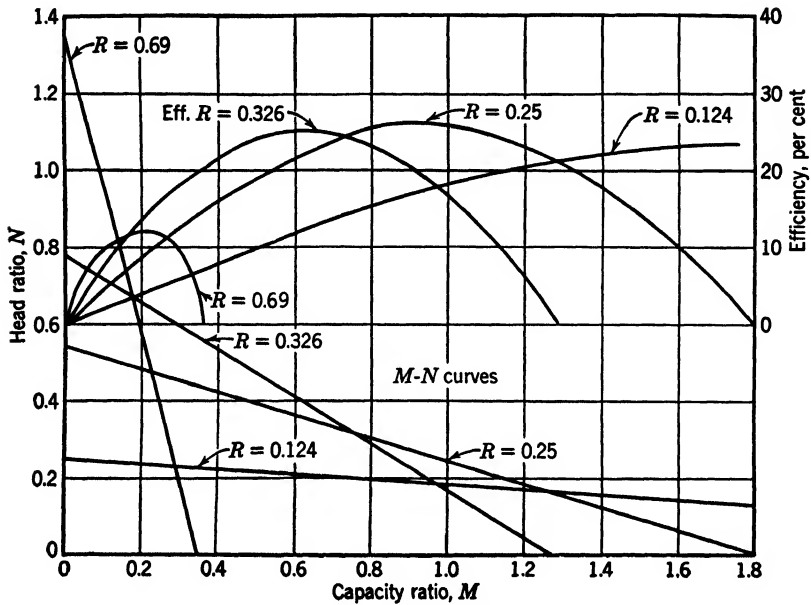


FIG. 18.5. Jet pump characteristics (Gosline and O'Brien).

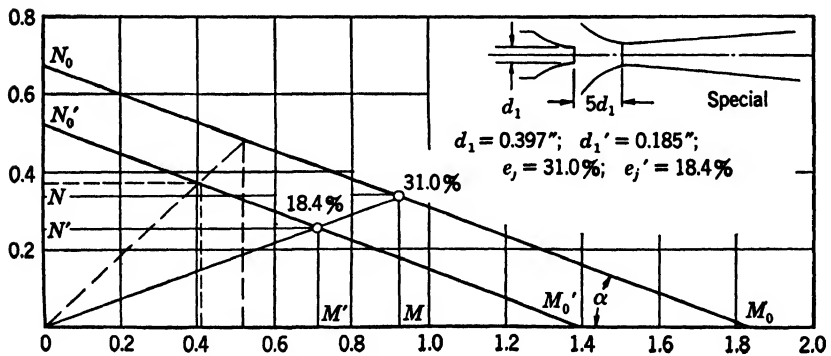


FIG. 18.6. Effect of size on efficiency of jet pumps.

the  $M$ - $N$  curves are straight lines and apply to all similar jet pumps. The slope of  $M$ - $N$  lines ( $\tan \alpha$ , Fig. 18.6) is determined by the value of  $R$ . The position of the  $M$ - $N$  lines is governed by the efficiency of the jet

pumps, more efficient pumps giving higher values of  $M$  and  $N$ , as is evident from the definition of efficiency of jet pumps (Fig. 18.6):

$$e_j = \frac{Q_2(H_d - H_s)}{Q_1(H_1 - H_d)} = MN \quad (18.5)$$

Since  $M$ - $N$  characteristics are straight lines they are completely defined by their intersections with the coordinate axes. Figure 18.7 gives

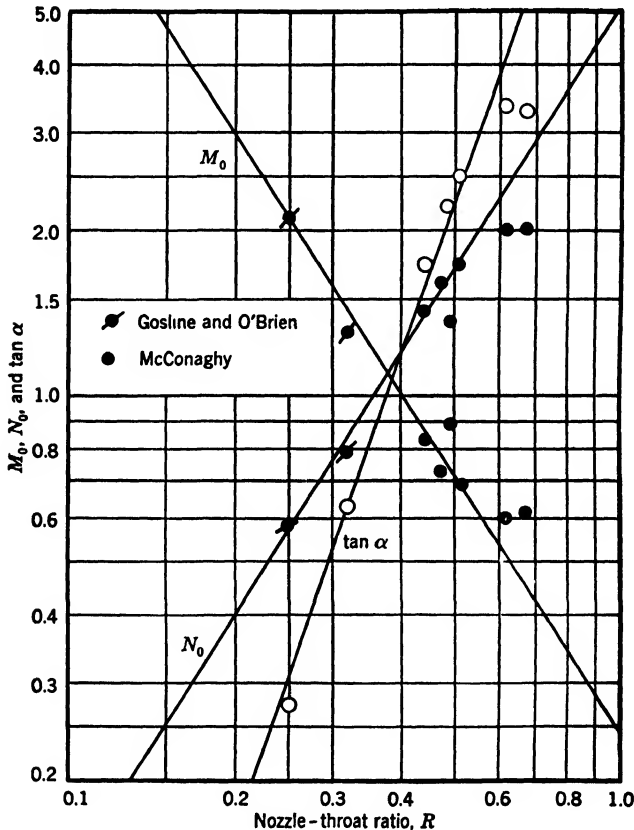


FIG. 18.7.  $M_0$  and  $N_0$  in terms of nozzle-throat ratio for 30 per cent peak efficiency.

values of  $M_0$  for  $N = 0$  and values of  $N_0$  for  $M = 0$  in terms of nozzle-throat ratios  $R$ . The fact that  $M$ - $N$  curves are straight lines results in the peak efficiency taking place at the values of  $M$  and  $N$  equal to half values of  $M_0$  and  $N_0$  respectively.

When the  $M$ - $N$  curve is established an efficiency curve can be easily plotted, and it is symmetrical about its peak. Since  $MN = e_j$ ,  $M = M_0/2$ , and  $N = N_0/2$  at b.e.p.,

$$M_0N_0 = 4e_j \quad (18.6)$$

where  $e_j$  is the jet pump peak efficiency. Thus selection of  $M_0$  and  $N_0$  fixes the efficiency of the jet pump. For a given nozzle-throat ratio, efficiency increases with the size of the pump. Efficiency also varies with the driving head as it appears in Fig. 18.4. But in every case  $M_0N_0 = 4e_j$ . Since the  $M$ - $N$  lines remain parallel it follows that for the same  $R$  and two  $M$ - $N$  curves

$$\frac{M_0N_0}{M'_0N'_0} = \frac{e_j}{e'_j} = \frac{M_0^2}{M_0'^2} = \frac{N_0^2}{N_0'^2}$$

and for all corresponding points on  $M$ - $N$  lines, such as b.e.p. (Fig. 18.6),

$$\frac{M}{M'} = \frac{N}{N'} = \sqrt{\frac{e_j}{e'_j}} = \frac{M_0}{M'_0} = \frac{N_0}{N'_0} \quad (18.7)$$

The corresponding points connected by equation 18.7 lie on radial lines drawn from the origin of  $M$ - $N$  coordinates.

Curves of  $M_0$  and  $N_0$  on Fig. 18.7 are plotted for 30 per cent efficiency. For any other values of efficiency, equation 18.7 should be used for  $M_0$  and  $N_0$  corrections. The maximum efficiency attained on commercial jet pumps in sizes employed for jet-centrifugal combination systems ( $0.25 < R < 0.625$ ) is about 35 per cent. Figure 18.7 gives also ratio  $N_0/M_0 = \tan \alpha$ ; this is the slope of  $M$ - $N$  lines, which does not depend upon efficiency of the pump.

Performance of jet pumps is affected by the nozzle position with respect to the throat, the optimum value occurring when this distance is equal to the nozzle diameter. Reduction of this distance below that value causes obstruction of the flow, and reduction of head-capacity and efficiency results. An increase of this distance above the one nozzle diameter has only a minor effect on the pump performance. Figure 18.6 shows a jet pump with the nozzle-to-throat distance equal to five times the nozzle diameter, and the nozzle-throat ratio  $R = 0.256$ . The values of  $M_0$  and  $N_0$  of this pump deviate only slightly from those given in Fig. 18.7, which apply to pumps with the nozzle-to-throat distance equal to about one nozzle diameter.

When the pressure at the nozzle discharge reaches the vapor pressure, jet pumps show the effects of cavitation in the same manner as the low

specific speed centrifugal pumps; that is, the head-capacity curve drops abruptly. Actual measurements of pressure at the throat show within a fraction of 1 ft. the vapor pressure.

### 18.3 PERFORMANCE OF A CENTRIFUGAL-JET PUMP COMBINATION \*

To proceed to the determination of the head-capacity characteristics of the combination when both centrifugal and jet pump performances are known, a number of additional notations should be made. From Fig. 18.2,

$H_p$  = centrifugal pump discharge head, which is the net head of the combination

$H$  = centrifugal net head

$H_1$  = head on the jet pump nozzle, driving head

$H_d$  = discharge head of the jet pump

$h_1$  = friction loss head in the centrifugal pump suction pipe, which is the discharge pipe of the jet pump

$h_2$  = friction loss head in the driving capacity pipe

All heads are taken above the jet pump suction level, which for simplicity is taken at the center of the jet pump suction nozzle:  $H_s = 0$ . It is convenient to consider the pipe between the jet pump discharge and the centrifugal pump suction as part of the centrifugal pump, to reduce the net centrifugal head  $H$  by the amount of loss in that pipe  $h_1$ , and to denote the difference between the two by

$$H_c = H - h_1 \quad (18.8)$$

This will be the net centrifugal head available to the system, and for a given length and size of suction pipe it can be established for the whole head-capacity range (Fig. 18.8). In this way the friction loss in the centrifugal pump suction pipe will be taken care of automatically.

The operating point of the system is determined by four conditions:

$$(1) \quad Q = Q_1 + Q_2 = Q_1(M + 1) \quad (18.9)$$

$$(2) \quad \frac{M}{M_0} + \frac{N}{N_0} = 1 \quad (18.10)$$

This is the equation of the jet pump head-capacity line, which is selected for a given nozzle-throat ratio and efficiency.

$$(3) \quad Q_1 = CA_1 \sqrt{2gH_1} \quad (18.11)$$

\* The method of determination of the characteristics of the centrifugal-jet combination was suggested in essence by McConaghy.<sup>3</sup>

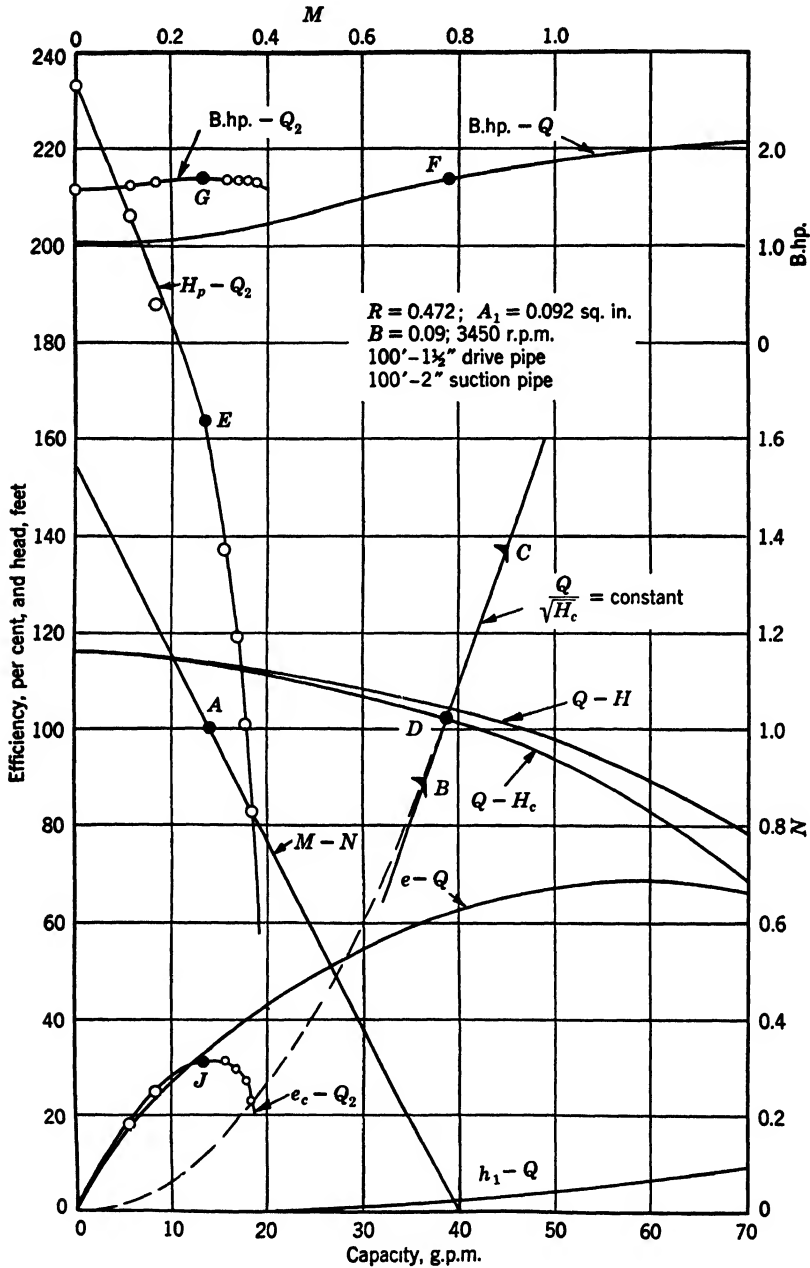


FIG. 18.8. Example of calculation of jet-centrifugal pump performance.

This is the discharge through the nozzle under the net head  $H_1$ , since  $H_s = 0$ , the small velocity head in the jet pump suction chamber being neglected.  $C$  is the nozzle discharge coefficient, selected from available data.

$$(4) \quad H_c = \frac{H_1}{N+1} [1 + B(N+1)] \quad (18.12)$$

where  $B$  is a numerical constant expressing the head loss  $h_2$  as a fraction of  $H_1$ . The development of the relationship between  $H_c$  and  $H_1$  as given by equation 18.12 follows:

From inspection of Fig. 18.2 it can be established that

$$H_p = H_1 + h_2 = H_d + H - h_1 = H_c + H_d \quad (18.13)$$

$$H_c = H_1 - H_d + h_2 \quad (18.14)$$

The value of the friction loss  $h_2$  can be expressed as a fraction of  $H_1$ :

$$h_2 = f \frac{LV_1^2}{d \cdot 2g} = f \frac{16L}{2gd^5\pi^2} Q_1^2 \quad (18.15)$$

where  $f$  is the friction coefficient,  $L$  is the length, and  $d$  is the diameter of the driving pipe.

From equation 18.11

$$H_1 = \frac{Q_1^2}{2gC^2A_1^2}$$

Combining the two,

$$\frac{h_2}{H_1} = \frac{16fLC^2A_1^2}{d^5\pi^2} = B = \text{constant} \quad (18.16)$$

$$h_2 = BH_1 \quad (18.17)$$

Then equation 18.14 becomes

$$H_c = H_1(1 + B) - H_d \quad (18.18)$$

Substituting for  $H_d$  its value from 18.3 gives the equation

$$H_c = \frac{H_1}{N+1} [1 + B(N+1)] \quad (18.12)$$

Now the number of variables is reduced by combining equations 18.9, 18.11, and 18.12:

$$Q = CA_1\sqrt{2gH_1}(M+1) \quad (18.19)$$

Squaring this and dividing by equation 18.12,

$$\frac{Q^2}{H_c} = \frac{2gC^2A_1^2(M+1)^2(N+1)}{1+B(N+1)} \quad (18.20)$$

For an arbitrary point on the centrifugal pump head-capacity curve ( $Q, H_c$ ) equations 18.10 and 18.20 are two simultaneous equations with  $M$  and  $N$  unknowns. Solution of these for  $M$  or  $N$  leads to a cubic equation, which cannot be solved algebraically. For a solution by trial it is more convenient to use equation 18.20 and reverse the procedure, that is, to substitute  $M$  and  $N$  values for an arbitrary point on the  $M$ - $N$  curve ( $A$  in Fig. 18.8). Then equation 18.20 becomes

$$\frac{Q}{\sqrt{H_c}} = \text{constant} \quad (18.21)$$

This means that equation 18.20 can be satisfied by a given centrifugal pump at any speed or impeller diameter. To find  $Q$  and  $H_c$  for a fixed r.p.m. of the pump an arbitrary value is assigned to  $Q$ , and  $H_c$  is obtained (point  $B$ ). Points of the same unit capacity ( $Q/\sqrt{H_c}$ ) lie on a square parabola with its apex at the origin of  $Q$ - $H_c$  coordinates. To determine its intersection with the  $Q$ - $H_c$  curve (point  $D$ ) another point  $C$  is located at an arbitrary capacity and connected with point  $B$  by the affinity relations. A straight line  $BC$  is drawn to intersect the  $Q$ - $H_c$  curve at point  $D$ .  $Q$  and  $H_c$  being known, the system head  $H_p$  and capacity  $Q_2$  (point  $E$ ) are found by using the relationships already established (or equations 18.23 and 18.24). The efficiency of the jet-centrifugal combination  $e_c$  (point  $J$ ) is obtained by dividing the output of the system by the brake horsepower of the centrifugal pump (points  $F$  and  $G$ ):

$$e_c = \frac{Q_2 H_p}{3960 \times \text{b.hp.}} \quad (18.22)$$

Any required number of points for the  $Q_2$ - $H_p$  curve can be obtained by this method by selecting different points on the  $M$ - $N$  curve.

#### 18.4 AFFINITY RELATIONS

**(a) Change in Pump Speed.** Equations 18.23 and 18.24 express all heads and capacities in terms of the centrifugal pump head  $H_c$  and the jet pump constants  $M$  and  $N$ .



$$\left. \begin{aligned} H_d &= H_c \frac{N}{1 + B(N + 1)} \\ H_1 &= H_c \frac{N + 1}{1 + B(N + 1)} \\ H_p &= H_c \frac{(N + 1)(B + 1)}{1 + B(N + 1)} = H_1(B + 1) \\ h_1 &= H_c \times \text{constant} = Q^2 \times \text{constant} \\ h_2 &= BH_1 \end{aligned} \right\} \quad (18.23)$$

$$\left. \begin{aligned} Q_1 &= \sqrt{H_c} \frac{CA_1 \sqrt{2g(N + 1)}}{\sqrt{1 + B(N + 1)}} = CA_1 \sqrt{2gH_1} \\ Q_2 &= Q_1 M \\ Q &= Q_1(M + 1) \end{aligned} \right\} \quad (18.24)$$

When centrifugal pump speed or impeller diameter is changed  $M$  and  $N$  values remain the same, and it can be stated from equations 18.23 that the net system head  $H_p$ , and the other heads  $H_1$ ,  $H_d$ ,  $h_1$ , and  $h_2$ , vary directly as the square of the speed or impeller diameter, or directly as the centrifugal head  $H_c$ . Similarly from equations 18.24 the capacity of the jet-centrifugal pump combination  $Q_2$ , and also  $Q_1$  and  $Q$ , vary directly as the speed or impeller diameter of the centrifugal pump or directly as  $\sqrt{H_c}$ .

**(b) Change in Size of Jet Pump.** If, for a given centrifugal pump, a larger jet pump of the same design ( $R = \text{constant}$ ) is used  $M$  and  $N$  remain the same except for the effect of change in peak efficiency.  $Q/\sqrt{H_c}$  will increase directly as the nozzle area  $A_1$  (equation 18.20). This means that the operating point of the centrifugal pump will move to a higher capacity and lower head. Since  $M$  remains the same  $Q$  will be split in the same ratio, or  $Q_1$  and  $Q_2$  will change directly as  $Q$ . All the heads,  $H_p$ ,  $H_d$ ,  $H_1$ ,  $h_1$ , and  $h_2$ , will change directly as  $\sqrt{H_c}$ .

**(c) Increase of Throat Size.** If, for a given centrifugal pump, the nozzle-throat ratio  $R$  is changed, for instance, by increasing the throat area by reborings,  $R$  will decrease. For b.e.p.,  $MN = e_j$  will essentially remain constant but  $M$  will increase and  $N$  will decrease. Thus, from equation 18.20, the centrifugal pump unit capacity  $Q/\sqrt{H_c}$  will increase (for simplicity assume  $B = 0$ ); this means that the operating point of the centrifugal pump will move to a higher capacity  $Q$  and

lower head  $H_c$ ; therefore  $H_p$  and all heads will decrease, because of the decrease of both  $N$  and  $H_c$  as shown by equations 18.23. Capacity  $Q_2$  will increase, but  $Q_1$  will decrease because of the decrease of the driving head  $H_1$ .

**(d) Increase of the Nozzle Size.** If the nozzle ratio  $R$  is increased by reborng the nozzle diameter, variation of heads and capacities will be in the opposite direction to that in case (c); that is, all heads will increase,  $Q_1$  will increase,  $Q_2$  will decrease, and  $Q$  will decrease.

**(e) Change in Size or Length of Pipes.** If the size or the length of the centrifugal pump suction pipe is changed so that the hydraulic loss  $h_1$  in this pipe is increased,  $H_c$  will be lower (Fig. 18.8). The decrease in  $H_c$  will be followed by a decrease in all heads and capacities. If the size or length of the drive capacity pipe is so changed as to increase its resistance  $h_2$ , the constant  $B$  will increase, and both heads and capacities will drop as indicated by formulas 18.23 and 18.24.

#### REFERENCES

1. The National Association of Domestic and Farm Pumping Equipment, "Manual of Water Supply Equipment," pp. 37-47, 1946.
2. J. E. GOSLINE and M. P. O'BRIEN, "The Water Jet Pump," *Univ. of Calif. Publ.*, Vol. 3, No. 3, pp. 167-190.
3. J. W. McCONAGHY, "Ingersoll-Rand Company's Development Report," C-HDA-9348, 1941 (not published).

## INDEX

- Absolute flow, 2
- Absolute velocity, 31
- Adjustable vane, 151, 320, 367
- Adjustment, axial, 214
- Affinity law, 27, 80, 310
  - jet-centrifugal, 422
- Air impingement, 254
- Airfoil, nomenclature, 147
  - properties, 155
  - theory, 158
- Angle, discharge, 51, 97, 182
  - entrance, 98
- Angle of attack, 147
- Angular velocity of vortex, 14
  - absolute flow, 68
  - relative, 68
- Aspect ratio, 147
- Axial flow design, 154
- Axial flow impeller, 22, 63, 66, 91
- Axial flow pumps, 143, 371
- Axial thrust, 218
  - balancing, 218, 223
  - of open impellers, 236
  
- Balancing, automatic, 225
  - dynamic, 352
- Balancing axial thrust, 218, 223
- Balancing drum, 140, 225
- Balancing shafts, 352
- Base circle, 126
- Bearing loss, 205
- Bernoulli's equation, 1
- Boiler feed, 298, 397
- Brake horsepower, 27, 354, 358
  - ratio, 153, 354
- Buoyancy force, 334
  
- Camber, 146, 147, 152
- Capacity, unit, 82, 86
- Capacity coefficient, 46
- Capacity constant, 96
- Capacity measurement, 5, 383, 405
- Capacity regulation, 319
- Casing, axial flow pump, 165
  - circular, 132
  - diffusion, 23, 138
  - distortion, 393
  - pump, 121
  - volute, 23, 122, 130
- Cavitation, 241
  - due to vibration, 253
- Characteristics, 25, 35
  - author's diagram of, 184
  - complete, 272
  - dimensionless, 45
  - Euler's, 44
  - jet pump, 414
  - theoretical, 35
  - type, 99
  - unstable, 296
- Chord, 147
- Chord-vane spacing ratio, 151
- Circulation, relative, 49
- Clutch, disengaging, 275
- Coefficient, capacity, 96
  - discharge, 198
  - drag, 156
  - friction, 4, 195
  - head, 45, 95
  - lift, 156
- Condensate pump, 234
  - throttling, 236
- Cone development, 108
- Constant, capacity, 96
  - design, 93, 141, 188
  - speed, 94
  - Thomas', 262
- Corrosion, 248
- Coupling, 274, 349
  - variable speed, 324
- Critical speed, 328, 336
  - secondary, 347
- Crossover, 136

- Damping of vibration, 334
- Darcy's formula, 3
- Deflection, dynamic, 341
  - static, 339, 341
- Depression, dynamic, 256
- Design, axial flow, 154
  - shaft, 328
  - sump, 363
- Design constants, 93, 141, 188
- Design procedure, 154
- Discharge coefficient, 198
- Disk friction, 201
- Distortion casing, 393
- Drag coefficient, 156
- Drum, balancing, 140, 225
- Dunkerley's formula, 337, 342
- Dynamic balancing, 352
- Dynamic deflection, 341
- Dynamic depression, 256
  
- Eddy loss, 174
- Efficiency, 27, 37
  - hydraulic, 37, 178
  - jet pump, 417
  - mechanical, 39
  - vane, 38, 46
  - volumetric, 38, 193
- Elasticity modulus, 351
- Elbows, flow through, 7
  - in series, 10
  - losses in, 18
  - non-reversing, 273
- Energy gradient, 10, 17, 133, 135
- Error triangles, 110
- Euler's characteristics, 44
- Euler's head, 35, 39
- Euler's velocity triangle, 35.
- Euler's work diagram, 47
- Expansion, heat, 391
  
- Fatigue of metals, 130, 248
- Floor clearance, 364
- Flow, absolute, 2
  - curvilinear, 5
  - pipe, 5, 195, 301
  - through elbows, 7
- Free vortex, 15, 70
- Friction, disk, 201
- Friction coefficient, 4, 195
  
- Gage, flow, 383
- Gas liberation, 2, 241
- Gradient, energy, 10, 17, 133, 135
  - hydraulic, 10
- Guide vanes, 163
- Gyroscopic action, 350
  
- Head, Euler's, 35, 59
  - input, 34
  - integrated, 65
  - negative, 271, 287
  - shut-off, 101
  - theoretical, 32, 52
  - total, 26
- Head-capacity equation, 176, 177
- Head coefficient, 45, 95
- Heat expansion, 391
- Horsepower, brake, 27
  - water, 27
- Hot-oil pumps, 388
  - testing, 390
- Hub ratio, 144
- Hydraulic gradient, 10, 12
- Hydraulic Institute, 268, 386, 398
- Hydraulic losses, 18, 170
- Hydraulic radius, 3
  
- Impeller, axial flow, 22, 63, 66, 91
  - design of, 103
  - mixed flow, 23, 69, 92, 106
  - open, 22, 213, 237
  - pitting of, 248
  - radial, 22, 58, 89
  - theory, 31
- Impeller approach, 39
- Impeller diameter, reduction of, 89
- Impelling ratio, 68, 188
- Impingement, air, 254
- Impulse action, 36
- Integrated head, 65
  
- Jet pump, 413
  - water system of, 413
  
- Kármán's formula, 202
- Kinematic viscosity, 79, 313
  
- Leakage, interstage, 233
- Leakage loss, 193
- Least resistance principle, 40

- Lift coefficient, 156
- Losses, bearing, 205
  - eddy, 174
  - hydraulic, 18, 170
  - leakage, 193
  - mechanical, 205
  - shock, 174
  - through tee, 18
- Materials, boiler feed, 399
  - corrosion-resisting, 251
- Mean camber line, 147
- Mean effective diameter, 166
- Mechanical losses, 205
- Metals, fatigue of, 130, 248
- Mixed flow impeller, 23, 69, 92, 106
- Model testing, 325
- Modulus of elasticity, 351
- Moment diagram, 339
- Momentum principle, 32
- Moody's formula, 326
- Motor, submersible, 378
- N.A.C.A., 155, 157
- Node, 333
- Noise, 242
- Nozzle, suction, 121
- Nozzle-throat ratio, 415, 423
- NPSH, 30, 269, 398
- Oil whip, 348
- Open impeller, 22, 213, 237
- Operating point of system, 301
- Paper stock pump, 43
- Parallel operation, 283, 299
- Performance, 27, 189
  - hydraulic, 170
  - jet-centrifugal, 419
  - jet pump, 415
- Pfleiderer's correction, 55
- pH number, 399
- Pipe flow, 5, 195, 301
- Pipe lines, throttling, 305
- Pitch, inlet, 66
  - outlet, 66
  - per second, 66
- Pitot tube, 383
- Pitting, vane, 248
- Power, balance of, 207
  - brake horsepower, 27
  - shut-off, 211
- Prerotation, 39, 162
- Pressure, "conduction," 11
  - "convection," 11
  - in elbow, 7
  - transition of, 11
- Pressure distribution, 48, 51
- Pressure energy, 13
- Pressure radiation, 11
- Pressure surges, 277
- Pressure swings, 296
- Propeller pumps, 23, 371
- Rachet, non-reversing, 277
- Radial impeller, 22, 58
- Radial ribs, 222
- Radial thrust, 128, 132, 146
- Radius, hydraulic, 3
- Reaction, generator, 60
  - turbine, 60
- Reduction, of channel area, 19
  - of impeller diameter, 89
- Regulation of capacity, 319
- Reverse rotation, 74, 277
- Reynolds' number, 3, 79, 316
- Ribs, radial, 222
- Rotation, motor, 277
  - reverse, 274, 277
- Rotometer, 41
- Salt-solution method of testing, 409
- Secondary critical speeds, 347
- Separation, 174, 241
- Shaft coupling, 274
- Shafts, balancing, 352
  - deflection of, 331
  - design of, 328
- Shock loss, 174
- Sigma, 262
- Similitude principle, 76
- Slope diagram, 340
- Solids, pumping, 14, 75
- Specific speed, 23, 29, 76, 99, 293
  - conversion factors, 88
- Speed, critical, 328, 336
  - secondary, 347
  - reverse, 274
  - specific, 23, 29, 76, 82, 99, 293

- Speed, specific (*Continued*)
  - conversion factors, 88
  - torque curve, 288
  - unit, 82, 86
  - variable, 307, 320, 323
- Speed constant, 94
- Starting pumps, 287, 290
- Static deflection, 341
  - moment diagram, 339
- Storage plants, 282
- Streamline, 2
- Stuffing box, 205, 334
- Submergence, 363
- Submersible motor, 378
- Suction nozzle, 121
- Sump design, 363
- Surges (pressure), 277, 296
- Swings (pressure), 296
  
- Tee, loss through, 18
- Terminology, 21
- Testing, of hot-oil pumps, 396
  - of models, 325
- Theoretical characteristics, 35
- Theory, airfoil, 158
  - impeller, 31
  - vortex, 14, 58
- Thoma's constant, 262
- Throat, 414, 423
- Throttling condensate pumps, 236
- Throttling pipe lines, 305
- Throttling pump suction, 247
- Thrust, axial, 218, 236
  - radial, 128, 132, 140
- Torque-speed curve, 288
  - effect on critical speed, 350
- Triangle, error, 110
  - velocity, 31, 35, 44, 186
- Turbine, efficiency of, 281
  - operation of, 280
  - reaction of, 60
  - water, 297
- Turbine pumps, 141
- Type characteristics, 99
  
- Unit capacity, 82, 86
- Unit peripheral velocity, 95
  
- Unit speed, 82, 86
- Unstable characteristics, 296
  
- Vanes, adjustable, 151, 320, 367
  - curvature of, 147
  - guide, 163
  - interference of, 161
  - non-active, 5
  - number of, 145, 152, 355
  - pitting of, 248
  - plain, 105, 119
  - spacing, 145
  - thickness of, 152
  - twist of, 149
- Variable speed, 307, 320, 323
- Variable speed couplings, 324
- Velocity, absolute, 31
  - angular, of vortex, 14
  - unit peripheral, 95
- Velocity distribution, 6, 48
- Velocity triangle, 31, 35, 44, 186
- Vibration, cavitation due to, 253
  - damping of, 334
  - natural period, 332
  - torsional, 351
- Viscosity, 313
  - conversion factors, 313
  - correction factors, 317
  - kinematic, 79, 313
- Viscous liquids, pumping, 310
- Volumetric efficiency, 38, 193
- Volute, 23, 122
  - double, 130
  - velocity distribution of, 50
- Volute angle, 126
- Vortex, angular velocity of, 14
  - forced, 15, 66
  - free, 15, 70
  - theory, 14, 58
  
- Water horsepower, 27
- Water system, of jet pump, 413
- Water turbine, 72, 137, 281, 297
- Wearing rings, 194
  - pressure at, 197
- Work diagram, Euler's, 47



